CELLULAR METAL MATERIALS

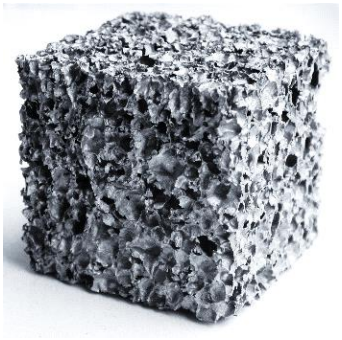

Iva Nová
Karel Fraňa
Jiří Machuta

This monograph is intended for the professional and scientific public, or even for doctoral students, to gain theoretical and professional knowledge in our country of a non-traditional, world of progressive technology and production of metal cellular systems.

This monograph was produced as a result of the solution and sustainability of the OP V V V excellent research: Hybrid Materials for Hierarchical Structures, Registration No: CZ.02.1.01/0.0/0.0/16_019/0000843.

Reviewers: Prof. Ing. Štefan Michna, Ph.D.
Ass. prof. Ing. Václav Machek, CSc.

“Vydala Technická univerzita v Liberci v roce 2024” a “ISBN 978-80-7494-729-2”.

CONTENTS

Foreword

This monograph covers the characteristics of manufacturing methods for metallic cellular and metallic porous materials. These materials currently have considerable industrial applications. The properties of these materials, based on their cellular or porous form, have been derived by analogy to the structure of natural substances. There are many of these substances, some of which we use almost every day and some of which have specific applications. Probably the most well-known method of preparing porous substances can be found in the baking industry. For example, bread, rolls, buns and other baked goods are characterized by their porous structure. Yeast contributes to the porous structure of bread by converting sugar to form carbon dioxide, which causes the baked goods to become porous. Another way of obtaining a porous structure in food is by the thermal decomposition of *sodium bicarbonate* that takes place during baking. The decomposition product of this substance is contained in baking powder, which also produces carbon dioxide.

Note: ***This means that baking cakes contributes to global warming.***

As in the previous cases, many other porous substances are prepared. Another possibility is the production of foamed metals, e.g. the production of foamed aluminium is based on the injection of gas into the melt followed by solidification of the foamed melt. Or another production method is based on the principle of "baking powder". This function is actually performed by e.g. titanium hydride (TiH_2), which is a very volatile substance. This substance decomposes at a certain temperature into titanium to form hydrogen. However, the production of foamed aluminium is incomparably very demanding, unlike baking a roll.

A somewhat unconventional principle of another method of producing porous substances is based on the joining of various particles. As, for example, tiny glass particles are heated briefly to the melting point of glass, a solid porous material is formed as a result of the particles melting at the point of contact. Porous materials can also be obtained by other ways of joining small particles. For this purpose, e.g. high-pressure compression can be used. One frequently used method is based on the removal of the liquid component from various substances. The higher the liquid content of the substance, the more porous the substance can be obtained. Therefore, in order to prepare such substances, it is necessary to master the preparation of the intermediate with the highest possible liquid content. This substance can be obtained, for example, by mixing clay and water. This produces a gel with a structure similar to a 'house of cards', with water molecules in the spaces between the 'cards'. Another method of preparing porous substances is based on the selective dissolution of one of the components of the solid phase (e.g. limestone formations).

Publication by *Karol Jedinák, Faculty of Science, Comenius University, Bratislava, February 17, 2009.*

Cellular metal systems, referred to as metal foams, with the production of and characterization are the subject of this book, are in a broad sense agglomerations

of gas bubbles. These bubbles are separated from each other first by thin liquid, later by thin layers of solidified metal.

Introduction

Nowadays, lightweight metal materials are increasingly used in industrial practice. It seems unbelievable that even this porous material can be used for structural purposes, and this is mainly because there is a tendency to use materials with considerable compactness without pores and micropores. However, it must also be remembered that nature has created porous organic substances such as bones, coral, etc., which, due to their cellular structure, are characterised by a relatively high stiffness.
Fig. 1 shows the structure of the bone and the structure of the plant stem.

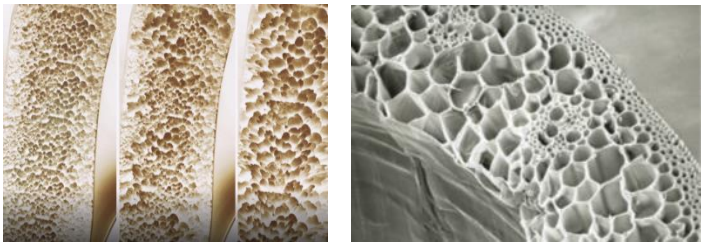

Fig. 1 Bone structure in longitudinal section and cellular structure of the plant stem [12]

Natural porous materials (bones, coral and cork) are synonymous with strong and lightweight structures. These are groups of materials with unique combinations of properties. As a result of the foam system being a non-linear stochastic distribution of material in space, it is not so easy to define their behaviour under different stresses when designing parts made of metallic foam materials. Metal foam products allow the use of hitherto little-known principles, whereby the method of manufacturing components allows the material to be more appropriately distributed throughout the volume of the component in an attempt to increase the cross-section and, hence the moment of inertia without increasing its mass.
For a long time, mankind has been trying to produce these materials industrially. In this field, scientists and engineers have followed the nature of nature and, in the last 30 years, have been intensively involved in the development and production of cellular metal systems - porous metals and metal foams ranging from laboratory curiosities to commercial components.
Fig. 2 shows different types of cellular metal structures (metal foams), which are produced by different technologies.
These lightweight metallic structures, containing 75 % to 95 % porosity, are usually divided into two distinct groups according to the appearance of the pores:
Metallic materials with closed pores are filled with gas (usually referred to as foams because of the foaming process required, such as putting bubbles into beer). These

materials have good strength and are mainly used for structural applications (e.g. in vehicles) and are also suitable as thermal insulation.

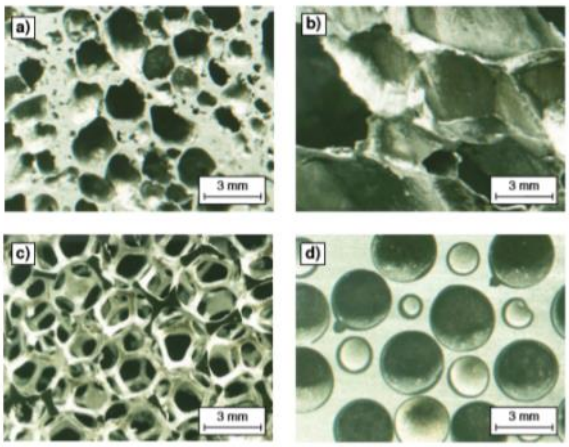

(a) closed-cell aluminium foam produced by powder metallurgy (product name: Alulight®), (b) molten metal by introducing gas into molten aluminium foam (product name: Cymat), (c) metallurgical melt open-cell aluminium sponge imaged by a precision casting process (product name: Duocel®), (d) syntactic bituminous foam produced by infiltration of ceramic hollow sphere packages by fusion metallurgy

Fig. 2 Cellular metallic structures made by different technologies, HARTMANN [12]

Metallic materials with open pores, connected cells (like a sponge, usually called porous metals). These materials are mainly used in applications where the permanent nature of porosity is used (e.g. vibration, filtration and catalysis at high temperatures, in medical devices) and are also suitable as sound insulation.
Fig. 3 shows a metallic material with closed and open pores.

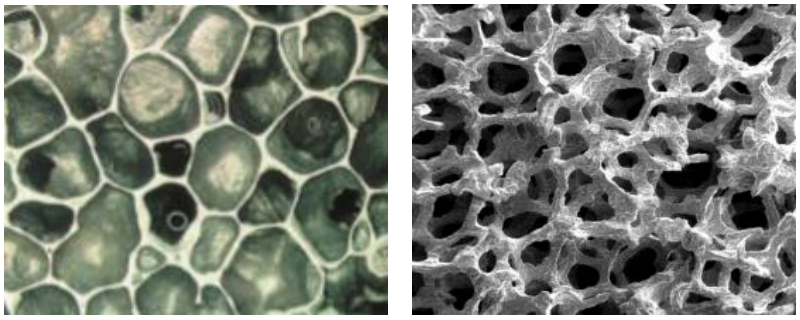

Fig. 3 Metallic material with closed and open pores [2]

Aluminium and its alloys are the most widely used in the production of metal cellular materials ("metal foams"). This is due to its relatively low density (ρ = 2700 kg.m^{-3}), low melting temperature (660 °C), relatively high stiffness, toughness and excellent corrosion resistance. These materials also exhibit good impact energy absorption and damping capabilities and are advantageously non-flammable and recyclable.

Cellular metal systems (cellular metal structures or metal foams) are nowadays to some extent a relatively new type of metallic material. They are characterised by special properties and find applications in a wide variety of industries, such as the automotive and transport industries. In particular, foams made of aluminium and its alloys are used in crumple zones and impact elements of road and rail vehicles. These foams are used because of their good ability to absorb impact energy. Due to the relatively high manufacturing difficulty and the complexity of developing new cellular metallic materials, the determination of their mechanical and physical values is very important. Initially, the values of these quantities were verified mainly experimentally. Although this approach gives reliable results, the major drawback is the financial complexity of special measuring equipment and the cost of the samples to be tested. Methodologies are gradually being developed and ways of testing their mechanical properties are being proposed.

The history of metal cellular systems (metal foams), the first mention of which dates back to 1926, [1]. It is generally stated that the origins of cellular metal systems date back to the late 1940s [2] when Benjamin Sosnick filed a patent for a "Mass of Metal" foam manufacturing process. His method took advantage of the fact that in alloys containing different phases with very different melting and boiling temperatures, the phases could melt and boil independently. In this process, a multi-phase alloy is heated, with the alloy composition chosen so that one of the components boils while the other merely melts. The alloy was in a pressure vessel during heating so that the metal in the gaseous state could not escape from the melt. The creation of pressure conditions led to the sudden boiling of the alloy, which could then be cooled. This produced a solid metallic mass full of closed pores. Since the 20th century, cellular materials have been constructed from metallurgical base materials [5], their properties have been systematically investigated and it has been determined for which technical applications they are applicable. Later, these cellular materials (cellular systems) came to be more favourably referred to as "foams" and, in the case of metallic systems, "metal foams", [3]. Over time, many patents have been published for their fabrication. These patents were focused on variations of foaming processes and today it is difficult to even assess whether all the proposed ideas would work in the manufacture of metallic cellular systems. Experts [6] and [7] now believe that the origin of metal foams (cellular metal systems) dates back to the 1940 s. According to BANHART [7], the development of aluminium foams started in the 1950s, at Bjorksten Laboratories (BRL). Also from the late 1950s, there are references to the development of aluminium foams in the USA, where 30 years later they started to be commercialized under the name of metal foams (cellular metals), [7].

From the late 1950 s to the 1970s, many patents were created and issued and many variations of metal foam production were designed. Whether anything was published alongside these patents is difficult to assess and trace.

Since the end of the 1980s, an increase in scientific activity can be seen, which has led to the revival of some old techniques, as evidenced by much higher publication

activity. Nowadays, it is observed that metal foam manufacturers and operators are trying to commercialise the production to a noticeable extent.
As pointed out by BANHART [3], the use of language in this area of research is often imprecise, BANHART [4] uses the term "foam" to mean a mixture of gas and solid phase in which the gas bubbles are isolated from each other, while the solid matrix is a random one that comes from the liquid phase in which the bubbles are arranged loosely. Nowadays, foam manufacturers try to characterize them, at least stating whether the foam has *open* or *closed* cells.

In the past, research and development work in the field of metal foams has been carried out mainly empirically, without detailed knowledge of the basic mechanisms of the foaming process. From the current literature, comprehensive characterizations, which are very successful, have been carried out and published by BANHART [5] and [7]. Obviously, the idea of foaming metals is very old, but several technologies for their production were proposed in the 1950s. Gradually since then, the basic innovations that are known today and that have led to the variety of processing methods are constantly being reviewed and innovated. The most important milestones in the development of foam technologies and some attempts to commercialize metal foams are presented. Continuous improvements in the production methods of aluminium foams have led to their recent industrial applications. Based on earlier developments, a number of new processing methods have been proposed.

In 2000, the book "Metal Foams" by ASHBY et al. was published [6]. This book is a basic and comprehensive literature for this time. The development of this book was supported by the British Council for Science and Research in dealing with ultralight metallic structures. Many researchers and groups have contributed to this book (Professor B. Budiansky, Professor H. Stone, Professor R. Miller, Dr. A. Bastawros, Dr. Y. Sugimura, Department of Engineering and Applied Science, Harvard University; Dr. T. J. Lu, Dr. Anne-Marie Harte, Dr. V. Deshpande, Centre for Micromechanics, Engineering Department, Cambridge University; Dr. E. W. Andrews and Dr. L. Crews, Department of Materials Science and Engineering, MIT; Professor D. Elzey, Dr. D. Sypeck and Dr. K. Dharmasena, Department of Materials Science and Engineering, UVA; Dr. John Banhart, Fraunhofer Institut Angewandte Materialsforschung, Bremen; Professor H.P. Degisher and Dr. Brigdt Kriszt of the Technical University of Vienna; Dr. Jeff Wood of Cymat Corp., Mississauga, Canada; and Bryan Leyda of Energy Research and Generation Inc., Oakland, CA). Much time has passed since then, and many researchers are now known to be addressing the issue of fabricating metallic cellular systems.
In addition to metal foams, there are also methods of producing metallic porous systems based on tiny "cores" cast into the melt. For this purpose, for example, particles of table salt NaCl - are used, which are poured directly into the melt or indirectly by mixing aluminium powder with table salt.

Today, there are a number of methods of manufacturing cellular metal materials (systems), which have different trade names and have been developed by different manufacturing or research companies. Such as Alporas, Cymat, Hydro/alco, Formgrip, Foamcarp, Foamcast, Alulight/Foaminal, Gasar, Duocel, etc.

A classification of the generally referred metallic cellular materials has been attempted by BANHART [3], [4], and GARCIA-MORENO [10]. They made a division of the methods of producing metallic foams based on the two, already mentioned, basic groups (closed or open cell foams), see Fig. 4.

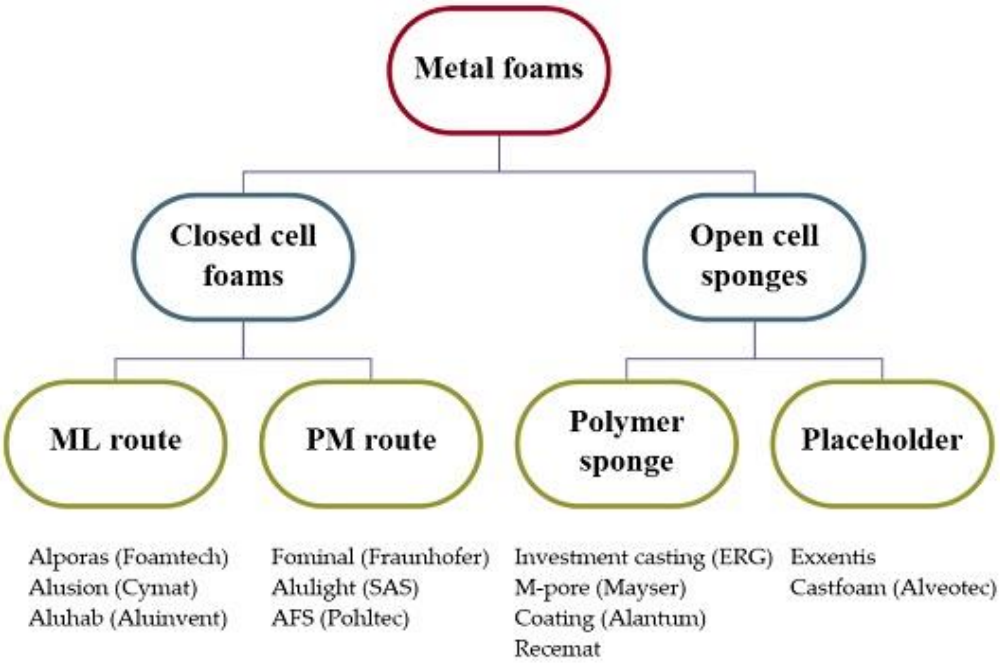

.

Fig. 4 Classification of metallic cellular materials (metallic foams) according to GARCIA-MORENO [10]

As reported by GERLY and CLYNE [11], two basic methods of producing closed-cell aluminium foams are currently based on molten aluminium. One process has been developed in Japan (US patent 4713277), which involves adding or incorporating calcium into molten aluminium. This produces dispersed calcium solids in the aluminium melt which are designed to increase the viscosity of the melt. In the next step, a foaming process is carried out. This adds a foaming agent to the aluminium melt (e.g. TiH_2 powder, the thermal decomposition of which produces a gas for foaming the melt). The second process has been patented by Alcan (US patent 5112697). The principle of this method is to bubble the aluminium melt with a gas, usually air. The aluminium melt must contain particles of silicon carbide which affect the retention of the froth cells rising to the surface of the melt. In this method, the foamed melt is fed onto a moving belt where solidification takes place.
The production of aluminium foam by Hydro Aluminium, Norway, is based on a similar production process. An alternative method for the production of closed-cell aluminium foams is given by powder metallurgy, see below. The characteristics of the production methods of cellular systems according to BANHART [4] are shown in Fig. 5.
Metal vapour – the principle in the production of metal foams from metal vapour (or gaseous metal compounds) is the condensation of the vapour formed in a vacuum on a "model" - polymer foam. The condensing metal covers the surface of the polymer

model and forms a layer of a certain thickness, depending on the specific gravity of the vapour and the time of its exposure. Subsequently, the polymer is removed by thermal or chemical treatment [4].

Metal powder – in this process, the powder remains in the solid phase throughout the production process and is only processed by sintering or other operations. This fact is crucial for the resulting morphology of the final internal cell structure. In the production of foams from the liquid phase, the surface tension produces predominantly closed pores, whereas foams produced by sintering metal powders have a structure with relatively round pores separated by thin walls of solidified melt. At present, the sintering of metal fibres or powders is the simplest method of producing porous metals and is widely used in powder metallurgy [4].

Ionised metal – the metal foam material is created in this process by electrically deposition of polymer foam with open pores. In order for plating to occur, the polymer foam must be electrically conductive. This is achieved by immersing the polymer foam in an electrically conductive graphite or carbon black-based solution. The final operation is annealing, where the polymer foam is removed [4].

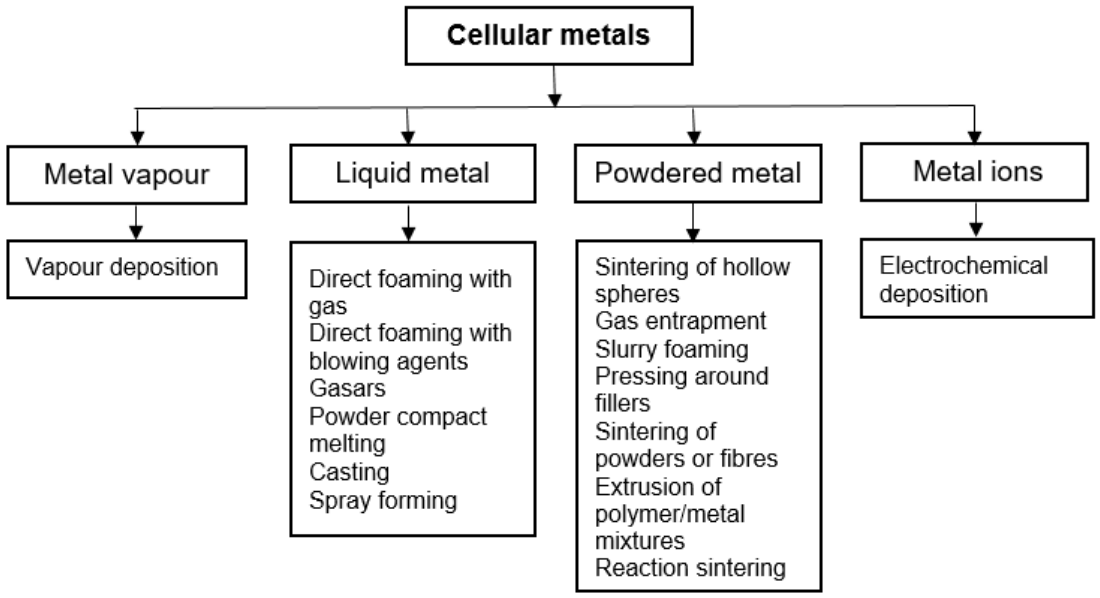

Fig. 5 Characteristics of manufacturing methods of cellular materials according to BANHART [4]

Liquid metal – one of the options for producing porous material from the liquid phase is direct frothing of the melt with gas or a frother. It is also possible to use foundry methods, e.g. technology using an evaporable disposable model or infiltration of liquid metal into a mould cavity filled with a solid material of defined shape and geometry (precursor, perform), which is removed after solidification of the metal leaving pores in the material structure. Another production option is the melting of powder mouldings containing a frother that releases a gas during decomposition [4]. Figure 6 shows an overview of metal foams or metal cellular systems.

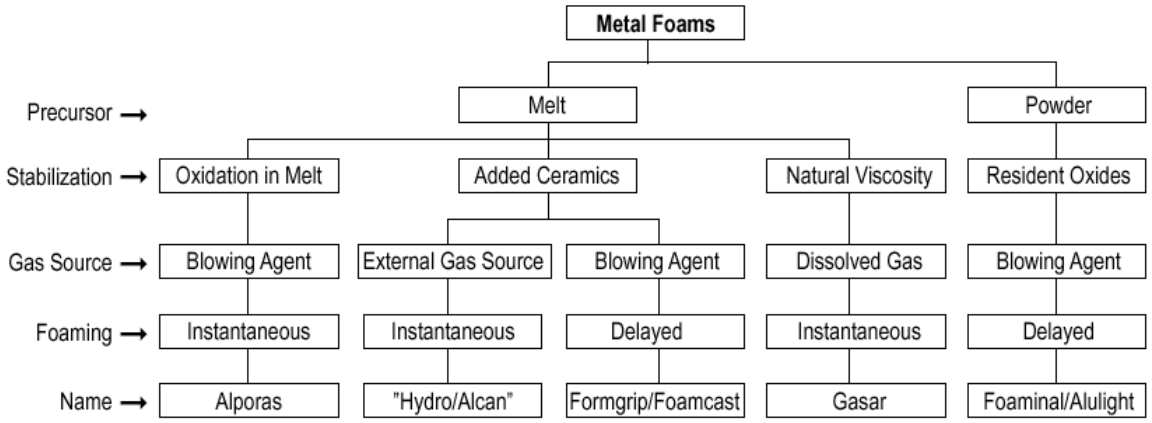

Fig. 6 Overview of cellular systems or metal foams according to [3] and supplemented according to the present

The "Slovak School", a research facility a collective of employees of the Institute of Materials and Mechanics of Machines of the Slovak Academy of Sciences in Bratislava has been involved in the development of aluminium foams for a long time. František Šimančík has been working on this development since 1993 and has created a methodology for the design and production of reinforced aluminium foams based on powder foaming systems. Reinforcing the foam significantly reduces its sensitivity to tensile stresses and virtually eliminates its sudden failure during tensile overload. This allows the use of aluminium foam as a load-bearing component in a variety of structural applications.

The expertise of Jaroslav Jerz, who graduated with a doctorate from the Technical University of Vienna in 1995, was used. He defended his doctoral thesis on "Gasification of aluminium and aluminium alloys by powder metallurgy". Today, this department is a world-renowned institution for the production of aluminium foams. Their other staff have also contributed to this.

Workers at VŠB TU Ostrava do not deal with the production of aluminium foams by classical (foaming) foaming methods, but focus on foundry methods that lead rather to the production of porous materials. They describe the foundry method used as the production of cast metal foams with an irregular arrangement of internal cells. The production of these porous materials is based on the production of precursors. Petr Lichý, Tomáš Elbel, Vlasta Bednářová, Ivana Kroupová and others participated in this development.

At present, the production of aluminium foams is also being dealt with by the staff of FS ČVUT in Prague, especially Aleš Herman. There are more than 500 workers in the world who continuously publish the results of their research activities focused on the production and properties of cellular metal systems, or aluminium foams.

1. CHARACTERISTICS OF CELLULAR METAL SYSTEMS AND THEIR PRODUCTION

Cellular (cellular) metal systems are often called "porous metals (metal foams)". They can exhibit various unique physical properties such as low apparent bulk density, high shock energy absorption, low thermal conductivity, high gas permeability and high specific stiffness, [1]. These materials can potentially be used in many areas, including lightweight construction, damping, shock absorption, thermal insulation, catalyst support, and biomedical implants. The structure of cellular metallic systems metallic "foams" - can be seen in Fig. 1.1.

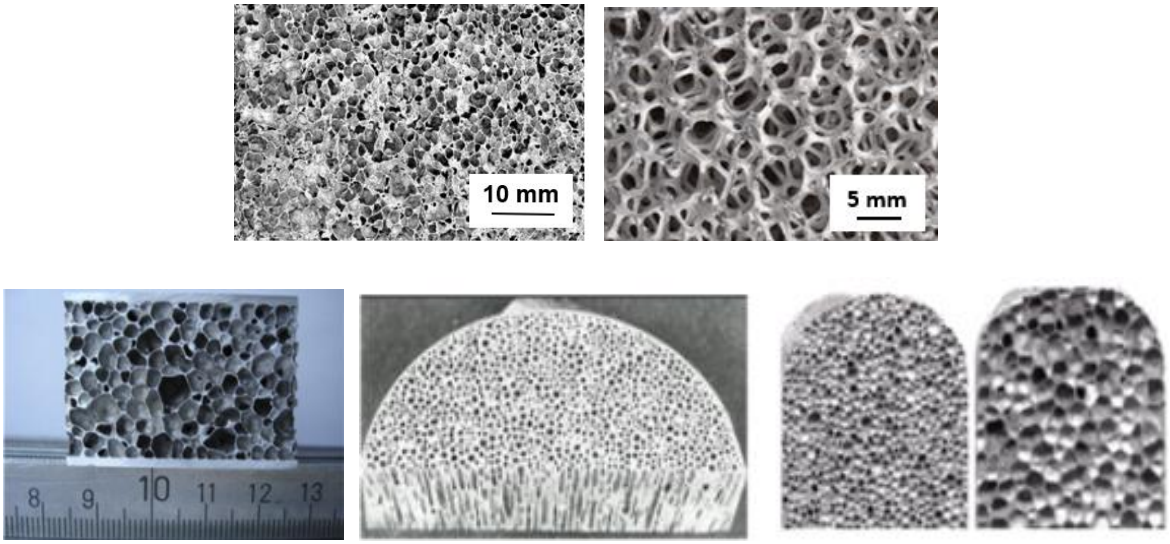

Fig. 1.1 Structure of cellular metallic systems metallic "foams" [1],[2]

As is evident from the appearance of the light metal cellular systems, a suitable gas or a suitable gaseous substance, or a substance which converts to a gaseous component on heating, is required for their production or "foaming" of the melt. Suitable substances include, for example, titanium hydride. Titanium hydride (TiH_2) is used as a foaming agent in the production of metal "foams" such as aluminium and zinc alloy foams.
Table 1-1 shows the basic methods of producing metal "foams" and lists their current producers, and the names of registered trademarks are given in parentheses.

Nowadays, thanks to metallographic methods, it is possible to evaluate metallographically very well the cells of cellular metal systems, see Fig. 1.2 (left). There are also now simulation programs such as CFD – Computational Fluid Dynamics (numerical simulation) created to numerically simulate fluid flow or heat transfer in a metallic cellular system with open cells, see Fig. 1.2 (right).
Table 1-1 Overview of the basic methods for the production of aluminium "foams"

Direct foaming	Indirect foaming
Technological procedure	***Technological procedure***
Alloy melting	Preparation of foam precursor
Alloy preparation by foaming	Melting of precursor or precursors
Formation of gas bubbles	Creating the entire foamed system
Foam collection	Solidification of foam
Solidification of foam	
Manufactured products	***Manufactured products***
Cymat, Canada (SAF)	Alm, Germany (AFS)
Foamtech, Korea (Lason)	Alulitgth, Austria (Aluligth)
Hütte Klainreichenbach (HKB)	Gleich - IWE, Germany
Austria (Metcomb)	Schunk, Germany
Shinko Wire Company, Japan (Alporas) distributor: Gleich, Germany	

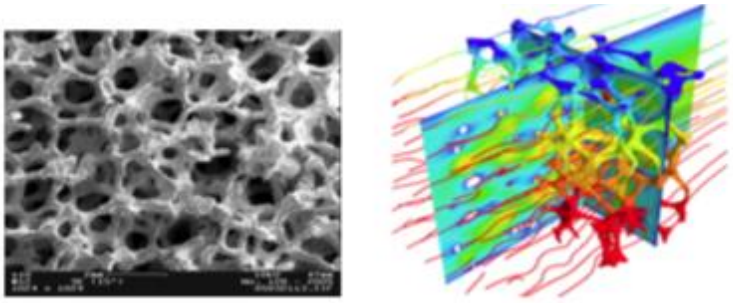

Fig. 1.2 Cellular metal structure (left), heat transfer and flow simulation results using CFD software on 3D open cell foam geometry (right)

The study of metal cellular systems (metal foams) has become attractive to researchers interested in scientific and industrial applications [1]. In this paper, different methods of producing these foams are presented and discussed. Some techniques are based on specially prepared molten metals with modification of their viscosity. Such melts can be foamed by gas injection or by the addition of gas-releasing superconductors, which cause the formation of bubbles during *in situ* decomposition. Another method is to prepare supersaturated metal-gas systems under high pressure and initiate bubble formation by controlling pressure and temperature. Finally, metal foams can be produced by mixing metal powders with superfluid, compacting the mixture and then foaming the compact by melting. Different foaming methods, foam stabilising mechanisms and some known problems with the various methods are described in this book. In addition, some possible applications of metallic foams are presented, which are known for their interesting combinations of physical and mechanical properties, such as high stiffness coupled with very low specific gravity or high compressive strength and good energy absorption characteristics. Although interest in these materials is increasing, there are some shortcomings in the characterisation of the term 'metal foam'. The

term is often used generically to describe materials that do not foam in the strictest sense. It is BANHART [1] who points out the correctness of the interpretation of the name "metal foams". According to BANHART [1], a distinction must be made:
Cellular metals: the most general term, referring to a metallic body in which any gaseous cavities are dispersed. The metallic phase divides the space into closed cells that contain the gaseous phase.
Porous metal systems *Porous metals: are a* special type of cellular metal confined to certain types of cavities. The pores are usually round and isolated from each other.
(***Solid) metal cellular systems*** *(solid metal foams) are* a special class of cellular metals that originate from liquid metal foams and therefore have a limited morphology. The cells are closed, round or polyhedral and are separated by thin layers.
Metal sponges: morphology of cellular metal, usually with interconnected cavities.
Generally, however, all of these systems are referred to in the technical literature under the collective term *metal foam* without further description.

The production of cellular metals in the most general sense, as described in published works [2], do not always involve foaming methods. The polymeric foam is first opened by a special treatment and then replicated to obtain the metallic structure. Replication can be done by metal vapour deposition, electroplating or casting. The result is a structure with open porosity rather than foam. The foaming process has nothing to do with the metallic state as only the polymer precursor has been foamed. Other structures can be used as templates for creating cellular materials: loose or sintered parts of inorganic or organic granular matter, hollow spheres or even regular polymer structures. Fig. 5 and Fig. 6 show an overview of the methods available for the production of metal foams [3], [4].

Significant factors in the production of metal cellular systems

One of the important factors for the production of metal cellular systems is whether it is used:

- molten metal;
- metal powder (although the actual foaming always takes place in the liquid state).

The second difference is the *source of the gas* that contributes to the foam or "porosity" of the metal system. The types of gas sources are:

- external gas source,
- The gas source can be in the form of a blowing agent (super fuel), which can be distributed in so-called "in-situ" (in certain locations).
- or dissolved gas is not used [1].

The third factor is the method of frothing, which can be instantaneous (that is, the addition of gas leads to instantaneous frothing) or an intermediate product is formed which can be frothed at a later stage (delayed frothing).

The fourth important factor is the foam stabilization mechanism, which is different for different methods. Some methods have been given a trade name, others

characterize "foam". Table 1-2 shows that there are about 5 basic types of "metal foam" production.

Table 1-2 Schematic of methods for the production of metal cell systems, or metal foams, redrawn from [1]

Production of cellular metal systems					
Starting substance (precursor)	***Melt of the relevant metal***				***Metal powder***
Foaming agent	**Stirring foaming agents into the melt**	**Gas injection into the melt**	**Melt injection and powder for gasification into shape**	**Hydrogen in the melt**	**Naphthenic acid in the form of powder**
Stabilization foaming	Oxidation in the melt	Addition of ceramics		Intrinsic viscosity	Residual oxides
Source gas	Gassing agent	External source gas	Gassing agent	Dissolved gas	Gassing agent
The gassing process	Instant	Instant	Delayed	Instant	Delayed
Business name	**Alpor**	**Hydro/Alcan**	**Formgrip Foamcast**	**Gasar**	**Foaminal/ Alulight**
Manufacturers	*Shinco Wire Company, Japan*	*Cymat Aluminium, Canada Metcomb, LKR Kleinreinchenbach, Austria*		*Ukraine*	*MEPURA patent, Alulight Austria IFAM, Fraunhofer Institute, Bremen, Germany*

The division of the production of "metal foams" is rather unclear in the literature, and the translation of the names from the English literature contributes to this. Therefore, the following simple division can be made, according to BANRART [1] and supplemented by the division of RAJAK [13]:

The basis of foam production is the melt

1) Methods of gas injection into the melt
   1.1 Hydro/Alcan method (Cymat)
   1.2 Metcomb method
2) Mixing the frother(s) into the melt
   2.1 Alporas method (Shinco Wire Company, Japan)
   2.2 Gasar method (Gascar), autoclave processing.

The basis of foam production is metal powder (powder metallurgy method)

3) Production of foams from moulded powders of mixtures of metal and foaming agent
   1.1 Pressing of powder mixtures and subsequent foaming in a mould in a hot oven (trade names of Alulight, ASF and ALM foams, IFAM technology);
   1.2 Low-pressure casting
   1.3 Rolling sheet metal into a semi-finished product
4) Gas melt supersaturation
5) Foam production using polymer templates

As can be seen from the above overview, there are in general a larger number of methods for the production of "metal foams", but chapters 1), 2), correspond to Table 1-2.
One of the most used methods according to BANHART [1] is shown in Fig. 1.3(b).

1.1 Methods of manufacturing cellular systems by direct melt filling (gassing)

[1], [2], [13]

1.1.1 Melt charging by feeding gas into the melt from an external source, HYDRO/ALCAN method, CYMAT

This method of producing "metal foams" is based on a starting material which is a melt of the relevant metal together with a stabilising agent. The stabilizer or stabilizing agent is usually a ceramic substance, e.g. SiC, Al_2O_3, etc. An external gas source is used, the gas is injected into the melt and the gassing process takes place immediately. Various gases can be used to form bubbles in the liquid aluminium. Air is the most commonly used, followed by carbon dioxide, oxygen, and inert gases. It is even possible to inject water into liquid aluminium under certain conditions, which is the source of bubble formation.

Only under certain conditions can metallic melts be foamed by forming gas bubbles directly in the melt. The gas bubbles formed in the metal melt quickly float to the surface of the melt due to the large buoyancy forces generated in the metal melt. Because metal melts have a high density against water. Therefore, there is a great danger of gas bubbles escaping outside the melt. This would invalidate the gassing process. Therefore, a so-called stabilizing agent must be added to the melt, which affects the conditions for maintaining a foamed melt at the melt-environment interface. In general, stabilizing agents are viewed as substances that modify or increase the viscosity of the melt. However, BANHART, oral communication 22.2.1918, does not consider the effect of the agent to affect viscosity, although it appears to do so. He also presents in literature. He regards this property as something other than an increase in the viscosity of the melt.

The protagonists of this method of producing metal foams state that an increase in the "viscosity" of the molten metal is used to prevent unwanted leakage of gas bubbles outside the melt (without the effect of its desired foaming). Generally, these "viscosity" influencing agents are added to the melt as fine ceramic powders alloying elements or other agents which contribute to forming a stabilizing property of the melt during foaming. Metallic melts may be foamed in one of three ways: by injection of gas into

the liquid metal from an external source, by the action of *in situ* gas generation in the melt by mixing of foaming (or supercharging) agents releasing gas into the molten metal, or by the action of gas which has previously been dissolved in the liquid. Fig. 1.3a) is a block diagram of the Alcan (Hydro/Alcan) process and Fig. 1.3b) is a picture diagram.

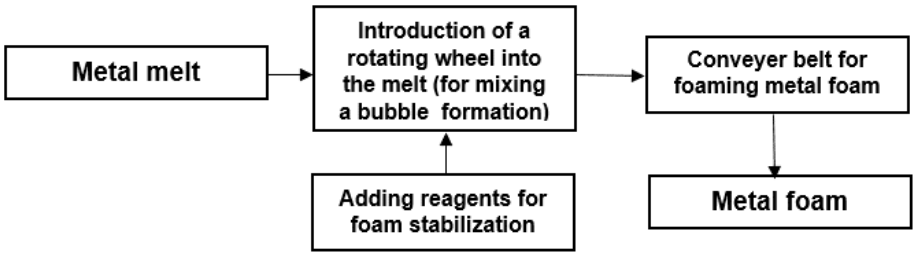

Fig. 1.3 a) Block diagram of the Alcan (Hydro/Alcan)+ foam stabilizing agent process is e.g. Al_2O_3 [13]

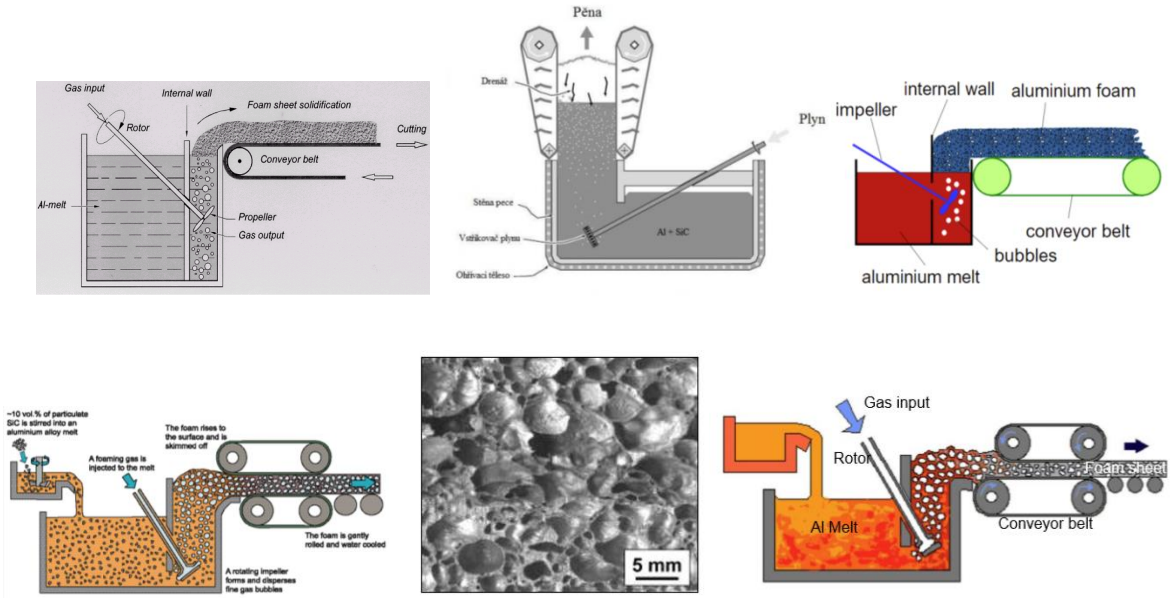

Fig. 1.3b) Method of manufacturing cellular systems - Foaming of Melts by Gas Injection (Hydro/Alcan) [2], AlSi9 alloy structure using direct gas foaming (bottom, middle), CURRAN [18], IBRAHIM [28]

This method of foaming aluminium and aluminium alloys is used by Hydro Aluminium in Norway and *Cymat Aluminium Corporation* in Canada, [3], [4]. In this process of producing "metal foam" (see Fig. 1.3a) and Fig. 1.3b), silicon carbide, aluminium oxide or magnesium oxide is used. Particles of these chemical compounds are used, as generally – but incorrectly used according to BANHART [1] to increase the "viscosity" of the melt. Therefore, the first step involves the preparation of an aluminium melt containing one of these substances, making it a Metal Matrix Composite (MMC). This first step reportedly requires a sophisticated mixing technique

to ensure uniform particle distribution. Different types of aluminium alloys can be used to prepare the melt.

The melt is foamed in a second step by injecting gases (air, nitrogen, argon) into the melt using specially designed rotary impellers or vibratory nozzles. These create very fine gas bubbles in the melt and distribute them evenly. The resulting viscous mixture of bubbles and metal melt floats to the surface. Above the surface of the melt, the foam is in a liquid state. As it reaches the conveyor belt, for example, its temperature drops and it turns into a solid foamed material. Due to the ceramic particles added to the melt, both the foam in its liquid state is relatively stable and the solidifying foam, which can be pushed off the surface of the melt (e.g. by a conveyor) and then subsequently solidifies and cools, acquires this stability. In this case, the typical thickness of the solidified foam is about 10 cm. The volume fraction of "reinforcing", i.e. ceramic particles, ranges from 10 % to 20 % by volume, with a mean particle size of 5 μm to 20 μm. The choice of particle size and content is most often made based on experience. The recommended particle size and content can be seen in Fig. 1.4.

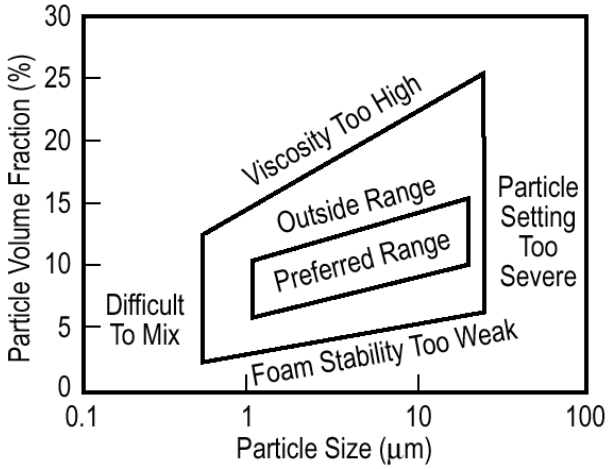

Fig. 1.4 Volume content of particles in relation to particle size [1]

The densities of aluminium foams produced in this way range from 0.069 g·cm^{-3} to 0.54 g·cm^{-3}, average pore sizes from 25 μm to 3 mm and wall thicknesses from 50 μm to 85 μm, [6]. The average cell size is inversely related to both average wall thickness and bulk density and can be affected by gas flow setting, impeller speed, nozzle oscillation frequency and the influence of other parameters. Fig. 1.5a) shows an example of foam produced according to this technology.

Cymat® Canadian company Cymat Corporation, which has obtained patents from Alcan and Norsk Hydro, and has also created parallel patents created by Norsk Hydro, produces foamed aluminium by the gas melt method from an external source. For the production of aluminium foam at CYMAT, the following sub-operations are important for the continuity of the different technological steps:

1) Melting and metallurgical preparation of melt containing ceramic particles (Metal Matrix Composite - MMC);
2) Introduction of gas or air into the MMC melt;

3) Creation of a gassed melt;
4) Solidification of gassed melt.

Smelting and metallurgical preparation of the melt - for this purpose, an aluminium alloy of the Al-Si type is used. Ceramic particles are added to the melt of this alloy, which prevent excessive fluidity of the aluminium alloy, or increase its viscosity, and at the same time are also referred to as stabilizing agents for stabilizing air bubbles, or for the formation of aluminium foam. Particles or powders of silicon carbide (SiC), magnesium oxide (MgO), aluminium oxide (Al_2O_3), titanium diboride (TiB_2), zirconium oxide (ZrO_2), silicon nitride (Si_3N_4) can be considered as ceramic particles. Other suitable solid materials which exhibit a similar stabilising effect may also be used. Ceramic particles are most commonly used at 10 to 20 % by volume, but the amount must not exceed 25 % by volume in the aluminium melt. The size of the ceramic particles shall be in the range of 0,5 μm to 25 μm, but a range of 1 μm to 20 μm is recommended. In practice, elongated particles with a ratio of 2:1 are more commonly used. Adding the particles to the aluminium alloy melt and mixing them thoroughly throughout the melt volume produces a composite material – Metal Matrix Composite - *MMC*. The ceramic particles are believed to aid foam stability through the following mechanisms:

- increase the viscosity of the aluminium melt;
- slow the flow of melt through the cell walls and help maintain a stable foam structure;
- promote force conditions, the repulsive force helps maintain the thickness of the cell wall between two adjacent gas cells;
- reduce the melt outflow that occurs due to the gravitational force around the gas bubble.

The authors [63] recommend SiC-based ceramic particles. They recommend heat treatment before their use. The heat treatment is based on heating them first to 950 °C for 1 hour, then to 650 °C for 2 hours.

SiC heat treated in this way is recommended for the foaming process. A quantity of 10 to 20 % by volume is mixed into the melt at a temperature of 650 to 680 °C with a rotary stirrer at a speed of about 14 00 rpm for 5 to 15 minutes. In doing so, the melt with ceramic particles (MMC – Metal Matrix Composite) is gradually heated until it reaches a temperature of 730 °C. This melting temperature is required for the foaming process. This heated and stirred melt is then poured into a frothing crucible (frothing device or frothing furnace). Tools such as ladle, and pan must be made of refractory material, the authors [63] used low carbon steel for the ladle, the surface of which was protected by a zirconium coating.

The gas supply to the melt – for this there are specific constructions, from the rotating wheel to the special oscillating nozzle system presented by e.g. ARC Leichtmetallkompetenzzentrum Rainshofen GmBH. The authors [63] used a nozzle to blow air into the melt. The gas is fed into the melt from an external source. This gas can be air, oxygen-enriched air, nitrogen, argon, etc.

Melt foaming from an external source – the foaming equipment includes a box-type furnace which is heated by resistance heat. It is constructed in such a way that a gas supply to the melt is created into the bottom of the filling cup using a nozzle. It is possible to use a relatively high cylindrical crucible (researchers [64] used a crucible of conical shape ∅ 170 mm, ∅ 140 mm and height 350 mm, the volume of the melt to be foamed was 1100 ml). Compressed air was blown into the melt of aluminium alloy with particles of the corresponding ceramic (of a certain amount) through a nozzle. The amount of air was monitored by a measuring device. The authors [63] used air whose quantity was 2 to 4 l/min, at a pressure of 0.2 MPa (for foaming they used SiC particles, about 5 μm 5, 10, 15 and 20 vol.%). The results obtained showed that the type of gas (often related to the type of ceramic particles), then the pressure or the amount of gas supplied, is important for successful melt foaming. This tends to be 1-3 l/min, the pressure tends to be 0.1 MPa and 0.2 MPa, for a quantity of 4 l/min the pressure tends to be 0.3 MPa. Flushing times and pressure values are not often reported in the literature. The temperature of the froth melt is usually 725 to 760 °C.
Once the crude MMC is melted, it is then transferred to a frothing device where the gas is injected into the melt and dispersed using rotating impellers or vibrating nozzles. Bubbles rise to the surface and the resulting cast metal foam mixture rises out out of the foaming device due to its density relative to the density of the molten MMC.

In the production of metal foam, the foam is simultaneously removed from the surface of the foamed melt, for example using a conveyor belt. While the foamed melt is being drawn off by the conveyor belt, it gradually cools to form a rigid porous metal structure.

The solidification of the liquid foam takes place under specific conditions, which are determined by the contact of the liquid foam with its surroundings.

CYMAT produces boards that solidify in the air. Furthermore, the foam can be solidified in a foundry mould, in a foaming cup after the foaming process is completed. Aluminium foam products manufactured by CYMAT are marketed as SAF – Stabilized Aluminium Foam. This method is shown in Fig. 1.5b). Stabilized aluminium foam cast by Cymat Technologies. It must contain less than 25 % stabilising particles by volume. MMC. Although this is a controversial subject, it is generally accepted that the presence of solid particles helps to "stabilize" bubbles. It is believed that the particles aid in foam stability. A rotary or vibratory pump takes care of the even distribution of fine gas bubbles in the melt. The presence of the particles in the foam helps to impede the flow of molten metal in the direction of gravity and also prevents the collapse of the cell walls, thus keeping the molten metal in.
The advantage of the direct foaming process is the ability to continuously produce large volumes of foam with low specific gravity that can be achieved. MMC foams are therefore likely to be cheaper than other cellular metal materials. A possible disadvantage of the direct foaming process is the potential need to cut the foam, thus opening the cells.

A foamed, pure metal melt that does not contain additives, using inert gas injection into the melt, can be a means of eliminating some of the undesirable side effects of stabilizing additives in metal melts, such as embrittlement, [2].

To maintain low viscosity, the melt-foaming process must be carried out at temperatures very close to the melting point. This can be achieved by bubbling gas through the melt, which is continuously cooled, e.g. in a continuous casting process. The bubbles are then trapped in the solidifying melt and form a foamed structure. In the liquid state, such systems are very unstable compared to metal-stabilized particles, which can remain liquid for some time.

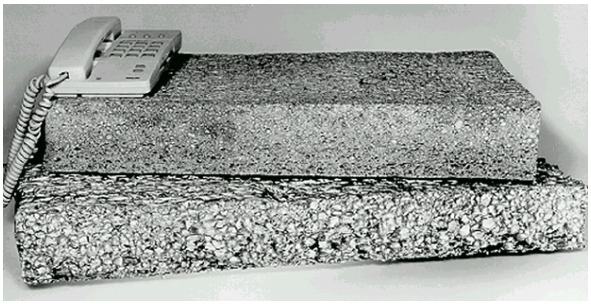

Fig. 1.5a) Cellular metal system produced by direct gas injection melt foaming, the plate can reach a thickness of up to 100 mm), manufacturer Hydro-Aluminium, Norway, BANHART [1]

Fig. 1.5b) Conveyor belt of the continuous aluminium foam production line by CYMAT [1]

1.1.2 Melt charging by feeding gas into the melt from an external source, METCOMB method

The method of producing aluminium foams under the *METCOMB* brand name was introduced in 2000 by the Austrian company LKR (Leichtmetall-Kompetenzzentrum Ranshofen) and the Hütte-Klein-Reichenbach metallurgical plant. This method is similar to the HYDRO/ALCAN method, but the METCOMB method differs from the melt straining method, which has been improved [14]. The basis of the new concept is the specific design of the gas injection nozzle, which leads to foaming with excellent gas cell size uniformity. The new concept of the method is also in the fact that the foam metal is introduced into the mould. Thus, complex foam structural parts with a closed outer layer (surface crust) can be produced.

The production of foamed aluminium under the commercial name *METCOMB*® is shown in Fig. 1.6a). The basis of the process is the formation of gas bubbles in the melt, which rise to the surface of the melt and accumulate in the mould cavity. The mould is then cooled, and the foamed melt solidifies in the mould. Depending on the application, a foamed metallic material with closed cells is formed. This process is protected by 5 patents and is focused on the production of complex three-dimensional parts and components. This is where this method differs most from the Cymat method, which produces continuously simple foam plates. Silicon carbide or aluminium oxide particles of around 20 % by weight are also used to increase the viscosity of the melt. The volumetric weight of products produced by the *METCOMB* method ranges from 400 to 900 $kg \cdot m^{-3}$. The *METCOMB* method is another method of producing foamed aluminium and aluminium alloys, similar to the already commercially used method of Cymat Aluminium Corporation, Canada Silicon carbide, aluminium oxide or magnesium oxide particles are used to stabilise the foaming melt. Typically, one of many common aluminium alloys is used to prepare the melt. The proportion of the melt volume that is foamed by the stabilising particles varies from 10 % to 20 %. The average particle size is between 5 µm and 20 µm.

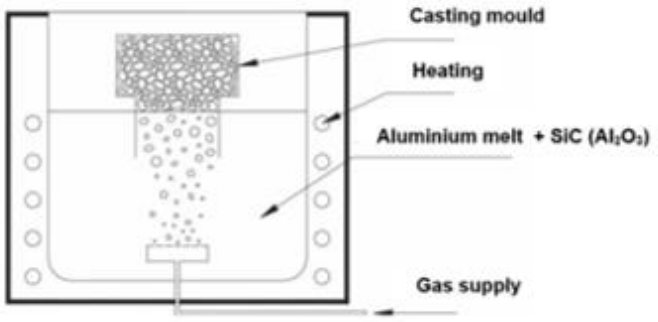

Fig. 1.6 a) Schematic of the Metcomb method [14]

The METCOMB method*, in which* the melt is foamed *by injecting gases* (air, nitrogen, argon), includes specially designed vibrating nozzles or specially designed rotating impellers. These special design elements create evenly distributed gas bubbles in the melt. The resulting viscous mixture of bubbles and molten metal or aluminium alloys floats to the surface of the melt. At this surface, it turns into a dry liquid foam which is fed into the mould. At the melt surface, the foam is relatively stable due to the presence of ceramic particles already added to the melt. The foamed material is either the shape of the cavity of the mould used or mounted on the foundry machine. These foamed products have a closed outer surface where the crust is located. Or the melt is foamed to produce foamed blocks. The desired shape can be separated from this foamed block. Due to the high content of ceramic particles, machining of these foams can be a problem. The advantages of this direct foaming method are the large volume of foam that can be continuously produced and the low density of the foam produced can be achieved.

Recently, this foaming (sparging) method has been applied at the Light Metals Competence Center (LKR) and the metallurgical plant in Kleinreichenbach, both production units in Austria [14]. The key point is the new gas injection concept, which leads to foams with excellent cell size uniformity.
In addition, by casting the foam into moulds, foam parts with complex shapes are formed and a closed outer crust can be formed. "Metcomb" is the trade name of this type of aluminium foam for its commercial use. Selected data related to the *Metcomb, Alporas,* and *Alulight* methods are summarized in Table 1-3.

Table 1-3 Comparison of the properties of aluminium foams produced by different methods, [1]

Comparison of the properties of aluminium foams produced by different methods			
Features	*Cymet or Metcomb, type of foam*	*Alpor type of foam*	*Alulight type of foam*
Shape of the system being monitored	Panels ≤ 16 x 1 x 0.2 m^3 episode, *Metacomb*	Blocks ≤ 2 x 0.6 x 0.5 m^3 10 mm thick sheets	Blocks ≤ 1 x 0.5 x 0.2 m^3 sandwich panels ≤ 2 x 1 x 0.02 m^3 AFS
Bulk weight [$kg \cdot m^{-3}$]	69 to 540	180 to 240	300 to 700
Pore diameter [mm]	3 - 25	2 to 10	2 to 10
Foam wall thickness [μm]	50-85	-	50 to 100
Materials of foams	Al alloys	Al, AlZnMg	metal alloys: Al, Zn, Pb, Sn
Reference	Ashby et al. (2000); Harte and Nichol (2001); Leitmaier et al. (2002); Kenny (1996);	Ashby et al. (2000); Miyoshi (1999);	Ashby et al. (2000); Baumgärtner (2000); Baumaister (2000); Stanczik et al. (2002); Seeliger (1991), (2001)
Foam information and foam distributors	www.comat.com; www.lkr.at www.hkb.at	www.metalfoam.co.kr www. gleich.de	www.alulight www.alm-gmbh.de (ASF); www.ifan.iwu.de www.lkr.at

Leitlmeier et al. [14] modified the *METCOMB* method. The foaming process by gas blowing using a new gas bubbling device that controls the formation of gas bubbles and the conduction of foam-stabilized particles on the melt surface into the mould, see Fig. 1.6a). It has also been shown that shallower depths of the "submerged gas" bubbling device lead to unstabilised bubbles and bubbles bursting on the melt surface. The immersion of the sparging system ("submerged gas" sparging) into the sparging device increases with decreasing particle content (Al_2O_3 and SiC). The use of nitrogen, as a foaming agent, resulted in more frequent bubble bursting before reaching the melt surface compared to the use of air or oxygen. It was also found that when nitrogen was used for foaming, SiC covered the wall surface. While the foams produced by oxygen

frothing of the melt, the cell wall surfaces and SiC particles were covered by a thin oxide layer. Fig. 1.6 b) shows an example of the stable processing condition of foam produced by *CYMAT as a* function of the distance of bubble movement on the SiC particle content in the melt.

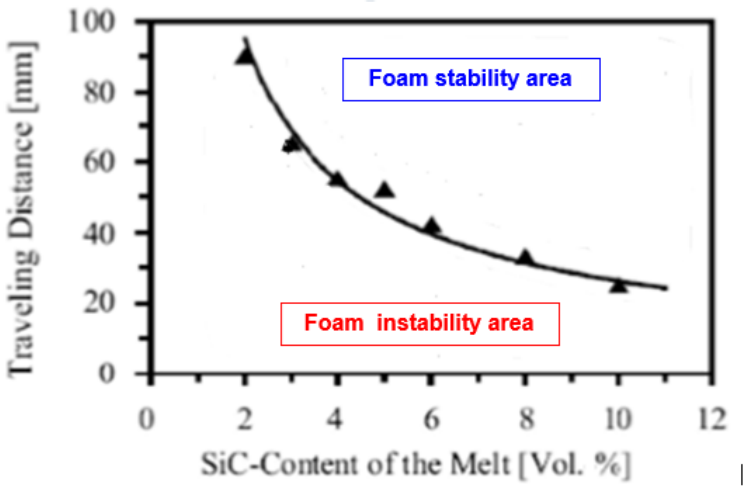

Fig. 1.6b) Stability criterion for aluminium foam (AlSi7Mg0.3 alloy, temperature 727 °C), LEITLMEIER, [14]

At small bubble movement distances and low SiC content, the bubbles lose stability, as shown in Fig. 1.6b). While bubble stability is achieved at long bubble motion distances and high SiC particle volume, see Fig. 1.6b). Fig. 1.6c) shows an example of aluminium foam-filled shaped profiles which were fabricated using the METCOMB method (manufacturer LKR Ranshofen).

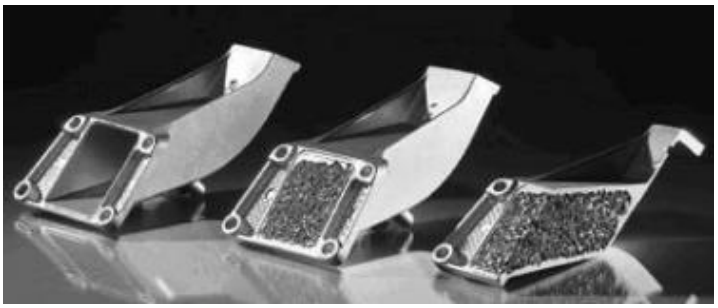

Fig. 1.6c) Example of aluminium foam-filled moulded profiles, METCOMB method (manufacturer LKR Ranshofen) [46]

Fig. 1.7) is an application of the *METCOMB* principle, the configuration for casting aluminium "foam" shows a crucible, rotating impellers and a ceramic shell mould attached to the crucible during casting. The entire assembly remains in the electric furnace during the aluminium "foam" process. The material used for the casting was a *composite material*, an aluminium alloy containing about 20 % silicon carbide particles. This alloy was melted in a graphite crucible in a furnace with resistance heating. The foaming equipment consisted of a stainless steel impeller connected to a

stainless steel shaft. The steel gear was driven by a hand drill (600 to 800 rpm· min^{-1}). During rotation, air was supplied to the melt just below the impeller by a steel pipe. The air flow rate was 6 to 7 l· min^{-1} and the air pressure was maintained at 0.2 MPa (2 bar). The function of the impeller was to specify the size of the air bubbles and their distribution in the melt. A ceramic shell mould was used to shape the aluminium foam, made in a conventional way from zircon and molachite refractory material with a shell mould thickness of 6 to 7 mm.

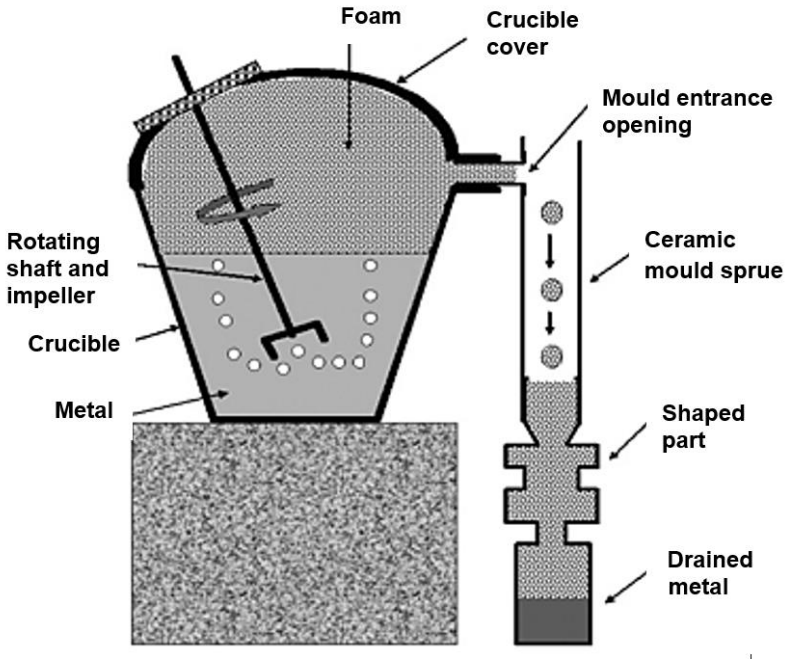

Fig. 1.7 Schematic of the METCOMB method principle, casting configuration showing the crucible, rotating impeller blades and ceramic shell mould made by the melt model method [17]

For casting, the ceramic mould was connected to the lid of the ceramic crucible by a 40 mm diameter mould extension channel. This extension channel was open and is shown as the 'mould inlet', see Fig. 1.7. The required temperature of the melt was 690 °C, and the temperature of the mould showed a stable temperature. The melt was briefly stirred with a rotating impeller to mix carbide particles that might settle on the bottom of the crucible during melting. Immediately thereafter, pressurized air was introduced into the airline to create bubbles in the melt or to froth the melt. The process continued until the space above the melt in the crucible was filled with foam. Then the mould began to fill with foam. Only when the mould channel was filled with foam did the rotation of the impeller stop. It is possible to extend the rotation of the wheel in this case by about 20 seconds to ensure that the mould is filled with foamed melt. The mould is then removed from the furnace to allow the foamed melt to solidify in the mould. Fig. 1.8 shows an example of the cast produced and its foamed structure produced by the application of the *METCOMB* method.

If the structure contains different pore sizes, this lack of homogeneity in pore size is probably related to the manual control of the foaming process.

In this foaming technology, it is necessary to find a suitable relationship between the fit and inclination of the rotating disc, the rotation speed and the speed and talk of the gas inlet. The volumetric weight of the foam produced is from 900 to 1200 kg·m^{-3}.

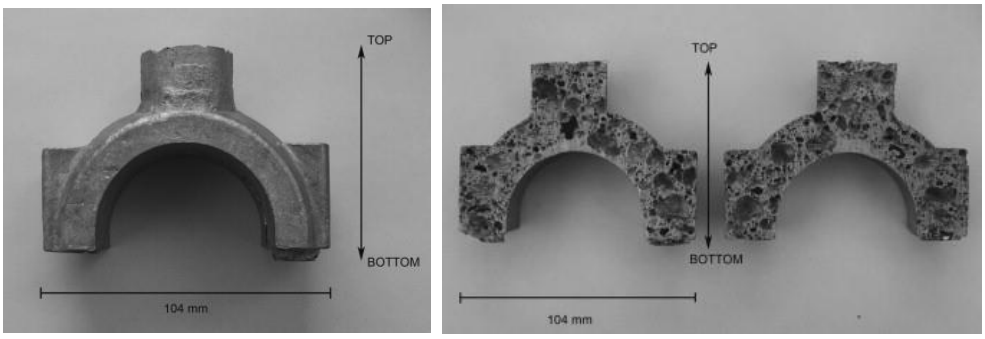

Fig. 1.8 Castings produced by METCOMB method and view of the obtained filler structure [17]

1.1.3 Melt foaming by adding a foaming agent to melts, ALPORAS method

Another method for producing "metal foams" is the *ALPORAS* method (Foaming of Melts with Blowing Agents), *Shinko Wire Company*, Japan. Illustrative diagram of the main steps of the preparation of the technology, in Fig. 1.9a) and block diagram in Fig. 1.9b), [13] CURRAN [18]. The ALPORAS method [21], [22] is classified as the direct addition of a foaming agent to a thickened melt, most commonly aluminium or its alloy. Aluminium foam is produced from molten aluminium with bubble stabilisation in the melt. To stabilize the bubbles, it is necessary to increase the viscosity of the melt and prevent bubbles from floating or escaping from the melt. To increase the melt viscosity, calcium is used, which acts as a melt thickener, that is, it contributes to increasing the viscosity of the melt, which is the starting substance of the process.

Stabilization of the process is realized by oxidation of the melt. The gas source is a gassing agent, in this case, titanium hydride (TiH_2). The use of a gassing agent makes the gassing process instantaneous. The gassing agent is added directly to the melt instead of being injected. The temperature of the melt causes the frothing agent to decompose and release the gas ($TiH_2 \rightarrow Ti + H_2$), in this case hydrogen, which is then the source of the frothing process (see Fig. 1.9a) [18]. Unfortunately, all aluminium foam manufacturing processes are patented and therefore, the literature information on foam production is very brief.

The process of aluminium foam production using the ALPORAS method can be described as follows:

1) A box-type melting furnace is used to prepare the aluminium melt (pure aluminium has a melting point of 660 °C). Approximately 1.5 % by weight of calcium is added to the aluminium melt with stirring. The calcium may also be in the form of a suitable alloy. The aluminium melt is assumed to have a temperature of 680 °C. At the

same time, air is introduced into the melt. A dispersion system of CaO and CaAlO particles$_4$ is formed, which are dispersed in certain areas of the melt.

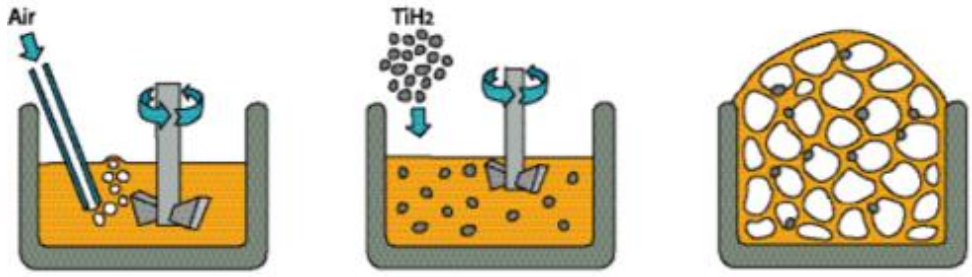

Fig. 1.9a) Schematic of the main steps of the direct melt filling process with the desired viscosity in the ALPORAS production method [18]

2) To the aluminium melt, which has a temperature of 680 °C, 1.6 wt. % of a foaming agent, what is TiH_2, is added and quickly mixed into the melt. The foaming process starts almost immediately, and the stirrer must therefore, be removed from the melt.
3) The setting time of the foam can be adjusted to some extent to control the level of porosity achieved.

The foaming agent is added directly to the molten metal as shown in Fig. 1.9a), provided that the TiH_2 foaming agent powder can be uniformly dispersed in the melt before the beginning of the onset of its decomposition to form hydrogen. The hydrogen will contribute to the formation of pores throughout the melt volume or, after solidification, throughout the metal volume. As with the direct method, the addition of air is necessary. Air is blown into the aluminium melt containing 1.5 wt. % calcium for 6 minutes at a temperature of 680 to 720 °C. The melt is stirred for several minutes, during which time its viscosity increases steadily as oxygen from the air combines with the calcium to form calcium oxide (CaO), calcium-alumina ($CaAl_2O_4$) or an intermetallic phase (Al_4Ca), which thickens the molten metal. Fig. 1.7a) shows the effect of stirring on the viscosity of aluminium melts with different amounts of calcium additions [10]. Calcium oxide (CaO) and calcium-aluminium oxide $CaAlO_4$, or Al_4Ca, are dispersed in certain areas of the melt due to melt stirring. These agents (CaO and $CaAlO_4$), when added to the foaming agent, stabilize the foamed melt (molten foam) against collapse, which is usually achieved by adding a reactive agent such as calcium [19] or magnesium [21]. Both of these elements exhibit a high affinity for oxygen, as known from the Ellingham oxide diagram. These elements are added to the melt under vigorous stirring. Figure 1.9b) shows a block diagram of the *ALPORAS* method.

The viscosity of molten aluminium can also be increased by bubbling (over-bubbling) oxygen, air or the use of other gas mixtures in the melt, which causes the formation of alumina, which also contributes to the increase in aluminium viscosity. Proper process setup is quite difficult and requires complicated temperature cycles and mechanical mixing.

Then, 1.6 wt% TiH_2 is added to the melt and held at 680 °C for 4 to 15 minutes. The resulting initial gas, H_2 does not have such a foaming effect, only after a certain time the foaming of the aluminium melt starts to take place [19].
An aluminium alloy containing Ca and TiH_2 is poured into a casting mould. The foamed melt is then cooled in the mould.

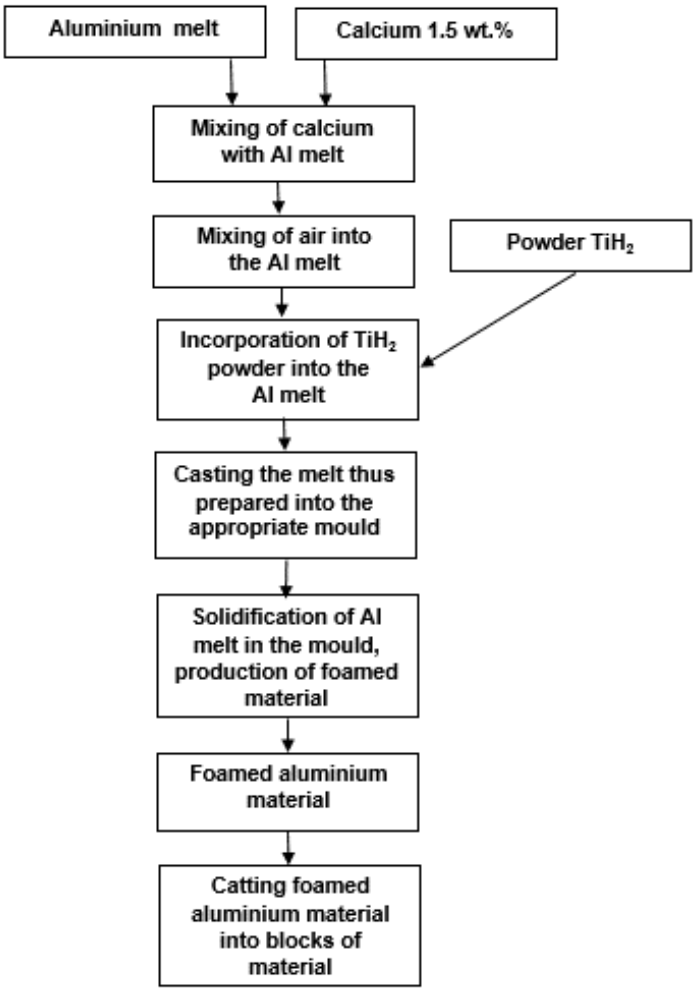

Fig. 1.9b) Block diagram of the ALPORAS method [13], [21]

Aluminium foam with a relatively uniform cell structure is obtained in batches up to 160 kg, with a density ratio of foamed material: unframed ($\rho_{F/}\rho_S$) = 0.05 to 0.3 and a closed cell size of 2 to 10 mm [18].
A certain disadvantage is the high price of the foaming agent and calcium. Although the efficient production of large blocks of foam in regular shapes is very challenging. This production is related to the requirement of mixing the entire volume to disperse the foaming agent. It also means that this production method cannot produce complex shapes. Attempts have been made to develop injection techniques using metal foam, whereby the melt is injected into the mould as it foams, but with limited success: the heating and cooling rates are difficult to control across the sample and the injection pressure is necessarily low to avoid crushing the molten foam, which favours an

irregular cell structure. Their bulk mass decreases significantly with distance from the injection site [22], [23].

Shinko Wire Company, Amagasaki, Japan, has been producing foams in this way since 1986 with production volumes of only 1,000 kg per day, see Fig. 1.9c). In the first step, approximately 1,5 % by weight of calcium is added to the aluminium melt (aluminium alloy) at 680 °C. Once the desired viscosity value has been reached, titanium hydride (TiH_2) is added (typically 1,6 % wt.). Titanium hydride, as already mentioned, serves as a foaming agent. As a result, thermal decomposition releases hydrogen gas in the molten metal (hot viscous liquid). The melt soon begins to slowly expand and gradually fills the frothing vessel. The foaming takes place at constant pressure. Once the mould has cooled below the melting point of the aluminium alloy used, the foamed aluminium melt is transformed into a solid aluminium foam which is removed from the mould and can be further processed, and cut into smaller blocks. The entire foaming process can take 15 minutes for a typical batch (2,050 x 650 x 450 mm^3). Careful adjustment of the process parameters has been shown to produce homogeneous foams, see the structure in Figure 1.10b).

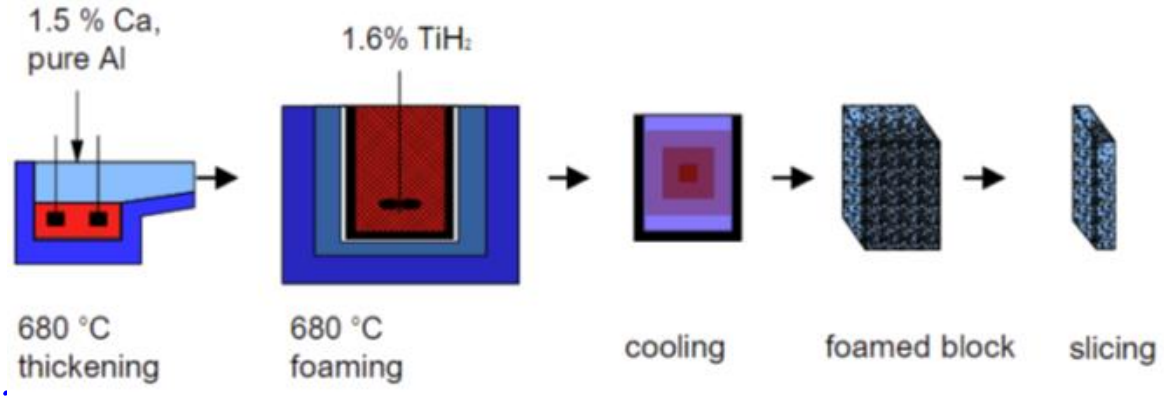

Fig. 1.9c) Commercial scheme of the Alporas cellular metal system production method (foam produced by direct melt foaming based on the addition of gas-releasing powders) *[1]*

Fig. 1.10a) shows the dependence of dynamic viscosity (apparent viscosity) on mixing time, [1]. Fig. 1.10b) is the structure of the cellular metallic material – foam structure (Southeast University China), as reported in [1]. Fig. 1.10c) is a section of aluminium foam produced by ALPORAS method (1.5 wt% Ca; 1.6 wt% TiH_2 foaming agent), [18].

Foams produced in this way – trade name *ALPORAS* – appear to be the most homogeneous aluminium foams currently available. An empirical relationship exists not only between average cell diameter and melt viscosity but also between final foam density and viscosity [9]. Typical densities after cutting off the sides of blocks of cast foam are between 180 $g \cdot cm^{-3}$ and 240 $kg \cdot m^{-3}$, with average pore sizes ranging from 2 mm to 10 mm. The blocks produced by the ALPORAS method have dimensions of 2050 x 650 x 450 mm^3, and their weight is about 160 kg. After removing the aluminium foam block from the mould, the blocks are divided into flat slabs of different thicknesses according to their intended use.

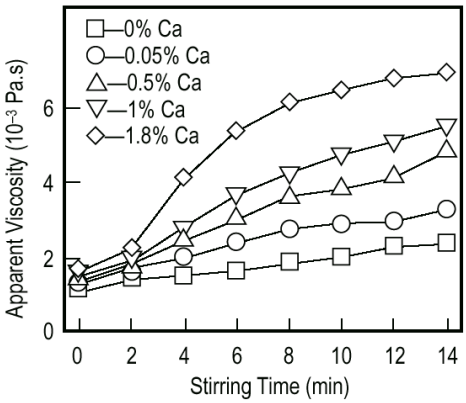

Fig. 1.10a) Dependence of dynamic viscosity (apparent viscosity) on mixing time [1]

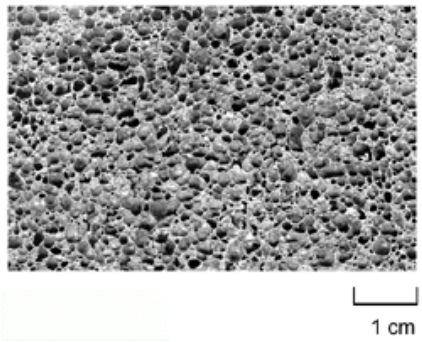

Fig. 1.10b) Structure of cellular metal system-foam structure (Southeast University China) [1]

Fig. 1.10c) Cutting of aluminium foam produced by the ALPORAS method (1.5 % wt. Ca; 1.6 % wt. TiH_2 foaming agent) [18]

1.1.4 Melt foaming by adding a foaming agent to melts, FORMGRIP, FOAMCARP, FOAMCAST methods

These methods (FORMGRIP, FORMCARP and FOAMCAST) are based on a melt of the respective metal; the source of the foaming gas is a foaming agent (superconductor) which is added to the melt. The melt gassing process is so-called delayed. First, a precursor is prepared which contains the foaming agent. The compact melt preparation process has recently been modified by incorporating titanium hydride particles into the aluminium melt instead of using powders to prepare the foam precursor material (the latter is typical for foam production by powder technology). To prevent premature hydrogen evolution from the foaming agent, the melt must either be rapidly cooled below its melting point after mixing or passivated to prevent the release

of gas before solidification. Conventional foundry alloys such as AlSi7Mg0.3, without ceramic additives, are used for the production of foamed castings. The cast part is compact and can be foamed by remelting in a manner analogous to the powder-based method. However, achieving a homogeneous distribution of TiH_2 powders after casting is challenging. This method also requires that the foaming agent powder (superconductor, e.g. TiH_2) undergo a heat treatment process (treatment) before its use, which creates an oxide barrier on the surface of each particle of the foaming agent and delays its decomposition. Powders treated in this way are added to the melt and must be stirred regularly to disperse them. This simultaneously results in a slow cooling of the melt [15]. In addition to the foaming agent, substances which stabilise the foam produced must also be added to the melt. For this purpose, e.g. silicon carbide is used. The foaming process can be influenced by changes in heating rates and final foaming temperatures, allowing a variety of different porous structures to be formed (see Fig. 6, Chapter Introduction). This process has been termed *"FORMGRIP"*, which is an abbreviation for foaming metals by releasing gas in the precursors. Fig. 1.9a) and 1.9b) show a schematic of the production of aluminium foam by the *FORMGRIP* method, the foaming agent being TiH_2.

The method known as *FOAMCARP* is analogous to the "FORMGRIP" method of aluminium foam production. Both methods are based on the processing of a melt, most often an aluminium alloy, and combine some of the advantages of using melt and powder to produce metal foams. A very important production step is the preparation of the precursor material. In the FOAMGRIP method, the production of the precursor is based on the presence of a foaming agent, which is TiH_2. In the FOAMCARP method, the production of the precursor is based on the presence of a foaming agent, which is $CaCO_3$, [18].

The process of aluminium foam production by FORMGRIP method can be described as follows:

1) Titanium hydride powder (TiH_2) is subjected to heat treatment in air to form a thin layer of rutile (TiO_2) on the surface of the powder. This is achieved by heating the TiH_2 powder to 400 °C and holding it at this temperature for 24 hours, followed immediately by heating to 500 °C for 1 hour).
2) SiC is used to increase the viscosity of the melt and acts as a surfactant to form bubbles.
3) Silicon carbide (SiC) is mixed into the molten aluminium alloy (usually AlSi12 alloy).
4) Heat-treated TiH_2 is then added to the melt.
5) The melt with both reagents is stirred, usually for 60 to 120 seconds, so that to disperse the particles of both reagents (TiH_2 and SiC).
6) Immediately after mixing, the melt is poured into a mould of a simple shape (e.g. cylinder ∅ 35 mm x 50 mm). The solidification and cooling of the melt in the mould produce a so-called solid foamable precursor, which is assumed to contain regularly dispersed SiC and TiH_2 particles.

7) A portion of this precursor is placed in a mould and heated above the melting temperature of the alloy used.
8) By heating the precursor in the mould above the melting point of the aluminium alloy, TiH_2 decomposes, releasing hydrogen, which fills the melt to form a foam that gradually fills the mould shape. The mould with the melt is allowed to cool. The resulting solid should be a rigid aluminum foam.

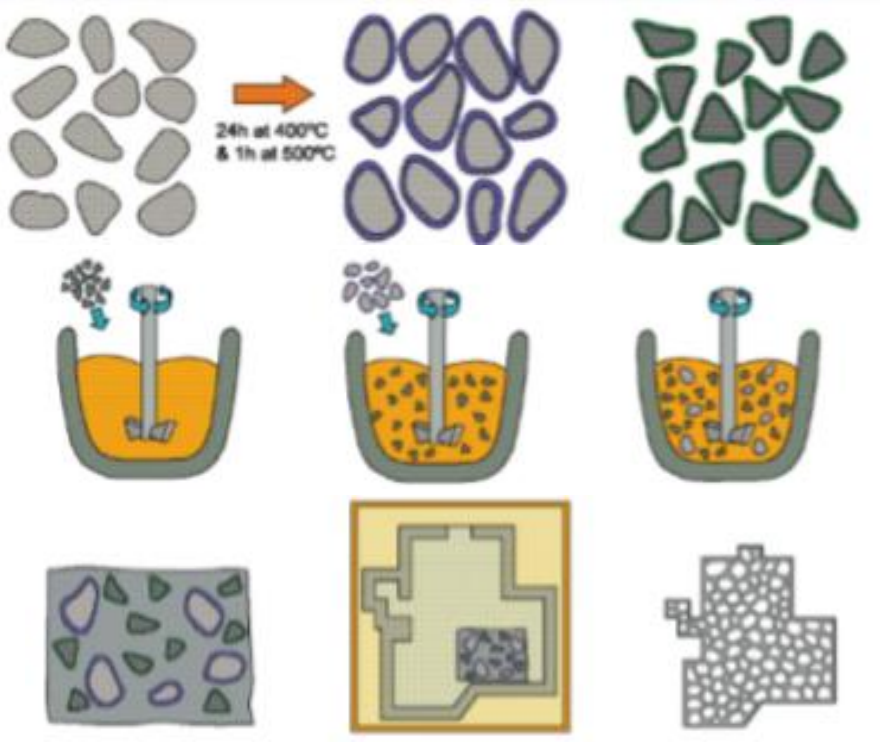

heating the TiH_2 powder to 400 °C and holding it at this temperature for 24 hours, followed immediately by heating to 500 °C for 1 hour

Fig. 1.11a) Schematic of the production of FORMGRIP aluminium foam, according to CURRANA [18]

Fig. 1.11c) shows the structure and range of foams produced by the FORMGRIP method, as influenced by temperature and foaming time [18].

The basis of the FORMGRIP method is the production of a foam precursor (also referred to as a semi-finished product). The foamable aluminium-based precursor material can be prepared either by using a melt prepared from a bun or a melt prepared by melting powder of the respective metal or metal alloy powder. The powder used abroad is called Duralcan (it is a mixture of aluminium powder, e.g. AlSi12, and 10 or 20 vol.% SiC powder). If preparing a melt from a bundle of alloy, then SiC must be added to the melt separately.

In preparing to use the precursor from the melt, the titanium hydride particles are mixed with the metal melt, and then the melt solidifies. The obtained precursor must be broken into small pieces and then can be foamed in a foaming mould. To avoid premature hydrogen evolution during stirring, the solidification must either be rapid or the superconductor must be passivated to prevent the release of too much gas at this

stage. One of the methods is also the use of a die-casting machine where the powder hydride is injected into the mould at the same time as the melt [24], this method is called *"FOAMCAST".* Alloys such as AlSi7 can be commonly cast without ceramic additives. However, achieving a homogeneous distribution of TiH_2 powders in the metal matrix is challenging.

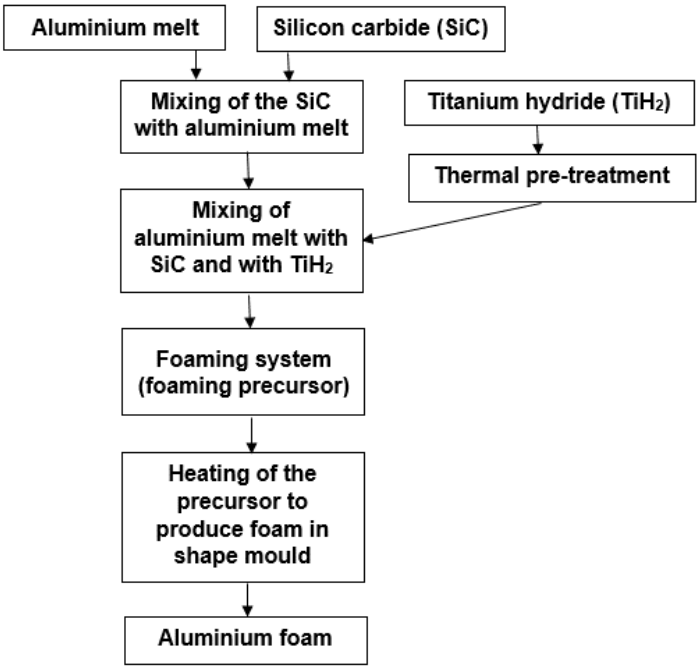

Fig. 1.11b) Schematic diagram of aluminium foam production according to FORMGRIP method [18]

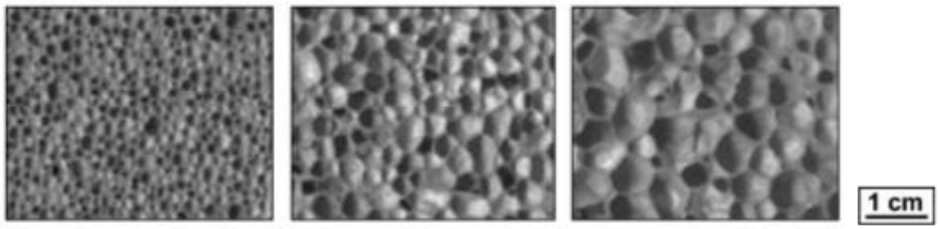

Fig. 1.11c) Structure and range of foams produced by FORMGRIP method, as influenced by temperature and foaming time [18]

Alternatively, TiH_2 powders can be added to the melt by relatively slow stirring and subsequent cooling, provided they are subjected to a heat treatment cycle that forms a zoxide barrier on each hydride particle to delay their TiH_2 decomposition until the foaming step [25]. To obtain a stable foam, 10 to 15 vol.% of SiC particles are added to the melt. The name of the FORMGRIP process is derived from the English name: *"Foaming of Reinforced Metals by Gas Release in Precursors"*. GERNELY et al. [26] and CURRAN [18] investigated the foaming of aluminium alloys using the foaming agent $CaCO_3$. This analogous process for the production of metal foams (to the

FORMGRIP process) is called "*FOAMCARP*" [26]. During foaming, thermal decomposition of $CaCO_3 \rightarrow CaO + CO_2$ occurs. The resulting CO_2 gas is also reduced by the presence of aluminium to CO, which causes surface oxidation of the foam cells [27] and forms an oxide layer on the foam cells.
Currently, a new technique for processing aluminium melt to produce aluminium foam, the FORMGRIP method, has been tested.
This method combines some of the advantages of melt-based metal foam production while applying the advantages of powder metallurgy [25]. This new technique involves the preparation of a precursor material by dispersing frother particles that thermally decompose after heating the precursor to form a gas (the frother particles are pre-thermally treated to delay the release of the gas) in liquid aluminium with the presence of SiC particles to stabilise the foam. Further, subsequent solidification of the foamed melt produces aluminium foam. Technologically, this is done by placing the precursor in a foaming mould. The mould is heated above the melting temperature of the metal. In the case of aluminium alloys, this is about 580 to 650 °C; for pure aluminium, it is above 660 °C. The foaming process takes place in a shaped foaming mould. For experimental purposes, a simple foaming mould is sufficient (see Figure 1.12b).

Fig. 1.12a) shows a schematic diagram of the production of aluminium foam according to the FORMGRIP method [25].

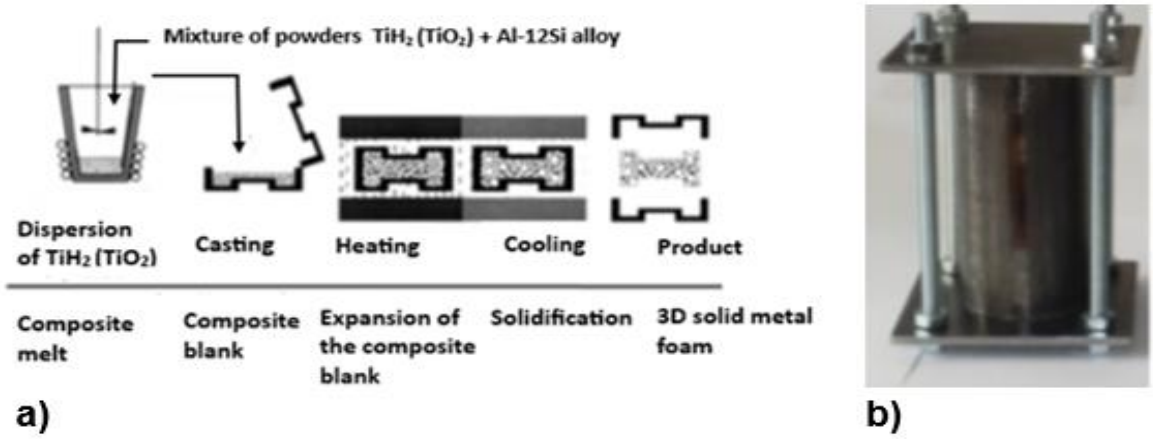

Fig. 1.12a) Pictorial diagram of the production of metal foams by FORMGRIP method, using a foaming precursor [25], b) example of a foaming mould

As can be seen from Fig. 1.10a), this technology consists of several technological steps:

1) The preparation of the composite melt is based on mixing the pre-prepared TiH_2 powder with AlSi12 aluminium alloy powder. SiC is further added, and this mixture is heated in a furnace. At the same time, it is required to ensure a homogeneous distribution of TiH_2.
2) Casting the melt thus prepared into a precursor mould and after solidification leads to the formation of a precursor composite.
3) Heating of the precursor in the frothing mould leads to the frothing of the melt and filling of the frothing mould space.

4) Cooling the foamed melt in the foaming mould produces an aluminium foam whose shape corresponds to the cavity of the foaming mould.

This method provides flexibility in the design of foam structures by controlling the amount and kinetics of the hydrogen evolution and foaming process that occurs during the foam production of the respective metal.

In the first stage, the pre-treated TiH_2 powder to powdered titanium dioxide (~30 μm diameter) is mixed with Al ± 12 % Si powder (~150 μm particle diameter). in a weight ratio of 1:4. Pretreatment of TiH_2 becomes a two-step heat treatment "oxidation sequence" to obtain titanium dioxide (rutile) on the surface of TiH_2 powder. This needs to be done by oxidation of TiH_2 powder with an oxygen supply at 400 °C for 24 hours. This is followed by oxidation of the TiH_2 powder at an elevated temperature of 500 °C for 1 hour. The titanium hydride is processed in air to form a titanium dioxide layer on its surface. The titanium hydride powder is stirred periodically during the pretreatment to ensure homogeneous oxidation. The powder thus prepared is then slowly cooled.

The oxidised powder is then mixed with aluminium powder or aluminium alloy powder that still contains a SiC component (e.g. AlSi12/SiC), which is used abroad under the trade name Duralcan. This powder has a melting point of 620 °C. This is followed by melting of the so-called 'composite mass' at 620 °C using conventional mechanical stirring (1200 $rpm \cdot min^{-1}$). The melt is stirred after the powder has been introduced for about one minute. The amount of foaming agent (FA) incorporated is 1,5 % wt. per 1 kg of composite mass, Order No. per 1 kg of metal. In the case of the *Duralcan* material, this process produces a composite precursor material having a relatively low porosity (P): the porosity is P = 23 %, 10 vol. % SiCp (SiCp is a foreign designation for a particular variety of SiC powder). Or the porosity is P = 14 %, 20 vol. % SiCp. In the second stage of the process, the foamable precursor material is placed in a graphite foaming mould (30 mm x 30 mm x 45 mm). The mould is heated to melt the aluminium alloy and, at the same time, to allow the pre-prepared foaming agent to also decompose to form hydrogen. Thus, the aluminium-foamed melt is gradually transformed into a cellular structure. Heating is carried out in a conventional laboratory furnace. The temperature is recorded using a thermocouple placed in the mould cavity. It is possible to heat treat the precursor materials according to different methods (T1 ± T6), see Fig. 1.12b).

The success of the production of this aluminium foam is the perfect and efficient preparation of the foaming precursor. It should be noted according to [25] that only a limited amount of hydrogen is released during the dispersion of the foaming agent (FA) with subsequent solidification of the aluminium.

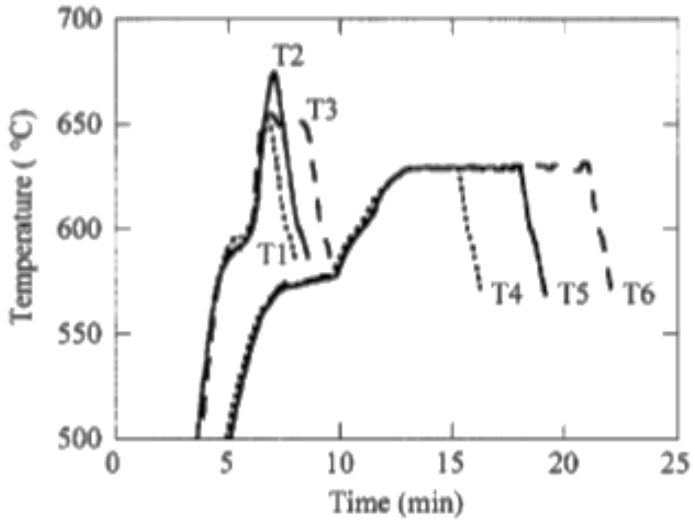

Fig. 1.12b) Overview of heat treatment methods T1 to T6 for the foaming process of aluminium precursor materials by FORMGRIP method [25]

The main factors controlling this are the thickness of the titanium dioxide layer formed on the surface of the foaming agent. Furthermore, the hydrogen concentration in the foaming agent, the initial melting temperature and the subsequent cooling rate.

The foaming agent (TiH_2) must be heat treated (a so-called hydride thermal pre-oxidation is carried out at temperatures of 454 to 482 °C for 5 to 20 min). Figure 1.12c) shows the thermogravimetric curves when TiH_2 powder is heated in argon to produce a pre-oxidised surface. This thermal treatment of the powder, as already mentioned, delays the evolution of hydrogen. Fig. 1.12d) shows the structures obtained.

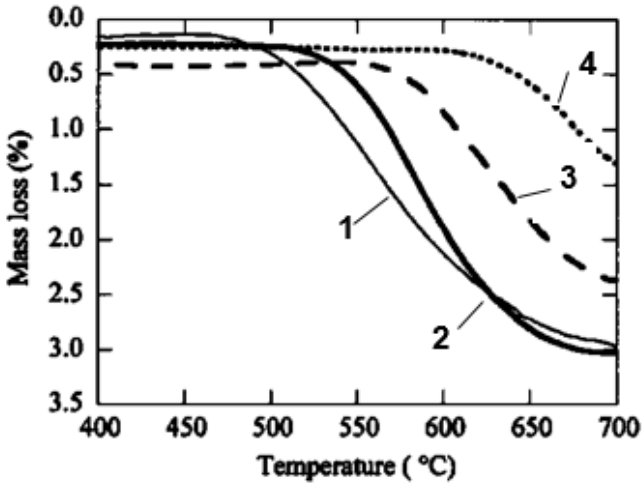

***1** - without HT TiH_2; 2 - TiH_2 oxidation for 24 hours, temperature 400 °C; 3 - TiH_2 oxidation 24 hours, temperature 400 °C and 1 hour, temperature 500 °C; 4 - TiH_2 oxidation 24 hours, temperature 400 °C and 3 hour, temperature 530 °C*

Fig. 1.12c) Thermogravimetric curves for heating the as-received and pre-oxidized TiH_2 powder in argon, showing the effect of powder pretreatment on the delay before hydrogen evolution (heating rate was 20 °C ± 1) [25].

The final structure of aluminium foam is the result of a set of three complex mechanisms: bubble nucleation, bubble expansion due to hydrogen evolution from gaseous hydride particles and the redistribution of gas in the composite or melt.
Figure 1.12d) shows the following partial conclusions. Foams containing higher amounts of silicon carbide particles, heated under the same conditions as those containing lower amounts, generally exhibit lower porosity values and smaller cell sizes, for example, *a)* with *e)* and *f)* with *g)*.
Higher precursor heating temperatures and longer heating times yield foams with higher porosity levels and larger average cell sizes, e.g., *(c)* with *(d)* and *(f)* with *(h).* Three main factors affect foam porosity and cell size, as can be seen in Fig. 1.12d) figures: (*a)* to (*h)*.

Important parameters for the production of aluminium foams are:
1) the amount and kinetics of hydrogen evolution,
2) melt viscosity,
3) critical thickness of the cell wall for its rupture (cell coalescence).

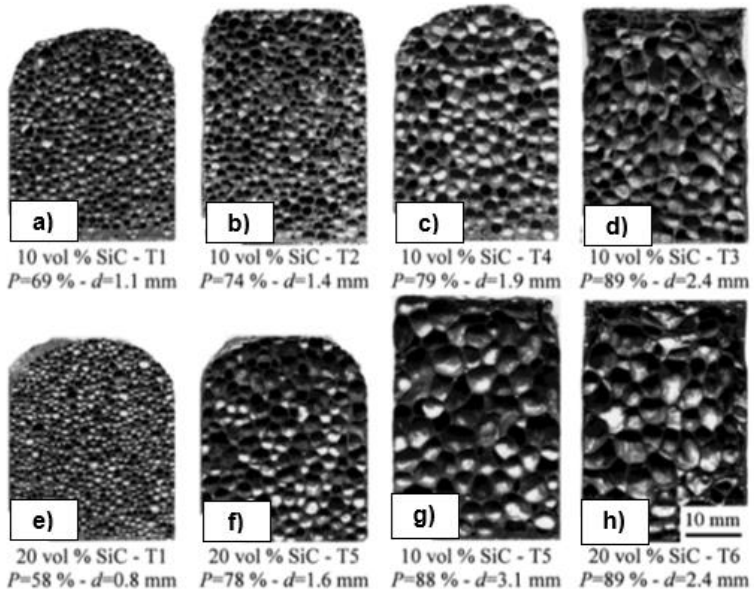

Fig. 1.12d) Structure of Al - 9Si/SiCp composite foams with SiC particles (10 % or 20 % by volume) and the effect of heat treatment T1 to T6, porosity (P) and pore diameter (d) of the foam [25]

To work successfully with a foaming agent, it is necessary to know its behaviour under different conditions. The temperature-pressure-concentration (T - p - C) dependence must always be evaluated for the foaming agent TiH_2. For example, from the investigation of the isotherm of the Ti - H system, it is clear that increasing the temperature from 600 °C to 700 °C increases the equilibrium pressure of hydrogen in the system by one order of magnitude [25].

Similarly, changing the hydrogen/titanium ratio (H/Ti) from 1.9 to 1.7 reduces the equilibrium pressure in the system at a constant temperature of about 606 °C by one

order of magnitude. These thermodynamic relationships show why the 20 °C difference in heating significantly increases the porosity of aluminium foam (see Fig. 1.12d), Figures c and *d.*

Another area of successful production of aluminium foams is the need to increase the viscosity of the melt to stabilise the liquid metal foams, this is usually done by incorporation or formation of suitable particles in the melt. These particles are SiC ceramic powder (5 to 20 μm in size). These particles increase the viscosity of the melt but also increase the viscosity of the surface of the aluminium foam cell. Or the melt viscosity when the particles are at the melt-gas interface.

A limited range of foams with high porosity but small gas cell size can be obtained by this method. This is related to the fact that the critical cell wall thickness is relatively large for composite foam systems. This prevents the cell walls from becoming thin without cell coalescence, which is a requirement for obtaining fine cells. For the microstructure of the foam section, see Fig. 1.12e).

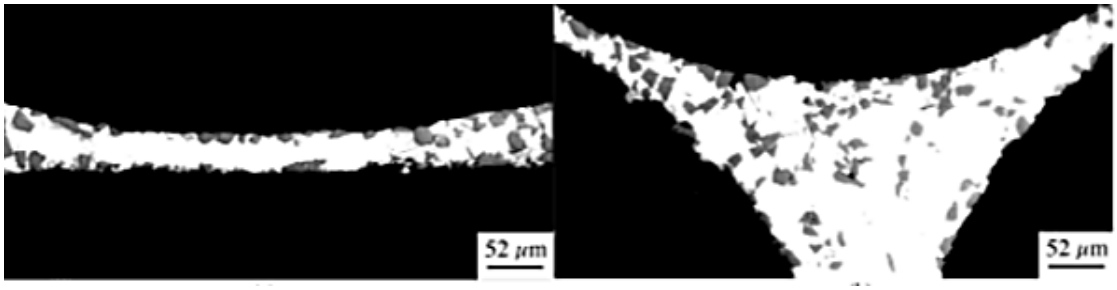

Fig. 1.12e) Sections of a microscopic structure illustrating the distribution of SiC stabilisation moieties in aluminium foam based on AlSi9 alloy, cell structure (left), cell boundaries (right), [25]

Figure 1.12e) shows that the critical cell wall thickness for rupture is affected by the presence and size of ceramic particles in the cell walls. In metal matrix composites, finer ceramic particles serve primarily to increase the viscosity of the melt of the aluminium alloy. Fig. 1.13 shows a schematic of the *FOAMCARP* (Foaming of Aluminium MMC by Chalk-Aluminium Reaction in Precursor) method, i.e. foaming of aluminium MMC $CaCO_3$ – reaction of aluminium in MMC (Metal Matrix Composites) precursor. In this case, the precursor is based on the use of $CaCO_3$, which decomposes with temperature to form CO_2. CO_2 acts as a foaming agent in the production of the foam.

Note: A compound that participates in chemical reactions.

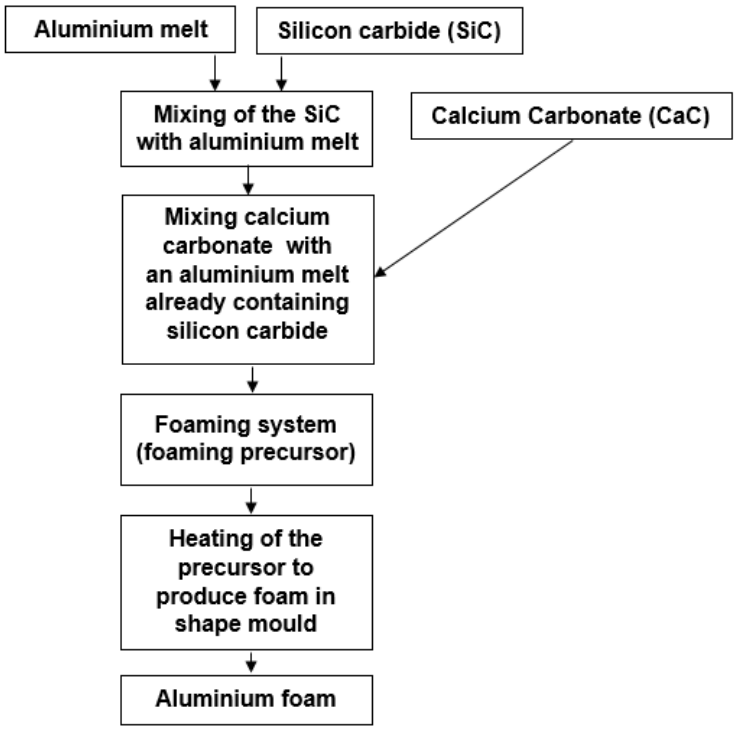

Fig. 1.13 Schematic diagram of aluminium foam production according to FOAMCARP method, [18]

1.1.5 Melt foaming based on eutectic solidification with dissolved gas, GASAR method

The GASAR (Gascar) method essentially began to develop in the 1980s, with contributions from both American and Soviet researchers. In 1996, a facility was assembled in Ukraine to implement the production of 50 kg of metal. At this time, the Japanese also started to deal with this meth, and since 2000 China, Korea and Brazil. The method is based on changing the solubility of hydrogen in the metal melt depending on the pressure. At the same time, the fact that some type of metal melts with hydrogen forms a eutectic system is exploited. By melting one of these metals in an atmosphere of hydrogen at high pressure (up to 50 atm, i.e. up to 5 MPa), a homogeneous hydrogen-filled melt is obtained. The process parameters must be chosen so that the hydrogen bubbles do not flow into the remaining liquid but remain near the solidification zone and are part of the solidified metal.

The resulting pore morphology is largely determined by the hydrogen content, its pressure in the melt, the direction and rate of heat dissipation and the chemical composition of the melt. In general, elongated pores are predominantly found in the material and are oriented in the longitudinal direction of the strained metal. In this foam production, the metal is melted in an autoclave and is brought under high pressure. This high pressure promotes the formation of a large number of hydrogen bubbles. The resulting melt, saturated with a large amount of hydrogen, is poured into a mould inside the autoclave. This is followed by the solidification of the melt-in a thermodynamically favourable direction (see Fig. 1.14) under reduced pressure. As

the solidification front penetrates the melt (at rates ranging from 0.05 to 5 mm·s^{-1}), the hydrogen content near the solidification plane increases, and bubbles form at the solidification front. The maximum porosity of the resulting "foam" system is low (about 5 to 75 %). The Gasar method is based on the melting of the respective metal (e.g. aluminium, nickel, copper, magnesium, chromium, molybdenum, cobalt, but also steel and ceramics) [11]. The melt stabilization process is based on the inherent viscosity of the melt. The gas that dissolves in the melt is hydrogen. The gassing process is instantaneous. This method became most widely used about ten years ago [11]. It is based on the equilibrium diagram of the metal and hydrogen concerned (see Fig. 1.13). And it takes advantage of the fact that some liquid metals form a eutectic system with hydrogen gas. This requires an autoclave in which a melt of the metal in question can be prepared, filled with hydrogen, and finally allowed to solidify directionally. If the vessel for producing the metal is cylindrical, both radial and axial pores can be produced in the material, depending on how the melt is cooled.

When one of the above metals is melted in a hydrogen atmosphere under high pressure, the result is a homogeneous melt filled with hydrogen. If the temperature is lowered, the melt eventually undergoes a eutectic transition to form a heterogeneous two-phase system (solid metal + gas). If the composition of the system is close enough to the eutectic concentration, a segregation reaction will occur at one temperature. At the moment the melt solidifies, it contains gas pores. The resulting pore morphology is largely dependent on the hydrogen content, the pressure above the melt, the direction and rate of heat dissipation, and the chemical composition of the melt. Fig. 1.15 shows a block diagram of the Gasar method.

Fig. 1.16 shows a diagram of the relevant equipment. Initially, the metal is melted *in an autoclave* beyond the boiling point, and later this high-temperature melt is brought into contact with high pressure to deal with the huge amount of hydrogen in the melt. After the solution, the saturated melt is transferred to a mould which is present inside the autoclave and solidification of the saturated melt is done under low pressure. Through this process, the hydrogen with which the melt has been saturated is "precipitated" as the melt solidifies at low pressures. The porosity of foams produced in this way is 5 % to 75 %. Generally, very elongated pores are formed, oriented in the direction of solidification (see Fig. 1.17). The diameter of the pores varies from 10 μm to 10 mm, the length of the pores varies from 100 μm to 300 mm, and the porosity varies from 5 % to 75 %. The pore size distribution tends to be uneven due to the simultaneous growth of small and large pores and their coalescence. The pores may be conical or even wavy. *The word 'gasar'* was designed to refer to porous materials formed by the eutectic solidification of a solid gas. Gasar is a Russian abbreviation that means "reinforced gas".

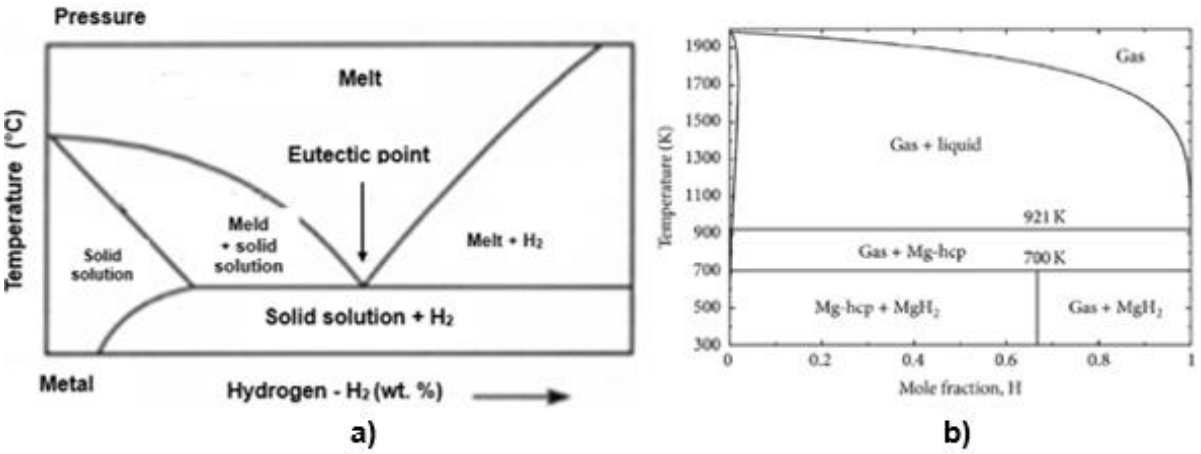

Fig. 1.14 Illustrative equilibrium diagram of metal - hydrogen a), system, magnesium - hydrogen b)

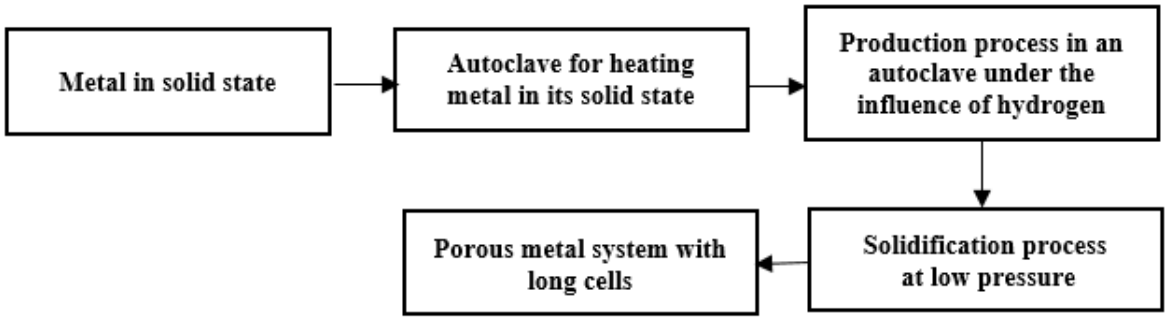

Fig. 1.15 Block diagram of the Gasar method [13]

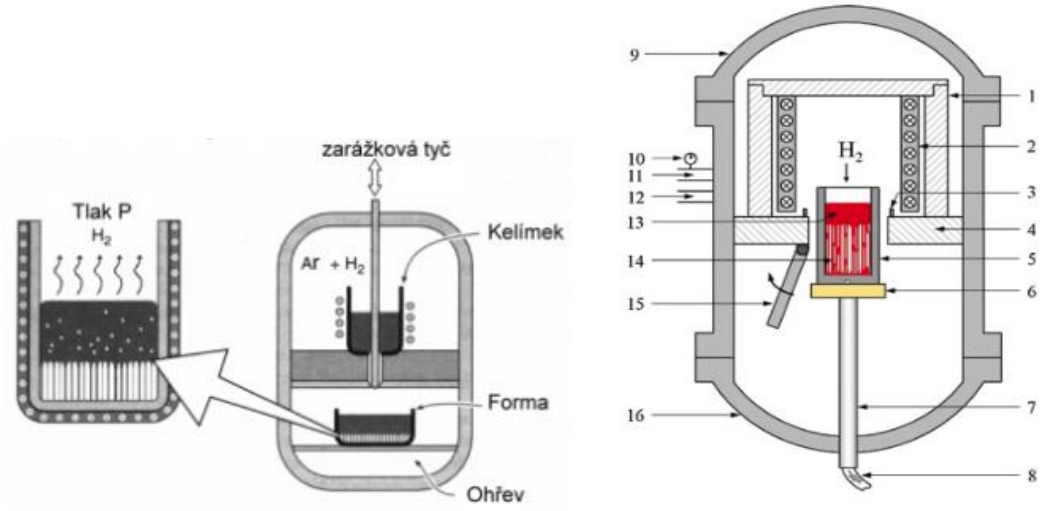

Tlak p H_2 - pressure p H_2; zarážková tyč – stop bar; kelímek - crucible, forma - mould, ohřev - heating

1. *Thermal insulation layer,* ***2.*** *Three-phase resistive graphite heater,* ***3.*** *Mould holder,*
4. *Thermal insulation layer,* ***5.*** *Graphite mould,* ***6****. Water-cooled copper crystallizer,* ***7****. Stop bar,*
8. *Cooling water,* ***9.*** *Upper furnace cover, 10. Manometer,*
11. *Gas inlet,* ***12.*** *Gas outlet,* ***13.*** *Molten Cu,* ***14****. Gasar Cu,*
15*. Rotation of the thermal baffle,* ***16****. Lower furnace cover.*

Fig. 1.16 Schematic diagram of the equipment for the production of foamed ingots by the Gasar method using directional crystallization (left), Bridgman method according to Gasar [15].

Fig. 1.17 Cellular metal system produced by the Gasar method, contains mostly elongated pores (cells), according to V. Shapovalov, as shown in [1]

Table 1-4 shows the technological parameters of the *GASAR* method for processing copper alloy ingots.

Table 1-4 Technological parameters of the GASAR method for copper alloy processing [1]

Technological parameters of Cu alloy processing							
Sample	Weight [kg]	D [mm]	P(H_2) [MPa]	P(Ar) [MPa]	T [K]	Speed [mm·s^{-1}]	Porosity [%]
a	19.98	150	0.36	0.12	1407	0	38.3
b	19.94					0.3	39.8
c	20.20					0.5	39.7
d	19.82					0.8	39.5
e	19.98					1.0	37.6
f	5.65	100				1.0	38.4

Fig. 1.18 shows the sections of the manufactured ingots according to the parameters given in Table 1-4.

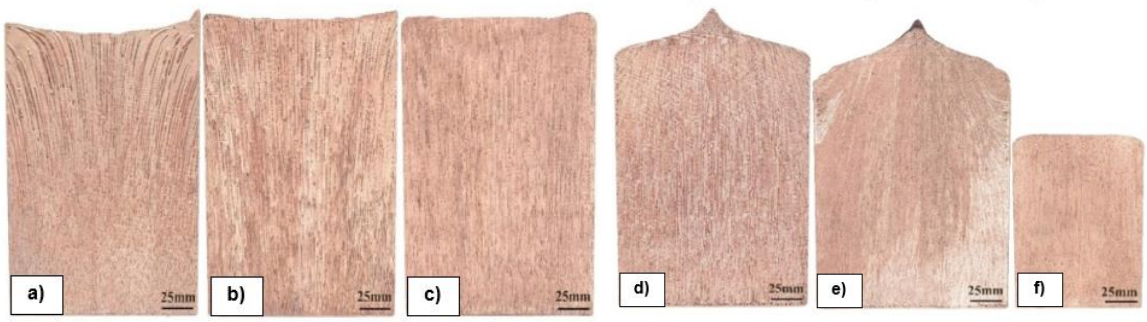

Fig. 1.18 Pore morphology on longitudinal sections of samples (a, b c, d, e, f) [1]

1.2 Methods of manufacturing cellular systems from metal powders [1], [2]

The production of cellular systems by powder metallurgy (PM) is nowadays an attractive way to produce metal foams from aluminium-based components. For this reason, a large number of shape applications can be produced. It is a method where the foaming of pure metals and their alloys is carried out without the need for stabilising

ceramic particles. These particles interfere with any mechanical cutting of the foamed materials produced in this way. The powder metallurgy method was patented by Allen et al. in 1963, [65]. It was further developed at the Fraunhofer Institute for Applied Materials Research (IFAM) in Bremen, Germany [3].

This technology is used to prepare metallic cellular materials, most often based on aluminium powders. The technology uses both metal powder and a foaming agent powder. Alternatively, inert gases containing a so-called precursor may be used in place of the foaming agent powder.

The powder metallurgy (PM) method can be used to produce foams of various metals and their alloys [4],[5],[6],[7] such as aluminium, zinc, tin, steel, etc. The production of aluminium-based metal foams is important for industrial applications due to their properties (bulk density, energy absorption capacity, vibration-damping corrosion resistance, etc.). Pure aluminium and its alloys are used for the production of aluminium foams. The good quality of aluminium foams depends on the choice of the right foaming agent (blowing agent) to ensure uniform physical properties. The production parameters at different stages often require appropriate adjustments. The first step is the preparation of a compact, dense and solid semi-finished product, which is called a foamable precursor. This is achieved by using a conventional technique that allows the production of a compact material (from a mixture of metal powder and a foaming agent (most commonly TiH_2 in an amount of 0.6 to 1 wt% and powder of the respective metal is used). The second step is the production of the metal foam by heating this foamable precursor at a temperature higher than its melting point. The PM method can be applied by two techniques [8].

The production of foams from metal powder can be divided into two groups:

1) The foaming is carried out with the gas released from the foaming agent (IFAM process);
2) Process containing trapped gas (e.g. McDonell Douglas).

In this method of PM foam production, high-purity (99.6 %) TiH_2 powder can be used

and a grain size of approximately 33 μm. Preferably, the TiH_2 powder is heat treated (24 hours at 400 °C and 1 hour at 500 °C) before the foaming process. Heat treatment and oxide layer formation dela – the evolution of gas or hydrogen during thermal decomposition of TiH_2. Furthermore, hydrogen must start to be released from TiH_2 at a temperature higher than the melting temperature of pure aluminium (660 °C) or at a temperature higher than the eutectic temperature of 577 °C when using Al-Si-based alloys [15].

The production of metal foams by powder metallurgy involves many methods, which are variously called, have been patented and have different designations.

1.2.1 Production of aluminium cellular systems by powder metallurgy, Fraunhofer Process – IFAM

The FRANHOFER process (*IFAM* process) for the production of metal foams by powder metallurgy (PM) was developed at the Fraunhofer Institute in Bremen, Germany and also patented [29], [30], [31]. It is characterized by the fact that after mixing the powders, this mixture of powders is compacted by unilateral compression, powder rolling or extrusion, depending on the desired shape. A similar powder metallurgy process is the *MEPURA* process (Alulight by Mepura, Ranshofen, Austria), which uses continuous extrusion technology to compact the powder mixture. A schematic of the production of foamed systems by the FRANKHOFER process is shown in Fig. 1.19.

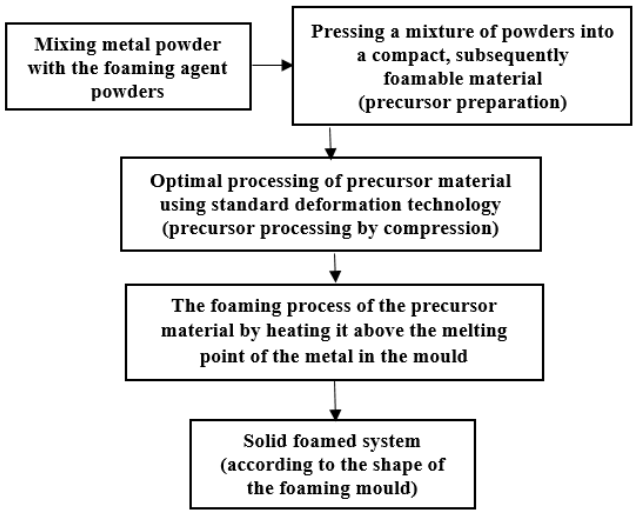

Fig. 1.19 Schematic of the production of metal foam by powder metallurgy, IFAM process [29]

For the production of "aluminium foam" by the PM (powder metallurgy) method. A powder of the relevant aluminium alloy is commercially available. This powder is mixed with the foaming agent powder (so that the aluminium powder is evenly represented in the mixture), and then this mixture of powders is compressed by a certain pressure. As a result, a semi-finished product (precursor) is obtained in which the foaming agent is homogeneously distributed in a dense, practically non-porous metal matrix. This foamable material can be further hot-worked into sheets, bars, profiles, etc., by conventional techniques such as rolling and extrusion. Finally, the foamed metal parts are obtained by simply heating the material above the melting points of the respective metal. The foamed materials with different pore densities are dependent on the content of the foaming agent and the foaming process parameters used. The porosity of these materials ranges from 50 % to 92 %, but for aluminium, a range of 80 % to 85 % is preferred. If metal hydrides are used as the foaming agents, in most cases, their content is sufficient at less than 1 wt.%. The method can be used for aluminium and its alloys, but also for other metals. Such as tin, zinc, brass, bronze and lead. Suitable frothing agents and process parameters must be used.

Other physical and mechanical properties have been characterized, [40]. This method has now been extended to metals with higher melting temperatures, such as iron and steel [41].

Fig. 1.20 shows a schematic of the IFAM metal fabrication method as presented by a German company, [1]. Fig. 1.21 shows aluminium foam pipes and profiles (IFAM, Germany), [45].

The structure of the metal foam produced by the Fraunhofer method (IFAM) is shown in Fig. 1.22.

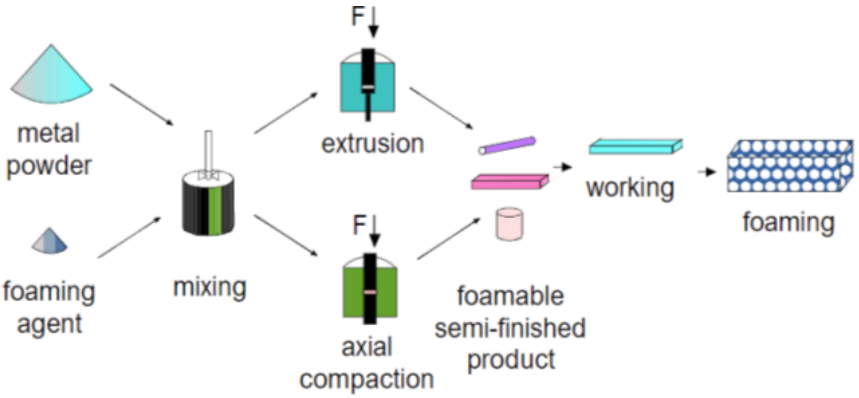

Fig. 1.20 Schematic diagram of aluminium foam production using IFAM technology, Germany KAMMER [45]

Fig. 1.21 Aluminium foam tubes and profiles, IFAM, Germany, KAMMER [45]

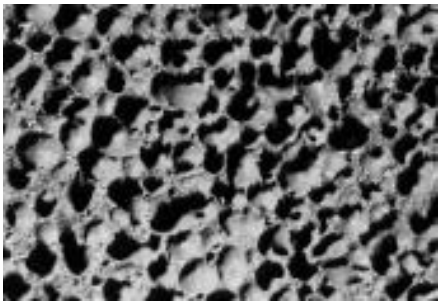

Fig. 1.22 Structure of foam made from metal powder by IFAM, (approximate scale 4:1) [40]

1.2.2 Production of aluminium cellular systems by powder metallurgy and gas-release foaming agent, ALULIGHT process (MEPURA patent)

As mentioned above, in the IFAM process (Fraunhofer-Institut Bremen, Germany), the material is compacted by unilateral compression, powder rolling or extrusion, depending on the desired shape. The MEPURA process (Alulight by Mepura, Ranshofen, Austria) [45] uses continuous extrusion technology to compact the mixture. The mixture is compacted into a compacted semi-finished product. The next step is heat treatment up to the melting temperature of the matrix metal and above the decomposition temperature of the foaming agent. At this temperature, the foaming agent decomposes and releases hydrogen gas. This gas leads to the production of a highly porous metal structure with closed cells. Cooling the melt below the melting point of the metal stops the foaming process. *The ALULIGHT method (MEPURA), the MEPURA* patent, or the MEPURA method (Alulight by Mepura, Ranshofen, Austria) is analogous to the *IFAM* method (*FRAUNHOFER).* Fig. 1.21 shows the IFAM aluminium foam products. A block diagram of the MEPURA technology is shown in Fig. 1.23. Fig. 1.24 shows an illustrative block diagram of the production of metal "foams" from powders by the MEPURA technology [45].

MEPURA technology starts by mixing metal powders (pure metal, alloy or powder mixture) with a foaming agent for aluminium and its alloys, usually 0.4 to 0.6 wt% TiH_2. The most common alloys for foaming are ductile alloys (1xxx series, pure aluminium; 2xxx series, Al-Cu alloys; and 6xxx series, Al-Mg-Si alloys). In addition, casting alloys (most commonly Al-Si alloys, i.e. silumines, e.g. AlSi7 and AlSi12, have excellent frothability due to their low melting temperature and good foaming properties.

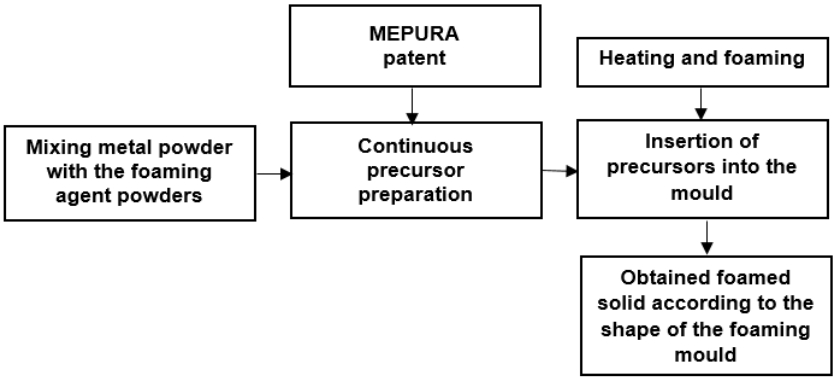

Fig. 1.23 Block diagram of the MEPURA method (Ranshofen, Austria) [45]

It has been shown, as reported by JERZ [56], that the pores produced using aluminium alloy intended for forming have a predominantly circular profile, with larger dimensions. In contrast, pores produced using foundry alloys are smaller and have an irregular shape. The walls between the pores are very thin, and their structure is uneven.

The patent or MEPURA process uses the technology of compaction of the mixture (metal powder and foaming powder). The compacted system (powder mixtures) is heat treated up to the melting point of the compacted metal and above the decomposition temperature of the foaming agent. At this temperature, the frothing agent decomposes

(e.g. if it is TiH_2, hydrogen gas is released). This gas helps the material to form into a highly porous structure with closed cells.
During the formation of the structure, the process slows down when the material reaches the melting point of the relevant metal and the process stops when it cools to below the melting point. The resulting metal foam porosity ranges from 65 % to 85 %. The production of metal foam with *MEPURA* technology depends on many factors. For example, the compaction conditions (technology, degree of deformation, temperature, pressure, time), the quality of the powders (particle type, particle size, alloy, mixing conditions), and the parameters of the foaming process (temperature, heating rate, cooling time, atmosphere).

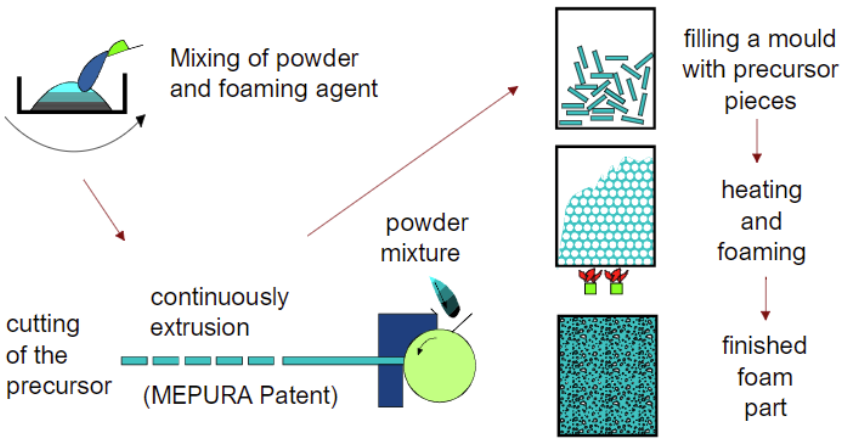

Fig. 1.24 Schematic diagram of the production of aluminium cellular powder foam systems by MEPURA technology (Company MEPURA, Austria), [32]

The foam bulk density can be controlled by the foaming agent content, temperature and heating rate [50].

As mentioned above, the first step of the MEPURA process is to mix the aluminium powder with the foaming agent powder. The next step is the formation of the precursor, i.e. the extrusion of the mixture of powders into a compact foamable system. In this process, however, the precursor is heated in the foaming cavity up to the melting point of the alloy. This leads to the formation of liquid foams which are injected in a controlled manner into the mould.

As can be seen from the above, aluminium foams are isotropic porous materials with several unusual properties that are particularly suitable for their technical applications (deformation elements of car bodies). Given their low density (approx. 500 to 1000 $kg \cdot m^{-3}$), the foams can float in water if they contain closed gas cells. The foams exhibit reduced conductivity for both heat and electricity. The strength is lower than conventional aluminium and decreases with decreasing density. The foams are stable at temperatures up to the melting point. They are non-flammable and non-toxic. In most foam manufacturing technologies, the properties can be varied over a wide range by controlling the manufacturing parameters. Some examples of properties are shown in Table 1-5.

The ALULIGHT method is a modified method of the MEPURA process. The first steps of this technology are comparable to the MEPURA process, i.e. mixing aluminium powder with a foaming agent and continuous extrusion into a compact foamable precursor. In this case, the precursor is heated in the foaming chamber up to the melting point of the alloy. This leads to the formation of a liquid foam, which is injected in a controlled manner into the mould, which is usually metallic, or exceptionally may be sand. This enables efficient small and large-scale production and prototyping. Such foam systems can form the inner parts of aluminium castings.

Table 1-5 Property values of aluminium foams (IFAM and MEPURA), [45]

Properties of aluminium foams (IFAM and MEPURA)				
Technological parameters and properties	**Pure Al 99,5**	**Pure Al 99,5**	**AlSi12**	
Foaming agent	Untitled	TiH_2	TiH_2	
Bulk weight [$kg \cdot m^{-3}$]	2700	400	540	840
Compressive strength [MPa]	76	3	7	15
Absorbed energy at 30 % compression [$MJ \cdot m^{-3}$], [$kJ \cdot kg^{-1}$]	- -	0,72 1,8	2,0 3,7	4,0 4,8
Tensile modulus of elasticity [MPa]	67 000 (MPa) (67 GPa)	2400 (2.4 GPa)	5000 (5 GPa)	14 000 (14 GPa)
Electrical conductivity [$m\ mm^{-1} \cdot \Omega^{-2}$]	34	2,1	unmeasured	
Thermal conductivity [$W \cdot m^{-1} \cdot K^{-1}$]	235	12	13	24

Fig. 1.25a) shows a block diagram of a more detailed production of aluminium foam by powder metallurgy, using the ALULIGHT method. It is a method that leads to the production of foamed aluminium with a continuous surface layer. This method is the most promising in terms of producing structural components with a continuous surface layer. Fig. 1.25a) simultaneously presents the technological process of LKR (Leicht-metallkompetenzzentrum Ranshofen, Austria) [55].

As already mentioned, and also evident from Fig. 1.25a), the production of aluminium foams by powder metallurgy consists of the fact that aluminium powder or aluminium alloy powder is first mixed with a foaming agent powder (TiH_2 or ZrH_2) in this method of aluminium foam production. Fig. 1.25b) shows the ratio of aluminium powder to the amount of foaming agent about the amount of semi-finished product obtained, which is subsequently foamed in a foaming mould.

From the mixture of powders thus formed, a foamable semi-finished product in the form of rods, wires or various other suitably sized profiles is produced by cold pressing and subsequent hot extrusion pressing (in the solid state) at a pressure of at least 200 MPa. The hot pressing process allows the formation of a protective layer on the surface of the foamable blank so that the function of the foaming agent is only apparent when the blank is melted.

Furthermore, this blank has the particles of the foaming agent evenly distributed and gas tightly sealed throughout the volume (due to hot pressing at high pressures).

When this frothing blank is placed in a frothing mould and heated in an electric furnace above the melting temperature of the relevant aluminium alloy (aluminium powder alloy), the frothing agent is melted.

Fig. 1.25c) shows an example of an electric resistance furnace for processing aluminium foams *[55].*

After melting the semi-finished product, the foaming agent (e.g. TiH_2) starts to release hydrogen due to its thermal decomposition, which forms bubbles in the aluminium melt, thus creating a foamed aluminium melt that fills the cavity of the respective mould. After filling the foaming mould with 'metal foam', the aluminium melt starts to flow out through the leaks in the mould. This is a signal that the melt foaming process has already taken place and the mould is filled with liquid metal foam. The subsequent rapid cooling of the mould results in a foamed solid mass of aluminium, according to the shape of the mould cavity, whose shape follows the cavity of the foaming mould. Various shapes of frothing mould are used for this purpose, see Fig. 1.25d).

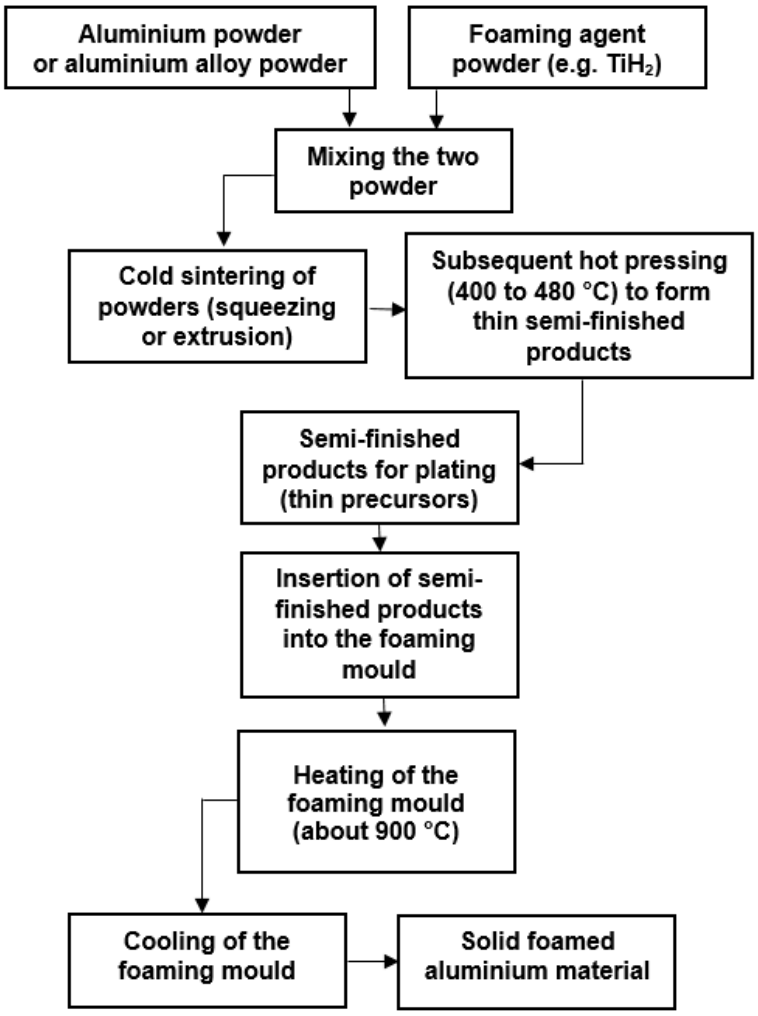

Fig. 1.25a) Block diagram of aluminium foam production by ALULIGHT method, CURRAN [18]

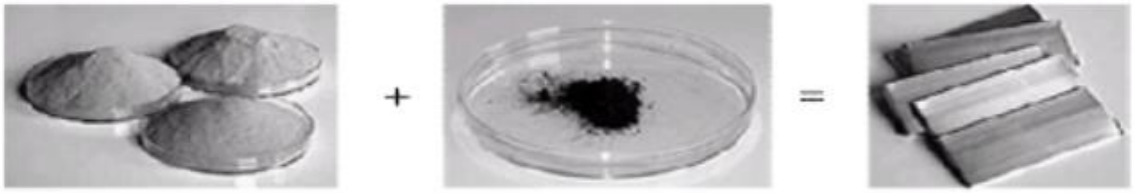

1 – 229 g aluminium powder; 2 – 1 g foaming agent; 3 – 320g foaming blank

Fig. 1.25b) Ratio between aluminium powder and the amount of foaming agent in the preparation of the foaming blank, [55]

Fig. 1.25c) Resistance electric furnace for realization of the foaming process of aluminium semi-finished products produced by powder metallurgy (LKR company), [55]

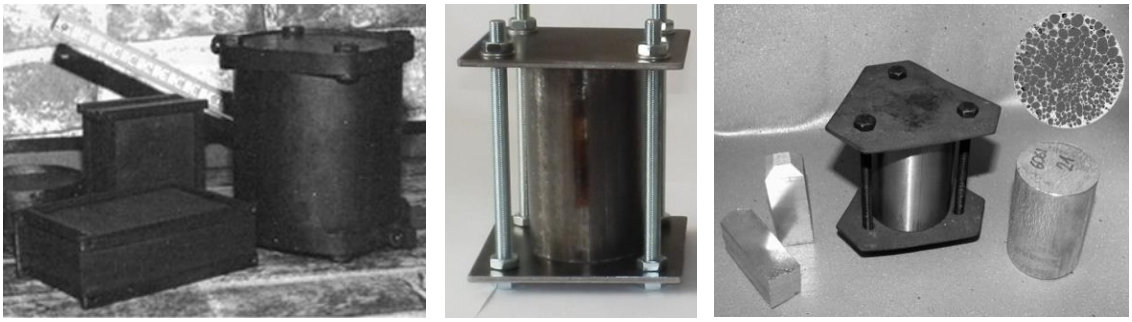

Fig. 1.25d) Foaming mould for the production of aluminium foams by powder metallurgy (left), JERZ [56], different designs of the foaming mould (middle), foaming blank, mould and cut made with aluminium foam (right), LEHMHUS [57]

The problem of aluminium foam production by powder metallurgy was also addressed by LEHMHUS [57]. He used the aluminium alloy powder AlMg1SiCu, which he purchased from MEPURA (Ranshofen, Austria). The aluminium alloy powder was mixed with 0.5 wt. % of titanium hydride powder (Chemetall, Hanau), which acted as a foaming agent. Next, foaming blanks (precursors) in the form of rods with rectangular cross-sections were formed by standard methods (cold and hot pressing). The blanks were inserted into a cylindrical steel foaming mould. The mould was placed in an upright position in a furnace with an atmosphere circulating at 730 °C. Thus, the heating of the semi-finished product and the decomposition of the frother occurred

gradually until the frothy melt filled the mould cavity. After the mould was cooled to room temperature, samples of cylindrical aluminium foam ∅ 45 x 60 mm were removed. The volumetric weight of the produced aluminium foam was 600± 30 [kg·m^{-3}].

The simple shape moulds used are shown in Fig. 1.25d). The produced foaming blanks (precursors) were placed in a cylindrical metal foaming mould, see Fig. 1.25 d), right. Fig. 1.25e) shows parts made of aluminium foam with a surface crust, which were produced by powder metallurgy, a method of LKR (Leichtmetall Kompetenzzentrum Ranshofen, Austria).

Fig. 1.25e) Aluminium foams with surface crusting, based on powder technology (AlSi12 and TiH_2 powder), size 150 x 50 x 10 mm, [55]

The production of aluminium foam by powder metallurgy using the ALULIGHT method is applied by the Institute of Materials and Mechanics of Machines *of the Slovak Academy of Sciences for the production of aluminium panels.* Fig. 1.26a) shows a block diagram of panel production using the ALULIGHT method.

Foamed aluminium and sandwich panels are produced by *powder metallurgy* (PM) technology, representing a new class of structural materials with huge application potential for the manufacture of lightweight structures. They are an alternative replacement for wood, plastics or various expensive sandwiches. Some of these properties are superior to those of polymer foam panels. They are more durable and more stable when exposed to elevated temperatures. They exhibit excellent fire resistance and do not produce toxic fumes in fire. They can potentially be used in the transport industry for lightweight rigid body structures for buses, trains, ships, cars, etc. The fracture resistance, damage resistance and energy absorption of the panels can even be improved by reinforcing their surface with steel wires without increasing their production costs.

The basis of production is the appropriate powders (metal and frother), the particle size of the powders and the ratio of metal powder to the amount of frother powder. The metal powder is most often aluminium or aluminium alloy powder. The frothing agent used is usually TiH_2 or ZrH_2, etc. The aluminium foam produced by the PM method, which was recently developed at the Institute of Materials and Mechanics of Machines of the Slovak Academy of Sciences for the Austrian company MEPURA GmbH, has the trade name ALULIGHT.

The preparation of the metal foam for the production of Alulight panels is as follows (see Fig. 1.26 a), involving dry mixing of metal powders (aluminium or its alloys) using powder frothers (typically TiH_2 and ZrH_2), cold compaction and then extrusion at a temperature of approximately 400 to 480 °C.

Thus, the foaming agent becomes uniformly distributed in the metal matrix. The extrusion process is useful in breaking up oxide films on the surface of metal powders. This product is considered a precursor material that is easily convertible to foam. This conversion is accomplished simply by heating the precursor to a temperature at which the metal alloy is converted to a melt. This heating breaks down the foaming agent and develops a gas, which is the basis for the foam formation. For the foam formed to retain its state, it must be stabilized by very *fine oxide particles* evenly dispersed in the precursor after it has been made. This is after it has been extruded.

After melting and foaming, the foam panel is quickly cooled to prevent the foam structure from collapsing. This technique requires special thin-walled moulds to withstand temperature changes. Larger parts, such as moulded panels, are therefore foamed specifically based on a specific set-up design that allows simultaneous moulding, heating and cooling. As mentioned above, foam panels can be reinforced with metal wires or mesh-like concrete. In this cassette, the reinforcing components (steel) are inserted into the mould together with the foamable PM precursor before foaming.

Panel properties – depend on the aluminium alloy used. The panels can be manufactured from different alloys of formed or cast pure aluminium, from 6000 series aluminium alloys or from AlSi12 aluminium alloys.

The mechanical properties of the panels can be optimised by suitable heat treatment of the alloy after foaming. Foam sandwiches can also be manufactured with plain or shaped aluminium cover sheets (Fig. 1.26b) on either one or both sides. This is the case if higher flexural strength or a specific surface quality of these products is required.

Another option is to reinforce the panel with metal wires or nets like concrete, see Fig. 1.26b). The adhesion is always diffusion bonded to the foam structure. One technological approach is that the reinforced panels or sandwiches are prepared during foaming in one technological operation, which significantly reduces production costs.

The extremely high stiffness-to-weight ratio of the panels and the high value of the abrasion properties are a guarantee for their technical applications. Resistance to fracture and damage can be substantially improved without excessive weight increase by the use of surface meshes and or wire reinforcements. In addition, the reinforcement panels can be easily connected, opening up huge potential for automotive applications, especially for lightweight body structures of future electric vehicles.

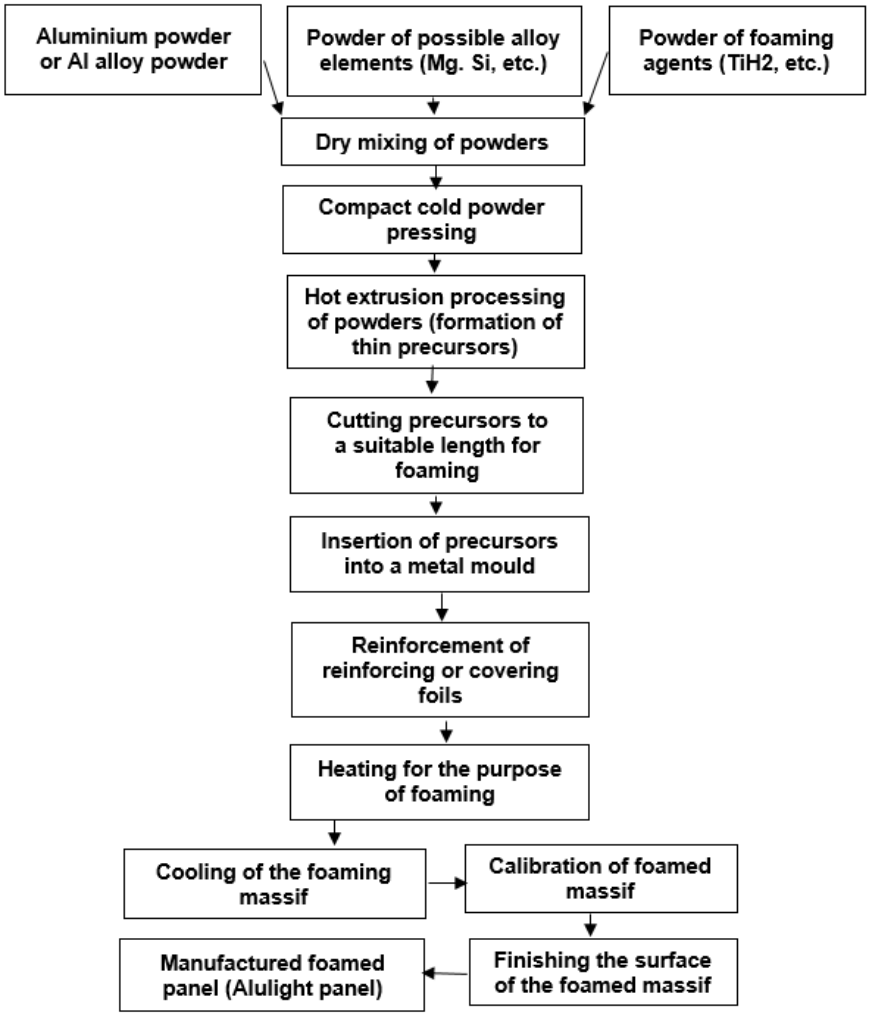

Fig. 1.26a) Block diagram of the production of ALULIGHT panels, ŠIMANČÍK [46]

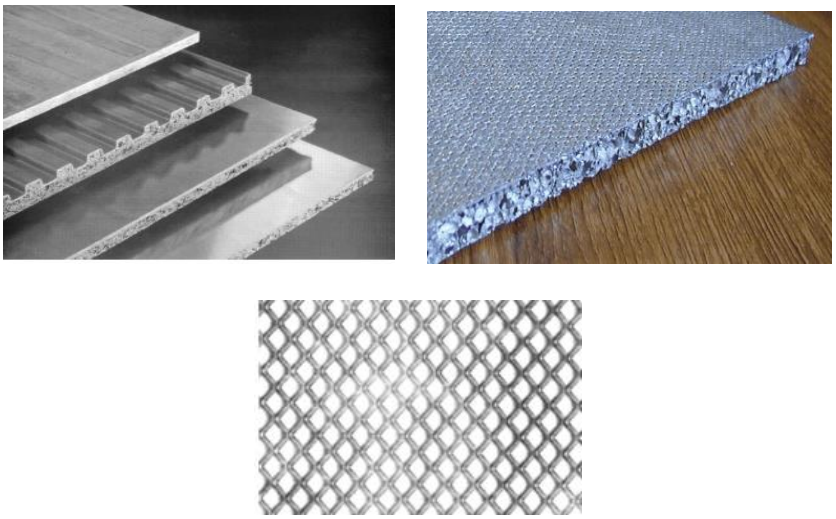

Fig. 1.26b) Aluminium foamed panels and sandwich panels (left); aluminium foamed panel whose surface is reinforced with stainless steel mesh (right), stainless steel net (below) ŠIMANČÍK [46]

1.2.3 Production of sandwich aluminium cellular systems

Aluminium Cellular Systems sandwiches, also referred to as Aluminium Sandwich Foam (AFS) sandwiches are products containing a highly porous aluminium alloy foam core and two aluminium alloy faceplates. The layers are firmly bonded together with a metallic connection. The use of such sandwich panels has been proposed for many industries, including automotive [47, 48], shipbuilding [49], rail and aerospace [50, 54]. Sandwich panels have various advantages when compared to dense material or bare foam. They are stiffer than dense sheets of the same weight [51]. Compared to bare foam without face sheets, the main advantage is that the outer shell allows the sandwich to bear the tensile load that occurs, e.g. when the panel is bent. Bare metal foam alone causes the exterior to perform poorly in tension and panel fractures. Aluminium foams reinforced with metal wires or mesh [52,53] improve this situation similar to AFS. They lead to better tensile properties but are less effective in accommodating compressive stresses. In sandwich panels, the porous foam core is hidden inside a dense material that prevents potential surface damage or corrosion problems. Provided the edges are sealed, the aluminium foam can be completely inaccessible to liquids and gases. Compared to sandwich panels, where the face plates are simply glued to a sheet of metal foam, the pure metallic nature of AFS is an advantage where flammability, heat resistance, weldability, recyclability or long-term stability is an argument. In the following, we briefly review advances in manufacturing technology and describe several promising applications of AFS in the transportation and defense sectors.

The production of AFS is based on the powder metallurgy method, on the expansion of metal precursors, which takes place due to the decomposition of the embedded foaming agent [54]. Such precursors allow the filling of complex moulds and thus the production of shaped parts of all kinds. They can also be used as load-bearing foam plates, provided that suitable shapes are available. If sandwich panels are required, metal faceplates can be attached to these plates.

The AFS manufacturing technique is moldless and requires no glueing step. Here, a three-layer composite is used, which contains a central foamable layer made from consolidated mixtures of metal powder and foaming agent powder and two full-face sheets, see Figure 1.27.

To ensure the flatness of the resulting AFS, it is recommended to carry out a hardening step after foaming. All manufacturing steps on an industrial scale are shown in Fig. 1.28a) and Fig. 1.28b) for better understanding. Powder-filled ingots, rolling process, rolled three-layer composite precursor, foam furnace.

Advantages of such an integrated process include the absence of any collisionally non-metallic joints, intrinsic non-flammability and the ability to create 3D-shaped parts by reshaping the three-layer composite before foaming or calibrating the AFS after hot foaming, [54]. Disadvantages are the limited combination of alloys for the core and faceplates due to the need to coordinate the melting temperatures of the core and faceplates. Special metal powders are used for this purpose with a large range of processing operations.

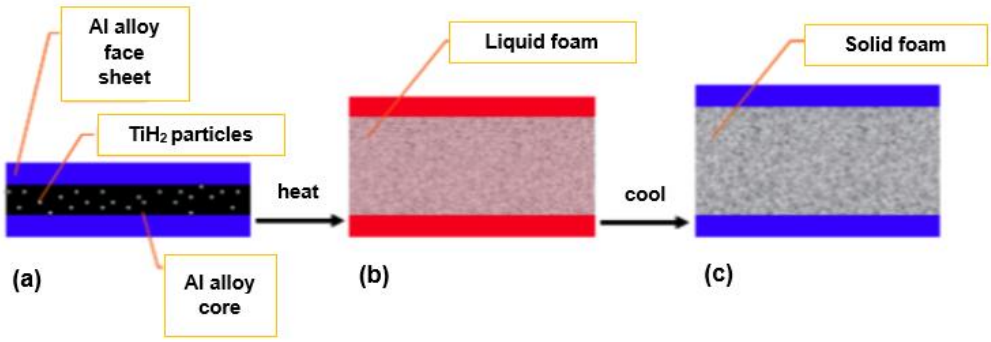

Fig. 1.27 The principle of aluminium foam sandwich (AFS) production, (production sandwich material) [54]

Possible ways to overcome this problem have been discussed [54], but no satisfactory solution has yet been demonstrated. The alloys that have been used for both core and faceplate fabrication are AlSi6Cu4 or AlSi6Cu6 aluminium alloys, as these alloys start melting at about 524 °C, which is a low temperature. Aluminium alloys with silicon and copper have low corrosion resistance and are therefore unsuitable. Al-Mg-Si alloys have proven to be suitable [8]. AlSi8Mg4 alloy (±1 wt. % Mg and Si) is also suitable as it has excellent foaming behaviour (good expansion, small and regular pores) [54].

AFS rolling ingots, Hot rolling, Precursor (3-17 mm), Foaming at 580 °C

Fig. 1.28a) AF precursor production process, top left: ingots filled with powdered frothing agent ready for rolling right: hot rolling is used to prepare the precursor, which is fed into the frothing furnace at 580 °C, [54]

AFS panels showing a favourable pore structure expressed by a predominant pore size in the range of 1 to 1.5 mm, see Fig. 1.28b), BANHART [54].

Fig. 1.28b Structure of an AFS sandwich panel, thickness approx. 10 mm, with all parameters maintained in the correct manufacturing process [54]

Fig. 1.29 shows examples of foam products from the Indian research institute AMPRI in Bhopal.

Based on long-term research on metal foams, it has been found that three groups of properties are favourable for metal foams [48]:

1) *Elastic Properties of Foam: The* Young's modulus (E) and other moduli (e.g., G) of metallic foams are typically measured using $(\rho^*)^2$, where ρ^* is the apparent bulk density of the foam [$kg \cdot m^{-3}$];
2) *Plastic properties of the foam:* collapse at nearly constant stress and associated collapse strength when observed by cyclic fatigue σ_c.
3) *Metal foams' functional properties* include thermal and electrical transport coefficients, electromagnetic or acoustic damping, etc*. Some of these are directly related to ρ** but may also depend in a complex way on the cellular morphology of the material produced.

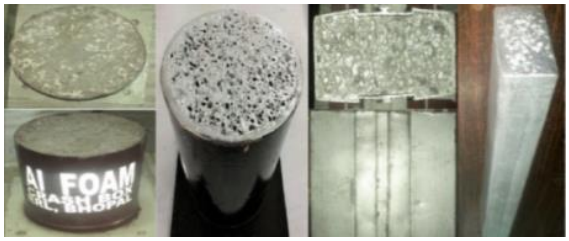

Fig. 1.29 Aluminium foam tubes and other profiles manufactured at the Advanced Materials and Process Research Institute (AMPRI) Bhopal, India [54]

1.3 Precursor production and foaming by mixtures of powders

When powder metallurgy is used for the production of cellular metal systems, the production of a semi-finished product for foaming, the so-called precursor.

1.3.1 Precursors (foam compact blowing agents)

This foam manufacturing process is another of the foam manufacturing processes that consist of an additional step of preparing a melt precursor that contains uniformly dispersed particles of foaming agent (superconductors). Later, during the melting of the precursor, the thermal decomposition of the frother forms gas bubbles at a local location in the material being processed. Because of these precursors, the production of foams of desired and complex shapes can be very easy, as is the case with direct melt foaming – the *CYMAT* method. By producing a precursor, the efficiency of the foaming process at a certain stage of metal foam production is positively affected. This precursor preparation is essentially achieved in two ways:

a) either by adding powders of the foaming agent to the melt, solidifying the melt to obtain a precursor, which must be further processed in a foaming metal mould at a certain temperature (always above the melting point of the metal used) and then cooling the mould to obtain the metal foam.
b) by compacting powder mixtures in the solid state or by forming compacted powder mixtures in the solid state using the tixo-casting process. The following three types of manufacturing processes use the above techniques to prepare precursors for further foaming.

1.3.2 Foaming due to mixtures of powders

In this manufacturing process [56], the main step for the preparation of the precursor starts with mixing the metal powders and the supercooled powders to prepare the unfinished dense product for the compaction process. The basic compaction processes used for the preparation of these precursors are single-stage compression, extrusion and powder rolling. Any of these methods can be used for compaction for better mixing of supercoater powders into metal powders without any air gaps and porosity. After preparing these precursors with the compaction process, they are heated to melt the metal powder present in the precursors so that the superfluids decompose. This decomposition of the frothers results in the development of a gas that causes the precursor to expand and form pores in the precursor. The precursor expansion process takes a lot of time as it is an important step in the manufacturing process it is created by porosity and is also greatly influenced by the temperature and size of the precursor material.

To achieve a favourable foam shape, the precursor material must be inserted into a mould. Otherwise, the result will be a block of metal foam with an undefined shape. When foaming inside closed moulds, almost any shape can be produced, e.g. tubes and other profiles can be filled with aluminium foam, as in Fig. 1.30. To achieve the desired foam shape, the precursor material must be inserted into the hollow mould. Otherwise, it would be a piece of metal foam with an undefined shape. Almost any shape can be made by foaming inside the closed mould. The foam and metal parts can be joined together during foaming. For example, tubes can be filled with aluminium foam in different ways. Another method is to produce sandwich panels consisting of foamed metal and sheet metal. These may be obtained by bonding face sheets to a foam sheet or a shell sheet of aluminum or steel sheet to a foam precursor. The latter method creates a metallic connection between all layers of the sandwich. The resulting "precursor sandwich" can be deformed in front of the foam, e.g. by deep drawing. Relatively complex foam sections can be obtained by injecting liquid-expanding foam into suitable moulds and allowing final expansion (Neumann AluFoam, Marktl, Austria), see Fig. 1.30.

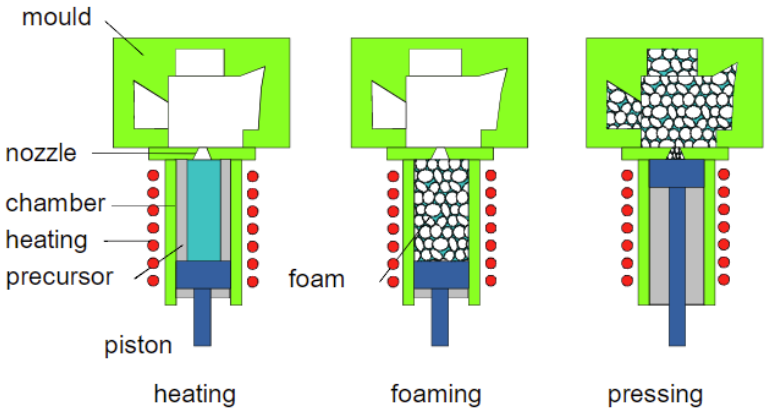

Fig. 1.30 Schematic diagram of aluminium foam production (Neumann, AluFoam, Austria), [2]

Trapped gas processes (McDonell Douglas) are also an option for the production of metal foams*.* In these technologies, a hermetically sealed container is filled with aluminium powder. The gas, e.g. argon, is then fed into the powder. The gas fills any gaps between the powder particles. When this mixture is heated, the powder particles melt and trap the gas. If the metal block thus produced is rolled and heated, the trapped gas expands and delivers the metal foam (McDonell Douglas).

1.4 Production of cellular systems from metal melts using polymer foam

1.4.1 Duocel method

Metal foams can also be produced without direct metal foaming [60], [61]. For this method of production, polymer foam is used as a starting point see the production process in Fig. 1.31. The polymer foam is processed into an open pore structure by manipulating the foaming process or by post-processing, a so-called reticular process (to form a network arrangement or honeycomb morphology). The resulting foam is then filled with a heat-resistant material slurry, e.g. a mixture of mullite, phenolic resin and calcium carbonate [61]. By drying, the polymer is removed, thereby creating a mould cavity. The molten metal is cast into the mould cavity, which accurately represents the structure of the original PU foam. The obtained metal foam is formed by open cells. After removal of the mould material (e.g. by water under high pressure), a metal foam is obtained which is an exact image of the original polymer foam. Fig. 1.31 shows the *DUOCEL* metal foam observed on an SEM microscope, produced by casting on a „lost pattern“.

Fig. 1.32 shows the structure of the metal foam sold by ERG Various grades are available, ranging from 2.5 to 16 pores per cm (10 to 40 ppi). Complex-shaped parts can be made by pre-moulding polymer foam. Aluminium alloys are usually used, but other metals (magnesium, zinc, copper, iron, nickel) can also be processed. Fig. 1.33 shows DUOCEL foams made by ERG, made from aluminium and copper. This produces foams with different densities and, where appropriate, morphologies, which are determined by the production of the polymer foam. The porosity of the obtained metal foam ranges from 80 % to 97 %. The reported production prices of these DUOCEL metallic porous systems are high.

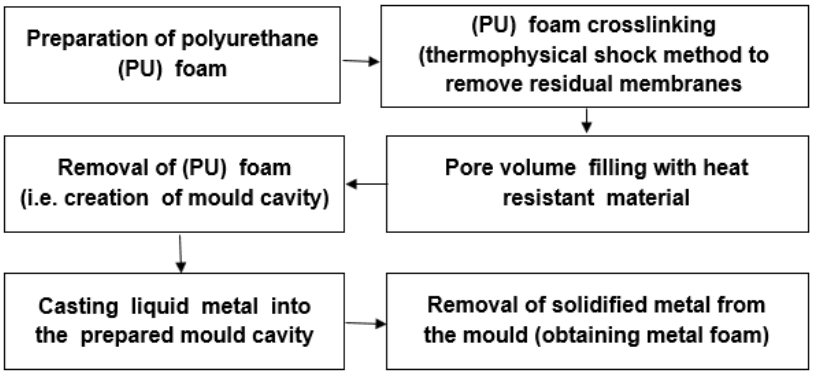

Fig. 1.31 Preparation of polymer foam for metal foam production using lost casting [61]

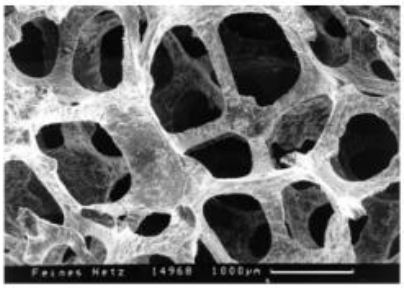

Fig. 1.32 Structure of DUOCEL metal foam obtained by SEM microscopy, [62]

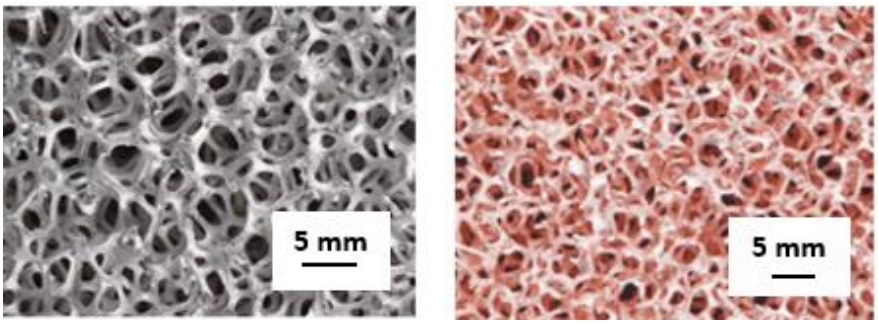

Fig. 1.33 DUOCEL foam made of aluminium and copper, ERG, [62]

Table 1-6 shows the mechanical values of DUOCEL copper foam (manufacturer ERG), [62].

Table 1-6 Mechanical values of DUOCEL copper foam (manufacturer ERG), [62]

DUOCEL copper foam (manufacturer ERG)	
Compressive strength [MPa]	0.903
Shear strength [MPa]	6.9
Compressive modulus of elasticity [MPa]	736
Tensile modulus of elasticity [MPa]	101
Heat capacity [J· kg^{-1}·K^{-1}]	3.86
Coefficient of thermal conductivity [W·m^{-1}·K^{-1}]	10.1
Coefficient of thermal expansion $[K]^{-1}$	$17.0 \cdot 10^{-6}$
Melting temperature [°C]	1083

2. METHODS OF PRODUCING POROUS METAL MATERIALS USING SHP

Porous (porous) materials referred to as 'open pore aluminium foams' are extensively studied by researchers at the Department of Materials Engineering, University of Sheffield. Under the designation "Open Cell Aluminium Foams by Space Holder Particles. The designation Space Holder Particles (SHP) is understood to mean "space holder technique". The workers here apply a method they call 'vacuum' (replication). Furthermore, two new methods have been introduced based on this principle, i.e. gas and mechanical infiltration. In the research on gas infiltration of melt between NaCl grains, infiltration pressures were determined to produce porous materials with pore sizes of 1.0 to 1.1 mm; 1.4 to 1.7 mm and 2.0 to 2.36 mm. Porous materials with a moderate porosity of 0.6 to 0.7 may be of interest as regenerators due to their high bulk heat capacity and large specific surface area. The replication process is an inexpensive and simple method of foam production that provides metallic foam with moderate porosity. Due to its simplicity, it provides many opportunities to investigate the effect of porosity, pore size and shape, or a combination of these.

A porous material is a material that has many open spaces in its structure, called pores or voids. The size of the pores varies from a few nanometres to many millimetres, depending on the purpose of the porous material. In engineering, a homogeneous material is often preferred, but in the natural world, there are the reverse effect occurs, meaning that pores have different sizes in the same structure, which is defined as a gradation of porosity [35], [36], [37], [38].

The most common terms used in this particular area of porous materials are: true specific gravity, which is the specific gravity of the material without pores or voids; bulk density is essentially the specific gravity of the material including open pores and voids; pore volume; pore size is the distance between the pore walls, their width or diameter; porosity is the ratio of the total pore volume to the apparent volume of the sample. The equations for determining these quantities are given in Table 2-1.

Table 2-1 Common equations used in the field of porous materials, LUNA [34]

Relations for determining the properties of porous materials, according to [34]	
Names	**Equations, quantities**
Actual specific gravity	$\rho_M = m / V_{MM;}$ [kg·m^{-3}]
Volume weight	$\rho_R = m / V_{MR;}$ [kg·m^{-3}]
Pore volume	$V_P = V_R - V_{M;}$ [m^3]
Porosity (porosity)	$\varepsilon = V_P / V_{R;}$ [1]
Surface (depends on the shape of the body), e.g. sphere	$A = 4 \cdot \pi \cdot r^2$ [m^2]
Specific surface area	$A_{Sp} = A/V_R$ [m^{-1}]

The characteristics of the porous material depend on the pore size. According to IUPAC (International Union of Pure and Applied Chemistry); Roquerol and Liu mention three classifications of materials: microporous, mesoporous and macroporous, their

definitions are given in publications [39], [40]. Microporous material has a pore size smaller than 2 nm; an example would be the medical professional making tape to cover a wound to prevent bacterial infection but still allowing air to pass through to create a sterile environment. The mesoporous material has a pore size between 2 and 50 nm. It is used in catalysis, separation, and adsorption and as hosts for certain molecules because of their uniform pore size [41]. Macroporous material has a pore size larger than 50 nm; it is commonly used for filters, anode material for fuel cells, stationary phases for various types of chromatography, bioreactors, microfluidic chips, filtering and heat transfer applications [42], in this work this type of material is used for heat transfer application.

The production of metallic porous materials involves several different methods, each of which involves the regular distribution of bodies of minute dimensions, which are most often soluble in water. In the English literature, these production methods are referred to as the "Space Holder Technique" (SHT) or Space Holder Particles (SHP). These tiny bodies can be, for example, NaCl. Their presence increases the porosity of the metal, which is based on the subsequent leaching of these particles in water. As a result, the density of the porous metal material thus produced is reduced. In some foreign publications, this method is referred to as the method using differently sized NaCl particles (A porous structure is formed by dissolving of salt from the aluminium matrix). These particles may be other materials that are burned out or melted during the production of the porous systems, etc. In the production of metallic porous materials, how the melt is brought between the grains of the water-leachable bodies is important. This may be by melt infiltration in a vacuum, melt infiltration during centrifugal casting or gravity casting. A special technology for the production of metallic porous systems is based on the use of a mixture of metal powder and particles that creates porosity in the metal material. Metallic porous materials are also in some cases referred to as metallic "foams" and their production is based on so-called replication, that is to say, on making an impression of, for example, the aforementioned NaCl particles. These technologies lead to the production of metallic materials with open cells (pores). Metallic porous materials are used for functional applications such as filtration, sound absorption, thermal insulation, heat exchange, energy absorption, and air and water purification.

2.1 Production of porous metal parts using molten metals and spatial formation of NaCl

As far as the production of metallic porous materials is concerned, this method is referred to in the literature as using NaCl space formations. Although the basic mechanism of melt infiltration between NaCl grains is different. At the same time, the amount of NaCl is also important. The use of 30 wt. % NaCl to produce a porous system yields a material with moderate porosity. As with the production of metal or aluminium foams, the production of porous aluminium material is not simple. Fig. 2.1 shows a relatively simple scheme for the production of porous metallic materials, as

presented by the manufacturer Alumeco Group [21]. This scheme represents the infiltration process of molten metal between NaCl particles.

Fig. 2.2 shows a pictorial diagram showing the possibility of higher production of the metallic porous material as presented in the production of the material known by the trade name ALUPOR. The pore size and the ratio between the maximum and minimum pore size are closely related to the obtaining of the corresponding mechanical properties and, where appropriate, filtration properties.

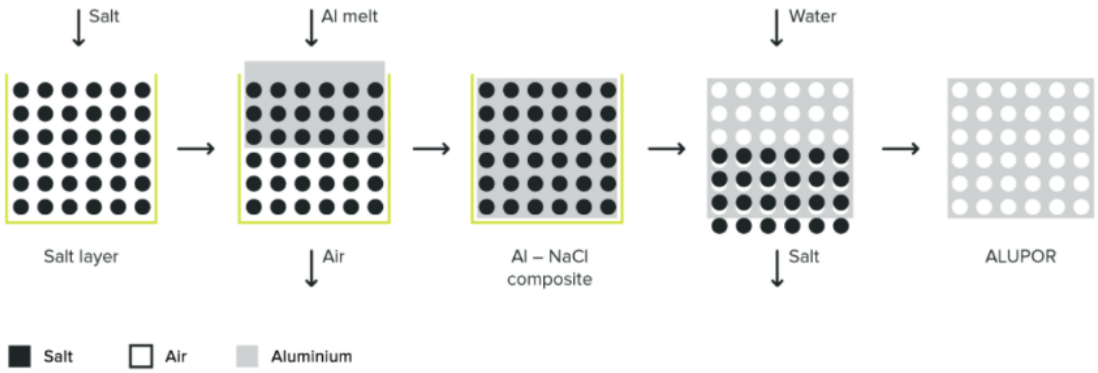

Fig. 2.1 Schematic of the production of the aluminium porous system, according to Ameco Group [21]

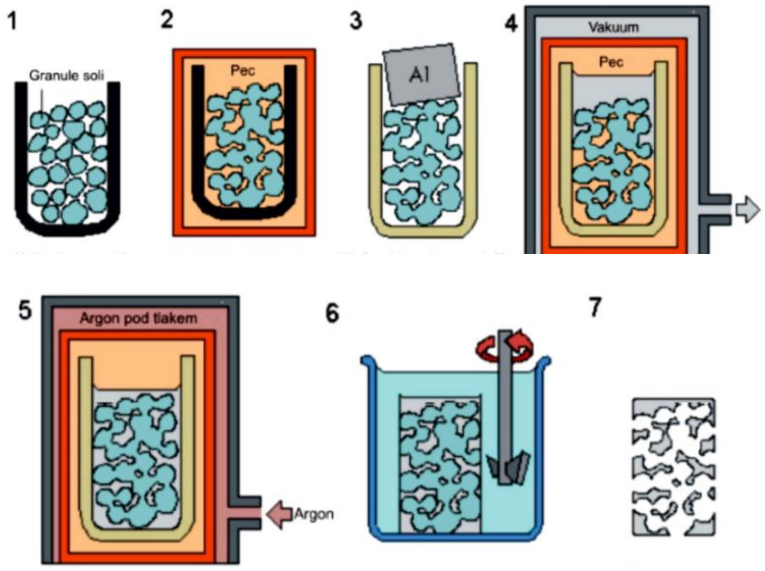

1- the crucible is filled with NaCl granules; 2 - sintering the grains of salt in the oven 3 - the aluminium bun is placed on the formed salt granules; 4 – the melting of aluminium in a vacuum furnace; 5 - after melting the aluminium, an overpressure of argon is set. The aluminium melt penetrates between the NaCl granules; 6 - the dissolution of NaCl granules from aluminium material; 7 - resulting porous material with open pores

Fig. 2.2 Schematic of the production of porous lightweight materials from aluminium and NaCl alloys according to CURRAN [18]

Fig. 2.3 shows a more detailed block diagram of the production of porous materials, according to which there is already a higher guarantee of obtaining the desired porous material. Fig. 2.4a) shows an example of the production of porous aluminium. The time of pouring the salt into the mould and the subsequent impregnation of the salt (NaCl) with molten aluminium to form the Al-NaCl composite system is part of the production step of porous aluminium, ALUPOR. Fig. 2.4b) shows the production of porous aluminium at the time of casting the aluminium melt onto the NaCl bed to form the Al-NaCl composite system, ALUPOR [20]. Fig. 2.4c) shows the porous aluminium material products (NaCl particles used in the fabrication process), Composite Material Ltd, ALUPOR. The manufacturer of these porous materials is Alumeco Group. The porosity of these porous materials is 55 % to 75 %. The bulk weight of the porous aluminium produced in this way depends on the degree of porosity, reaching a value of 1,000 $kg \cdot m^{-3}$ to 1,400 $kg \cdot m^{-3}$, which is almost a third or half the specific weight of fully compact aluminium.

Porous cellular metal materials have gained considerable industrial application in the last decade and further methods for their production are being sought. Lightweight metal-based systems, particularly aluminium and its alloys, are materials of choice for the manufacture of structural components and parts in many industries due to the unusual combination of properties they offer, i.e. low weight, high energy absorption capacity, high stiffness and high damping. These materials are used in a variety of applications, some of which are based on significant mechanical properties (in particular, closed cell foams), while others are based on rheological properties and transport processes, which are enabled by the accessibility of open pores for fluid penetration and flow (open cell foams). Or porous metallic materials.

Porous aluminium serves as an effective replacement for sintered metals, aluminium foams and metal sponges. It is a 100 % open porous material and is suitable for the replacement of sintered metal filters with filtration from 5 to 200μ m. These materials can be used to produce filters operating at temperatures of 250 to 300 °C. Applications of this material are for heat exchangers, vacuum tables, energy absorbers and shock absorbers. Today, not only the Alumeco Group but also Exxentis, Schweiz, is professionally involved in these metal porous systems.

These metallic porous materials are, in some cases, referred to as metallic foams produced by replication. Replication is one of the processing techniques used to produce porous metal systems (with open pores). For example, an aluminium alloy such as AlSi12 or AlSi7Mg etc. is used to produce aluminium foam or porous aluminium material. From these alloys, a cylindrical cast is prepared, which is also placed in a cylindrical mould on an infiltration layer of NaCl or the melt is poured into a mould with NaCl and gradually infiltrated between its grains, see Fig. 2.1.

Professionally produced porous materials using NaCl particles have the commercial designation *EXXCENTIS* or *ALUPOR.* Exxcentis is a Swiss company. The material under the designation ALUPOR - Composite Material Ltd, Sverdlovsk region, Russia. Its technical partner is Alumeco Group, Denmark.

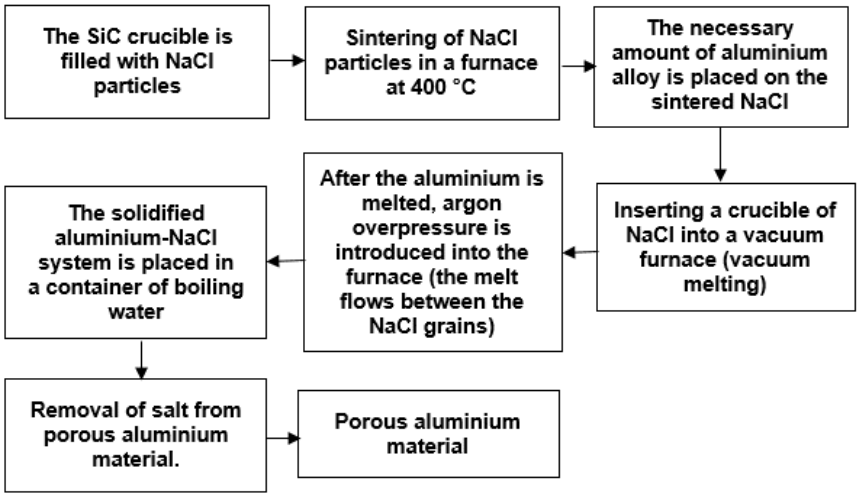

Fig. 2.3 Schematic of the production of NaCl-based metallic porous systems, CURRAN [18]

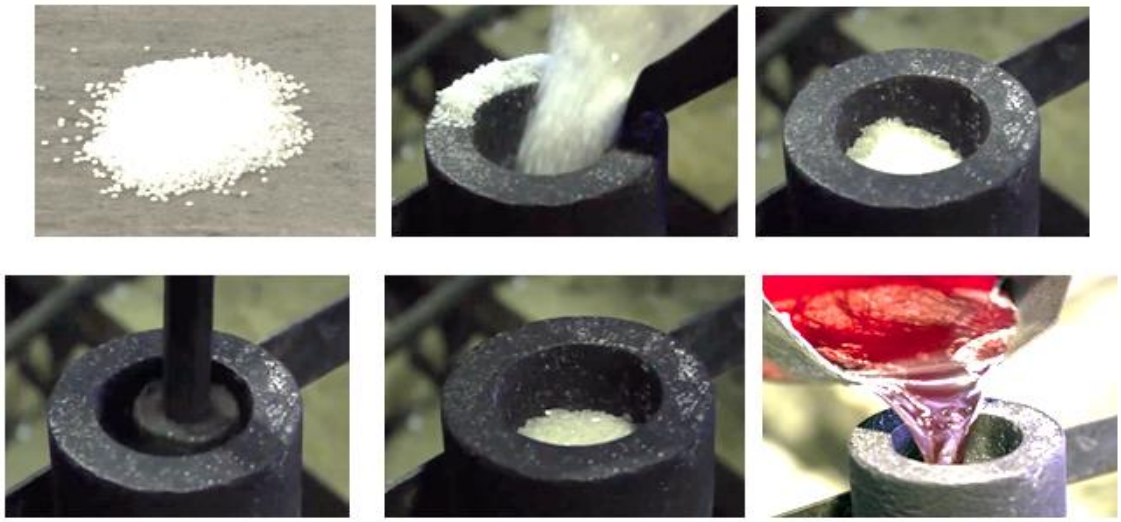

Fig. 2.4a) Production of porous aluminium, at the time of pouring the salt into the mould and subsequent impregnation of the salt with the aluminium melt to form the Al-NaCl composite system, ALUPOR

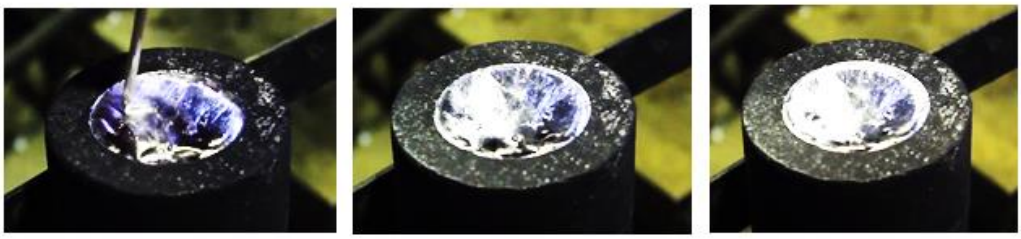

Fig. 2.4b) Production of porous aluminium, after casting the aluminium melt onto a NaCl bed to form the Al-NaCl composite system, ALUPOR [20]

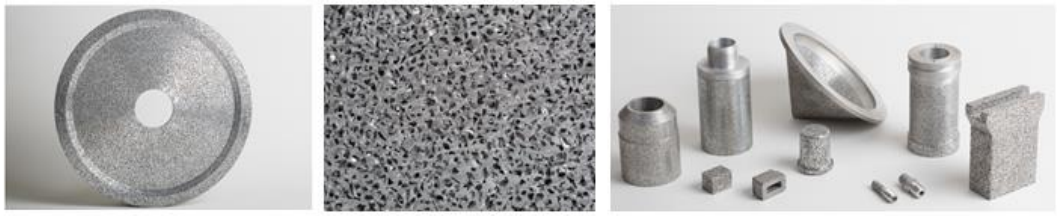

Fig. 2.4c) Products made of porous aluminium material (NaCl particles used in production), Composite Material Ltd., ALUPOR [20]

Researchers at the University of Sheffield are manufacturing porous aluminium systems [15]. Subsequently, the production of an aluminium porous system using table salt particles is also described. Here, the salt particles work on the principle of "salt nuclei" to form a porous solid aluminium porous material. The principle is that an aluminium tablet (approx. ∅ 50 x 30 mm) is heated in a cylinder-shaped mould together with table salt, which is poured into the bottom of the mould. The mould or tube is approx. 145 mm high and is closed on both sides by flanges held in place by 4 screws. The upper flange is fitted with an outlet for the connection of hoses in the shape of a T. One outlet is used for the connection of a vacuum pump to create a vacuum in the working space of the cylindrical part of the mould. The other outlet of the T-tube is for the supply of argon. Approximately 300 to 500 ml of salt is required for the experiment. Then a tablet of the appropriate metal e.g. aluminium or its alloy is inserted. Fig. 2.5a) shows an example of fine salt (bedding salt) and infiltration salt (salt for the production of porous metal systems), NaCl, as well as a diagram of the mould and the mould. Fig. 2.5b) is a diagram of the mould with two flange-shaped caps.

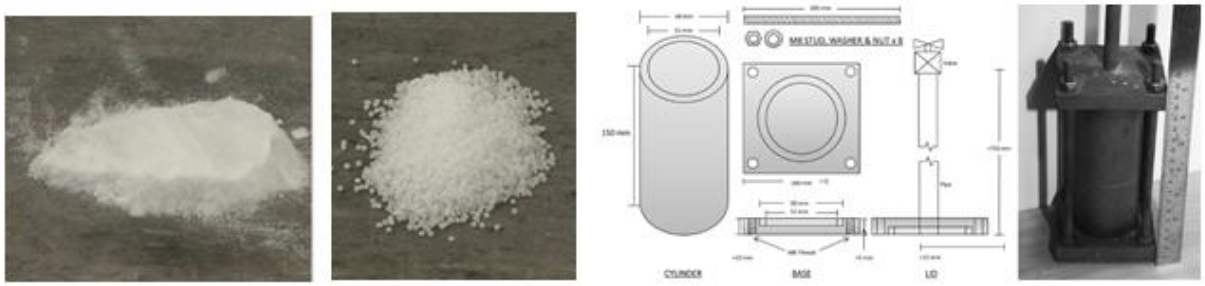

Fig. 2.5a) Different types of salt or salt bodies and technical data for mould-making [15]

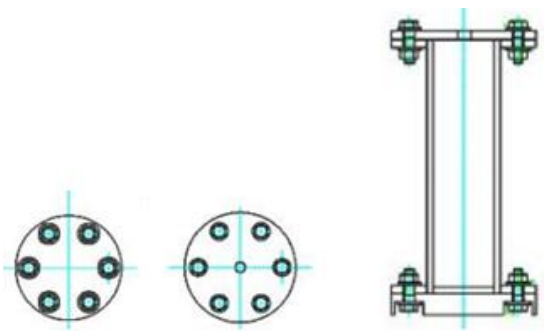

Fig. 2.5b) Diagram of the mould for the production of aluminium porous systém [15]

Fig. 2.6 is a diagram of the mould and the salt and aluminium tablet layers. Fig. 2.7 shows the table salt, the aluminium tablet and the mould. The production is based

on the principle of melt infiltration between NaCl grains, which is supported by both vacuum and argon atmosphere. This production of porous aluminium materials is referred to by the researchers as replication. A schematic illustration of the preparation process of the porous aluminium materials produced is shown in Fig. 2.8.

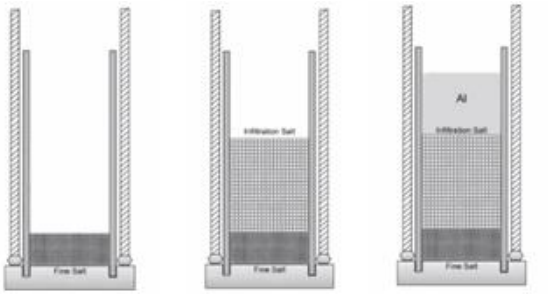

Fig. 2.6 Diagram of filling the mould cavity with fine salt, porosity salt (infiltration salt) and aluminium, LUNA [15]

Fig. 2.7 Table salt - NaCl, aluminium tablet and mould [15]

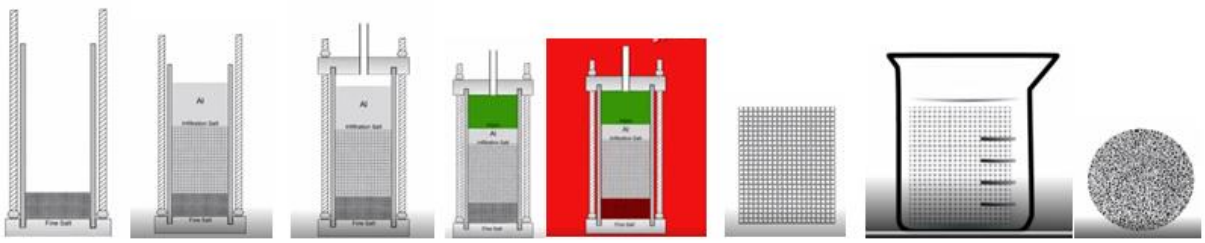

1) *fine salt is put at the bottom of the preparation;* ***2) the*** *necessary amount of infiltration salt is then poured in;* ***3) an*** *aluminium tablet of a certain size is placed on the infiltration salt; 4**)** vacuum conditions are created in the closed mould for melting the tablet; 5**)** the mould is placed in the furnace,* ***6)*** *infiltration of the melt between the grains of the infiltration salt - NaCl,* ***7)*** *manufactured system (infiltrated aluminium between the grains of the salt) 8**)** insertion of the composite material, aluminium with salt into water, dissolution of the salt occurs, 9**)** manufactured porous aluminium system*

Fig. 2.8 Schematic of the production of an aluminium porous system (replication process), LUNA [15]

Fig. 2.9 to Fig. 2.13 are partial examples of the necessary production equipment.

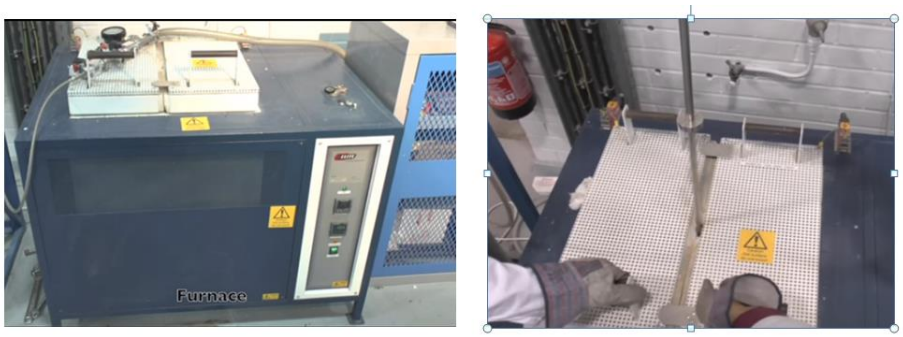

Fig. 2.9 Resistance furnace of special design with a split door in the upper part of the furnace, [15]

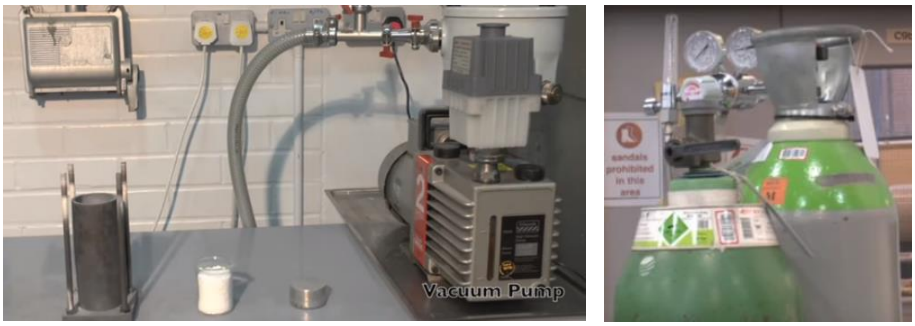

Fig. 2.10 View of mould, table salt, aluminium tablet and argon pressure vessel, LUNA [15]

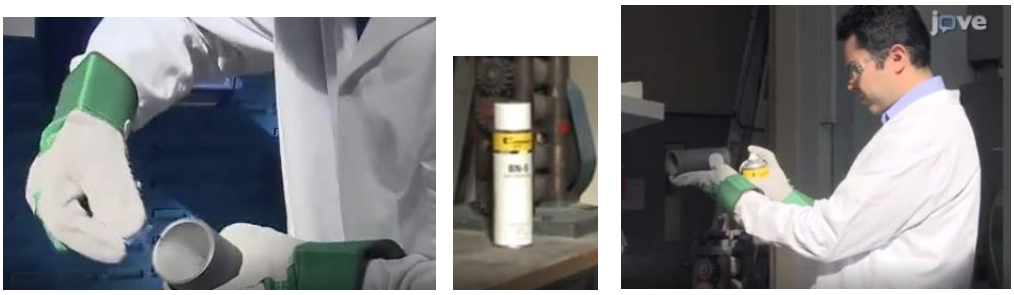

Fig. 2.11 Treatment of the mould cavity before the technological process of the porous system production, LUNA [15]

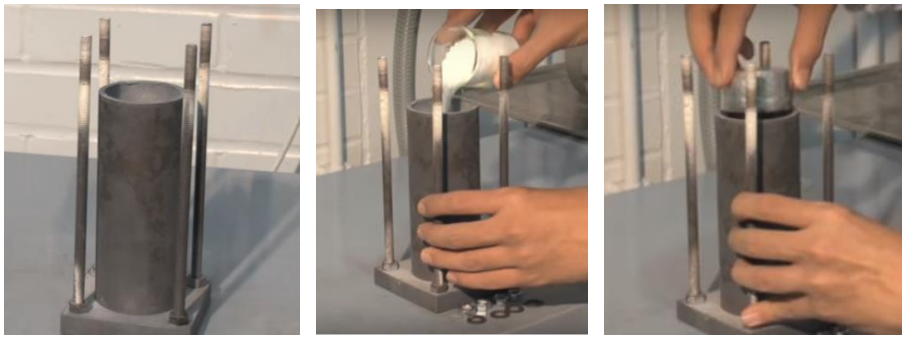

Fig. 2.12 The mould, pouring the curing salt into the mould and inserting the aluminium tablet into the mould [15]

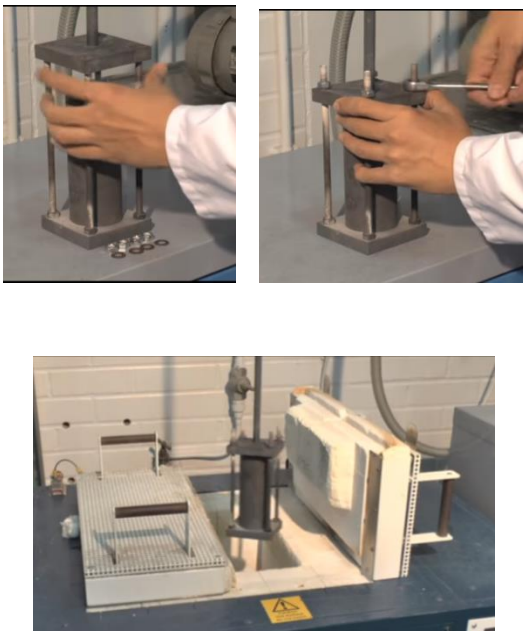

Fig. 2.13 Assembling the upper flange and clamping with 4 screws, inserting the mould into the furnace [15]

Fig. 2.14 is a schematic of the equipment for the production of porous aluminium materials. Fig. 2.15 to Fig. 2.17 show examples of the vacuum system controls, gauge readings, oven temperature settings, for the infiltration process, and for removing the mould from the oven. Fig. 2.18 shows the aluminium porous materials ("foams") produced. The material is from the publication by Luna et al [15].
After the mould is placed in the oven, the air must be sucked out of the mould working area. This is done using a vacuum pump and a special line with a pressure gauge. And the air is sucked out or a vacuum is created.

As can be seen from the above, researchers at the University of Sheffield are producing aluminium porous systems based on melt infiltration between NaCl grains in a special mould using vacuum and argon; a schematic of the plant is shown in Fig. 2.14.

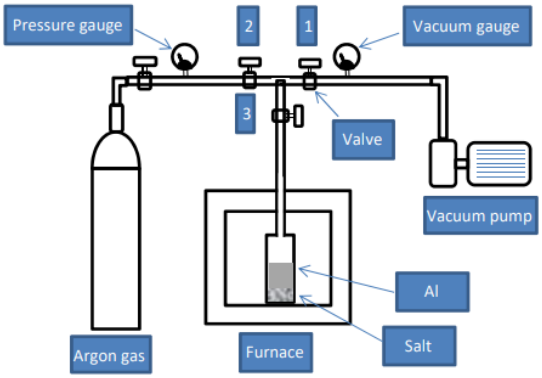

1,2,3 - valves
Fig. 2.14 Schematic of the plant for the production of porous aluminium materials using grains of salt NaCl [15]

Valve 1 regulates the suction of air from the mould and contributes to the vacuum in the mould. The corresponding piping with valve 1 and vacuum gauge is connected to the vacuum pump. During the vacuum process, *valve 2* is closed to prevent access of argon and at the same time to prevent damage to the argon pressure gauge and the vacuum gauge. *Valve 3* is used to isolate the mould from the system and to detect gas leaks from the piping system. Quick-release clamps are placed between them and valve 3 so that the mould can be isolated from the system. The vacuum pump is designed to provide a vacuum up to 750 torr. The furnace is electric with heating control and program settings for different heating methods.

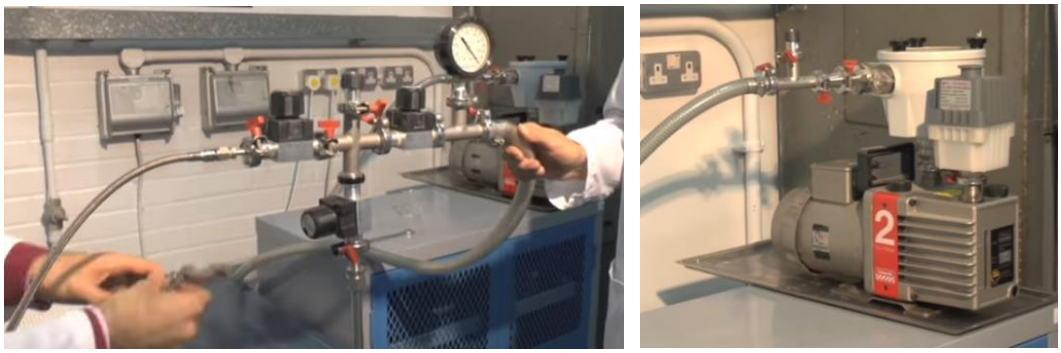

Fig. 2.15 View of the vacuum system for extracting air from the assembled mould, [15]

Fig. 2.16 T distribution system, flowing into the mould; switching on the vacuum pump and creating a vacuum until the gauge needle reaches "0", [15]

The temperature in the furnace must be approximately 50 °C higher than the melting temperature of the alloy used (e.g. Al, 660 °C). The heating time of the mould containing the aluminium tablet and salt is 1.5 to 2 hours. After this time has elapsed (1,5 to 2 hours), the argon supply valve is opened, and argon is fed into the mould, the molten aluminium being forced between the grains of salt, which is helped by the vacuum created in the mould. The mould is removed from the box-shaped furnace with a special jig; see Fig. 2.17 (left) and Fig. 2.17 (right) show the heated mould from which the manufactured material containing the cast grains of table salt is removed.
The researchers [15], to remove the hot mould from the furnace, created. A special simple fixture in the form of a modified rod attaches it to the nut on the air suction tube in the upper flange.

Fig. 2.17 View of the open furnace, when removing the mould with special preparation (left), removed mould (right), [15]

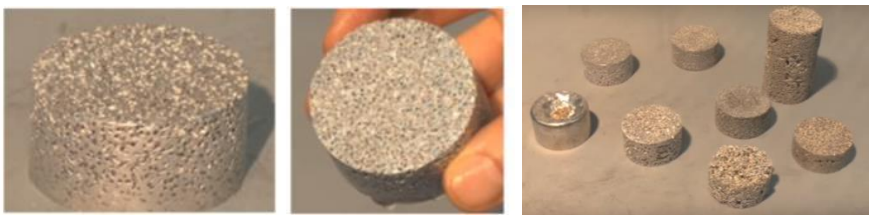

Fig. 2.18 View of the fabricated aluminium porous ("foam") material LUNA, [15]

The replication process, where molten metal is infiltrated between grains of removable preform material, allows a considerably high degree of control and has been used to good effect to elucidate some of these relationships. However, this process has many steps that are dependent on the individual production technology. The demonstration of the production of an aluminium porous material by University of Sheffield researchers has aimed to describe all stages of porous material production, including the use of all materials and equipment that are relatively easy to apply in a research environment. It also aims to show how lightweight metallic materials can be produced efficiently and simply. The obtained metal blanks with coated grains of table salt are finally placed in water and boiled for about 30 to 60 minutes to dissolve the table salt (leaching of salt nuclei). After drying, the porous aluminium material is obtained. In this way, aluminium porous materials can be obtained (open cell systems with a pore size of 1 to 2.36 mm, with a porosity of 61 % to 77 %. Fig. 2.19 shows cross-sections of samples of fabricated porous aluminium materials. The Swiss company Exxentis is also involved in the production of porous materials, see Fig. 2.20a) to Fig. 2.20d), [17]. Fig. 2.21 shows products made from porous aluminium material with salt particles promoted by Material Distric, Narden [19].

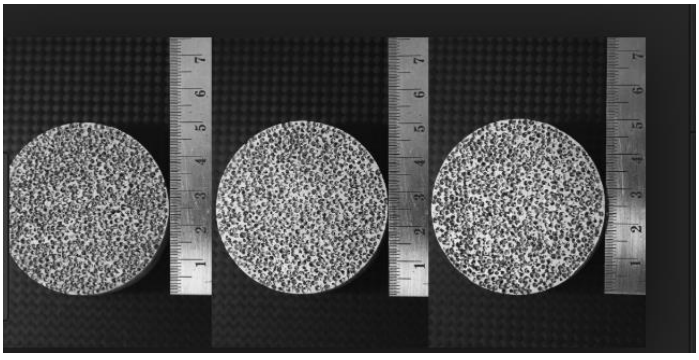

Fig. 2.19 Aluminium porous systems produced by University of Sheffield staff, LUNA, [15]

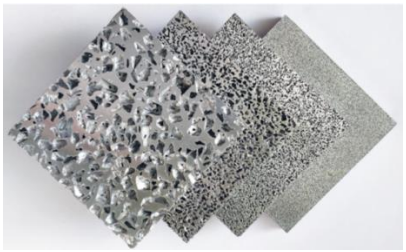

Fig. 2.20a) Aluminium porous systems, manufactured by Exxcentis, [17]

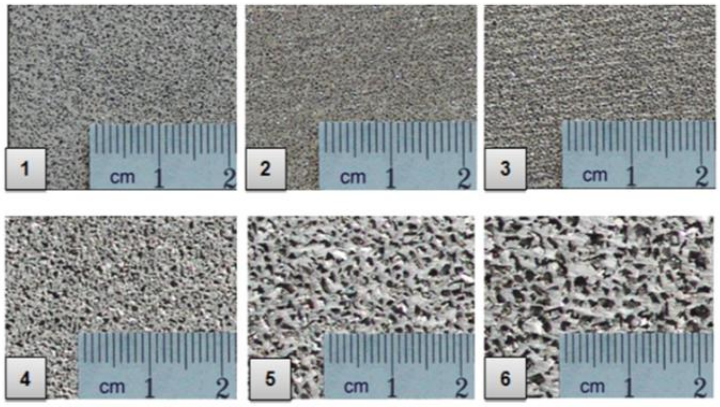

Pore sizes in the material:
***1** - 0.10 to 0.35mm; **2** - 0.20 to 0.40 mm; **3** - 0.35 to 0.63 mm; 4 – 0.35 to 1.00 mm; **5** – 0.63 to 1.60 mm and **6** – 0.63 to 3.00 mm*

Fig. 2.20b) Aluminium porous systems, manufactured by Exxcentis [17]

Fig. 2.20c) Structure of porous aluminium materials based on Al-NaCl, (produced by Alumeco Group and Exxcentis) [17]

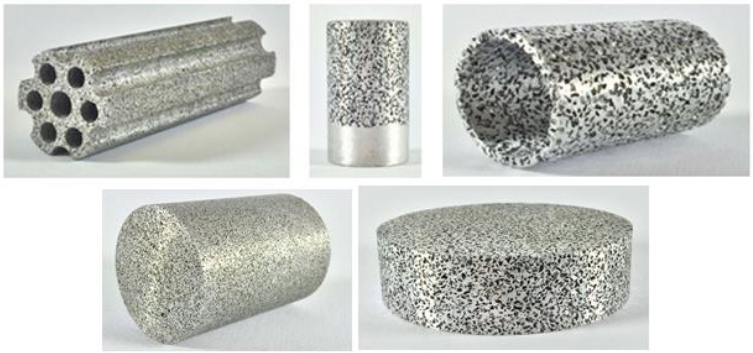

Fig. 2.20d) Products made of porous aluminium material, manufactured by Exxcentis, [17]

Fig. 2.21 Products made of porous aluminium material with salt particles promoted by Material District, Narden [19]

The above porous aluminium materials serve as an effective replacement for aluminium foams or aluminium sponges. It is a 100 % open porous material with pore sizes ranging from 5 to 200μ m. This aluminium material can withstand temperatures from 250 to 300 °C. As can be seen from the above, spatially ordered particles are used for the production of metallic porous lightweight materials with open cells (porous materials). These spatial formations cause porosity or porosity in the final effect of the material. Some technologies for the production of these materials are based on the use of a powder of a given metal or metal alloy (e.g. aluminium alloy). The particles of the metal powders used must be smaller than the particles to form the porosity of the material, as the designation implies [9]. The metal powder must be thoroughly mixed with the sodium chloride particles. During the processing of the powder with NaCl particles for the formation of spatial porosity of the material, after the powder is melted and solidified, these particles are subsequently removed by chemical or thermal means [2,3,4,5,6]. The shape of the "space holder" particles controls the morphology of the porous structure of the material. In addition to the widely used NaCl particles, carbonate particles, carbamide particles, expanded polystyrene granules, magnesium particles, polystyrene spheres, and more recently, sucrose crystals can also be used [7,8].

Material District, Naarden [19], as well as other manufacturers, use NaCl particles to produce porous aluminium systems. After the aluminium has solidified, the NaCl is removed by placing the solidified NaCl particles in water. The sodium chloride is leached out, making the material porous. Depending on the size of the NaCl grains, the porosity of the aluminium produced may vary. The NaCl particles must be spread out as the metal material solidifies so that all the empty spaces (cells of the porous material) are interconnected after the subsequent leaching of NaCl.

The porous material can be used in filtration systems, lighting devices, wall decorations, acoustic solutions, etc. The properties of the produced material are: compressive strength 7 to 40 MPa (depending on the pore size), bulk weight 1350 $kg \cdot m^{-3}$, thermal conductivity coefficient is 40 to 45 [$W \cdot m^{-1} \cdot K^{-1}$], [19].

2.2 Production of porous metal parts using metal flakes and spatial sucrose formations

For the production of porous aluminium materials, aluminium alloy flakes can also be used instead of aluminium melt or aluminium powder, as used by PAPATONIOU [1]. For this purpose, sucrose, known as crystalline raw cane sugar, was used instead of the traditionally used NaCl. The aim of using sucrose was to test the production of an aluminium porous material in a simple, economical and environmentally friendly way. The method involves mixing the powder, pressing, leaching and sintering. The parameters for optimizing the production of aluminium porous material were investigated. With the premise of producing high-quality open-cell aluminium porous materials with excellent environmental and favourable economic effects.

The use of aluminium flakes with sucrose resulted in a porous material with a porosity of 80 vol% with open cells. Relatively low compaction přes

sures are required to produce this material. The main parameter of the technology used was the determination of the compaction pressure for the production of the precursor and its sintering temperature. Fig. 2.22 shows a schematic of the production process according to [1], which is as follows:

1) The preparation of aluminium flakes and the determination of a certain amount of sucrose, which creates porosity in the metal system;
2) Mixing aluminium flakes with sucrose particles;
3) Pressing of a mixture of both mixed ingredients (aluminium flakes and sucrose), pressing pressure 200 MPa. Obtaining a mixture of the pressed ingredients;
4) Water washout dissolving (using agitator 100 rpm, water temperature 60 °C)
5) Creation of a precursor for the production of porous material.
6) Sintering of the precursor in the furnace, burning of sucrose - i.e. obtaining porous material. Sintering temperature 620 °C to 740 °C (heating rate 10 °C· min^{-1}, cooling rate 3 °C·min^{-1}).
7) Obtaining porous material.

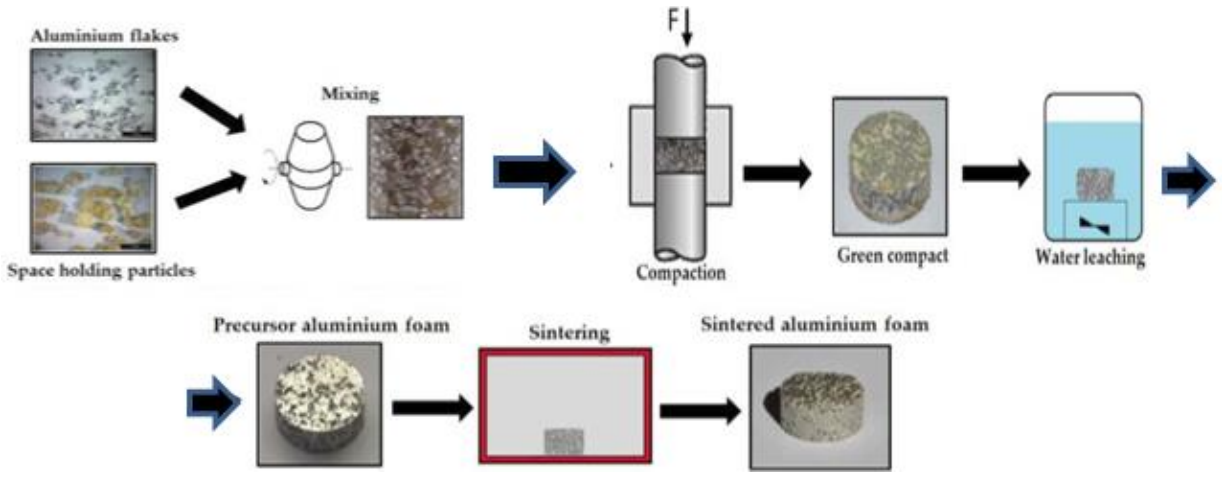

Fig. 2.22 Schematic of the production of porous aluminium using sucrose, [1]

Fig. 2.23 shows an example of the particles of both ingredients used.

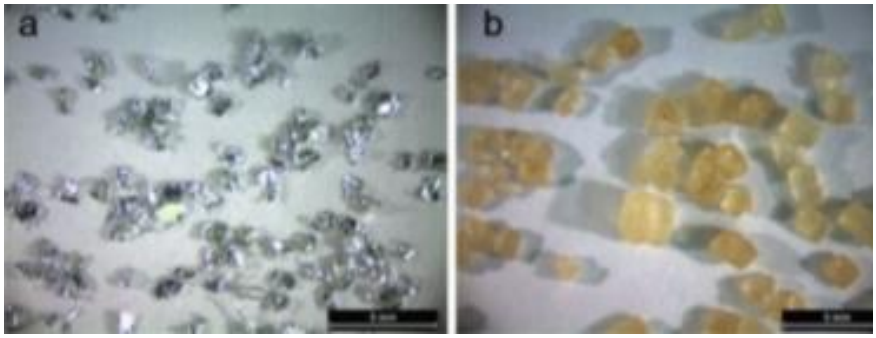

Fig. 2.23 Materials used in the open cell aluminium foam manufacturing process: a) flaked aluminium particles, b) sucrose particles, [1]

Pressing - a pressing pressure of 200 MPa was suitable for the production of stable precursors. Cracks were formed when a pressure of 250 MPa was used see Fig. 2.24 (red arrows) [1].

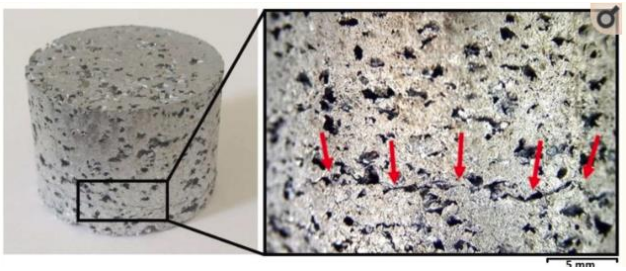

Fig. 2.24 The obtained porous aluminium system and its structure produced by pressing with a pressure of 250 MPa, cracks are evident, according to [1].

Sintering was carried out at temperatures between 620 and 740 °C. During sintering, each compacted sample must be heated slowly at a rate of 10 °C· min^{-1} until the appropriate temperature is reached and maintained for 3 hours. After sintering, the precursors are cooled to a temperature of about 20 °C with a cooling rate of 3 °C·min^{-1}. It has been found that a porosity of 78,9 % of the obtained aluminium material is obtained at a sintering temperature of 620 °C, and a porosity of about 76,8 % when a sintering temperature of 740 °C is used. Fig. 2.25 shows the samples after sintering.

Dissolution during the dissolution process, the sucrose particles were easily dissolved in distilled water to leave open cells in the precursor. A magnetic stirrer with a heating plate at 100 rpm in^{-1} and 60 °C for two hours was used to dissolve the "space-holding particles". During dissolution, the water was heated to 60 °C. After the dissolution process, the precursor was left in the oven for one hour to remove any remaining distilled water. After drying for one hour, the weight of the precursor was determined by weighing to the nearest 0.001 g to determine if any sucrose particles remained within the porous structure. The measurements showed that after the entire dissolution

drying procedure, no sucrose particles in the matrix of the aluminium 'foam'. Porous test samples ∅ 25 x 15 mm were produced using this technology.

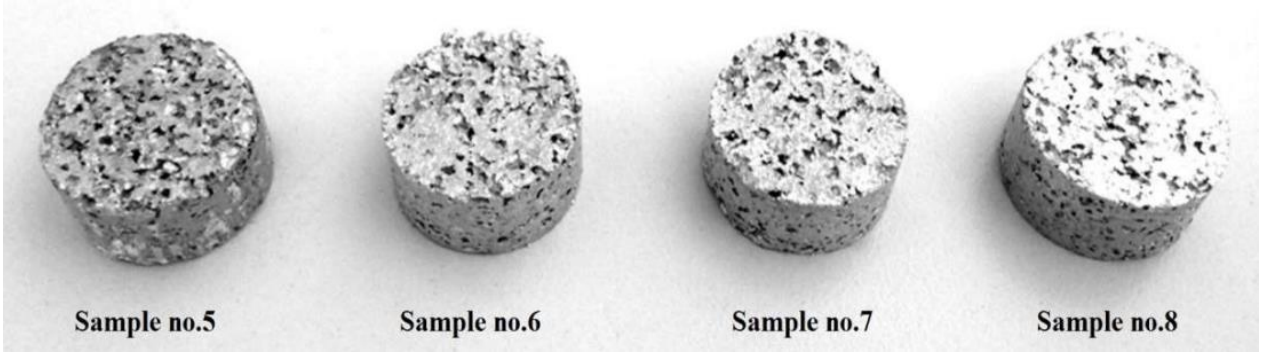

Fig. 2.25 Aluminium-based samples with sucrose after sintering, [1]

Table 2-2 lists the properties of the samples produced, according to [1]. The sample numbers always represented the respective group. Samples of groups 1, 2 and 4 were not tested.

Table 2-2 Values of selected quantities of aluminium samples produced using sucrose [1]

Monitored values of selected variables of aluminium porous samples ∅ 25 x 15 mm					
A sample from the group	**Pressing pressure [MPa]**	**Sintering temperature [°C]**	**Absorbed energy per volume [kJ·dm^{-3}]**	**Absorbed energy per mass [kJ· kg^{-1}]**	**Porosity [%]**
3	200	without sintering	0.39	0.62	79.8± 1.8
5	200	620	0.41	0.67	79.9± 1.6
6	200	660	0.78	1.32	78.1± 1.7
7	200	700	0.94	1.41	77.2± 1.5
8	200	740	1.16	1.85	76.8± 1.3
9	200	780	the material collapsed during the test		

Fig. 2.26a) shows the microstructure of the fabricated samples (open-cell aluminium porous material) at a sintering temperature of 740 °C.

Determination of the density of the produced porous material (ρ_P) - was made based on known physical quantities:

$$\rho_P = \frac{m_P}{V_P}, \tag{2.1}$$

where denotes:ρ_P is the bulk mass of porous material [kg ·m^{-3}] or [g·cm^{-3}]; m_P is the mass of porous material [kg] or [g]; V_P is the volume of porous material [m^3] or [cm^3].

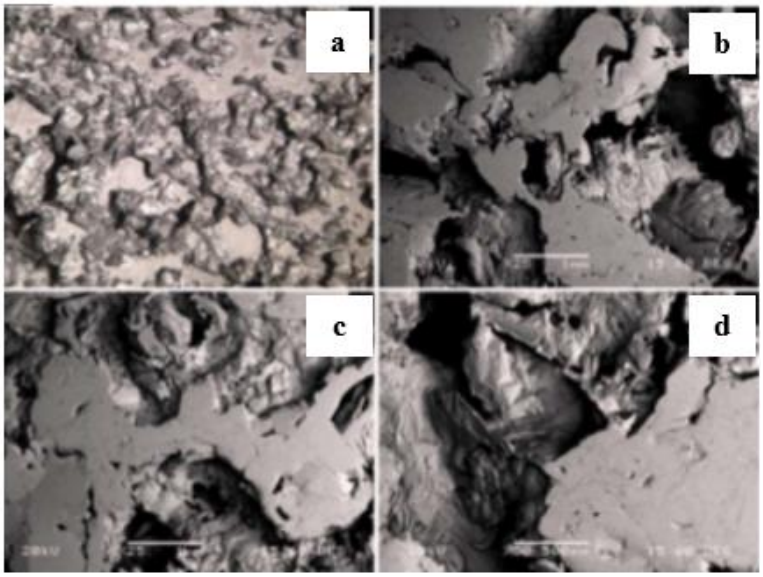

a - optical stereoscopic image illustrating irregular porous morphology;
b to d - morphology and internal structure of cell walls

Fig. 2.26a) Morphology and microstructure of fabricated samples of aluminium porous material at sintering temperature 740 °C [1]

Fig. 2.26b) is the XRD analysis, i.e. the X-ray diffractogram of the precursor sample (2) and the porous sample (1).

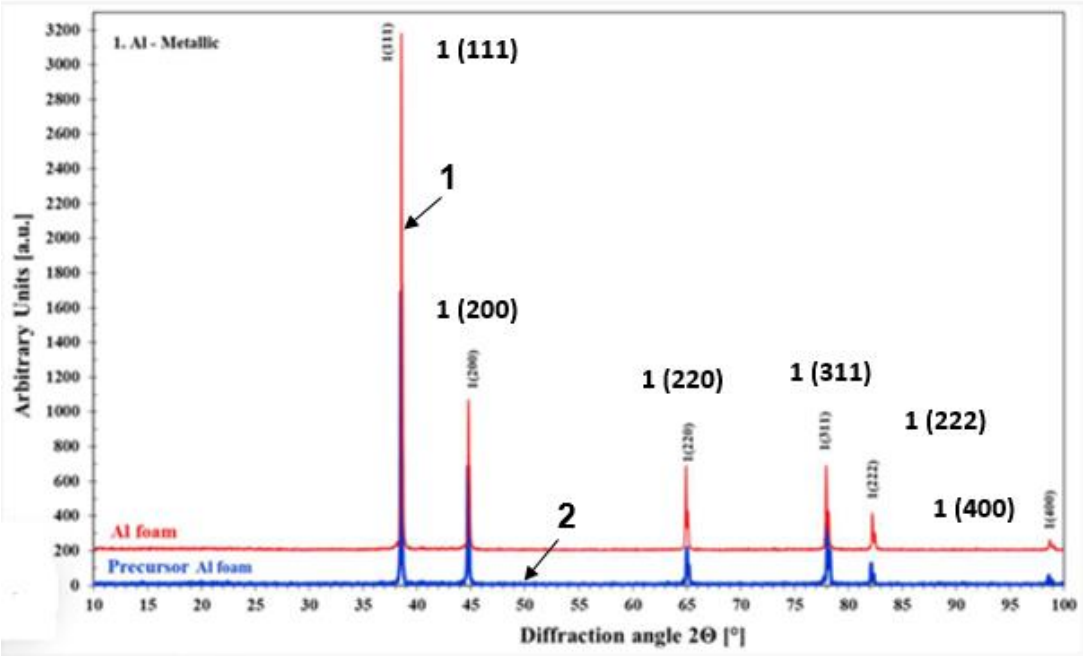

Fig. 2.26b XRD analysis - X-ray diffractogram of precursor and sample - blue and porous sample - red (bottom) [1]

The determination of the porosity (total porosity) of the produced porous material (P_P) can be calculated:

$$P_P = 1 - \frac{\rho_P}{\rho_{K.M}}, \tag{2.2}$$

where it reads: P_P is the porosity of the material produced [1]; ρ_P is the bulk density of the porous material [kg·m^{-3}] or [g·cm^{-3}]; $\rho_{K.M.}$ is the density of the compact metallic material [kg·m^{-3}] or [g·cm^{-3}], i.e. the material without porosity. If pure aluminium is used, then $\rho_{K.P.}$ = 2700 [kg·m^{-3}] or 2.70 [g·cm^{-3}].

Fig. 2.27 shows the porosity of the material produced as a function of the sintering temperature. One set of three aluminium porous samples was produced for each sintering temperature to ensure the reproducibility of the results. For all samples, the total porosity was determined to be between 77 and 80 %, using equation (2.2), as shown in Fig. 2.27a), where the dependence of the total porosity on the sintering (sintering) temperature. Total porosity includes macroporosity derived from sucrose particles. Therefore, to measure macroporosity, the sample surfaces were first treated with electrostatic discharge to visualize their internal structure. The fabricated samples were then examined macroscopically using an optical stereoscope and the macroporosity was determined using an image processing program - open Image. The average macroporosity value of all samples ranged from 63 % to 65 %, as can be seen in Fig. 2.27b). At the same time, the microporosity of the samples was determined as a function of sintering temperature (sintering), which ranged from 13 to 15 %, as shown in Fig. 2.27c). Microporosity was determined by subtracting the macroporosity from the total porosity of the sample [1]. The porosity measurement patterns indicate that there is a small decrease in total porosity, macroporosity and microporosity with increasing sintering temperature.

Subsequently, using Image software, an image of the structure of the fabricated samples (with open cells) was processed and the mean macroporosity value was further determined (see Fig. 2.28. Fig. 2.28a). This shows the fracture macrostructure of the fabricated porous material. Fig. 2.28b) shows the structure with the porosity indicated, which was determined using the Image P_{makro} = 64% software.

The determination of the compressive strength of the samples of the produced porous material was carried out based on tensile strength:

$$\boldsymbol{\sigma = \frac{F}{(A \cdot P_P)}}, \tag{2.3}$$

where: F is compressive force [N]; A is the area on which the compressive force was applied [m^2]; P_P is the porosity of the material after the sintering process [1].

As can be seen from equation (2.3), the area affected by the compressive force is influenced by the porosity of the specimen. Fig. 2.29 shows the stress-strain

relationship of fabricated porous aluminium materials. Fig. 2.29 essentially shows the compressive stress resistance of porous aluminium samples after their sintering process at 620 °C, 660 °C, 700 °C, and 740 °C.

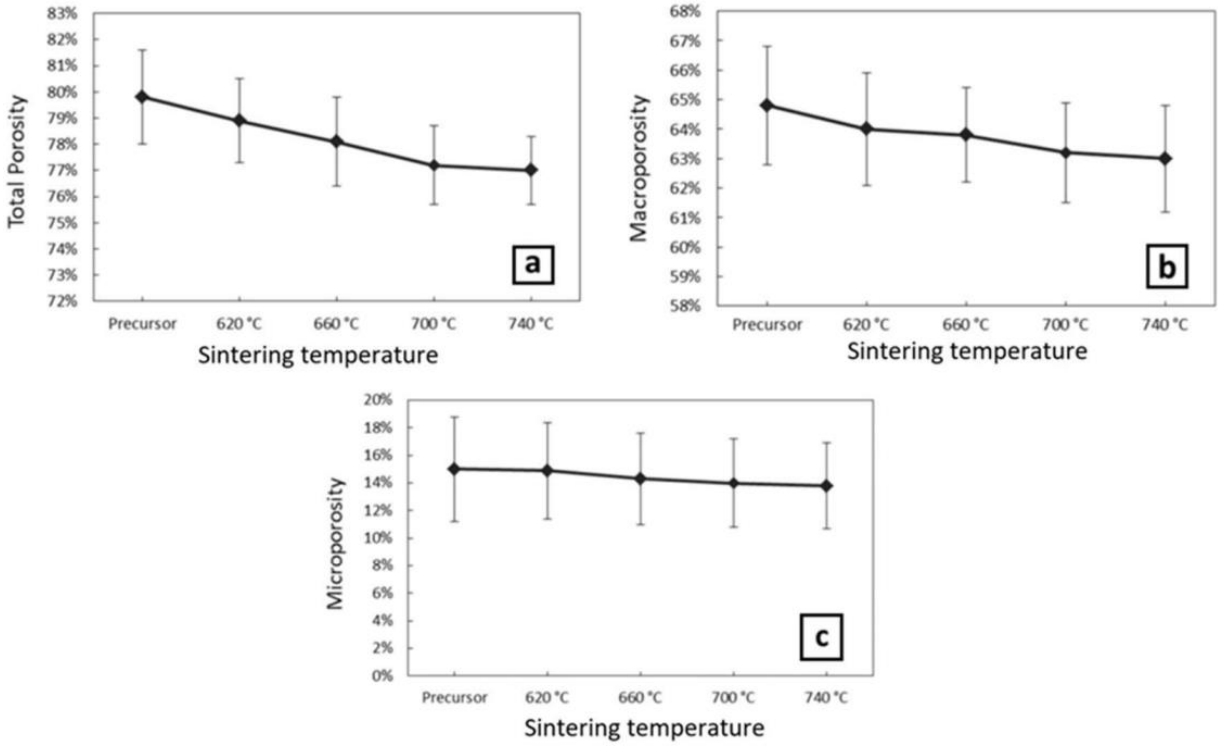

Fig. 2.27 Porosity of the manufactured material determined by different methods: a) according to equation (2.2); b) macroporosity determined by the scientific image processing program – The open Image, c) microporosity calculated by subtracting macroporosity from total porosity, [1]

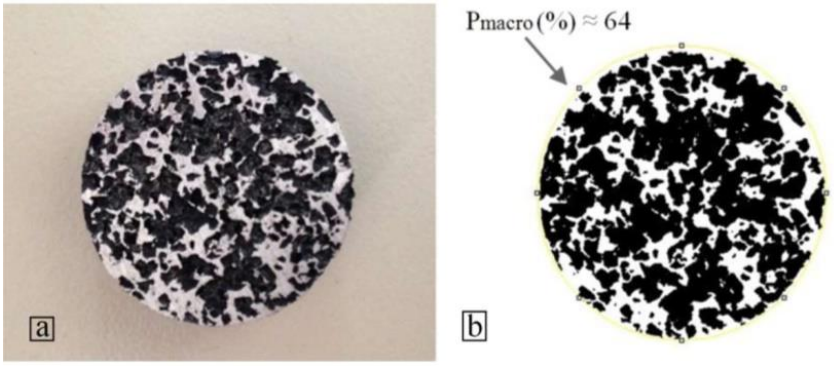

Fig. 2.28 Macrostructure: a) fracture of the fabricated porous material; b) porosity monitoring of the structure using Image P_{makro} = 64 % [1]

The obtained stress-strain curves are characterized by a typical initial elastic response, followed by a slight increase in stress with a large deformation with a positive slope, and finally a transition to squeezing of the material. Porous specimens without the sintering process show significant high stresses at the "plate", which is expected due

to the angular morphology of the material flows during compression. To more accurately examine the elastic region, the strain scale for the elastic region was divided into strain units; see Fig. 2.29 above. It was found that the strain changes in the elastic region are non-linear, which was explained by the authors [1] by the manifestation of material defects during the pressing process. Furthermore, the energy absorbed by the material produced was also monitored.

Fig. 2.30 shows the energy absorption values of porous aluminium samples by volume and by weight at different sintering temperatures. Energy absorption is an important parameter to verify the usefulness of the produced porous material as a possible energy absorbing "capacitor".

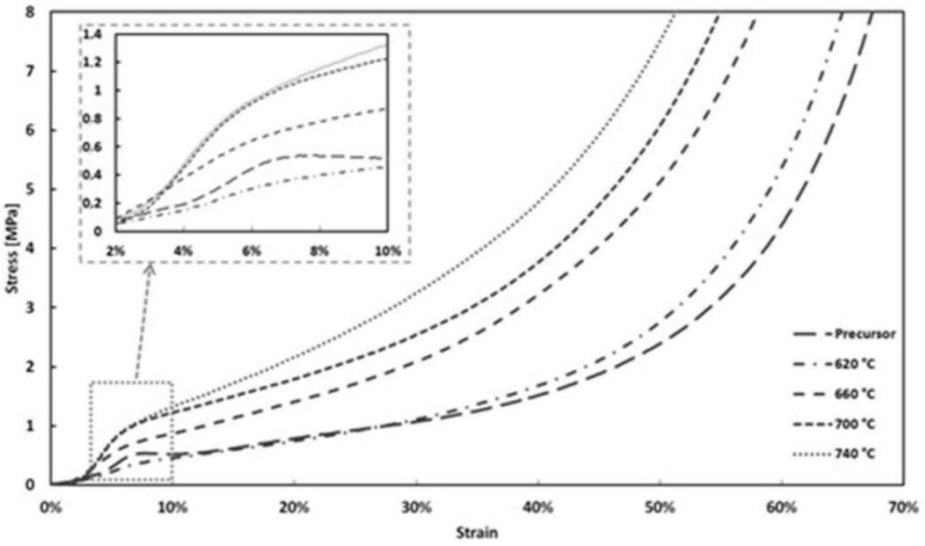

Fig. 2.29 Stress-strain relationship of aluminium porous materials produced at different sintering temperatures [1]

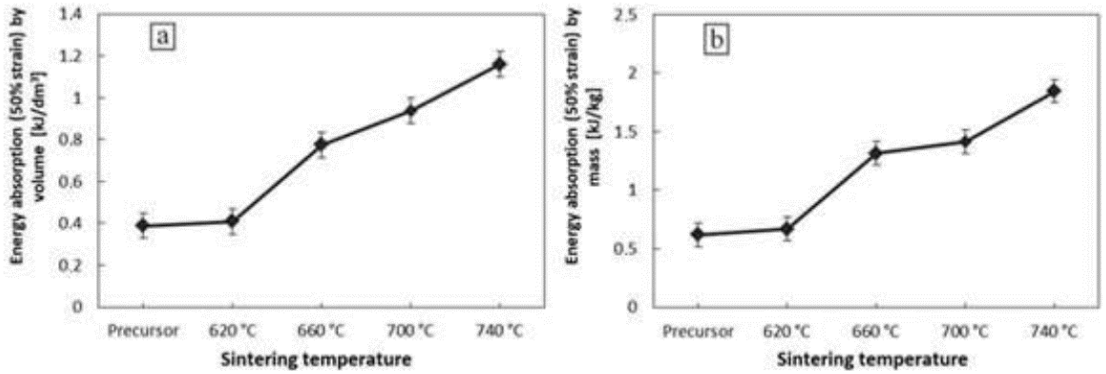

Fig. 2.30 Absorbed energy values of aluminium porous samples by volume (a) and by weight (b) at 50 % stress, samples were manufactured at different sintering temperatures [1]

The use of aluminium alloys as the main material of this process allows the production of porous aluminium materials with excellent open cell structure. In doing so, sucrose particles (which form the Space Holder Particles SHP) are used. To produce these materials, low pressing pressures are required without the need for any binding additives to improve the sintering process. As can be seen from the above, sucrose crystals can be used to produce aluminium porous materials. The shape of the internal pores (cells) of the material produced is related to the mean size, geometry and volume of the sucrose particles used. The manufacturing process provides a simple, inexpensive and environmentally advantageous method for the production of porous materials.

2.3 Production of aluminium porous systems by infiltration using centrifugal forces

WANG et al. [22] fabricated an aluminium porous system by a special infiltration casting method. This method allows very good control of the topology of the fabricated porous system (shape, size and pore distribution). This method usually uses a removable pre-form with an interconnected porous structure into which the molten metal infiltrates under external pressure. This is the basis for the production of open-cell porous material. Infiltration casting was first used to produce "metal foams" or metallic porous systems in 1961 (Polonsky et al.), as reported in [22]. Since that time, 4 different methods of producing pre-ingots and 4 different devices have been developed. A detailed review of infiltration casting for the production of metallic porous materials can be found in reference [23]. FABRIZIO et al. [24] used a hydraulic cylinder to provide a pressure of 2.5 MPa and produced aluminium porous materials by replicating a NaCl precast.

LARA-RODRIGUEZ et al. [25] developed a replication casting device and successfully produced magnesium open-cell porous materials with a pore size of about 3.3 mm at an argon pressure of 1.96 bar (0.196 MPa). The conventional infiltration casting method mainly uses mechanical pressure (piston or gas), but it is not enough to effectively overcome the surface tension of liquid metals, and the residual gas in the gaps or cavities of the pre-form is difficult to completely displace. For this reason, it is difficult to achieve complete filling of the preform with molten metal. It is known that in supergravity fields (created by a centrifugal device) mass transfer can be significantly increased. Due to these properties, supergravity technology has been successfully applied in many fields (e.g. in the chemical industry) so far. In terms of material preparation, supergravity infiltration, also known as centrifugal casting, is one of the simplest
and most efficient technology for the production of complex metal parts, functionally graded materials and metal matrix composites (MMC).

To produce porous aluminium systems, YANG et al [22] assembled a centrifugal casting plant (see Fig. 2.31). The assembly consists of a resistance furnace with a cylindrical alumina chamber of 40 mm diameter and 150 mm length. For monitoring The heating furnace and counterweight were symmetrically attached to the centrifugal

rotor. The dashed line shown in Fig. 2.31b) indicates the furnace and counterweight in the stationary state, and these change from vertical to horizontal rotation when the centrifugal rotor is switched on.

As reported by WANG et al. [22], during infiltration, it is important that the effects of centrifugal force positively influence the relative density and structure of the resulting porous material. It should also be noted that the minimum centrifugal force is determined by several parameters, such as the NaCl particle size and the infiltration temperature. It is difficult to isolate the effect of specific parameters (NaCl particle size and infiltration temperature) on the minimum centrifugal force using conventional centrifugal casting, where the infiltration temperature cannot be precisely controlled.

During fabrication, it is important to position the embedded NaCl preform so that it is towards the centre of rotation in the supergravity field due to its lower density of NaCl (2165 $kg \cdot m^{-3}$ at 20 °C) than the specific gravity of aluminium (2700 $kg \cdot m^{-3}$ at 20 °C).

A graphite crucible consisting of two small crucibles was used in the infiltration experiment. The two small crucibles had the same inner diameter of 21 mm, and there were 20 filter holes with a diameter of 0.5 mm at the bottom of the upper crucible. To simplify the production process, sintering of the pre-form with NaCl particles was avoided. The preform was placed in the lower graphite crucible, while about 30 g of aluminium blocks were placed in the upper graphite crucible. The crucibles were mechanically connected (screws). The entire crucible was then heated at 710 °C for 20 minutes in a centrifugal resistance furnace (see Fig. 2.31) to completely melt the aluminium blocks. Later, the device was started and set to the desired rotation speed. The centrifugal force exerted causes the molten aluminium to pass through the filter holes and infiltrate the cavities before the NaCl is pressed. The rotation of the device lasted 10 minutes initially, the temperature was 710 °C and later, the temperature decreased at a cooling rate of 15 $°C \cdot min^{-1}$. When the temperature was below 500 °C (the aluminium was completely solidified), the centrifugal device was switched off. and the graphite crucible containing the sample was removed and cooled in air. The formed rigid aluminium-NaCl (Al/NaCl) composite system was removed from the bottom crucible. Finally, the NaCl particles were removed from the composite by dissolving them in water to obtain the final sample of porous aluminium material.

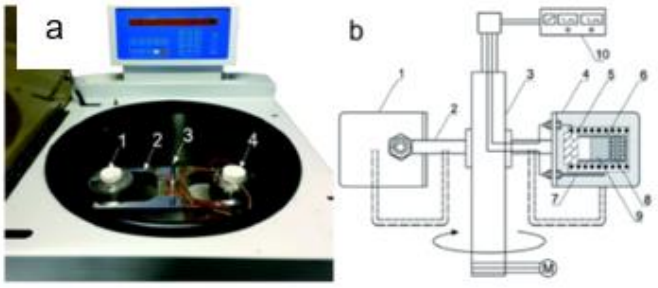

1- counterweight, 2 - centrifugal rotor, 3 - axis of rotation, 4 - resistance heating furnace, 5 - resistance furnace coil, 6 - graphite crucible, 7 - R-type thermocouple, 8 NaCl preform, 9 - aluminium melt (aluminium alloy), 10 - temperature controller

Fig. 2.31 a) centrifugal device, (b) diagram of the centrifugal device [22]

To quantify the supergravity field, the gravity coefficient G was determined, which is defined as the ratio of the centrifugal acceleration to the normal gravitational acceleration:

$$G = \frac{\sqrt{g^2+(\omega^2 \cdot r)^2}}{g} = \frac{\sqrt{g^2+\left(\frac{N^2 \cdot \pi^2 \cdot r}{900}\right)^2}}{g}, \quad (2.4)$$

where denote: g is normal gravitational acceleration (9.81 $m \cdot s^{-2}$); ω is the angular velocity of the radius [s^{-1}]; r is distance from the centrifugal axis to the centrer of the NaCl preform, (in this work r = 0.25 m); N is rotational velocity, [rpm. min^{-1}].

During infiltration, supergravity rotation provides sufficient centrifugal pressure to achieve full infiltration. The centrifugal pressure acting on the preform surface (Pc) due to centrifugal force can be calculated:

$$P_C = \frac{\rho \cdot \omega^2 (L_2^2 - L_1^2)}{2} = \frac{\rho \cdot N^2 \cdot \pi^2 (L_2^2 - L_1^2)}{1800}, \quad (2.5)$$

where: ρ is the density of molten aluminium; L_2 and L_1 are the level of molten aluminium measured from the centre of rotation.

A more detailed description can be found in [26]. In [22], where aluminium was used and its specific gravity at 710 °C is 2373 $kg \cdot m^{-3}$, the values were L_2 = 0.24 m and L_1 = 0.206 m. In combination with equation (2.1), the centrifugal pressure can also be expressed

$$P_C = 705 \cdot G \quad (2.6)$$

The maximum speed can be reached from 0 $rpm \cdot min^{-1}$ to 1891 $rpm \cdot min^{-1}$, which is the maximum as reported in reference [22]. The generated gravity coefficient increased from 1 to 1000, and the centrifugal pressure increased from 0 kPa to 705 kPa. The paper [22] presents the results of infiltration casting in a supergravity field. The experiment yielded castings of a porous aluminium system that varied in pore size based on the use of NaCl particles (200, 400 and 600μ m). A centrifugal pressure of Pc = 353 kPa (G = 500) was used in the experiment resulting in different pore sizes and their metallic structures. As can be seen from Fig. 2.32 (a) to Fig. 2.32 (c), a homogeneous pore distribution can be observed not only on the surface of the castings but also in their transverse and longitudinal direction, see Fig. 2.32 (d) to Fig. 2.*32* (f). The cross-sectional structures of the obtained porous aluminium systems were obtained by scanning electron microscopy.
WANG et al. [22] observed aluminium infiltration during casting in a supergravity field, where molten aluminium is forced to penetrate the NaCl preform channels. He obtained three kinds of results: no infiltration, partial infiltration and full infiltration.

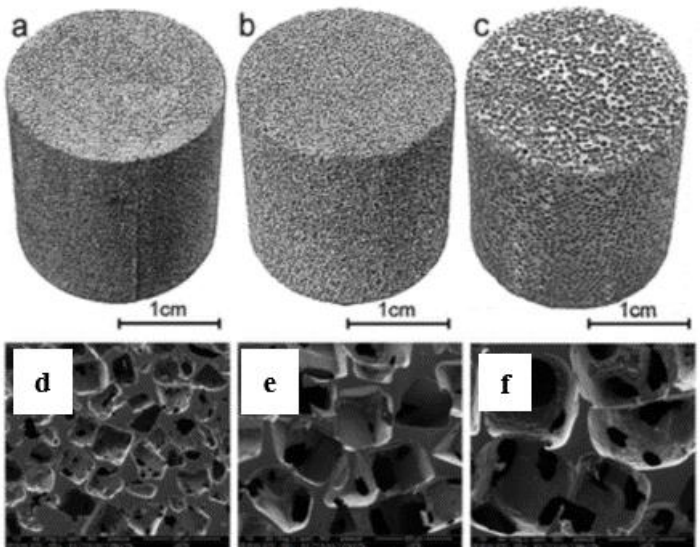

Fig. 2.32 Aluminium porous systems (open cell) with different NaCl particle sizes were used: (a) and (d) 200μ m; (b) and (e) 400μ m; c) and f) 600μ m; pressure = 353 kPa (G = 500) was used, cross-sectional structures were obtained using SEM, [22]

To evaluate the effect of the supergravity field on the extent of infiltration, the effect of centrifugal pressure (Pc) and gravity coefficient (G) on the relative densities of the final aluminium foams see Fig. 2.33 was plotted for three types of aluminium porous systems.

As can be seen from Fig. 2.33, the relative bulk density increases gradually with increasing centrifugal pressure coefficient and gravity (G). Thus, for example, from Fig. 2.33 for a NaCl particle size of 600 μm, the following can be observed. The NaCl preform cannot be infiltrated by molten aluminium until the Pc is above 8 kPa (G = 11). The relative bulk mass increased rapidly to 0.21 with increasing Pc to 32 kPa (G = 45), while above 32 kPa, the relative bulk mass also increased but relatively slowly. At a maximum centrifugal pressure of 705 kPa (G = 1000), the relative bulk density of the porous aluminium foam system with a NaCl pore size of 600 μm reached its peak, i.e. 0.24. Table 2-3 shows the values of selected physical quantities.

Table 2-3 Values of produced physical quantities of porous aluminium systems infiltration in a supergravity field, P_C = 705 kPa (G = 1000) [22]

Values of produced physical quantities of porous systems∅ 40 x 50 mm			
Pore size [μ m]	**Porosity [%]**	**Relative bulk density [1]**	**Volume weight [kg·m^{-3}]**
200	66	0.34	920
400	71	0.29	780
600	76	0.24	650

Figure 2.34 shows the structures, obtained by SEM microscopy, of a porous aluminium system fabricated using NaCl particles of size 600 μm, with different centrifugal pressures, (a) and (d) 30 KPa; (b) and (e) 353 kPa; (c) and (f) 705 kPa.

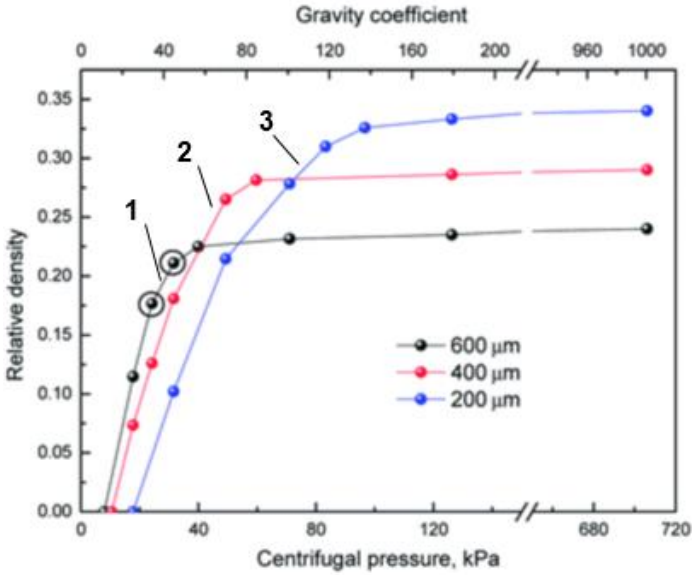

1 *– 600 μm;* ***2*** *– 400 μm;* ***3*** *– 200 μm*

Fig. 2.33 Dependence of the effective centrifugal pressure and gravity coefficient on the relative density of the porous system [22]

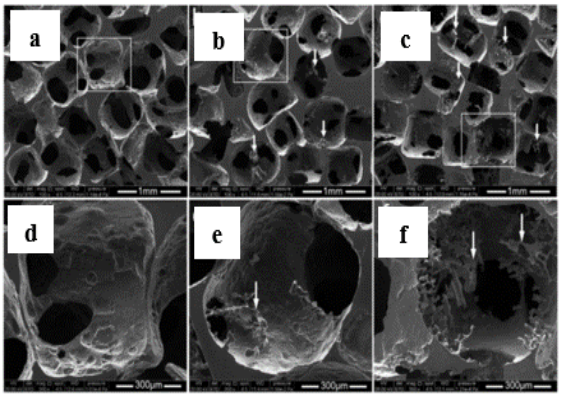

Fig. 2.34 Structure of a porous aluminium system made using NaCl particles of size 600μ m, with different centrifugal pressures, a) and d) 30 kPa; b) and e) 353 kPa, c) and f) 705 kPa [22]

The fabricated samples of the porous aluminium systém ∅ 40 mm x 50 mm were pressure-coated. The results obtained are shown in Fig. 22.35. Table 2-4 shows the mechanical property values of the fabricated samples with pore sizes (200, 400 and 600μ m) of the porous aluminium systems described above, produced by infiltration in a super gravity field (centrifugal casting).

Fig. 2.36 shows the dependence of the yield strength of a porous aluminium alloy on the relative density according to various authors and the results of [22].

From the work [22], it is clear that by infiltration casting in a supergravity field, it is possible to produce a porous aluminium material (replicated aluminium foam) with open pores with a relative density between 0.24 and 0.34 using NaCl particles of 200,

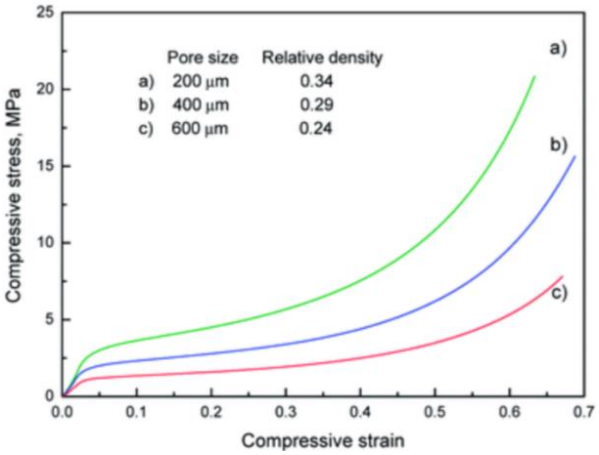

Compressive stress - compressive strain; compressive strain - strain from compressive force Pore size 200, 400 and 600μ m; Relative density: 0.34, 0.29 and 0.24

Fig. 2.35 Compressive stresses of 50 x 50 mm∅ samples made with different NaCl particle sizes (200, 400 and 600μ m), P_C = 705 kPa [22]

400 and 600 μm, at an applied centrifugal pressure of P_C = 705 kPa (G = 1000). Fig. 2.36 shows the dependence of the yield strength of a porous aluminium alloy on the relative density according to different authors and the results of [22].

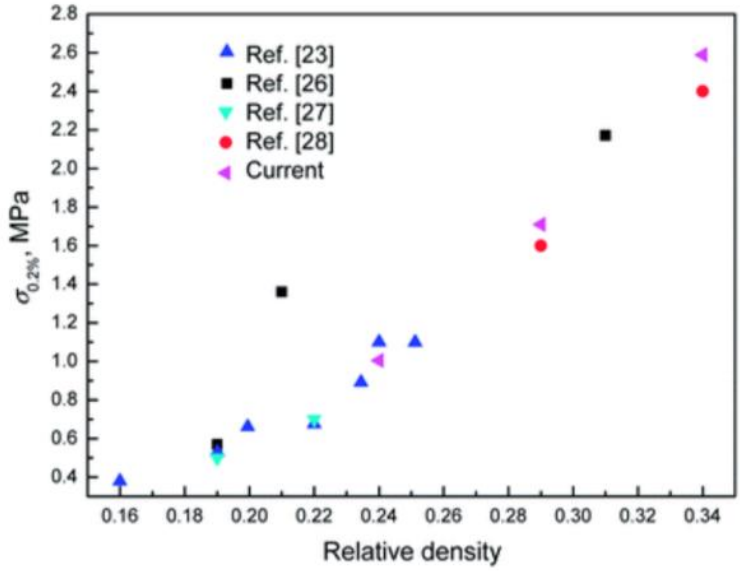

Fig. 2.36 Dependence of the yield strength of a porous aluminium alloy on the relative density according to different authors and results according to [22]

Reference for Figire 2.36 [23] *DESPOIS, J. MARMOTTANT, A. SALVO, L. and A. MORTENSEN. Influence of the Infiltration Pressure on the Structure and Properties of Replicated Aluminium Foams, Mater. Sci. Eng., A, 2007, 462, pp. 68-75.* ***[26]*** *JAMSHIDI-ALASHTIR and G. ROUDINI. Producing Replicated Open-cell Aluminum Foams by a Novel Method of Melt Squeezing Procedure. Mater. Lett., 2012, 76, pp. 233-236.* ***[27]*** *GOODALL, R. DESPOIS, J.F. MARMOTTANT, A. SALVO, L. and A. MORTENSEN. The effect of pre-forprocessing on replicated aluminium foam structure and mechanical properties, Scr. Mater., 2006, 54, 2069-2073.* ***[28]*** *GOODALL, R. MARMOTTANT, A. SALVO, L. and A. MORTENSEN. Spherical Pore Replicated Microcellular Aluminium: Processing and Influence on Properties, Materials Science Engineering, A, 2007, 465, pp.124-135.*

Table 2-4 Mechanical properties of porous aluminium system samples [22]

Mechanical properties of samples of porous aluminium systems				
Pore size [μm]	Yield strength $R_{p0,2}$ [MPa]	Limit of strength R_m [MPa]	Young's modulus value [MPa]	Redesign when pressed (ε_D)
200	2.59	5.35	93.3	0.51
400	1.71	3.37	67.5	0.53
600	1.01	1.94	39.2	0.54

2.4 Production of aluminium porous materials by the controlled infiltration method atmosphere

PIMIENTO et al. [27] describe the fabrication of aluminium porous materials (with open cell pores) that were produced by infiltration processes using controlled atmosphere devices for metal fusion and infiltration processes.
The material characteristics of the fabricated porous aluminium material samples were monitored. For this purpose, the methodology developed by BAFTI and HABIBOLAHZADEH [28] was used.

The determination of the density of the material produced is based on a basic physical formula:

$$\rho = \frac{m}{V}, \tag{2.7}$$

where: m is the weight of material produced [kg]; V is the volume of material produced [m^3].

Determination of the theoretical density of the composite material (aluminium and NaCl):

$$\rho_T = (\rho_{Al} \cdot W_{Al} + [\rho_{NaCl} \cdot (1 - m_{Al}) \tag{2.8}$$

where: ρ_{Al} is density of aluminium (2700 kg·m^{-3}); W_{Al} is the corresponding percentage of the aluminium fraction [1]; ρ_{Al} is density of NaCl (2165 kg·m^{-3});

Determination of porosity of composite material (aluminium and NaCl):

$$P_k = 1 - \frac{\rho_K}{\rho_T}, \tag{2.9}$$

where: ρ_K is density of the composite material, [kg·m^{-3}]; ρ_T is theoretically determined density of the composite material (aluminium and NaCl), [kg·m^{-3}].

The determination of the porosity of a porous material (P_P), e.g. aluminium, can be made based on equation (2.2).

The authors [27] determined the topologies of NaCl particles using digital images and determined the morphologies and size of NaCl particles. They also determined the shape of the cells forming the porosity of the material. Using scanning electron microscopy (SEM Jeol JSM 6610 HLV), they observed the interconnectedness of the cells of the porous material. For each porous aluminium material sample produced, the dimensions were measured, and its weight and the bulk weight in the composite (Al-NaCl) state were determined. Similarly, the masses of the resulting aluminium porous samples were determined after leaching (splitting NaCl in water). Their bulk mass was calculated. The weights were determined by weighing to the nearest $\pm$ 0.001 g. Based on these data, the specific gravity of the compact material $\rho_{K.M.}$, the bulk weight of the porous aluminium materiál ρ_P, the porosity of the compact material P_K and the porosity of the fabricated material P_P were determined using equations (2.2), (2.8) and (2.9).

The authors [27] used pure aluminium (purity 99.8 %) in the form of ingot for the experiments. Equiaxial granules of NaCl in three particle sizes (Group I, particle size range from 4.7 to 4.0 mm; Group II, particle size range from 4.0 to 3.3 mm; and Group III, particle size range from 3.3 to 2.0 mm) were used to create the porosity of aluminium (translated as *Space Holder Particles (SHP)*. The obtained aluminium porous materials showed in all cases a highly porous structure with interconnected porosity cells. The maximum porosity value was 73.7 %, and the minimum density value was 0.71 $g \cdot cm^{-3}$ (710 $kg \cdot m^{-3}$). This work shows that sodium chloride particles of a certain size are required to produce porous materials with high cell interconnectivity. For this, a device that allows controlled atmosphere metal fusion and infiltration processes is suitable. An inert gas atmosphere is suitable for this purpose, which protects the metal against rapid oxidation. The production equipment used has been separated from the heating furnace. The authors have described the basic principle, the equipment itself is described very briefly. Internally, the plant consists of a metal container with a hole in the bottom and a metal mould. Fig. 2.37 shows the basic container-mould system, in which a metal container containing aluminium is placed on a metal mould containing a bed of NaCl particles. The vessel and mould are interconnected. The vessel-mould system is then placed in a conventional vertical electric furnace with a controlled inert gas atmosphere. In the experiments, each size group of NaCl was placed in a metal crucible so that the crucible was filled.

The aluminium melt was placed inside a metal container with a hole in the middle of the bottom (see Fig. 2.37). Fig. 2.38 shows the sodium chloride particles of the sizes used, in three size ranges: a) is from 4.7 to 4.0 mm; b) is a range from 4.0 to 3.3 mm; and c) is a range from 3.3 to 2.0 mm.

The metal container with aluminium was placed on top of the metal mould with NaCl to ensure continuous contact of the NaCl particles. The mould-vessel system was introduced into a vertical electric furnace to melt the aluminium at 700 °C for 30 minutes. When the aluminium was melted, the bed of NaCl particles was infiltrated with liquid aluminium by gravity. After the infiltration process, the mould-vessel system was cooled to obtain an Al-NaCl compact.

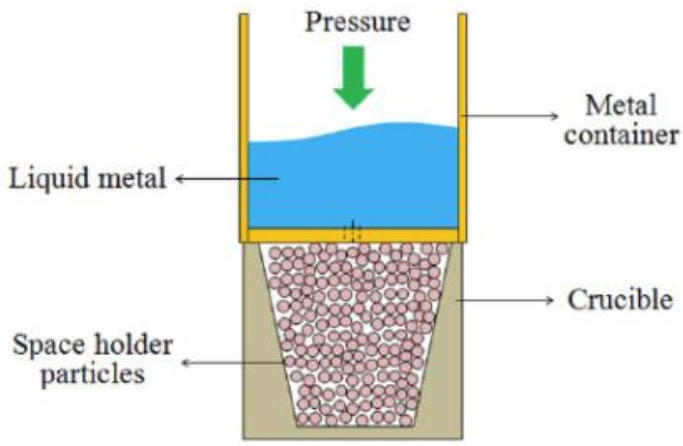

Fig. 2.37 Schematic of the container/mould equipment used for processing aluminium "foams" with open pores, according to [27]

Fig. 2.38 View of NaCl particle sizes used for the production of porous aluminium systems (aluminium "foams"): (a) NaCl particle size from 4.7 to 4.0 mm; (b) NaCl particle size from 4.0 to 3.3 mm; and (c) NaCl particle size from 3.3 to 2.0 mm [27].

The amount of NaCl in the compact material was leached by immersion in a water bath at 25 °C for two hours to form a porous aluminium material with interconnected cells. Finally, to determine the volume of NaCl in each porous material, NaCl (sodium chloride) was leached. The leached salt - i.e. sodium chloride was dried in an oven at 105 °C until the observed mass was stable. This mass of NaCl was monitored for feedback. The NaCl content for each aluminum foam obtained was 53.1 % by volume for particle size I, 54.1 % by volume for particle size II, and 56.4% by volume for particle size III.

Fig. 2.39 shows samples of cylindrical aluminium porous systems that were produced by the infiltration process using NaCl particles with a particle size of 4.7 to 4.0 mm, see Fig. 2.38 (a). With NaCl particle sizes of 4.0 to 3.3 mm, see Figure 2.38 (b) and with NaCl particle sizes of 3.3 to 2.0 mm, see Figure 2.38 (c). Fig. 2.39 (a), left and right, shows the cast samples obtained, consisting of both aluminium and sodium chloride. Fig. 2.39 (b), left and right, shows the cast samples formed with aluminium and sodium chloride after machining. Fig. 2.39 (c), left and right, shows fabricated samples from which sodium chloride has been removed by dissolution in water. A relatively uniform distribution of cells can be observed in the samples. As a result of this production technology, aluminium porous samples with homogeneous cell

distribution were obtained. It is expected that the porous aluminium material produced in this way, with a highly homogeneous structure, will exhibit relatively high mechanical properties.

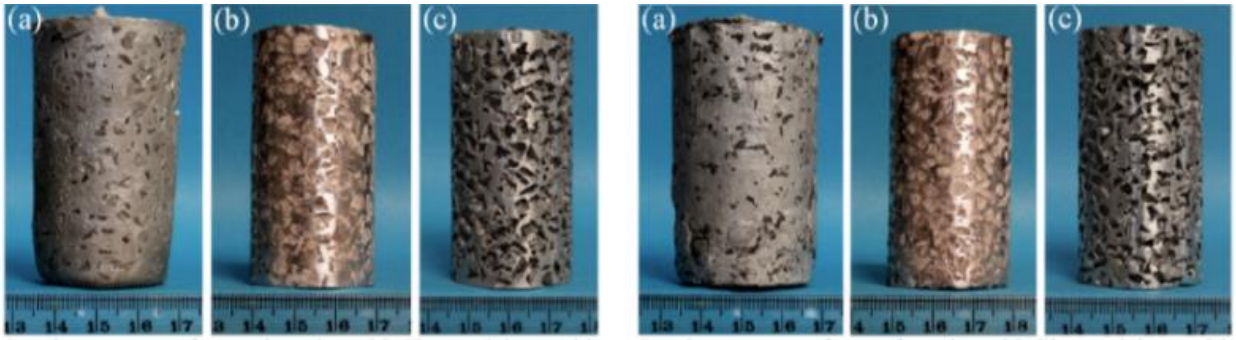

Left: (a) (b), (c) - samples produced using NaCl particles with particle size range I (4.7-4.0 mm); Right: (a), (b), (c) - samples produced using NaCl particles with particle size range II (4.0-3.3 mm).

Fig. 2.39 Fabricated aluminium samples after the infiltration process: (a) obtained Al-NaCl extrusions, (b) obtained Al-NaCl extrusions after machined processes, and (c) obtained aluminium porous systems after NaCl leaching in water, [27].

Fig. 2.40 shows the interconnectedness of the cells obtained using NaCl particles ranging from 4.0 to 3.3 mm. The areas enclosed by the yellow lines show the approximate form of the equiaxial NaCl particles used to produce the porous aluminium materials. It can be seen that the cell (pore) sizes in the samples using both types of NaCl particle sizes are quite consistent. At the same time, Fig. 2.40 also shows the interconnection with the second cell, which is outlined by the red oval. This second cell is also connected to the third cell, which is marked by the green oval. Both of these interconnections correspond to the black area in Fig. 2.40, which creates an open cell structure, and virtually all of the cells are connected.

Fig. 2.41 shows the densities of ρ_T (theoretically determined bulk mass of the porous material), ρ_K (bulk mass of the composite system: aluminium NaCl), and ρ_P (bulk mass of the produced porous material) as a function of NaCl content. From Fig. 2.41, it can be seen that the values of all three observed densities decrease with increasing NaCl content (ρ_T, ρ_K, ρ_P).

The reduction ρ_T can be explained by the lower density of NaCl, which is 2165 kg·m^{-3}, compared to the density of aluminium of 2700 kg·m^{-3}. Since the proportion of NaCl particles in the composite material (aluminium-NaCl) increases, the reduction of ρ_T. On the other hand, ρ_K is lower than ρ_T. This reduction can be explained based on two reasons:

a) lower density of NaCl compared to aluminium;
b) the formation of void spaces that may be present between the aluminium and NaCl particles.

Fig. 2.42 shows the dependence of the porosity of P_P and P_K on the NaCl content. Both porosities increase with increasing sodium chloride content. The porosity of P_K is the porosity of compact materiál, and the porosity of P_P is the porosity of porous

material. The increase in P_K is mainly associated with the decrease in NaCl particle size.

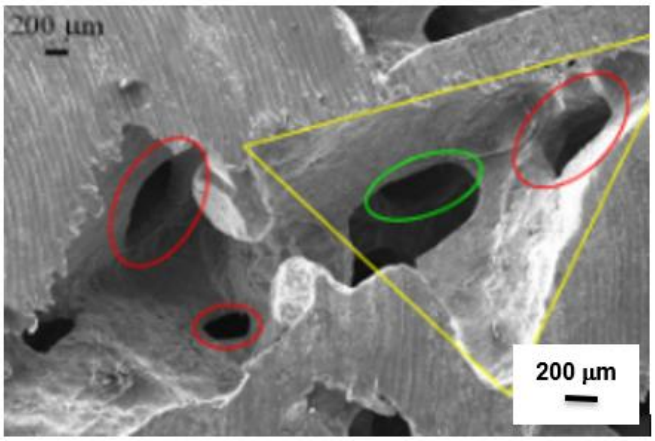

Fig. 2.40 Structure of the aluminium porous system fabricated using NaCl particle sizes ranging from 4.0 to 3.3 mm and subsequent leaching; the yellow line shows the interconnection of the cells, the interconnection with the second cell is delineated by the red oval and the interconnection with the third cell is indicated by the green oval; scanning electron microscope [27]

As the particle size decreases, the contact points between the NaCl particles increase, and the void spaces within the compact space located around these contact points also increase. As a result, the liquid metal is unable to surround (wet) the NaCl particles due to its surface tension and thus, the liquid metal cannot infiltrate these small void spaces within the NaCl bed. The porosity of P_P aluminium porous materials after the sodium chloride dissolution process in water also indicates a continuous increase in porosity of the porous material with increasing NaCl content in the metal volume.
In the case of higher NaCl content in the metal material, after the dissolution of NaCl. A larger void space is formed in the metal material, which leads to the growth of material porosity. On the other hand, it is observed in Fig. 2.42 that the difference in porosity between samples with high NaCl content (56.4 vol. %) and those with lower NaCl content (53.1 vol. %) also increases when the NaCl content in aluminium is also increased. This tendency is attributed to the sum of two effects.

a) the increase in void spaces found around NaCl particles, which increases with decreasing NaCl particle size and increasing NaCl content.
b) the empty spaces left by NaCl particles after their leaching, which increase with increasing NaCl content.

The results [27] shows that the fabricated aluminum open-cell porous materials containing cells (pores) between 65.3 % and 73.7 % of the fabricated volume, with a minimum density of 710 [$kg \cdot m^{-3}$].

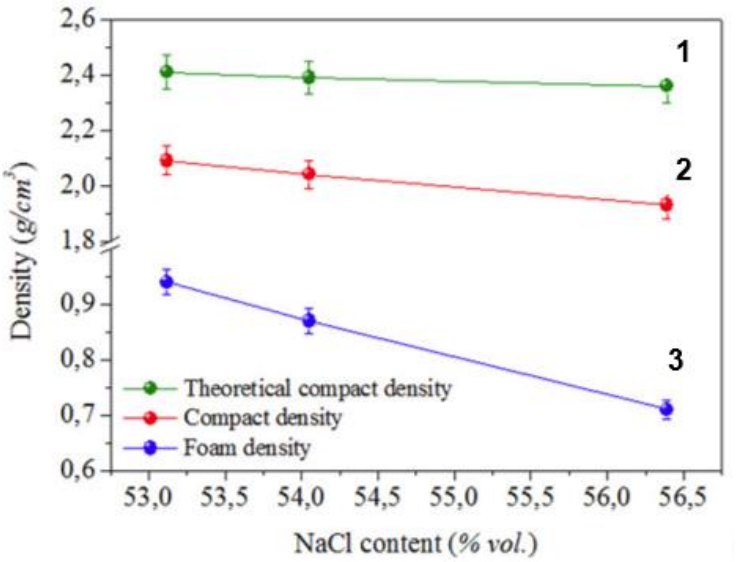

Straight line 1: the bulk mass of the composite material (compact), theoretically determined (ρ_T);
Straight line 2: specific gravity of composite material (aluminium and NaCl) (ρ_K);
Straight line 3: bulk mass of porous material (compact) (ρ_P);

Fig. 2.41 Variations of the density of aluminium system samples as a function of NaCl content [27]

These materials can be produced by a special method of infiltrating liquid aluminium into a bed of NaCl particles. All these fabricated porous aluminium samples exhibited a highly interconnected porous structure. This high intercellular connectivity was due to the contact between the NaCl particles in the bed, which was supported by the specific fabrication. This is done by placing a metal container with aluminium in a metal mould with NaCl particles. This configuration prevented the movement of the NaCl particles due to density effects between the aluminium and NaCl particles.

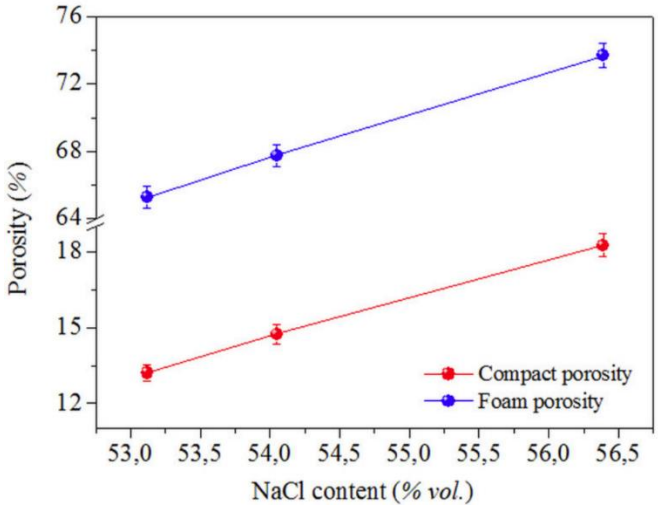

The upper straight line is the porosity of the fabricated aluminium porous system;
The lower line is the porosity of the compact system: aluminium-NaCl.

Fig. 2.42 Variants of sample porosity as a function of NaCl content, [27]

The presented results show that the use of infiltration processes is an excellent method for obtaining aluminium porous materials with high porosity and a homogeneous distribution of cells (pores). The achieved structure of porous aluminium material with open cells is important for applications where mass or energy transport is essential.

2.5 Production of aluminium porous materials by the gravity infiltration method casting into a metal mould

The team of authors [29] dealt with the production of porous metallic materials with open cells by gravity casting into a metal mould. This technology is also based on the use of NaCl particles. For this purpose, the authors [29] used aluminium alloy A356 (AlSi7 Mg0.3) and different amounts of sodium chloride particles. Sodium chloride is a favourable ecological material, it is relatively inert to aluminium and its use is also associated with low economic costs. Before the experiments, the morphology and microstructure of the NaCl particles were observed (see Fig. 2.43).

The aluminium alloy used (A356 - AlSi7Mg0.3) was taken from a bun. It was melted in a graphite crucible, which was placed in an electric resistance furnace. The alloy was gradually heated in the furnace, which was set at 850 °C with a temperature increment of 25 °C·min^{-1} for two hours to homogenize the melt. Then, the molten aluminium alloy A356 was cooled down to 680 °C. At the same time, the NaCl salt particles were weighed according to their mass distribution and preheated at 680 °C for 15 min in the furnace. Then, the appropriate amount of NaCl was added to the molten aluminium alloy A356. These appropriate amounts of NaCl are given in Table 2-5. Table 2-5 also shows the ratio of NaCl and alloy A356 used.

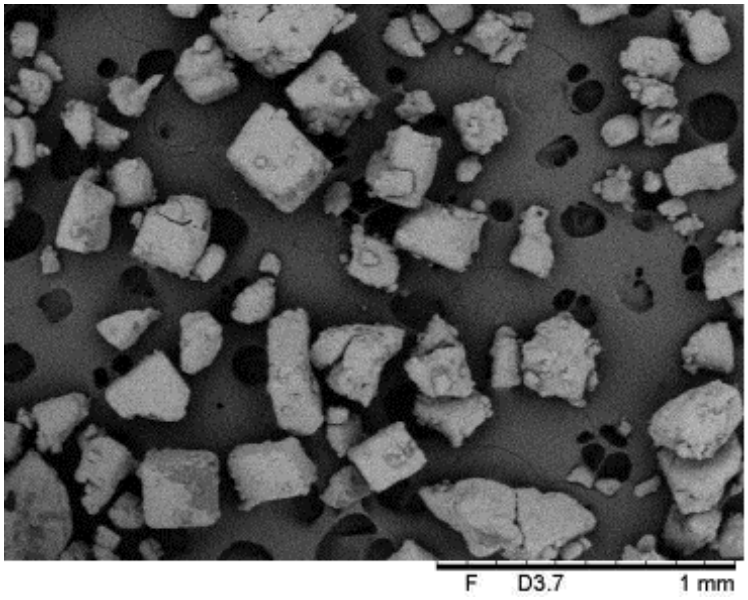

Fig. 2.43 Morphology of sodium chloride used (square appearance) [29]

Table 2-5 NaCl particle ratio for melt mixing [29]

Composition of NaCl particles used for mixing into the aluminium melt			
Ratio (NaCl: A356 alloy)	0.2:1	0.6:1	1:1
Normal casting, NaCl: A356 alloy (in grams)	10:50	30:50	50:50

The measured mixture of NaCl and A356 alloy melt was manually stirred for one minute to obtain a uniform distribution of salt particles in the melt of the aluminium alloy used. Further, during the casting process, argon was used and flushed at a rate of 1.0 $l \cdot min^{-1}$ for one hour to ensure a homogeneous distribution of NaCl in the melt. The molten aluminium alloy A356 containing NaCl was allowed to cool in a crucible at room temperature for 30 minutes. The solidified material was then of the produced "composite" (NaCl-solidified alloy A356) removed from the crucible. This 'composite' was incubated in water at 90 °C for approximately 1 hour. This removed the NaCl particles, resulting in a porous aluminium material with open pores. All porous material samples were produced in this way. The morphology was observed on a light and scanning microscope and microstructure of the produced porous materials. Furthermore, porosity and bulk density were investigated on the fabricated porous material. The bulk density decreased with increasing porosity of the fabricated material due to increasing NaCl content. Table 2-6 shows the average pore sizes left by NaCl particles in aluminium alloy A 356. Table 2-7 shows the corresponding densities.

Table 2-6 Average pore sizes in aluminium porous material samples from A356 alloy with open cells [29]

Average pore size in A356 samples			
Sample of premium material	10 NaCl-A356	30 NaCl-A356	50 NaCl-A356
Average pore size [μm]	203.90	209.40	223.60

Table 2-7 Bulk density values of porous A 356 alloy samples [29]

Bulk density values of porous A 356 alloy samples				
Sample of premium material	A 356	10 NaCl-A356	30 NaCl-A356	50 NaCl-A356
Bulk weight [$kg \cdot m^{-3}$]	2690	2670	2610	2490

The density of the A356 alloy without salt particles is expected to be the highest, i.e. 2690 [$kg \cdot m^{-3}$]. Also, as expected, the bulk density of the porous A356 alloy sample decreased with increasing NaCl. As reported by [29], the lower bulk density can be attributed to the larger pore size, as shown in Table 2-6. Also, the higher amount of NaCl provided more pores and thus, a lower bulk density of the material produced was achieved. As expected, the lowest bulk density was exhibited by the porous A 356 alloy sample, which was fabricated with the highest NaCl particle content, i.e. 50 g NaCl, and exhibited a bulk density of 2490 [$kg \cdot m^{-3}$]. Fig. 2.44 shows the bulk mass of the fabricated open-cell aluminium porous alloy A356 samples that were fabricated with different amounts of NaCl (0, 10, 30 and 50 g).

Fig. 2.45a) shows the porosity of the fabricated open-cell aluminium porous A356 alloy specimens using different amounts of salt (0, 10, 30 and 50 g NaCl). For this

purpose, stereo microphotography of open-cell aluminium porous A356 alloy samples at 20x magnification with different NaCl contents was used.
The surface of the fabricated aluminium porous material samples with different sodium chloride particle contents was observed on a scanning electron microscope with (a) A356-10 gNaCl, (b) A356-30 gNaCl, (c) A356-50 g NaCl, see Fig. 2.45b.

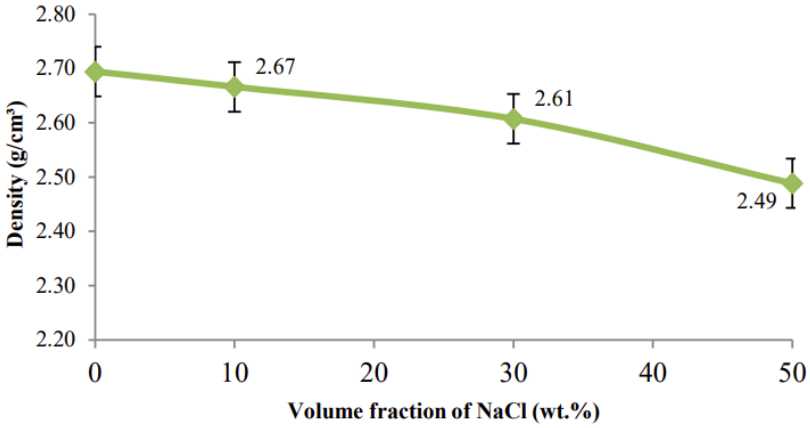

Fig. 2.44 Dependence of the density of the porous A 356 alloy sample on the NaCl content [29]

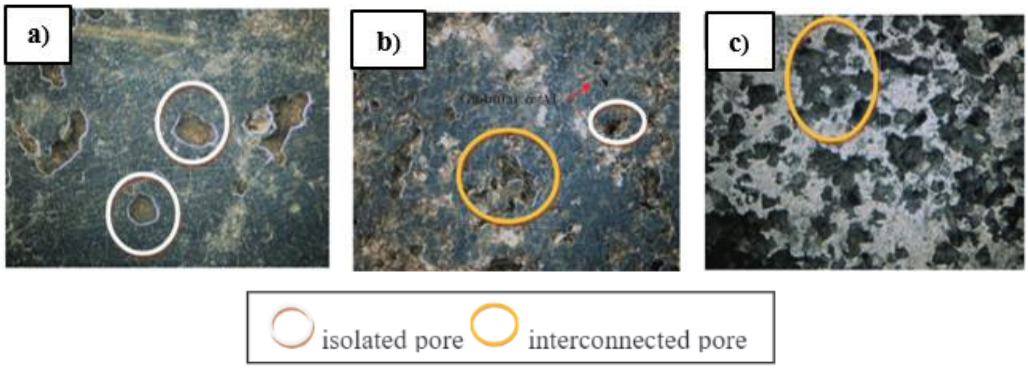

Isolated pore; interconnected pore

a) A 356 - 10 g NaCl; b) A 356 - 30 g NaCl; c) A 356 - 50 g NaCl

Figure 2.45a) Macrostructure of aluminium porous samples made from A 356 alloy with different NaCl contents (grams), magnification 20 times, left. Microstructure of aluminium porous samples made from A 356 alloy with different NaCl contents (grams), scanning electron microscope SEM

The authors [29] do not provide a methodology for monitoring porosity, but the calculation according to equation (2.2) was likely used. Fig. 2.46 shows the porosity of the fabricated A356 Al alloy samples with different amounts of NaCl. From Fig. 2.46, it is clear that the porosity of the fabricated samples increases with increasing NaCl content.

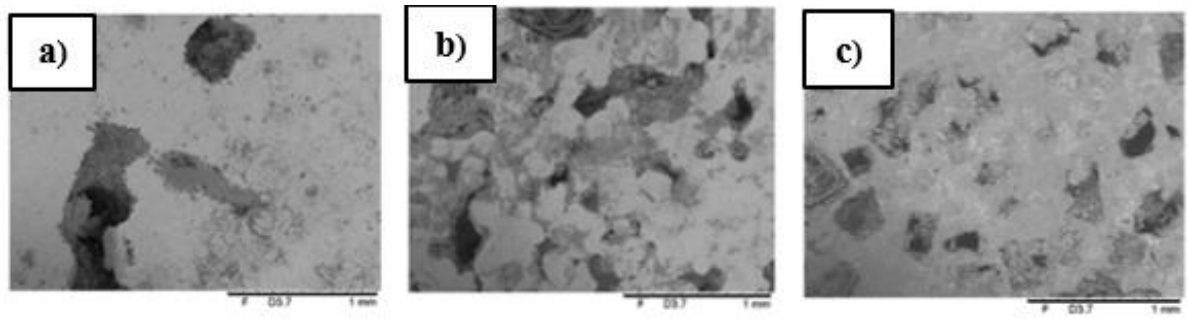

Fig. 2.45b) Surface structure of fabricated samples of porous aluminium materials, SEM with different NaCl content, a) A356 -10g NaCl, b) A356 - 30 g NaCl, c) A356 - 50 g NaCl

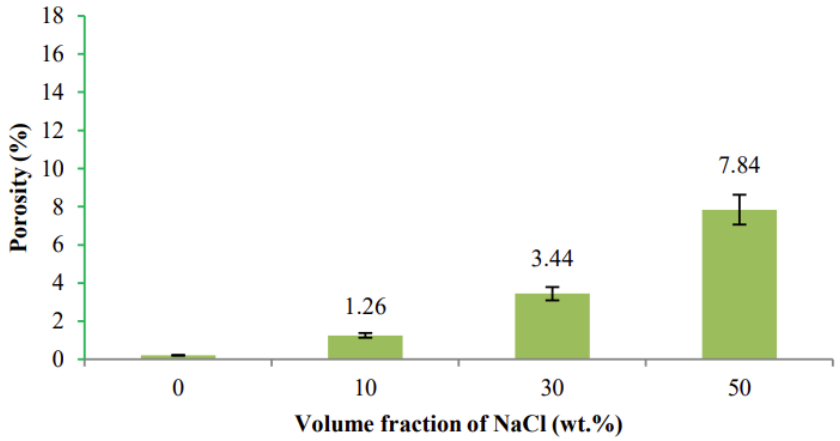

Fig. 2.46 Dependence of the porosity of the porous A 356 alloy sample on the NaCl content, [29]

The sample of the alloy without NaCl has essentially no porosity in theory, yet the sample showed a porosity of 0.22 %. The other aluminium alloy samples showed porosities ranging from 1.26 % to 7.84 % depending on the increasing amount of NaCl. The highest porosity was obtained using 50 NaCl - A356, which showed a porosity value of 7.84 %. It is a great pity that the authors of AIDA et al. [29] do not give the relationships that lead to the determination of both the density and porosity of the porous materials produced, which they call aluminium "foams". The porosity values given are very low compared to those given by the authors [30] and [31]. It should be noted that the authors of [29] give some NaCl values in grams and some in % wt.

2.6 Production of porous metal materials using metal powder and NaCl space formations

MOHAMMED and ALJUBOURI [11] also produced aluminium porous materials using salt particles. Aluminium powder (aluminium alloy) was used for this purpose with a particle size of 3.63 μm (0.00363 mm). This aluminium powder was mixed with NaCl particles (see Fig. 2.47). NaCl particles with sizes ranging from 300 to 400 μm, i.e. 0.300 to 0.400 mm, were used to produce the porous aluminium material. For the

experiments, aluminium powder was mixed with sodium chloride particles in the ratio of 30, 40, 50, 60, 70 and 80 wt.%. Fig. 2.47 shows the shape of NaCl particles and aluminium powder observed on a scanning electron microscope.

After perfect mixing of the two ingredients (Al powder and NaCl) for about 1 hour in a mixing machine, the prepared mixture was pressed at a pressure of 200 MPa in a specially made jig (with a cavity ∅ 30 x 50 mm) on a hydraulic press to achieve the desired shape of the resulting pressed "composite system" (aluminium and NaCl).

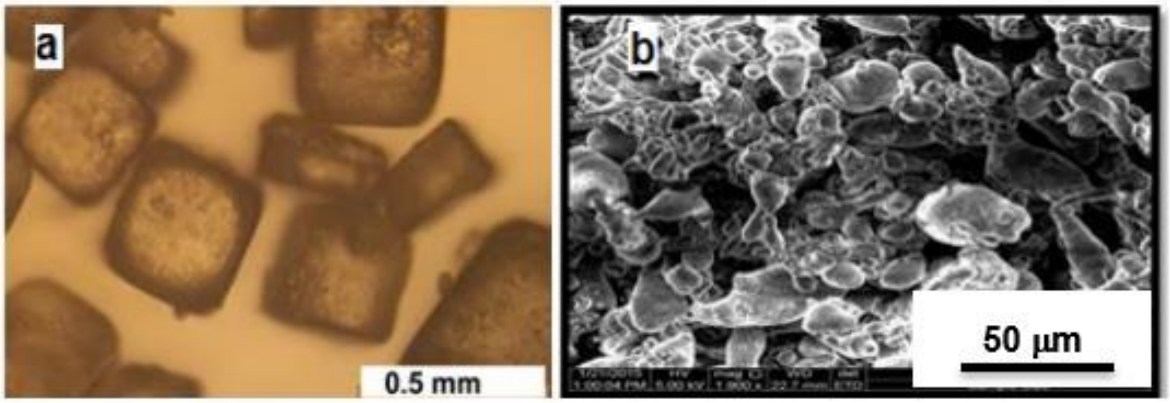

Fig. 2.47 Shape of NaCl particles (a); aluminium powder used for the production of aluminium porous materials (b), observed on SEM microscope, [11]

If it is a pressing of metal powder and sodium chloride, it can be done either by unidirectional or both directional pressing of the mixture of metal powder and sodium chloride. However, this depends on the appropriate design of the jig, which is always necessary to produce a pressed metal porous material using NaCl. Fig. 2.48 shows the Al-NaCl composite system before and after sintering (sintering).

Fig. 2.48 Aluminium samples in the production of porous material a) after sintering; b) after dissolution of NaCl; note: the pictures are not of good quality even in the original publication [11]

This was followed by heating in an oven of the compacted composite material, under an argon atmosphere at 650 °C for 2 hours. This process was carried out for sintering. After sintering, sodium chloride was removed from the compacted material

and thus treated. The samples were placed in boiling water at a temperature of approximately 95 °C for 10 hours. The boiling water gradually dissolved the sodium chloride from the aluminium material.

Fig. 4.49 shows the porosity and density values obtained for the samples of the porous materials produced. As is generally assumed, and Fig. 4.49 confirms this, the porosity of the samples increases with increasing NaCl content. Conversely, the bulk density of the porous aluminium material samples decreases with increasing NaCl content. The porosity of the sample that was made using 80 wt% NaCl is very high, reaching 81%, the material shows high porosity but very low density. Fig. 2.50 shows the dependence of strength on porosity of the fabricated aluminium porous materials.

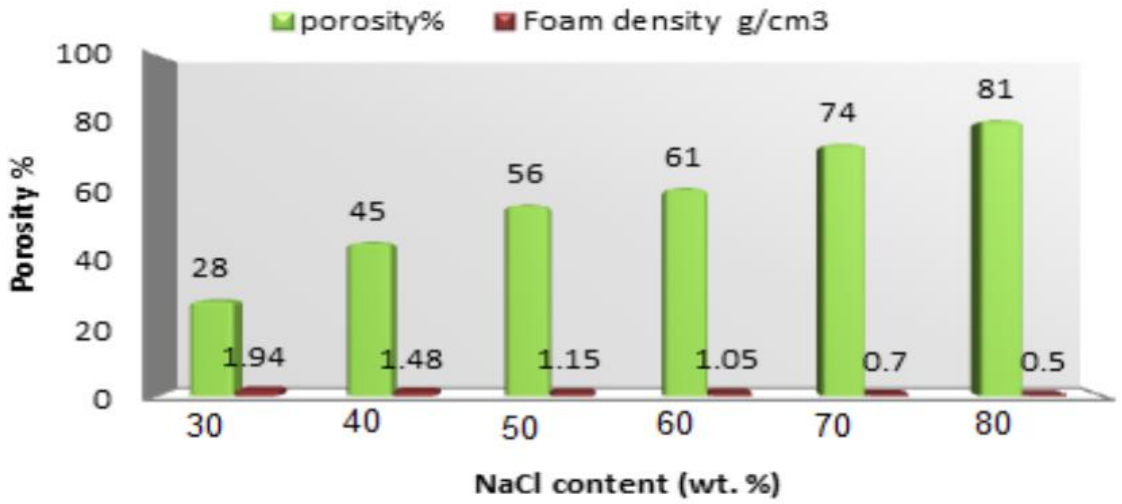

Fig. 2.49 Effect of NaCl content on porosity and density of aluminium materials, [11]

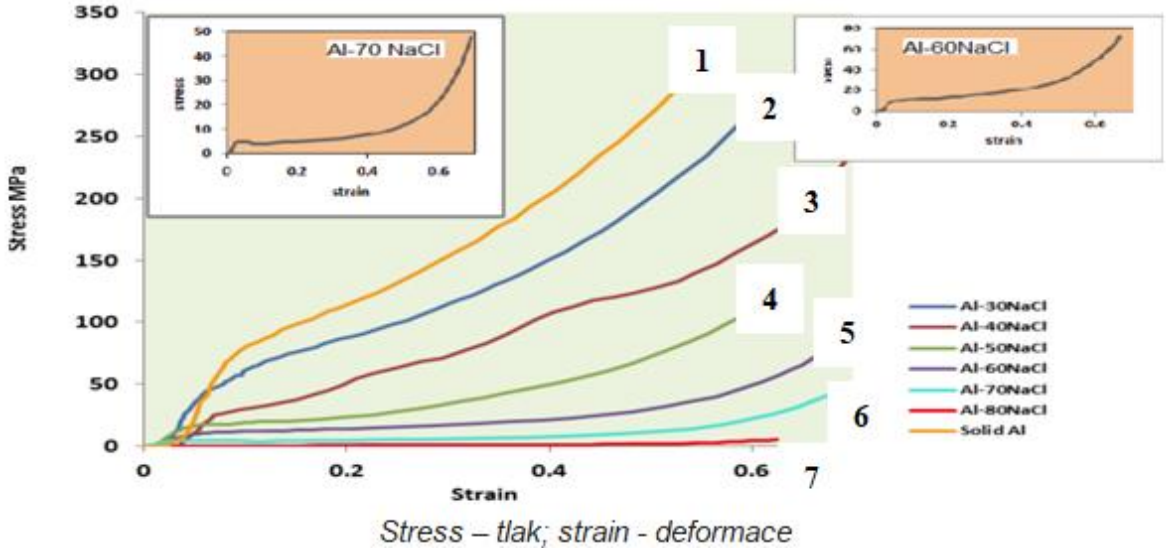

***1** - solid aluminium; **2** - 30 NaCl; **3** - 40 NaCl; **4** - 50 NaCl; **5** - 60 NaCl; **6** -70 NaCl; **7-** 80 NaCl*

Fig. 2.50 Compressive strength (MPa) of aluminium porous material samples related to porosity, res. NaCl content (without NaCl yellow, upper curve) [11]

Table 2-8 shows the values of compressive strength and Young's modulus of elasticity of the fabricated aluminium porous material samples (aluminium powder to sodium chloride ratio of 30, 40, 50, 60, 70 and 80 wt %).

Fig. 2.51 shows the microstructure of samples of aluminium porous materials produced on the basis of different ratios of aluminium powder and NaCl, wt.%. It has been shown that when a higher content (wt. %) of NaCl was used in the ratio of aluminium cladding to NaCl, a larger size was achieved in the material produced as well as higher pore sizes.

Table 2-8 Compressive strength and Young's modulus values of fabricated aluminium porous material samples using different NaCl contents

Compressive strengths, E values and mean pore size of samples of porous aluminium materials made with different ratios of aluminium powder and NaCl [wt. %]							
Sample	***Al***	***Al 30 NaCl***	***Al 40 NaCl***	***Al 50 NaCl***	***Al 60 NaCl***	***Al 70 NaCl***	***Al 80 NaCl***
Compressive strength [MPa]	60.5	32.7	24.7	9.4	6.5	3.8	0.26
Young's modulus of elasticity [GPa]	1.45	1.32	0.62	0.46	0.25	0.14	0.023
Mean pore size [mm]	-	0.29	0.30	0.35	0.41	0.46	-

At high NaCl content, most of the NaCl particles were in contact with each other. A continuous dimensionless network of pores was formed after NaCl desulfurization.

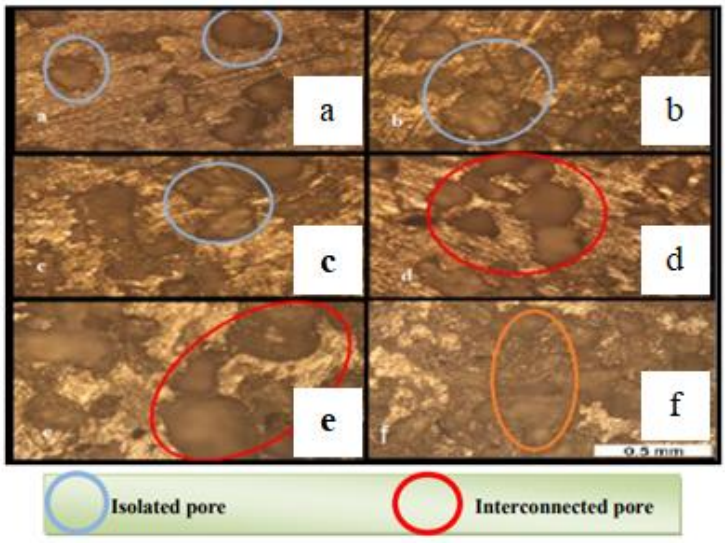

Insolate pore - isolated pores; Interconnected pore - connected pores
a) Al-30NaCl; b) Al-40NaCl; c) Al-50NaCl; d) Al-60NaCl; e) Al-70NaCl; f) Al-80NaCl

Fig. 2.51 Microstructure of aluminium porous material samples produced on the basis of different NaCl content by weight, determined by light microscopy [11]

In contrast, isolated pores with a thick cell wall were observed when 30 wt% NaCl was used. At 80 wt% NaCl, the pores found were mostly interconnected and showed thinner cell walls. The values of the mean pore sizes are shown in Table 2-8.

Also, the issue of the fabrication of open-cell aluminium porous materials and the use of the pressing process has been addressed by NANSAARNG and SOPHA [30]. For this purpose, they used aluminium powder with a purity of 99.8 % and a particle size of 0.6 mm. They also used sodium chloride particles with two particle sizes of 0.6 mm and 0.3 mm. The aluminium powder to NaCl was mixed in a 2:1 ratio. This mixture was compressed in the mould with a force of 40 kN to form cylindrical speci ∅ 25 x 40 mm (see Fig. 2.52).

sample produced using 0.6 mm NaCl particles (left)
sample produced using NaCl particles with a particle size of 0.3 mm (right)

Fig. 2.52 Samples of porous aluminium materials∅25 x 40 mm with NaCl particle sizes of 0.6 mm and 0.3, produced by the pressing process [30]

The samples thus produced [30] were heat treated in an oven at 720 °C for one hour. Then, the samples were stripped of NaCl and subjected to compression testing and microstructure monitoring. At the same time, the porosity of the fabricated samples was calculated, according to the relations of [30], which the author refers to as apparent porosity (porosity).

$$P_Z = \left(\frac{M-D}{V}\right) \cdot 100\ [\%], \tag{2.10}$$

where: P_Z is apparent porosity [%]; M is mass of melt [kg]; D is mass of solid material [kg]; V is total volume [m].

The density calculation was performed according to the relation:

$$B = \frac{D}{V}. \tag{2.11}$$

Table 2-9 shows the weight, bulk density and apparent porosity. Sample ***1*** was made with a 2:1 ratio of ingredients: 0.6 mm particle size aluminium powder and 0.6 mm particle size NaCl. Sample ***2*** was again made with 2:1 ingredients, namely, aluminium powder with a particle size of 0.6 mm and NaCl particles with a particle size of 0.3 mm. This sample designation is also valid for other tables. Since the aluminium samples were removed immediately after their production, the salt particles were removed by dissolving them in water. Therefore, their weight in the undried and dried states was monitored.

Table 2-9 Apparent porosity values [30]

Apparent porosity values of porous aluminium samples				
Sample	**Weight (moist) [g]**	**Weight (dry) [g]**	**Volume weight [kg·m^{-3}]**	**Apparent porosity [%]**
1.	19.96	13.94	1174	51.37
2.	19.39	13.65	1118	51.35

Table 2-8 shows small differences in the determined weight and bulk weight of the samples. In fact, the authors [30] did not accurately characterize the dimensions of the samples studied and this is then a problem for the assessment of the determined results. With the same dimensions of both samples, it is obvious that NaCl with larger particles will create more porosity of the material or sample, and thus, its bulk mass will be lower. At the same time, the structure of the produced porous (porous) aluminium samples was also observed on a scanning electron microscope (see Fig. 2.53).

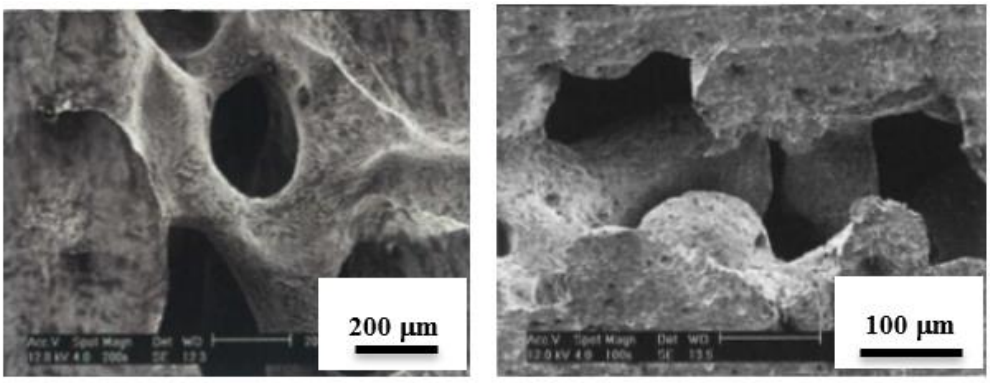

Fig. 2.53 Structure of porous aluminium material produced using NaCl particles of 0.3 mm (left) and 0.6 mm (right); SEM electron microscope

Table 2-10 shows the density values of the produced porous aluminium materials with NaCl particle sizes of 0.3 and 0.6 mm.

The bulk weight of the samples thus produced ranged from 1100 to 1200 [kg·m^{-3}] with porosities of 50 to 52 % and compressive strengths of 16 to 17 MPa. The results

reported in [30] provide a basis for monitoring the properties of porous aluminium materials.

Table 2-10 Bulk density values of produced porous aluminium samples [30]

Values of selected physical quantities of porous aluminium samples				
Sample	**Weight (dry) [g]**	**Volume weight [g·cm^{-3}]**	**Volume weight [kg·m^{-3}]**	**Volume [cm^3]**
1.	13.94	11.74	1174	1.19
2.	13.65	11.18	1118	1.22

Table 2-11 shows the compressive strength values of the fabricated porous aluminum specimens. The samples used for compressive strength monitoring were ∅ 22.4 mm.

Table 2-11 Compressive strength values of fabricated porous aluminum specimens [30]

Compressive strength values of porous aluminium specimens			
Sample	**Sample area [mm^2]**	**Total load [N]**	**Compressive strength [MPa]**
1.	394.0	6531	16.6
2.	390.5	6745	17.3

Also, HUSSAIN and SUFFIN [31] dealt with the production of porous aluminium materials based on the sintering of a mixture of aluminium and NaCl particles, with a subsequent process of dissolution of the salt particles. The aim of their research was to observe the effect of the amount of NaCl on the morphology of the formed cavities or the porosity of the fabricated samples. In their experiments, the researchers [31] used pure aluminium powder (99.8 % purity) with a particle size of 35 μm (0.035 mm) and NaCl particles of 1 mm. The pure aluminum powder with NaCl particles was mixed in a ball mill for 1 hour according to the composition used as shown in Table 2-12.

Table 2-12 Powder ratio in the preparation of porous aluminium samples [31]

Ratio of mixed powders of aluminium and NaCl		
Porous material designation	**Amount of pure aluminium powder [% wt]**	**Amount of NaCl [% wt]**
Al-20 NaCl	80	20
Al-40 NaCl	60	40
Al-60 NaCl	40	60
Al-80 NaCl	20	80

A small amount of ethanol was added during mixing to prevent the segregation of the powder. The respective mixture was pressed at 200 MPa in a metal tool to obtain a cylindrical compact material. Next, the cylindrical compact material was sintered in a tubular electric furnace at 570 °C under an argon atmosphere for

5 hours. The obtained compact aluminium material with NaCl particles was then placed in water at 90 °C for 1 hour to dissolve or wash out the sodium chloride particles.
The authors of [31] present the relations for the determination of the density and porosity of the obtained porous material, which they adopted from the authors of [32]. The bulk density (ρ_P) was determined by the double weighing method in air and water, according to Eq:

$$\rho_P = \left(\frac{w_a}{w_c - w_b}\right) \cdot \rho_{liquid}, \tag{2.12}$$

where: w_a is the weight of material on air [g]; w_c is the weight of material and water [g]; w_b is the weight of water loss [g].

To determine the porosity of the porous material (or aluminium "foam"), the researchers [31] used relation (2.2), which they expressed in [%], see relation (2.13):

$$P_P = \left[1 - \frac{\rho_P}{\rho_{Al}}\right] \cdot 100\ [\%], \tag{2.13}$$

where denotes:ρ_P is density of the prepreg material [g·cm^{-3}]; ρ_P is density of pure aluminium 2.7 [g· cm^{-3}]; ρ_{liquid} is density of water 1.0 [g· cm^{-3}].

Fig. 2.54 shows the density and porosity relationships of the fabricated porous aluminium materials using different NaCl contents obtained by researchers [31].

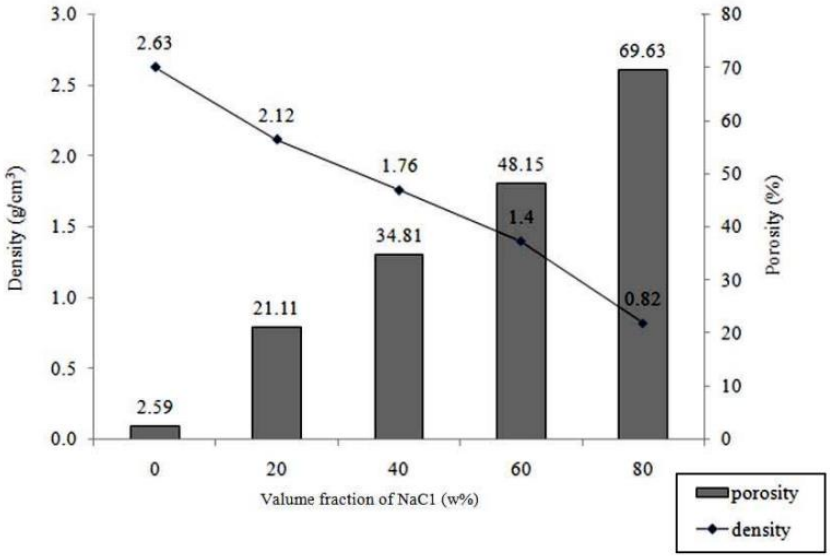

Fig. 2.54 Dependence of density and porosity of produced porous aluminium materials on the volume fraction of NaCl used, according to the results of [31]

Fig. 2.55 shows the microstructure of the samples obtained using a light microscope. The researchers [31] observed connected and unconnected cells. The interconnected cells were better at removing NaCl particles. Fig. 2.55 shows that the

microstructure of the porous aluminium samples produced (aluminium 'foams') varies in the size and shape of the pores (cells). The shape of the pores replicated the initial cubic shape of the NaCl particles. It was observed that the following sequence of foam means reflected the pore size in ascending order: Al-20NaCl, Al-40NaCl, Al-60NaCl and Al-80NaCl. From these findings, it can be concluded that by increasing the NaCl particle content in the production of porous aluminium materials (aluminium "foams"), larger cells and higher pore sizes can be obtained. As noted by the researchers [31], isolated pores were mainly seen to a large extent in aluminium material when using Al-20 NaCl. On the contrary, a large amount of interconnected pores was observed in the aluminium material when using Al-80NaCl. This observation suggests that a higher NaCl particle content is more conducive to the formation of interconnected pores. At the same time, it is important to observe the relationship between pore size, cell walls and density of the fabricated porous aluminium material. This relationship affects the properties of the fabricated porous aluminium materials.

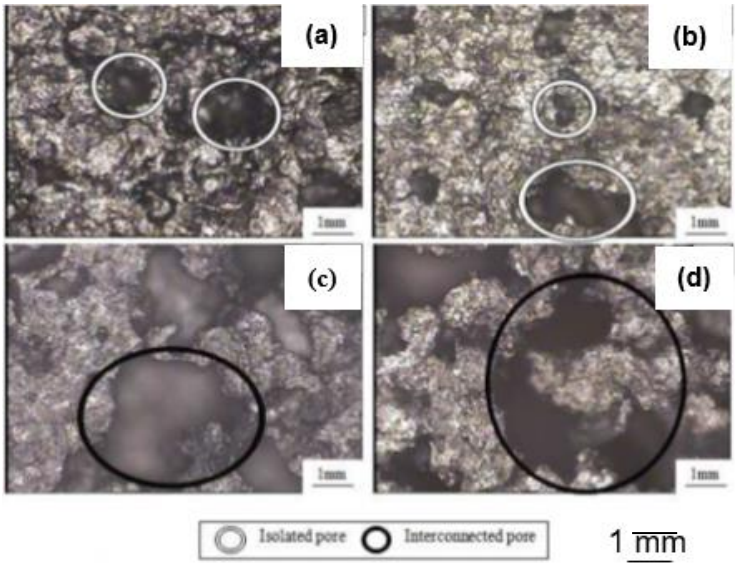

insolated pore - marked areas above, interconnected pore - marked areas below

Fig. 2.55 Structure of fabricated porous aluminium materials (aluminium "foams") with different NaCl contents: (a) Al-20NaCl; (b) Al-40NaCl; (c) Al-60NaCl; (d) Al-80NaCl; obtained using light microscopy, [31]

Fig. 2.56 shows the microstructure and pore characteristics of the fabricated samples, which were observed using a scanning electron microscope (SEM).

The values of the monitored quantities are shown in Table 2-13. In addition to density, the average pore (cell) size [μm] of the fabricated aluminium porous samples was also monitored. At the same time, the values of the average pore (cell) wall thickness [μm] were also monitored.

As can be seen from the values shown in Table 2-13, the bulk density of the porous material decreases with increasing NaCl content. Its minimum value is 1300 [kg·m^{-3}], which is close to the density value of 1174 [kg·m^{-3}] measured by NANSAARNG and SOPHA researchers [30].

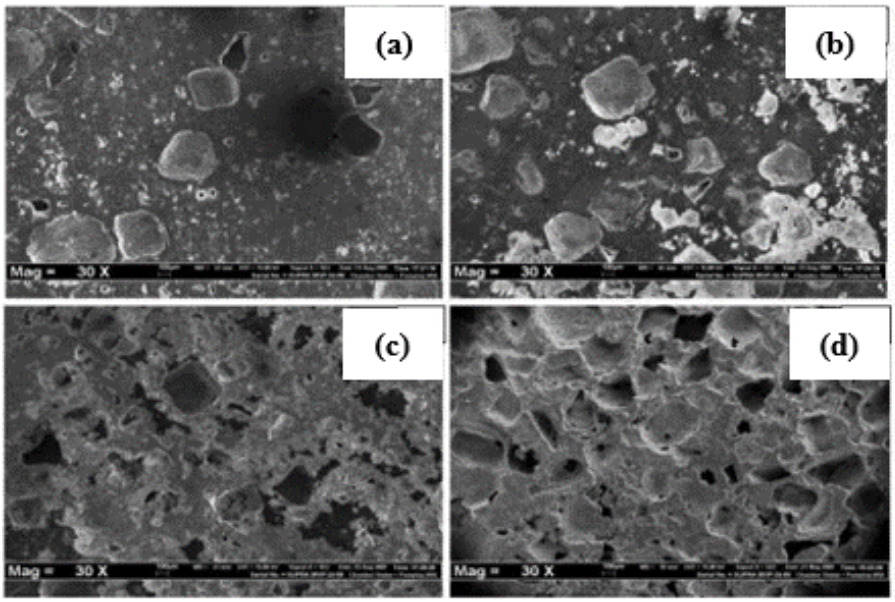

Fig. 2.56 Microscopic observation of the pores of aluminium porous materials (aluminium "foams") using different NaCl contents: (a) Al-20NaCl; (b) Al40NaCl; (c) Al-60NaCl; (d) Al-80NaCl [31]

Table 2-13 Density values, average pore size, the average pore wall thickness of fabricated aluminium porous samples [31]

Characteristics of porous aluminium material				
Al-NaCl ratio	***Al-20NaCl***	***Al-40NaCl***	***Al-60NaCl***	***Al-80NaCl***
Bulk weight [g· cm^{-3}]	1.99	1.90	1.69	1.30
Average pore (cell) size [μm]	403.75	422.50	446.86	500.25
Average pore (cell) wall thickness [μm]	148.33	117.14	98.57	75.07

It is also clear from this table that the average pore (cell) size increases with increasing NaCl content in the respective experimental fraction, with a maximum value of about 500 [μm]. Conversely, the average pore (cell) wall thickness decreases with increasing NaCl in the respective experimental fraction, with a minimum value of about 75 [μm]. Both these values are associated with the fraction of NaCl in the fraction. Thinner cell walls and larger pore (cell) sizes lead to a lower density of porous material (aluminium "foams"). Cell wall thickness decreases with increasing NaCl content in experimental practice. Fig. 2.57 shows graphical stress-strain relationships for porous aluminium materials made with different NaCl content in the fraction: Al-0NaCl; Al-20NaCl; Al-40NaCl; Al-60NaCl and Al-80NaCl, left. Fig. 2.57 also shows the graphical absorbed energ strain relationship for porous aluminium materials produced with different NaCl content in the fraction: Al-0NaCl; Al-20NaCl; Al-40NaCl; Al-60NaCl and Al-80NaCl, right.

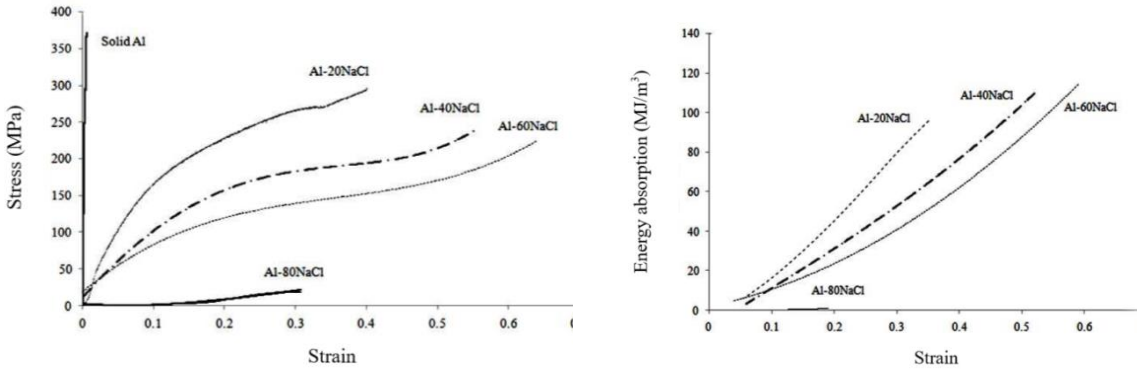

Fig. 2.57 Compressive stress-strain relationship (left); absorbed energy-strain relationship (right) in the context of NaCl fraction (Al-0NaCl; Al-20NaCl; Al-40NaCl; Al-60NaCl and Al-80NaCl) [31]

Fig. 2.57 shows the stress-strain curves obtained by compression testing of samples of porous aluminium materials made using different NaCl contents. In the course of observing the stress-strain relationship, the material behaviour can theoretically be divided into three regions: *region I* - linear elastic deformation, *region II* - more gradual deformation and region *III* - material compaction. From these stress-strain curves the compressive strength, yield strength and modulus of elasticity can be determined. The obtained values of mechanical properties are shown in Table 2-14. As expected, it was found that increasing the NaCl particle content in the production of porous aluminium samples significantly decreases the yield strength value. The reference curve of pure aluminium shows the highest yield strength. As can be seen from Fig. 2.57, the modulus of elasticity (elastic modulus), which is indicated by the slope of the curve (stress-strain), decreases with decreasing porosity of the samples, [31]. This phenomenon is explained by the authors [31] by the fact that elastic deformation can easily occur at high porosity, resulting in a decrease in elastic modulus. As expected, the elastic modulus is highest for pure aluminium compared to porous aluminium samples.

Table 2-14 Mechanical properties of aluminium porous samples [31]

Mechanical properties of aluminium porous samples					
Al-NaCl ratio	***Al-0NaCl***	***Al-20NaCl***	***Al-40NaCl***	***Al-60NaCl***	***Al-80NaCl***
Compressive strength [MPa]	370.9	27.2	245.7	222.5	197.2
Compressive yield strength [MPa]	299.1	176.1	144.4	144.5	134.9
Yield Strain [1]	0.004	0.113	0.199	0.354	0.203
Modulus of elasticity [GPa]	161.3	1.59	0.73	0.41	0.080

If we compare the corresponding values of the quantities between Table 2-8 and Table 2-14, we can see that some of them are close, some do not correspond at all, such as the values of the modulus of elasticity for pure aluminium, which are very different.

Fig. 2.58 shows a graphical dependence of the absorbed energy as a function of the NaCl content of the fraction. This figure shows the total energy absorption of the foams during the compressive strength test. The results were calculated based on the area under the stress-strain curves, see Fig. 2.57 (left). The porous Al-80 NaCl sample clearly showed the lowest energy absorption compared to the other porous samples, with a value similar to that of the pure aluminium sample. In addition, this sample exhibits a brittle material behavior as shown by the small area under the stress-strain curve, which is consistent with low energy absorption. As explained by the authors [31], this trend may be related to the presence of residual NaCl particles in the porous sample Al-80NaCl, which were not completely dissolved during the dissolution process. The observation of the authors [31] showed that 1 h of salt dissolution is not sufficient to completely dissolve the amount of NaCl particles in the porous Al-80NaCl sample. NaCl is an ionic compound that is brittle due to the rigid interactions between charged ions that hold the charged particles in fixed positions. As a brittle material, the remaining NaCl affects the properties of aluminum porous materials. In addition, the excessive NaCl content caused the cell walls of the porous samples to be too thin and, thus, weak. Referring to Table 2-14 and the morphological observation of the structure of the Al-80NaCl porous aluminum sample, it can be seen that this sample exhibits the thinnest cell wall thickness (75.07μm) compared to the other aluminium porous samples. The weak cell walls of the Al-80NaCl aluminium porous sample did not allow further loading during the compression test.

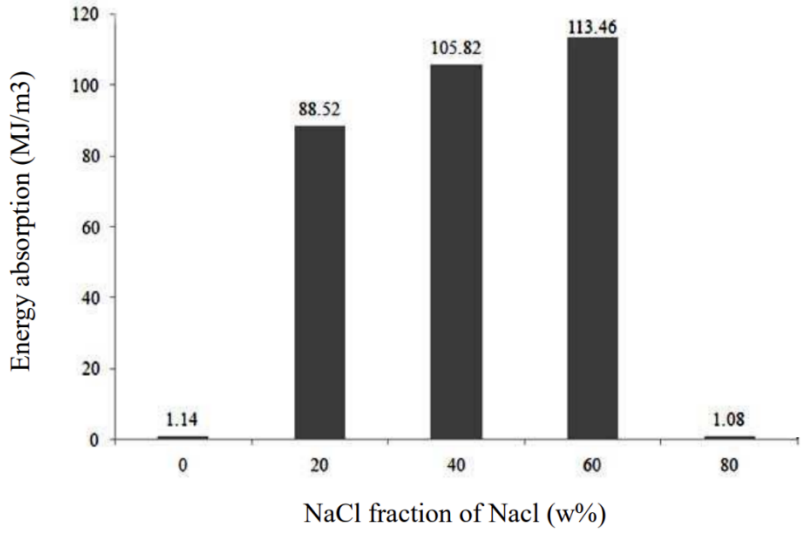

Fig. 2.58 Dependence of absorbed energy on the mass % of NaCl in the fraction [31]

From the authors' publication [31], the finding from mechanical testing that the compressive stress (stress-strain curve) of the porous aluminium Al-20NaCl sample was the highest, as shown in Fig. 2.57, is of practical benefit. By observing the absorbed energy, see Fig. 2.58, which shows that the cellular structures of Al-20NaCl porous aluminium sample exhibit an energy absorption of 88.52 [$MJ \cdot m^{-3}$], but the absorbed energy of Al-40NaCl porous aluminium sample is higher, it is 105.82

[MJ·m^{-3}]. The porous aluminium sample with higher porosity, i.e. Al-60NaCl, shows the highest absorbed energy, which shows an absorbed energy of 113.46 [MJ·m^{-3}]. From these values, it is clear what amount of wt. % NaCl should be contained in the fabricated aluminium porous materials. The research [31] clearly showed that the Al-60NaCl aluminium porous sample absorbed the highest energy compared compared to the other samples. This is due to the porosity and cell walls of this aluminium porous sample in which a more homogeneous pore structure was formed than other aluminium porous samples, as illustrated in Fig. 2.56. During the compression of the porous aluminium sample, there was still a phase of cell wall bending and a subsequent phase of cell wall collapse. A large amount of energy (absorbed energy) was required for this to occur, and this occurred at a point where there was a very gradual increase in stress on the stress-strain curve, see Fig. 2.57 (left), as confirmed by XIAO et al. [33]. Therefore, the microstructure of the Al-60NaCl aluminium porous sample suggests its behaviour for compressive stress and a better energy absorption behaviour.

Table 2-15 compares the mechanical and physical properties of various foamed and porous materials.

Table 2-15 Values of mechanical and physical properties of various foamed and porous materials

Values of the mechanical and physical properties of various foamed and porous systems				
Feature	**Baked bronze**	**CYMAT**	**DUOCEL (Al foam)**	**ALUPOR**
Porosity [%]	30-40	80-98	80-98	55-75
Bulk weight [kg·m^{-3}]				1000 - 1400
Cell type of porosity	Open	Closed	Open	Open
Achieved average pore size [μm]	3-250	200-50000	20-5000	100-5000
Minimum pore diameter [μm]	5	42	25-35	40-60
Compressive strength [MPa]	60-200	5	25	35-109
Young's modulus of elasticity [MPa]	150 000 200 000	1300	150	1000 up to 4000
Young's modulus of elasticity [GPa]	150-200	1.3	0.15	1.0-4.0
Coefficient of thermal conductivity [W·m^{-1}·K^{-1}]	4.68		5.8	35-50
Electrical conductivity [Sm·m^{-1}]	1.0· 10^{6} up to 5.0· 10^{6}	1.2· 10^{6}	1.4· 10^{6}	3.55·10^{6} up to 4.78·10^{6}
Coefficient of thermal expansion [K^{-1}]	18.0·10^{-6}	23.6·10^{-6}	23.6·10^{-6}	23.6·10^{-6}

Nowadays, porous aluminium materials, like aluminium foams, find considerable use in many areas of engineering due to their excellent physical and mechanical properties (low thermal conductivity, low bulk density, high specific strength, good acoustic properties and good electrical insulation properties).
The cellular structure of Al foams is required for functional applications such as filtration, sound absorption, thermal insulation, heat exchange, air and water purification, and energy absorption. The annex*, Table P1,* lists companies involved in the manufacture or provision of metal cellular systems (metal foams).
Table 2-16 shows a selection of some properties of selected aluminium foams.

Table 2-16 Property values of selected aluminium foams

Feature	*Aluminium foam marking*		
	ALPORAS	**CYMAT METCOMB**	**ALULIGHT**
Typical product dimensions [m]	blocks 2.0 x 0.6 x 0.5	panels 1.6 x 1.0 x 0.2	blocks 1.0 x 0.5 x 0.2
Bulk weight [kg·m^{-3}]	180 to 240	69 to 540	300 to 700
Pore diameter	2 to 10	3 to 25	2 to 10
Wall thickness between pores [μm]	50	50 to 85	50 to 100
Other suitable alloys for the production of metal foams	aluminium and its alloys only	aluminium alloys	zinc alloys tin alloys

3. PHYSICAL NATURE OF THE FOAMING PROCESS

In this chapter, a rather detailed description of the foaming process for the production of metal foams "in situ" by feeding gas into the melt from an external source is given. In addition to the technological aspects, the physical phenomena occurring in the various stages of the foaming process. These facts are important for the actual production of the metal foam. At the beginning of this chapter, it is necessary to recall the basic methods for the production of cellular metallic materials, which can be classified into four categories according to the state of the metal during foam production (molten metal, solid metal powder, metal vapour and metal ion methods). The basic methods that are applied in the current production of metal foams are: direct melt foaming method from an external gas source, direct melt foaming using gas released due to thermal decomposition of the foaming agent, remelting of the foamed metal precursor composite with the molten material, melting of the powder compact mixture containing the foaming agent.

Fig. 3.1a) shows examples of selected types of cellular systems made with different technologies.

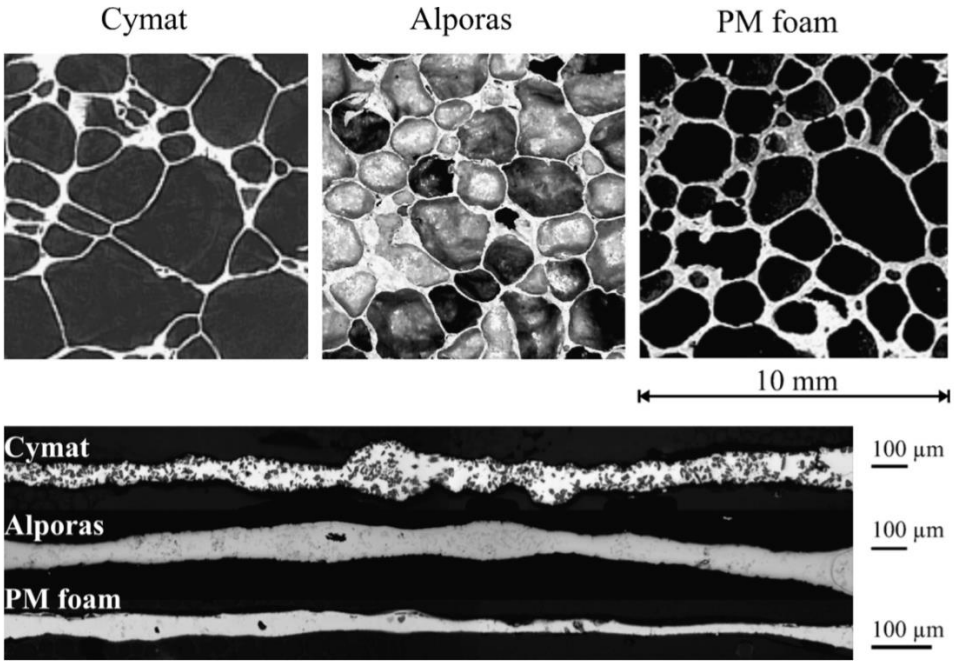

Fig. 3.1a) Selected cellular aluminium materials; ***Cymat:*** *melt fuming with SiC particles with gas from an external source;* ***ALPORAS:*** *melt with calcium fumed with TiH fuming agent₂* ***;*** ***PM*** *- powder metallurgy, metal powder and TiH fuming agent₂ are compressed*

A description of the physical nature of the frothing process can be made based on melt gassing from an external gas source. In the foundry equipment, the relevant aluminium alloy is melted and a certain amount of stabilising agent is added. This produces a metal matrix composite of aluminium alloy with 10 to 20 vol. % particles of stabilising agent, which is usually SiC or Al_2O_3. This is then followed by a transfer to a froth pan, which has a special design with a built-in rotating device for feeding gas from

an external source into the melt. The gas is fed into the melt using special nozzles. The dispersed bubbles rise upwards. Here, they accumulate on the melt surface and form a foam. The escape of gas from the bubble and its collapse are prevented by adding ceramic stabilising particles to the melt.

3.1 Physical description of the metallic cellular system

A metal cellular system (metal foam) is a two-component system that is a mixture of gas bubbles dispersed in a melt of metal. Once the melt has solidified, it is a two-component system consisting of gas bubbles that are dispersed in the solidified metal, most commonly aluminium or aluminium alloy. Essentially, it is the dispersion of a gas in another substance. Metal foam is formed by the bubbling of molten metals through the gas. Its stability is maintained by adding ceramic particles to the melt before it is foamed. Fig. 3.1b) shows a schematic of a physical model of a metal foam, indicating all the elements and laws involved in its formation.

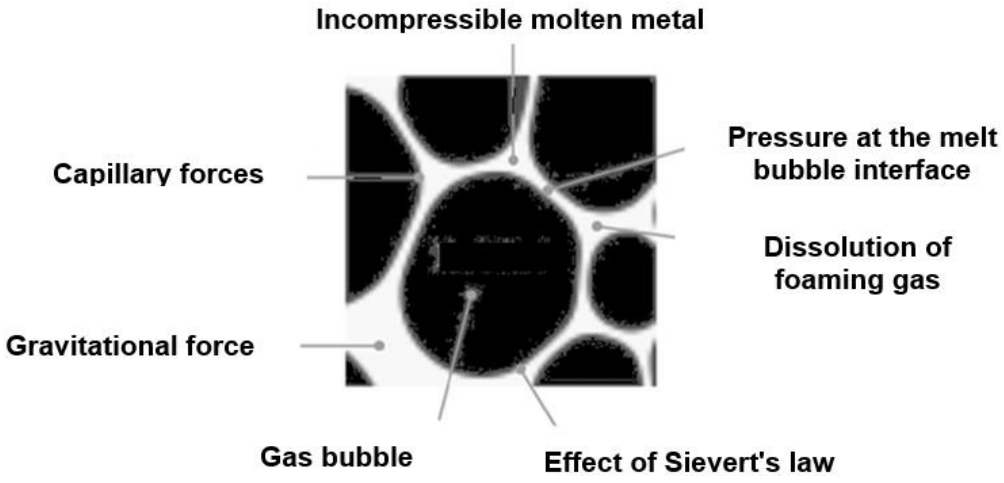

Fig. 3.1 b) Physical description of bubble behaviour in a metal melt

3.2 Physics of the foaming process

Frothing by feeding gas into the melt of the metal (most commonly, aluminium alloy) - the generation of gas "in situ" is a process that goes through various stages of development, the frothing process as seen in Fig. 3.1c). At the very beginning, the expansion starts with the nucleation of bubbles induced by excessive gas supply to the melt to realize the melt foaming process. This gas is released and dissolved in the metal melt due to the increase in temperature (or the decrease in external pressure, which takes place during foaming in the presence of the decomposition of the foaming agent), increasing the concentration of dissolved gas in the melt. As a result, the gas contributes to the formation of bubbles in the melt. The amount of gas in the bubbles increases as their volume increases. During growth, the bubbles begin to interact with each other. The forces that affect the interaction of the bubbles result from the law of hydrodynamics and are on. This means that they depend on the expansion velocity and the viscosity of the melt.

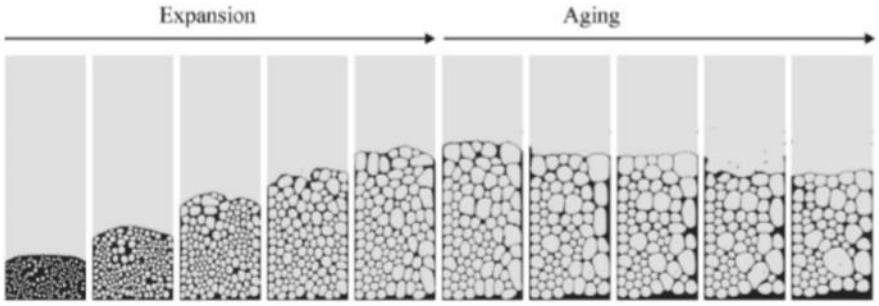

Expansion, Aging

Fig. 3.1c) Stages of metal foam development (nucleation, growth, thickening and disintegration, 2D simulation, LBM), according to KÖRNER [1]

These forces try to deform the bubbles and counteract their surface tension, the aim of which is to create or restore the spherical shape of the bubble. When the relative bulk density reaches a certain value, the bubbles turn into foam structure components and take on more and more of a polygon shape. This process is associated with cell coalescence, which leads to foam compaction and eventually to foam collapse.

3.2.1 Basic equations for foam development

Foam development is the process of applying the fundamental laws of physics. Foam is a two-phase system consisting of a gas and a metal melt (according to the IFM, it is a three-phase system consisting of a gas-metal melt-metal solid phase). Due to the large difference in gas and melt densities, the dynamics are insignificant and can be neglected for most practical applications.

***a) Hydrodynamics of an incompressible* fluid**

The hydrodynamics of an incompressible liquid (melt) is given by the Navier-Stokes equation [1]:

$$\partial_\alpha \cdot v_\alpha = 0 \tag{3.1}$$

$$\partial_\alpha \cdot v_{\alpha+} \left(v_\beta \cdot \partial_\beta\right) \cdot v_\alpha = -\frac{1}{\rho} \partial_\alpha \cdot p + \nu \cdot {\partial_\beta}^2 \cdot v_\alpha + g_\alpha, \tag{3.2}$$

where: ρ is density of melt [kg·m^{-3}], v is velocity, p is pressure, υ is kinematic viscosity, and g is gravitational acceleration (g = 9.81 m·s^{-2}).

Equations (3.1) and (3.2) express the law of conservation of mass and momentum. The solution (NSR) gives the pressure and velocity field in the melt. The gas pressure $\mathbf{p_i}$ in the bubble labelled **" i "** can be determined from the gas equation of state:

$$p_i = \frac{n_i \cdot R \cdot T}{V_i}, \tag{3.3}$$

where: R is the universal gas constant (R = 8.314 J· $mol^{-1}·K^{-1}$), n_i is gas mass, T is temperature [K], and V_i is the volume of the bubble "i" [m^3].

Momentum transfer takes place at the melt-gas interface (region Γ). At this phase interface, the velocity must be the same in both the melt and the gas:

$$v_G\,(x) = v_F\,(x), \qquad \text{for all } x \in \Gamma \qquad (3.4)$$

where it means: v_G is velocity in gas, v_F is velocity in melt (fluid).

In addition to momentum, a balance of forces must be maintained. The force exerted by the pressure of the gases contributes to this balance. The gas pressure force is counteracted by the forces from capillary pressure, melt pressure and the force due to the viscosity of the fluid (see Fig. 3.2).

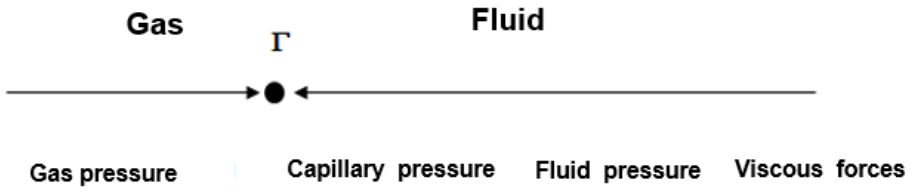

Fig. 3.2 Schematic of the forces and pressures between gas and fluid in the formation of a gas bubble, [1]

Since the gas is only capable of exerting normal forces but cannot transmit tangential stresses, the boundary conditions are divided into normal and tangential components:

$$p - 2 \cdot \rho \cdot \partial_n \cdot v_n = p_i - 2 \cdot \sigma \cdot \kappa \qquad (3.5)$$

$$\partial_n \cdot v_n = \partial_t \cdot v_n = 0, \qquad (3.6)$$

where: v_t, v_n are the tangential and normal components of the velocity, ρ is melt density [$kg·m^{-3}$], 2·σ·κ is capillary pressure [Pa], κ is average curvature, and σ is the surface melt tension [$N·m^{-1}$].

Equation (3.6) follows from the absence of tangential stresses. The left-hand side of equation (3.5) is the normal force exerted by the melt. It is the sum of the pressure and viscous forces. The right-hand side is the gas pressure, which is reduced by the capillary pressure 2·σ·κ.

b) Gas solubility

In addition to the laws of hydrodynamics, gases are also necessary for the development of foam, such as the gas supply to the melt or the gases obtained from the decomposition of the foaming agent. In general, we are interested in the ultimate

solubility of the gas in the melt. According to KÖRNER [1], the amount of dissolved gas in the melt is governed by the diffusion equation:

$$\partial_t C + v_\alpha \cdot \partial_\alpha C - \partial_\alpha (D \partial_\alpha C) = Q \quad (3.7)$$

where it reads: C = C(x,t) is the gas concentration field, D is the gas diffusion coefficient in the metal melt [$m^2 \cdot s^{-1}$], Q = Q(x,t) is the presence of the foaming gas (or gas obtained by decomposition of the foaming agent).

Equation (3.7) is a differential equation, and boundary conditions must be formulated for its solution. Generally, Dirichlet or von Neumann boundary conditions are used. In the case of foam production, it is convenient to use Dirichlet boundary conditions where the concentration is given at the gas-melt interface, then the equilibrium concentration at the interface can be solved using Henry's law:

$$C(x,t)_\Gamma \propto p_i, \quad (3.8)$$

where it reads: $C(x,t)_\Gamma$ is the gas concentration at the melt-gas interface at x location x and time t; p_i is the partial pressure of the gas "i".

The mathematical notation (3.8) should be read to mean that the gas concentration at the melt-gas interface is equal to some constant multiplied by the gas pressure i: $C(x,t) = k \cdot p_i$. This is exactly what Sievert's law describes:

$$C(x,t)_\Gamma = K \cdot p_i, \quad (3.9)$$

where: K is Sievert's constant.

The monitoring of hydrogen solubility due to thermal decomposition of hydride-based foaming agents (TiH_2, MgH_2, CaH_2, ZrH_2) in metal melts, mainly aluminium, in the production of metal cellular systems (aluminium foams) is presented in the following section.

In the context of foaming the aluminium melt with a foaming agent using powder metallurgy, the maximum possible volume of gas released from the foaming agent can be calculated based on the percentage of the foaming agent that will be released per kilogram of aluminium:

$$V = n \cdot \frac{R \cdot T}{p} = \frac{m}{M} \cdot \frac{R \cdot T}{p} \ [m^3], \quad (3.10)$$

where: n is the number of moles, T is absolute temperature [K], m is the quantity of the foaming agent [g], M is the molar mass of the foaming agent [$g \cdot mol^{-1}$], R is universal gas constant (R = 8.314 $J \cdot mol^{-1} \cdot K^{-1}$], p is pressure (most often p = 101 325 Pa); V is volume of the released gas [m^3].

For the production of aluminium foam by powder metallurgy, 0.5 to 1 wt. % of foaming agents is used. The gas volume using 1 % wt TiH_2 can be determined according to equation (3.10) by substituting the necessary values, which are m = 10 g, M = 49.91 [g· mol^{-1}], R = 8.314 J· mol^{-1}·K^{-1}, p = 101 325 Pa, T = 933 K, i.e. the melting temperature of aluminium. The maximum possible volume is $1.534 \cdot 10^{-2}$ [m^{-3}]. The volume V_S [m^{-3}] of 1 kg of aluminium can be determined by calculating 1/2700 = $3.70 \cdot 10^{-4}$ [m^{-3}], 1 kg of aluminium and the specific gravity of aluminium is 2.700 kg·m^{-3}. Based on these calculations, the relative density of aluminium foam can be determined:

$$\rho_{REL} = \frac{V_S}{V+V_S} \, [1], \tag{3.11}$$

where: V_S is the volume of the solid phase of 1 kg of aluminium ($V_S = 3.70 \cdot 10^{-4}$ [m^{-3}], V is the volume of gas [m^{-3}], which is given by the percentage or mass of the foaming agent.

$$\rho^* = \rho_{REL} \cdot \rho_S, \tag{3.12}$$

where: ρ^* is the volumetric mass density of the produced foam [kg·m^{-3}]; ρ_{REL} is relative volumetric mass density [1], and ρ_S is the density of foamed material [kg·m^{-3}].

The thermal decomposition of the foaming agent results in a steady increase in the hydrogen concentration due to the lack of hydrogen transport to the surfaces of the precursors (foaming masses in the production of aluminium foams), leading to hydrogen supersaturation of the melt. When the critical hydrogen concentration is exceeded, heterogeneous nucleation occurs in aluminium, which is the basis for the aluminium crystallization mechanism. Crystallization nuclei are formed almost immediately after the foaming process starts. The subsequent increase in porosity is obtained by pore growth, which is a consequence of the presence of gas in the pores. Hydrogen in aluminium for thermodynamic equilibrium in Fig. 3.3.
The solubility of hydrogen in aluminium is determined by thermodynamic equilibrium. This is quantified by Sievert's law. Sievert's law relates the partial pressure of hydrogen p_{H2} and the dissolved hydrogen S (solubility) in aluminium:

$$S = K_S(T) \cdot \sqrt{p_{H2}}, \tag{3.13}$$

where: S is the solubility of hydrogen [cm^3 H_2·(100 g Al)$^{-1}$]; K_S (T) is the equilibrium constant for the given metal [cm^3 H_2·(100 g Al)$^{-1}$·$Pa^{-1/2}$]; p_{H2} is the partial pressure of H_2 in the surrounding gas atmosphere [Pa].

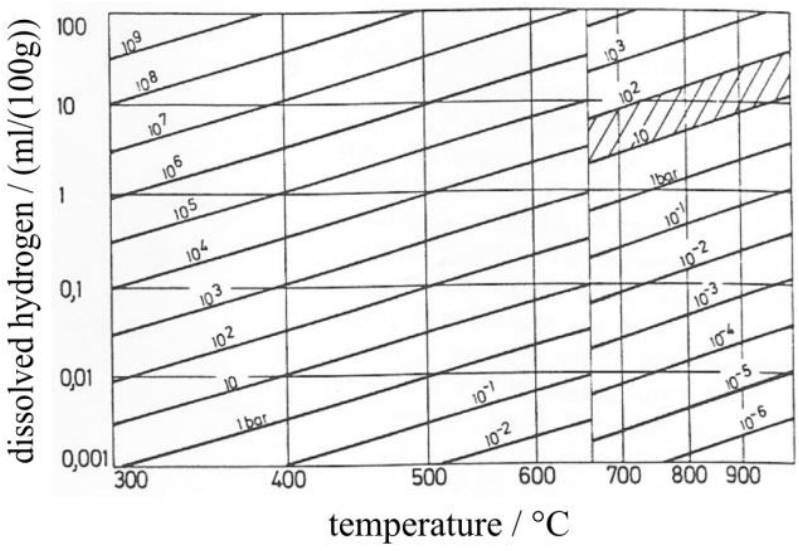

Fig. 3.3 Dependence of hydrogen solubility in aluminium on pressure and temperature according to LUTZE [4]

The solubility constant K_S is different for liquid and solid aluminium. The solubility coefficient of hydrogen K_S, which is a function of temperature, can be determined. The values are different for solid and liquid aluminium as reported by TALBOT [10], based on the following equations:

Coefficient of solubility of hydrogen K_S in liquid aluminium:

$$K_S\ (T) = 10^{(-\frac{2760}{T}+2.768)} \tag{3.14}$$

Hydrogen solubility coefficient K_S in solid aluminium:

$$K_S\ (T) = 10^{(-\frac{2580}{T}+1.399)} \tag{3.15}$$

By substituting into equations (3.14) and (3.15), for an aluminium temperature of 1000 K (727 °C) it can be determined that K_S (T) for the melt is 1.02 and K_S (T) for the solid state is 0.066.

The solubility of hydrogen in the aluminium melt in the production of aluminium foam can be determined by the equation:

$$\left(\frac{C}{C^0}\right) = K_S(T) \cdot (\frac{p_{H2}}{p^0})^{1/2}, \tag{3.16}$$

where it reads: C is the concentration of hydrogen in aluminium; C^0 is the concentration or volume of atomic gas under standard conditions, T = 273 K, p^0 = 101325 Pa, K_S is the coefficient of solubility of hydrogen in aluminium, C^0 = (1/100) [$cm^3.g^{-1}$], i.e., the volume of atomic gas that falls per 100 g of metal.

The square root in equation (3.16) affects the compensation of interstitially dissolved hydrogen atoms with H_2 molecules at the gas-phase/melt interface (in this case, aluminium). Under normal hydrogen pressure ($p_{H2} = p^0$), the equilibrium concentration approaches 0.77 (0.85) cm^3 /100 g, i.e., $7.6 \cdot 10^{-4}$ [$mol \cdot kg^{-1}$] = $1.8 \cdot 10^{-3}$ [$mol \cdot l^{-1}$], at 700 °C (973 K).

The comparison of hydrogen stored in TiH_2 with dissolved hydrogen at equilibrium is very small. Examining the above calculation using equation (3.10), about 1.5 % of the hydrogen is dissolved in the aluminium. The outer surfaces of the precursor may have a significantly lower hydrogen value depending on its partial pressure in the atmosphere and its concentration around the TiH_2 particles.

The solubility of hydrogen in aluminium and its alloys is variable and depends on the temperature of the alloy, the chemical composition and the partial pressure of hydrogen in the surrounding atmosphere. The amount of dissolved hydrogen is determined in units of cm^3 per 100 g of metal. This value of 1 cm^3 per 100 g of metal corresponds to a concentration of 0.9 ppm. Aluminium and its alloys show a significant difference between the solubility of hydrogen in the solid and liquid state. As reported by ROUČKA [7], in the solid state at 660 °C, the solubility of hydrogen in Al is only 0.036 cm^3/100 g.

In molten aluminium at 660 °C, the solubility of hydrogen is 0.77 cm^3/100 g, which is about 20 times higher. Other authors, e.g. AMBRIZ [8], report a value for the maximum solubility of hydrogen in aluminium of 0.69 cm^3/100 g (see Fig. 3.4 left).

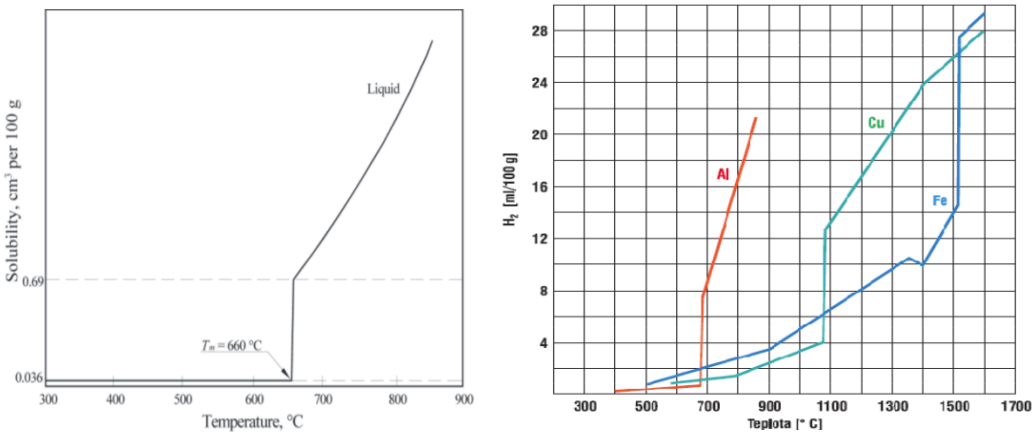

Fig. 3.4 Solubility of hydrogen in pure aluminium according to AMBRIZ [8] (left), According to KOUKAL [9], right

The temperature dependence of the hydrogen solubility in aluminium at a pressure of 101325 Pa can be obtained by applying the van´t Hoff isobar as reported by KALOUSEK [11]:

$$\frac{d(\log K_S)}{d(\frac{1}{T})} = -\frac{\Delta H^0}{R}, \qquad (3.17)$$

where it reads: ΔH^0 is the difference in the standard enthalpy of solubility of hydrogen in the aluminium melt [J·mol^{-1}]; T is temperature [K]; K_S is the equilibrium constant of hydrogen in the aluminium melt.

Based on the ratio of the respective equilibrium constants and the solubility of hydrogen in liquid aluminium and the solubility under equilibrium conditions, one can write:

$$\frac{K_S}{K^0{}_S} = \frac{S}{S^0} \tag{3.18}$$

By integrating the van´t Hoff isotherm equation (3.16) and using equation (3.17), we can write:

$$\log S = -\frac{\Delta H^0}{R \cdot T} + C, \tag{3.19}$$

where it reads: C is the integration constant.

The change in the standard enthalpy of solubility of hydrogen in molten aluminium ΔH^0 is considered to be independent of temperature. Table 3-1 shows the values required by various authors as reported by LIU [20] for the calculation according to equation (3.19).

Table 3-1 Values for calculating the solubility of hydrogen in aluminium according to different authors

Calculation of hydrogen solubility in aluminium by various authors						
$\log S = -\frac{\Delta H^0}{R \cdot T} + C$						
ΔH^0		**Constanta C**	**S^0**	**Reference gas**	**Sample weight**	**Used Reference**
[kcal·mol^{-1}]	[kJ·mol^{-1}]	[1]	[ml/100g]	[1]	[g]	
5 365	22. 45	2.72	0.881	helium	100	TALBOT [14]
5 067	21. 21	2.62	0.998	helium	100	OPIE and GRANT [13]
5 484	22. 95	2.80	0.911	neon	30-40	RANSLEY and NEUFELD [12]
5 921	24. 78	3.07	1.026	argon	300	LIU [20]

The work of RANSLEY and NEUFELD [12] in 1948, for the determination of the solubility of hydrogen in pure aluminium, was the basic work of this research. In 1950 OPIE and GRANT [13] concluded that the solubility of hydrogen in aluminium is given by a general equation:

$$log_{10}\ S = -\frac{A}{T} + C, \tag{3.20}$$

where denotes: S is the solubility of hydrogen in aluminium [cm^3 per 100 g of metal]; A is constant, which represents the enthalpy of hydrogen solution in liquid or solid aluminium; C is an integration constant.

Table 3-2 shows the values for the calculation of log S according to different authors.

Table 3-2 Equations for determining the solubility of hydrogen in both molten and solid aluminium

Values in the equation for determining the solubility of hydrogen in both molten and solid aluminium					
$log_{10} S = -\frac{A}{T} + C$		**Enthalpy of solubility ΔH [J·mol^{-1}]**	**Method**	**Year of publication**	**Reference**
Constant A	**Constant C**				
Hydrogen in liquid aluminium					
2760	2.796	52 840	Sievert	1948	RANSLEY and NEUFELD [12]
2713	2.528	51 940	Rapid quenching	1967	GRIGORENKO et al [16]
2980	3.070	57 050	Sievert	1995	LIU et al [20]
Hydrogen in solid aluminium					
2080	0.788	39 820	Sievert	1948	RANSLEY and NEUFELD [12]
3300	2.105	63 180	Saturation and extraction	1968	EICHENAUER et al [15]
3340	2.220	63 940	Vacuum solid extraction	1979	ICHIMURA et al [19]

***Note:** S is the solubility of hydrogen under standard conditions per 100 g of melt in cubic centimetres.*

Equilibrium hydrogen concentrations are found roughly at the pore interface, which neglects the bubble surface tension as implied by the theory of bubble formation in molten aluminium. The outer surfaces of the precursor can be much lower according to the partial pressure of hydrogen in the atmosphere, and the concentration around TiH_2 particles can be remarkably increased due to the continuous release of gas. These pressure gradients cause the dissolved gas to diffuse into the pores and atmosphere. The controlling factor is the diffusion coefficient:

$$D = D_0 \cdot \exp\left(-\frac{\Delta H}{R \cdot T}\right) [m^2 \cdot s^{-1}], \quad (3.21a)$$

where it reads: D_0 is diffusion frequency factor [$m^2 \cdot s^{-1}$], ΔH is the activation energy of diffusion [J· mol^{-1}], R is the gas universal constant (R = 8.314 $J \cdot mol^{-1} \cdot K^{-1}$), and T is diffusion temperature [K].
The values for calculating the diffusion of hydrogen in aluminium are given in Table 3-3. The interaction of the straining agent on the diffusion length can be determined from Eq:

$$\delta_{dif} = \sqrt{4 \cdot D \cdot t}, \quad (3.21b)$$

where it reads: D is the diffusion coefficient [$m^2 \cdot s^{-1}$], and t is diffusion time [s].

Table 3-3 Values for calculating hydrogen diffusion in aluminium

Values for calculating hydrogen diffusion in aluminium			
Metal for hydrogen diffusion	**D frequency factor value$_0$ [m s]$^{2\cdot-1}$**	**Diffusion activation energy HΔ [J· mol^{-1}],**	**Literature**
Liquid aluminium	3.8· 10^{-6}	19 260	EICHENAUER and MACROPOULOS [5]
Solid aluminium	1.1· 10^{-5}	40 950	EICHENAUER et al. [6]

For a temperature of 700 °C, which is the existing temperature of the aluminium melt (660 °C and superheating), the diffusion coefficient is D = 3.51· 10^{-7} [$m^2 \cdot s^{-1}$].

3.2.2 Gas bubble formation in molten metal

When observing the formation of a bubble in a melt, the analogy of the formation of an isolated gas bubble in water can be learned. The view presented of an isolated bubble in water is a simplified picture, but the formation of foam bubbles in a melt can be imagined as a combination of the interaction of individual gas bubbles.

a) Bubble expansion in a viscous liquid

A simplified view of the behaviour of an isolated growing bubble in a liquid is often used to gain a first understanding of expansion, especially of polymer foams [1]. The evolution of bubbles in the environment vicinity of a gas source adapted for metallic ALPORAS foams has been studied [36]. The physical-mathematical description of gas bubble growth is very complicated. The process depends on diffusion, momentum and mass balance. After introducing a complete system of equations, asymptotic solutions for simplified growth with limited applications are presented in this section. An isolated spherical bubble is considered an infinitely extended incompressible Newtonian fluid (the behaviour can be described by the law of viscosity) with constant viscosity. Gravity is neglected here. The dissolved gas forms a bubble due to thermodynamic equilibrium at the gas-melt interface and due to diffusion. The system is isothermal and the physical properties remain constant. Then, the continuity and momentum equations must be combined in spherical coordinates to the Rayleigh equation, according to THIESE [29]. According to the research of KÖRNER [1], bubble expansion may be suppressed by viscous, capillary or inertial forces during foam production (e.g. Integral Foam Moulding). This can be based on experience. For example, if a heated bottle of mineral water is opened, the formation of gas bubbles is very rapid. It is also expected that gas bubbles will develop very quickly, e.g. within
a fraction of a second. The viscosity of the semi-liquid metal plays an important role during the solidification of the melt in the production of metal foam, which is much higher compared to a completely liquid melt. In addition, the surface tension of metals is also about ten times higher than that of water.

In her investigations of the melt foaming process, KÖRNER [1] studied the effect of relevant pressures on the gas bubble. In doing so, she considered the expansion kinetics of an isolated bubble having a radius R. The bubble was observed in an

infinitely expanded incompressible liquid with viscosity and under pressure. The high symmetry of this problem allows the introduction of spherical coordinates, thus reducing the governing Navier-Stokes equations (3.1) and (3.2), to the so-called Rayleigh´s equation according to KÖRNER [1], which describes the time evolution of the bubble for radius R, using the first and second derivatives:

$$\dot{R} \equiv \frac{dR}{dt};\ \ \ddot{R} \equiv \frac{d^2R}{dt^2}. \tag{3.22a}$$

The notation of the Rayleigh´s equation according to THIESE [29]:

$$\boldsymbol{R \cdot \ddot{R} + \frac{3}{2}\dot{R}^2 + 4\nu \cdot \frac{\dot{R}}{R} = \left(p_G - p_\infty - \frac{2\cdot\sigma}{R}\right)/\rho,} \tag{3.22b}$$

where: R = R(t) is bubble roundness growth function, ν is kinematic viscosity, p_G is the gas pressure in the bubble, p_∞ is the melt pressure on the bubble, σ is melt surface tension, and $\rho$is the melt density.

The notation of the Rayleigh´s equation according to KÖRNER [1]:

$$\boldsymbol{R \cdot \ddot{R} \cdot \rho + \frac{3}{2}\dot{R}^2 \cdot \rho + 4 \cdot \nu \cdot \rho \cdot \frac{\dot{R}}{R} + \frac{2\cdot\sigma}{R} = p_i - p_0,} \tag{3.23}$$

where: p_i is bubble pressure; p_0 is atmospheric pressure.

The individual terms in equation (3.23) define these pressures:
Inertial pressure:
$\boldsymbol{R \cdot \ddot{R} \cdot \rho + \frac{3}{2}\dot{R}^2 \cdot \rho;}$
Viscous pressure:
$\boldsymbol{4 \cdot \nu \cdot \rho \cdot \frac{\dot{R}}{R};}$
Capillary pressure:
$\boldsymbol{\frac{2\cdot\sigma}{R}};$
Bubble overpressure:
$\boldsymbol{p_i - p_0}.$

Comparing equations (3.22b) and (3.23) in this notation, they are identical, but THIES in his paper [29] gives the multiplication on the right-hand side ρ.

The Rayleigh equation essentially expresses the balance between inertial, viscous and capillary forces that prevent the bubble from expanding. The important parameter is the overpressure inside the bubble. The question is what is the dominant position of the inertial, viscous or capillary forces. If they do, then they inhibit the expansion of the bubble. If not, then the inertial and viscous forces on the left-hand side of equation (3.26) are very small, and a balance between bubble pressure, external pressure and

capillary pressure can be assumed. In metal foam production, these forces depend on the material and also on the process parameters of the foaming process.

To estimate the pressures, it is necessary to assume that the temporal increase in the volume of the bubble ***V*** is proportional to its area:

$$\frac{dV}{dt} = \dot{V} = 4 \cdot \pi \cdot R^2 \cdot \frac{dR}{dt}, \qquad \textit{with the condition } \dot{R} = \frac{dR}{dt} = konst. \tag{3.24}$$

Under this assumption, the time t_f necessary to reach the final bubble radius R_f is given by:

$$t_f = \frac{R_f}{\dot{R}} \tag{3.25}$$

Fig. 3.5 shows the graphical dependence, according to equation (3.23), of the so-called inertial viscous and capillary pressure for a gas bubble (bubble velocity $\dot{R}$ = 0.0025 m·s^{-1}; kinematic viscosityν = 0.001 m^2·s^{-1}; surface tension of the aluminium melt σ = 0.8 N·m^{-1}; density of the aluminium meltρ = 2400 kg·m^{-3}), which propagates in the aluminium melt. A bubble velocity of 0.0025 m·s^{-1} corresponds to the evolution of a bubble with a radius of 500 µm (0.5 mm) during a time instant of 0.2 s.

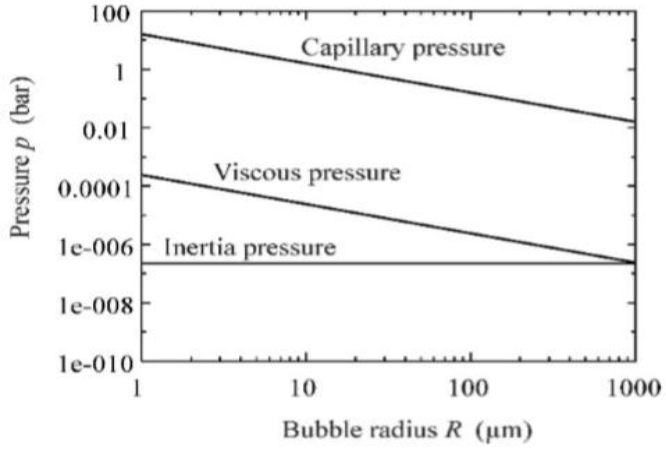

Bubble velocity: $\dot{R}$ = 0.0025 m·s^{-1}; kinematic viscosity: ν = 0.001 m^2·s^{-1}; surface tension of the aluminium melt: σ = 0.8 N·m^{-1}; density of the aluminium melt: ρ = 2400 kg·m^{-3}; 1μm = 0.001 mm, [1]

Fig. 3.5 Pressure dependence during expansion of one bubble in an aluminium melt

It is also possible to observe the effect of the diffusion process on the growth and expansion of the gas bubble in the viscous melt. The dissolved gas in the melt diffuses into the bubble at thermodynamic equilibrium at the gas-melt interface. The diffusion is described by the equation:

$$\partial_t c + u \cdot \partial_r c = \frac{D}{r^2} \partial_r (r^2 \partial_r c), \tag{3.26}$$

where: c is concentration; D is diffusion coefficient [$m^2 \cdot s^{-1}$]; u is radial velocity ($u = \dot{R} \cdot R^2/r^2$).

Equation (3.26) is valid for the condition r > R. The following equation solves the stability relation of the mass on the bubble surface:

$$\frac{d}{dt}\left(\frac{4}{3} \cdot \pi \cdot \frac{1}{V_m} \cdot R^3\right) = 4 \cdot \pi \cdot R^2 \cdot D \cdot \left(\frac{\partial c}{\partial r}\right)_{r=R}, \quad (3.27)$$

where: V_m is the molar volume of the ideal gas ($V_m = RT/p^0$); c is concentration [$mol \cdot m^{-3}$].

Equations (3.28) and (3.29) depend on the initial and boundary conditions. Thus, for example, R(0) = R_0 or 0; $\dot{R}(0) = 0$; c(r,0) = c(∞,t) = c∞; c(R,t) = c_R is given by Sievert's law (3.16).

As stated by THIES [29], surface tension can only play a significant role in the early stages when the bubble is very small. This is when the factor $2\sigma/(R\, p_{0\infty})$ is large. The solution simplifies when a stationary diffusion process is assumed. Also, the concentration away from the bubble remains constant, c∞, then equation (3.28) gives a solution of the form c (r) = k_1 /r + k_2. Using the boundary conditions, the constants k_1, k_2 and the concentration gradient (∂c / ∂r) r = R = (c∞ -c_R) / R = cΔ / R. For the radius R, one can write:

$$R(t) = \sqrt{2 \cdot c_\Delta \cdot V_m . D \cdot t + R_0^2}, \quad (3.28)$$

According to [1], the parameter β can be introduced the symptotic solutions is set as follows.$\sqrt{1/2 \cdot c_\Delta \cdot V_m} \to 0$. If $\beta >> 1$ the following approximation can be written:

$$R(t) \cong 2 \cdot \sqrt{\frac{3}{\pi}} \cdot c_\Delta \cdot V_m \cdot \sqrt{D \cdot t} + R_0 \quad (3.29)$$

For the foaming process, according to [1], in the production of metal foams, the following values can be used, the temperature of the aluminium melt is 700 °C + 273 = 973 [K]: $V_m = RT / p^0 = 8.314 \cdot 973 / 101\,325$ [$m^3 \cdot mol^{-1}$] = 0.08 [$m^3 \cdot mol^{-1}$]; $c_\Delta = 7.6 \cdot 10^{-4}$ [$mol \cdot kg^{-1}$] = $2.4 \cdot 10^3$ [$kg \cdot m^{-3}$] =1.9 [$mol \cdot m^{-3}$] assuming a supersaturation of approximately one atmosphere in a 700 °C aluminium melt. The parameter β is about 0.3, which is, unfortunately, in the middle of the two asymptotic solutions. The result of the calculation according to [29] is:

$R(t) = 3{,}2 \cdot 10^{-4}\sqrt{t/s}[m]$ $\quad for\ the\ equation\ (3.28),$

$R(t) = 1{,}7 \cdot 10^{-4}\sqrt{t/s}[m]$ $\quad for\ the\ equation\ (3.29).$

For example, calculating a bubble of size about ∅ 1 mm, its evolution takes 10 to 35 s, depending on the chosen equation. Actual melt-foaming times range from a few seconds to several minutes, depending on the chosen heating rate. In the powder metalurgy-based foaming process, hydrogen is usually continuously supplied to the melt by the decomposition of TiH_2. It should be added that the temperature of the process affects the decomposition of TiH_2 and, consequently, the hydrogen concentration in the melt. The value of the hydrogen concentration at the bubble surface is a fundamental parameter for bubble growth.

The equilibrium of a spherical bubble is based on equation (3.23). The behaviour of the bubble in the melt can be evaluated based on Laplace's law according to THIESE [29]:

$$p_G - p_L = \sigma \cdot k = \frac{2 \cdot \sigma}{R}, \tag{3.30}$$

where: p_G is the gas pressure in the bubble; p_L is pressure in the melt; σ is surface tension at the interface of the melt-gas systems (the surface tension of molten aluminium is 0.9 $N \cdot m^{-1}$); 2/R is local curvature of the bubble, κ is constant, resp. resistance, which results from the average local curvature (in the case of equal radii); p_l is pressure in the melt, which consists of hydrostatic pressure ($p_H = h \cdot \rho \cdot g$) and atmospheric (or ambient) pressure p_0 (p_0 = 101 325 Pa).

The melt pressure p_L is calculated based on hydrostatic pressure and atmospheric pressure:

$$p_L = h \cdot \rho \cdot g + p_0, \tag{3.31}$$

whe: h is the distance between the centre of the bubble and the atmosphere (i.e. to the surface of the melt), g is gravitational acceleration 9.81 $m \cdot s^{-2}$, p_0 is atmospheric pressure (101325 Pa or 10^5 Pa).

Substituting equation (3.31) into equation (3.30) gives the relationship for calculating the pressure in the bubble.

$$p_G - (h \cdot \rho \cdot g + p_0) = \frac{2 \cdot \sigma}{R}, \tag{3.32a}$$

$$p_G = \frac{2 \cdot \sigma}{R} + (h \cdot \rho \cdot g + p_0), \tag{3.32b}$$

Based on equation (3.32b), the pressure in the bubble can be calculated informatively for the following values of the quantities: p_0 = 101 325 Pa; h = 0.1 m; σ = 0.9 $N \cdot m^{-1}$; R = 10 μm = $1.0 \cdot 10^{-5}$ m; ρ = 2400 $kg \cdot m^{-3}$ (density of the aluminium melt). The result of the calculation of p_G is 283679 Pa (283.7 kPa). Of this, the internal pressure of the gas in the bubble is 180,000 Pa (180 kPa), the hydrostatic pressure is 254 Pa (254 kPa), and the atmospheric pressure is 101,325 Pa (101.4 kPa). At the

beginning, when the bubble nucleus is formed, there is a value of R on the order of about
R = 10 µm. The effects of surface tension contribute significantly to the formation of a gas bubble. The hydrostatic pressure is, in comparison, compared to the ambient pressure. However, it is responsible for the buoyant force acting on the bubble. Under stationary conditions, the buoyancy force is given by Stoke's law, and the velocity of bubbles in the melt is given by equation (3.35).

b) Bubble exposed to gravity

The bubbles quickly dissolve in the liquid. This effect can be caused by a density gradient (e.g. during IFM Integral Foam Moulding), see Fig. 3.6b).
In the following, a single gas bubble is observed in the infinite melt space. The bubble rises against the pull of gravity and eventually reaches a stationary velocity ***v***, where the gravitational force is balanced by the buoyant force. If the deformation of the bubble is negligible, the stationary rising velocity ***v*** results from the balance of force between the gravitational force given by Stokes's law and the buoyancy [32]. The stationary velocity ***v*** for the emergence of an air bubble to the surface of the melt can be derived by assuming that forces are acting on the gas bubble*:*

a) buoyant force of the bubble - $F_{VZ;}$
b) resistive force of the bubble - F_{OD}

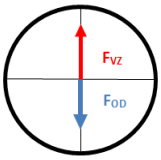

Fig. 3.6a) Schematic of the forces acting on a bubble of radius R

$$F_{VZ} = V_B \cdot \rho_K \cdot g, \qquad (3.33\ a)$$
$$F_{OD} = 4 \cdot \pi \cdot R \cdot \eta \cdot v, \qquad (3.33\ b)$$

where it reads: R is the radius of the gas bubble [m], η is the dynamic viscosity of the melt
[Pa· s; kg·s^{-1}·m^{-1}], v is velocity of the gas bubble escape to the melt surface [m·s^{-1}]; V_B is the volume of the air bubble [m^3], assuming the air bubble is spherical then $V_B = 4/3 \cdot \pi \cdot R^3$; ρ_K is the density of the melt being gassed [kg·m^{-3}], g is the gravitational acceleration [m·s^{-2}], and ν is the kinematic viscosity of the melt [m^2·s^{-1}], $\nu = \eta / \rho$.

Illation of the (stationary) velocity of the air bubble in the melt under the conditions $F_{VZ} - F_{OD} = 0$, i.e. $F_{VZ} = F_{OD}$:

$$V_B \cdot \rho_K \cdot g = 4 \cdot \pi \cdot R \cdot \eta \cdot v \qquad (3.33c)$$

$$v = \frac{1}{3} \cdot \frac{R^2 \cdot g}{\nu} \qquad (3.33d)$$

The quadratic dependence of the bubble radius to determine the stationary velocity clearly shows that a small bubble radius contributes to a smaller stationary velocity. Conversely, a large value of kinematic viscosity also contributes to a lower value of stationary velocity.

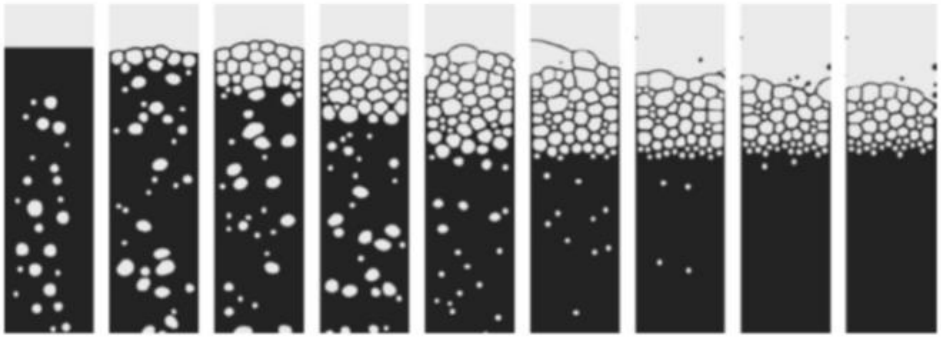

Fig. 3.6b) Schematic of a bubble exposed to gravity and illustration of the foam formed (2D - LBM simulation), according to [1]

If the bubble velocity satisfies the assumption of equation (3.33d), the bubble distance ***d*** can be determined:

$$d = \int_0^{tf} v\big(R(t)\big) \cdot dt = \int_0^{tf} \frac{g}{3 \cdot \nu} \cdot R^2 \cdot dt = \frac{g}{9 \cdot \nu} \cdot \dot{R}^2 \cdot t_f^3 = \frac{g}{9 \cdot \nu} \cdot R_f^2 \cdot t_f \qquad (3.34)$$

R =$\dot{R}t$; $\dot{R} = konst.$, assumption R_f =0.5 mm; dynamic viscosity of the aluminium melt: η = 0.001 [Pa·s], the kinematic viscosity of the aluminium melt is 0.001/2300 = $4.35 \cdot 10^{-7}$ $m^2 \cdot s^{-1}$; t_f = 0.2 s; g = 9.81 $m \cdot s^{-2}$; distance: d = $5.45 \cdot 10^{-5}$ m, i.e. 0.0545 mm, (density of molten aluminium: ρ = 2400 $kg \cdot m^{-3}$).

THIESE [29] gives an essentially analogous relationship for determining the bubble velocity according to Stokes' law:

$$v = C \cdot \frac{g \cdot R^2}{\nu}, \qquad (3.35)$$

where: ν is the kinetic viscosity of the melt; C is a factor depending on the bubble surface; C = 1/3, i.e. for a bubble moving in the melt. If C = 2/9, then the motion of the solid particle in the melt is solved.

In a melt of pure aluminium, the kinematic viscosity is $\nu = 6 \cdot 10^{-7}$ [$m^2 \cdot s^{-1}$] at 700 °C [43]. The viscosity value depends on the melt temperature. If the melt temperature increases by 100 °C, the viscosity value decreases by 20%. This means that at a temperature of 800 °C, the viscosity of a pure aluminium melt will be about $\nu = 4.8 \cdot 10^{-7}$ [$m^2 \cdot s^{-1}$].

A spherical bubble with a size of ∅ 50μm, that is, a volume of 20 833 [mμ^3], moves with a velocity ***v*** of 10 mm·s^{-1} (v = 0.01 m·s^{-1}).

c) Interaction between bubbles

The primary interaction between bubbles is the result of hydrodynamic forces produced by the velocity field, which is induced by the motion of the bubbles or their expansion. As a result, bubbles deform, but capillary forces try to restore the spherical shape of the bubbles due to the minimization of surface energy.

Transient gas cell walls, the simplest situation of two expanding bubbles, is shown in Fig. 3.7. This fig. also shows the evolution of transient cell walls. Transient cell walls result from the rapid expansion of bubbles, which brings the system into equilibrium to form a round bubble. Transitional cell walls evolve dynamically and are intrinsically unstable; that is, they disappear if the system takes a long time to reach an equilibrium state.

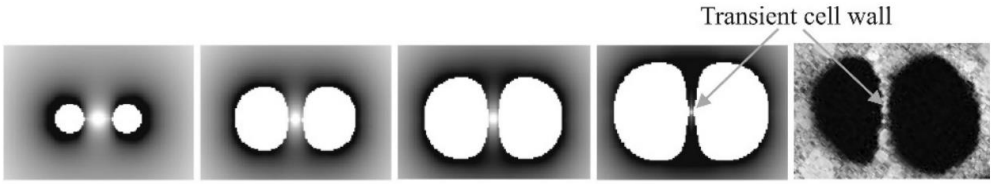

Fig. 3.7 Schematic of the interaction between two bubbles and the evolution of the transition cell wall, left: 2D-LBM simulation (white is the bubble, grey color around indicates the velocity field; small velocities are indicated by light grey color, large velocities are indicated by dark grey color); right: there are two gas bubbles in solidified magnesium, AZ91 alloy, KÖRNER transition walls, [1]

The conditions in the melt for asymmetric bubble growth and the bubbles become increasingly deformed as they expand. The magnitude of this effect depends on the surface tension of the melt, the viscosity of the melt, the growth rate and the size of the bubbles.

Fig. 3.8 shows a schematic of the capillary forces in the transition wall of a gas bubble (cell). The pressure difference between the cell walls and the plane edges leads to a rapid thinning of the cell wall (overpressure is indicated by **+ (plus)**; under pressure is indicated by **- (minus)**, [1]. Capillary pressure differences lead to overpressure in the walls and low pressure at their boundaries. Low pressure leads to rapid thinning of the cell wall and eventually to cell wall rupture. In the production of metal foams, the melt will rearrange under the influence of capillary forces. The formation of transient cell walls is an important mechanism in the formation of the resulting metal foam.

In principle, it should be possible to produce highly porous, foamed metallic structures without the formation of transient cell walls.

For this reason, it is important to address the durability of transient cell walls in the production of metal foams.

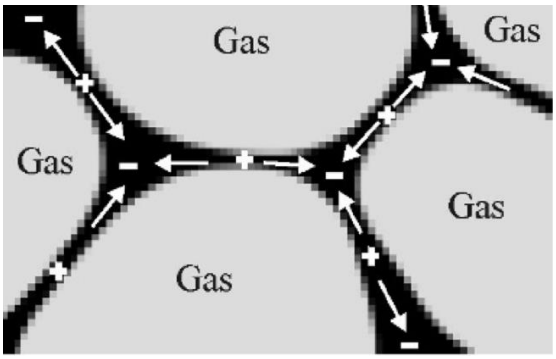

*Fig. 3.8 Schematic of capillary forces in the transition wall of a gas cell; the pressure difference between the cell walls and the edges of the planes leads to a rapid thinning of the cell wall (overpressure is marked **+ (plus)**; pressure is marked **- (minus)**, [1]*

The solution of the durability of cell wall transitions was performed by KÖRNER [1]. She performed the calculation using a simple cell wall model. If R_{PI} denotes the radius of curvature of the cell surface, then the pressure difference Δp between the surface boundary and the cell wall can be determined:

$$\Delta p = \frac{\sigma}{R_{PI}}, \tag{3.36}$$

where: σ is surface tension; R_{PI} is the radius of curvature of the bounded area.

Cell wall thinning rate $\dot{d}$ is defined according to [21], and at the same time, the relation (3.36) can be substituted after p.Δ

$$\dot{d} = \frac{2 \cdot d^3 \cdot \Delta p}{3 \cdot \eta \cdot R^2} = - \frac{2 \cdot d^3 \cdot \sigma}{3 \cdot \eta \cdot R^2 \cdot R_{PI}}, \tag{3.37}$$

where: R is the curvature of the surface projection of the bulb; η is the dynamic viscosity of the melt; Δp is the pressure difference between the wall and the volume, which is defined by the capillary pressure, its calculation is according to equation (3.36).

The integration of equation (3.37) gives the time ***t***, which is the thinning time of the cell wall. In doing so, some stability of the cell wall thickness is still maintained even though the cell wall thickness changes from an initial thickness d_i to a final thickness d_f:

$$t = \frac{3 \cdot \eta \cdot R^2 \cdot R_{PI}}{4 \cdot \sigma} \cdot \left[\frac{1}{d_f^2} - \frac{1}{d_i^2} \right] < \frac{3 \cdot \eta \cdot R^2 \cdot R_{PI}}{4 \cdot \sigma} \cdot \frac{1}{d_f^2} \tag{3.38}$$

By plugging the specific data into equation (3.37), the observed time t can be calculated.

Reference [1] suggests a calculation with the following values given: σ = 0.8 $N \cdot m^{-1}$; $\eta = \nu \cdot \rho$; ρ = 2.4 $g \cdot cm^{-3}$ (2400 $kg \cdot m^{-3}$); R_{Pl} = 100 µm; R = 250 µm; d_f = 10 µm. The wall thickness thinning time given by KÖRNER [1] is $t < 10^{-4}$ s.

Based on the above, our wall thinning calculation was performed, according to equation (3.38). The following values were used for the calculation: surface tension of the aluminium melt σ = 0.8 $N \cdot m^{-1}$; dynamic aluminium viscosity $\eta = \nu \cdot \rho = 1.44 \cdot 10^{-3}$ [$kg \cdot m^{-1} \cdot s^{-1}$]; kinematic aluminium viscosity $\nu = 6 \cdot 10^{-7}$ [$m^2 \cdot s^{-1}$]; density pure aluminium melt ρ = 2400 $kg \cdot m^{-3}$; R_{Pl} = 100 µm (R_{Pl} = 0.1 mm = 0.0001 m), R = 250 µm (R = 0.25 mm = 0.00025 m); d_f = 10 µm (d_f = 0.01 mm = 0.00001 m).

$$t < \frac{3 \cdot 1{,}44 \cdot 10^{-3} \cdot 6{,}25 \cdot 10^{-8} \cdot 1{,}0 \cdot 10^{-4}}{4 \cdot 0{,}8 \cdot 1{,}0 \cdot 10^{-10}} < 8{,}44 \cdot 10^{-5}\, s;\ \ to\ je\ cca\ \ t < 10^{-4}$$

This result shows that cell wall thinning is a very rapid process. The thinning time is so short that the development of extensive straight cell walls requires additional stabilization to reduce thinning. However, when the viscosity is strongly increased, e.g. by three orders of magnitude, that is, in the case of solidification, as reported by [1], the cell wall thinning time approaches the same time scale as the entire foaming process. Thus, the short production time of the metal foam, combined with the increased viscosity during melt solidification, has the potential to promote the formation of transient cell walls without further stabilization. This is probably the reason why stabilizing agents must be used during foaming.

3.3 Theoretical Basis for Stability Description of Metallic Cellular Systems

From a theoretical point of view, there is no universal description of foam stability, as stated by KÖRNER [1]. Initially, it was assumed that the stability of the foam was due to adsorbed surfactants that affected the mechanical-dynamic properties of the surface layer. The first approaches to explain foam stability were based on the idea of Gibb´s and Marangoni, who started from the idea of the importance of viscosity and surface elasticity. However, these early theories failed to explain the high stability of the formation of thin films in the cell wall of metal foam. This issue was addressed by Russian researchers in the middle of the 20th century, and the influence of static disjoint pressure induced by intermolecular forces was studied. At the same time, it became clear that it was necessary to distinguish between the dynamic and static stability of the foam. Dynamic stability is generated by forces that develop, for example, during viscous tension, whereas static stability includes all mechanisms that generate static forces, such as electrostatic repulsion. Particular emphasis must be placed on the role of solid particles with replication on foam stabilisation. The stability of metallic foams has been controversially discussed in the literature, but a definitive, generally acceptable stability theory is still lacking, as reported by [1].

The following section summarizes the main aspects of metal foam stabilization, to which is the mechanism of the barrier effect caused by particles enclosed in cell walls contribute [22]. For different foaming methods, the particles act as a barrier that supports the foam formation mechanism. They can be either solid particle (fragile mesh or endogenous particles). Their barrier effect always induces an uncoupling pressure, which is responsible for foam stabilization. This realisation is the basis for explaining the stabilisation of foam produced mainly by *IFM (Integral Foam Moulding).* The first studies to reveal the mechanisms of metal foam stabilization were focused on monitoring the importance of the viscosity and surface tension of the melt [23]. High melt viscosity values retard cell wall thinning and thus have a positive effect on foam durability. It has been confirmed that the stabilization of metal foam is closely related to a high melt viscosity value [24]. This idea was supported by several experimental observations [23], [24]. Fig. 3.9 shows aluminium foams; the top part is the cell structure of the foam, and the bottom part is the cell wall. On the left is foam produced by direct frothing of melt containing SiC particles, [26]; on the right is foam produced by powder metallurgy using TiH frothing agent$_2$ [27].

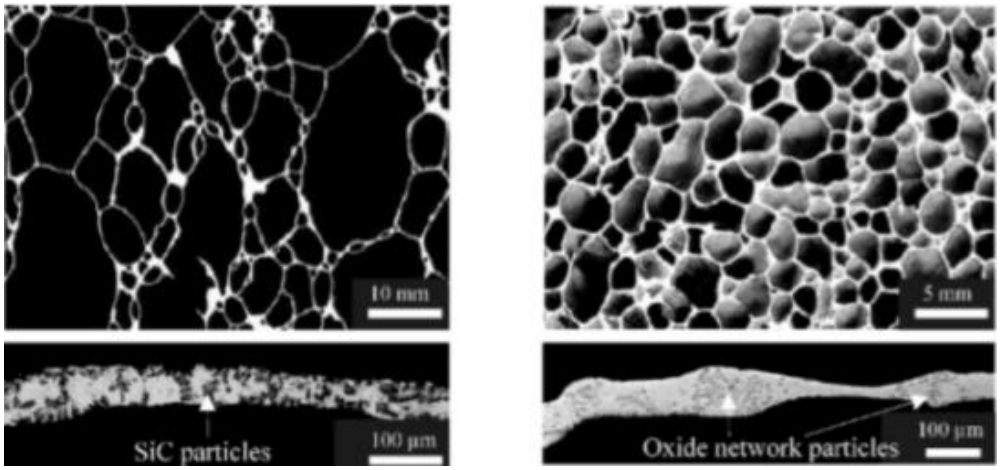

Fig. 3.9 Aluminium foam, top is the cell structure of the foam, bottom is the cell wall; left: is foam produced by direct frothing of melt containing SiC particles, [26]; right: is foam produced by powder metallurgy using TiH frothing agent$_2$ [27].

During the process, for example, calcium is added to the aluminium melt and stirred for several minutes until the viscosity reaches a certain value that is 3 to 4 times higher than the initial viscosity. Subsequently, a foaming agent in the form of TiH_2 is added. The quality of the resulting metal foam is very sensitive to the viscosity of the melt [25]. Another example is aluminium foams reinforced with SiC particles [26], see Fig. 3.9. These foams are produced by gas injection into a composite melt of a metal matrix. The particle size typically ranges from 5 to 20 μm.

If the particle volume is too low, the gas injected into the melt contributes to the disappearance of bubbles in the upper parts of the melt. Achieving a stable foam is

only possible when the volume fraction of SiC particles is sufficiently high, which is also supported by a high melt viscosity value.

The basic characteristics of metal foams are closely related to the following criteria:
High stability - in general, the metal foamed mass is stable. Foams produced by various methods can be kept in a liquid state for more than one hour without changing their internal structure [22]. On the other hand, real-time X-ray diffraction reveals that cell wall rupture processes take place within 50 ms [28]. These properties are characteristic of stable foams, where their stability is mainly due to the static interfacial force, [1].
Thick cell wall foams, typically metal foams, exhibit thick cell walls of about 101 to 102 μm (0.101 to 0.102 mm), see Fig. 3.9. The cell walls contain a relatively large volume fraction of material.
The critical cell wall thickness of PM foams (foams produced by powder metallurgy) depends on several circumstances. During the production of metallic foams based on powder compacts (PM foam), cell coalescence processes take place throughout the expansion process [28].
Wall rupture occurs when the walls have an average thickness of 50 μm and thinner cell walls are even more unstable.
Special cell wall foams, which are often typical of metallic foams, exhibit strong and irregular thickness changes along the cell walls [22], see Fig. 3.9. These walls are highly unstable. This instability is also influenced by the capillary forces manifested.
Non-ideal but stable cellular structures are cellular structures that are far from thermodynamic equilibrium if we assume that the surface energy of the structure must be minimized to produce foam, see Fig. 3.9. Cell wall mobility and boundaries exhibit planar formations and are very attenuated.

As stated by KÖRNER [1], the relationship between the mean cell diameter D and the phase ratio ∅**:**

$$D \propto \emptyset = \frac{1}{\rho_{REL}} - 1, \; pro\, \emptyset > 1, \tag{3.39}$$

where: ρ_{REL} is the relative density of the foam.

Mean cell diameter D and phase ratio are correlated [22].

3.4 Dynamic stabilization of cellular systems by surfactants

The thickness of the gas cell walls (cell walls) is closely related to the surfactants that are absorbed in the melt-cell wall interface. These surfactants control the mechanical-dynamic properties of the surface layer, which exhibits surface elasticity and surface viscosity. Surface viscosity affects the relaxation rate of applied external stress, while surface elasticity is a measure of the energy stored in the surface layer due to surface tension. One of the effects of surfactants is to retard cell wall thinning by increasing surface viscosity [2] and surface elasticity. High concentrations of

surfactants, polymers or particles on the surface cause high adhesive or cohesive bonding which increases both surface viscosity and surface elasticity see Fig. 3.10.

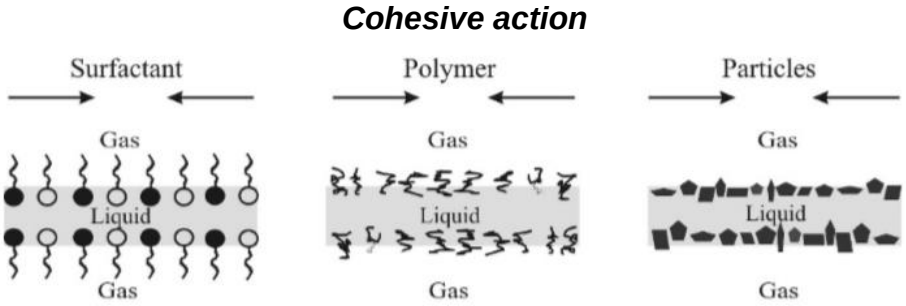

Fig. 3.10 Schematic of the effect of different types of surfactants acting at the melt-gas interface. Mixed surfactant system (left); polymer influence (centre); particle influence (right), after LANGE, [2].

According to [2], the effect of surface viscosity on the rate of cell wall thickening can be explained as follows. For high values of surface viscosity, the two adsorption layers behave almost like rigid membranes and are unable to follow the vertical motion of the liquid. In this case, the "drainage" between the solid walls follows the rules for the liquid. If the surface viscosity is low, the absorption layer is mobile and can eliminate the movement of the liquid. The starting point for cell wall rupture is a local thinning of the wall (film-like thinness). This thinning must eliminate stabilizing forces. Theories describing stabilization have been described by Gibbs and Marangoni, and reference is made in reference [3]. Gibbs describes the fact that local thinning of the film also leads to a local reduction in the surfactant representation. Fig. 3.11 shows a schematic of the Gibbs-Marangoni mechanism of dynamic foam stabilization (a) the original state of the thin film; b) the higher local surface tension due to local thinning of the layer; c) the difference, resp. Surface tension gradient that pulls surfactant molecules into the thinned section; d) surface film repaired by surface transport mechanism). The surface tension gradient induces forces that are affected by the surfactant concentration.

If the surfactant concentration is too low, the induced force is also low. At very high surfactant concentrations, the result is maximum foam stability as a function of surfactant concentration, [2] and [3]. In addition to the forces induced by the surface tension gradient, there is another effect that is attributed to Marangoni. When the surfactant concentration is locally reduced, inhomogeneously dispersed solids move over the surface.

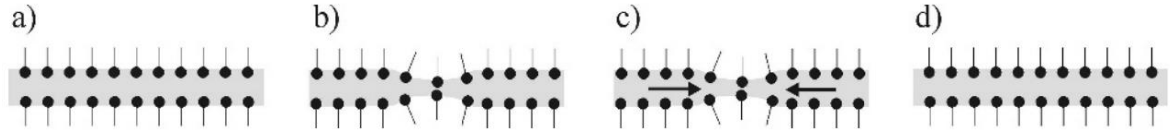

Fig. 3.11 Schematic of the Gibbs-Marangoni mechanism of dynamic foam stabilization, a) original state of thin film, b) higher local surface tension due to local thinning of the layer, c) difference or gradient of surface tension pulls surfactant molecules into the thinned section, d) surface film corrected by surface transport mechanism

As a result, the thin liquid film near the surface is transported due to viscous tensile forces. Thus, a current is present near the surface from regions of low surface tension (high concentration) to regions of high surface tension (low concentration). As stated by KÖRNER [1], it is important to keep in mind that both Gibbs and Marangoni effects are not sufficient to explain the existence of stability of foams where the thickness of the cell walls is more or less constant. This means that both effects only characterize the wall behavior of transient foams. These effects are not able to explain the stability of permanent foams.

3.5 Stabilization of cellular systems foam by static forces

A prerequisite for the development of permanent foam is the presence of static stabilizing forces. These forces act against suction and represent a kind of vacuum in the cell walls. The different sources of static forces are discussed according to KÖRNER [1] in the following.

The uncoupling pressure, equilibrium or static stability of thin films or cell walls is extremely important. Foam films gradually drain away by gravitational or capillary forces. Since capillary forces always tend to reduce film thickness, there must be an additional force, termed "disjunctive pressure" Π, to counterbalance the capillary forces. If the "disjunctive pressure" Π is positive (repulsive forces), film formation is suppressed. Otherwise, attractive forces act. In general, the "disjunctive pressure" Π is calculated as the sum of three components [1]:

$$\Pi = \Pi_{EL} + \Pi_{W} + \Pi_{ST} \, , \tag{3.40}$$

where: Π_{EL} is repelling the electrostatic force of two layers on both surfaces; Π_{W} is the force due to van der Waals interaction; Π_{ST} is the force from spherical or structural interaction caused by a spherical barrier in the layer.

The range of forces Π_{EL} and Π_{W} is very small 10^{-9} m or even smaller. As a result, foams stabilized by electrostatic repulsion of two layers develop very thin stable cell walls (<1 nm), which are commonly referred to as "black films".

We observe the magnitude of the uncoupling pressure concerning the wall thickness ***d***. The stability of the wall is guaranteed as $\partial\Pi/\partial d < 0$. For the growth of instability and subsequent wall rupture, it is necessary that $\partial\Pi/\partial d > 0$. The behaviour of the uncoupling pressure depends on other circumstances. Fig. 3.12 shows one typical example where wall rupture occurs for the case $d < d_{crit}$ (wall thickness is less than the critical size). Thus, wall breakage is only possible when the "capillary" pressure exceeds the maximum uncoupling pressure. For Π, see Fig. 3.12, the stability criteria for the metal foam cell wall are given in reference [21].

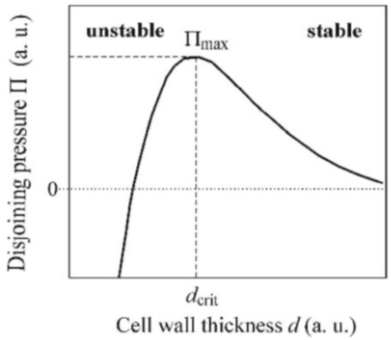

Cell wall thickness d (a.u.), approx. 10^{-10} m

Fig. 3.12 Schematic diagram of the magnitude of the uncoupling pressure as a function of cell wall thickness [1]

The cell wall (the cell wall is stabilized if the wall thickness is greater than the critical size (d_{crit}). Smaller wall thicknesses lead immediately to cell wall rupture. The equilibrium cell wall thickness can be calculated:

$$\frac{\sigma}{R_{PI}} - \Pi(d) = 0, \tag{3.41}$$

where: σ is surface tension, R_{PI} is the radius of curvature, Π (d) is disconnection force at cell wall thickness d.

Consequently, the equilibrium thickness is not only determined by the disjunctive pressure but also by the magnitude of the suction effect due to surface tension. The magnitude of the dissipative pressure can be estimated from the average curvature and surface tension. High disjunction pressure leads to small radii of curvature R_{PI} of the cell boundary surfaces. Thus, very sharp surfaces on the cells are an indication of the presence of high uncoupling (disjunction) pressure. The thickness of the cell wall is satisfactory if a balance is achieved between the forces of the so-called suction effect and the disjunction pressure [1].

3.6 Stability of gas bubbles through stabilising particles

Most metal foams are created based on two-phase systems: gas with melt and containing a stabilizing agent (surfactant). However, we study foams as three-phase systems: gas, melt and solid particles. The dispersed particles in the melt, which are used for the production of metallic cellular materials, can stabilize the foams but also destabilize the BINKS [30].

3.6.1 Effect of dispersed particles on melt viscosity

The dispersed particles greatly increase the viscosity of the melt. The kinematic viscosity of a melt with dispersed particles can be determined:

$$\nu = \nu_0 \cdot (1 + 2{,}5 \cdot V_{REL}), \qquad \textit{for } V_{REL} < 0 \tag{3.42}$$

where denotes: ν_0 is the kinetic viscosity of the melt without particles; V_{REL} is the relative volume of particles (solid fraction content).

Equation (3.42), shows that the increase in viscosity is relatively modest up to a relative particle volume of about 10 %. For higher relative particle volume contents, there is as yet no analytical description available for the determination of viscosity. Particle size and shape are very important in this regime. RAVI [42] provides a relationship for determining dynamic viscosity with stabilizing particle content. This viscosity is referred to by the term "effective dynamic viscosity" and can be determined:

$$\eta_E = \eta_0 \cdot (1 + 2{,}5 \cdot \varphi + 10{,}25 \cdot \varphi^2), \qquad (3.42\ a)$$

where: η_0 is the dynamic viscosity of the melt without particles; φ is the volume fraction of the suspended particles.

According to WANGA [43], the effective dynamic viscosity can be calculated:

$$\eta_E = \eta_0 \cdot \left[\left(\frac{\xi \cdot \left(1+D_P^{0,95}\right)}{0.01+37.35 \cdot D_P^{0,95}}\right) \cdot \varphi\right], \qquad (3.42b)$$

where: ξ is a relative factor that includes the diameter of the particle; φ is the volume fraction of the suspended particles; D_P is the diameter of the particle [cm], and the dynamic viscosity must be based on cm.

There are various approaches that model the effect of higher particle content on melt viscosity. The most widely used is the Krieger-Doughert model for spherical particles in metallic melt [37].

$$\boldsymbol{\nu = \nu_0 \cdot \left(\frac{V_{REL}}{V_{REL}^{CRIT}}\right)^{-2{,}5 \cdot V_{REL}^{CRIT}}}, \qquad (3.43)$$

where it reads: V_{REL}^{CRIT} is critical relative particle volume, for constrained computational model networking.

Various modifications of the Krieger-Doughert model are available in the literature [38]. Chen and Fan [39] give the viscosity for a suspension of particles dispersed in a semi-liquid metal melt:

$$\boldsymbol{\nu = \nu_0 \cdot \left(\frac{V_{REL}}{V_{REL}^{CRIT}}\right)^{-2{,}5}}, \qquad (3.44)$$

Fig. 3.13a) shows the relative viscosity (ν/ν_0) as a function of the relative particle volume (V_{REL}), taking into account the critical relative paren volume (V_{REL}^{CRIT}). For low V_{REL}, the Krieger-Doughert model approaches equation (3.42), the so-called Einstein

equation. The relative viscosity ratio is very steep over a relatively narrow range of V_{REL}. Moreover, the increase in melt viscosity is relatively small up to a particle content of 30 %.

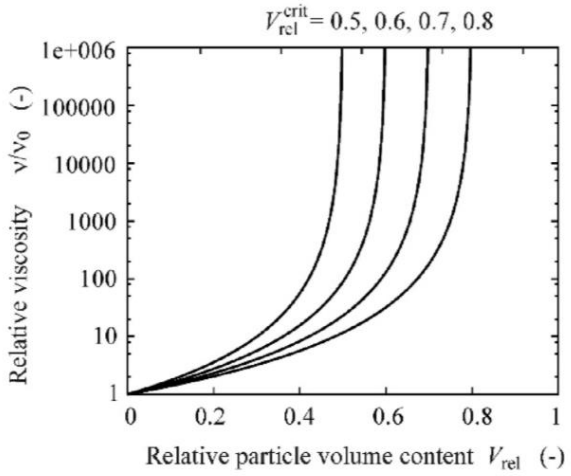

Fig. 3.13a) Viscosity of semi-liquid metal suspensions, determined according to equation (3.44), where the relative viscosity (ν_0 / ν) is a function of the relative volume of the particles, according to [1]

Fig. 3.13b) shows the relationship between the dynamic viscosity (referred to as apparent dynamic viscosity by SONG [44]) of the melt and the amount of different calcium contents mixed into the melt (stirring speed 700 rpm at a melt temperature of 973 K).

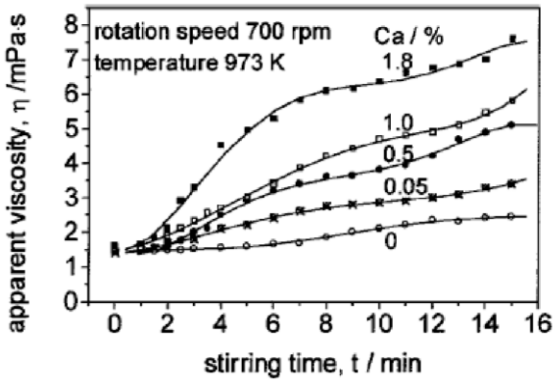

Fig. 3.13b) Relationship of dynamic viscosity of aluminium melt at different calcium content and melt mixing time (mixing speed 700 rpm at melt temperature 973 K), SONG [44]

Foam stabilization is influenced by the particles due to their ability to bridge cell walls. This effect begins to operate when the thickness of the cell wall is approximately equal to the diameter of the particles. The effect of the particles depends on their contact angleΘ with the fluid and also depends on the shape of the particles. Fig. 3.14 indicates the effect of spherical particles.

Fig. 3.14 Schematic of the effect of contact angle on effective particle bridging, a) the stability condition is 90° for $\theta \leq$; b) the instability condition is $\theta >$ 90°, according to IPA [33].

DIPPENAAR [34] was one of the first to systematically investigate the effect of contact angle and particle shape on the stabilising potential of foam. Spherical particles with $\theta \geq 90°$ stabilize foam walls (sometimes referred to as films in the literature), while the condition for particles $\theta > 90°$ accelerates foam breakdown. As stated by KÖRNER [1], the reason for stabilization is the capillary pressure that sucks the melt onto the particle. Destabilization results from the convex curvature of the surface which removes the melt from the particle. Non-spherical particles with special shapes can lead to film rupture even at the condition $\theta \leq 90°$. Therefore, it is important to observe the melt-wetting behaviour of the particles in combination with the particle shape when producing metal foam.

A high viscosity value slows down the formation of the cell wall, see equation (3.42), thus having a positive effect on the lifetime of the foam. Research [40] has shown that metal foam stabilization and high melt viscosity are closely related. This finding has been supported by experimental observations, e.g. during the production of *Alporas* foam [36], calcium is added to the aluminium melt and the melt is stirred for several minutes. This achieves the necessary increase in viscosity, which is 3 to 4 times the viscosity without stabilizing particles (viscosity of the initial melt). In this method of producing Alporas foam, a foaming agent is subsequently added, which is TiH_2. The quality of the resulting metal foam is very sensitive to the viscosity of the melt [1]. Another example is aluminium foams reinforced with SiC particles [41], see Fig. 3.15.

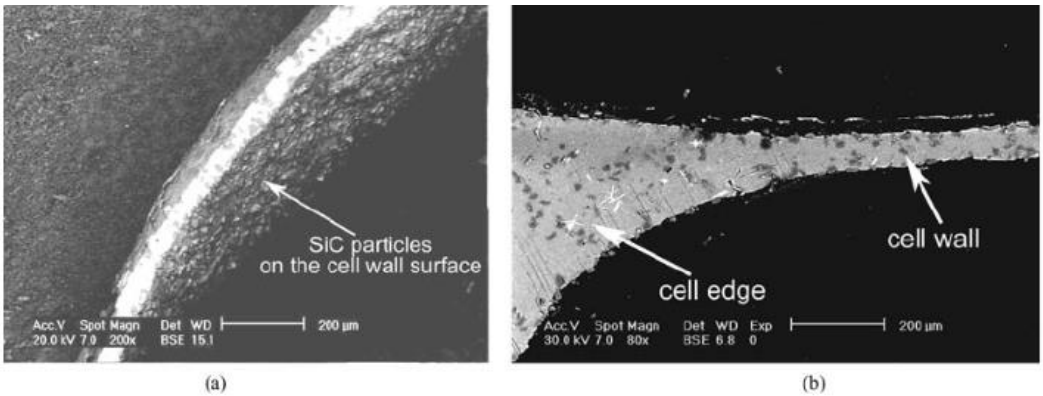

Fig. 3.15 Microstructures of aluminium foam with SiC particles a) gas cell wall surface; b) inner parts of the gas cell wall, 10 wt. % SiC was used; REM electron microscope, the foam was produced by powder metallurgy, according to [41]

The above theory of the physical nature of the foaming process relates to the production of cellular metallic materials ("metal foams"). As mentioned in the introduction, there are currently several technologies for implementing the foaming process. These foams are produced, for example, by feeding gas into a composite melt which, when solidified, forms the metal matrix of the cellular material. The size of the particles used, which positively influence the viscosity of the melt, ranges from 5 to 20 μm. If the volume of the stabilizing particles is too low, the gas fed into the melt forms bubbles in the melt which rise to the surface of the melt, where they disappear. The stability of the produced metal foam is maintained if the volume content of the stabilising SiC particles is satisfactory.

A satisfactory particle content favourably influences the viscosity of the melt, which must be sufficiently high. In direct melt foaming (e.g. Metcomb method), an amount of SiC stabilising agent of about 10 to 20 % by volume is used. In the production of metal foams by the transfer metallurgy (PM) method, a quantity of stabilising particles is also used, preferably in an amount of 10 to 20 wt. % when SiC is applied.

4. FOAMING AGENTS FOR THE PRODUCTION OF CELLULAR METAL MATERIALS

This chapter lists the foaming agents that are used for the production of cellular metal materials. In this context, it should be noted that there are various methods of producing cellular metallic materials, as can be seen, for example, from Table 1-2. The source of gas for the production of these materials is either gas from an external source, gas dissolved in the melt, or gas obtained from the decomposition of a frothing agent.

It is generally known that pure liquids or metal melts do not foam. An essential prerequisite for the development and production of foam is the necessary gas, which can be obtained, for example, by the presence of a foaming agent. In general, foaming agents can be specific adsorbed cations or anions from inorganic salts, polymers, and other particles, which can often cause foaming even at extremely low concentrations, as reported by KÖRNER [1] based on Pugh's research. From a thermodynamic point of view, foams are predisposed to achieve high interfacial free energy, but at the same time, they are also prone to low stability and decomposition. According to [1], two different classes of foams are distinguished concerning kinetics and the underlying mechanisms:

Unstable or transient foams with low durability in seconds. In this case, surfactants slow down the foaming process and weakly prevent the film between the melt and the gas bubble from bursting. As mentioned above, it is assumed that the melt foaming is the result of the Gibbs-Marangoni *effect* (Section 4.3.1. KÖRNER [1]), where the cell wall is stabilized during thinning due to the material moving towards the weakened region as a result of a local increase in the surface tension of the melt. The flow is essentially a response to the melt surface tension gradient. As a result of the viscous flow, it can carry a significant amount of the underlying fluid or melt along with it to restore the thickness of the foam walls.

Permanent or metastable foams have a theoretical shelf life of hours to days. In these systems, cell wall thinning times are relatively short compared to their lifetime. Stability is controlled by the balance of interfacial forces. These forces are balanced only after the melt's solidification is complete.

Essential for the success of the foaming process (integral foaming) of the produced cellular metal system or material is the availability and use of a suitable foaming agent (superconductor), which should have the following properties:

- ***High equilibrium dissociation pressure*** gas pressure for the produced "foam" (foam pressure) rises with the equilibrium pressure of the foaming agent (blowing agent).
- ***High foaming efficiency:*** A smaller amount of foaming agent is needed to be used for the metal melt foaming process.
- ***High value of the kinetics of rapid decomposition***, the kinetics of decomposition determines the effectiveness of the foaming agent.

- ***It must not have a detrimental effect on the alloy used***: the addition of the foaming agent must not affect the composition of the alloy. Elements that could lead to degradation of the alloy or to problems in the recycling of the metal product must be avoided.

Table 4-1 provides an overview of straining agents for the production of cellular metallic materials.

Table 4-1 Tensioning agents for the production of cellular metal systems, according to KOIZUMI [5]

Foaming agents for the production of metal "foams"				
Foaming reagents	***Sample***	***Particle size [μ m]***	***Gas***	***The equation of formation Gas***
Titanium hydride	TiH_2	26	H_2	$TiH_2 \rightarrow Ti + H_2$
Magnesium hydride	MgH_2	10	H_2	$MgH_2 \rightarrow Mg + H_2$
Magnesium hydroxide	$Mg(OH)_2$	7.4	H_2O	$Mg(OH)_2 \rightarrow MgO + H_2O$
Magnesium carbonate hydroxide	$4MgCO_3 \cdot Mg(OH)_2 \cdot 5HO_2$	11	H_2O CO_2	$4MgCO_3 \cdot Mg(OH)_2 \cdot 5H_2O \rightarrow 6H_2O + CO_2 + 5\ MgCO$
Calcium hydride	CaH_2	10	H_2	$CaH_2 \rightarrow Ca + H_2$
Zirconium hydride	ZrH_2	20	H_2	$ZrH_2 \rightarrow Zr + H_2$
Magnesium carbonate	$MgCO_3$	11	CO_2	$MgCO_3 \rightarrow MgO + CO_2$
Dolomite	$CaMg(CO_3)_2$	15	CO_2 CO_2	$CaMg(CO_3)_2 \rightarrow CaCO_3 + MgO + CO_2$ $CaCO_3 \rightarrow CaO + CO_2$
Calcium carbonate	$CaCO_3$	13.5	CO_2	$CaCO_3 \rightarrow CaO + CO_2$

Many metal-based foaming agents have been tested for the fabrication of cellular metal systems (or aluminium foams): TiH_2, SrH_2, MgH_2, $CaCO_3$ [7],[8],[9]. For example, titanium hydride, TiH_2, exhibits a decomposition temperature close to the melting temperature of aluminium alloys. Titanium hydride, TiH_2, is not always suitable for the gasification process due to too low decomposition kinetics at the melting temperatures of some aluminium alloys, [12]. Sometimes it is more appropriate to use foaming agents such as magnesium hydride MgH_2 for these purposes. Detailed thermodynamics and decomposition kinetics of MgH_2 are given in the publication by BINKS [6]. The thermodynamics provides information on the achievable foaming pressure, while the kinetics determines the rate ratios and time dependence of the decomposition of the foaming agent. Table 4-2 shows some important data on the foaming process.

Table 4-2 Properties of different hydrides [13]

Selected properties of hydrides for the production of metal "foams"			
Hydrogen, first name hydride	**Density [g·cm^{-3}]**	**Hydrogen [wt. %]**	**Volume weight of hydrogen [H atoms· cm^{-3}· 10 ^{22}]**
H_2, liquid (20 K)	0.071	100	4.2
MgH_2	1.40	7.6	6.7
TiH_2	3.80	4.0	9.1

MATIJASEVIC [2] dealt with the problem of foaming agents. He concluded that aluminium foams produced based on the technology of decomposition of powders of foaming agents usually have uneven cells, which can lead to lower mechanical properties of these cellular materials. This may be due to thermal or temperature gradients during the foaming process. These temperatures are in turn not favourable for melting and processing the melt of the metal, rep metal alloy. Foam production also seeks to improve the homogeneity of the cell size of aluminium foams. In this context, there is also an effort to accommodate selective oxidation of the foaming agent (e.g. titanium hydride - TiH_2), which affects the formation of more uniform cell sizes of aluminium foams. It has been found [2] that the uniformity of cell size distribution is improved (individual cell walls are smoother and less wavy) when the foaming agent is heat-treated before foam production. Fig. 4.1 shows, according to [2], the temperatures modifying the foaming process of metals. The left part of the figure shows the range between solidus and liquidus for three commercially used aluminium-based materials [3], [4] (pure aluminium, AlSi7 and AlSi6Cu4). The right part of the figure shows the range of temperatures between the onset and maximum hydrogen release from the TiH_2 powder and the precursor (containing pure Al and TiH_2). Also shown are the values of the pre-treated TiH_2 foaming agent (heated to 480 °C for 180 min at a constant heating rate of 10 K·min^{-1}). These data were derived from experiments [2]. According to [2], many factors affect the aluminium foam production. The most crucial is the use of a *suitable foaming agent* that releases gas at a certain temperature to ensure high expansion and thus the formation of uniform foam porosity.

By long-term use of TiH_2 in air at a certain temperature and for a certain period, it was found:

- The onset of foam formation is delayed by pre-heat treatment with TiH_2. In the current configuration, the delay can be up to 45 seconds, corresponding to a temperature difference of 45 K.
- It takes longer to achieve a given volume of foam.
- The final expansion of the foam increases. Bubbles η = 4.5 to 5.5; uniformity of the foam formed (pores were more uniform and cell walls smoother) was found.

The importance of the foaming agent in its addition to the melt is linked to a different manufacturing process for aluminium foams invented by the Japanese Shinko Wire Company (patented in 1986 as Alporas®). The whole process takes place in furnaces and consists of several parts.

In the first stage of production, 1 to 2 wt. % of calcium solids (or manganese) are added to the molten aluminium at 670 to 690 °C, which begins to oxidize rapidly to form finely dispersed particles of the chemical compounds (CaO, $CaAl_2O_4$ and Al_4Ca) to thicken the aluminium melt and thus increase its viscosity. It is only when the frothing agent, TiH_2, is added to the melt in an amount of 1 to 2 wt % (particle size 5 to 20 μm) that small bubbles are formed. Proper process flow is ensured by maintaining the given temperature, pressure and time.

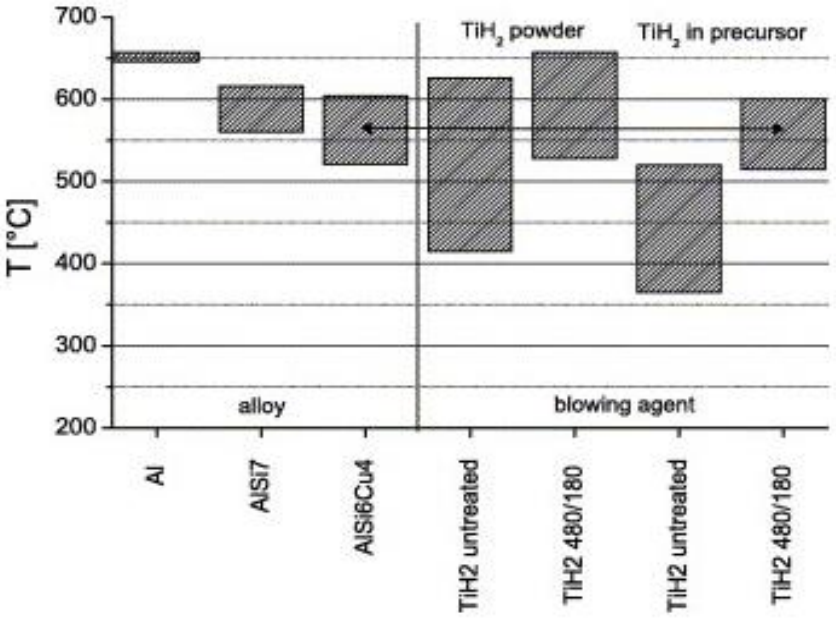

Fig. 4.1 Process temperatures; left - melting temperatures of selected metals; right - TiH_2 powder temperatures and Teploy TiH_2 in the precursor, [2]

It usually takes about 10 minutes to dissolve titanium hydride. The melt must be prepared for the addition of the powdered frothing agent. When the foaming process is complete, the melt must solidify properly and uniformly, otherwise, hydrogen will leak from the pores, and foam instability will occur. Subsequent cooling produces cellular aluminium.

Depending on the application, *Alporas* produces mostly metal "foams" with closed cells. The cell size can be varied from 0.5 to 5 mm, depending on changes in TiH content$_2$ or the foaming and cooling time of the melt (the products are 2400 × 700 × 450 mm foamed aluminium parts). The specific weight of the aluminium foam produced can be as low as 200 kg·m^{-3} to 250 kg·m^{-3}. The variance of the mechanical properties reported by the manufacturer is relatively small and this is also evidence of the evenly distributed structure of the material. Cutting large parts in a certain way loses their surface integrity and thus their tensile strength. Cutting results in rapid wear of the cutting tools. *Alporas* cellular material is also a difficult material to recycle because it contains relatively large amounts of calcium.

4.1 Characteristics of titanium hydride

Titanium hydride (TiH_2) is a chemical compound of titanium and hydrogen. Hydride is highly reactive and must be kept away from heat and strong oxidants.
Titanium hydride usually refers to the inorganic compound TiH_2 and related non-stoichiometric materials [14] [15]. It is commercially available as a stable grey-black powder that is used primarily in pyrotechnics [16] in the production of metal foams and in other fields. When titanium hydride is heated, which is applied, e.g. in powder metallurgy, titanium hydride releases hydrogen, which froths and thus foams the metal alloy [16]. Titanium hydride (TiH_2), the most commonly used commercial foaming agent, decomposes into titanium and hydrogen gas at temperatures above 400 °C.
Thermal decomposition of titanium hydride:

$$TiH_{2(s)} \Rightarrow Ti_{(s)} + H_{2(g)} \quad (4.1)$$

$$\Delta G^0_T = 453 - 0.58\ T, [kJ \cdot mol^{-1}], \quad (4.2)$$

where denotes: ΔG^0_T is change in Gibbs energy [$kJ \cdot mol^{-1}$]; T is temperature [K].

The change in Gibbs or free energy ΔG^0_T for reaction (4.1) is plotted as a function of temperature, see Fig. 4.2. In Fig. 4.2, all elements are assumed to be in their standard state, with gases being produced at atmospheric pressure, which helps to characterize the situation inside the cells in the liquid foam.
Direct decomposition of TiH_2 in a hydrogen gas atmosphere thus takes place at ~750 °C. In practice, foam formation with TiH_2 occurs rapidly at lower temperatures and intermetallic compounds TiAl and $TiAl_3$ are formed at the interface between the TiH_2 particles and the melt. As reported by CURRAN [41], other reactions also take place.
The change in Gibbs energy (ΔG) for several possible alternative reactions between foaming agent particles and melt components is also shown in Fig. 4.2, assuming the unit activity of Al and Si.

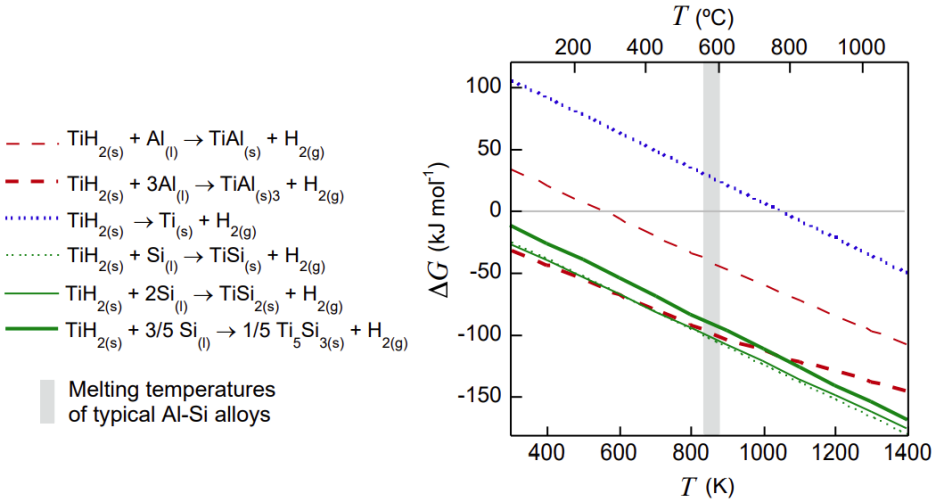

Fig. 4.2 Gibbs energy change for G for the thermal decomposition of the TiH_2, equation (4.1) and for several possible TiH_2 reactions developing gas in the Al-Si alloy melt (calculated with data from reference [48], all components have unit activity and p_{H2} = 1 atm, [41]

In the commercial method of producing non-stoichiometric $TiH_{(2-x)}$, the titanium metal sponge is treated with hydrogen gas at atmospheric pressure (0.1 MPa) at a temperature of 300 to 500 °C. The hydrogen absorption is exothermic and rapid and changes the colour of the grey/black sponge. The brittle product is ground to a powder that has a composition around $TiH_{1.95}$ [3].
In the laboratory, titanium hydride is produced by heating titanium powder under flowing hydrogen at 700 °C, and the idealized equation, according to [16] is: $Ti + H_2 \rightarrow TiH_2$.
Other methods of titanium hydride production include electrochemical and ball milling [5] [6]. Fig. 4.3 shows a titanium hydride and a schematic of its crystal cell.

Fig. 4.3 Titanium hydride, a very reactive chemical compound (melting point 450 °C, density = 3760 kg·m^{-3}, molar mass 49.91 g·mol^{-1}), cubic crystal lattice FCC TiH_2 with the tetrahedral arrangement of hydrogen atoms [20]

There is also $TiH_{1.95}$, which is not water and air, is slowly attacked by strong acids, and is degraded by hydrogen fluoride and hot sulfuric acids. It reacts rapidly with oxidizing agents, and this reactivity leads to the use of titanium hydride in pyrotechnics [16].

In the general case, TiH_x. When TiH_x approaches stoichiometry, it exhibits a distorted tetragonal structure, which is referred to as the ε phase. This composition is very unstable in terms of partial thermal decomposition if not maintained under a pure hydrogen atmosphere. Otherwise, the composition decomposes rapidly at room temperature until it reaches the approximate composition of $TiH_{1.74.}$ This composition adopts a fluorite structure and is referred to as theδ -phase and only very slowly decomposes thermally at room temperature until it reaches the approximate composition of $TiH_{1.47}$.
Titanium dihydride has been investigated, and the α (α-titanium) phase has a hexahedral crystal lattice (HCP) at room temperature. Hydrogen initially occupies tetrahedral interstitial sites in titanium. When the H/Ti ratio approaches 2, the titanium hydride transitions to β phase with a cubic crystal lattice (FCC). In the δ phase, hydrogen atoms eventually fill all tetrahedral sites to achieve the confining stoichiometry of TiH_2. The different phases of titanium hydride are described in Table 4-3.

Table 4-3 Characteristics of titanium hydride phases [20]

Characteristics of titanium hydride at 500 °C				
Pfase	**Hydrogen [% wt.]**	**Hydrogen [% at.]**	**TiH_x**	**Type of crystal cell**
Alpha (α)	0 to 0.2	0 to 8	-	HCP
Alpha and beta ($\alpha+\beta$)	0.2 to 1.1	8 to 34	$TiH_{0,1}$ to $TiH_{0,5}$	-
Beta (β)	1.1 to 1.8	34 to 47	$TiH_{0,5}$ to $TiH_{0,9}$	BCC
Beta and Delta ($\beta+\delta$)	1.8 to 2.5	47 to 57	$TiH_{0,9}$ to $TiH_{1,32}$	-
Delta (δ)	2.7 to 4.1	57 to 67	$TiH_{1,3}$ to TiH_2	FCC

When titanium hydride contains 4.0% hydrogen at a temperature below 40 °C, it transforms into a tetragonal crystal lattice (BCT) called titanium [20].

When titanium hydrides with less than 1.3% hydrogen (known as hypereutectoid titanium hydride) cool, the φ - titanium phase transforms back into the α - titanium phase, resulting in excess hydrogen.

The powder of the foaming agent TiH_2 for the production of cellular metal systems (metal "foams") is supplied by e.g. Chemetall GmbH, Frankfurt, purity 99 %. The physical and chemical properties, together with the average particle size of the powder, are given in Table 4-4.

Table 4-4 Physical and chemical properties along with the average particle size of TiH_2 powder

Physical and chemical properties and average size TiH powder particles$_2$						
Density [kg· m^{-3}]	***Chemical analysis [%]***	***Colour***	***Temperature decomposition [°C]***	***Particle size distribution [μ m]***		
				D (v. 90)	D (v. 50)	D (v. 10)
3760	98.8	grey	400	30.79	14.14	3.18

Fig. 4.4 shows the appearance (morphology) of the TiH_2 powder, which was obtained using a scanning electron microscope (SEM). This image shows the angular morphology of the powder particles; the particle size is variable, and the powder surface is irregular.

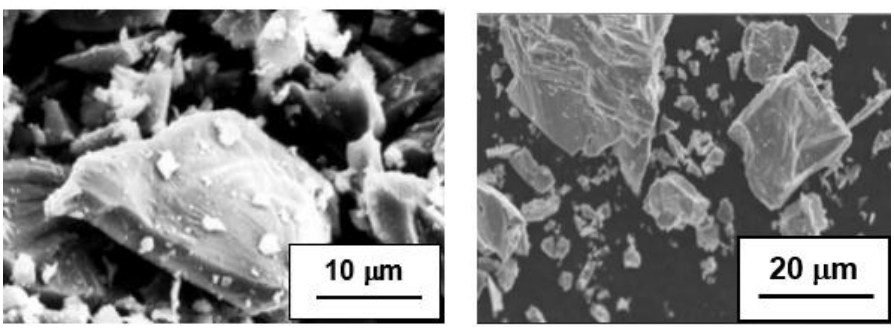

Fig. 4.4 Appearance of TiH powder particles$_2$ (scanning electron microscope) [31]

For research purposes and technical applications of the pre-prepared TiH_2 powder, it was isothermally heated in air at different temperature conditions and heating times (temperatures: 480 °C, 500 °C, 520 °C; times: 90, 180 and 360 minutes). For transmission electron microscope (TEM) and diffraction observations the powders were cold pressed into small tablets of 6 mm diameter and then heat treated in air, see Figure 4.5. The curves in Figure 4.5 correspond to TiH_2 or the sub-stoichiometric compound TiH_X.

Titanium hydride powder processed in this way shows two decomposition peaks. The release of gas starts already at 400 °C. Heat treatment at 480 °C for 180 minutes completely eliminates the first stage of decomposition and increases the temperature at which maximum gas release occurs. The decomposition of TiH_2 is prevented due to the slow diffusion of hydrogen through the oxide layer. Longer treatments up to 360 minutes or treatments at higher temperatures up to 520 °C shift the position of the peaks to even higher temperatures. Practical applications have shown that the decomposition properties of the defoaming agent - TiH_2 - can be tailored by a suitable choice of heat treatment parameters.

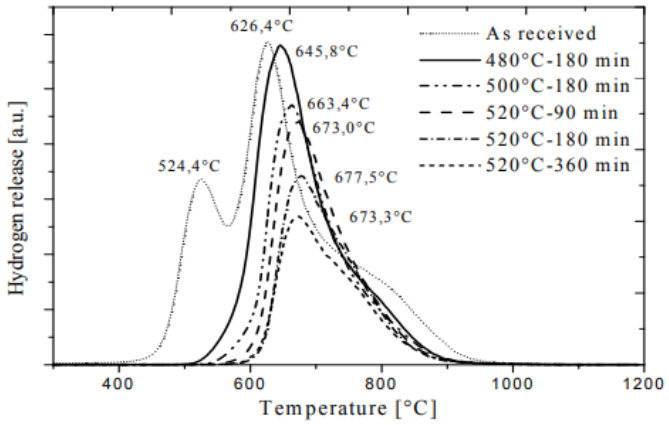

Fig. 4.5 Mass spectrometry of TiH_2 powder sample during thermal pre-treatment at different heating conditions in argon atmosphere, heating rate 10 $K \cdot min^{-1}$ [31]

The XRD curves of TiH_2 samples processed in the air at 520 °C for 90, 180 and 360 minutes are shown in Fig. 4.6. From the powder diffraction files of the powders, the phase composition was observed as $TiH_{1.924}$ with FCC crystal structure, TiH_2 powder with crystal lattice ($a = 4.45 \cdot 10^{-10}$ m) was identified. After heating in air, the peaks are shifted to larger angles, indicating hydrogen loss.

The oxidation results in Ti_3O and TiO_2 (titanium dioxide rutile), which are characterized by hexagonal and tetragonal crystal structures.

Colour changes were also observed during the thermal pre-preparation of TiH_2 powder in the air. Initially, the dark grey powder turned blue at 480 °C. It further turned black at 500 °C and showed a light brown colour at 520 °C and a dark brown colour above this temperature. The colouring of the powder indicates that the oxidation process takes place at the surface of the powder, where the surface oxide is formed. The composition, amount and thickness of the oxidation products are sensitive to the

method and rate of heating and the time delay in maintaining the temperature at the appropriate level. The oxidation layer on the surface of TiH_2 powder is about 100 nm, see Fig. 4.7.

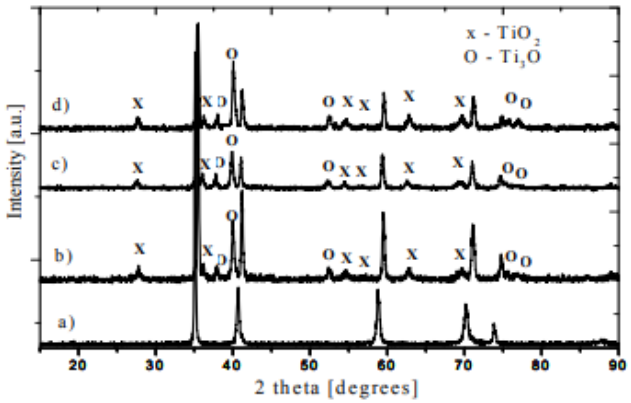

a) heating in air at 520 °C; (b) heating in air at 520 °C, residence time 90 min; (c) heating in air at 520 °C, residence time 360 min.

Fig. 4.6 XRD curves for TiH_2, powder samples heated in air at 520 °C at different time delays [31]

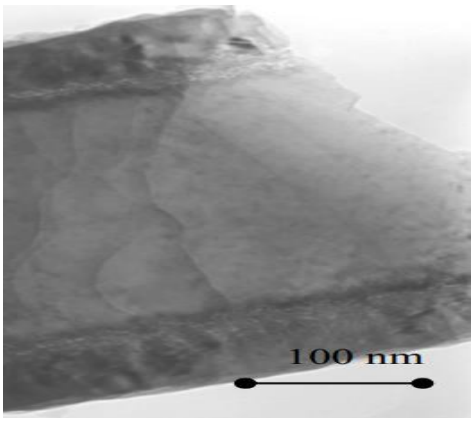

Fig. 4.7 Oxidation layer of 100 nm thickness on the surface of TiH particle$_2$ [31]

When TiO_2 was formed, the amount of oxides remained constant, while the hydrogen concentration increased significantly. The structure of titanium hydride changed to β-phase at higher temperatures due to the loss of the original amount of hydrogen. After cooling the sample "TiH_2 ", the sample consists of a mixture of α Ti and $TiH\delta_{1,5}$. The measurements were carried out "in situ". The advantage of the measurement is the possibility to accurately observe the phase transition using only one sample for the whole temperature range.

The action of titanium hydride in aluminium can be seen in Fig. 4.8. Here a section of a sample of foamed aluminium ∅ is 110 x 300 mm, the gasification temperature of TiH_2 is 993 K (720 °C), the melting temperature of aluminium is 660 °C.

The weight of Al foamed in this way is 1000 g, and the addition of titanium hydride is 1.0 wt. %, the addition of Ca is 2.0 wt.%. It was made by a special process, it was stirred at 1000 rpm min^{-1}, the stirring time was 20 s, and the foaming time was 10 s.

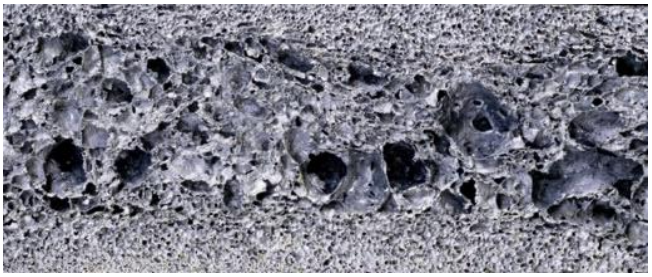

Fig. 4.8 Section through a foamed aluminium sample∅110 x 300 mm. Al melting temperature (660 °C), gasification temperature of TiH_2 is 993 K (720 °C), YANG [24]

The foaming process was also monitored by YANG [24], who used a foaming temperature of 940 K, a foaming agent amount of 1.0 % wt., and the mixing of the melt with the foaming agent took 30 to 80 s. A special mixing device operating at a speed of 1000 rpm· min^{-1} was used. The porosity of the aluminium "foam" obtained was approximately 55.0 %. It was shown that if the amount of foam pores (cells) increases, the size of the foam cell walls decreases. When the foaming agent was mixed into the melt for 40 s, a foam with relative cell size (D is about 4 mm) was formed and high porosity (P = 88.8 %) as shown in Fig. 4.9 (a). Whereas, when the foaming agent was added for 80 s, a slowing down of the foaming process was observed, contributing to the formation of small foam cells with their size (D < 1 mm) and low porosity P = 65.2%, as illustrated in Fig. 4.9 (b).

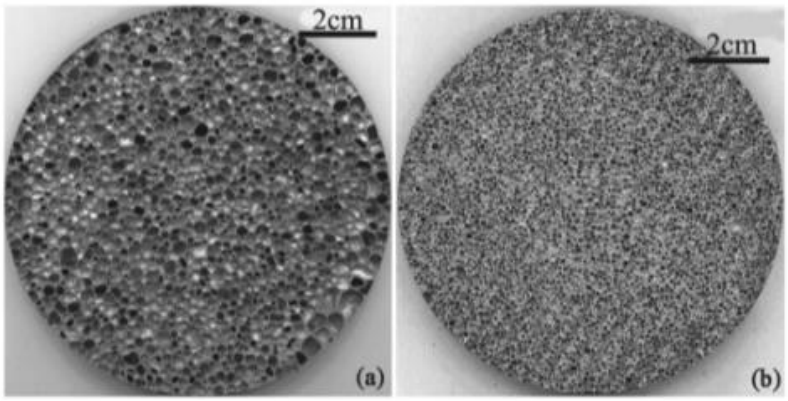

Fig. 4.9 Cutting of two aluminium foams with different pore structures, foaming time 150 s, (a) - the foaming agent mixing time was 40 s; (b) the foaming agent mixing time was 80 s, [24]

The porosities of the samples in Fig. 4.9 (a) and 4.9 (b) are 88.8 % and 65.3 %, respectively. The pore size of the sample (a) is about 4 mm, and that of the sample (b) is <1 mm. The foaming process temperature during fabrication is 940 K (i.e. 667 °C,

slightly above the melting temperature of aluminium). The amount of the foaming agent TiH_2 used was 1.0 wt%, and the amounts of Ca were 2.0 wt%.

The gas released from the decomposition of titanium hydride is one of the key factors affecting the foaming process of Al alloy. As part of the research, a set of decomposition kinetic equations of titanium hydride was obtained by separating the temperature programmed decomposition (TPD) spectrum obtained by a specially designed TPD device, see its schematic in Fig. 4.10, with argon used as the carrier gas and a thermal conductivity cell as the detector. According to these equations, the decomposition and hydrogen release characteristics of titanium hydride at a fixed temperature (400 °C) and elevated temperature are quantitatively described, which can be applied to predict the foaming by melting of Al and providing a theoretical basis for the production of a three-dimensional "foam" shape of an Al alloy.

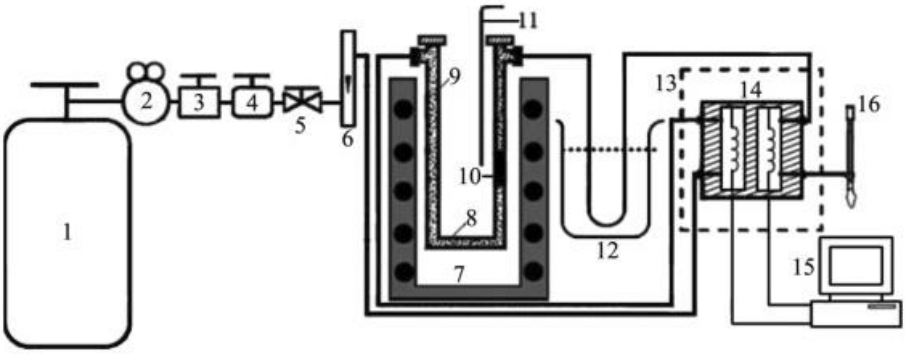

(1) is an argon tank, (2) a pressure reducing valve, (3) a special valve, (4) a control valve, (5) (9) quartz sand, (10) titanium hydride, (11) a thermocouple, (12) a cooling paste, (13) a housing, (14) a thermal conductivity cell, (15) a workstation-computer station, and (16) a medium flow meter.

The argon flow rate is 1 → 2 → 3 → 4 → 5 → 6 → 14 → 8 → 12 → 14 → 16

Fig. 4.10 Schematic representation of a temperature-programmed device for monitoring TiH_2 decomposition [24]

4.2 Characteristics of ZrH_2 Zirconium Hydride

Zirconium hydride (ZrH_2) is a chemical compound formed by combining zirconium and hydrogen. Zirconium hydrides are formed when the metal interacts with hydrogen gas. Changing the amount of hydrogen and the form of its presence in the zirconium hydride (precipitated phase) controls properties such as the hardness, ductility and tensile strength of the resulting zirconium hydride. Zirconium hydride with increased hydrogen content may be harder and stronger than zirconium, but such zirconium hydride is also less ductile than zirconium.

While this reaction occurs even at room temperature, homogeneous bulk hydrogenation is usually achieved by annealing at temperatures between 400 and 600 °C for a period of between several hours and several weeks [25]. At room temperature, zirconium hydrates oxidize rapidly in air and even under a high vacuum. Zirconium hydrides are soluble in hydrofluoric acid or alcohol; they react violently with water, acids, oxidizing agents or halogenated compounds [26].

As a pure powder, zirconium hydrides are used as hydrogenation catalysts, powder metallurgy and catalysts in vacuum tube production.

Zirconium hydride is used in powder metallurgy where the gas acts as a hydrogenation catalyst and reducing agent. It is also used as a frothing agent in the production of metal cellular systems. Other uses include acting as a fuel in pyrotechnic components, namely pyrotechnic initiators.

Thermal decomposition of zirconium hydride:

ZrH_2 (s) $\Rightarrow$ Zr (s) + H_2 (g) (4.3)

ΔG^0_T = 169.000 - 134.7· T, [J·mol^{-1}], (4.4)

To determine the decomposition temperature of ZrH_2, one can write:
$\Delta\ G_T^0$ = 169000-137.7· T = 0.
T = 169000/137.7 = 1227 K, i.e. 954 °C.

Fig. 4.11 shows an example of a fabricated metal "foam" using the foaming agents ZrH_2 and TiH_2.

Fig. 4.11 Metal foam (metal cellular system) fabricated using ZrH foaming agent$_2$ (left); porous aluminium foam structure fabricated using TiH_2, the area shown is 80 x 80 mm, (right), Nanjing University, Southeast China

MATIJASEVIC et al. [27], evaluated foaming agents of hydrides (Ti, Zr, Hf) in the framework of the production of aluminium "foams" by powder metallurgy (mixing and compaction of powder mixtures at different conditions) with subsequent melting of the powder precursor. Before compaction, ZrH_2 was subjected to an oxidation treatment to adjust its thermal decomposition characteristics. The *zirconium hydride* pretreatment was found to have a positive effect on foam production with a better and more uniform distribution of foam cells (pores). These results confirmed that zirconium hydride is also a good foaming agent. It is potentially a serious competitor to titanium hydride, which is currently the most commonly used foaming agent in metal foam production. When using foaming agents, the aim is to obtain a regular structure of the foamed material. Also, metal foams with non-uniform cells can find interesting technical applications. One of the reasons for the non-uniform cell structure may be the temperature difference between the decomposition temperature of the foaming agent and the melting temperature of the metal used (most often, aluminium alloy). This difference causes the formation of irregular, cracked pores, which have their origins in the early expansion stage of foam production. To minimize the temperature mismatch

between the decomposition temperature of the foaming agent and the melting temperature of the metal in question, this temperature difference can be reduced by adding an alloying metal agent. Alternatively, the thermal decomposition temperature of the foaming agent may be favourably influenced, for example, by heat treatment. MATIJASEVIC et al. [27] also report the observation that if the foaming agent powder is preheated in air, then an oxide layer is formed on its surface (this layer slows down the release of gas from the foaming agent particles during their thermal decomposition). Thus, the thermal decomposition of e.g. TiH_2 releases hydrogen in an ideal way, i.e. during the foaming process, but also when the respective metal is melted [28].

In this context, it should be noted that the term "hydride" is described as a binary combination of hydrogen and metal or something similar to metal) [29]. From the nature of hydrogen bonding, hydrides can be divided into three main groups (covalent or volatile (salt) hydrides, ionic hydrides and metal hydrides). Metal hydrides are used for foaming and also exhibit the properties of metals (high thermal conductivity, electrical resistance, hardness, crystal structure etc.). Metal hydrides have other uses beyond their use as a foaming agent (in nuclear applications as chemical reducing agents, for deoxidation and desulphurisation of molten iron alloy material and for use as high energy fuels). Interestingly, zirconium hydride contains twice as many hydrogen atoms per unit volume as liquid hydrogen. Titanium, thorium and zirconium hydride are effectively used as foaming agents for the production of metallic cellular systems.

Knowledge of the use of ZrH_2 for the fabrication of metallic cellular systems is reported in [27]. The hydrogen release from ZrH_2 powder in the untreated state and after various pretreatments in argon and air was monitored (for this purpose, a Netzsch STA 409C simultaneous thermal analyzer for differential temperature analysis - DTA and for gravimetry - TGA and mass spectrometry - MS).
For this purpose, ZrH_2, powder supplied by *Chempur* GmbH, Karlsruhe, (purity 99.7%, < 45 μm) was used. The powder was examined in the "untreated" state and after several pre-treatments. Pretreatments of ZrH_2 powder were carried out isothermally, at different temperatures (400, 480, 520 °C) and times (90 and 180 min), using an argon atmosphere (purified with zirconium active material, 10^{-12} ppm) inside a tube furnace. Furthermore, a chamber furnace with an air atmosphere was used.
Next, the foaming precursors were prepared by mixing aluminium powder (Eckart, purity 99.74

%, <160μ m), silicon powder (Olschlager, purity 98.5 %, <100 μm) and copper powder (Chempur, purity 99.8 %, <250 μm) in such quantities to obtain *AlSi6Cu4 alloy* (90 wt% Al, 6 wt% Si and 4 wt% Si). In addition, a powder of a foaming agent was added in the amount of 0.5 wt% ZrH_2. The foaming agent was either in an untreated state or in a state after one of the various air pretreatments. When working with powdered foaming agents, it is important to take care to prepare and treat the powders consistently. For powders based on powder metallurgy, a long mixing time, about 90 minutes, in the mixing equipment is necessary to achieve homogeneity of distribution of all powder

components, including the powder of the foaming agent. The powder mixtures thus prepared must be further compressed. Pressing must be carried out in two stages.
The first stage of pressing must be carried out at room temperature (approx. 20 °C). For this purpose, a press mould is suitable so that a roll of the compressed mixture of all the necessary powders is pressed out. The size of this roll must be as appropriate, e.g. approx. ∅ 35 x 50 mm. The roll of the powder mixture thus pressed is then placed in an oven and heated to a temperature of 450 °C at a rate of 10 °C.min^{-1} and heated at this temperature for about 30 minutes.
The second stage of pressing is carried out under hot conditions. For this purpose, a sample heated to 450 °C is used and after a bob of 30 minutes, a pressure of 200 MPa is applied to the sample. This produces a very compact semi-finished product (foamable or foaming precursor).
This foaming precursor is then fed into a furnace at 650 °C. This temperature is related, for example, to the melting temperature of the aluminium alloy AlSi6Cu4 ($T_{melt.}$ = 650 °C). A thermocouple can be installed in the precursor to monitor the temperature of the straining process. The foaming process is completed when the sample or precursor reaches the expected foaming time (t_f time foaming finish) and the required foaming temperature (T_f is temperature foaming). The detailed preparation and methodology of the experiments are explained in the reference [31].

The results that were determined from the thermal analysis of DTA and TGA showed that no further oxidation occurs because the thermal analysis was performed using argon. ZrH_2 powder was found to release only hydrogen. The maxima of the mass spectrometric curves are observed during the decomposition of ZrH_2.

Fig. 4.12 (a) shows the behaviour of the powders as they decomposed, the unheat treated ZrH_2 powder as well as the behaviour of the ZrH_2 powder pre-heat treated under argon (an argon stream and a heating rate of 5 K· min^{-1} was used).

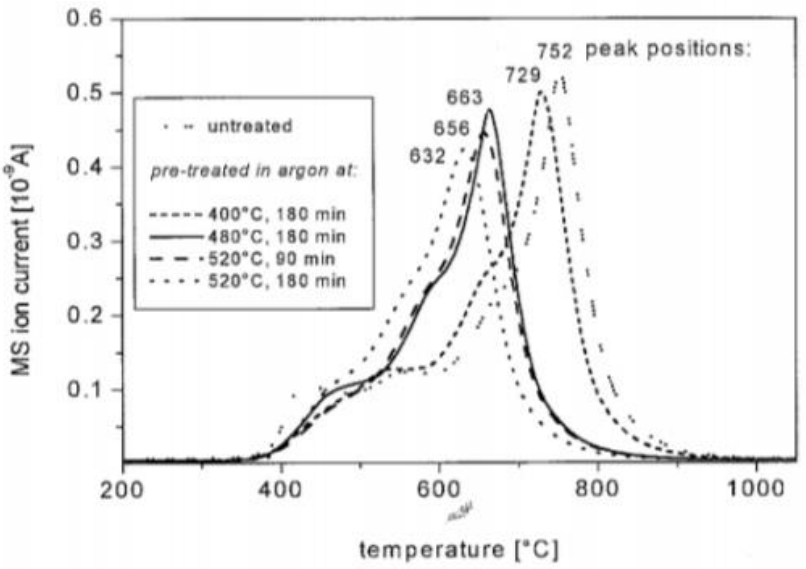

Fig. 4.12 (a) Mass spectrometric analysis of pre-treated ZrH_2 foaming agent powders (they were pre-treated in an Ar atmosphere); heated from 30 °C to 1050 °C, at a rate of 5 K· min^{-1}

in an argon atmosphere (low temperature, temperature range omitted); peak temperature positions are given in °C; a curve for untreated ZrH_2 powder is included [31].

Based on mass spectroscopy (MS), three peaks of the temperature curves of the untreated powder can be observed. The first hydrogen evolution step (monitored by mass spectrometry), using the 1 % criterion, starts at 205 °C, with a relative maximum at 436 °C. The second dehydrogenation step starts at about 480 °C and reaches a maximum of 552 °C. The third dehydrogenation step starts at about 580 °C with a small shoulder and reaches a maximum of 752 °C. Fig. 4.12 (b) shows an analogy of ZrH powders$_2$, with pretreatment in air.

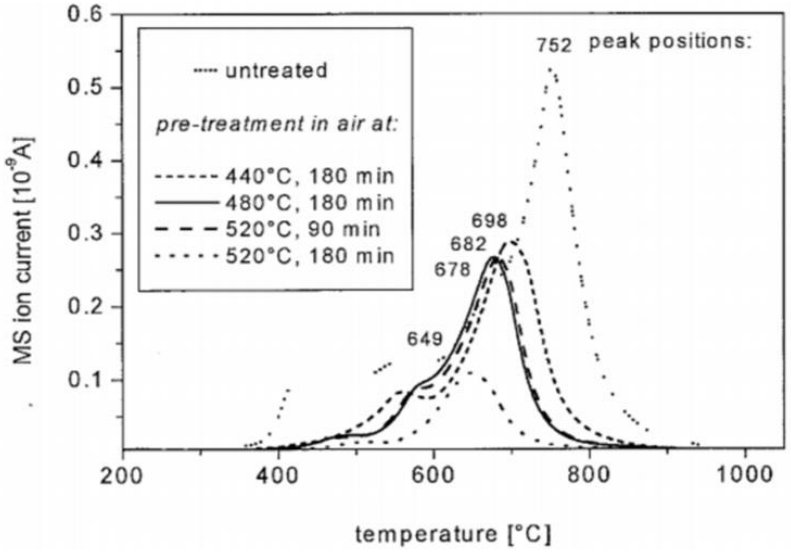

Fig. 4.12 (b) Mass spectrometric analysis of pre-treated ZrH_2 foaming agent powders (which have been heated from 30 °C to 1050 °C, at a rate of 5 K· min^{-1} in an argon atmosphere (low temperature is temperature range omitted), positions of temperature peaks are given in °C; also included is a curve for untreated ZrH_2, powder [31].

Fig. 4.12a) also shows that heat treatment at 400 °C for 180 minutes eliminates the first stage of decomposition, leaving only two peaks. The double peak structure remains the same for the process at higher temperatures or longer times. The remaining two peaks are shifted to lower temperatures compared to the untreated ZrH_2 powder. By observing the curves with prior argon pretreatment, it can be seen that at 205°C the effect of treatment under argon is not apparent, with all temperatures starting between 205°C and 211°C. The levels of gas released outside the peaks for the untreated powders start at 400 °C and end at about 950 °C.
For ZrH_2 pre-treated powders, the gas release starts in the temperature range of 480 °C to 520 °C and ends at about 900 °C.

As can be seen in Fig. 4.12b), the ZrH_2 foaming agent powders pretreated in air show a different behaviour in their decomposition than that observed when the powders were pretreated with argon. Heat treatment for 180 min at 400 °C in air eliminates the first stage of decomposition. However, unlike the process under argon,

pretreatment of the powders in the air significantly changes the gas evolution temperature. Treatments up to 180 min at higher temperatures (up to 520 °C) increase the onset of decomposition by 258 K, while peak temperatures decrease by up to 103 K.

For all treatments, the gas release is less than for untreated powders and ceases earlier, at about 850 °C for the 400 °C treatment and about 800 °C for the 480 and 520 °C treatments, 90 min, about 750 °C for the 520 °C treatment, 180 min compared to about 950 °C for the untreated powder.

Fig. 4.13 shows the correlation between the foaming time and the final temperature at which the experiments were carried out and "stopped" to achieve the required foam expansion of 60 %. The data were measured on samples with both air pretreatment and different amounts of ZrH_2. The heating conditions were the same in all cases. The final foaming temperature (T_f) was shown to increase steadily with foaming time (t_f). As a result of the observation, the precursor containing a pre-heat treated foaming agent (a higher temperature for a longer time) also needs a higher temperature and longer foaming time for the foaming process to take place in a given volume of metal.

The effect of oxidation on the quality level of the foaming agent ZrH_2 was monitored on the nature of the pores (cells) formed during the foaming process (see Fig. 4.13). The untreated ZrH_2 foaming agent produced pores with jagged boundaries and a non-uniform pore size distribution. The changes in the shape of the pores are remarkable in the context of increasing hydride oxidation. The pores become more spherical and have smooth surfaces even at shorter ZrH_2 pretreatment times. At the same time, the increasing oxidation of this hydride has a positive effect on the distribution and size of the pores.

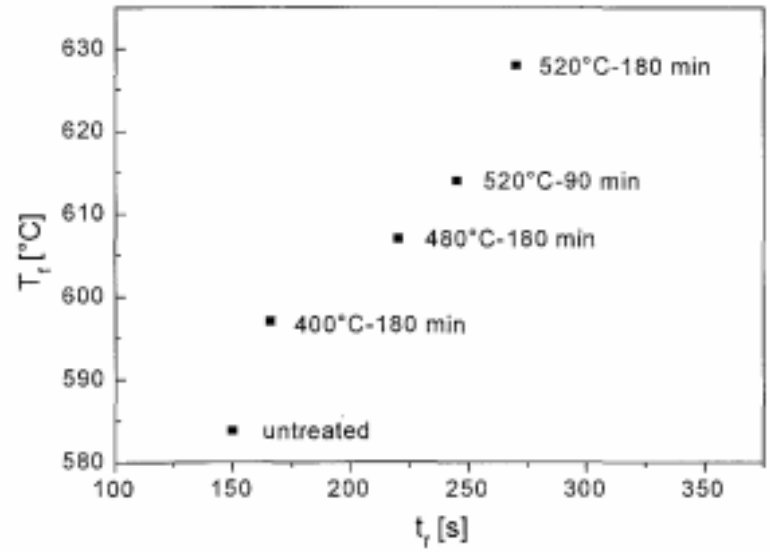

Fig. 4.13 Final temperatures T_f (foaming agent) of the samples at foaming time t_f for the production of aluminium foam from AlSi6Cu4 alloy, using foaming agent ZrH_2 to achieve foaming of 60 %, ZrH_2 was pre-heated in the air according to different methods, and the temperature in the furnace was 650 °C, [31]

ZrH_2 foaming agent powders pre-heat treated at temperatures 520 °C produce more uniform foam pores than powders pretreated at lower temperatures. Pre-thermal

treatment of ZrH_2 in air results in foams with a more spherical and homogeneous pore distribution. Fig. 4.14 shows an example of aluminium foams produced using the ZrH_2 foaming agent.

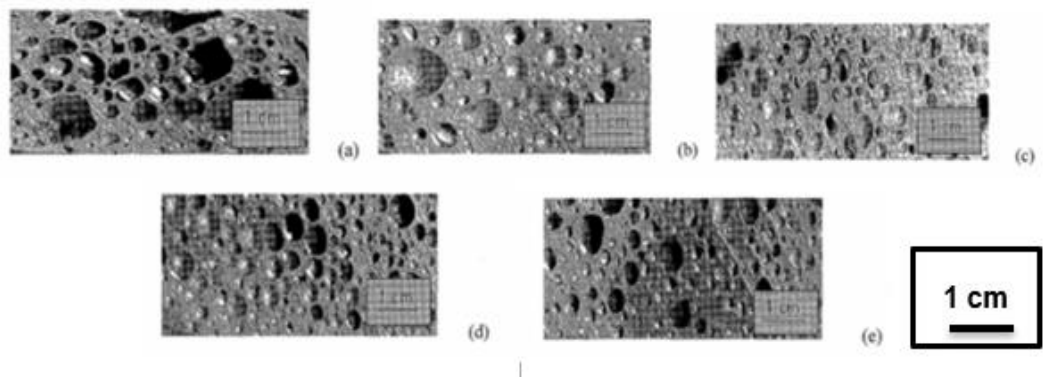

(a) untreated ZrH_2 (porosity P = 58 %), (b) pre-treated ZrH_2 in air 400 °C, 180 min (P = 50%), (c) 480 °C, 180 min (P = 50 %), (d) 520 °C, 90 min. (P = 53 %), (e) 520 °C, 180 min (P = 52 %),

Fig. 4.14 Aluminum foams made from AlSi6Cu4 alloy using decomposed ZrH_2 gases (the direction of expansion of the gases was from the bottom to the top), [27]

4.3 Characteristics of dolomite $MgCa(CO_3)_2$

The researchers PAPADOPOULOS et al [35], tried to apply the foaming agent dolomite ($MgCa(CO_3)_2$) or ***carbonate-magnesium-calcium*** in the production of metallic cellular systems***.*** Dolomite is a naturally occurring mineral. It is a very effective foaming and stabilizing agent for the production of aluminium foam systems. The thermal decomposition of dolomite occurs in two stages:

Stage 1: $CaMg(CO_3)_2 \Rightarrow MgO\ (s) + CO_2\ (g) + CaCO_3\ (s)$ (4.5)
Stage 2: $CaCO_3\ (s) \Rightarrow CaO_{(s)} + CO_2\ (g)$ (4.6)

Dolomite and its thermal decomposition can also be written in this way:
$CaCO_3 \cdot MgCO_3\ (s) \Rightarrow CaO\ (s) + MgO\ (s) + CO_2\ (g)$ (4.7)

The decomposition of *dolomite $MgCa(CO_3)_2$*, or $CaCO_3 \cdot MgCO_3$ produces calcium oxide, magnesium oxide and carbon dioxide. The course of thermal decomposition is influenced by the flow of gases from the decomposing dolomite. The temperature of the first stage of thermal decomposition of dolomite is about 750 °C. The temperature of the second stage of decomposition of dolomite is determined by the thermal decomposition of $CaCO_3$, which corresponds to a temperature of about 900 °C.
Dolomite as a frothing agent has several notable advantages over the current use of titanium hydride as a frothing agent. The characteristic cellular structures and microstructural features of the foams produced have been investigated with a dolomite foaming agent. Furthermore, the properties of the foams produced with

the dolomite foaming agent were investigated. Foams with titanium hydride-based foaming agents were also produced by the same technological method. The structure of the foams produced using dolomite-based foaming agents is characterized by smaller cell sizes with thinner cell walls. The use of the $MgCa(CO_3)_2$ foaming agent also leads to a significant increase in the stability of the molten foams with a large range of foaming process temperatures and leads to an almost complete absence of influence on the melt (melt flow) even at extended foaming times. Many of these properties are attributed to the cell surfaces covered by the thin oxide film formed during the foaming process.

Researchers [32], in experiments, produced metal foams based on titanium hydride and dolomite-based melt foaming processes.

The foam based on the foaming agent TiH_2 was produced by the following process: calcium (1.8 % wt.) was added to a prepared 720 °C aluminium melt with an average particle size of 1190 μm (supplied by *Aldrich* Chemical Company). The calcium particles were dispersed in molten Al (commercial Al composition: 99.8 wt.% Al and 0.15 wt.% Fe). The addition of Ca increased the viscosity of the melt, and the melt was stirred with Ca for 8 minutes at a speed of about 700 $rpm \cdot min^{-1}$. To the melt at a temperature of about 680 °C, a powder of the foaming agent TiH_2 (1.5 to 2 wt. %) with a mean particle size of about 44 μm was then added. The melt was stirred for 10 minutes at a speed of 1200 $rpm \cdot min^{-1}$ to achieve uniform distribution of the powder. Further, the melt was kept in the furnace for 3 minutes to allow thermal decomposition of the titanium hydride, the resulting gas evolved in the melt causing it to swell or foam. This frothy melt is allowed to solidify and cool in the air after removal from the furnace.

The preparation of foamed aluminium based on dolomite was carried out analogously. First, aluminium was melted at a temperature of 720 °C (commercial composition: 99.8 wt. % Al and 0.15 wt. % Fe), then powdered dolomite $MgCa(CO_3)_2$, in an amount of 1.5 to 3 % wt., was added to the melt at 650 °C. The melt was stirred at a speed of 1200 $rpm \cdot min^{-1}$ for 90 seconds to achieve uniform distribution of the powder in the melt. Then, the melt was put into the furnace and maintained at a certain temperature in the furnace for 13 minutes to allow the dolomite to undergo thermal decomposition to form CO_2 gas, which will form aluminium melt foaming or aluminium foam. The temperature progression of the heated foamed material was monitored using a K-type thermocouple placed directly in the melt. The equipment used for the foaming processes (using hydride and dolomite foaming agents) consists of a resistance furnace, a stirrer which is driven by a motor, can provide different stirring speeds. In the evaluation of the produced aluminium "foams", the specific gravity of the produced foam ($\rho_{Al.F.}$) and the relative specific gravity of the produced foam ($\rho_{Al.F.}/\rho_{B.M.}$) and its porosity P were monitored (see Table 4-5).

From Table 4-5, it can be seen that for a comparable amount of foaming agent, metal foams made with dolomite have higher porosity than those made with titanium hydride foaming agent.

While observing the behaviour of dolomite powder, the kinetics of gas release from this powder were also monitored. The effect of the purity and particle size of the frothing

agent of the dolomite powder was also assessed. At the same time, the influence of the purity of the particle size of the powdered dolomite on the kinetics of the foaming process.

Table 4-5 Average values of the properties of the produced aluminium foams (bulk density and porosity) produced using the two foaming agents $MgCa(CO_3)_2$ and TiH_2 PAPADOPOULOS [33]

Physical properties of manufactured aluminium foams				
Sample	**Foaming agent [% wt.]**	**Specific gravity $\rho_{Al.F.}$ [kg·m^{-3}]**	**Relative the specific weight of the foam $\rho_{Al.F.}/\rho_{B.M.}$ [1]**	**Porosity P [%]**
A1	$MgCa(CO_3)_2$; 1.5	467	0.17	82.1
A2	$MgCa(CO_3)_2$; 3.0	773	0.29	71.4
A3	TiH_2; 1.5	625	0.23	70.0
A4	TiH_2; 2.0	571	0.22	68.9

The microstructure of the dolomite powder was obtained on a scanning electron microscope (SEM) and is shown in Fig. 4.15. The natural dolomite powder is white in colour and fine, with an average particle size of 46 μm. The measured particle size distribution of $MgCa(CO_3)_2$ powder is shown in Fig. 4.16a). Fig. 4.16 b) is an X-ray diffractogram of powdered dolomite used to make Al "foam" with closed cells [32].

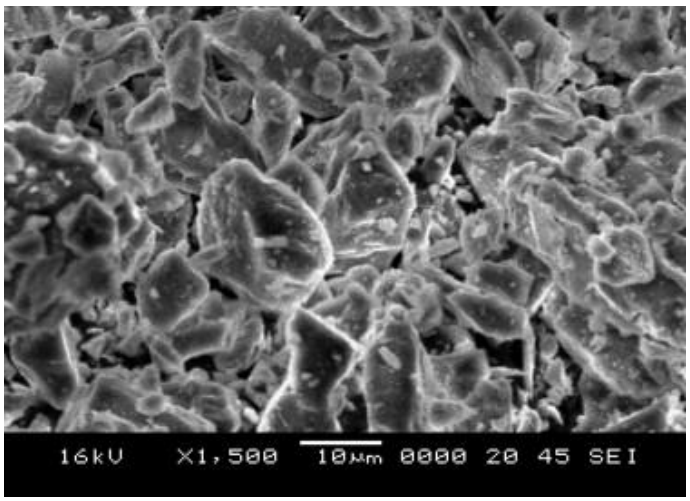

Fig. 4.15 Powdered dolomite frother used, SEM electron microscope [32]

The thermogravimetric analysis (TG) of the frothing agent, $MgCa(CO)_{32}$ dolomite powder, is shown in Fig. 4.17. Thermogravimetric curves were obtained using CO_2 atmosphere (red curve) and in the air (black curve), the heating rate was 20 °C min^{-1}. From this analysis, the melt temperature for foaming can be determined based on the thermal decomposition of the foaming agent. According to the curve of thermogravimetric analysis of dolomite, the initial temperature for the development of CO_2 is about 630 °C. The thermal decomposition of powdered dolomite frothing agent samples is strongly influenced by the rate at which CO_2 is used for frothing. This rate

is dependent on the particle size of dolomite, the efficiency of thermal pre-preparation of the powder, and the sample size [33].

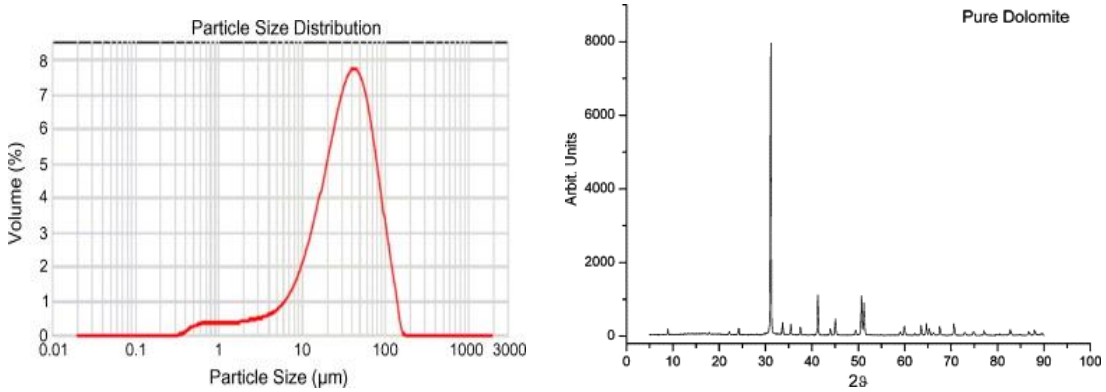

(a) (b)

Fig. 4.16 (a) Measured size distribution of the dolomite foaming agent used for foaming; (b) X-ray diffractogram of powdered dolomite used for the production of closed-cell Al foam [32].

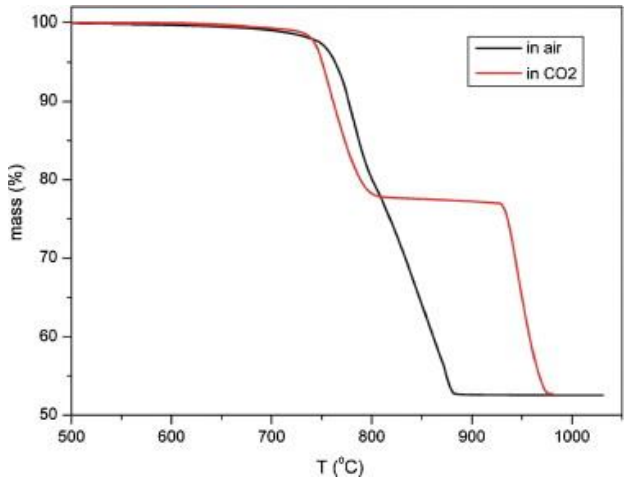

Fig. 4.17 Thermogravimetric curves (TG) of dolomite powder analysis [32]

On the other hand, in connection with the analysis of dolomite, it should be noted that the direct decomposition of TiH_2 in a hydrogen gas atmosphere occurs at a temperature of about 490 °C. In practice, rapid sintering with TiH_2 at lower temperatures leads to the formation of intermetallic phases TiAl and $TiAl_3$ [33] at the interface between titanium hydride and the metal matrix, suggesting parallel reactions. The above characteristics show that the onset temperature of CO_2 evolution from dolomite powder is higher than that of hydrogen from titanium hydride.

The cell morphology (pore) of the foam formed using the foaming agents $MgCa(CO_3)_2$ and titanium hydride were also investigated. The macrostructures of the produced foam cell longitudinal sections obtained by applying the two foaming agents dolomite and titanium hydride, metal foams are shown in Fig. 4.18. The foams obtained using dolomite exhibit smaller cell (pore) size than that exhibited by the titanium

hydride-based foam, although the foaming time was approximately 13 min using dolomite and only 3 min using titanium hydride. Apart from the difference in scale, all samples have similar 'polyhedral' cell structures, with straight or gently curved cell surfaces and apparently smooth cell surfaces.

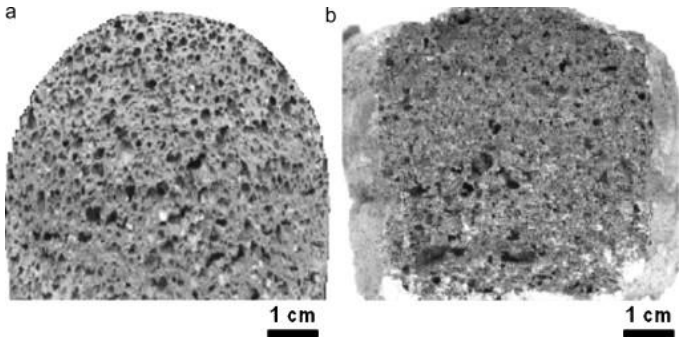

(a) foam produced on the basis of the foaming agent TiH_2 (foaming of a foamable precursor with 1.8 wt. % SiC particles, T_f = 720 °C, t_f = 3 min, $\rho_{Al.F.}$ = 569 kg m^{-3} and $\rho_{Al.F.}/\rho_{B.M.}$ = 0.219. (b) Foam is produced by the foaming agent $MgCa(CO_3)_2$, by foaming a foamable precursor with 2 wt.% SiC particles, T_f = 720 °C, t_f = 13 min., $\rho_{Al.F.}$ = 773 kg m^{-3} a $\rho_{Al.F.}/\rho_{B.M.}$ = 0.29

Fig. 4.18 Longitudinal section through the cellular structure of titanium hydride and dolomite-based foams, [32]

Research [32], which focused on the use of titanium hydride (TiH_2) compared to dolomite ($MgCa(CO_3)_2$, confirmed that the use of titanium hydride foaming agent for the production of aluminium foam involves high raw material costs and hazards due to the specific nature of this powder. Careful process control is required to obtain reproducible cell structures with strong sensitivity to variations in the foaming process and the risk of heating. Titanium hydride-based foams have smooth surface walls with no visible irregularities. However, the chemical decomposition of dolomite is more gradual at temperatures corresponding to the formation of aluminium melts. Dolomite acts as a foaming and stabilising agent. Its main purpose is that of a frother, and at the corresponding decomposition temperatures, its decomposition reaction takes place to form carbon dioxide. The reaction of CO_2 with liquid aluminium leads to the formation of thin layers of solid oxides and increases the mechanical stability of gas cells [33]. The reduced foaming rate of dolomite also improves the control of the foaming process. When dolomite is used, the risk of a turbulent foaming process is much lower, and material costs are also low. Its thermal decomposition, which occurs at higher temperatures (about 750 °C), intensively releases carbon dioxide, see equations (4.5), (4.6) and (4.7), as the above shows, the technology of the foaming process using dolomite is more feasible than that using titanium hydride.

4.4 Characteristics of calcium carbonate

Calcium carbonate ($CaCO_3$) is a white crystalline substance that is used, among other things, as a foaming agent to produce cellular metal systems (metal cellular materials

and metal foams). The crystalline modifications are identical to the mineral lattices for **calcite** (*I-modification*), **aragonite** (*II-modification*) and **vaterite** (*III-modification*).
In nature, calcium carbonate occurs under the name limestone. Heating or thermal decomposition of calcium carbonate (at a certain temperature and pressure) produces calcium oxide and carbon dioxide:

$$CaCO_3\,(s) \rightarrow CaO\,(s) + CO_2\,(g) \qquad (4.8)$$

The carbon dioxide produced by equation (4.8) is the source of the bubbles for the frothing of metal melts.
The determination of the temperature at which calcium carbonate decomposes into calcium oxide and carbon dioxide can be made by knowing the Gibbs energy value for this reaction.
The general equation to express the change in Gibbs energy is:

$$\Delta G_T^0 = A + B \cdot T \log T + C \cdot T\,, [J] \qquad (4.9)$$

where: A is constant, for $CaCO_3$; C is the constant, for $CaCO_3$; T is temperature [K].

The constants for equation (4.9), which relates to determining Gibbs energy change for the thermal decomposition of calcium carbonate, are A is 165777; constant B = 0 and constant C = 141.68.

$$\Delta G_T^0 = 165777 - 141.86 \cdot T \qquad (4.10)$$

To determine the decomposition temperature of $CaCO_3$, one can write: $\Delta G_T^0 = 165777 - 141.86 \cdot T = 0$.
T = 165777/141.86 = 1169 K, i.e. 896 °C.

According to CURRAN [41], the equation for the Gibbs energy change for the thermal decomposition of $CaCO_3$ is:

$$\Delta G_T^0 = 161000 - 137 \cdot T \qquad (4.11)$$

To determine the decomposition temperature of $CaCO_3$, according to equation (4.11), one can write: $\Delta G_T^0 = 161000 - 137 \cdot T = 0$.
T = 161000/137 = 1175 K, i.e. 902 °C.

For the foaming of aluminium alloys using calcium carbonate, the melt temperature must be close to 896 °C to 902 °C so that the thermal decomposition of the calcium carbonate can be used for foaming.

The equilibrium maximum partial pressure of CO_2 can be calculated using the equation:

$$logp_{Co2} = \frac{84\,100}{T} + 71{,}56 \text{ [MPa]}, \quad (4.12)$$

where: p_{CO2} is the partial pressure of CO_2 [MPa], and T is temperature [K].

The partial pressure p_{CO2} for the thermal decomposition of $CaCO_3$, as a function of temperature, is shown in Fig. 4.19. For the melting temperature of pure aluminium ($T_{melt.\ (Al)}$ = 660 °C): 1000/(660 + 273) = 1.07, for the melting temperature of AlSi12 ($T_{melt.\ (AlSi12)}$ = 577 °C): 1000/(577 + 273) = 1.17, see the grey markings in Fig. 4.19.

The decomposition rate of $CaCO_3$ is relatively slow. Purity and particle size have little effect on this rate. Experimentally, it is shown by [40], that thermal decomposition is strongly influenced by the carbon dioxide atmosphere. In connection with the foaming of aluminium or magnesium melts, attention must be paid to the thermodynamic laws of calcium carbonate decomposition in the melts of these metals. It has been confirmed by research that the thermal decomposition of the foaming agent $CaCO_3$ is thermodynamically advantageous only when it is accompanied by a subsequent reaction of the foaming gas with the metal melt.
The complete decomposition of $CaCO_3$ produces 0.56 kg of CaO and 0.44 kg of CO_2 (20 g of $CaCO_3$ produces *11.2 g of* CaO and *8.8 g of* CO_2). Calcium carbonate decomposition starts slowly above 600 °C, but higher temperatures accelerate the process until the thermodynamic decomposition temperature is reached.

According to the mineralogical composition, limestones are divided into high percentage limestones with over 98% $CaCO_3$; moderately contaminated with 90 to 98% CaCO3; moderately contaminated with 80 to 90% $CaCO_3$ and highly contaminated below 80% $CaCO_3$. Of the polluting components, silica (usually in the form of quartz), iron and aluminium compounds are most commonly present with $CaCO_3$. Magnesium oxide is a separate group, which, although not counted as an impurity, is a component that usually accompanies $CaCO_3$ as a homogeneous impurity.

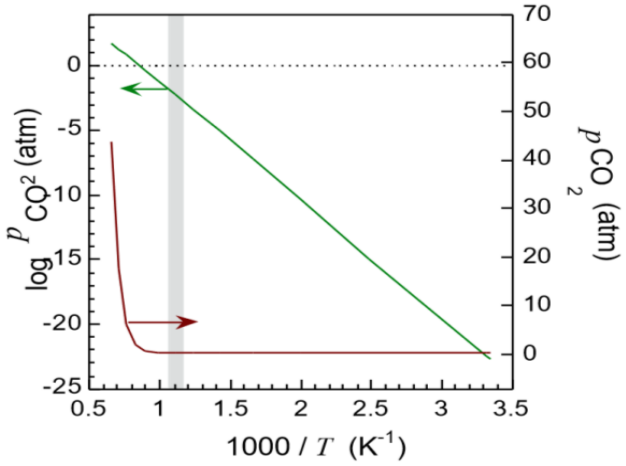

Fig. 4.19 Equilibrium partial pressure p_{CO2} for the thermal decomposition of $CaCO_3$, the grey markings indicate the melting temperatures of Al-Si type aluminium alloys [40]

Depending on the magnesium oxide content, we then speak of magnesian limestone, dolomitic limestone and then dolomite, which is an equimolar mixture of $CaCO_3$ and $MgCO_3$.
The dissociation of calcium carbonate takes place at a temperature that depends on the partial pressure of CO_2. The resulting CO_2 gradually begins to surround the decomposing calcium carbonate. To decompose $CaCO_3$, enough heat must be supplied to the system so that the pressure of CO_2 released from the calcium carbonate exceeds the partial pressure of carbon dioxide from the surrounding atmosphere. If the pressure of the CO_2 released is in equilibrium with the pressure of the oxide surrounding the $CaCO_3$, then the pressure of CO_2 equals the maximum pressure of dissociation for a given temperature, and is chemical equilibrium occurs. Equilibrium is reached when the ratio of the concentrations of the species formed and the starting species equals the equilibrium constant for a given temperature. In heterogeneous reactions, the equilibrium constant of the reaction is determined only by the concentrations (activities) of the gaseous products since the activity of a solid pure substance under standard conditions is equal to one. If the concentration or activity of the gaseous component is replaced by the partial pressure of CO_2, then the equilibrium constant will be equal to the partial pressure of CO_2. Thermodynamically, the decomposition of calcium carbonate can occur as early as 600 °C when the decomposition pressure of CO_2 is greater than the partial pressure of CO_2 in the normal atmosphere surrounding the calcium carbonate. Because the total pressure of the atmosphere is much higher than the tension of the carbon dioxide released at 600 °C, this gas can only be removed from the reaction space by diffusion, a very slow process.

Reactivity of the foaming gas (CO_2) - the reaction with aluminium is considered, where CO_2 (g) is reduced to form CO (g) and a film of α - Al_2O_3 is formed on the surface of the gas cell with the aluminium melt (at 650 °C this process is thermodynamically favourable with the condition ΔG^0_T = - 779 000 [J· mol^{-1}]), according to Eq:

$$2Al\ (l) + 3\ CO_2\ (g) \Rightarrow Al_2O_3\ (s) + 3\ CO\ (g) \qquad (4.13)$$

$$\Delta G^0_T = -\ 840\ 000 - 66.0 \cdot T\ [J \cdot mol^{-1}]. \qquad (4.14)$$

Another possibility is the reaction based on equations (4.8) and (4.13), resp. between $CaCO_3$ and Al:

$$2\ Al\ (l) + 3CaCO_3\ (s) \Rightarrow Al_2O_3\ (s) + 3CaO\ (s) + CO\ (g) \qquad (4.15)$$
$$\Delta G^0_T = -\ 300\ 000 - 417 \cdot T\ [J \cdot mol^{-1}]$$

Reaction (4.13) can take place over the entire surface of the gas cell [41], but reaction (4.15) is only chargeable in a small region of the solid-liquid contact area [41].
In Fig. 4.20, the free energy change, $G\Delta^0_T$, as a function of T for several possible reactions in molten foams of aluminium alloys.

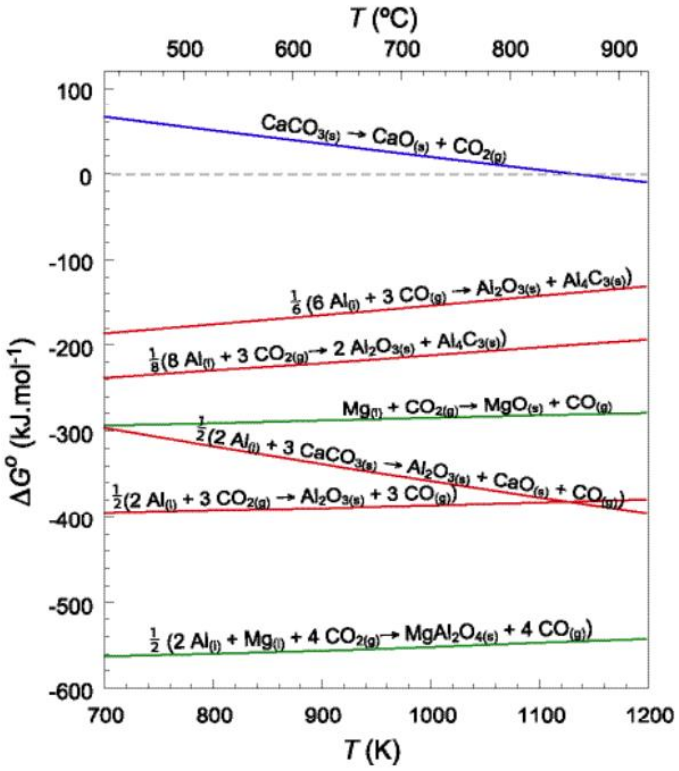

Fig. 4.20 Gibbs energy change $G\Delta^0_T$ as a function of temperature for several possible reactions in molten foams ($G\Delta^0_T$ relates to 1 mol of Mg or Al), all elements are assumed to be in the standard state, [41]

The Gibbs energy change ($G\Delta^0_T$) in Fig. 4.20 refers to 1 mol of Mg or Al, all elements are assumed to be in the standard state.

The use of the foaming agent $CaCO_3$ is currently being investigated by many researchers, e.g. GERAMIPOUR [42], who studied open-cell aluminium foam. This foam was produced using a low-capacity foaming agent, i.e., $CaCO_3$ and powder metallurgy. The fabrication procedure was carried out in a standard manner.

Powder mixtures of aluminium and $CaCO_3$ were cold compacted into compacted cylindrical precursors and prepared for the foaming process at specific temperatures under air atmosphere. In this context, the effects of several parameters were investigated: pressure for precursor preparation, suitable content of foaming agent, temperature and time of the foaming process, microstructure, linear expansion, relative weight

and compressive strength of the aluminium foam samples produced.

Fig. 4.21 shows the $CaCO_3$ particles, which are typically used for the foaming process. The purer the $CaCO_3$, the closer its decomposition temperature is to the theoretical temperature.

A uniform distribution of aluminium foam gas cells with a size of less than 100 μm was obtained, forming semi-open structures with relative masses ranging from 55.4 % to 84.4 %. Increasing the compaction pressure between 127 and 318 MPa and using a foaming agent up to 15 % (weight fraction) resulted in an increase in linear expansion, compressive strength and compaction density.

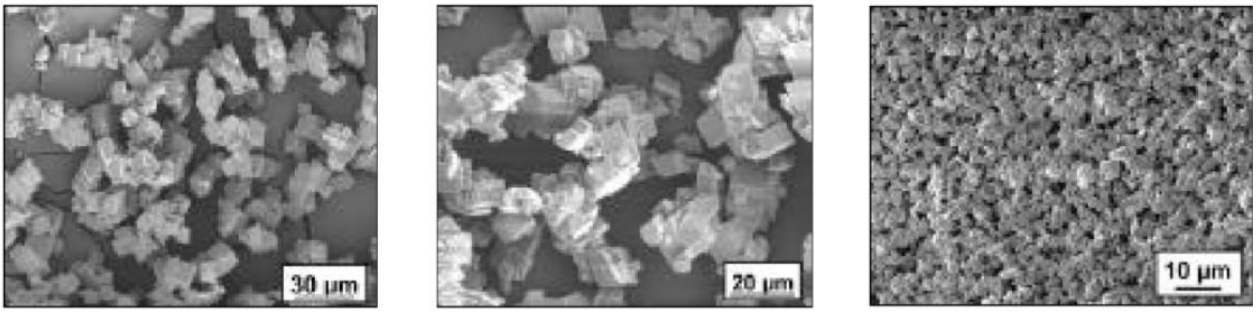

(a) 99.95-100.05% pure $CaCO_3$ (b) Precipitated 99.5% pure $CaCO_3$ (c) Ground 98% pure $CaCO_3$

$CaCO_3$ purity is higher than 99.95 % (left); precipitated form of $CaCO_3$ with 99.5% purity (middle), small particles of $CaCO_3$ with 98% purity (right)

Fig. 4.21 $CaCO_3$ powder particles of different particle size and purity, observed by scanning electron microscope [42]

Changing the foaming process temperature from 800 to 1000 °C induced an increase in all the parameters studied except compressive strength and relative bulk density. The results showed that the suitable foaming process temperature is 900 °C, and the foaming process time is 10 to 25 minutes. The DTA curve of $CaCO_3$ was monitored to determine the appropriate foaming process temperature (see Fig. 4.22a). This curve shows the temperature characteristics of the $CaCO_3$ foaming agent. There are two endothermic regions on the curve. One is at temperatures of 30 to 250 °C, and the other is at temperatures of 670 to 900 °C. The first relates to moisture loss and the second to $CaCO_3$ decomposition reactions.

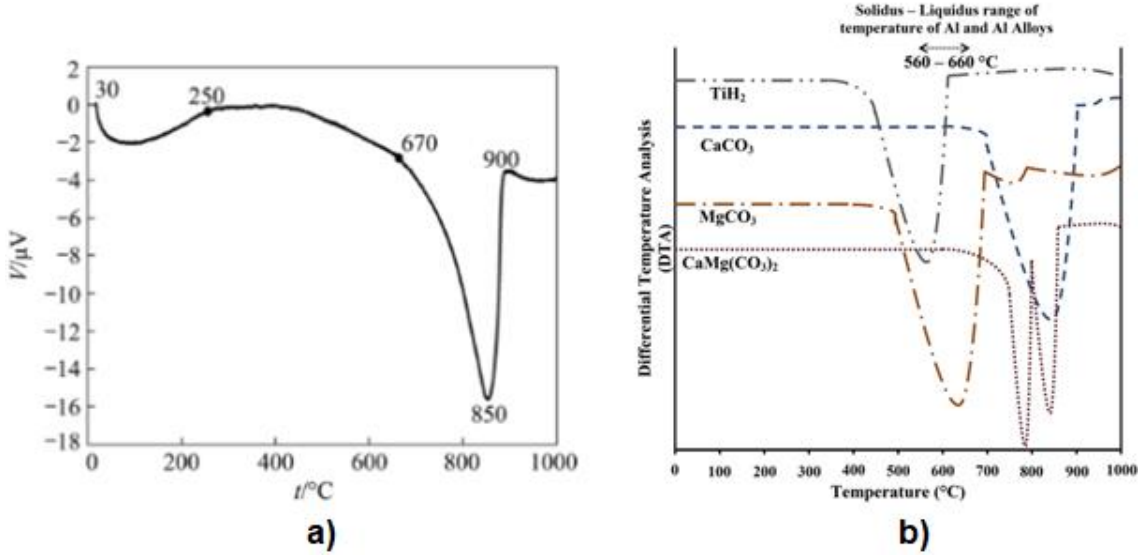

Fig. 4.22 Differential thermal analysis curve of $CaCO_3$ frother a) according to GERAMIPOUR [42]; b) DTA curves of different frothers when heated according to SOLOKI [49]

The thermal decomposition and release of CO_2 gas began at about 670 °C, and was completed at about 900 °C. The maximum rate of thermal decomposition of the $CaCO_3$ frother was at 850 °C.

Based on the temperature results resulting from the DTA curve, the temperatures (800 °C, 900 °C and 1000 °C) were selected for the experiments testing the $CaCO_3$ foaming process.

SOLOKI [49] observed the behavior of different foaming agents (see Fig. 4.22 b). This figure shows the differential thermal analysis (DTA) curves for the foaming agents: TiH_2, $CaCO_3$, $MgCO_3$ and $CaMg(CO_3)_2$. These curves were also observed concerning the liquid (melting) taplots of aluminium alloys (from 560 to 660 °C). The curve for TiH_2 shows an endothermic reaction starting at 410 °C (685 K) and ending at 605 °C (878 K), peaking at 570 °C (843 K). The curve for $CaCO_3$ shows an intense broad endothermic reaction starting at 625 °C (898 K) and ending at 890 °C (1163 K). The curve for $MgCO_3$ indicates a strong endothermic reaction that starts at 400 °C (673 K) and ends at 690 °C (963 K), peaking at 650 °C (923 K).
Several much smaller endothermic reactions can also be observed in the curve. The $CaMg(CO_3)_2$ curve shows two endothermic reactions, both sharper than those shown by the $CaCO_3$ or $MgCO_3$ curves. The first endothermic reaction on the $CaMg(CO_3)_2$ curve starts at 600 °C (873 K) and peaks at 780 °C (1053 K). The second endothermic reaction on the $CaMg(CO_3)_2$ curve peaks at 830 °C (1103 K) and ends at about 900 °C (1173 K).

Furthermore, HAESCHE et al. [35] have conducted investigations with the foaming agents: $CaCO_3$, $CaCO_3$ + CaO, $CaMg(CO_3)_2$. These foaming agents are characterized by a low purchase price. Two different aluminium alloys, AlSi9Cu3 and AlMg4.5Mn, were investigated. For foam production using $CaCO_3$, the AlMg4.5Mn alloy proved to be unsuitable in terms of its melting temperature. On the contrary, the AlSi9Cu3 alloy was shown to be suitable, precisely when using the foaming agents limestone and especially dolomite. These frothers are suitable for the production of precursors (small cylindrical bodies). Furthermore, CaO (calcium oxide) added for foam stabilisation is effective only for foaming agents with a lower decomposition temperature. An amount of 5 wt. % $CaMg(CO_3)_2$ without further stabilizing additives show an excellent foaming effect. The results obtained from the experiments carried out are shown in Fig. 4.23.

Fig. 4.23 shows the specific gravities of the samples of the produced aluminium foams made of aluminium alloy AlSi9Cu3 with different content of foaming agents: ($CaCO_3$, $CaCO_3$ + CaO, $CaMg(CO_3)_2$) at 3 and 5 wt.%, at foaming temperatures of 750 °C, 800 °C and 825 °C, according to HAESCHE [35]. Fig. 4.24 shows the structures of the foamed aluminium alloy AlSi9Cu3 using a foaming agent of 5 % wt. $CaCO_3$and a stabilising agent of 3 wt. % CaO. Using a foaming agent of 5 % wt $CaMg(CO_3)_2$ and a stabilizing agent of 3 wt.% CaO, the temperature of the foaming process was 825 °C [35].

Compared to the standard foaming agent TiH_2, a slight increase in the foaming process temperature is recommended. This measure is supported by a comparison of thermal analyses performed on all foaming agents. Foams with somewhat irregular gas cells (pores) were obtained. The large number of small pores is typical of the use of the dolomite frother as opposed to the calcium carbonate frother used. Currently, the advantages of the dolomite frothing agent over calcium carbonate are mainly explained for obtaining small pores. Based on the obtained knowledge, clear

interactions between $CaCO_3$ and $MgCO_3$, which form $CaMg(CO_3)_2$ and variations in their initial decomposition temperature and the reaction progress of the foaming agent (superconductor) $CaMg(CO_3)_2$ can be expected. The chemical compound MgO is very good for foam stabilization. There are differences in the amount of gas released for the foaming process.

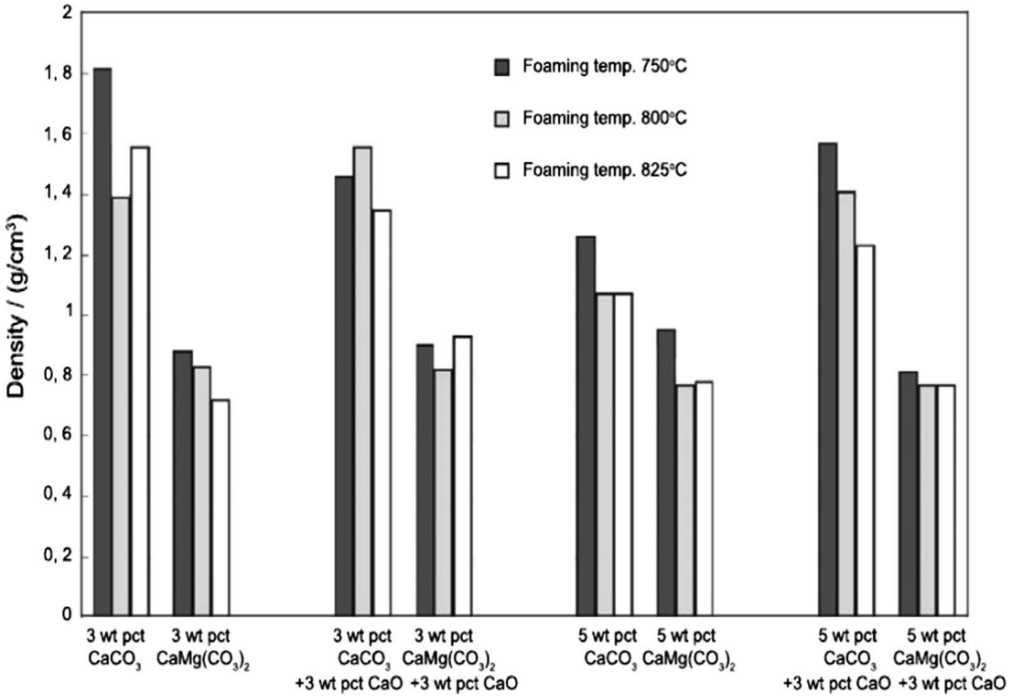

Foaming temperature: 750 °C is the black column, 800 °C is the grey column, 825 °C is the white column

Fig. 4.23 Densities of aluminium foam samples of AlSi9Cu3 alloy using different foaming agents $CaCO_3$, $CaCO_3$ + CaO, $CaMg(CO_3)_2$ at 3 and 5 wt.%, at foaming temperatures of 750°C, 800°C and 825°C, according to HAESCHE, as reported by SOLOKI, [49]

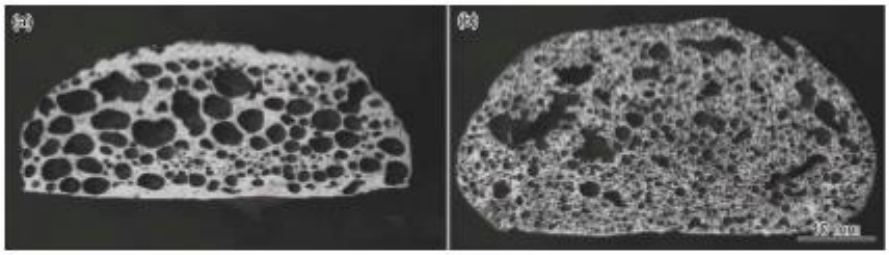

Fig. 4.24 Structure of aluminium foams made of AlSi9Cu3 alloy; left: with a foaming agent of 5 % wt.$CaCO_3$ and a stabilising agent of 3 % wt.CaO; right: with a foaming agent of 5 % wt. $CaMg(CO_3)_2$ and a stabilising agent of 3 % wt. CaO, foaming process temperature 825 °C, according to HAESCHE, as reported by SOLOKI, [49]

The method of producing metal foams where a foaming agent $CaCO_3$is added to the melt is also called FOAMCARP (*Foaming* of *Aluminium MMC* by *Chalk-Aluminium Reaction* in *Precursor*), i.e. foaming of aluminium MMC by $CaCO_3$ aluminium reaction

in the precursor (MMC Metal Matrix Composites). This method of producing metal foams, as is generally known, is based on the production of a precursor (a starting substance from which the final product is formed by chemical transformation).

The precursor production is based on the preparation of an aluminium melt first, which is mixed with a small amount of SiC, and then a foaming agent, which is $CaCO_3$, is added to the melt. After the solidification of the melt treated in this way, a foaming precursor (semi-finished product) is formed. By heating the precursor in the foaming mould to a certain temperature, the foaming process in the mould will occur and foamed aluminium will be formed. CURRAN [41] conducted research using a foaming agent $CaCO_3$ To assess the effect of purity and particle size of the $CaCO_3$ foaming agent on the kinetics of the foaming process, powders with particle sizes between 5 μm and 70 μm with different purities were analyzed and monitored using a scanning electron microscope (SEM), microphotographs of the different powders are shown in Fig. 4.25.

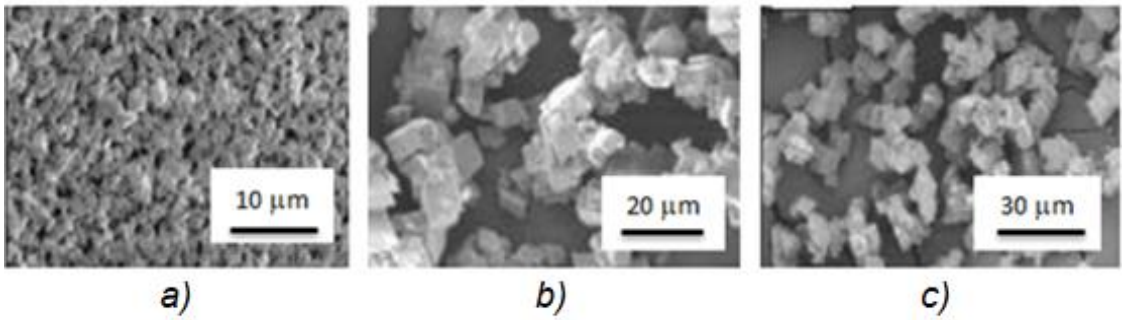

a) ground $CaCO_3$, purity 98 %, b) precipitated $CaCO_3$, purity 99.5 % c) pure $CaCO_3$, purity 99.9 %

Fig. 4.25 $CaCO_3$, different forms of its particles used in the FORMGRIP metal foam manufacturing process, monitored by SEM CURRAN [41]

At the same time, the effect of the foaming agent TiH_2 (see Fig. 4.26a), which was heat treated according to the time-temperature regime, was also analyzed (see Fig. 4.26b). The CaCO foaming agent$_3$ was used to produce aluminium foams by the FOAMCART process, and the TiH_2 foaming agent was used to produce aluminium foams by the FORMGRIP process.

Two materials were used for the foams under the name *Duralcan*^{TM} Al-SiC with Metal *Matrix Composites* (*MMCs*). One was designated F3S10S and the other F3S 20 S, the difference being the ceramic particle content, see Table 4-6.

Table 4-7 shows the chemical composition of the F3S10S and F3S20S alloys used to produce the foams.

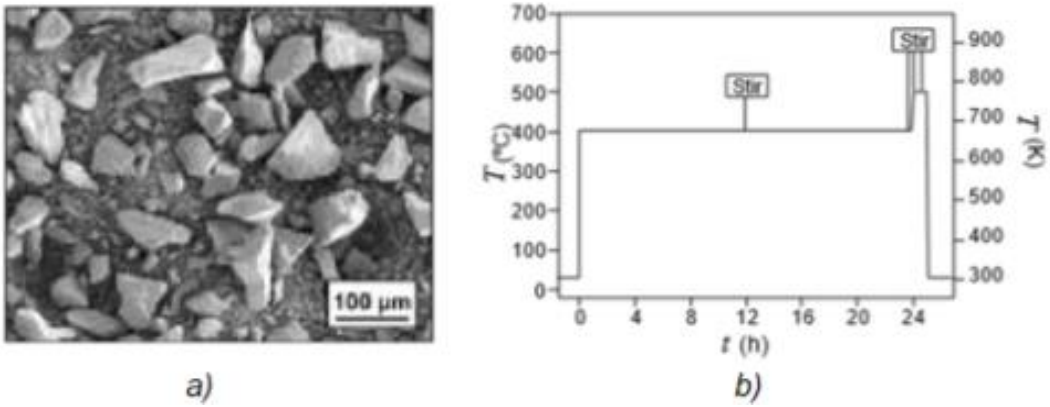

Fig. 4.26 a) the used heat-treated foaming agent TiH_2; b) the heat treatment mode of TiH_2 powder before its use in the FORMGRIP process (24 hours at 400 °C and 1 hour at 500 °C, resistance furnace in the presence of air) CURRAN [41]

Table 4-6 Characteristics of Duralcan™ powders [41]

Composite material Duralcan™ based on Al-SiC with metal matrix (Material Matrix Composites - MMCs)				
Mark Alloys	**Chemical Ingredients**	**SiC content [wt. %]**	**Particle size range [µm]**	**Average particle size [µm]**
F3S 10S	Al-Si9-Mg	10	3 to 19	9.3
F3S 20S	Al-Si9-Mg	20	5 to 24	12.8

Note: *F3S10S and F3S 20S have the same chemical compositions but differ in the SIC content of the composite.*

At the same time, Table 4-7 also lists other alloys that can be used in the production of metal foams.

Table 4-7 Overview of alloys for the production of aluminium foams [41]

Chemical composition of aluminium alloys used for the production of metallic "foams" [wt. %]									
Alloy designation	**Chemical designation**	**Si**	**Fe**	**Cu**	**Mn**	**Mg**	**No**	**Zn**	**Sn**
1050	Pure Al	0.25 max.	0.4 max.	0.05 max.	0.05 max.	0.05 max.	-	-	-
LM 6	AlSi 12	10.0 13.0	0.6 max.	0.1 max.	0.5 max.	0.1 max.	0.1 max.	0.1 max.	0.05 max.
LM 10	AlMg10	0.25 max.	0.35 max.	0.1 max.	0.1 max.	9.5 11.0	0.1 max.	0.1 max.	0.05 max.
LM 25	AlSi7Mg	6.5 7.5	0.5 max.	0.1 max.	0.3 max.	0.20 0.45	0.1 max.	0.1 max.	0.05 max.
6061	AlMg1SiCu	0.4 0.8	0.7	0.15 0.40	0.15 max.	0.8 1.2	-	0.25 max.	-
F3S 10 S	AlSi9Mg	8.5 9.5	0.2 max.	0.2 max.	0.03 max.	0.45 0,65	0.03 max.	0.03 max.	0.03 max.
F3S 20 S	AlSi9Mg	8.5 9.5	0.2 max.	0.2 max.	0.03 max.	0.45 0.65	0.03 max.	0.03 max.	0.03 max.

The frothing agent titanium hydride powder (325 mesh) containing particles smaller than 44 μm was supplied by *Goodfellow* Cambridge Limited of England. Before the foaming process, this powder was heat treated in the air at 400 °C and 500 °C, each time at a dose of 5 g in open ceramic crucibles according to the time-temperature regime in Fig. 4.26 b. Heat-treated (pre-prepared) TiH_2 powder was mixed into the aluminium melt or added to the aluminium powder.

The frothing agent used, $CaCO_3$, was obtained from *Alfa Aesar* Johnson Matthey GmbH. Three $CaCO_3$ frothers were obtained with relatively high purity (ground powder with a purity of 98 %, powder with a purity of 99.5 % and high purity powder with a purity above 99.95 %).

The production of aluminium foam by the FOAMCARP process, where the first step is the production of a foamable precursor, the process is shown schematically in Fig. 4.27 and described verbally below.

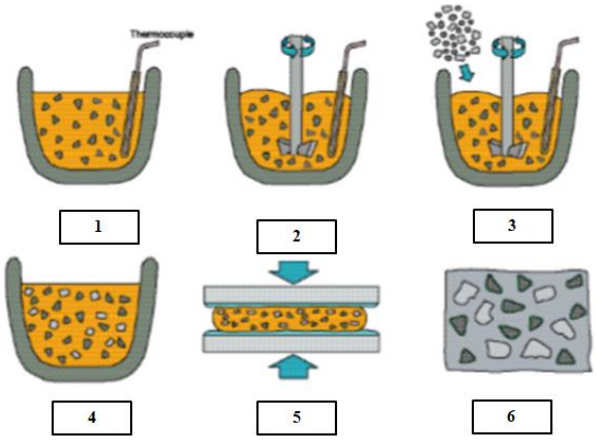

Fig. 4.27 Schematic diagram of the precursor production process for the FOAMCARP method of aluminium foam production using $CaCO_3$ CURRAN [41]

1. A quantity of 1 kg of aluminium alloy (e.g. AlSi12, $T_{tání}$ = 577 °C) is placed in a graphite crucible, which is heated in a furnace to a temperature of 645 °C (about 60 °C higher than the melting point of most alloys used). Temperature measurements are made using a K-type (NiCr-Ni) thermocouple in an alumina shroud placed in the crucible on the melt side. Induction heating of the material can also be carried out, which is effective and ensures a slight floating of the SiC particles in the melt.
2. When the melt temperature reaches about 645 °C, the furnace is switched off, and the melt is stirred at 450 rpm·min^{-1} using a stainless steel stirrer.
3. A $CaCO_3$ frother is added to the 635 °C melt. A suitable amount of $CaCO_3$ is about 3 % wt (33 g $CaCO_3$ per 1100 g melt). Because neither $CaCO_3$ nor TiH_2 frothers are normally well dispersible (dispersible) in the metal melt (most commonly, aluminium melt), aluminium powder (in this case, for example, AlSi12 powder)

must still be added to the melt. A ratio of 1:2 of aluminium powder to $CaCO_3$ has proven successful. This means that 66 g of AlSi12 powder must be added to 33 g of $CaCO_3$. and a stainless steel propeller agitator is introduced at the same time. The mixture of the two powders is stirred into the melt at a speed of about 450 rpm· min^{-1} for 60 seconds to achieve a dispersive and preferably regular distribution of the particles of both powders ($CaCO_3$ and SiC) in the melt. The melt is cooled by stirring. The mixture of powders is added to the melt at its temperature of 635 °C. The melt is also stirred immediately for about 60 seconds. At the same time, the stirring is assumed to cool the melt to a temperature of 580 °C.

4. The AlSi12 melt with $CaCO_3$ powder is stirred, and the $CaCO_3$ particles are gradually dispersed in the melt. Stirring stops at about 580 °C. This produces an increasingly viscous melt.
5. The viscous melt thus obtained is poured onto a boron nitride-coated heat-resistant plate. A heat-resistant plate is also applied to the surface of the melt, compressed to form a layer about 25 mm thick, which solidifies in air.
6. A foamable precursor containing AlSi12 % wt. and 10 % vol. SiC and 3 % wt. of the foaming agent $CaCO_3$ are obtained.

A stainless steel stirrer must be used for mixing to prevent the dissolution of the iron during mixing and its transfer to the melt. The melt is also in contact with the graphite crucible during mixing. Since the melt mixing is carried out in air, a small amount of surface oxide may also be introduced into the melt.
The precursor thus produced attained a relative density of $\rho_{REL.}$ = 0.8 to 0.85, this porosity being partly due to the introduction of gas into the melt during mixing and partly due to the premature release of a small amount of foam gas.

Production of aluminium foam by the FOAMCARP process, the second stage of the process, involves the processing of a foamable precursor. Precursors with dimensions (60 × 60 × 25 mm) were placed in a foaming mould, as shown in Fig. 4.28 (right) and subjected to heat treatment to melt the aluminium alloy AlSi12 and simultaneously foam it by thermal decomposition of the foaming agent $CaCO_3$, see Fig. 4.28 (left). After the solidification of the melt, the foamed AlSi12 alloy was obtained. For the foaming process, stainless steel moulds were shaped, and the interior of the moulds was coated with a protective layer of nitride boride. The temperature during foaming was monitored by a thermocouple inserted into a drilled hole in the precursor material.
The foaming precursor is heated to the appropriate temperature, at which point the AlSi12 alloy in the precursor is melted, and the $CaCO_3$ (s) $\Rightarrow$ CaO_2 (s) + CO_3 (g) is decomposed to form a foamed melt by placing the mold assembly. The time dependence of temperature during precursor heating is shown in Fig. 4.28 (left). The main variable is the foaming temperature (T_{foam}), which is the temperature equal to the temperature in the furnace at the time of the foaming process. The foaming time is defined as the time that occurs between the moment of foaming (the temperature reaches T_{foam}) and the moment when the foamed aluminium alloy (AlSi12) is removed

from the furnace. In experiments where the heating of the precursors was interrupted, it was found that a limited foaming process occurs before the foaming temperature T_{foam} is reached.

In the following situations, it was necessary to determine the required precursor heating parameters based on the wide range of temperatures and foaming times obtained.

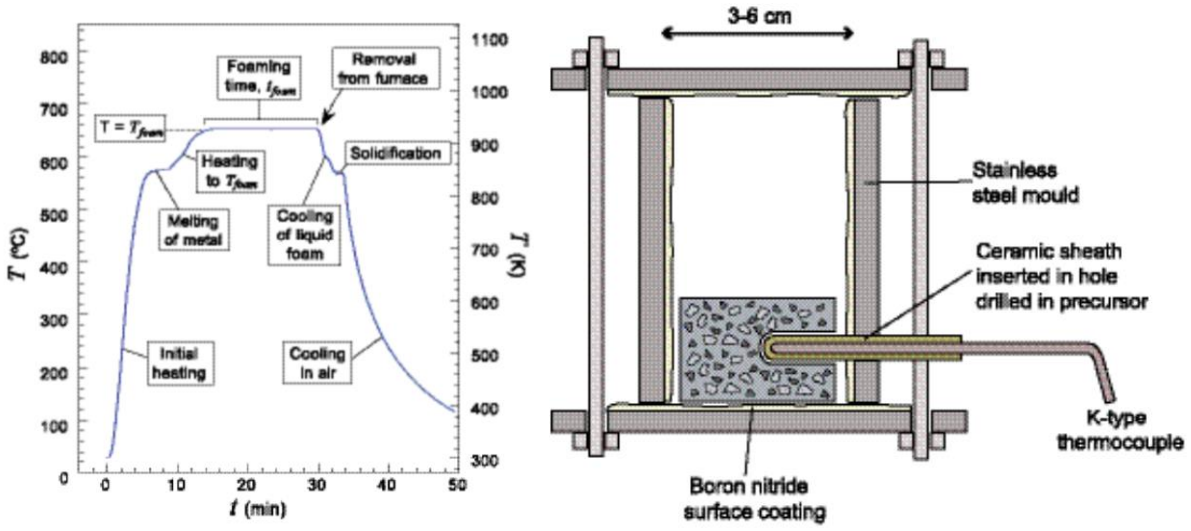

Fig. 4.28 Time dependence of the foaming process temperature with foaming temperature T_{foam} = 650 °C and foaming time t_{foam} = 900 s, FOAMCARP CURRAN foaming method (left) and foaming mould (right), CURRAN [41]

In the *FORMGRIP* process, TiH_2-based foams are typically produced by heating the precursors at 630 °C for 1 to 2 min, depending on the desired ratio (density of foam/density compact material). $CaCO_3$ foams require a longer foaming time, which is about 5 to 15 minutes. The foaming process temperature is slightly higher, at 650 °C for satisfactory production of aluminium foam (from AlSi12 alloy). To monitor the temperature in the precursor during the foaming process, it is advantageous to introduce a thermocouple into the precursor. At the end of the foaming process, the thermocouple is removed, and the foaming mould containing the foam is allowed to cool in air.

According to Curran [41], *induction heating* can also be used to heat *precursors during the foaming process.* Aluminium foams can be produced in this way; see the schematic of the experimental setup shown in Fig. 4.29 a). The device consists of an inductor coil into which a graphite crucible containing the foaming precursor is inserted. The temperature during the foaming process can also be measured by a thermocouple inserted in the precursor to monitor the temperature evolution and to control the foaming process if necessary. The foam produced is cooled in the air.

Induction heating of melts in direct metal melting - small samples of various alloys can also be heated by gas supply from an external source after induction melting, as described above and shown schematically in Fig. 4.29 b). The metal alloys are melted

and heated to the temperature of the foaming process by induction heating. The heating rate is then reduced to maintain an approximately constant temperature with a tolerance of ± 20 °C, and the foaming gases are introduced into the metal melt at a controlled rate. The resulting foamed metal melt can be fed into a mould which is subsequently cooled in air.

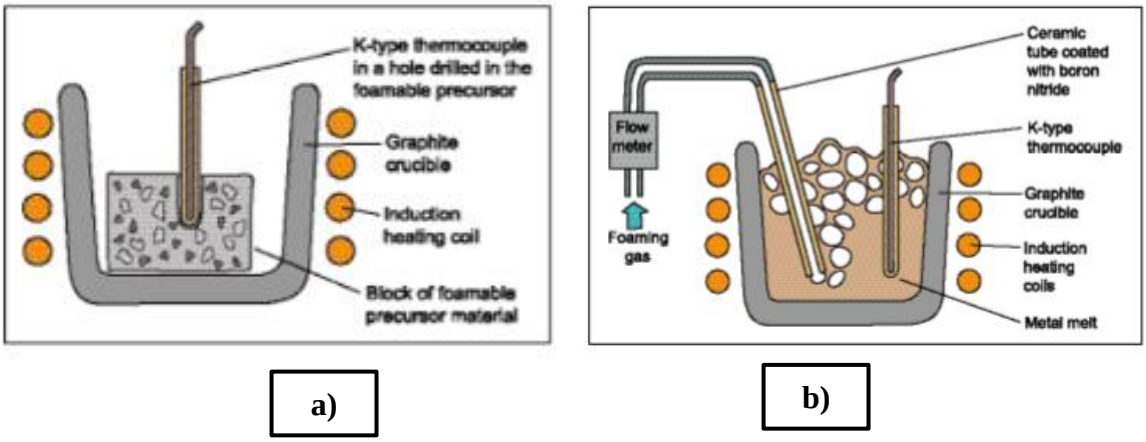

Fig. 4.29 a) Experimental set-up for induction heating of foaming precursors; b) experimental equipment for direct frothing of the melt after its induction melting

From the English description in Fig. 4.29 a), the induction heating of the foaming precursor is evident. This happens in the graphite crucible in which the precursor block material is heated. A hole is drilled in the precursor to accommodate a K-type thermocouple which monitors its temperature as it heats. Fig. 4.29 b) shows the induction heating of the melt fed directly from an external gas source. The melt is heated in a graphite crucible. The melt temperature is measured with a K-type thermocouple.

Research conducted by CURRAN [41] has shown that calcium carbonate is an effective foaming agent for aluminium, with several notable advantages over the currently used titanium hydride. Using the $CaCO_3$ foaming agent, the characteristic cellular structures of, in this case, aluminium foam were fabricated and investigated. Two methods were used to produce aluminium foams carried out by CURRAN [41]. The FOAMCARP method (process), which applies the CaCO foaming agent$_3$ and the FORMGRIP method (process), which uses the TiH foaming agen t$_2$. The foams produced by the two methods were compared. The results obtained for the foams produced in this way were compared. By comparing the results it is possible to see remarkable differences in terms of the structure of the foams produced and the influence of various parameters on the process. The most significant design feature of the calcium carbonate-based foams is the smaller cell size and thinner walls separating the gas cells from each other. The use of the foaming agent $CaCO_3$ leads to a significant increase in the stability of the molten foams. Many of these properties are attributed to the surfaces of the cells, which are covered with a thin oxide film formed early in the foaming process. The composition and morphology of the oxide film have

also been studied. At the same time, the implications in terms of the role of SiC were discussed and the effects of various parameters on and stability of the molten foams were investigated.

Based on the monitoring of the effectiveness of the $CaCO_3$ foaming agent, calcium carbonate was found to be a highly effective foaming agent for aluminium. Using it, aluminium foams can be produced with a similar level of porosity to aluminium foams produced using titanium hydride, but with several significant advantages.

The chemical decomposition of calcium carbonate is more gradual than the thermal decomposition of titanium hydride at the melting temperature of aluminium. This means that the FOAMCARP process for the production of aluminium foams is based on the production of a foaming precursor and its heating or heat treatment. For the production of the precursor, the foaming agent $CaCO_3$ is used in its natural state without prior heat treatment. This is in contrast to the publication of NAKAMURA [43], see Fig. 4.30, which instead carried out surface treatment of $CaCO_3$ before its foaming effect, a two-step process, to promote melt wettability in the production of aluminium foam. In contrast to CURRAN [41], NAKAMURA [43] considered the surface treatment of $CaCO_3$ before its foaming agent as very necessary. Fig. 4.31 shows the foams produced according to CURRAN [41] from an aluminium alloy AlSi9Mg0.5 and untreated $CaCO_3$ foaming agent.

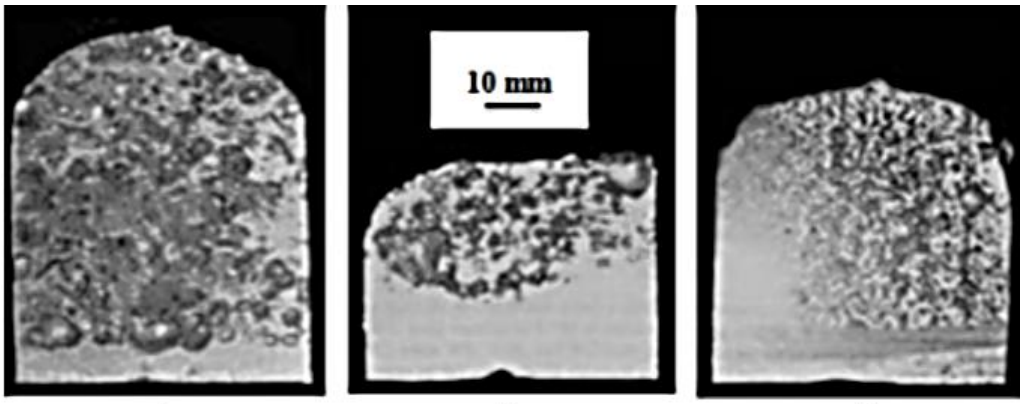

Fig. 4.30 Sections of aluminium foams using foaming agents: a) titanium hydride; b) calcium carbonate; c) pre-treated calcium carbonate, [43]

As mentioned above, the reduced speed of the $CaCO_3$ foaming process improves the control of the foaming process. CURRANO [41] found that foam production from AlSi9Mg0.5 alloy is most efficient with the addition of 10 % vol. SiC particles (denoted SiCp) and 3.3 % wt. of powdered $CaCO_3$ with a particle size of 20 μm, as it is difficult to ensure the dispersion of particles smaller than 10 μm.

The optimum heating time of the foaming precursor, for its foaming purpose in the production of aluminium foam (t_{foam}), is from 600 to 900 seconds (i.e. 10 min to 15 min) at a temperature of 650 °C. As shown above, this temperature is lower than the theoretical assumptions based on calculations using Gibb's energy change.

Fig. 4.31 Longitudinal sections of cylindrical bodies of foams produced using a foamable precursor (containing10 % vol. SiC particles with a size of 9 μm, and 3.3 % wt.$CaCO_3$ dispersed in AlSi9Mg0.5 matrix) with different temperatures (T_{foam}) and time of foaming process (t_{foam}). The respective technological conditions of foam production influenced the density of the produced foam (ρ_{foam}) and the relative density of the produced foam (ρ_{foam} /ρ_{compac}) CURRAN, [41]

The temperature thus calculated is about 900 °C. A frothing temperature of 650 °C for the thermal decomposition of $CaCO_3$ during the frothing process may be sufficient when there is significant contamination of the aluminium melt due to the presence of various process components. For the production of aluminium foams using a titanium hydride foaming agent, a suitable foaming time (t_{foam}) of 60 to 180 seconds at a temperature (T_{foam}) of 630 °C is suitable. The FOAMCARP method can produce aluminium foams with a highly homogeneous cell structure, with a relative specific gravity ($\rho_{foam}/\rho_{compac}$), of about 0.15 to 0.2, using an AlSi9Mg0.5 alloy. From the partial results, it can be seen that at the foaming temperature (T_{foam}) = 650°C and the foaming time (t_{foam}) = 300 s, the foam bulk density (ρ_{foam}) = 671 [kg·m^{-3}], relative bulk density, (ρ_{foam} /ρ_{compac}) = 0.25 was obtained. With increasing foaming foam(t_{foam}) of about 900 s at the same foaming temperature (T_{foam}) of 650 °C, the specific gravity of the foam (ρ_{foam}) = 410 [kg·m^{-3}] was reduced, and thus the relative specific gravity (ρ_{foam} /ρ_{compac}) = 0.15. With an increase in the foaming temperature (T_{foam}) = 750 °C and a foaming time (t_{foam}) = 300 s, again a lower specific gravity (ρ_{foam}) = 285 [kg·m^{-3}] and also a lower relative specific gravity ($\rho_{foam}/\rho_{compac}$) = 0.12 was produced. Again, an increase in the length of the foam produced can be observed. At a foaming temperature (T_{foam}) = 750 °C and with a longer foaming time (t_{foam}) = 900 s, aluminium foam is produced with a bulk mass (ρ_{foam}) =314 [kg·m^{-3}] and a relative specific gravity (ρ_{foam} /ρ_{compac}) = 0.11.

The use of the foaming agent $CaCO_3$ in the production of aluminium foams was also investigated by KEVORKIAN [40]. He successfully replaced the foaming agent TiH_2 powder with calcium carbonate ($CaCO_3$). Fig. 4.32 shows $CaCO_3$ and its TG and DSC curves. These curves show that the thermal decomposition of this $CaCO_3$ is above 800 °C.

For the production of foams, [40] used several calcium carbonate powders with different average particle sizes (38, 72 and 120 µm). Foam precursors were produced with different $CaCO_3$ powder contents (3 to 10 % vol.). The precursors were produced by melt and powder metallurgy methods. The precursors obtained by powder metallurgy showed excellent homogeneity and a density ≥ 98 %. For the precursors produced by powder metallurgy, 3 to 7 vol. % $CaCO_3$ were used with an average particle size of 38 µm and a density ≥ 99 %. The efficiency of the foaming process of the experimentally prepared precursors was evaluated by assessing the relative density of the foams obtained (apparent volume weight of the foam divided by the density of the compact aluminium).

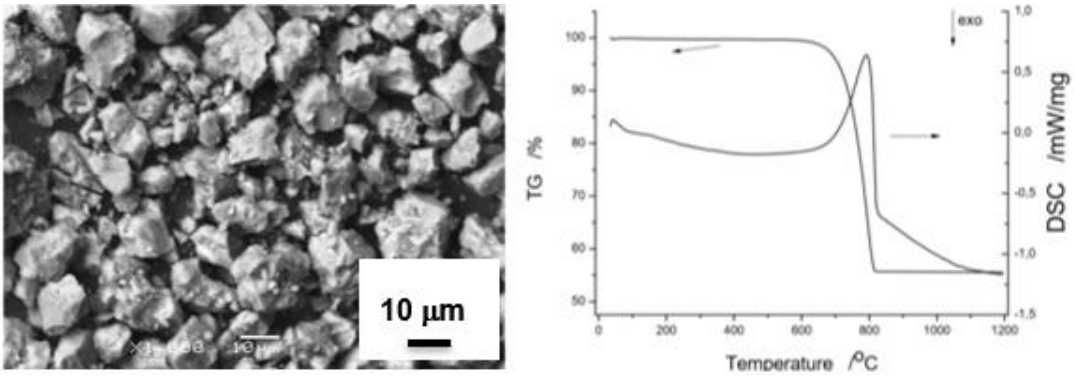

Fig. 4.32 CaCO particles$_3$, viewed with a scanning microscope (left); thermogravimetric curve - TG and differential scanning calorimetry curve-DSC for $CaCO_3$ (right) [40]

The experimental findings showed that the apparent specific gravity of the foam samples is inversely proportional to the specific gravity of the foamed precursor. Thus, foamable precursors with higher specific gravity led to foamable samples with lower apparent specific gravity and higher foaming efficiency. Higher foaming efficiency leads to the formation of "foam" with finer pores. The mechanical properties (compressive strength and energy absorption) of foam samples are also strongly influenced by foaming efficiency. For the range of foams analysed, about 550 $kg \cdot m^{-3}$, the compressive strength reached up to a value of about 13 MPa for samples with a lower foaming efficiency of about 79.6 %. This is in contrast to the maximum energy absorption value achieved for the foams with the highest foaming efficiency. From the results obtained, it is clear that the properties of aluminium foam are strongly dependent on its porosity. By comparing the properties of foams obtained through the foaming agents TiH_2 and $CaCO_3$, it was found that the microstructure, compressive strength and impact energy absorption are comparable when using both foaming agents. The evaluation of $CaCO_3$-based foaming powders for the production of aluminium foams was also addressed by LAZÁRA et al. [44], who conducted a systematic study on the evaluation of foamability using an alternative mixture of carbonates in molten aluminium. Foams were produced by varying the carbonate content, mixing it into the molten aluminium and then carrying out a foaming process.

In addition, the addition of small amounts of TiH_2 in combination with these carbonates was also tested. The experimental results suggest that using the $CaCO_3$ foaming agent, with the correct technological regime, it should be possible to obtain aluminium foams of similar quality to those obtained using the TiH_2 foaming agent, but at a lower cost. This confirmed the conclusions of the research [41]. At the same time, [44] states that when using a TiH_2 foaming agent, it is always necessary to use a stabilising agent, which is e.g. SiC (particle size 5 to 25 μm). In this context, MIYOSHI [45] mentions two effects of using $CaCO_3$, that is, the foaming and stabilizing effect of the produced foams.
As confirmed by GERGELY et al. [46], when using the foaming agent TIH_2, it must be heat treated beforehand.

Research carried out by Lazaro et al [44] confirmed that the decomposition of $CaCO_3$ shows an elevated onset temperature, see Fig. 4.33, compared to TiH_2 (not shown) with its thermal decomposition or early gas release resulting in dispersion problems, too rapid expansion etc.

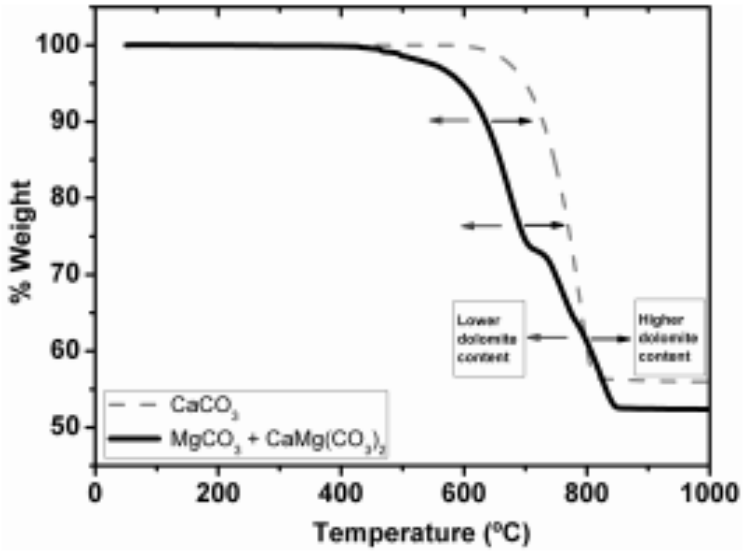

Fig. 4.33 Thermogravimetric curves, dashed curve belongs to $CaCO_3$, solid curve belongs to the mixture $MgCO_3$ + $CaMg(CO_3)_2$, [44]

The authors [44] used a foaming agent they called an alternative carbonate designed and evaluated in this publication, referred to *as "flotation sterile", i.e. sterile flotation.* It consists of a mixture of coarse powders of magnesite and dolomite (where the particles are smaller than 250 μm). The main advantage of this froth flotation reagent, compared to commercial TiH_2 or $CaCO_3$ froth flotation reagents, is that *$MgCO_3$ and $CaMg(CO_3)_2$* by-products (CaO, MgO) can be recovered based on their origin. The thermogravimetric curve in Fig. 4.33 for the mixture $MgCO_3$ + $CaMg(CO_3)_2$ shows that thermal decomposition occurs between temperatures of 500 and 850 °C (that is, between the thermogravimetric curves for TiH_2 and for $CaCO_3$) and occurs in two steps.
The first step - the decline corresponds mainly to the decomposition of magnesite. The *second step* corresponds to both magnesite decomposition and dolomite

decomposition. The change in the dolomite content of the powder of the thermogravity curve can be shifted to higher or lower temperatures and offers additional possibilities for selecting the correct powder of the frother depending on the properties of the alloy used. In addition, "sterile flotation" decomposition directly produces both CaO and MgO, as opposed to calcium carbonate, which produces only CaO. This offers several other advantages. For one its use is not limited to Al-Mg alloys, which is necessary to ensure acceptable froth stability and efficiency in the $CaCO_3$ froth flotation process [47].

The foaming processes of the researchers [44] for the production of aluminium alloy foam were applied to an alloy type AlCu4Mg1Mn1) with a weight of 500 g, and a melting temperature of 660 to 680 °C. A graphite crucible was used for foaming, and several experiments were carried out with the content of the foaming agent ranging from 0.7 to 5 % wt. of a mixture of $MgCO_3$ + $CaMg(CO_3)_2$ foaming agent powders. Each time the appropriate amount of frother was added to the melt and the melt was stirred for 1 to 3 minutes, at a stirrer speed of 600 rpm·min^{-1}. After mixing, the crucible was maintained at the appropriate temperature for some time while the expansion process was taking place. The crucible with the foamed melt was then removed from the furnace and cooled in air until the melt solidified. If two-stage foaming is used, then immediately after the first melt stirring, another foaming agent is added and stirred for 30 seconds. The crucible is then left in the furnace again for some time and the melt is maintained at a certain temperature, which has been selected based on the relevant TG found (see Fig. 4.33). While the melt is maintained at a certain temperature, the expansion process takes place. The melt is then removed from the furnace and cooled in air until it solidifies. Fig. 4.34 shows the results of researchers [44] two-stage foaming using $MgCO_3$ + $CaMg(CO_3)_2$.

Fig. 4.35 shows sections of foam samples that were produced at different conditions (% powder, mixing time, foaming time) *(a)* 1.5 % wt. 1 min, 60 s; *(b)* 2.5 % wt., 1 min, 60 s; *(c)* 5 % wt., 1 min, 60 s; *(d)* 1.5 % wt., 1 min, 30 s; *(e)* 1.5 % wt., 1 min, 120 s; *(f)* 1.5 % wt., 3 min, 120 s, according to LAZAR, [44], using a mixture of the foaming agents $MgCO_3$ + $CaMg(CO_3)_2$ and the aluminium alloy AlCu4Mg1Mn1.

It can also be observed in Fig. 4.35 that there is an unstressed area, almost at the same height, on the fabricated foamed AlCu4Mg1Mn1 alloy parts. The melt mixing time was also evaluated in this context. It was found that if the stirring time is increased from 1 minute to 3 minutes, then excessive oxidation is caused by the melt. This corresponds to Fig. 4.35 (f). The effect of the foaming time is evident from Fig. 4.35 (a), Fig. 4.35 (d) and Fig. 4.35 (e), which show the structure of the samples when 1.5 % wt. of the foaming agent is used. From these results it is evident that the amount of foaming agent and the foaming time have a positive effect on the foaming process, see the foaming in Fig. 4.35 (b), 2.5 %wt. of foaming agent and a foaming time of 60 seconds contributed to this foaming. The foaming in Fig. 4.35 (e) was contributed by 1.5 % wt. of the foaming agent and a foaming time of 120 seconds. From the results of the authors [44], it is clear that the expansion rate of this mixture of foaming agents is very low but constant. This slow growth, caused by the gradual decomposition of the

foaming agent mixture, shows its high stability when compared to the $CaCO_3$ foaming agent.

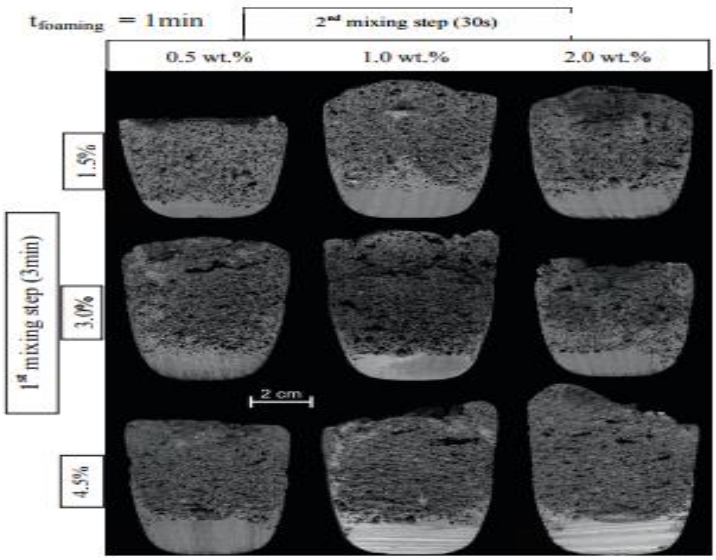

Fig. 4.34 Cutting through manufactured foams in one-stage and two-stage foaming [44]

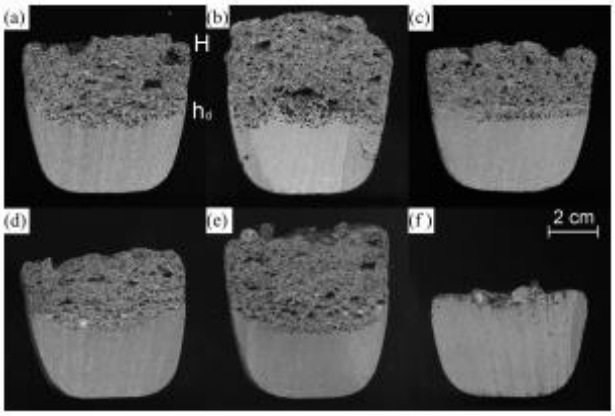

Fig. 4.35 Sections of foam samples produced at different conditions in order of value (% powder, mixing time, foaming time) (a) 1.5 % wt., 1 min, 60 s; (b) 2.5 % wt., 1 min, 60 s; (c) 5 % wt., 1 min, 60 s; (d) 1.5 % wt., 1 min, 30 s; (e) 1.5 % wt., 1 min, 120 s; (f)1.5 % wt., 3 min, 120 s, frothing agent $MgCO_3$ + $CaMg(CO_3)_2$; AlCu4Mg1Mn1 [44]

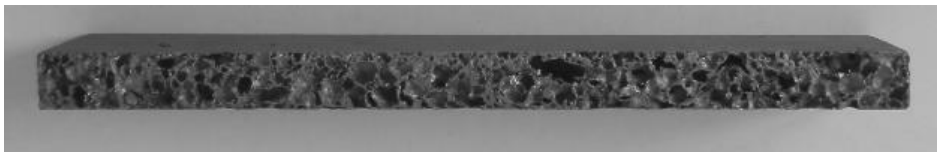

Fig. 4.36 Foam cut by powder metallurgy using TiH_2 foaming agent

As can be seen from Section 4.4, there is a great deal of research effort to produce aluminium "foams" using the foaming agent $CaCO_3$. It is clear from the results obtained and published to date that the quality of foam shown in Figure 4.36 has not been achieved. This foam was produced by powder metallurgy using the foaming agent TiH_2.

5. METALS FOR THE PRODUCTION OF CELLULAR MATERIALS

5.1 Metals and metal alloys for the manufacture of cellular materials

For the production of metallic cellular materials (metal foams and porous metallic materials), mainly low-density metals are used. Because the specific gravity of the ceramic particles used to form the walls of the air bubbles is comparable to the density of the molten metal. This is particularly important for the production of metal foams that are based on direct gas foaming from an external source. For example, the density of aluminium alloy melts ranges from 2300 to 2380 [$kg \cdot m^{-3}$], while the density of small SiO_2 particles of 0.1 mm shows a specific gravity of about 2600 [$kg \cdot m^{-3}$]. These particles are moving in the bottom or sedimenting at the bottom of the froth cups. It is, therefore, important that the frothing gas is brought to the bottom of the crucible.

For the production of aluminium cellular materials (aluminium foams), several aluminium alloys are used [23], e.g. EN AW 1060, EN AW 3003, EN AW 6016 or EN AW 6061, AlMg1Si0.6, which are forming alloys. According to [23], the most commonly used alloy for direct melt foaming is A 356 (EN AC 42 100 - AlSi7Mg0,3), 1 % wt. magnezium can be added to this alloy. This small amount of magnesium slightly reduces the density of the melt, which is advantageous for direct frothing of the melt with gas from an external source. In addition, the alloy EN AC 42 200 can be used, this alloy contains 0,6 % wt. of magnesium. It has been found that when aluminium alloys intended for forming are used, the foams produced have a smaller gas cell size than when foundry alloys are used. AlSi12 alloy can also be used for the production of powder metallurgy-based cellular materials.

For the production of foams by direct melt foaming, the above alloys are most often used for the production of the so-called Metal - Matrix - *Composite (MMC).* This means that the respective metal is mixed with an appropriate amount of ceramic material (SiC, Al_2O_3, MgO etc.) after melting and the melt is thoroughly mixed so that the added ceramic material particles have as homogeneous a distribution as possible in the melt. After the melt has solidified, this material is called a *metal matrix composite.* Using EN AC 42 100 alloys, it has been shown [24] that it is a good idea to heat treat the SiC particles (10 μm in size) before preparing this metal matrix composite material. Heating and holding at 950 °C for 1 hour and then holding at 650 °C for 2 hours.

The heat treatment is done to reduce the absorbed gases in the SiC particles. When using the aluminium alloy AlSi7Mg0,3 for the production of aluminium foams (temperature 650 to 680 °C), it is also necessary to add particles of ceramic material to the melt. Subsequently, it is necessary to mix them with the melt at a speed of 1400 $rpm \cdot min^{-1}$. After the solidification of this alloy, a metal matrix composite is produced. As in the other example, this composite is subsequently melted and stirred again when the melt reaches 700 °C. This is due to the need for a homogeneous arrangement of SiC particles in the melt. Depending on the circumstances, an additional 5 % vol. of SiC particles may be added to this melt and then the melt is foamed in the presence of a foaming medium or a foaming agent.

In these cases, the influence of ceramic particles on the properties of the foams produced is most often monitored. Experiments, where 10 vol. % SiC, 15 vol. % and 20 vol. % SiC were added to the melt were observed. During foaming, the melt temperature was 730 °C and air was always blown into the melt at a rate of 2 to 4 $l \cdot min^{-1}$ at a pressure of 0.2 MPa. The results showed that with the addition of 5 vol. % SiC, the porosity of the produced foam reaches 96 %, the wall thickness of the gas cell is about 100 μm and the specific gravity of the produced foam of aluminium alloy (AlSi7Mg0.3) is 100 [$kg \cdot m^{-3}$]. When 10 vol. % SiC was used, a porosity of 94 % was obtained the wall thickness of the gas cell was 180 μm and the specific gravity of the aluminium alloy foam produced was 160 [$kg \cdot m^{-3}$]. Using 15 vol. % SiC, a foam porosity of 90 % was obtained, the cell wall thickness was 250 μm and the specific gravity of the aluminium alloy foam was 250 [$kg \cdot m^{-3}$]. Using 20 vol. % SiC, the porosity of the foam produced was 88 %, the cell wall thickness was 370 μm and the specific gravity of the aluminium alloy foam was 320 [$kg \cdot m^{-3}$]. The cell size ranged from 18.5 to 20.5 mm.

5.2 Physical properties of metal melts

Melts of metals and their alloys are media whose kinematic viscosity is of the order of a Newtonian fluid, therefore metal melts are governed by the laws of hydromechanics.

5.2.1 Viscosity of metal melts

Viscosity characterizes the internal resistance to the flow of a melt (liquid) caused by the internal friction of the melt particles as they move. Thus, the higher the viscosity (internal friction) of the melt, the slower the melt flows, it has less fluidity. As the temperature of the melt increases, its viscosity decreases and thus the melt has a higher fluidity. Viscosity is divided into two groups (dynamic and kinematic).

Dynamic viscosity (internal friction) characterizes the resistance that a fluid imposes on the actual movement (flow) or other mutual change of the particles of a liquid medium. It corresponds to the force required to cause a certain displacement of the flowing medium (a mass of 1 kg displacement in a time unit of 1 s by a length of 1 m). The unit is 1 Pa.s (Pascal second, $kg \cdot m^{-1} \cdot s^{-1}$). The dynamic viscosity η (éta) is calculated from Eq:

$$\eta = \frac{\tau}{\frac{dv}{dy}} \; [kg \cdot s^{-1} \cdot m^{-1}, \; N \cdot s \cdot m^{-2}, Pa \cdot s \,]; \tag{5.1}$$

where: τ is tangential stress acting between the fluid layers in the direction of the medium motion; dv/dy is the magnitude of the velocity gradient perpendicular to the fluid flow motion.

.

Dynamic viscosity is the ratio of the tangential stressτ acting between the layers (particles) of the fluid in the direction of the medium motion to the magnitude of the velocity gradient dv/dy perpendicular to the flow.
The dynamic viscosity of pure aluminium is about 0.0012 to 0.0013 [Pa·s].
Kinematic viscosity ϑ (theta) better describes the effect of the melt on its flow velocity. Kinematic viscosity can be calculated from the relationship:

$$\vartheta = \frac{\eta}{\rho} \ [m^2 \cdot s^{-1}] \tag{5.2}$$

where: ρ is the density of the melt [kg·m^{-3}] (aluminium melt has a density of about 2380 kg·m^{-3}).

The kinematic viscosity of aluminium is about 5.04·10^{-7} to 5.65·10^{-7} [m^2·s^{-1}]. The viscosity of melts or liquids decreases exponentially with temperature. The temperature dependence of viscosity is expressed by the Arrhenius equation [20]:

$$\eta = \eta_0 \cdot \exp\left(\frac{E_A}{R \cdot T}\right) \ [Pa \cdot s], \tag{5.3}$$

where: η_0 is frequency factor [Pa·s], E_A is the activation energy of the viscous flow required to overcome potential barriers during the transition of particles between moving layers [J·mol^{-1}], R is universal gas constant 8. 314 [J·mol^{-1}·K^{-1}], T is temperature [K].

It is known from metallurgical practice that an increase in the melt temperature of an aluminium alloy by 100 °C leads to a reduction in its viscosity of about 20 %.

Equation (5.3) is suitable for determining the dynamic viscosity of molten inorganic alloys at temperatures where the viscosity is low (below 1 kPa s) [21].
The quantity of dynamic viscosity is in units of [Pa· s] according to the SI system. It is also sometimes given as [kg·s^{-1}·m^{-1}]. Dynamic viscosity according to various authors, especially in the natural sciences, is also given in *mPa· s, i.e. milli Pascal second = 0.001[Pa·s].*

The dynamic viscosity values of pure aluminium are known, but little is known about the viscosity values of aluminium alloys, e.g. based on Al-Si. These alloys have received attention e.g. by SHIRANGAM [17]. Also little published are viscosity values as a function of temperature. It is known from physical laws that the viscosity of substances or metal melts decreases with increasing temperature. Fig. 5.1, Fig. 5.2, Fig. 5.3 show the temperature dependence of the viscosity of various Al-Si alloys.

The viscosity values of the melt at the values used for its superheat are of the order of magnitude similar to the viscosity of water. This allows the application of the laws of hydromechanics to the melt flow in the mould channels (inlet system). A higher value of melt viscosity slows down its flow through the channel.

Foreign particles (e.g. slag) in the melt increase its viscosity. The viscosity of metal melts is deliberately increased in the production of metal foams by adding various substances (SiC, Al_2O_3, MgO, etc.).

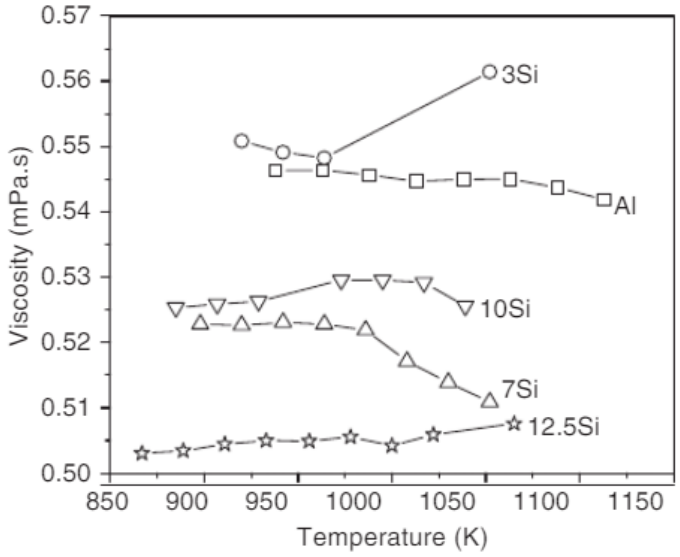

Fig. 5.1 Viscosity values of aluminium and aluminium-silicon alloys as a function of temperature according to SRIRANGAMA et al. [17]

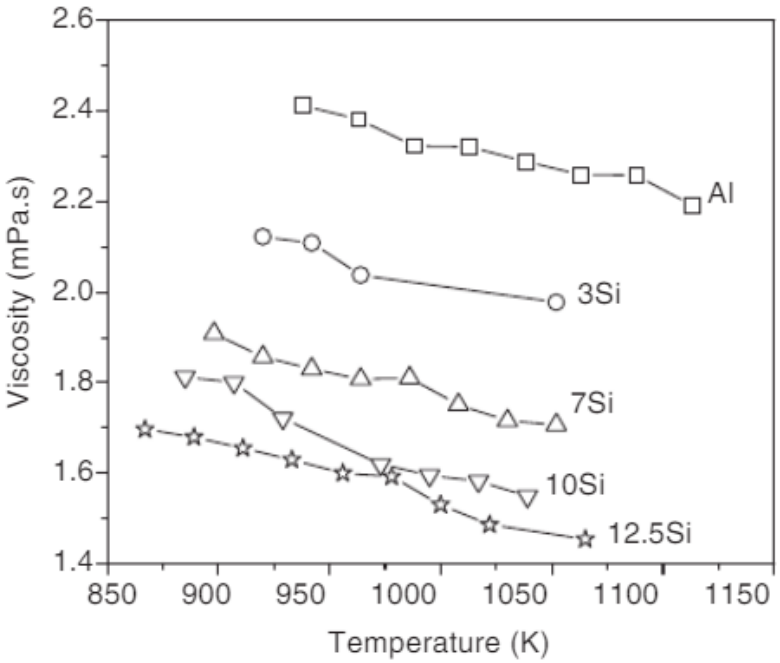

Dynamic viscosity 1.42 mPa·s = 0.00142 Pa·s, [kg·s^{-1}·m^{-1}]; kinematic viscosity is calculated by dividing dynamic viscosity by density (kinematic viscosity is 0.00142 divided 2380 is 5.9·10^{-7} [m^2·s^{-1}])

Fig. 5.2 Viscosity values of aluminium and sub eutectic aluminium-silicon alloys according to the empirical model [17]

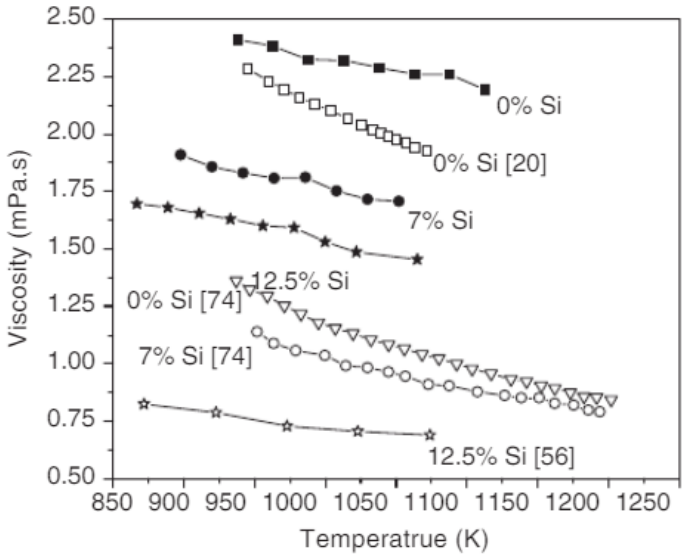

Note *- the bibliography is for this fugure only:*
[20] IIDA, T. and R.I.L. GUTHRIE. The Physical Properties of Liquid Metal, Clarendon Press, 1988.
[56] SONG, X. BIAN, X. ZHANG, J. and J. ZHANG. Journal of Alloys and Compounds 479, 2009, p. 670.
[74] SKLYARCHUK, V. et al. International Journal of Thermophysics. 30 (2009), p. 1400.

Fig. 5.3 Comparison of viscosity values of Al and Al-Si alloys experimentally determined with viscosity values reported in the literature, according to SRIRANGAMA et al. [17].

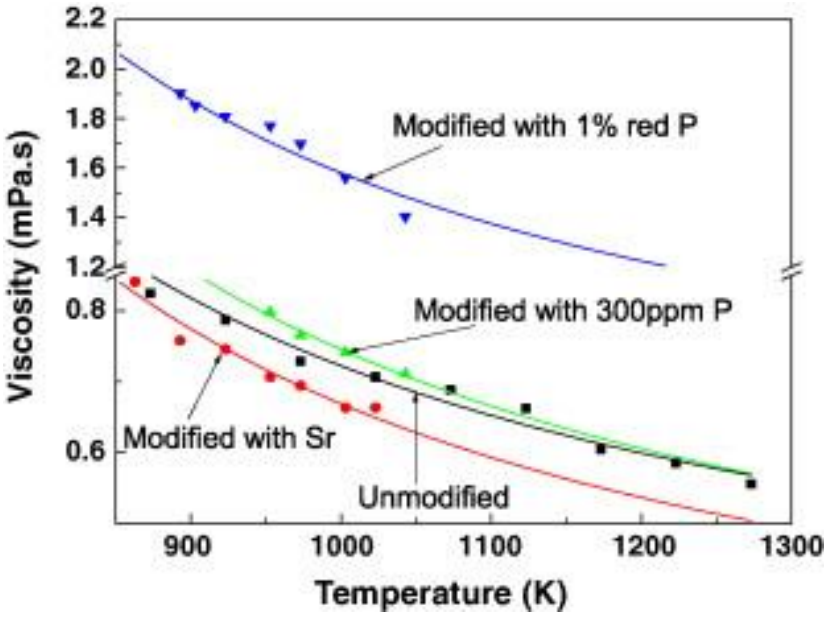

Fig. 5.4 Dependence of dynamic viscosity on temperature for memodified AlSi12 alloy (for indicative assessment of values), [19]

Table 5-1 lists the dynamic and kinematic viscosity values of various metal melts for comparison of aluminium with other non-ferrous metals.

Table 5-1 Dynamic and kinematic viscosity values of different metal melts Kalousek [1]

Melt viscosity values of selected metals				
Metal (metal alloy)	**The specific gravity of melt [kg· m^{-3}]**	**Temperature [°C]**	**Dynamic viscosity η [Pa·s]**	**Kinematic viscosity ϑ [m^2·s^{-1}]**
Aluminium	2410	750 700	2.70·10^{-3} 3.00·10^{-3}	1.06·10^{-6} 1.25·10^{-6}
Copper	8450	1150	3.80·10^{-3}	0.45·10^{-6}
Zinc	6650	500	3.68·10^{-3}	0.54·10^{-6}
Tin	10645	400	1.37·10^{-3}	0.20·10^{-6}
Iron	7400	1600	4.00·10^{-3}	0.53·10^{-6}
LLG (cast iron)	6900	1310	2.65·10^{-3}	0.30·10^{-6}
LKG (cast iron)	6800	1260	2.10·10^{-3}	0.29·10^{-6}

Table 5-2 shows the characteristic melt values of AlSi12 aluminium alloy and strontium and phosphorus-modified AlSi12 alloy. The quantities listed in Table 5-2 denote: η_0 is the pre-exponential factor in the Arrhenius equation, see (5.3), η_L is the viscosity at liquidus temperature, Ea is the activation energy for viscous flow, and T_L is the liquidus temperature, [20]. These values are used to calculate the dynamic viscosity according to equation (5.3).

Table 5-2 Characteristic values of unmodified AlSi12 melt and strontium and phosphorus-modified AlSi12 melt [20]

Characteristics of modified and unmodified AlSi melt				
Aluminium alloy	**Frequency factor η_0 [Pa·s]**	**Activation energy E_A [J·mol^{-1}]**	**Liquid temperature T_L [K]**	**Dynamic viscosity η_L [Pa· s]**
AlSi12	2.343·10^{-4}	9316.49	843	8.902·10^{-4}
AlSi12 300 ppm P (0,03 % P)	2.145·10^{-4}	10361.53	865	9.058·10^{-4}
AlSi12, P	3.427·10^{-4}	12709.34	870	1.986·10^{-3}
AlSi12 0,2 Sr	1.789·10^{-4}	10962.12	844	8.531·10^{-4}

5.2.2 Surface tension of metal melts

It results from the uniform application of forces on the surface of the melt particle σ [N.m^{-1}]. If the melt has a large surface tension, it tends to form a spherical shape and has a large wetting angle $\Theta > 90°$. Then this melt particle contacts the substrate over a small area. Conversely, a melt with a small surface tension has a small wetting angle$\Theta < 90°$ and contacts the substrate over a large area of the particle. If the melt is in contact with the mould and exhibits a large wetting, then we say the mould is metallophilic. If the melt does not wet the mould much then we call it metallophobic.

This type of mould is disadvantageous for filling with melt as the melt does not exactly follow the shape of the mould cavity.
The surface tension of metal melts can be calculated based on an empirical formula, according to KALOUSEK [1]:

$$\sigma = \alpha \cdot \frac{\rho}{M_{m(x)}} = 7{,}87 \cdot 10^{-6} \cdot \frac{\rho}{A_{r(x)} \cdot M_u} \; [N \cdot m^{-1}], \tag{5.4}$$

where: α is coefficienta experimentally determined ($7.87 \cdot 10^{-6}$ J·m·mol^{-1}], ρ is the density of the molten metal [kg·m^{-3}], and$_{r(x)}$ is the molar mass of the metal in question, and M_u is the molar mass constant 10^{-3} [kg· mol^{-1}].
Based on equation (5.4), the surface tension of aluminium, whose relative atomic mass is 26.98, can be calculated. One mol of Al = $26.98 \cdot 10^{-3}$ [kg· mol^{-1}]. Specific gravity of molten aluminium = 2410 [kg·m^{-3}]. This calculation can be used to determine the surface tension of aluminium to be 7.0310^{-1} [N·m^{-1}].

Relatively few researchers have investigated the surface tension of aluminium and aluminium alloys, but FERREIRA et al. [14] have investigated the surface tension of pure Al, Si and Al-Si alloys. To do this, they used the oscillating droplet method combined with electromagnetic levitation. However, the surface tension of the alloys in the Al-rich composition is strongly affected by oxygen adsorption at the same oxygen partial pressure. With increasing Si concentration, the surface tension of the alloy approaches the values of the oxygen-reduced surface. In Fig. 5.5, Fig. 5.6 and Fig. 5.7 are the temperature dependences of the surface tension of aluminium, silicon and ternary and quaternary aluminium alloys.
The researcher SHI [16] presents a relationship for calculating the surface tension of molten aluminium alloys, Al-Si type:

$$\sigma = 967{,}81 - 180{,}94 \cdot w - 1{,}81 \cdot t - 0{,}14 \cdot T, \tag{5.5}$$

where: σ is the surface tension of molten silumin (Al-Si) alloy, w is the amount of degassing agent, t is degassing time, and T is the temperature of melt during degassing.

The authors KOBATAKE et al. [22], observed the surface tension of pure metals Al, Si as well as melts of Al-Si alloys. For this, they used the oscillating drop method in combination with electromagnetic levitation. However, they concluded that the surface tension of the Al-rich composition alloys is strongly affected by oxygen adsorption at the same oxygen partial pressure. With increasing Si concentration, the surface tension of the alloy approaches the values of the surface that is affected by oxygen.
These authors [22] give an overview of published values of aluminium surface tension, according to different authors, as shown in Table 5-3. In this table, the surface tension, σ_L, and its temperature coefficient (temperature coefficient surface tension) σ_T, of liquid aluminium measured by methods (SD by sessile drop, LD by large drop, EML by electromagnetic levitation, ESL by electrostatic levitation, ADL by aerodynamic

levitation, μ_G by oscillating drop method under microgravity) are reported. A similar situation is shown in Table 5-4, where the surface tension of silicon is given.

Table 5-3 Surface tension values of aluminium according to different authors as reported by KOBATAKE [22]

Surface tension values of clay according to different authors				
Author	**Method**	**σ [N m].$^{-1}$**	**$\sigma_T/10^{-4}$ [N m K].$^{-1}.^{-1}$**	**Literature**
GOUMIRI	SD	0.865	-1.20	[28]
LEVIN	SD	0.866	-1,50	[29]
POPEL	SD	0.930	-1.46	[30]
YATSENKO	SD	0.865	-1.60	[31]
CORDOVILLA	MBP	0.865	at 1073 K	[32]
SARAVANAN	MBP	0.850	-1.5	[33]

Note: *MBP - maximum bubble pressure method in a nitrogen atmosphere.*

Table 5-3 shows the surface tension according to different authors. Also listed in this table is the temperature coefficient (σ_T) of the aluminium melt measured near the aluminium melting temperature using methods (*SD* sessile drop; *MBP* maximum bubble pressure).

Table 5-4 Silicon surface tension values according to different authors, according to Kobatake [22]

Silicon surface tension values according to different authors						
Author	**Method**	**Substance in a cup**	**The atmosphere used**	**σ [N·m^{-1}]**	**$\sigma_T/10^{-4}$ [N·m^{-1}·K^{-1}]**	**Reference**
KINGREY	SD	MgO	He H_2	0.740 0.860	-	[24]
DZHEMILEV	SD	Al_2O_3	He	0.750	-	[25]
ELYUTIN	SD	BN	He	0.833	-0.84	[26]
MUKAI	SD	BN	By	0.830	-7.40	[27]

Note: *BN is a special substrate; its composition is unknown.*

Table 5-5 shows the surface tension values of the Al-Si system, including pure aluminium and silicon, according to [22].

Table 5-5 Surface tension values of Al-Si, pure aluminium and silicon, KOBATAKE, [22]

Surface tension values of Al-Si alloys according to different authors			
Material	**Liquid temperature T_L [K]**	**σ_L [N·m^{-1}]**	**$\sigma_T/10^{-4}$ [N·m^{-1}· K^{-1}]**
Al	933	$9.79 \cdot 10^{-1}$	-2.71
Si	1685	$8.26 \cdot 10^{-1}$	-4.12
AlSi12	842	$8.24 \cdot 10^{-1}$	-0.31
AlSi20	957	$8.53 \cdot 10^{-1}$	-1.16
AlSi30	1084	$8.38 \cdot 10^{-1}$	-0.83

		$8.48 \cdot 10^{-1}$	-2.11
AlSi40	1420	$8.21 \cdot 10^{-1}$	-1.99
AlSi50	1422	$8.06 \cdot 10^{-1}$	-1,39
AlSi60	1424	$8.34 \cdot 10^{-1}$	-1.27
AlSi65	1479	$8.24 \cdot 10^{-1}$	-0.27
AlSi80	1574	$8.22 \cdot 10^{-1}$	-0.37
AlSi90	1630	$7.86 \cdot 10^{-1}$	-1.50

Fig. 5.5 shows the temperature dependence of the surface tension of the aluminium melt.

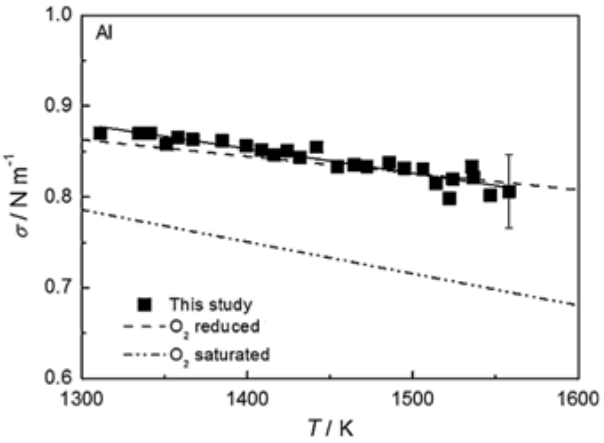

Dashed and dotted curves, after LEVINA E.S. et al. [35]

Fig. 5.5 Surface tension of aluminium melt as a function of temperature, according to KOBATAKE [22] and LEVIN [35]

Fig. 5.6 shows the surface tension dependence of the melt of Al-Si alloys with different aluminium contents.

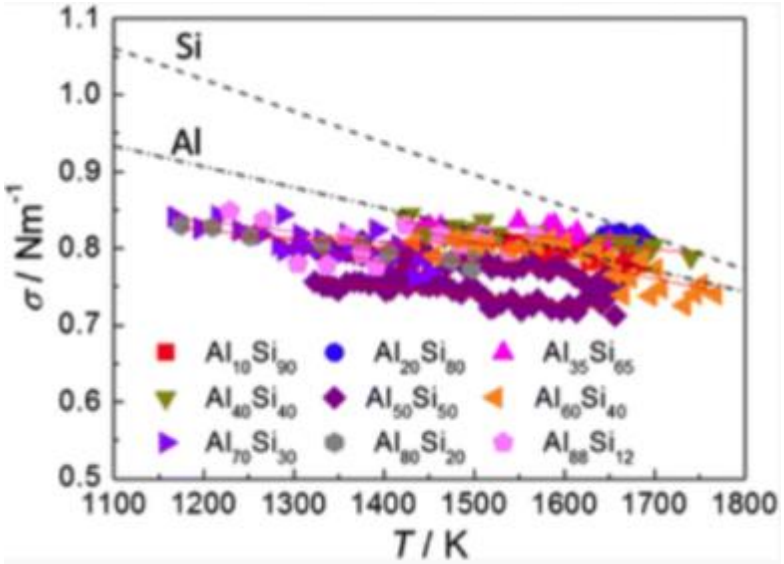

Fig. 5.6 Surface tension dependence of Al-Si alloy melt with different aluminium content, KOBATAKE [22]

Fig. 5.7 compares the surface tension waveform of liquid aluminium and liquid silicon as a function of temperature according to EGRYHO as reported by [22], with the values according to KAPTAYE [14], Fig. 5.8 shows the temperature dependence of the surface tension of the Al-Si ternary and quaternary systems according to [14].

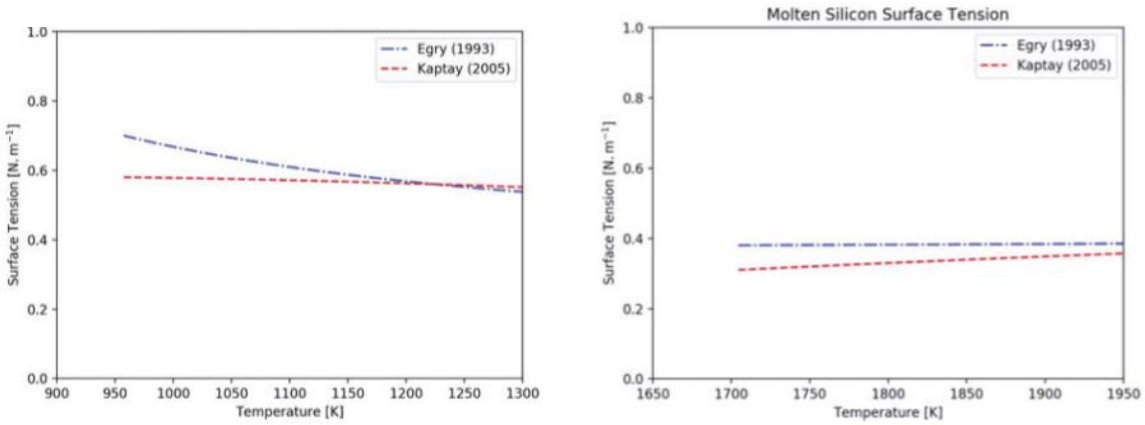

Fig. 5.7 Comparison of the temperature-dependent surface tension of liquid aluminium with the values of EGRYHO (1993) with the values of KAPTAYE (2005), according to [22], left and comparison of the temperature-dependent surface tension of liquid silicon with the values of EGRYHO (1993) with the values of KAPTAYE (2005), according to [22], right

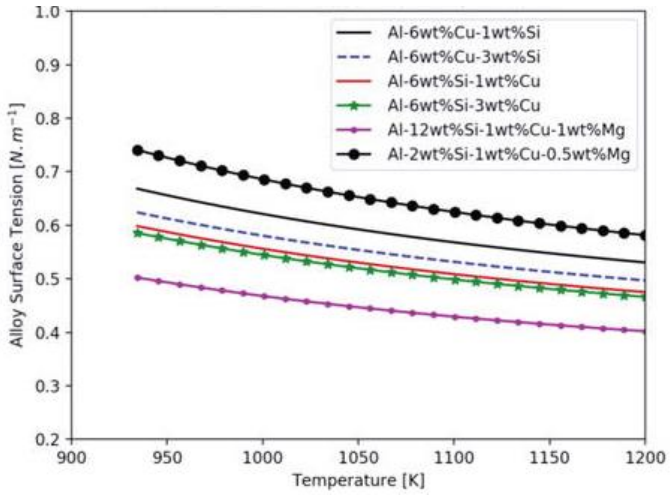

Fig. 5.8 Surface tension dependence on temperature for ternary alloys (Al-Cu-Si) and quaternary alloys (Al-Cu-Si-Mg), [22]

In order to verify the correctness of equation (5.5), experiments were carried out with a eutectic Al-Si alloy, [16]. The surface tension of the melt was monitored. The surface tension and temperature were measured on a physical property analyzer. Before the experiments, the melt of the alloy was degassed. The amount of degassing agent ***w*** was (0.10; 0.20; 0.30; 0.40 and 0.50 wt. %) as shown in Table 5-6. It was found that degassing reduces the surface tension

of the molten Al-Si alloy. The surface tension of the Al-Si alloys was calculated according to relation (5.5) taking into account also the amount of degassing agent, degassing time and degassing temperature. Table 5-6 shows the measured and calculated surface tension values of Al-Si alloy according to [16]. Table 5-7 shows the surface tension values of metal melts according to KALOUSEK [1].

Table 5-6 Surface stress values calculated and measured according to [16]

Surface tension of the Al-Si alloy values calculated and measured						
Number	**Quantity w [%]**	**Time [min]**	**Temperature [°C]**	**Surface tension σ [N·m^{-1}]**		**Deviation [%]**
				calculation	***measured***	
1	0.10	10	730	$8.294 \cdot 10^{-1}$	$8.346 \cdot 10^{-1}$	- 0.6
2	0.20	8	746	$8.127 \cdot 10^{-1}$	$8.164 \cdot 10^{-1}$	- 0.5
3	0.30	10	735	$7.925 \cdot 10^{-1}$	$8.012 \cdot 10^{-1}$	- 1.1
4	0.35	9	721	$7.873 \cdot 10^{-1}$	$7.847 \cdot 10^{-1}$	0.3
5	0.40	12	735	$7.708 \cdot 10^{-1}$	$7.781 \cdot 10^{-1}$	- 0.9
6	0.50	12	738	$7.523 \cdot 10^{-1}$	$7.468 \cdot 10^{-1}$	0.7

Table 5-7 Surface tension values of metal melts according to KALOUSEK [1]

Surface tension values of selected metals		
Metal (metal alloy)	**Temperature [°C]**	**Surface tension [N·m^{-1}]**
Aluminium	660 660 660 750	1.07 1.05 0.65 0.49
Copper	1180	1.10
Tin	500	0.53
Magnesium	680	0.55
Steel (0.3 % C)	1520	1.50
Cast iron with flake Graphite	1300	1.10

Note: ***water (20 °C) 0, 073 [N·m^{-1}].***

The pores formed in the low viscosity aluminium melt tend to coalesce into larger bubbles and the buoyancy force pushes them to the surface of the melt. In the production of foamed aluminium, it is necessary to prevent the foam from collapsing before it solidifies. Therefore, stabilising agents of ceramic origin are added to the melt during foaming. Alternatively, substances are added which form stabilising particles. The stabilising particles positively influence the foam against collapsing. The literature indicating the amount of these particles added to the melt is not uniform. This is because it is often not clear whether these particles are added to the melt as a weight or volume percentage.

For example, the production of aluminium foam by direct blowing of gases into the melt from an external source, the *Cymat* corporation method, applied by a Canadian company, is referred to in the literature as *SAF* Stabilization Aluminium Foam. The foam contains 10 % to 20 % ceramic particles of 5 to 20 μm in size.

5.3 Overview of metal melt viscosity enhancers

Silicon carbide is a compound of carbon with silicon (SiC) found very rarely in nature as the mineral *moissanite.* It is often mistakenly stated that there is a quadruple bond between the C and Si atoms in this compound. Due to the spatial structure of the solid formed by the tetrahedra, the bond is simple; there is no separate SiC molecule. The melting point of silicon carbide is 2730 °C and the specific gravity is 3210 kg m^{-3}. Silicon carbide is produced by reacting carbon with silicon:

$C + Si \Rightarrow SiC$

or the reaction of silica with carbon:

$SiO_2 + 3C \rightarrow SiC + 2CO$ (at 2 000 °C)

possibly by the reaction of silicon with carbon monoxide:

$Si + 2CO \rightarrow SiC + CO_2$.

Silicon carbide is used for the production of metal foams, especially for the production of aluminium alloy foams. In metal foams it acts as a viscosity increasing agent and affects the surface tension of metal melts, especially aluminium alloys. It is a high quality material. Silicon carbide comes in different colours (black, green etc.) Black silicon carbide is harder and more brittle relative to green silicon carbide. The production of black silicon carbide is done by melting silica sand and petroleum coke at temperatures above 2000 ˚C in a resistance furnace. It is removed from the furnace in its coarse state and is crushed and sorted into grades with precise grain size. Grains in the range of F10 to F220 are sorted on sieve classifiers, micro grains F-240 to F-3000 are sorted by sedimentation in a water bath. The sorting is carried out in accordance with FEPA, Standard 42 GB 1984 R 1993. The grain sizes produced according to FEPA are F-12 to F-1500. Fig. 5.9 shows a view of the silicon carbide and its particle. SiC with a particle size of 5 to 20 μm is suitable for foam manufacturing purposes.

Fig. 5.9 Black silicon carbide powder (left), black particles silicon carbide (right)

The grain size of silicon carbide is shown in Table 5-8. Table 5-9 shows the chemical analysis of silicon carbide.

Table 5-8 Overview of silicon carbide grain sizes

Grain size of black silicon carbide			
(98% SiC; 0.2% Fe_2O_3 ; 0.2% free C; 0.001% Fe, 1.6% other) *Bulk specific gravity 1200 to 1600 [kg·m^{-3}]*			
Designation	**Grain size [μm]**	**Designation**	**Grain size [μm]**
F14	1700 - 1400	**F150**	106 - 90
F16	1400 - 1180	**F180**	90 - 75
F20	1180 -1000	**F220**	75 - 63
F24	850 – 710	**F240**	70 - 22
F30	710 – 600	**F280**	59 - 22
F36	600 – 500	**F320**	49 - 17
F40	500 – 425	**F360**	40 - 12
F46	425 – 355	**F400**	32 - 8
F54	355 – 300	**F500**	25 - 5
F60	300 – 250	**F600**	19 - 3
F70	250 – 212	**F800**	14 - 2
F80	212 – 180	**F1000**	10 - 1
F90	180 - 150	**F1200**	7 - 1
F100	150 - 125	**F1500**	5 - 0.8
F120	125 - 106		

Table 5-9 Chemical analysis of silicon carbide

Characteristics of SiC					
Chemical composition by weight [%]				*Mechanical properties*	
SiC	**Fe_2O_3**	**free C**	**free Fe**	**Hardness Mohs**	**Bulk weight [kg·m^{-3}]**
98	0.2	0.2	0.001	9.5	120 -160

Calcium (Ca) is a reactive, low-density, silvery metal that belongs to the group of *alkaline earth metals*. Its melting point is 842 °C, specific gravity 1550 kg·m^{-3} It is relatively soft and its properties are more similar to those of alkali metals. Calcium is very reactive and in nature forms only calcium compounds Ca^{2+}. When heated, it readily combines with nitrogen to form calcium nitride Ca_3N_2 and with hydrogen to form calcium hydride Ca^{2+} and with a large number of elements to form compounds at higher temperatures.

Calcium is used as an agent to increase the viscosity of the aluminium melt. Mainly in the production of metal cellular systems (metal foams) by the *ALPORAS* method. Approximately 1,5 % by weight of calcium is added to the aluminium melt at 680 °C and the melt is stirred for 6 to 10 minutes in air at a temperature of 670 to 690 °C. When calcium is added to the melt, chemical reactions start to take place to form CaO_2, $CaAl_2O_4$, or Al_4Ca, and the viscosity of the melt increases significantly. This metallurgical treatment of the melt contributes to a higher intensity and successful foaming process.

Aluminium oxide (Al_2O_3) is a crystalline substance, usually white in colour, which is formed by the combustion of aluminium or by the dehydration of aluminium hydroxide. Alumina occurs naturally as the very hard mineral corundum, crystallizing in a trigonal (dome) system. Its specific gravity is about 4100 $kg \cdot m^{-3}$. The melting point of Al_2O_3 is about 2050 °C, so it is very heat resistant. It is also characterized by an amphoteric structure. It is produced from *bauxite*. It is non-toxic in nature and has considerable technical applications. A type of corundum is emery. Gemstones found in nature are blue *sapphire* and red *ruby*.
For the production of metal foams, it is used as an agent that increases the viscosity of the melt and favourably affects its surface tension. This effect is based on the principle that Al_2O_3 particles adhere to the melt. For the purpose of producing metal foams, 12 to 15 wt% Al_2O_3 is used.

Magnesium oxide (MgO) is a white crystalline substance found in nature as the mineral *periclase*. MgO crystallises in FCC, its melting point is 2800 °C. Magnesium oxide is easily prepared by burning a thin magnesium sheet burning in air under a brilliant white flame. The reaction produces a white *hygroscopic powder*.
For the production of aluminium foams, it is used as a reagent for the stability of aluminium foam.

In the first step for the preparation of the foamed melt by direct gas injection from an external source, it is important to add one of the following substances (stabilising agents: silicon carbide, aluminium oxide or magnesium oxide). SiC particles are widely used for this purpose. Their addition to the melt is to increase its viscosity, or even to increase the surface tension, which favourably affects the foaming process. For example, patent 4 973 358 A, which relates to the production of foamed aluminium by gas from an external source, specifies the addition of a number of particles depending on the aluminium alloy used, see Table 5-10.

Table 5-10 Amount of stabilising agent used for the production of aluminium foams

Amount of stabilising agent used for the production of aluminium foams					
Manufacturer / Method	**Quantity Stabilization reagents**	**Used Alloy**	**Temperature melt [°C]**	**Size particles SiC [μm]**	**Revolutions (RPM) [min^{-1}]**
Hydro Aluminium/ Cymat Aluminium	12 % vol. *SiC*	AlSi7	750	-	-
MMC (metal matrix composites) melt	10 to 20 vol. % *SiC or Al_2O_3*	AlSi10Mg	not stated	5 - 20	-
LKR Metcomb	10 to 20 vol. % *SiC or Al_2O_3*	not specified	not specified	not specified	not specified
Shinko Wire Company ALPORAS	1,5 wt. % Ca	not specified	680	not specified	not specified

Fig. 5.3 shows an example of a set of influences on the choice of ceramic particle size for the stability of aluminium foam produced by the direct melt foaming method, often referred to as MMC (Metal Matrix Composites), according to [3].

Currently, scientists are looking into the importance of the chemical and process parameters that are necessary to obtain a stable metal foam. From experimental evidence, it is clear that all metal foams must be stabilized by solid additives. The mechanism by which these particles contribute to the stabilizing effect has not yet been convincingly explained. In addition, the role of viscosity or surface tension of the metal melt is questionable.

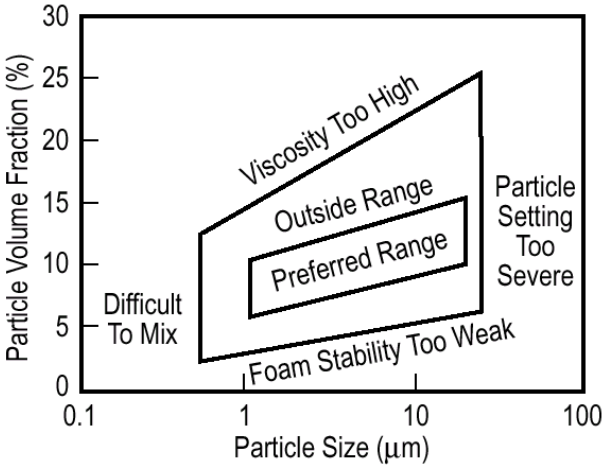

Particle Volume Fraction – volume fraction of particles; Particle size - particle size; difficult to mix; particle setting too severe - large particle size; preferred range - suitable size; outside range - out of range; foam stability too weak - foam stability too weak; viscosity too high - viscosity too high

Fig. 5.10 Selection of particle size and content for the production of MMC (metal matrix composites) foams, JIN [3]

Foam liquid metals always contain some kind of solid inclusions, either micrometre-sized particles or nanometer-sized oxide particles, which are located inside or on the surface of the gas cell films. In the first case, the particles are added to the melt at some stage in the processing process, while in the latter case, the particles for the formation of the oxide films are usually introduced into the material as a by-product of powder production. For example, as reported by BABCSÁN [4], the production of metal foams such as *"Cymat", "Formgrip"* and *"Metcomb"* is analogous to some "dirty" foamed materials studied today, where particles stabilize the foam melt. For the production of stable foam from metal melts where foaming is carried out by blowing gas from an external source into the metal melt, a minimum amount of solid particles is necessary, as reported by BABCSÁN [4] following the work of Ip, Wang and Togura. The first principles of foam stability in its production, based on the reported limits for their particle size and volume content, which are necessary for the formation of metal foam, were published by JIN [3]. In this literature, there are several theories explaining the stability of metal foam. For example, GERGELI et al [6] state that the viscosity of the melt is critical for foam production. The viscosity is influenced by the amount of particles. Melt viscosity increases with particle content but also with decreasing temperature. All these effects also slow down the vertical movement of bubbles in the melt.

For metal foam production, it would be beneficial for the solid particles to contribute to the formation of a flatter curvature of the foam wall boundaries, which reduces the effect of the suction of the molten metal from the cell wall to the melt boundary. It has been shown that the melt-wetting angle must be within a certain size range (size not shown) provided that the particles present stabilize the interface: melt-gas bubble, KAPTAY [9]. The addition of ceramic particles to the aluminium alloy melt can significantly reduce the surface tension due to their distribution in the metal melt [8]. Another stabilising effect of the oxidized surface of the aluminium melt (formation of Al_2O_3) on the surface of the melt gas cell walls, is produced by the reaction of the metal melt during oxidation with the applied feed gas, see Fig. 5.11 (showing foam after solidification), was observed by BABCSÁN et al. [8]. This confirms the finding that high-temperature surface layers are duplexes. The amorphous oxide formed as the first layer can be transformed into secondary crystals within the oxide layer or can nucleate into primary crystals below the amorphous layer.

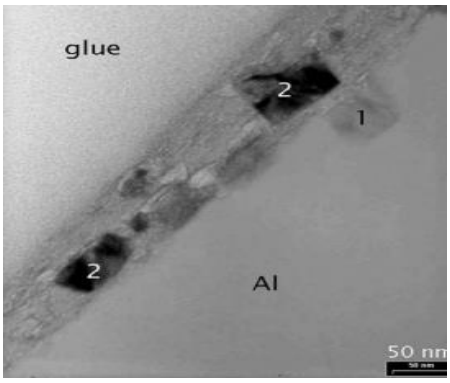

Fig. 5.11 Oxide layer on a cell of foam "produced by the Cymat method" containing 1: primary oxide and 2: secondary oxide particles, BABCSAN [8]

For foams produced by powder metallurgy (PM), i.e. from powder compacts, BABCSÁN [4] states, based on the experience of Arnold et al. that the stability of the foam is created by "networks" of solid alumina particles. Micro-gravity experiments have been carried out which have shown that an important effect of the solid stabilizing particle is to prevent the surfaces of the foam cells from aggregating into larger units.
The distribution of particles and the forces between them are well known from the distribution of particles in water suspensions (the transparency of water and its low temperature have contributed to this research).
Investigating the distribution of particles in metal melts is challenging (this is affected by the high temperature at which the melts exist), so the distribution and dispersion of particles can be observed on metals after they have solidified using metallographic methods. In such studies, it must be taken into account that even during the solidification of the metal, the distribution of particles may change, e.g. due to pressure effects or other influences. It is envisaged that, for example, the use of a new method

based on synchrotron radiation (magnetic braking radiation) could be used to observe the behaviour of particles even at high temperatures.

Particles can agglomerate on the surface of rising gas bubbles and metal melt during foam production. In the *Metcomb* method (gas injection into the melt from an external source), the volume fraction of particles in the foam mass from the bottom of the vessel where the gas bubbles are fed to the surface of the metal melt was also monitored. In this context, it was found that only from a certain distance from the bottom of the vessel (no specific value given) can a stable foam be formed. The minimum coverage of the bubble surface by the stabilising particles must be at least 50 %. BABCSAN et al. [8] also investigated the surface coverage of bubbles with stabilising particles in the production of the metal foam *"Metcomb".* It was found that the maximum coverage of the used stabilizing particles SiC or Al_2O_3 is 45 % using a foaming gas, nitrogen. This value decreases significantly with the use of gases that exhibit an oxidizing effect during foaming [8].

5.4 Effect of particle size and volume fraction

The particle size of stabilizing agents in the production of metal foams has been investigated by many researchers, e.g. BABCSAN et al. [4] carried out investigations on foams produced by the "*Formgrip*" method. He investigated the effect of particle size of stabilizing agents by X-ray radioscopy. Precursors containing two types of SiC particles were foamed under the same conditions and observed at specific locations. It was found that bubble coalescence was much more pronounced for the precursor containing coarse particles of stabilizing agents, see Fig. 5.12, which was obtained using a synchrotron beam, [4].

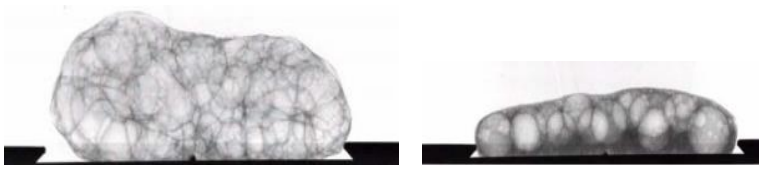

Fig. 5.12. Melts of aluminium foams: with SiC stabilising agent with a particle size of 13 µm (left); with SiC stabilising agent with a particle size of 70 µm (right) used in the production of "Formgrip" foams with precursor: AlSi9Cu3 + 10 wt. % of the stabilizing agent SiC and + 0.5 wt. % of the foaming agent TiH_2 (X-ray image was obtained using a synchrotron beam), BABCSAN [4]

At a certain point (ex-situ) in the solidified metal foam, the cell walls were observed using a scanning electron microscope (SEM). It was found that there is very little coverage of particles of 13µm in the solidified foam wall (see Fig. 5.13, left). On the contrary, a large number of particles with a size of 70 µm can be found on the surface (see Fig. 5.13, right).

While the 13 µm particles separated on the surface of the cells and only small amounts could be loaded on the surface. Stabilizing SiC particles of 13 µm particle size produced cell walls of approximately 85 to 100 µm thickness. Also, the final cell wall

thickness varied with the particle size of the stabilizing agent. Using a SiC stabilizing agent with a particle size of 70 m, the cell wall thickness reached up to 300 μm. Cell wall sections of these two sizes are shown in Fig. 5.14. For completeness, it should be noted that each foam had a different manufacturer. Except for the difference in the size of the stabilizing SiC particles, other trace elements in the SiC (e.g., the presence of iron) or other technological factors may play a large role.

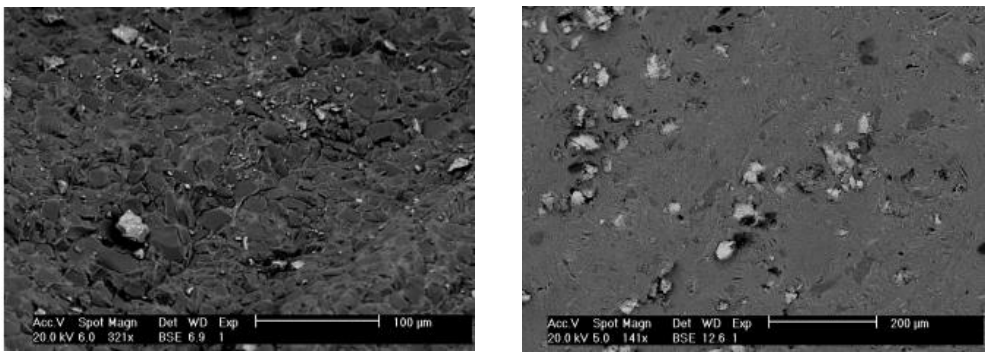

Fig. 5.13 View of the cell wall of the metal foam prepared by the "Formgrip" method containing 10 vol. % of stabilizing SiC particles of 13 μm (left); view of the cell wall surface of the metal foam prepared by the "Formgrip" method containing 10 vol. % of stabilizing SiC particles of 70 μm (right) [4]

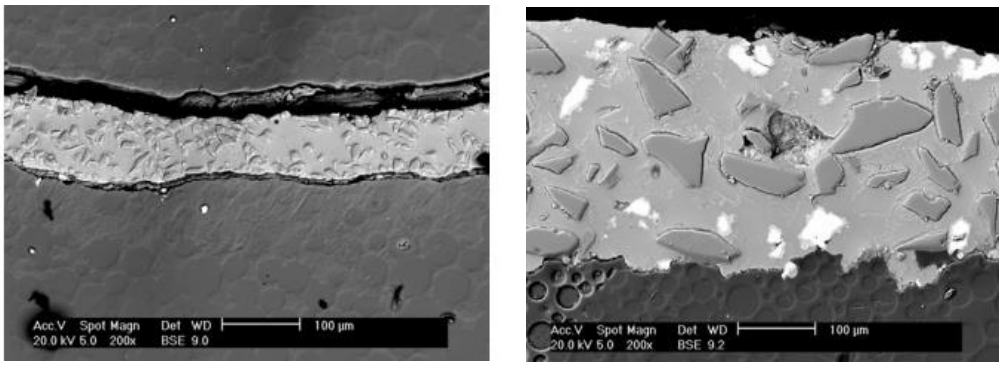

Fig. 5.14 Cell wall section of a metal foam cell made from the "Formgrip" precursor containing 13 μm SiC stabilising agent particles, SEM left; containing 70 μm SiC stabilising agent particles, SEM right, [4]

The size of the SiC stabilisation particles was also investigated in his PhD thesis by YÜSEL [12], who observed their size on a scanning electron microscope SEM, see Fig. 5.15, Fig. 5.16 and Fig. 5.17. These particles were monitored for the production of aluminium foam by powder metallurgy using a foaming agent TiH_2 of 0.5 to 1 wt. %. Fig. 5.18 shows sections of aluminium foams that were produced by powder metallurgy.

Research has shown that when blowing gas directly into the melt from an external source, it is necessary to use a larger amount of stabilising agent, or ceramic particles, which will provide a greater proportion of the so-called inclusions that are necessary to obtain a stable foam than is the case with methods of producing metal foams, e.g. powder metallurgy (where a compact precursor or powder compact is used). The

powder compacts used for foaming contain thin oxide films that have previously coated the surface of the metal powder particles. After the extrusion of the powder compounds (carried out under heat), these thin oxide films are further compacted and converted into oxide fibres with a diameter of about 20 nm and a length of 4 to 100 nm, as reported by BABCSAN et al. [4] based on the investigations carried out by Kim et al. These oxides are homogeneously distributed in the precursor.

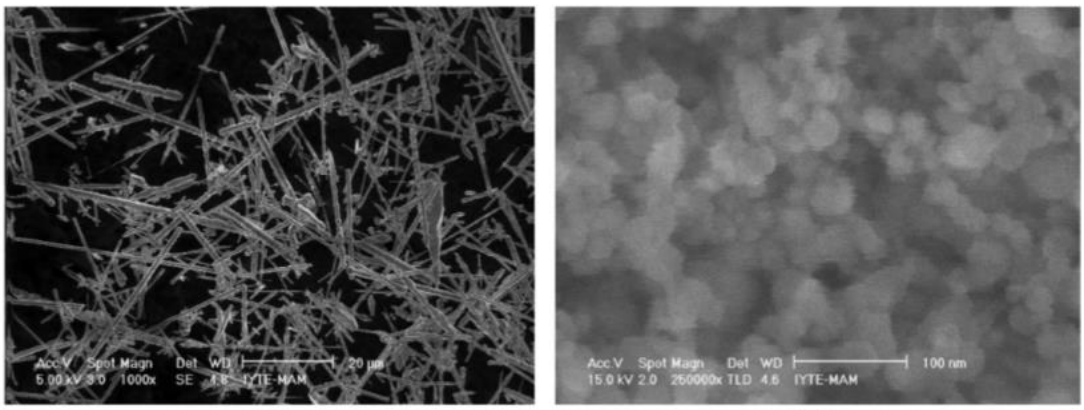

Fig. 5.15 SiC particles (a) whiskers 1.5 μ m to 182 μm, (b) SiC powder 30 μm, determined by SEM, YÜKSEL [12]

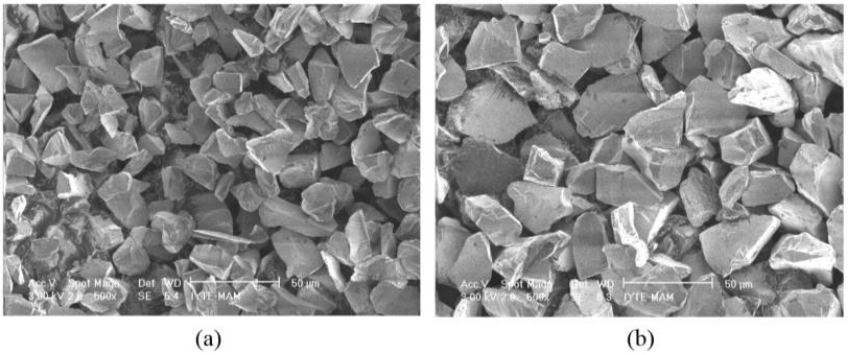

Fig. 5.16 SiC powder (a) particle size 10 to 20 μm; (b) particle size 20 to 30 μm, determined by SEM YÜKSEL [12]

Melting and stirring of molten metal (without the presence of a foaming agent) leads to the agglomeration of oxide films, as reported by BABCSÁN et al. [4] based on the studies of Arnold. In general, it has been confirmed that oxides promote the production of metal foams.

MALEKJAFARIAN et al. [13] investigated the effect of using SiC on the stability of fabricated metallic aluminium foam. The mechanical properties of the foam thus produced were also monitored. The aluminium foam was produced by direct melt foaming with gas from an external source. A SiC stabilizing agent with a particle size of 10 μm was used to stabilize the foam. The stabilizing agent was heat-treated before the actual foam production. The SiC particles were heated to 950 °C for 1 hour. Subsequently, they were heated only to 650 °C for 2 hours. This heat treatment of the

SiC particles was carried out to improve their wettability with the melt and also to remove adsorbed gases from their surfaces.

LEITLMEIER et al. [7] report that at least 10 vol% of stabilizing SiC particles with a size of 9 μm is required in aluminium foams that are produced by bubbling gas from an external source in a metal melt when stabilizing foam produced from a 727 °C melt. Research has shown that a minimum of 8 vol. % of SiC particles of 10 to 15 μm are required to stabilize aluminium alloy foam. For aluminium (aluminium alloy) melt temperatures from 735 to 775 °C, a minimum amount of 10 vol. % of SiC (particle size 10 μm to 15 μm) is already required.

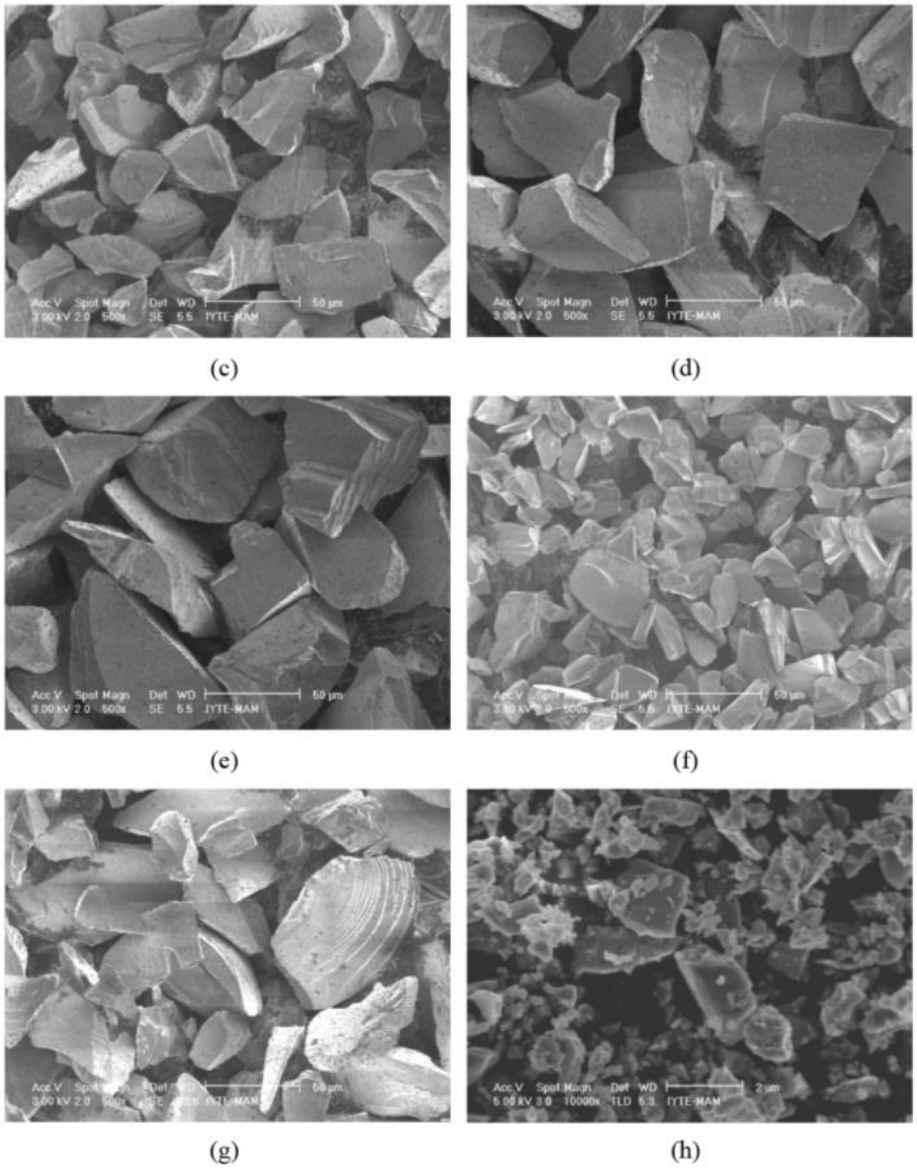

Fig. 5.17 SiC powder (c) particle size 35 μm to 45 μm; (d) particle size 45 μm to 56μm (e) particle size 56 μm to 74 μm; (f) particle size 3 μm to 40 μm (g) particle size 26 μm to 74 μm; (h) particle size 0.2 μm to 2μm, determined by SEM, YÜKSEL [12]

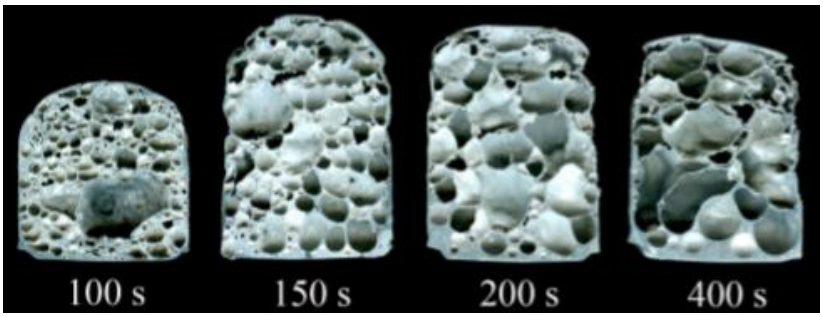

Fig. 5.18 Sections with aluminium foams produced by powder metallurgy (5 wt.% SiC, size 3 μm to 40 μm; 1 wt. % TiH_2 and Al powder, at foaming process 100 s, 150 s, 200 s and 400 s) [12]

Fig. 5.19 shows the SiC particles used. Fig. 5.20 shows the effect of SiC volume on the compressive strength of the produced aluminium foam.

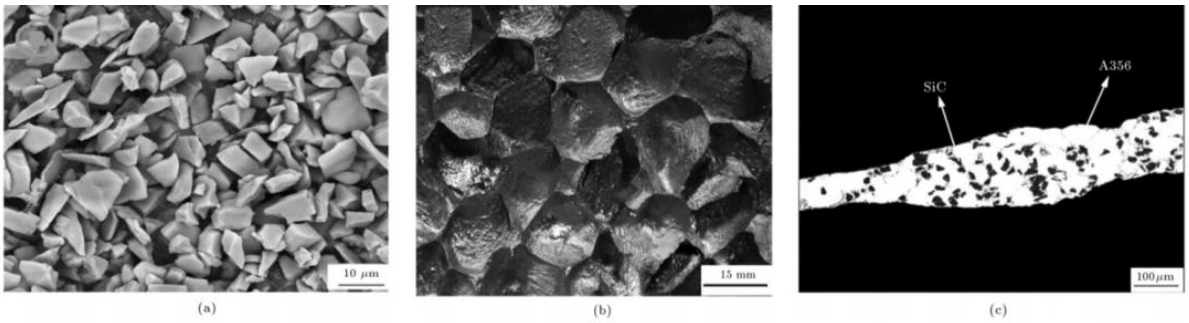

Fig. 5.19 SiC stabilising agent particles, a) SiC particles viewed under a microscope; c) view of a cell wall section of aluminium foam in which SiC particles are dispersed; a) macrostructure of aluminium foam produced by direct gas injection into the aluminium melt [13]

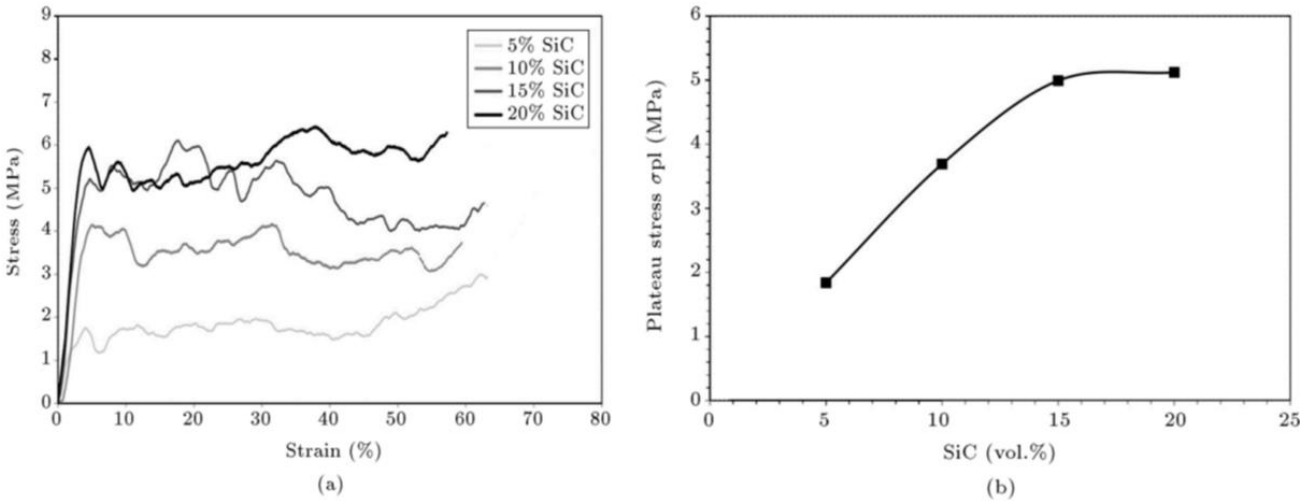

Fig. 5.20 a) Stress-strain curves of aluminium foams obtained from the pressure test at different vol. % SiC; b) Effect of volume % of SiC on the compressive strength of fabricated aluminium foam [13]

In both cases, the depth of the injector immersion from the bottom of the vessel was 3 cm, BABCSÁN et al. [8] concluded that when using the stabilising agent Al O_{23} in the aluminium melt, a minimum amount of 5 vol. % with a particle size of 11μ m is required, producing a stable foam at a melt temperature of 700 °C, with an injector depth from the bottom of 18 mm.

In the case of metallic foam of the "*Alporas*" type, the size and volume fraction of these inclusions are estimated to be about 1μ m and 1 vol. %. Fig. 5.21 shows the oxide networks decorated with secondary phases in the cross-section of the *"Alporas"* foam cell, as determined by scanning electron microscopy SEM.

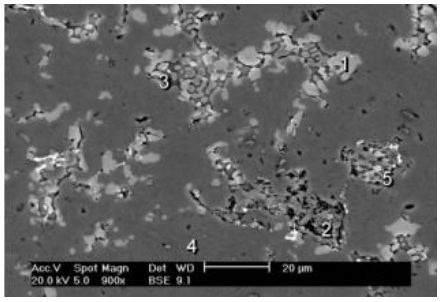

Fig. 5.21 Oxide networks decorated with secondary phases in the etched cross-section of the "Alporas" foam cell, SEM, [4]

The above facts provide clear evidence that there is a lower volume fraction of inclusions when the metal foam is produced using powders (formation of oxide films) than when the melt is formed from an external source and ceramic particles are added. Small particles are difficult to mix with the aluminium melt, as reported by BABCSAN [4] based on the findings of researchers Wu and Reddi on stabilising particles. Fig. 5.22 shows the relationship between the volume and size of stabilising particles used by different researchers (Waigang, Leitlmer, Ip and Babcsan) in the production of metal foams.

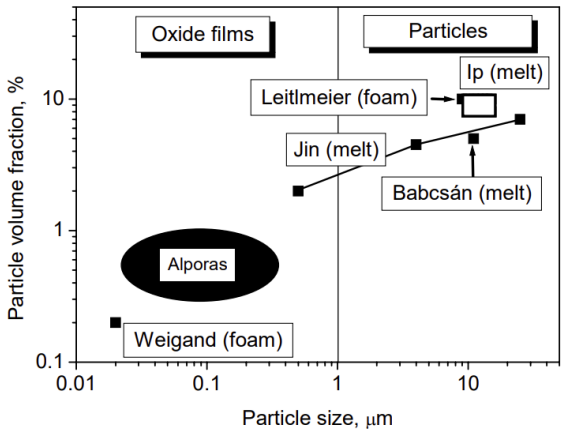

Leitlmeier (foam), according to [7]; Jin (melt) - melt according to [5]; Babcsan (melt), according to [4]; Weigand (foam) - foam according to the author WEIGAND

Fig. 5.22 Stability diagram for metal foams regarding fraction and particle size (data from various authors measured in foam or melt are included) [4]

Fig. 5.22 shows the relationship between the size and volume of particles in the fraction (providing foam stability) according to the authors who studied melt or foam: Leitlmeier (foam), approx. 10 vol. % of particles, size 8 μm [7]; JIN (melt), approx. 5 vol. % particles, size 4 μm, [5]; BABCSAN (melt), ca. 5 vol. % particles, size 10 μm, [4]; Alporas foam, ca. 0.2 to 1 vol. % particles, size 0.02 to 0.3 μm for oxide film formation, [4]; WEIGAND (foam), ca. 0.2 vol. % particles, size 0.02 μm for oxide film formation, [4].

5.5 Composition of particles and effect of reaction layers on particles

5.5.1 Composition of particles

Foam stabilisation depends on the appropriate particles and their stabilising effect, which is mainly determined by the chemical composition of the particles. These particles are Al_2O_3, SiC and MgO. This means that these chemical compounds (Al_2O_3, SiC and MgO) are the stabilising particles of the foam. The particles increase the stability of the liquid aluminium foam produced by gas injection from an external source. The foaming of pure Al and its alloys, which is based on the application of powder metallurgy (powder compacts), can be stabilised with TiB_2, Al_2O_3 and SiC reagents, respectively, as reported by BABCSAN [4] based on the findings of Kennedy. It is well known that, in addition to the particle composition, the stabilisation effect is also influenced by the wetting angle (angle of contact with the melt) [9].

For the melting of aluminium, SiC and Al_2O_3 contact angles are emphasised by several authors, as reported by BABCSAN [4], according to the conclusions of Laurent and also according to the researcher Shen. The range of contact angle varies from 60 to 90°. KENNEDY [10] studied the effect of a contact angle of 98° on TiB_2 particles in pure aluminium at 900 °C. As it is known from metallurgy and smelting of aluminium, when the temperature reaches 780 °C, Al_2O_3 oxides are intensively formed on its surface. According to CAPTAYE [9], for non-oxidized melts, the contact angle between the melt and the TiB_2 particle can be a very small wetting angle.

Experiments have been carried out, as reported in [4], using TiB_2 particles in the production of aluminium foam by gas foaming from an external source into a 700 °C AlSi10 aluminium alloy melt. 15 wt. % of TiB_2 with a particle size of 3 to 6 μm was added to the melt. It was found that TiB_2 was not an effective stabiliser for the production of this aluminium foam, as illustrated in Fig. 5.23. Fig. 5.23 shows the irregular residues of the metal foam bubbles produced by the foaming of the AlSi10 alloy containing the stabiliser particles (15 wt. % TiB_2 particles of size 3 to 6 μm), observed by light microscopy.

In the production of this foam, TiB_2 particles were found to fall out of the bubble surfaces, leaving significant amounts of TiB_2 on the melt surface.

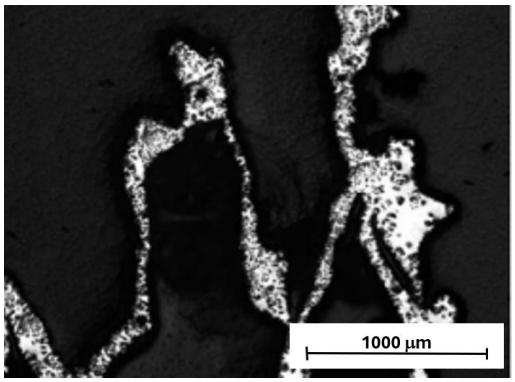

Fig. 5.23 Irregular bubble residues of aluminium foam from AlSi10 alloy with the presence of stabilising TiB_2 particles, determined by light microscopy), [4]

Research shows that not only the chemical composition of the particles but also other influences (or the presence of other particles among the particles of stabilizing agents) can affect the quality of metal foam production.

5.5.2 Effect of reaction layers on particles

Monitoring of the effect of reaction layers on stabilizing particles was carried out during the production of aluminium foam by MMC method, respectively *Duralcan* method - by injection of external gas into the melt. For this purpose, a melt of aluminium alloy AlSi0.8Mg0.8 and 10 vol. % of stabilizing agent Al_2O_3 was used. As can be seen in Fig. 5.24 (left), thicker aluminium foam cell walls were formed with more aggregated Al_2O_3 particles than was the case with the modified MMCs method, which used the aluminium alloy AlSi10Mg (with a higher Si/Mg ratio) and 12.5 vol. % Al_2O_3 stabilizing agent, see Fig. 5.24 (right).

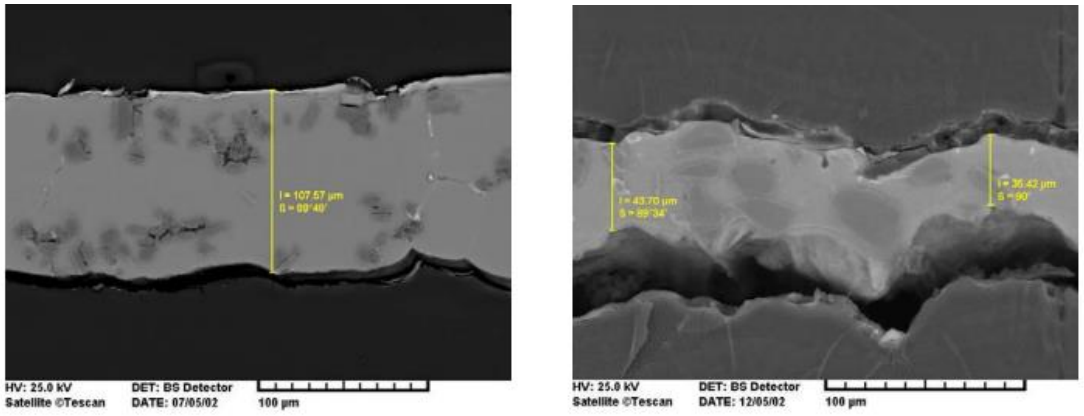

Fig. 5.24 Cell wall section of an aluminium foam (with a cluster of Al_2O_3 particles coated with spinel Al_2MgO_4) from an alloy with a low Si/Mg ratio, SEM, left;
Section through the wall of an aluminium foam cell (Al_2O_3 particles are free of spinel $Al\ MgO_{24}$) in a high Si/Mg ratio aluminium alloy, SEM, right, [4]

Particle sections on cell walls showed that a spinel layer (Al_2MgO_4) forms on alumina particles for low Si/Mg ratio (see Fig. 5.25, left). If more Si is present in the aluminium alloy, then the assumption is that a spinel Al_2MgO_4 layer will not form on the Al_2O_3 particles, resulting in thinner cell walls with inhibition of cluster formation. Local conglomeration of Al_2O_3 particles was observed in the cell wall section (MMC method), which increases the cell wall thickness (see Fig. 5.26). SiC particles, identified by EDS, are visible on the cell wall surface.

It has also been shown that SiC loses its stability capability with the amount of melt superheat. XRD analysis showed that Al_4C_3 BABCSANE formation occurs at high melt temperatures [11]. The formation of carbide on the surface of the stabilizing particle can affect the contact angle between the particle and the melt. This may take it out of its area of action. Regarding the effect of the straining process and the type of gas for the straining process (MMCs, Duralcan). It was found that the stability of metal foam depends not only on the properties of the stabilizing particles but also on the gas used for the foaming process. If the gas is hydrogen, which is used in the production of metal foams by powder metallurgy with the use of a foaming agent, which is usually TiH_2, it is necessary to take into account the fact that the thin films of the gas cell walls often break and the resulting foam collapses.

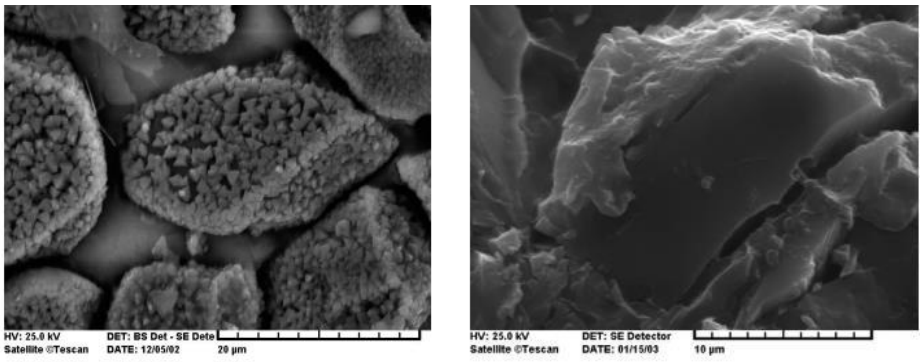

Fig. 5.25 Spinel Al_2MgO_4, on the surface of an A_2lO_3 particle in an aluminium foam cell wall with a low Si/Mg ratio, SEM (left); Al_2O_3 particle without spinel in an aluminium foam cell wall with a high Si/Mg ratio, SEM (right), [4]

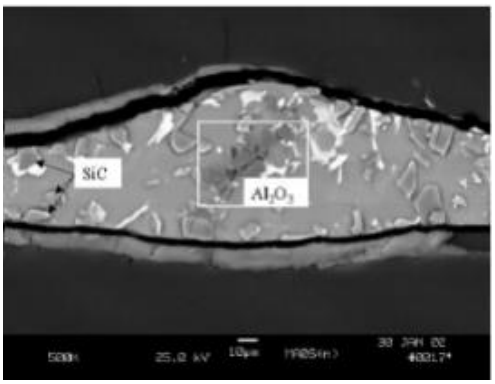

Fig. 5.26 Cell wall section of aluminium foam (made from Duralcan MMCs, foamed with air), presence of stabilising SiC particles with the addition of Al_2O_3, SEM [11]

The basic parameters for the production of stable metal foam can be divided into two groups. The *role of solid inclusion* (i.e. particles and or thin non-metallic films) is important. Furthermore, *the role of surface skin formation.* The role of surface skin formation has been investigated in the literature for metal foams produced by gas injection as reported by BABCSAN [4]. In this chapter, the effect of solid inclusions on the stability of the foam is considered. Based on the research, it can be concluded that solid inclusions affect the stability of foam due to their wettability, shape and their distribution in the melt (network formation, clustering or segregation). In addition to particle concentration and size, recent research has shown that both the composition of the stabilizing particles and the composition of the metal melt affect the stability of metal foams. It is assumed that not only the composition of the melt and its temperature, but also the possible effect of other technological influences, BABCSAN [4], affect the behaviour of the stabilizing particles.

6. CHARACTERISTICS OF PHYSICAL AND MECHANICAL PROPERTIES OF CELLULAR METALLIC MATERIALS

6.1 Physical properties of metals for the production of foamed materials

6.1.1 Bulk weight of foamed material

The volume weight of the foamed metal material is one of the important physical quantities of the foam, which influences other quantities and their values, such as the value of mechanical properties and the total weight of the manufactured part. Through compression tests, it has been confirmed that the higher the bulk density of the foam, the greater its stiffness and the more resistant the metal foam is to mechanical stresses, especially in compression. At the same time, it also depends on other parameters, such as the thickness of the crust (if the foam has a crust) and the pore size of the metal foam. In engineering practice, a low bulk density is advantageous. For example, the bulk density of aluminium foams is in the range of 400 to 600 $kg \cdot m^{-3}$. According to ORT [11], and GIBSON [12] research, this range of bulk weights achieves acceptable results from all aspects investigated. At the same time, it should be noted that the higher the bulk density of the foam, the higher the total cost of production. For example, a foam product with a surface crust made of AlSi12 alloy with a volume weight of 400 $kg \cdot m^{-3}$, in the shape of a cylinder ∅ 50 mm x 100 mm, produced by LKR, currently has a price of about 5 €. This considers piece production without the need for a new foaming mould.

6.1.2 Foam packing size (crust thickness)

The surface coating, or crust, significantly affects the properties of the foam. This envelope is achieved by a suitable choice of foam production technology (the last stage of production involves very rapid cooling of the foaming mould). For example, foam produced by blowing foaming gas into the melt does not have this crust. The size of the crust of the foamed part cannot be determined in advance. The overall size of the part has a significant influence on the size of the crust. The larger the part, the greater the thickness of the crust. The size and effect of the crust on the properties of powder metallurgy foams were investigated by ORT [11], and it was concluded that in the case of the specimens for the compression test, which were in the shape of cylinders ∅ 50 x 100 mm, the crust thickness was 0.18 mm. It can be concluded that a crust thickness of 0.18 mm is the minimum value of the foam part envelope [11]. It is not possible to produce castings with a smaller crust thickness. For example, according to [10], at Leichmetall - Kompetenzzentrum (LKR) Ranhofen, a foamed magnesium alloy part was produced by the vacuum method (molten scrap is poured into the crucible, and the foaming is carried out using a vacuum). The foamed part follows the shape of the mould (which in this case is the crucible in which it is foamed). The resulting foamed part had dimensions of Ø 80 x 150 mm, and the thickness of the crust was about 20

mm, which is a significant increase over the AlSi12 foam part that was produced by powder metallurgy.

By using a certain technology, the thickness of the foam packaging can be significantly reduced. The thickness of the shell (crust) has a significant effect on all the variables and their values that are examined on the foamed part. The assumption is that the greater the thickness of the crust (foam cover), the higher the mechanical values of the foamed part. This is particularly important when examining foamed parts for automotive applications.

6.1.3 Amount and cell size of foamed material (porosity)

The amount and size of the gas cells of the produced foam (porosity) are also an important physical quantity that defines its behaviour and mechanical properties. The cell size of the foam can be influenced by the production technology. The range of cell size and quantity is typically between 60 % and 80 %. For the production of metallic, rep. aluminium foams *by powder metallurgy*, a porosity value of around 80 % is typical. Again, there is a direct proportionality: the higher the porosity of the foam produced, the lower its total weight, but at the same time, the mechanical property values decrease in direct proportion.

Pore size plays a major role, especially in compressive stress testing of strained material. The findings of [11] show that when compressive tests (compression tests) were performed on a foam sample with 81% porosity, the following conclusion. When using samples with lower porosity e.g. 60 %, the gas cells (pores) of the foam are more condensed and have a smaller volume, but the total number of cells is higher. This internal structure of the foam has a significant effect, especially on the higher velocity in the compression test (1 $m \cdot s^{-1}$ and higher loading velocities). In the compression test, the specimens deform, especially along the cell boundaries and the resulting strength of the whole foam is affected. If the foam specimen had approximately 20 % more gas cells, the deformation could proceed along the foam crust, and thus, the deformation would not damage the internal structure of the foam part as much. This phenomenon can be observed when the foam is loaded with a pressure of 1 $m \cdot s^{-1}$, where the thickness of the crust plays an even greater role. If the test specimen had a crust thickness of at least 0.5 mm, this would be a sufficiently rigid surface for the internal cell structure. This suggests that the resulting foam stiffness could more than double. However, this claim needs to be verified by further experimental tests.

6.2 Prediction and determination of metallic cellular material values

6.2.1 Determination of the bulk density of cellular materials

The bulk density of cellular systems (foams) is determined by physical calculation according to a known relationship:

$$\rho = \frac{m}{V}\ [kg \cdot m^3], \qquad (6.1)$$

where: V is the volume of the foam sample [m^3] and m is the weight of the foam sample [kg].

From formula (6.1), the specific gravity can be determined directly by finding the weight of the body *m* by weighing and, at the same time, finding the volume *V* of the body. For simple geometric shapes, the volume can be found by calculating the measured length dimensions of the solid.
In other cases, the volumes of the bodies are determined from direct measurement of the volumes of the liquids. Into these liquids are immersed the observed bodies on which the volume is determined. It is necessary to have the liquid in a graduated container (e.g. a graduated cylinder). However, if a volumetric vessel must be used to determine the volume, the direct method of determining the specific gravity tends to be inaccurate (the relative error in measuring the volume is usually 1 % or more; the accuracy of weighing, which is around 0,1 %, remains unused). Therefore, for more accurate monitoring of specific gravity, the low-precision direct method is replaced by indirect methods, the so-called second weighing (the task is also called hydrostatic). The hydrostatic method is a method suitable for determining the specific gravity of irregularly shaped bodies. It is based on the validity of Archimedes' law. The measurement consists of weighing the body twice on a modified laboratory balance. The first weighing of the body under examination is carried out in the air, the weight being denoted by m_v.
For balance in the air:

$$V \cdot g \cdot (\rho - \rho_{V)} = m_V \cdot g \cdot \left(1 - \frac{\rho_V}{\rho_Z}\right), \qquad (6.2)$$

where: ρ is the observed density of the body [$kg \cdot m^{-3}$]; V is the volume of the observed body [m^3]; ρ_V is the density of the air [$kg \cdot m^{-3}$]; ρ_Z is the density of the weight [$kg \cdot m^{-3}$]; m_V is the mass of the body determined by weighing it in air [kg].

In the second weighing, the test object is completely immersed in a liquid of known density ρ_k. The most commonly used liquid is distilled water, the specific gravity of which is tabulated. The body is balanced with a weight of weight m_k.
For balance after the second weighing can be written:

$$V \cdot g \cdot (\rho - \rho_{K)} = m_K \cdot g \cdot \left(1 - \frac{\rho_V}{\rho_Z}\right), \qquad (6.3)$$

After mathematical modifications of equation (6.3), a relationship can be established to determine the density of the observed body:

$$\rho = \left(\frac{\rho_K \cdot m_V - \rho_V \cdot m_K}{m_V - m_k}\right), \qquad (6.4)$$

where denotes: ρ_K is the specific gravity of known liquid [kg·m^{-3}]; m_K is the weight of known weights when weighed in liquid [kg]; ρ_V is the specific gravity of air [kg·m^{-3}]; m_V is the weight of known weights when balanced in the air [kg].

6.2.2 Determination of the relative specific gravity of cellular material

Relative specific gravity of *foam* (ρ_{REL}) - is the ratio of the density of the foamed material (aluminium foam - Al. P.) to the density of the unfoamed material (B.M.):

$$\rho_{REL} = \frac{\rho_{Al.P.}}{\rho_{B.M.}}, \tag{6.5}$$

where: ρ_{REL} is the relative specific gravity of metal foam [1]; $\rho_{Al.P.}$ is the relative specific gravity of foam (porous metal material) [kg·m^{-3}]; $\rho_{B.M}$ is the density of base (nano foamed) material [kg·m^{-3}].

6.2.3 Determination of porosity of metallic cellular materials (P)

Porosity (P) is the difference between the density of the unstressed material and the specific gravity of the stressed material (aluminium foam - Al. P.) to the density of the unstressed material (B.M.):

$$\boldsymbol{P} = \left(\frac{\boldsymbol{\rho_{B.M} - \rho_{Al.P.}}}{\boldsymbol{\rho_{B.M.}}}\right) \cdot \mathbf{100}\ [\%] \tag{6.6}$$

Table 6-1 shows the empirical relationships for determining the values of the mechanical property quantities of cellular systems (metal foams), which are divided into two groups according to the nature of the foam cells (open and closed).

Table 6-1 Relationships for calculating mechanical properties of metallic cellular systems according to ASHBYHO [2]

Relationships for determining the mechanical properties of metallic cellular materials		
Greatness	*Foams with open Cells*	*Foams with closed cells*
Young's modulus of elasticity E [MPa]	$E = (0.1 \div 4)E_S \cdot \left(\frac{\rho}{\rho_S}\right)^2$	$E = (0.1 \div 4)E_S \cdot \left[0.5 \cdot \left(\frac{\rho}{\rho_S}\right)^2 + 0.3 \cdot \frac{\rho}{\rho_S}\right]$
Shear modulus G [MPa]	$G \approx \frac{3}{8} \cdot E$	$G \approx \frac{3}{8} \cdot E$
Compressibility modulus K [MPa]	$K \approx 1.1 \cdot E$	$K \approx 1.1 \cdot E$
Flexural modulus E_f [MPa]	$E_f \approx E$	$E_f \approx E$
Poisson numberμ [1]	$0.32 \div 0.34$	$0.32 \div 0.34$
Compressive strength σ_c [MPa]	$\sigma_c = (0.1 \div 1.0) \cdot \sigma_{C,S} \cdot \left(\frac{\rho}{\rho_s}\right)^{3/2}$	$\sigma_c = (0.1 \div 1.0) \cdot \sigma_{C,S} \cdot \left[0.5 \cdot \left(\frac{\rho}{\rho_s}\right)^{\frac{2}{3}} + \left(\frac{\rho}{\rho_s}\right)\right]$

Tensile strength σ_t [MPa]	$\sigma_t \approx (1.1 \div 1.4) \cdot \sigma_c$	$\sigma_t \approx (1.1 \div 1.4) \cdot \sigma_c$
Intermediate fatigue stress σ_E [MPa]	$\sigma_E \approx (0.5 \div 0.75) \cdot \sigma_c$	$\sigma_E \approx (0.5 \div 0.75) \cdot \sigma_c$
Deformation to compaction ε_D	$\varepsilon_D = (0.9 \div 1.0) \cdot [(1.0 - 1.4) \cdot \left(\frac{\rho}{\rho_S}\right) + \left(\frac{\rho}{\rho_S}\right)^3]$	$\varepsilon_D = (0.9 \div 1.0) \cdot [(1.0 - 1.4) \cdot \left(\frac{\rho}{\rho_S}\right) + \left(\frac{\rho}{\rho_S}\right)^3]$
Loss factor η [1]	$\eta = (0.95 \div 1.05) \cdot \frac{\eta_S \cdot \rho_S}{\rho}$	$\eta = (0.95 \div 1.05) \cdot \frac{\eta_S \cdot \rho_S}{\rho}$
Hardness H [MPa]	$H = \sigma_C \cdot \left(1 + 2 \cdot \frac{\rho}{\rho_s}\right)$	$H = \sigma_C \cdot \left(1 + 2 \cdot \frac{\rho}{\rho_s}\right)$
Fracture initiation J_{IC} [J·m^{-2}]	$J_{IC} = (0.1 \div 0.4) \cdot \sigma_{y,s} \cdot \left(\frac{\rho}{\rho_s}\right)^{(1.3 \div 1.5)}$	$J_{IC} = (0.1 \div 0.4) \cdot \sigma_{y,s} \cdot l \cdot \left(\frac{\rho}{\rho_s}\right)^{(1.3 \div 1.5)}$

Because the mechanical values of aluminium foam depend on many factors (e.g., specific gravity of the foam, nature of the metal alloy etc.), the relationships for the calculations in Table 6-1 should be taken as informative.

Table 6-2 Relationships for the calculation of electrical properties of metallic cellular systems, according to ASHBYHO [2]

Relations for the determination of thermal properties of metallic cellular materials		
Greatness	*Foams with open Cells*	*Foams with closed Cells*
Melting point $T_{TÁ}$ [°C]	as for unwritten materials	as for unwritten materials
Maximum operating temperature T_{MAX} [K]	as for unwritten materials	as for unwritten materials
Minimum operating temperature T_{MAX} [K]	as for unwritten materials	as for unwritten materials
Specific heat capacity c_P [J·kg^{-1}·K^{-1}]	as for unwritten materials	as for unwritten materials
Thermal conductivity λ [W·m^{-1}·K^{-1}]	$\left(\frac{\rho}{\rho_s}\right)^{1.8} < \frac{\lambda}{\lambda_s} < \left(\frac{\rho}{\rho_s}\right)^{1.65}$	$\left(\frac{\rho}{\rho_s}\right)^{1.8} < \frac{\lambda}{\lambda_s} < \left(\frac{\rho}{\rho_s}\right)^{1.65}$
Coefficient of thermal expansion α [K^{-1}]	as for unwritten materials	as for unwritten materials
Latent heat L [J·kg^{-1}]	as for unwritten materials	as for unwritten materials
Relationships for determining the electrical properties of metallic cellular systems		
Electrical resistance R [10^{-8}·Ω· m]	$\left(\frac{\rho}{\rho_s}\right)^{-1.6} < \frac{R}{R_s} < \left(\frac{\rho}{\rho_s}\right)^{-1.85}$	$\left(\frac{\rho}{\rho_s}\right)^{-1.6} < \frac{R}{R_s} < \left(\frac{\rho}{\rho_s}\right)^{-1.85}$

6.3 Compressive stress test of cellular systems

Due to their cellular structure, the mechanical properties of metallic cellular systems are different compared to conventional (compact) metals. Therefore, conventional test methods such as tensile testing cannot be used to monitor the mechanical properties. The most important test for cellular metallic materials is the compressive test (see Fig. 6.1). Based on this test, the compressive force-path dependence (see Fig. 6.2), and the compressive strengths of 3 Alporas foam samples were monitored. For the

compressive test, the compressive stress-strain dependence (see Fig. 6.3a) is very often given, where 3 regions are visible on the strain curve. In Fig. 6.3b), the area of deformation work under the so-called "change" curve is indicated.

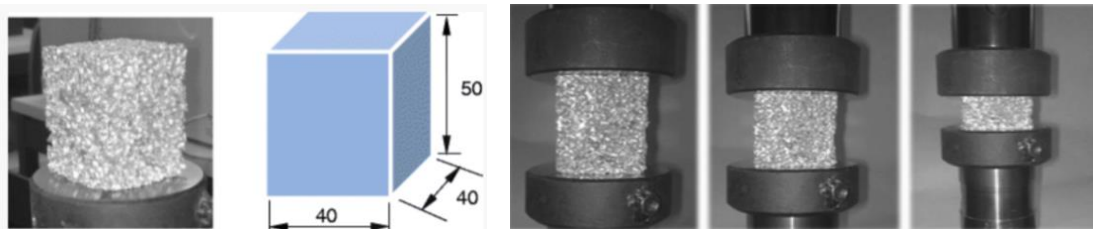

Fig. 6.1 Compression test of metal cellular systems (metal foams), in this case Alporas aluminium foam [13]

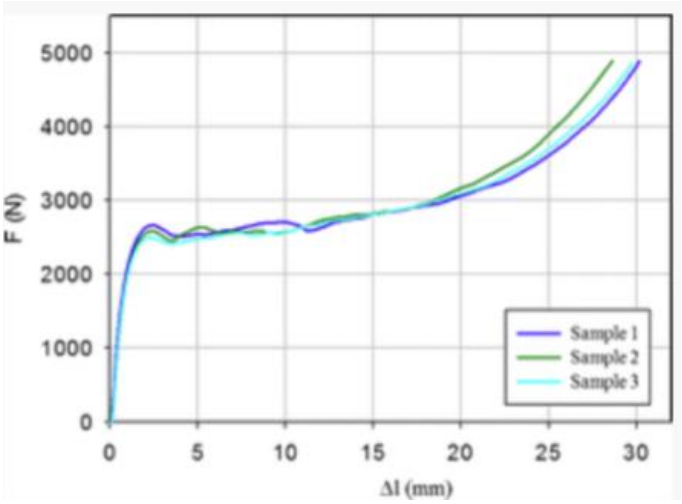

Fig. 6.2 Dependence of compressive force and path, while observing the maximum force to determine the compressive strength of 3 Alporas foam specimens [13]

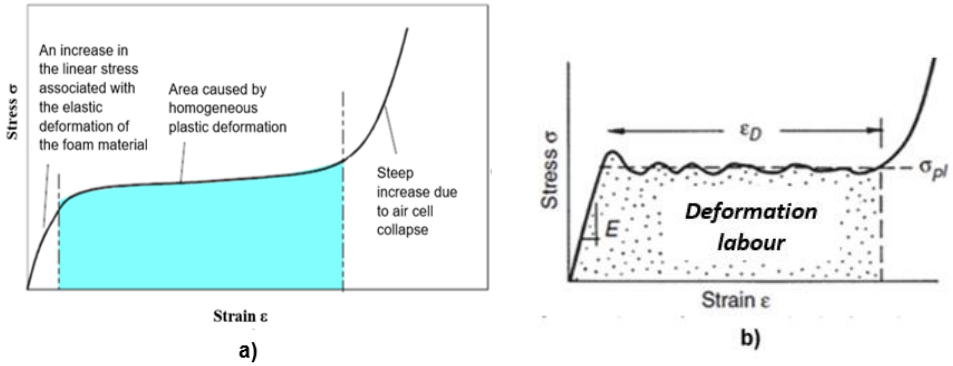

Fig. 6.3 Schematic of the stress-strain relationship for aluminium foam

In Figs. 6.3(a) and 6.3(b), there are three significant regions, (I), (II), and (III), which represent (I) a linear increase in stress at the onset of deformation, (II) a flat regime of nearly constant stress, and (III) a steep increase in compressive stress. This behaviour was found to be typical of cellular metallic systems (metal foams) with both open and

closed cell walls. The area under the change curve, Fig. 6.3b represents the strain work: $Q_{AB} = \int_0^{\varepsilon_P} \sigma \cdot d\varepsilon$.

In the first area, the linear increase is not only due to elastic deformation, as it is of compact metals. In foams, irreversible (plastic) deformations can occur at low stresses.
The second area shows a gradual increase in compressive stress, which is caused by homogeneous plastic deformation.
The third area shows a sharp increase in stress, which is caused by the deformation of the walls of gas cells until the cells gradually collapse. Opposite cell walls begin to touch each other.

It has been shown that the tensile strength of the foam is almost the same as the stress at which it corresponds to the second region. Therefore, this stress is used as the main value of the properties of foams. Due to the particular shape of the curve (compressive stress-strain), especially the second region, metal foams are able to absorb large amounts of energy at relatively low stresses (the potential for energy absorption increases with increasing area under the second region). Metal foams behave like polyurethane foams, except that their strength or stress is about 30 times higher at the same level of porosity. It has been shown that there are several factors that affect the behaviour of foam in compression testing. It is mainly the density of the foam and the choice of metal alloy.

In Fig. 6.4a) and Fig. 6.4b) are the compressive stress-strain curves of the strained material made of a magnesium alloy (AZ 31: 3.14% Al; 0.72% Zn; 0.45% Mn; 0.05 % Si; residual magnesium) with uniform porosity (60%) and the dimensions of the test specimens were 30 × 30 × 30 mm but with different pore sizes (1.2; 1.5; 1.8 and 2.0 mm) and varying porosities of 60 %, 65 %, 70 % and 75 % (mean pore sizes of about 2.0 mm), [3]. As can be seen from Fig. 6.4, the compressive stress-strain curve for magnesium alloys also contains three regions. The strength of the second region is an important aspect for evaluating the energy absorption characteristics of the foam. As can be seen in Fig. 6.4(a), the second region (middle plateau) stress increased from approximately 19 MPa to nearly 20 MPa as the pore size changed from 1.2 mm to 1.5 mm, and then decreased linearly with increasing pore size. To maintain porosity, as the pore size decreases, the number of pores increases, resulting in a smaller cell edge thickness. For a sample with a pore size of 1.2 mm, the cell margins may be too small to deliver sufficient melt, which will significantly degrade the mechanical properties. Therefore, the strength in region II (plateau) decreases [3].

As for the 1.8 and 2.0 mm samples, the larger pore size will cause inhomogeneous density in the foams [3], resulting in lower strength of the second region. From Fig. 6.4(b), it can be seen that the strength in region II decreases with increasing porosity of the material, which is a characteristic behaviour of metallic foams. The yield strengths for porosities of 60 %, 65 %, 70 %, and 75 % are 21 MPa, 17 MPa, 13.5 MPa, and 2.3 MPa, respectively.

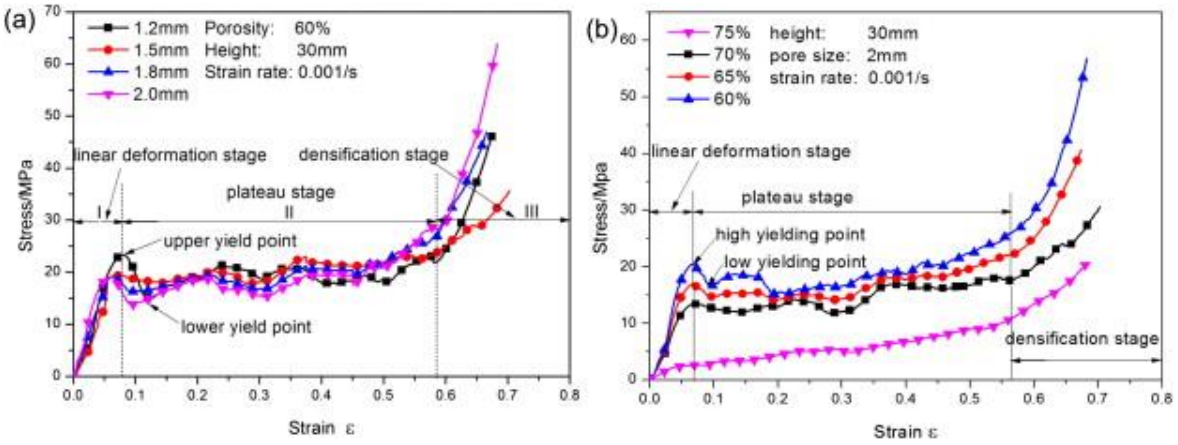

Fig. 6.4 Compressive stress-strain diagrams for AZ 31 magnesium alloy material (a) with different pore sizes (1.2, 1.5, 1.8 and 2.0 mm); (b) with different porosities of 60%, 65%, 70% and 75%, [3].

For foamed materials produced by powder metallurgy, it is clear from research that the lower the specific gravity of the foam, the longer the second region. At the same time, it is also clear that the stress in the second region is lower for low specific gravity. This means that the force or stress increases with increasing specific gravity. Similar results have been found for other alloys and foams produced by other technologies. Also, the content of alloying elements has a great influence on the mechanical properties of the foam. As also shown by research [1], lower stress values are exhibited by commercially produced foams from pure aluminium. The same behavior was found for foams produced with other technologies. The compressive stresses of foams with open or closed cells are almost the same when foams made of the same alloy with the same specific gravity are compared.

The methodology for compressive strength testing of aluminium foams produced by powder metallurgy was developed at *LKR Leichtmetall-kompetenzzentrum-Ranshofen GmbH*, Austria and is carried out on test rigs. A cylinder-shaped test body ∅ 17 mm, 50 mm long is used. A speed of 0,01 $m.min^{-1}$ is recommended for the jaw of the compression machine, which produces the compressive force (see Fig. 6.5):

In region 1, that is, at low stress, the material deforms almost elastically because the cellular (cell) walls are elastic. *Region 2* is the stable region of deformation under average compressive loading, the beginnings of twisting, buckling or breaking of the foam cell walls occur. *In region 3, a* rapidly increasing compressive load occurs at which the cell walls collapse in on themselves. For loads at the beginning of the second part of the load-deflection curve (steady-state level), when significant plastic deformation begins, the stress can be calculated and defined as the plastic pressure at which the cellular (cell) system collapses. The area under the curve represents the energy required to achieve permanent plastic deformation of the aluminium foam. The amount of energy consumed in deformation up to the point at which the stress on the specimen reaches its maximum value is important in terms of comparing the ability of the material to absorb impact energy. This ability is closely related to specific gravity. When the specific gravity is low, the foam will deform completely before it can absorb

the required amount of energy. Conversely, when the specific gravity is high, the compressive stress reaches a critical value at a small deformation.

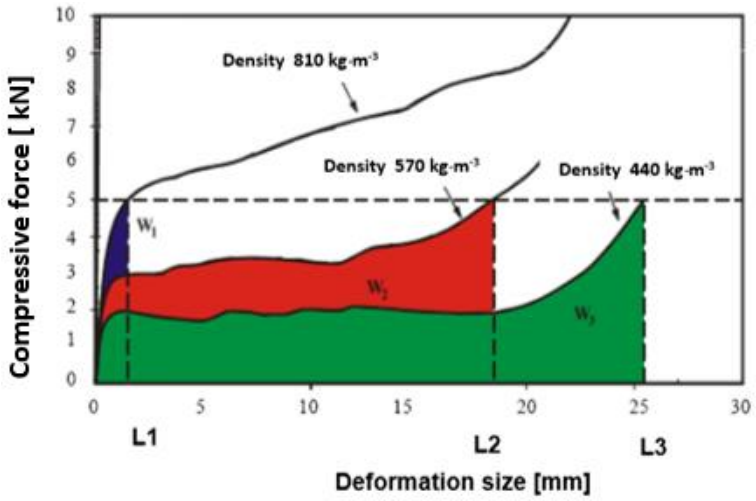

Fig. 6.5 Examples of compressive force-deformation curves obtained from tests of aluminium foams in compression at different densities. The coloured areas represent the energy (W) required for plastic deformation ($W_2 > W_3 > W_1$) [1].

Fig. 6.5 and Fig. 6.6 show the behaviour of aluminium foams with different densities ($\rho = 440$ kg·m^{-3}; $\rho = 570$ kg·m^{-3}, and $\rho = 810$ kg·m^{-3}) in compression testing [1]. These results confirm, as stated above, that the bulk density of the foam, the longer the second region. At the same time, it is also clear that the lower the foam bulk density, the lower the stress in the second region.

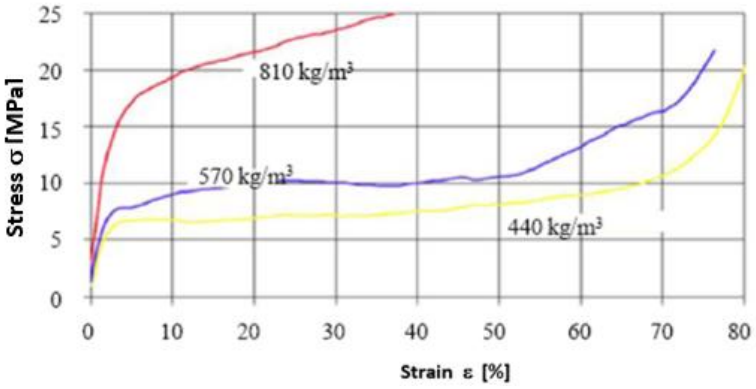

Fig. 6.6a) Behaviour of aluminium foams with different densities (ρ = 440 kg·m^{-3}; ρ = 570 kg·m^{-3} and ρ is 810 kg·m^{-3}) in compression test, [1]

The surface of the foam also has a significant influence on its characteristic properties. Metal foam that is covered with a continuous surface (e.g. obtained by casting) has the character of a sandwich material. In this case, the surface layer acts as a reinforcement, which increases the strength of the material compared to the foam itself. This phenomenon is applied, for example, to sandwich material composed of steel or aluminium plates, with aluminium foam filling the space between them.

Similarly, the stiffness of the tubes is increased if they are provided with foam filling of the inner space.

This is because the foam prevents premature compression of the pipe and thus increases the amount of energy it can absorb. Moreover, in the advanced stages of deformation, when the foam is fully compressed, it still prevents further deformation. This implies that a smaller diameter pipe with foam filling has the same absorption capacity as a larger diameter pipe without foam filling than an empty pipe of even larger diameter [3]. Fig. 6.6(b) shows the stress-strain relationship for tubes with aluminium foam inside their compartments of different specific gravity (570 kg·m^{-3}, 490 kg·m^{-3}) and tubes without foam inside it their compartments.

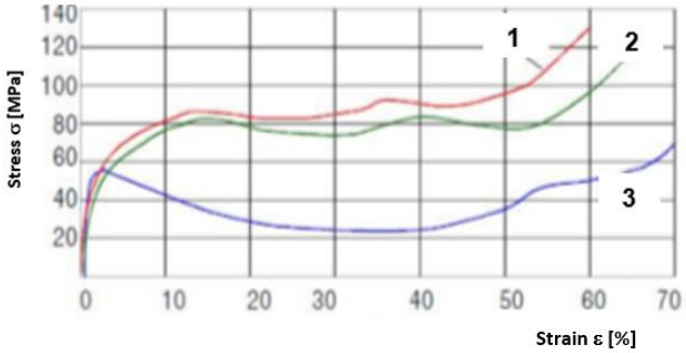

1 *- tube with aluminium foam filling (volume weight 0.57 g· cm^{-3});* ***2*** *- tube with aluminium foam filling (volume weight 0.49 g· cm^{-3});* ***3*** *- tube without filling*

Fig. 6.6b) Stress-strain relationship for a tube with aluminium foam inside its compartment of different specific gravity (570 kg·m^{-3}; 490 kg·m^{-3}) and a pipe without foam inside its compartment [3]

Fig. 6.7 shows the compressive strain (strain-stress dependence) for aluminium foams produced by different technologies (Alcen, Alporas, Alulight and Durocel) according to ANDREWSE [15].

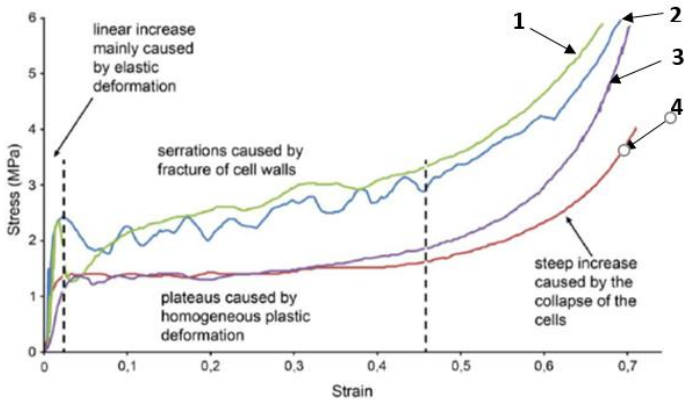

1 - ALULIGHT, 2 - ALCAN, 3 - DUOCEL, 4 - ALPOPAS

Fig. 6.7 Compressive stress-strain of aluminium foams for foams produced by different technologies Alcen, Alporas, Alulight and Durocel, according to [4] and ANDREWSE [15]

6.3.1 Behaviour of cellular systems in compression test

ORT research [11] focused on determining the appropriate loading rate for the compression test. Therefore, its tests applied loading rate values in a wide range from 0.001 $m \cdot s^{-1}$ up to 20 $m \cdot s^{-1}$. The reason for this was to observe the behaviour of the aluminium foam with a crust when loaded at different compression speeds.
When loaded at a velocity of 0.001 $m \cdot s^{-1}$, the superior ability of the aluminium foam was evident, with the specimen deforming regularly. As the loading rate increased during the compression test, the deformation pattern of the foam changed. When a velocity of 1 $m \cdot s^{-1}$ was applied, and the sample was already significantly deformed, but the core, which consisted of a cellular structure, remained together. At a loading speed of 20 $m \cdot s^{-1}$, the sample was completely destroyed and "crushed" into several small pieces. The resulting curves, which appear in the compressive stress-strain diagram, or the path dependence of the compressive force, demonstrate identical compression curves when all compression rates are used. Of course, the values of the compression force increase proportionally at higher compressive stresses almost exponentially.

As the specific gravity of the foam increases, the pressure under which the foam collapses increases significantly. This can be improved by appropriate heat treatment. The collapsing method for aluminium foam, the twisting or cracking of the cell walls, may be influenced by the composition of the base alloy or the heat treatment. Foams based on the use of an aluminium alloy (e.g. AlSi12) are prone to cell wall cracking while forming alloys are in turn prone to cell wall bending and twisting.
Initial peaks on the compressive force-trajectory curve were observed on different alloys using increasing loading rates. At a loading rate of 0.001 $m \cdot s^{-1}$, the "inertial" property of the foam is likely to be manifested. Initially, a higher force is probably applied to the surface of the foam than to its internal structure, so the cell surface is not yet deformed. Fig. 6.8 shows an example of the compressive stress-strain curves obtained by the ORTEM [11] compressive test at a loading rate of 0.001 $m \cdot s^{-1}$ (60 $mm \cdot min^{-1}$) using 3 test specimens ∅ 50 x 100 mm, with a surface crust of 0, 18 mm, made of AlSi12 aluminium alloy, with a density of 385 $kg \cdot m^{-3}$ [11]. Zwick T1FR250SN, GTM 4138 transducers, range 20 kN were used for the compression test. Software Zwick Test Expert v.12.0, MS Excel. The average compressive stress value was determined to be 0. 263 MPa.
Furthermore, ORT, [11] in the research glued test specimens of aluminium foam with crust (made by powder metallurgy) between two sheet metal specimens and observed their fracture toughness.
The term *fracture toughness,* see Table 6-1, refers to the resistance of the material to crack initiation and subsequent growth. It is based on fracture mechanics and is essentially a material characteristic that can be used to calculate the load capacity of a component with a crack. From a practical point of view, toughness can be characterised as the ability of a material to absorb energy before failure or before reaching a certain limit state.

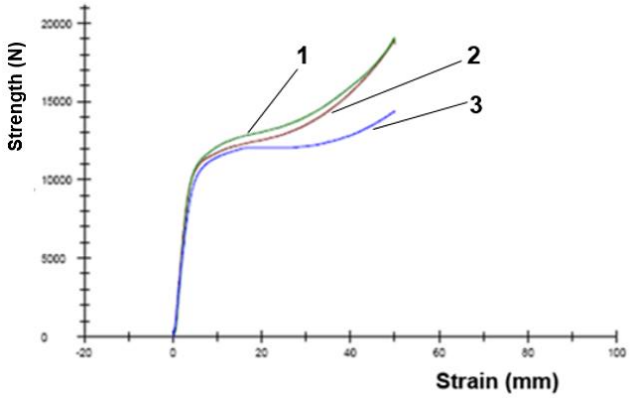

1 - *sample of AlSi12 foam (∅ 50 x 100 mm, density 385 kg·m^{-3});*
2 - *sample of AlSi12 foam (∅ 50 x 100 mm, density 385 kg·m^{-3});*
3 - *sample of AlSi12 foam (∅50 x 100 mm, density 385 kg·m^{-3})*

Fig. 6.8 Compressive stress-strain relationship of test specimens ∅50 x 100 mm with a surface crust of 0.18 mm, made of aluminium alloy AlSi12, with a density of 385 kg·m^{-3} [11]

Therefore, the fracture type is divided into *tough* and *brittle* according to the energy dependence. Under fast shock loading, most materials can absorb less energy than under slow loading. As the loading rate increases, the material becomes brittle. The formation of brittle fractures depends on many factors. The most important are low temperature, loading rate, material thickness, the presence of indentations or defects, and material quality.

Table 6-3 lists the mechanical properties of foams that have been produced by different technologies as reported by ASHBY [2].

The tests carried out by GUDEN and YÜKSEL [14] were aimed at monitoring the compressive strength of closed-cell aluminium foam samples. μThe aluminium foams were produced by powder metallurgy using a foaming process from powder extrusions (precursors), the method is patented and called the *Franhofer process IFAM,* see chapter 1.1.2.1 and SiC powder with a quantity of 10 wt. % with a particle size of 23 μm. For this purpose, a foaming agent TiH_2 was used in an amount of 1 wt. % with a particle size smaller than 37μm. The process was based on the production of two different materials. One was produced as a composite using (10 wt. % SiCp/Al), the other was produced as a non-composite using Al. To produce the composite material, the appropriate amount of the basic components, i.e. Al powder with 10 wt. % SiC and 1 wt% of the foaming agent TiH_2 was mixed. This resulted in the composite, which is further referred to as 10 wt. % SiCp/Al. The fabricated precursors for the production of foam samples for the compression test were prepared using plate-shaped precursors with a size of 70 × 70 × 8 mm. The precursors were pressed in a mould, at 350 °C for 30 min under a pressure of 220 MPa. These precursors were subsequently loaded into a steel mould (so-called foaming mould) where the foaming process was carried out at 750 °C. This produced a liquid aluminium foam. After solidification of this foam in the cooling foaming mould, samples of the cellular material 'aluminium foam' were obtained.

Table 6-3 Values of selected mechanical properties of aluminium foams produced by different methods as reported by ASHBY [2]

Mechanical properties of aluminium foams produced by different methods according to [2]					
Property	**CYMAT (Alcan)**	**MEPURA (Alulight)**	**Shinko Whire (Alpor)**	**ERG (Duracel)**	**INCO**
Material for foam production	Al + SiC	Al-Mg-Si	Al-5Ca-Ti	Al1Mg0.8Si+T6	Ni
Relative bulk density ρ_{REL} [1]	0.02- 0.2	0.1 – 0.35	0.08-0.1	0.05-0.1	0.03-0.04
Foam cell structure	Closed cells	Closed Cells	Closed cells	Open cells	Open Cells
Bulk weight ρ [kg·m^{-3}]	70-560	300-1000	200-250	160-250	260-370
Young's modulus of aluminium foam E [GPa]	20-2000	1700-12000	400-1000	60-300	400-1000
Shear modulus G [MPa]	1-1000	600-5200	300-350	20-100	170-370
Compressive strength Rm_D [MPa]	40-7000	1900-14000	1300-1700	900-3000	600-1100
Tensile strength Rm [MPa]	0.05-8.5	2.2-30	1.6-1.9	1.9-3.0	1.0-2.4
Tensile yield strength $Rp_{0,2}$ [MPa]	-	-	-	-	-
Ductility ε [1]	0.01-0.02	0.002-0.04	0.01-0.06	0.1-0.2	0.03-0.1
Modulus of elasticity of volume K [MPa]	20-3200	1800-13000	900-1200	60-300	400-1000
Moore's stress σ_{MOR} [MPa]	0.04-7.2	1.9-25	1.8-1.9	0.9-2.9	0.6-1.1
Poisson's constant η [1]	0.31-0.34	0.31-0.35	0.31-0.36	0.31-0.37	0.31-0.34
Fatigue limit $\sigma_C{}^C$ [MPa]	0.02-3.6	0.95-1.3	0.9-1.3	0.45-1.5	0.3-0.6
Deformation compaction ε_D [1]	0.6-0.9	0.4-0.8	0.7-0.82	0.3.-0,9	0.9-0.94
Fracture toughness K_I [MPa·m$^{1/2}$]	0.03-0.5	0.3-1.6	0.1-0.9	0.1-0.2	0.6-1.1
Maximum operating temperature T_{MAX} [K]	500-530	400-430	400-420	380-420	550-650
Minimum operating temperature T_{MIN} [K]	1-2	1-2	1-2	1-2	1-2
Specific heat capacity c_P [J·kg^{-1}· K^{-1}]	830-860	910-920	830-870	850-950	450-460
Coefficient of thermal expansionα [·10^{-6}· K^{-1}]	19-21	19-23	21-23	22-24	12-13
Latent heat of fusion L [kJ·kg^{-1}]	355-385	380-390	370-380	380-395	280-310
Coefficient of thermal conductivity λ [W·m^{-1}·K^{-1}]	0.3-10	3.3-3.5	3.3-4.5	6.0-11	0.2-0.3
Electrical resistance R [10^{-8}·Ω· m]	90-3000	20-200	210-250	180-450	300-500

The samples thus produced were subjected to a pressure test (see Fig. 6.9a) and Fig. 6.9b), and the deformation of their gas cells was observed.

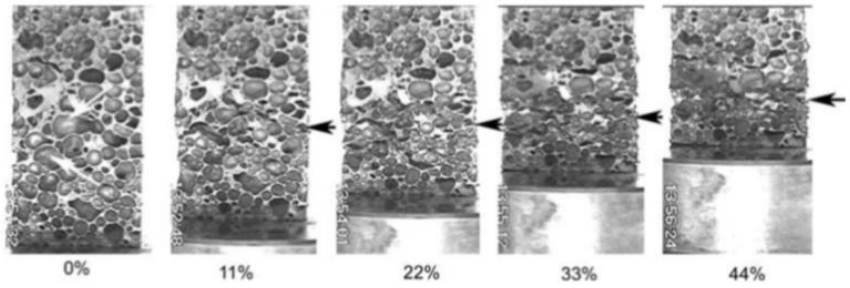

Fig. 6.9 a) Deformation of aluminium foam samples at different percentage pressure coating [14]

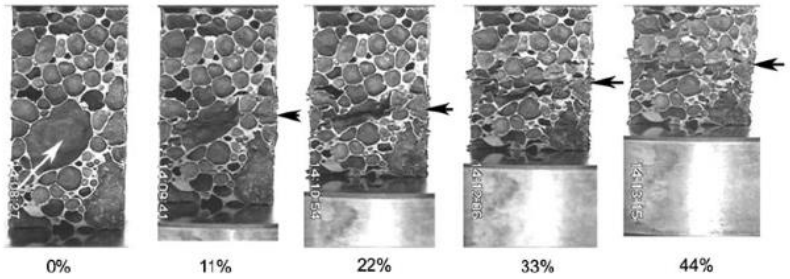

Fig. 6.9 (b) Deformation of aluminium foam samples with 10 % SiC styling agent (10 % SiCp/Al) at different compressive stresses [14]

Fig. 6.10 shows the deformed cells of samples produced by powder metallurgy. Fig. 6.10a) is related to Fig. 6.9a), Fig. 6.10b) is related to Fig. 6.9b). In Fig. 6.10b), deformed aluminium "foam" cells were produced using 10 wt. % SiC are shown. Compressive deformation of this cellular material resulted in the bending of the cell walls and, in some cases, cell breakage. It was found that the addition of SiC (10 %) to produce the composite precursor increased the expansion of the compact aluminium foam. Compression tests performed on foamed aluminium and aluminium materials with 10 % SiCp/Al showed [14] that adding SiC induces a more brittle deformation behaviour of the foam walls compared to pure aluminium foam.

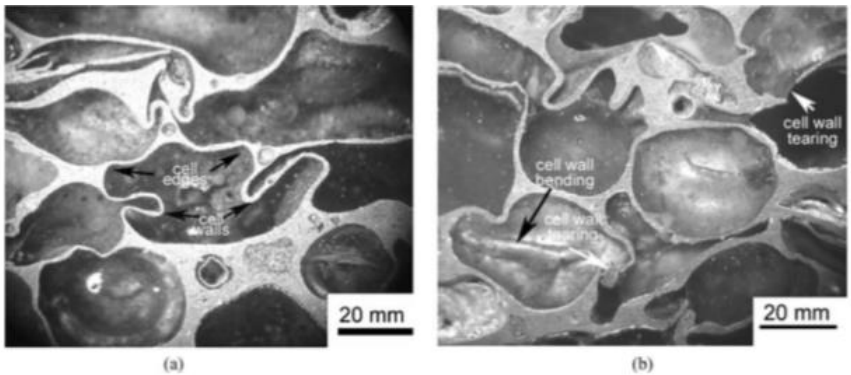

Fig. 6.10 Deformed microstructure of aluminium under compressive loading, a) aluminium foam, b) aluminium foam with 10 % wt. SiC (10 % wt. SiCp/Al) [14].

The results showed that the Al foam samples behaved similarly to the foam with open cells. The composite (10 % SiCp/Al) foam samples exhibited values of foam behaviour between open and closed cells during cell boring.

KOVAČÍK et al. [17] researched the mechanical properties of closed-cell aluminium foam samples at higher temperatures (100 to 550 °C). The aluminium foam samples were embedded by powder metallurgy using a sputtering agent TiH_2. The samples are shown in Fig. 6.11 and were made using three aluminium materials. Pure aluminium Al99, 5 %, see Fig. 6.11 (a), AlMg1Si0.6 alloy, see Fig. 6.11 (b) and AlSi12 alloy, see Fig. 6.11 (c). The dimensions of the samples were 8 x 70 mm (i.e. 1960 mm^2 area).

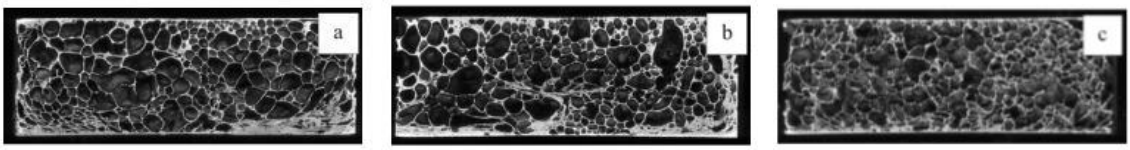

(a) - pure aluminium Al99, 5 %; (b) - AlMg1Si0.6 alloy, (c) - AlSi12 alloy

Fig. 6.11 Cross-sectional view of aluminium foam specimens (area 1960 mm^2) used for compressive loading at specific temperatures [17]

The specimens were tested on a 10 kN ESH servohydraulic testing machine (ESH 2094, ESH testing Ltd., UK) with a constant crosshead speed of 5 $mm \cdot min^{-1}$ at the Department of Materials Science and Metallurgy, University of Cambridge. The heating of the samples was carried out using a computer-controlled infrared heating furnace. The samples were heated individually to 100 °C, 200 °C, 300 °C, 400 °C, 500 °C and 550 °C, and the heating rate was 5 $°C \cdot min^{-1}$. Since the thermocouple could not be placed in the aluminium foam during the experiment to monitor the heating temperature, it was placed just next to the sample. The temperature stabilization inside the foam was first checked using a reference foam sample. At a given temperature, the sample was held at that temperature for 15 minutes before the compression test began. Fig. 6.12 shows the observed graphical stress-strain relationships for specific temperatures for the three types of materials used to make the foams: Al 99,5 %, AlMg1Si0.6 and AlSi12.

Figs. 6.12 a), 6.12 b) and 6.12 c) show the effect of temperature on the compressive stress-strain relationship up to the macroscopic failure of aluminium foams at constant specific gravity and strain rate $3 \cdot 10^{-3}$ [s^{-1}]. At room temperature, the mechanical and physical properties of aluminium foams depend mainly on the corresponding properties of the metal or metal alloy from which the foam is made. It has been hypothesized and also found that increasing the temperature of the "foam" results in a decrease in its compressive strength.

The absorbed energy causes an increase in the compaction deformation (the deformation is extended at relatively constant stress, i.e. the length of the plate) at a constant specific gravity. The activation energy for the compression of aluminium foams is dependent on the specific gravity (with a maximum in a certain specific gravity range) depending on the composition of the foam.

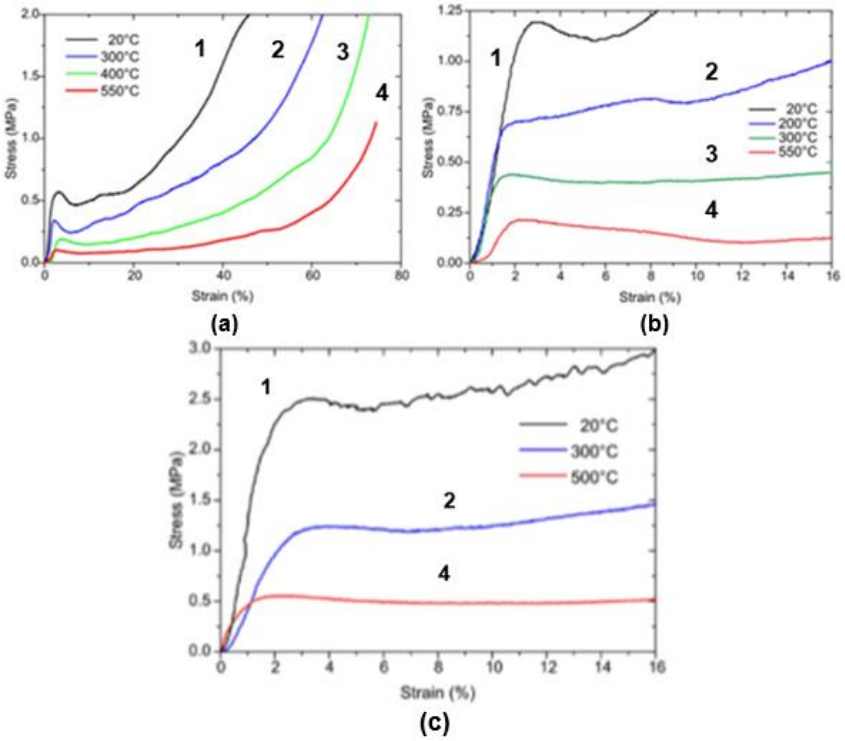

1 *– 20 °C;* ***2*** *– 200 °C;* ***3*** *– 300 °C;* ***4*** *– 550°C;*
4 *– 500 °C, viz obr. (c)*

(a) - Pure aluminium foam samples, Al 99.5%, specific gravity (308 ± 19) kg· m^{-3};
(b) - samples of aluminium alloy AlMg1Si0.6, specific gravity (412 ± 15) kg· m^{-3}
(c) AlSi12 alloy samples, specific gravity (465 ± 8) kg· m^{-3}

Fig. 6.12 Stress-strain relationship of aluminium foams with different specific gravity when heated to the appropriate temperature (e.g. 20 °C, 300 °C, 400 °C and 550 °C), according to [17]

The characteristic exponent T_f for the compressive strength of aluminium foams was also found to be a temperature-dependent variable. The compressive strength deformation (deformation to macroscopic failure of the foam) is almost independent of temperature or decreases at constant specific gravity depending on the matrix of the aluminium alloy. The absorbed energy per unit volume of aluminium foams decreases significantly with increasing temperature due to a decrease in the compressive strength value at constant specific gravity.

Foam properties are further affected by anisotropy and heterogeneity of the foam structure and cell wall imperfections (cracks, voids and fractures) as reported by [18]. MARKAKI [19], in his doctoral thesis, observed the microstructural fracture of cell walls of foams in tensile testing. He concluded that foam made of AlSi12 alloy breaks due to tensile rupture and the effect of cleavage fracture. The AlMg1Si0.6 alloy foam behaves as a tough material. Brittle fractures usually occur when foams made from aluminium foundry alloys are subjected to compressive stress. Later brittle failure of cell walls in the pore layers adjacent to the previously fractured layer (cracks grow) leads to multiple stress drops on the notched stress-strain curve in the "plate" region (Fig. 6.12c). The magnitude of the deformation of the first stress drop depends on the

average size of the foam gas cells [20]. In contrast, for foams made from forming alloys, the plastic behaviour of almost all cell walls leads to a subsequent stretching of the whole foam sample through the weakest bonds, resulting in a smooth "plateau" region, see Fig. 6.12a) and Fig. 6.12b). With larger gas cell sizes of the foam, e.g. pure aluminium, see Fig. 6.12, a first stress drop is soon observed in the curves, which is probably due to some heterogeneity of the gas cells.

6.3.2 Modulus of elasticity of metallic cellular materials

The modulus of elasticity of a material, or Young's modulus, generally represents the internal resistance of a material to elastic deformation. The higher the modulus of elasticity, the greater the stress in the material required to produce deformation. A distinction is made between materials with a high modulus of elasticity and materials with a low modulus of elasticity. From the stress-strain diagram, in terms of Hooke's law, $\sigma = E \cdot \varepsilon$, where$\sigma$ is the stress;ε is the strain (e.g., relative elongation or relative shortening etc.), E is Young's modulus. $E = \sigma/\varepsilon$; $tg\alpha = \sigma/\varepsilon$, which implies that $E = tg\alpha$. The larger the angle α, the higher the elastic modulus the material should have.

The modulus of elasticity, in combination with the geometry, is an important property for estimating the stiffness of the finished metal product. The specific modulus of elasticity (E/ρ) of aluminium foams is much lower than that of compact aluminium. For example, the specific modulus of foam made from pure Al99.5 aluminium is about 6 GPa (6000 MPa), while compact pure aluminium exhibits about 70 GPa. When producing foam from pure aluminium by powder metallurgy, the value of the modulus is 2.4 GPa (2400 MPa) with a specific weight of foam of 400 $kg \cdot m^{-3}$ (0.4 $g \cdot cm^{-3}$). Fig. 6.13 shows a diagram of the compressive stress-strain relationship for a porous material with the region for calculating the Young's modulus E marked, [12].

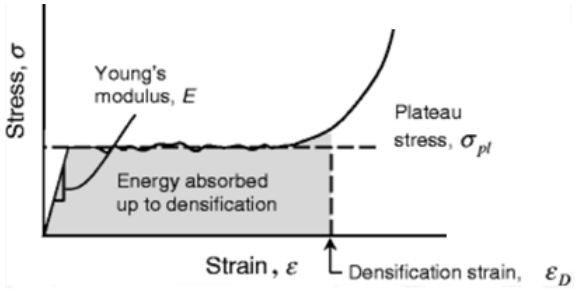

Fig. 6.13 Schematic diagram of the compressive stress-strain relationship for a porous material, showing the region for calculating Young's modulus E [12]

As shown in Fig. 6.14, the elastic modulus of the foam increases with increasing specific gravity. This effect appears in foams produced both by powder metallurgy and by melt foaming.

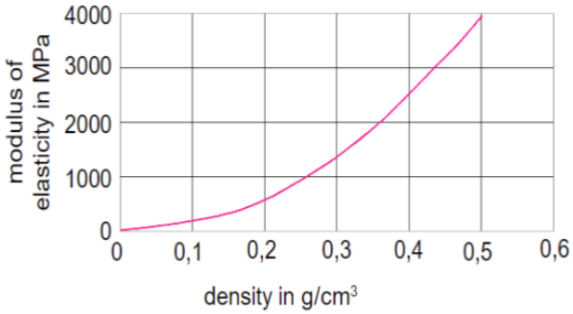

modulus of elasticity modulus of elasticity, density-specific gravity

Fig. 6.14 Dependence of modulus on specific gravity for commercially produced aluminium foam (Norsk Hydro method, Norway) [5]

Fig. 6.15 shows the Young's modulus values published by ASHBY [2]. Young's modulus was measured about the corresponding specific gravity for metal foams (red bubbles) compared to solid light alloys (purple), steels (dark green), polymers (blue) and polymer foams (light green).

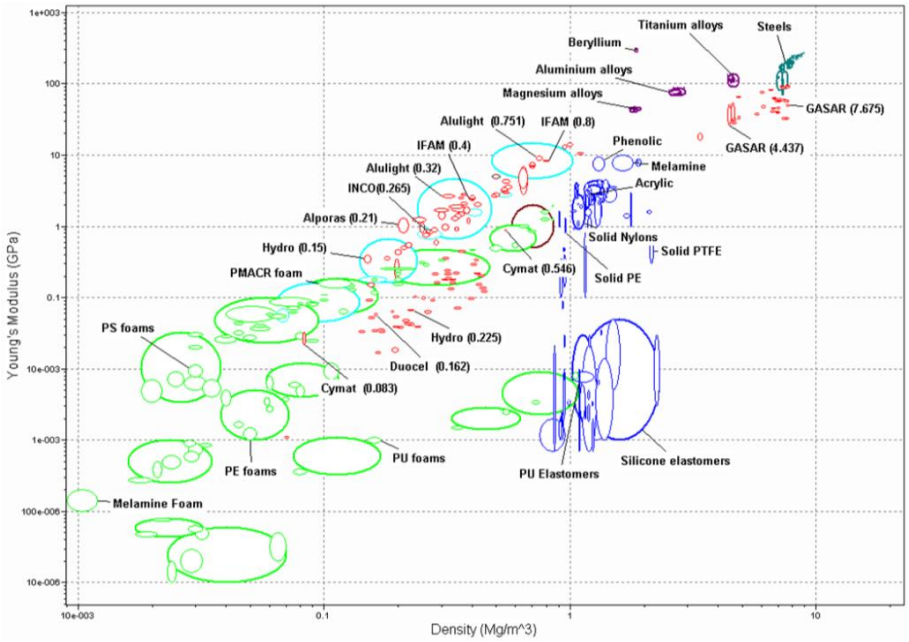

Fig. 6.15 Young's modulus values for aluminium foams produced by different methods according to ASHBY [2]

6.4 Physical and chemical properties of metallic cellular materials

6.4.1 Physical properties

The physical and chemical properties of foams are different from those of compact metals. However, these differences can provide advantages for some industrial applications. Due to the cellular structure, the coefficient of thermal and electrical conductivity is generally lower than that of a compact metal. This is because the foam

cells are gas-filled and the walls of these cells are the lowest volume fraction of the respective foam. A far greater proportion of the mass of the foam is made up of its gas-filled cells (pores). At the same time, the walls of the foam cells are coated with an oxide layer. It is therefore understandable that the conductivity increases with the higher specific gravity of the foam.

The thermal conductivity values of the foam are estimated to be 1/10 of the specific gravity ($g \cdot cm^{-3}$) exhibited by a compact metal of the same alloy. Further processing of the foam, where oxidation takes place, may lower the thermal conductivity of the foam even further. The coefficient of thermal expansion is the same as that of the compact metal, which means that the foams do not lose their shape up to relatively high temperatures. Due to the low thermal conductivity, the foams can be used as thermal insulation materials.

Another advantage of metal foams is their excellent sound damping and vibration absorption. The fineness and homogeneity of the foam's gas cells contribute to increased vibration absorption. Also, the higher connectivity between the foam air cells and the open cell walls leads to better sound absorption efficiency. Therefore, extensive research is being conducted on these foams. For example, Alporas foam shows
a large sound absorption coefficient, which is equivalent to a glass wave, [3]. The permeability of various foam media is influenced by the structure and size of the gas cells (porosity). It is directly proportional to the size of the gas cells for a specific amount and the size of cells (pores), which is also referred to as porosity, [9].

6.4.2 Chemical properties

Aluminium foams, in particular, are non-flammable and non-toxic. Their corrosion behaviour is comparable to that of compact aluminium alloys, but research is currently being carried out to provide further information. It has been found that the oxidation layer protects the foam against corrosion. At the same time, the foam remains stable within the pH due to this layer. The foams exhibit pH ranging from 4.8 to 8.5 [8]. An important observation is that all foam properties depend on the specific structure of the material. This structure develops during the manufacturing process, and as a result, the manufacturing process has a great influence on the properties of the foam. Foams of different manufacturing technologies can have different properties even if they are made from the same alloy. Therefore, for the application, it is advisable to specify all the desired properties of the foam and to select the manufacturing technology and alloy [3].

The characteristics and properties of specific metallic cellular materials (metallic foams and metallic porous materials) depend mostly on the material used, the relative specific gravity and the nature of their cells. Furthermore, whether the cells are open or closed depends on the thickness of the cell walls.

7. DESIGN AND MANUFACTURE OF METAL CELLULAR MATERIALS ON THE QUIVER

An excellent project has been funded for the development of science and research at the Technical University of Liberec (TUL) for the years 2018 to 2022. Excellent Research. Reg. CZ.02.1.01./0.0/0.0/16_019/ 0000843: "Hybrid materials for hierarchical purposes". In the area of research objective 2: Metal-based materials and structures, research activity 01: *Cellular lightweight metallic structures* was applied.

An important research activity in this project was the formation of an interdisciplinary team involving the study of special technological procedures and the design and manufacture of equipment for the processing of light metal materials and structures (cellular metal structures). Among the most considered materials were aluminium alloys and zinc alloys.

The main focus of this project was to address the methods of producing metal foams:

a) Monitoring the effects of straining agents in the production of aluminium cellular materials. Methods of frothing metal melts based on the gas produced by the thermal decomposition of the foaming agent.
b) Method for the production of metal foams by powder metallurgy PM (metal powder based and foaming agent powder).
c) Study of properties and theoretical calculations of thermal decomposition and diffusion properties of straining agents in aluminium and its alloys.
d) Numerical simulation calculations of the foaming process based on direct gas filling from an external source.
e) Production of metallic porous materials.
f) Experimental foaming of various aluminium alloys with air or argon.

In the course of the project about direct melt foaming, experimental production equipment was to be designed, constructed and tested. Part of this research activity of this project was to achieve the production of porous aluminium material. Another objective of this project was to address the production of porous metallic materials based on NaCl or other agents forming after solidification of metals and their subsequent removal, small cavities that cause porosity in the material.

7.1 Monitoring the effects of straining agents on the production of aluminium, cellular materials

7.1.1 Theoretical calculations of the amount of gas released by the blowing agents

This research work in our project builds on Chapter 4. As is evident from this chapter, many metal-based straining agents are used to fabricate cellular metal systems: TiH_2, SrH_2, MgH_2, and ZrH_2 [1,2].

Calcium carbonate $CaCO_3$, which is also described in detail in Chapter 4, is a commonly used foaming agent in production.
When the foaming agent is heated to a suitable temperature, other important processes occur in the production of metal "foams". These are the decomposition of the foaming agent to form a gaseous component, its diffusion and the activity of the gaseous component to form heterogeneous bubbles in the metal melts. The most commonly used foaming agent production for aluminium foams is titanium hydride.

In the framework of our "*Hybrid materials for hierarchical purposes"* ("HYHI") project, the foaming capacity of the foaming agent was calculated. At the same time, it is necessary to take into account how much of the respective agent is used in the production of the metal foam. For example, TiH_2 is used for the foam production of 1.5 wt. %. The calculation can be made for 1 kg of metal, e.g. aluminium. The equation of state can be applied to the calculation:

$$p \cdot V = n \cdot R \cdot T, \tag{7.1}$$

where: p is pressure (i.e. 101 325 Pa); V is the volume of gas [m^3]; n is several moles [mol]; R is the universal gas constant (R = 8. 314[$J \cdot K^{\cdot -1} \cdot mol^{-1}$]); T is temperature [K], for the melting temperature of pure aluminium T = 933 K.

In equation (7.1), n = m/M can be substituted for the number of moles:

$$p \cdot V = \frac{m}{M} \cdot R \cdot T, \tag{7.2}$$

where m is the mass of the foaming agent [g]; M is the molecular mass of the foaming agent.

For example, the foaming agent TiH_2: 0.10 wt. % TiH_2 is 1 g; 0.20 wt.% TiH_2 is 2 g; 1.50 wt.% TiH_2 = 15 g. The molecular weight of the foaming agent M_{TiH2}: Ti + $2H_2$ = 47.90 + 2·1.008 = 49.91 [$g \cdot mol^{-1}$].

At the same time, the relative bulk density of the foamed aluminium material can be calculated:

$$\rho_{r} = \frac{V_S}{V+V_S}, \tag{7.3}$$

where: V_S is the volume of metal to be foamed [m^3], for pure aluminium V_S = 1 kg / 2700 $kg \cdot m^{-3}$ = $3.704 \cdot 10^{-4}$ [m^3]; V is the volume of gas released by the decomposition of the foaming agent [m^3].

For the solid state of aluminium, its density can be calculated based on a well-known physical relationship:

$$\rho = \frac{m}{V}, \tag{7.4}$$

where: ρ is solid density [kg·m^3]; m is mass of the sample [kg]; V is volume of the raft [m^3].

Thus, for example, to determine the relative density of foamed aluminium, it is necessary to use relation (7.2). Thus, for example, using a foaming agent of 0.5 wt %, m = 1 g, M_{TiH2} = 49.91 [g· mol^{-1}], one can write:

$$V = \frac{1}{49.91} \cdot \frac{8.314 \cdot 933}{101325} = 1.535 \cdot 10^{-3}\ [m^3] \tag{7.5}$$

$$\rho_r = \frac{3.704 \cdot 10^{-4}}{1.535 \cdot 10^{-3} + 3.704 \cdot 10^{-3}} = 1.94 \cdot 10^{-1} \tag{7.6}$$

The density of foamed aluminium ($\rho_{Al.F.}$) from aluminium foam can be calculated using the equation:

$$\rho_{Al.F.} = \rho_r \cdot \rho_{Al} = 1.94 \cdot 10^{-1} \cdot 2700 = 523\ [kg \cdot m^{-3}] \tag{7.7}$$

In the theoretical calculations of the straining effects, the relative bulk weight and the bulk weight of the strained aluminium material were determined. For this purpose, the use of foaming agents was assumed: TiH_2, SrH_2, MgH_2, ZrH_2, $MgCO_3$ and $CaCO_3$. The calculation of the gaseous effect can usually be expressed per kilogram of aluminium. Equations (7.1) and (7.2) were used to determine the maximum volume of gas released from the respective frother. To determine the relative density (7.3). Further, to determine the density of the respective aluminium foam, equation (7.6) or its analogous form. The results of the calculations are given in Table 7-1 to Table 7-5.

Table 7-1 Theoretical calculation of the straining effect of titanium hydride for 1 kg of aluminium

Theoretical calculation of the straining effect of titanium hydride for 1 kg of aluminium						
Foaming agent	**Gassed metal**	**Amount of foaming agent [wt. %]**	**Gas volume V [m^3]**	**Volume of solid metal (aluminium) V_S [m^3]**	**Relative bulk density ρ_r [1]**	**Volumetric weight of foamed aluminium $\rho_{Al.F.}$ [g·cm^{-3}]**
Titanium hydride (TiH_2)	Aluminium	0.50	0.0077	$3.70 \cdot 10^{-4}$	0.0460	0.124
		0.75	0.0115		0.0312	0.084
		1.00	0.0153		0.0236	0.064
		1.25	0.0192		0.0189	0.051
		1.50	0.0230		0.0158	0.043
		1.75	0.0268		0.0136	0.037
		2.00	0.0307		0.0119	0.032

Table 7-2 Theoretical calculation of the foaming effect of magnesium hydride for 1 kg aluminium

Theoretical calculation of the foaming effect of magnesium hydride for 1 kg of aluminium						
Foaming agent	**Gassed metal**	**Amount of foaming agent [wt. %]**	**Gas volume V [m^3]**	**Volume of solid metal (aluminium) V_S [m^3]**	**Relative bulk density ρ_r [1]**	**Volumetric weight of foamed aluminium $\rho_{Al.F.}$ [$g \cdot cm^{-3}$]**
Magnesium Hydride (MgH_2)	Aluminium	0.50	0.0145	$3.70 \cdot 10^{-4}$	0.0248	0.067
		0.75	0.0218		0.0170	0.046
		1.00	0.0291		0.0126	0.034
		1.25	0.0363		0.0101	0.027
		1.50	0.0436		0.0078	0.021
		1.75	0.0509		0.0072	0.019
		2.00	0.0582		0.0063	0.017

Table 7-3 Theoretical calculation of the straining effect of zirconium hydride for 1 kg of aluminium

Theoretical calculation of the straining effect of zirconium hydride for 1 kg of aluminium						
Foaming agent	**Gassed metal**	**Amount of foaming agent [wt. %]**	**Gas volume V [m^3]**	**Volume of solid metal (aluminium) V_S [m^3]**	**Relative bulk density ρ_r [1]**	**Volumetric weight of foamed aluminium $\rho_{Al.F.}$ [$g \cdot cm]^{-3}$**
Zirconium hydride (ZrH_2)	Aluminium	0.50	0.0041	$3.70 \cdot 10^{-4}$	0.0827	0.220
		0.75	0.0062		0.0567	0.150
		1.00	0.0082		0.0431	0.012
		1.25	0.0103		0.0348	0.094
		1.50	0.0123		0.0292	0.078
		1.75	0.0144		0.0251	0.067
		2.00	0.0164		0.0220	0.059

Table 7-4 Theoretical calculation of the foaming effect of calcium carbonate for 1 kg aluminium

Theoretical calculation of the foaming effect of calcium carbonate for 1 kg of aluminium						
Foaming Agent	**Gassed metal**	**Amount of foaming agent [wt. %]**	**Gas volume V [m^3]**	**Volume of solid metal (aluminium) V_S [m^3]**	**Relative bulk density ρ_r [1]**	**Volumetric weight of foamed aluminium $\rho_{Al.F.}$ [$g \cdot cm^{-3}$]**
Calcium carbonate ($CaCO_3$)	Aluminium	0.50	0.0038	$3.70 \cdot 10^{-4}$	0.0882	0.238
		0.75	0.0057		0.0606	0.164
		1.00	0.0076		0.0461	0.400
		1.25	0.0096		0.0373	0.101
		1.50	0.0115		0.0312	0.084
		1.75	0.0134		0.0269	0.072
		2.00	0.0530		0.0236	0.064

Table 7-5 Theoretical calculation of the foaming effect of magnesium carbonate for 1kg aluminium

Theoretical calculation of the foaming effect of magnesium carbonate for 1 kg of aluminium						
Foaming agent	**Gassed metal**	**Amount of foaming agent [wt. %]**	**Gas volume V [m^3]**	**Volume of solid metal (aluminium) V_S [m^3]**	**Relative bulk density ρ_r [1]**	**Volumetric weight of foamed aluminium $\rho_{Al.F.}$ [$g \cdot cm^{-3}$]**
Magnesium carbonate ($MgCO_3$)	Aluminium	0.50	0.0045	$3.70 \cdot 10^{-4}$	0.0754	0.204
		0.75	0.0068		0.0515	0.139
		1.00	0.0091		0.0391	0.106
		1.25	0.0114		0.0316	0.085
		1.50	0.0136		0.0264	0.071
		1.75	0.0159		0.0228	0.062
		2.00	0.0182		0.0199	0.054

Based on the values given in Tables 7-1 to 7-5, the corresponding graphical dependencies were constructed and are shown in Fig. 7.1 to Fig. 7.3. Fig. 7.1 shows the graphical dependence of the gas volume on the amount of foaming agent (foaming agent or superconductor, TiH_2, SrH_2, MgH_2, ZrH_2, $MgCO_3$ and $CaCO_3$). Fig. 7.2 shows a graphical dependence of the relative density ρ_r on the amount of the respective foaming agent. Fig. 7.3 shows the dependence of a densityρ on the amount of the respective foaming (frothing) agent. In both cases, the foaming agents used were (TiH_2, SrH_2, MgH_2, ZrH_2, $MgCO_3$ and $CaCO_3$) in 1 kg of aluminium.

In the case of this work, only a theoretical assumption was made to predict the behaviour of the foaming agent. The gas released, expressed in V [m^3] by heating the foaming agent, depends on the type of foaming agent (blowing agent) used for hydrides TiH_2, MgH_2, CaH_2, ZrH_2 it is hydrogen. For carbonates $CaCO_3$, $MgCO_3$ is carbon dioxide.

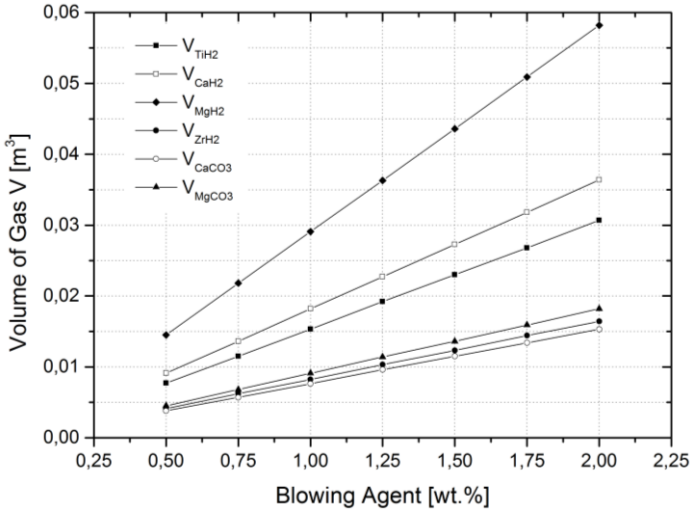

Fig. 7.1 Dependence of the amount of released bulk gas on the amount of foaming agent

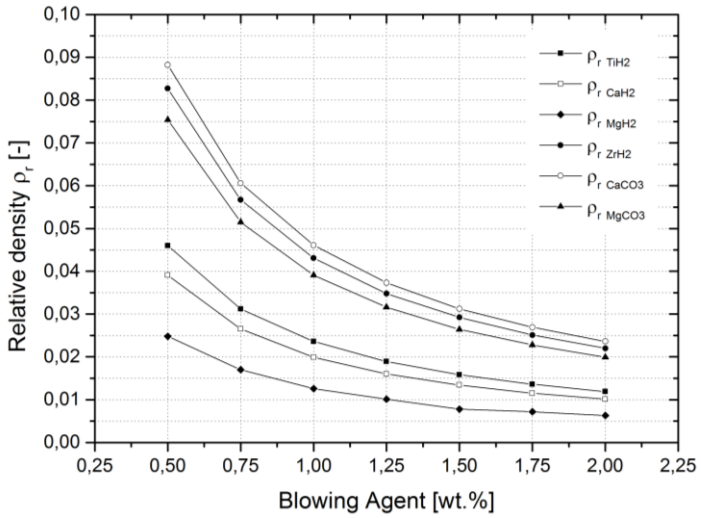

Fig. 7.2 Dependence of the relative density of aluminium foam on the amount of foaming agent

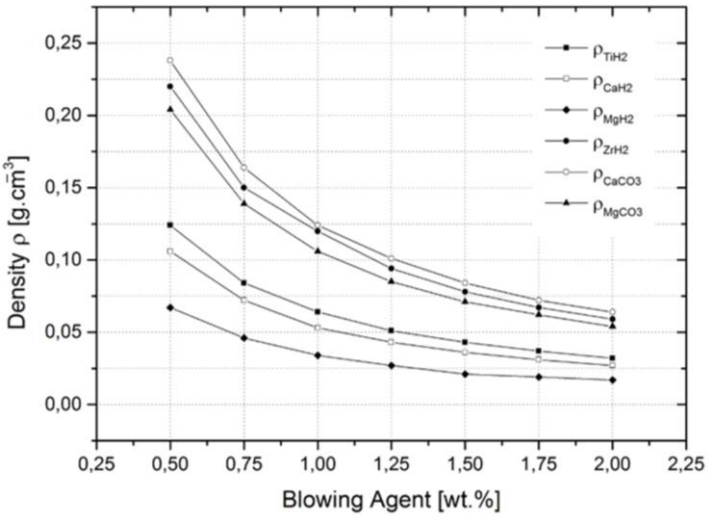

Fig. 7.3 Dependence of the density of aluminium foam on the amount of foaming agent

From these theoretical calculations of the behaviour of selected straining agents for the production of metal cell systems, or aluminium "foams", it can be seen that the MgH_2 straining agent shows the greatest gas evolution 2 wt. %, the calculated volume of gas released is 0.0582 [m^3]. When using a 0.5 % wt. foaming agent, the calculated volume of gas released was 0.0145 [m^3].

On the other hand, the CaCO foaming agent$_3$ showed the lowest volume of gases released. Using this foaming agent of 2 % wt., the calculated volume of gas released was 0.0530 [m^3]. Using the $CaCO_3$ 0.5 wt. % foaming agent, the volume of gas released was 0.0038 [m^3]. According to practical experience with the production of aluminium "foams", titanium hydride is most commonly used. Depending on the technology used, the content can vary from 0.5 to 1 % wt. Thermal decomposition of the hydrides produces hydrogen, which is the basic foaming agent.

In addition, the relative bulk density of aluminium foam (ρ_r) and the bulk density of aluminium foam (ρ) were determined based on calculations and the use of physical relationships with respect to the density of aluminium in the solid state and the appropriate foaming agent.

From the theoretical calculations, it is clear that the most suitable foaming agent is MgH_2, which leads to the lowest density of aluminium foam. However, a foaming agent TiH_2 with a content of 0,5 to 1,0 % wt. is commonly used in the production of aluminium foams. For example, for a foaming agent containing 0.5 % wt. TiH_2, the relative bulk density ρ_r = 0.0460 and corresponds to an aluminium foam density of 0.124 [$g.cm^{-3}$]. The densities of the "foam" produced are also dependent on the production technology. Density values starting from 0.20 to 0.25 [$g.cm^{-3}$] (produced by the Alporas method) or from 0.30 to 0.40 [$g.cm^{-3}$] are used according to [3], [4].

As can be seen from the aluminium foam density tables above (ρ), theoretical calculations show that higher foaming occurred with higher levels of foaming agent. For example, using 0.5 % wt. TiH_2 at first glance means that half the amount, i.e. 2.5 g of TiH_2 powder, is not involved in foam formation. However, the difference may be due to two factors. The first factor is that the ideal reaction temperature is 933 K (i.e. 660 °C), at which the melting point of aluminium does not occur. The second factor may be the loss of hydrogen to the surrounding environment.

Observed issues have been published:

NOVÁ, I. FRAŇA, K. MACHUTA, J. and I. NOVÁKOVÁ. Theoretical Calculations of the Foaming properties of Powder Agents for the production of Aluminium Foams. Manufacturing Technology, Vol 19, No. 1, 2019, 119-122. ISSN 1213-2489, Scopus.

NOVÁ, I. FRAŇA, K. SOBOTKA, J. SOLFRONK, P. KOREČEK, D. a I. NOVÁKOVÁ. Production of Foaming Process in the Production of Aluminium Faoams. Manufacturing Technology. 2019, Vol. 19, No. 4. pp. 655-659. 119–122. ISSN 1213-2489, Scopus.

NOVÁ, I. FRAŇA, K. SOLFRONK, P. KOREČEK, D. and J. SOBOTKA. Properties of Aluminium Cellular Materials Produced by Powder Metallurgy Using the Foaming Agent TiH_2. Manufacturing Technology, Vol 22, No. 4, 2022, 444–450, ISSN 1213-2489, Scopus.

7.1.2 Hydrogen diffusion and its calculations for the foaming process of aluminium cellular materials

Furthermore, within the framework of our research project "HYHI", theoretical calculations of hydrogen diffusion processes of selected powdered foaming agents (TiH_2, CaH_2, MgH_2, ZrH_2), which can be used for the production of aluminium foams, were carried out. Hydrogen for the production of metal cell systems in the case of aluminium "foams" can be obtained by thermal decomposition of titanium hydride, magnesium hydride, calcium hydride and zirconium hydride. Our main research objective was to perform hydrogen solubility calculations according to the relationships

reported by various researchers. In addition, the diffusion of hydrogen in aluminium was investigated. Calculations of diffusion coefficients were performed. At the same time, the diffusion paths of hydrogen as a function of temperature were calculated. and diffusion time. In addition, by calculating the diffusion of hydrogen in solid and liquid aluminium, the results were obtained for the duration of the expected effect of the powder supercoolant (0.75, 1.0, 1.25, 1.50, 1.75 and 2.0 % wt.).

7.1.2.1 Solubility of hydrogen in aluminium

The solubility of hydrogen in pure liquid aluminium dates back to the pioneering work of Ransley, Talbot and others. It is essentially the concentration of hydrogen usually expressed as ml or cm^3 H_2 for 100 g of aluminium. The solubility of hydrogen in aluminium and its alloys is variable and can be written down:

$$H_2\ (gas) \leftrightarrow 2H_{Al} \quad \text{(solution in aluminium)} \tag{7.8}$$

The solubility of hydrogen in aluminium and its alloys is variable and depends on the temperature of the alloy, the chemical composition and the partial pressure of hydrogen in the surrounding atmosphere. The amount of dissolved hydrogen is determined in units of cm^3 per 100 g of metal. This value of 1 cm^3 per 100 g of metal corresponds to a concentration of 0,9 ppm. Aluminium and its alloys show a significant difference between the solubility of hydrogen in the solid and liquid state. As reported by ROUČKA, [5] in the solid state at 660 °C, the solubility of hydrogen in Al is only 0.036 cm^3/100 g. In molten aluminium at 660 °C, the solubility of hydrogen is 0.77 cm^3 /100g, about 20 times higher. Other authors, e.g. AMBRIZ [3], give a value for the maximum solubility of hydrogen in aluminium of 0.69 cm^3/100 g, see Fig. 7.4 (left).

The solubility of hydrogen in aluminium is determined by thermodynamic equilibrium. This is quantified by Sieverts law. Sieverts law relates the partial pressure of hydrogen p_{H2} and the dissolved hydrogen S (solubility) in aluminium.

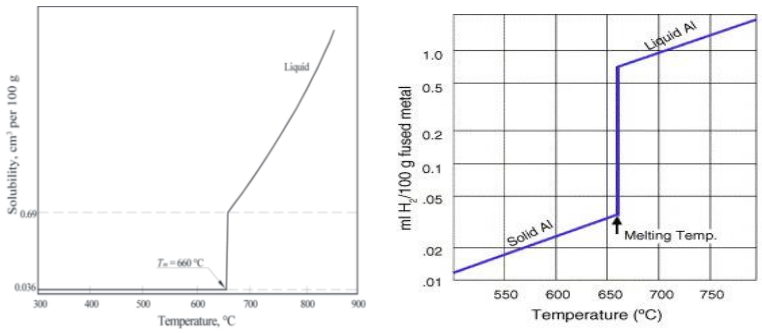

Fig. 7.4 Solubility of hydrogen in pure aluminium according to AMBRIZ [3] (left), according to Electric Company [1], (right)

$$S = K_S(T) \cdot \sqrt{p_{H2}}, \tag{7.9}$$

where denotes: S is solubility of hydrogenin the aluminium [cm^3 H_2·(100 g Al)$^{-1}$]; K_S (T) is equilibrium constant for the given metal [cm^3 H_2·(100 g Al)$^{-1}$·$Pa^{-1/2}$]; p_{H2} is partial pressure of gas in the surrounding atmosphere [Pa].

In the production of aluminium cellular systems, hydrogen is dissolved in the aluminium. The solubility of hydrogen in aluminium is determined by thermodynamic equilibrium.

$$\left(\frac{S}{S^0}\right) = K_S\,(T) \cdot \left(\frac{p_{H2}}{P^0}\right), \tag{7.10}$$

where denotes: S is solubility of hydrogen in the aluminium (liquid or solid); S^0 is atomic volume in cm^3 per 100 g of material at standard state T = 273 K; P^0 is standard pressure 101325 Pa (1/100) [cm^3g^{-1}]; C^0 is molar unit (1/100) [cm^3g^{-1}] = $2.1\cdot10^{-3}$ [mol·l^{-1}] = $8.9\cdot10^{-4}$ [mol·kg^{-1}], the density of molten aluminium is 2.4 g·cm^{-3} and density of solid aluminium is 2.7 g·cm^{-3}; K_S (T) - solubility coefficient for the solid and liquid states of aluminium, according to [6], [7]:

Solid state:

$$K_S\,(T) = 10^{\left(-\frac{2580}{T}+1.399\right)}, \tag{7.11}$$

Liquid state:

$$K_S\,(T) = 10^{\left(-\frac{2760}{T}+2.768\right)}, \tag{7.12}$$

where denotes: R is universal gas constant, R = 8.314 [J· mol $^{-1}$· K^{-1}]; T is temperature [K].

By substituting into equations (7.11) and (7.12), for an aluminium temperature of 1000 K it can be determined that K_S (T) for the melt is 1.02 and K_S (T) for the solid state is 0.066.

Under normal hydrogen pressure (p_{H2} = p^0), the equilibrium concentration approaches 0.77 (0.85) cm^3 /100 g, i.e.,$7.6\cdot10^{-4}$ [mol·kg^{-1}] = $1.8\cdot10^{-3}$ [mol·l^{-1}], at a temperature of 700 °C (973 K). The comparison of hydrogen stored in TiH_2 with dissolved hydrogen at equilibrium is very small. Examining equation (7.8), less than 1 % of the hydrogen is dissolved in the aluminium.

Equilibrium concentrations are found roughly at pore interfaces that neglect bubble surface tension. The outer surfaces of the precursor may have a significantly lower hydrogen value depending on its partial pressure in the atmosphere and related to its concentration around TiH_2 particles.

The temperature dependence of the solubility of hydrogen in aluminium at a pressure of 101 325 Pa can be obtained by applying the van Hoff isobar as reported by Kalousek [20]:

$$\frac{d(\log K_S)}{d(\frac{1}{T})} = -\frac{\Delta H^0}{R}, \quad (7.13)$$

where it reads: ΔH^0 is the standard enthalpy of solubility of hydrogen in the aluminium melt; T is temperature [K]; K_S is the equilibrium constant for the aluminium melt.

Based on the ratio of the respective equilibrium constants and the solubility of hydrogen in liquid aluminium and the solubility under equilibrium conditions, one can write:

$$\frac{K_S}{K^0{}_S} = \frac{S}{S^0}, \quad (7.14)$$

By integrating the van Hoff isotherm equation (7.13) and using equation (7.14) we can write:

$$\log S = \frac{\Delta H^0}{R \cdot T} + C, \quad (7.15)$$

where it reads: C is an integration constant; $H\Delta^0$ is considered temperature dependent.

Table 7-7 shows the values for the application of the calculation according to equation (7.15) according to different authors as reported by LIU [8]. Special equipment using a reference gas is required to determine these values.

Table 7-7 Values for calculating the solubility of hydrogen in aluminium by various authors, Liu [17]

ΔH^0		**Constant C**	**S^0**	**Reference gas**	**Sample weight**	**Author calculation methods**
[kcal·mol^{-1}]	**[kJ·mol^{-1}]**	**[1]**	**[ml/100g]**	**[g]**	**[g]**	
5.365	22.45	2.72	0.881	helium	100	TALBOT [9]
5.067	21.21	2.62	0.998	helium	100	OPIE [11]
5.484	22.95	2.80	0.911	Neon	30-40	RANSLEY [10]
5.921	24.78	3.07	1.026	argon	300	LIU [8]

The work of RANSLEY and NEUFELD [10] in 1948, for the determination of the solubility of hydrogen in pure aluminium, was the basic work of this research. In 1950, OPIE AND GRANT [11] concluded that the solubility of hydrogen in aluminium is given by a general equation:

$$log_{10}\ S = -\frac{A}{T} + C, \quad (7.16)$$

where denotes: S is the solubility of hydrogen in aluminium [cm^3 per 100 g of metal]; A is a constant that represents the heat of the solution of hydrogen in liquid or solid aluminium; C is an integration constant.

Table 7-8 shows the equations for calculating log S according to various authors.

Table 7-8 Equations for the determination of hydrogen solubility in molten and solid aluminium by various authors

Number equation	$log_{10} S = -\frac{A}{T} + C$		Entalpie solution ΔH [J. mol^{-1}]	Method	Year of publication	Published by
	Constant A	Constant C				
Hydrogen in liquid aluminium						
1	2760	2.796	52 840	Sievert . method	1948	RANSLEY et al [10].
2	2550	2.620	48 820	Sievert. method	1950	OPIE et al. [11].
3	3086	2.969	59 080	saturation and extraction	1961	EICHENAUER et al [4].
4	2713	2.528	51 940	rapid cooling	1967	GRIGORENKO et al [13].
5	2970	2.817	56 860	rapid cooling	1987	FEICHTINGER et al [14].
6	2700	2.720	51 690	modif. Sievert. met.	1988	TALBOT et al. [9].
7	2692	-1.320	-	-	1995	ANYALEBECHI et al [13].
8	2980	3.070	57 050	Sievert. method	1995	LIU et al. [8].
9	2392	2.256	45 800	rapid cooling	1995	IMABAYASHI et al [21].
Hydrogen in solid aluminium						
10	2080	0.788	39 820	Sievert. method	1948	RANSLEY et al [10].
11	3342	1.961	58 240	saturation and extraction	1961	EICHENAUER et al [4].
12	3300	2.105	63 180	saturation and extraction	1968	EICHENAUER et al [18].
13	3340	2.220	63 940	solid state extraction under vacuum	1979	ICHIMURA et al [15].
14	5040	4.976	96 490	gradual diffusion	1983	HASHIMOTO et al [2].
15	3320	2.220	-	modif. Sievert. method	2004	TALBOT et al [16].

***Note**: S is the solubility of hydrogen under standard conditions in cubic centimetres per 100 g of melt.*

The values of log_{10} S for the calculation of hydrogen solubility in aluminium according to ANYALEBECHI [12] differ from other authors mainly in the value of the constant C, which is -1.32.

7.1.2.2 Computational methods for experimental applications of hydrogen in molten aluminium in the production of cellular materials

The solubility of hydrogen in the aluminium melt was monitored as a result of our experiments aimed at monitoring the foaming process in the production of aluminium cellular systems (aluminium foams). The solubility of hydrogen in the pure aluminium melt was calculated based on the temperatures required for the foaming technology of molten aluminium. For these purposes, all available equations (see Table 7-8), were used to solve for the solubility of hydrogen in molten aluminium.
The calculated log S and S values are shown in Table 7-9. Table 7-10 shows the calculated log S and S values for the solubility of hydrogen in solid aluminium.

Table 7-9 Calculated values of the solubility of hydrogen in pure aluminium melt (log S and S) based on values from different authors

Monitoring of hydrogen solubility in aluminium melt [cm^{-3} /100 g Al]											
Calcul number	**933 K**		**943 K**		**953 K**		**963 K**		**973 K**		**Calculation according to reference**
	660 °C		***670 °C***		***680 °C***		***690 °C***		***700 °C***		
	log S	***S***	***log S***	***S***	***log S***	***S***	***log S***	***S***	***log S***	***S***	
I.	- 0.158	0.695	- 0.127	0.746	- 0.096	0.802	- 0.066	0.859	- 0.037	0.918	[10]
II.	- 0.113	0.771	- 0.084	0.824	- 0.056	0.879	- 0.028	0.938	- 0.0007	0.998	[11]
III.	- 0.338	0.459	- 0.303	0.498	- 0.268	0.540	- 0.234	0.583	- 0.202	0.628	[12]
IV.	- 0.380	0.417	- 0.349	0.448	- 0.319	0.480	- 0.289	0.514	- 0.260	0.550	[14]
V.	- 0.366	0.431	- 0.333	0.465	- 0.299	0.502	- 0.267	0.541	- 0.235	0.582	[15]
VI.	- 0.174	0.670	- 0.143	0.719	- 0.113	0.771	- 0.084	0.824	- 0.055	0.881	[9]
VII.	was not counted										[13]
VIII.	- 0.124	0.752	- 0.090	0.813	- 0.057	0.877	- 0.024	0.946	0.0073	0.983	[8]
IX.	- 0.308	0.492	- 0.281	0.524	- 0.254	0.557	- 0.228	0.592	- 0.202	0.628	[19]

Table 7-10 Calculated values for the solid-state hydrogen solubility of pure aluminium (log S and S) based on values from various authors

Monitoring the solubility of hydrogen in solid aluminium [cm^{-3} /100 g Al]											
Calculation number	**933 K**		**943 K**		**953 K**		**963 K**		**973 K**		**Calculation according to reference**
	660 °C		***670 °C***		***680 °C***		***690 °C***		***700 °C***		
	log S	***S***	***log S***	***S***	***log S***	***S***	***log S***	***S***	***log S***	***S***	
X.	- 2.842	0.0014	- 2.303	0.0049	- 1.903	0.0125	- 1.595	0.0254	- 1.441	0.0362	[10]
XI.	- 3.871	0.0013	- 3.005	0.0009	- 2.362	0.0043	- 1.867	0.0135	- 1.621	0.0239	[12]
XII.	- 3.654	0.0002	- 2.798	0.0016	- 2.164	0.0068	- 1.675	0.0211	- 1.432	0.0370	[22]
XIII.	- 3.609	0.0002	- 2.743	0.0018	- 2.101	0.0079	- 1.606	0.0248	- 1.360	0.0437	[21]
XIV.	- 3.820	0.0002	- 2.513	0.0031	- 1.544	0.0286	- 0.797	0.1596	- 0.426	0.3750	[2]
XV.	- 3.574	0.0003	- 2.713	0.0019	- 2.075	0.0084	- 1.583	0.0261	- 1.338	0.0415	[9]

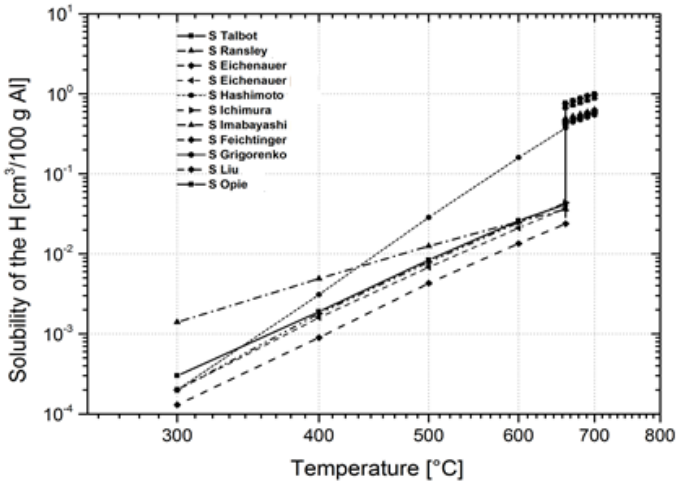

Fig. 7.6 Hydrogen solubility in aluminium at different temperatures, calculation performed according to the equations of various authors

7.1.2.3 Calculation of hydrogen diffusion in liquid aluminium

Monitoring the diffusion of hydrogen in aluminium melt is one of the important processes in the production of cellular metal systems (metal foams). The diffusion of hydrogen corresponds very well to the mechanism of hydrogen diffusion, where jumps of hydrogen atoms are due to thermal activation.

The diffusion coefficient of hydrogen in aluminium (solid and liquid) can be determined using the well-known Arrhenius equation:

$$D = D_0 \cdot \exp\left(-\frac{\Delta H}{R \cdot T}\right), \qquad (7.17)$$

where denotes: D_0 is frequency factor of diffusion [$m^2 \cdot s^{-1}$]; ΔH is activation enthalpy [$kJ \cdot mol^{-1}$]; R is universal gas constant R = 8.314 [$J \cdot K^{-1} \cdot mol^{-1}$], T is temperature [K].

Table 7-10 shows the values needed to calculate the diffusion coefficient of hydrogen in the solid and liquid state of aluminium (frequency factor D_0 and activation enthalpy ΔH).

Table 7-11 Values for determining the hydrogen diffusion coefficient in pure aluminium

Values for the determination of the hydrogen diffusion coefficient in pure aluminium				
Frequency factor D_0 [$m^2 \cdot s^{-1}$]	**Activation enthalpy ΔH [$kJ \cdot mol^{-1}$]**	**Stages**	**Temperature range [°C]**	**Reference**
$1.10 \cdot 10^{-5}$	40.95	rigid	to 660	[4]
$1.01 \cdot 10^{-5}$	47.70	rigid	450 - 625	[23]
$1.90 \cdot 10^{-5}$	40.00	rigid	450 - 590	[24]
$2.50 \cdot 10^{-6}$	90.00	rigid	450 - 590	[25]
$4.58 \cdot 10^{-6}$	37.03	rigid	300 - 640	[21]
$3.80 \cdot 10^{-6}$	19.26	liquid	over 660	[12]

Note: Hydrogen diffusion coefficient in the solid state of pure aluminium: D = 0.11 exp (- 9780/RT) [$cm^2 \cdot s^{-1}$], [12].

The diffusion path of a hydrogen atom in aluminium can be calculated from the relation [6]:

$$l = \sqrt{D \cdot t} \qquad (7.18)$$

where denotes: D is diffusion coefficient of hydrogen [$m^2 \cdot s^{-1}$]; t is diffusion time [s].

a) Calculation of the diffusion coefficient of hydrogen in aluminium

To address the decomposition of hydride-based straining agents, calculations of the diffusion coefficient of hydrogen in solid and liquid aluminium at different temperatures (20 °C, 100 °C, 200 °C, 300 °C, 400 °C, 500 °C, 550 °C, 600 °C, 610 °C, 620 °C, 630 °C, 640 °C, 650 °C, 660 °C, 670 °C, 680 °C, 690 °C, 700 °C and 720 °C) were performed. The temperature range from 660 °C to 700 °C can be considered very important for the production of aluminium 'foams'. The formula (7.17) and the values of the corresponding quantities in Table 7-11 were used for the calculation according to [4] and [12]. The calculated values of the diffusion coefficients for each temperature and solid and liquid phase, respectively, are given in Table 7-12.

Table 7-12 Values of the calculated diffusion coefficient of hydrogen in aluminium

Calculated values of the hydrogen diffusion coefficient in aluminium					
Diffusion coefficient D [$m^2 \cdot s^{-1}$]	**Frequency factor D_0**	**Activation enthalpy**	**Temperature**		**Stages**
			[K]	**[°C]**	

	[$m^2 \cdot s^{-1}$]	ΔH [$kJ \cdot mol^{-1}$]			
$5.511 \cdot 10^{-13}$	$1.1 \cdot 10^{-5}$	40.95	293	20	solid
$2.025 \cdot 10^{-11}$			373	100	
$3.300 \cdot 10^{-10}$			473	200	
$2.025 \cdot 10^{-9}$			573	300	
$7.291 \cdot 10^{-9}$			673	400	
$1.881 \cdot 10^{-8}$			773	500	
$2.783 \cdot 10^{-8}$			823	550	
$3.910 \cdot 10^{-8}$			873	600	
$4.150 \cdot 10^{-8}$			883	610	
$4.411 \cdot 10^{-8}$			893	620	
$4.680 \cdot 10^{-8}$			903	630	
$5.016 \cdot 10^{-8}$			913	640	
$5.280 \cdot 10^{-8}$			923	650	
$3.154 \cdot 10^{-7}$	$3.8 \cdot 10^{-6}$	19.26	**933**	**660**	liquid
$3.230 \cdot 10^{-7}$			943	670	
$3.344 \cdot 10^{-7}$			953	680	
$3.412 \cdot 10^{-7}$			963	690	
$3.534 \cdot 10^{-7}$			973	700	
$3.572 \cdot 10^{-7}$			983	710	
$3.690 \cdot 10^{-7}$			993	720	

Fig. 7.7 Dependence of the value of the diffusion coefficient of hydrogen in aluminium on temperature in decadic and logarithmic coordinates.

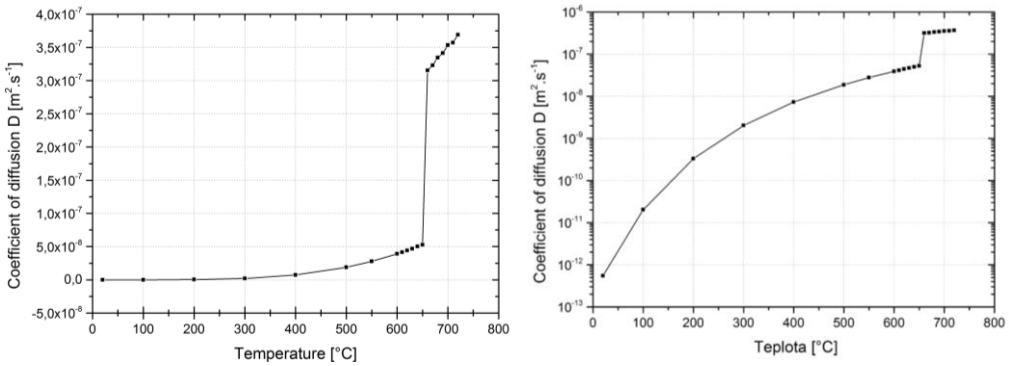

Coefficient of diffusion - diffusion coefficient; Temperature - temperature

Fig. 7.7 Dependence of the hydrogen diffusion coefficient in aluminium on the temperature in decadic and logarithmic coordinates

b) Calculation of diffusion paths of hydrogen in aluminium

According to formula (7.18), the diffusion paths of hydrogen in aluminium were calculated at different temperatures for time points of 10 [s], 20 [s], 30 [s], 40 [s], 50 [s] and 60 [s] (see Table 7-13).

Table 7-13 Calculation of hydrogen diffusion paths in aluminium at time instants 10, 20, 30, 40, 50 and 60 [s]

Calculation of hydrogen diffusion paths in aluminium at 10, 20, 30, 40, 50 and 60 s								
Number path calculation	**D [$m^2 \cdot s^{-1}$]**	**Temperature [°C]**	***L = (D· t)$^{1/2}$ [m]***					
			10 [s]	**20 [s]**	**30 [s]**	**40 [s]**	**50 [s]**	**60 [s]**
1	$5.511 \cdot 10^{-13}$	20	$2.348 \cdot 10^{-6}$	$3.320 \cdot 10^{-6}$	$4.066 \cdot 10^{-6}$	$4.695 \cdot 10^{-6}$	$5.250 \cdot 10^{-6}$	$5.751 \cdot 10^{-6}$
2	$2.025 \cdot 10^{-11}$	100	$1.423 \cdot 10^{-5}$	$2.012 \cdot 10^{-5}$	$2.465 \cdot 10^{-5}$	$2.846 \cdot 10^{-5}$	$3.183 \cdot 10^{-5}$	$3.486 \cdot 10^{-5}$
3	$3.300 \cdot 10^{-10}$	200	$5.746 \cdot 10^{-5}$	$8.124 \cdot 10^{-5}$	$9.950 \cdot 10^{-5}$	$1.149 \cdot 10^{-4}$	$1.285 \cdot 10^{-4}$	$1.407 \cdot 10^{-4}$
4	$2.025 \cdot 10^{-9}$	300	$1.423 \cdot 10^{-4}$	$2.012 \cdot 10^{-4}$	$2.465 \cdot 10^{-4}$	$2.846 \cdot 10^{-4}$	$3.182 \cdot 10^{-4}$	$3.486 \cdot 10^{-4}$

5	$7.291 \cdot 10^{-9}$	400	$2.700 \cdot 10^{-4}$	$3.818 \cdot 10^{-4}$	$4.677 \cdot 10^{-4}$	$5.400 \cdot 10^{-4}$	$6.038 \cdot 10^{-4}$	$6.614 \cdot 10^{-4}$
6	$1.881 \cdot 10^{-8}$	500	$4.337 \cdot 10^{-4}$	$6.134 \cdot 10^{-4}$	$7.512 \cdot 10^{-4}$	$8.671 \cdot 10^{-4}$	$9.698 \cdot 10^{-4}$	$1.063 \cdot 10^{-3}$
7	$2.783 \cdot 10^{-8}$	550	$5.275 \cdot 10^{-4}$	$7.461 \cdot 10^{-4}$	$9.132 \cdot 10^{-4}$	$1.055 \cdot 10^{-3}$	$1.180 \cdot 10^{-3}$	$1.292 \cdot 10^{-3}$
8	$3.910 \cdot 10^{-8}$	600	$6.253 \cdot 10^{-4}$	$8.843 \cdot 10^{-4}$	$1.084 \cdot 10^{-3}$	$1.251 \cdot 10^{-3}$	$1.398 \cdot 10^{-3}$	$1.532 \cdot 10^{-3}$
9	$4.150 \cdot 10^{-8}$	610	$6.442 \cdot 10^{-4}$	$9.110 \cdot 10^{-4}$	$1.116 \cdot 10^{-3}$	$1.288 \cdot 10^{-3}$	$1.440 \cdot 10^{-3}$	$1.578 \cdot 10^{-3}$
10	$4.411 \cdot 10^{-8}$	620	$6.642 \cdot 10^{-4}$	$9.393 \cdot 10^{-4}$	$1.150 \cdot 10^{-3}$	$1.328 \cdot 10^{-3}$	$1.485 \cdot 10^{-3}$	$1.627 \cdot 10^{-3}$
11	$4.680 \cdot 10^{-8}$	630	$6.841 \cdot 10^{-4}$	$9.675 \cdot 10^{-4}$	$1.185 \cdot 10^{-3}$	$1.368 \cdot 10^{-3}$	$1.530 \cdot 10^{-3}$	$1.676 \cdot 10^{-3}$
12	$5.016 \cdot 10^{-8}$	640	$7.082 \cdot 10^{-4}$	$1.001 \cdot 10^{-3}$	$1.244 \cdot 10^{-3}$	$1.416 \cdot 10^{-3}$	$1.584 \cdot 10^{-3}$	$1.735 \cdot 10^{-3}$
13	$5.280 \cdot 10^{-8}$	650	$7.266 \cdot 10^{-4}$	$1.028 \cdot 10^{-3}$	$1.259 \cdot 10^{-3}$	$1.453 \cdot 10^{-3}$	$1.625 \cdot 10^{-3}$	$1.780 \cdot 10^{-3}$
14	$\mathbf{3.154 \cdot 10^{-7}}$	**660**	$\mathbf{1.776 \cdot 10^{-3}}$	$\mathbf{2.512 \cdot 10^{-3}}$	$\mathbf{3.076 \cdot 10^{-3}}$	$\mathbf{3.552 \cdot 10^{-3}}$	$\mathbf{3.971 \cdot 10^{-3}}$	$\mathbf{4.350 \cdot 10^{-3}}$
15	$3.230 \cdot 10^{-7}$	670	$1.797 \cdot 10^{-3}$	$2.542 \cdot 10^{-3}$	$3.113 \cdot 10^{-3}$	$3.594 \cdot 10^{-3}$	$4.019 \cdot 10^{-3}$	$4.402 \cdot 10^{-3}$
16	$3.344 \cdot 10^{-7}$	680	$1.829 \cdot 10^{-3}$	$2.586 \cdot 10^{-3}$	$3.167 \cdot 10^{-3}$	$3.638 \cdot 10^{-3}$	$4.089 \cdot 10^{-3}$	$4.479 \cdot 10^{-3}$
17	$3.412 \cdot 10^{-7}$	690	$1.847 \cdot 10^{-3}$	$2.612 \cdot 10^{-3}$	$3.200 \cdot 10^{-3}$	$3.695 \cdot 10^{-3}$	$4.130 \cdot 10^{-3}$	$4.524 \cdot 10^{-3}$
18	$3.534 \cdot 10^{-7}$	700	$1.880 \cdot 10^{-3}$	$2.659 \cdot 10^{-3}$	$3.255 \cdot 10^{-3}$	$3.760 \cdot 10^{-3}$	$4.204 \cdot 10^{-3}$	$4.604 \cdot 10^{-3}$
19	$3.572 \cdot 10^{-7}$	710	$1.890 \cdot 10^{-3}$	$2.673 \cdot 10^{-3}$	$3.274 \cdot 10^{-3}$	$3.780 \cdot 10^{-3}$	$4.226 \cdot 10^{-3}$	$4.629 \cdot 10^{-3}$
20	$3.690 \cdot 10^{-7}$	720	$1.921 \cdot 10^{-3}$	$2.717 \cdot 10^{-3}$	$3.327 \cdot 10^{-3}$	$3.842 \cdot 10^{-3}$	$4.295 \cdot 10^{-3}$	$4.705 \cdot 10^{-3}$

The results of the calculation of the diffusion paths of hydrogen as a function of temperature and time during the foaming of aluminium are interpreted graphically, see Fig. 7.7.

Based on the value of hydrogen diffusion coefficient in aluminium at different temperatures, the hydrogen diffusion paths at 60 [s] and 120 [s] were calculated. Based on the calculations, it was determined that the diffusion path of hydrogen in solid aluminium varies from $1.063 \cdot 10^{-6}$ [m] at a diffusion time of 60 [s] in solid aluminium at 20 °C to $1.780 \cdot 10^{-6}$ [m] at 650 °C.

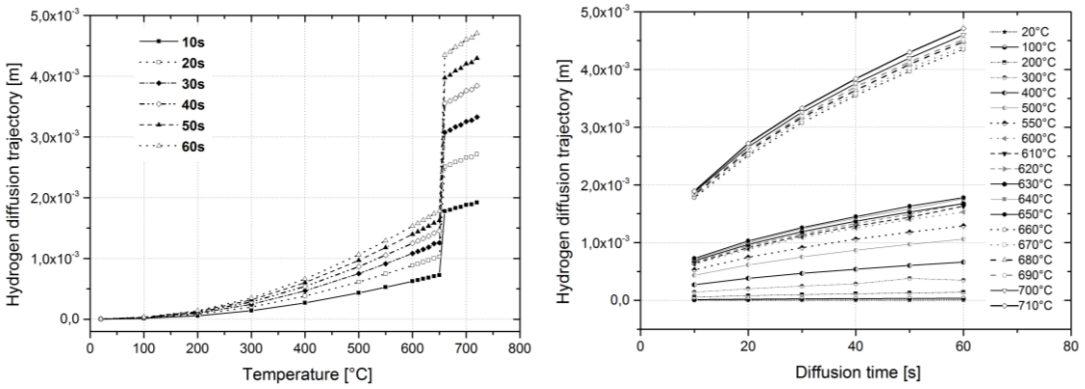

Fig. 7.7 Calculated values of diffusion paths of hydrogen in pure aluminium in the production of cellular systems as a function of temperature (left), as a function of time (right)

In the liquid state of aluminium, the diffusion paths of hydrogen range from $4.350 \cdot 10^{-6}$ [m] at 660 °C to $4.705 \cdot 10^{-6}$ [m] at 720 °C. At 500 °C this hydrogen path is $1.063 \cdot 10^{-3}$ [m], i.e. 1.1 [mm]. The hydrogen diffusion paths at a diffusion time of 120 [s] range from $5.49 \cdot 10^{-6}$ [m] at 20 °C to $2.517 \cdot 10^{-3}$ [m] at 650 °C. At 500 °C this hydrogen path is $1.502 \cdot 10^{-3}$ [m], i.e. 1.5 [mm]. For a temperature of 500 °C, the diffusion paths of hydrogen in aluminium differ by about 40 %. In the liquid state of aluminium, these diffusion paths of hydrogen range from $6.152 \cdot 10^{-3}$ [m] at 660 °C to $6.654 \cdot 10^{-3}$ [m] at 720 °C. In the production of metal cellular systems (especially aluminium foams) by powder metallurgy, the thermal decomposition of the foaming agent is of considerable

importance. These reagents are hydrides. Thermal decomposition of hydrides leads to the formation of hydrogen gas, which causes porosity (cellularity) of the metal system.

This paper focuses on the solubility and diffusion of hydrogen in pure aluminium and is the basis for the theoretical knowledge of aluminium foam production. In powder metallurgy for the production of aluminium foams, hydrogen is a product of the thermal decomposition of the frothers (TiH_2, SrH_2, MgH_2, etc.). Hydrogen is a very important simple diatomic gas. It has different solubility in the solid and liquid states of the respective metal.

The solubility of hydrogen in metals increases with increasing temperature (dissolution is an endothermic process). This means that the solubility of hydrogen in aluminium and aluminium alloys is variable and dependent on temperature, chemical composition and the partial pressure of hydrogen in the surrounding atmosphere. Aluminium and aluminium alloys show a significant difference between the solubility of hydrogen in the solid and liquid states. As reported in [26], in the solid state at 660 °C, the solubility of hydrogen in Al is only 0.036 cm^3 /100 g of aluminium. In molten metal at 660 °C, the solubility is 0.77 cm^3 /100 g of aluminium, that is, about 20 times higher. According to AMBRIZA [3], the solubility of hydrogen at 660 °C is only 0.69 cm^3 /100 g of aluminium. According to OPIE [11], the solubility of hydrogen in liquid aluminium is 0.77 cm^3/100 g of aluminium. According to RANSLEY [10], in the liquid state the solubility of hydrogen in liquid aluminium is 0.695 cm^3/100 g aluminium and according to TALBOT [6], in the liquid state the solubility of hydrogen in liquid aluminium is 0.67 cm^3/100 g aluminium.

The diffusion paths of hydrogen in liquid and solid aluminium were also investigated. It was confirmed that at low temperatures with short diffusion times, the diffusion paths of hydrogen are very small (20 °C, 10 s) is $2.35 \cdot 10^{-6}$ [m]. With increasing temperature and time the diffusion paths increase (660 °C, 10 s) is $1.8 \cdot 10^{-3}$ [m], (720 °C, 60 s) is $4.7 \cdot 10^{-3}$ [m].

When producing a sample of a cellular metal system that is a few centimetres long, the hydrogen transport time requires a relatively long time. This is a rather important observation. Therefore, in powder metallurgy for the production of aluminium foams, it is necessary to ensure the homogeneity of the foaming agent throughout the volume of foamed material produced.

Observed issues have been published:
NOVÁ, I. FRAŇA, K. JELÍNEK, M. Physical metallurgical of diffusion and solubility of hydrogen to determine its optimal foaming properties for the production of aluminium foams. (Ready for publication in 2025).

7.2 Production of porous aluminium materials using sodium chloride and evaluation of their physical and mechanical properties

In the framework of the excellent project OP VVV: Excellent Research. CZ .02.1.01./0.0/0.0/16_019/ 0000843: "Hybrid materials for hierarchical purposes" (research objective 2: Metal-based materials and structures, within research activity

01: *Cellular lightweight metallic structures)* We dealt with the production of porous aluminium materials.

7.2.1 Application of foundry technology and its verification

The design of the technology took into account all the difficulties of melting aluminium alloys, including its high affinity for oxygen. For the preparation of porous aluminium material, a combination of the foundry method and the use of filler material was used. This material was sodium chloride with a particle size of 2 to 3 mm (see Fig. 7.8).

Production of aluminium porous by the foundry method

A special preparation was used to produce a porous aluminium alloy, with a cavity ∅ 60 x 100 mm, see Fig. 7.9, which was filled with a defined amount of "filling material", i.e. sodium chloride. A cylindrical sample of aluminium alloy AlSi12 was also inserted into the jig. The jig was placed in a classic resistance furnace. The furnace was heated to 850 °C.

Fig. 7.8 Sodium chloride used for the production of porous aluminium

Prior to insertion into the furnace, the bolts and nuts on the fixture were treated with a graphite release material so that the fixture could be easily loosened and disassembled after the formation of the porous aluminium system. EN AC - 44300 aluminium alloy (AlSi 12) was used for its production, the elemental content is given in Table 7-14. The chemical composition was identified by Bruker Q4 Tasman spark emission spectrometer.

Table 7-14 Chemical composition of the aluminium alloy used

Chemical composition of alloy EN AC 44300 (AlSi12) [wt. %]										
Si	***Fe***	***Mn***	***Cu***	***Zn***	***Ti***	***V***	***Mg***	***At***	***Pb***	***Al***
11.9	0.45	0.41	0.05	0.11	0.10	0.008	0.001	0.005	0.005	86.96

Fig. 7.9 Preparation and furnace for the production of porous aluminium systems

The experiments carried out at our workplace are among the first ones, therefore non-standard conditions for the production of porous pure aluminium were observed. As can be seen from Fig. 7.10, the method chosen did not produce the expected results.

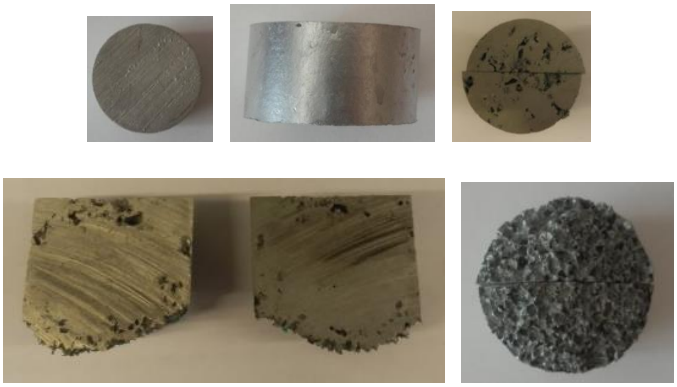

Fig. 7.10 Compact AlSi12 alloy specimen taught for foaming and fabricated porous AlSi12 alloy specimen

This experiment confirmed that the production of aluminium porous materials using sodium chloride is only possible using melt infiltration between sodium chloride grains. In the framework of the project, a different technology was applied.

7.2.2 Production of an aluminium porous system by pressing the melt between the grains sodium chloride

Due to previous production failures, further experiments were based on the use of melt pressure, which was forced into the cavity of a foundry mould filled with sodium chloride. The foundry mould (see Fig. 7.11), is made from EN 1.2343 steel (CSN 19 552), with a cavity of ∅ 60 x 50 mm. It was necessary to develop the necessary methodology to ensure homogenisation of the salt distribution in the mould. The melt was melted in a graphite crucible, and a classic resistance furnace was used for melting. To produce the cellular aluminium system, or porous aluminium alloy AlSi 12, the mould was preheated to 200 °C and filled with a defined amount of 'filler material', i.e. sodium chloride. A measured amount of melt was poured into the mould, and the melt in the mould was compressed; a pressure of 100 MPa was developed.

Fig. 7.11 Equipment for pressing the melt into a mould with sodium chloride

After solidification, the casting was cut transversely and placed in a water bath to dissolve the salt. Next, the weight of the produced porous sample was monitored with a thickness of 10 mm. The macrostructure of the cross-section is shown in Fig. 7.12.

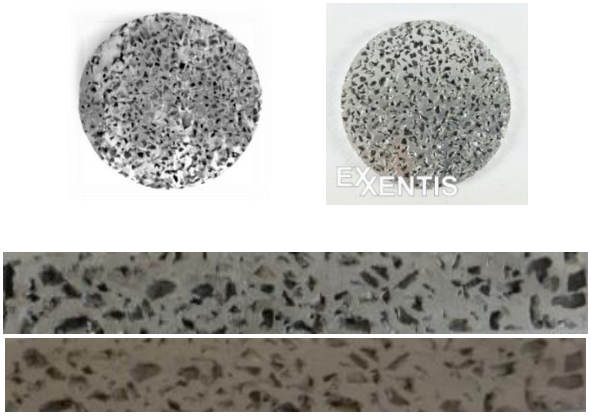

Fig. 7.12 Macrostructure of a porous sample of aluminium alloy AlSi 12, ∅60 x 10 mm, left; aluminium alloy cut by EXXENTIS, right; cross-section through the manufactured sample, bottom

Furthermore, the porosity of the fabricated AlSi12 alloy sample was observed using an Olympus DSX 500 microscope. Fig. 7.13 shows the porosity at different locations in the cross-section of the sample.

Fig. 7.13 Section through a fabricated porous material of aluminium alloy AlSi 12, viewed with an Olympus DSX 500 microscope, magnified 10 times

Fig. 7.14 shows a plan view of the porous aluminium alloy material AlSi12.

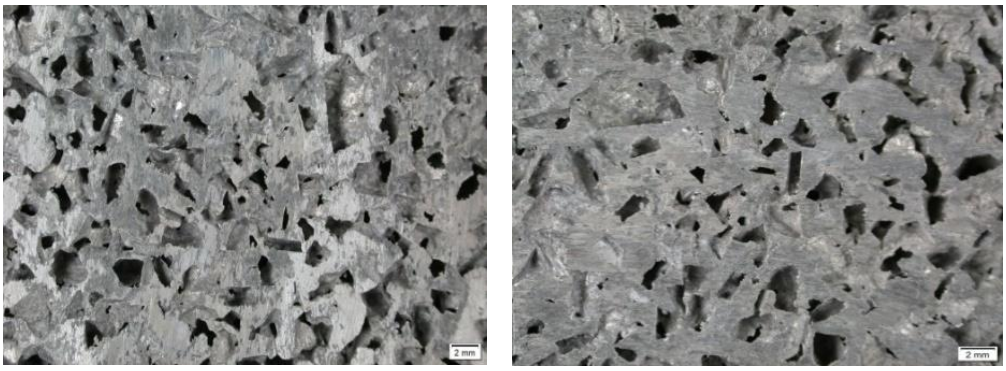

Fig. 7.14 Porosity of aluminium samples cut out from the surface of the sample circle determined with an Olympus DSX 500 microscope

7.2.2.1 Evaluation of the properties of porous aluminium alloy AlSi12

For the evaluation of the properties of the produced porous aluminium alloy system, a methodology for the determination of the relevant physical-material characteristics or the relevant quantities was developed. The evaluation of the fabricated aluminium porous materials concerns the determination of these quantities:

a) Determination of the bulk density of the porous material ($\rho_{Al.P.}$) - is done based on a physical calculation, according to a known relationship

$$\rho_{Al.P.} = \frac{m_{Al.P.}}{V_{Al.P.}}, \tag{7.19}$$

where: $\rho_{Al.P.}$ is a bulk mass of porous material [kg·m^{-3}]; $m_{Al.P.}$ is mass of porous material [kg]; $V_{Al.P.}$ is volume of porous material [m^{-3}].

b) Determination of the relative bulk density of porous material (ρ_R)

$$\rho_R = \frac{\rho_{Al.P.}}{\rho_{B.M.}}, \tag{7.20}$$

where: ρ_r is a relative bulk mass of porous material [1]; $\rho_{Al.P.}$ is a bulk mass of porous material [kg·m^{-3}]; $\rho_{B.M\ (Al)}$ is density of base material without porosity [kg·m^{-3}].

c) Determination of the bulk density of a discretised structure of porous material

$$\rho_{Al.P.} = \frac{\rho_{B.M.} \cdot V_{Al.P.}}{V_{B.M.}}, \tag{7.21}$$

where it reads: $V_{Al.P}$ is the volume of porous material [m^3]; $V_{B.M.}$ is the volume of base material without porosity [m^3].

d) Determination of the porosity of the material (P)

The porosity of a material is the ratio of the difference in density of the base material and the porous material (porous aluminium Al. P.) to the density of the base (non-porous) material (B.M.):

$$\boldsymbol{P} = \left(\frac{\boldsymbol{\rho_{B.M)} - \rho_{Al.P.}}}{\boldsymbol{\rho_{B.M.}}}\right) \cdot \mathbf{100}\ [\%] = \left(\mathbf{1} - \frac{\rho_{Al.P.}}{\rho_{B.M.}}\right) \cdot \mathbf{100}\ [\%] \qquad (7.22)$$

e) Determination of Young's modulus of elasticity in the tension of porous aluminium material AlSi12, according to [1] and [2]

$$E_{M.P.} = k \cdot E_{B.M.} \cdot \left(\frac{\rho_{M.P.}}{\rho_{B.M.}}\right)^{m}, \qquad (7.23)$$

where it says: $E_{Al.P.}$ is Young's modulus of elasticity of the strained material [MPa], $E_{B.M.}$ is Young's modulus of elasticity of the base material [MPa], $\rho_{Al.P.}$ is bulk mass of the porous material [kg·m^{-3}]; $\rho_{B.M.}$ is density of the base material [kg·m^{-3}]; k is constant for calculating the elastic modulus k is (0.1 to 4), m is the constant for calculating the elastic modulus m is 2 [2], m is 1.5 to 1.7 [1].

f) Calculation of the thermal conductivity coefficient of porous material AlSi 12

Based on equation (7.24), calculations were performed.

$$\lambda_{Al.P.} = \lambda_{B.M.} \cdot \left(\frac{\rho_{Al.P.}}{\rho_{B.M.}}\right)^{a}, \qquad (7.24)$$

where: $\lambda_{B.M.}$ is the coefficient of thermal conductivity of the base material AlSi12 ($\lambda_{B.M.}$ = 150 W·m^{-1}·K^{-1}]; a is constant (a = 1.65 to 1.85) [4], a = 2 [3].

Based on equations (7.19) to (7.24), selected values of the properties of the fabricated porous AlSi12 alloy were calculated. These values are shown in Table 7-15.
The production of aluminium porous systems is associated with complexity and considerable difficulty in ensuring the homogeneity of structure. These complications are, to some extent, related to the high affinity of aluminium for oxygen. The methods described in the literature did not prove successful in our experimental conditions. Therefore, a non-standard method of pushing the melt into the moulds was resorted to with the available amounts of NaCl proving to be viable. This method can only be used when the forming press can be applied with a pressure range of at least 100 MPa.

The values found for the porous material AlSi12 are: bulk density $\rho_{Al.P}$ = 1074 [kg·m^{-3}]; relative bulk density$\rho_{REL\ (AlSi12)}$ = 0.40; porosity P (AlSi12) = 60 %, Young's modulus $E_{Al.P.}$ (AlSi12) = 3667 [MPa] and thermal conductivity coefficient $\lambda_{Al.P.\ (AlSi12)}$ = 25 [W·m^{-1}·K^{-1}]. These values are in agreement, which are presented by the manufacturers of porous aluminium [5].

Table 7-15 Observed and calculated values of porous material AlSi12

Calculation of physical values of porous material from AlSi12 alloy	
Features	**Value**
Bulk weight of AlSi12 ∅ 60 x 10 mm (base material) $\rho_{B.M.(AlSi12)}$ [kg·m^{-3}]	2660
Volume AlSi12,∅ 60 x 10 mm (base material) $V_{B.M.(AlSi12)}$ [m^3]	2.82· 10^{-5}
Weight AlSi12,∅ 60 x 10 mm (base material) $mB_{.M.(AlSi12)}$ [kg]	0,075
Volume of porous material AlSi12∅ 60 x 10 mm, $V_{Al.P.(AlSi12)}$ [m^3]	2.89· 10^{-5}
Weight of porous material AlSi 12∅ 60 x 10 mm $mAl_{.P.(AlSi12)}$ [kg]	0.031
Bulk weight of porous material AlSi12∅ 60 x 10 mm, $\rho_{Al.P.(AlSi12)}$ [kg·m^{-3}]	1074
Relative bulk density of AlSi 12 porous material ∅ 60 x 10 mm, $\rho_{REL(AlSi12)}$ [1]	0.40
Porosity of porous material AlSi 12 ∅ 60 x 10 mm, P [%]	60
Young's modulus of *porous material* AlSi12, ∅ 60 x 10 mm, $E_{Al.P.(AlSi12)}$ [MPa]	3667
Thermal conductivity coefficient of AlSi 12, $\lambda_{Al.P.(AlSi12)}$ [W· m^{-1}·K^{-1}]	25

Note: $E_{B.M.(AlSi12)}$ ***- Young's modulus,*** E_{AlSi12} ***= 75 000 [MPa].***

Another option for more viable production of aluminium porous materials is focusing on the use of vacuum and protective argon atmospheres. Again, special equipment is required for this. As can be seen from Fig. 7.12 on the left, our fabricated porous structure made of aluminium material (AlSi12 alloy) is comparable to the aluminium porous material professionally produced by Exxentis.

This issue has been published:
NOVÁ, I. FRAŇA, K. SOBOTKA, J. SOLFRONK, P. KOREČEK, D. and I. NOVÁKOVÁ. Production of Porous Aluminium Using Sodium Chloride. Manufacturing Technology. 2019, Vol. 19, No. 5. pp. 817-822.

7.2.3 Production of porous aluminium material by pressing sodium chloride grains into the aluminium alloy melt when using the new cut mould

This part of the research activity deals with the presentation of the results of long-term research on the production of porous aluminium materials. As it is known, these materials are mainly characterized by lower density and corresponding mechanical properties. Based on the developed methodology, samples of porous aluminium materials were produced. For this purpose, different sizes of sodium chloride particles (with an average size of 2, 4, 6 and 9 mm) were used. The most preferred foundry alloy AlSi12 was used for the production of aluminium porous material. In the experiments, samples of porous aluminium material in the shape of a cone were produced. The cavity of the foundry mould was in the shape of a cone (diameters: D = 0.047 m, d = 0.040 m, height v = 0.040 m). The samples produced were analysed. Their weight and volume were monitored, and their bulk density and relative bulk density were calculated. Their porosity was also determined. Based on empirical relationships, Young's modulus and thermal conductivity values were calculated. The compressive strength of the selected samples was monitored. The Young's modulus value was determined from the measured stress-strain curve. The porosity of the fabricated samples was also evaluated microscopically.

7.2.3.1 Experimental production of aluminium porous materials

In the experiments on the production of aluminium porous materials using sodium chloride, the vacuum system (infiltration of the melt between sodium chloride particles, abroad this method is called SHP Space Holder Particles) was not used.
At our workplace, the Department of Mechanical Engineering Technology, Faculty of Mechanical Engineering Technical University of Liberec, we also deal with the production of porous metal materials within the framework of a grant project.
In this case, an unconventional technology based on pressing sodium chloride into the aluminium alloy melt in a foundry mould was designed and tested for the production of aluminium porous materials. For this purpose, the aluminium alloy (EN AC-44300) AlSi 12 (melting point approx. 577 °C) with a density of 2650 [kg·m^{-3}] was used.

The chemical composition of the AlSi12 alloy used (EN AC-44300) was determined on a Bruker Q4 Tasman emission analyser (see Table 7-16).

Table 7-16 Chemical composition of aluminium alloy AlSi12

Prescribed chemical composition of AlSi 12 alloy										
Si	*Fe*	*Mn*	*Cu*	*Zn*	*Ti*	*V*	*Mg*	*At*	*Pb*	*Al*
EN AC 44300 (AlSi12) [wt%]										
10.5-13.5	0.45-0.90	0.55	0.08	0.15	0.15	-	-	-	-	-
Determined chemical composition of AlSi12 alloy										
12.1	0.43	0.46	0.04	0.12	0.10	0.007	0.001	0.005	0.004	86.96

For the pressing of sodium chloride, a foundry mould made of EN 1.2343 steel was used (see Fig. 7.15, left). The working cavity of the mould is of a simple shape, a conical cone so that samples of the porous system produced can be easily removed from the mould. A schematic of the conical mould cavity can be seen in Fig. 7.15, right.

The mould consists of four parts, as shown in Fig. 7.16. *Cylindrical part:* outer diameter 90 mm, height 110 mm, ∅ punch holes 40 mm, ∅ holes 47 mm for pushing the porous part out of the mould. *Punch:* ∅ 38 x 80 mm. *Dimensioning pad with cone*: ∅ 100 x 45 mm, cone: ∅ D_1 = 51 mm, ∅ D_2 = 46 mm, height 25 mm.
Two samples of sodium chloride No. I and No. II were used for the experiments. Medium-size particles of 3 to 5 mm and 1 to 3 mm were separated from sample No. I. From sample No. II, particles of 5 to 7 mm and 8 to 10 mm were separated (see Fig. 7.17). In terms of physical properties, the melting temperature of sodium chloride is important for our purpose of producing porous material, which is about $T_{melting}$ = 801 [°C]; enthalpy of melting $\Delta H_{melting}$ = 488 000 [J.kg^{-1}].

The chemical analysis of both sodium chloride samples was performed by X-ray fluorescence method, on XRF equipment, Bruker S8 Tiger, Billerica, MA, USA.

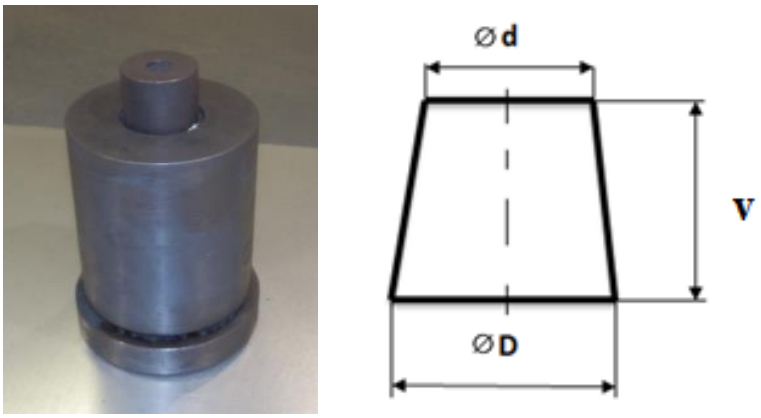

∅D = 47 mm;∅d = 40 mm; h = 40 mm

Fig. 7.15 Diagram of the conical mould cavity

Fig. 7.16 View of the individual parts of the mould

(A: 8 to 10 mm; B: 5 to 7 mm; C: 3 to 5 mm; D: 1 to 3 mm)

Fig. 7.17 Particle sizes of sodium chloride for the production of aluminium porous materials

Table 7-17 Chemical composition of NaCl samples used.

Mark Samples NaCl	Chemical composition of NaCl [wt.%]						
	Cl	At	Ca	S	Si	K	Br
I.	58.8	40.7	0.17	0.13	0.08	0.04	0.08
II.	58.9	40.6	0.21	0.14	-	-	0.15

Thermal analysis of materials (TG / DTA - thermogravimetry / differential thermal analysis) of samples I. and II. NaCl was performed on Discovery Series equipment, TA Instruments, New Castle, DE, USA. Both samples (I. and II.) were heated at a heating

rate of 10°C/min in flowing air. The results of thermal analysis and differential thermal analysis of sample I and II. NaCl are shown in Fig. 7.18.

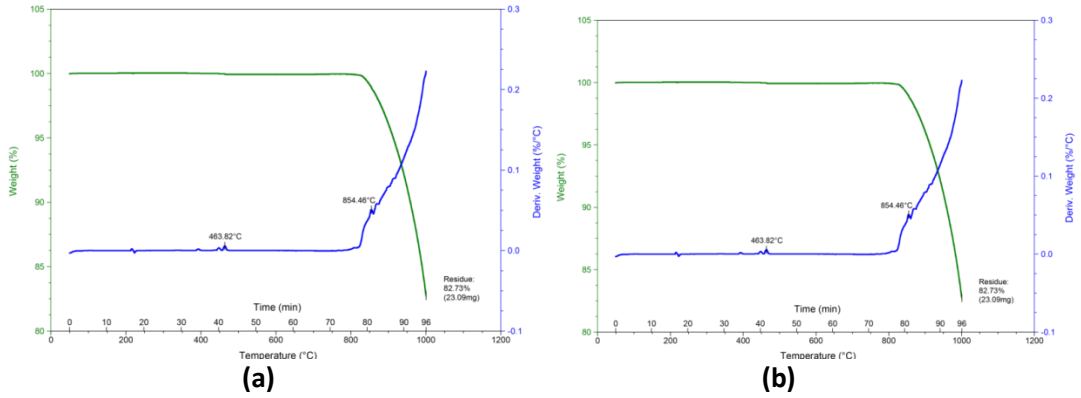

Fig. 7.18 Results of thermal analysis of sodium chloride samples Na Cl I. (a) and NaCl II. (b).

Sample production was carried out in a mould with a conical cone cavity (see Fig. 7.15). The volume of the conical mould cavity was calculated using a well-known formula:

$$V = \frac{1}{12} \cdot \pi \cdot v \cdot (D^2 + D \cdot d + d^2). \tag{7.25}$$

A) Determination of sodium chloride and aluminium for the production of porous aluminium alloy samples, production of porous aluminium material samples

By substituting the values shown in Fig. 7.15, right, into Equation (7.24), a volume (V) equal to 5.689· 10^{-3} [m^3] was calculated. In the production of the aluminium porous material, it was assumed that 50% of the mould volume (*V)* would be filled with aluminium alloy (AlSi12), and 50% of the mould volume will be filled with sodium chloride (NaCl). It can be calculated that the volume for the alloy is:

$$V_{SLIT} = 0.5 \cdot V = 2.987 \cdot 10^{-5}\ [m^3], \tag{7.26}$$

$$V_{NaCl} = 0.5 \cdot V = 2.987 \cdot 10^{-5}\ [m^3]. \tag{7.27}$$

A well-known physical relationship was used to calculate the mass *m of* sodium chloride:

$$m = \rho \cdot V, \tag{7.28}$$

where: m is mass of sodium chloride [kg]; ρ is specific gravity [kg·m^{-3}]; V is volume [m^3].

Table 7-18 shows the calculated sodium chloride volume values and melt volume of AlSi12.

Table 7-18 Calculated sodium chloride volume and melt volume AlSi12

Calculation of the mass of sodium chloride		
Mass of NaCl m_{NaCl} [kg]	**The volume of NaCl V_{NaCl} [m^3]**	**The specific gravity of NaCl ρ_{NaCl} [$kg \cdot m^{-3}$]**
0.065	$2.987 \cdot 10^{-5}$	2165
Calculation of the weight of aluminium alloy AlSi 12		
Weight AlSi12 m_{AlSi12} [kg]	**Volume AlSi12 V_{AlSi12} [m^3]**	**Specific gravity AlSi12 ρ_{AlSi12} [$kg \cdot m^{-3}$]**
0.079	$2.987 \cdot 10^{-5}$	2650

Aluminium alloy AlSi12 was melted in a graphite crucible in a resistance melting furnace "Classic". The superheat temperature of the melt was 720 to 750 °C. The melt was metallurgically treated with refining salts before being cast into the foundry mould, and after the temperature was measured, the melt was poured into the foundry mould. Before pouring the melt into the mould cavity, the mould was preheated to working temperature and treated with a protective graphite spray (Molybkombin UMF T4 spray). A measured amount of AlSi12 alloy melt was then poured into the preheated casting mould, and a measured amount of sodium chloride was poured in, see Fig. 7.19 (left, centre).

The mould with the melt and sodium chloride was then placed under a hydraulic press, and the sodium chloride was forced into the aluminium alloy melt by the press, see Fig. 7.20 (right). It is important for the injection that a pressure of about 100 to 150 MPa can be exerted on the salt in the mould. At the same time, the hydraulic press must be well adjusted for pressing, including the ram parameter setting (see Fig. 7.20, right). Fig. 7.20 (left) shows the hydraulic press and a detailed view of its monitor, which gives an overview of the necessary pressing parameters (see Fig. 7.20, centre).

Fig. 7.21 and Fig. 7.22 show porous materials produced using both types of sodium chloride particles by casting them into the AlSi12 melt. The casting of sodium chloride into the aluminium alloy melt produced a two-phase system. This was followed by boiling the salt out of the samples at about 110 °C for about 60 minutes. The porous aluminium samples thus formed were subjected to analysis. Fig. 7.22 shows the samples that were analysed.

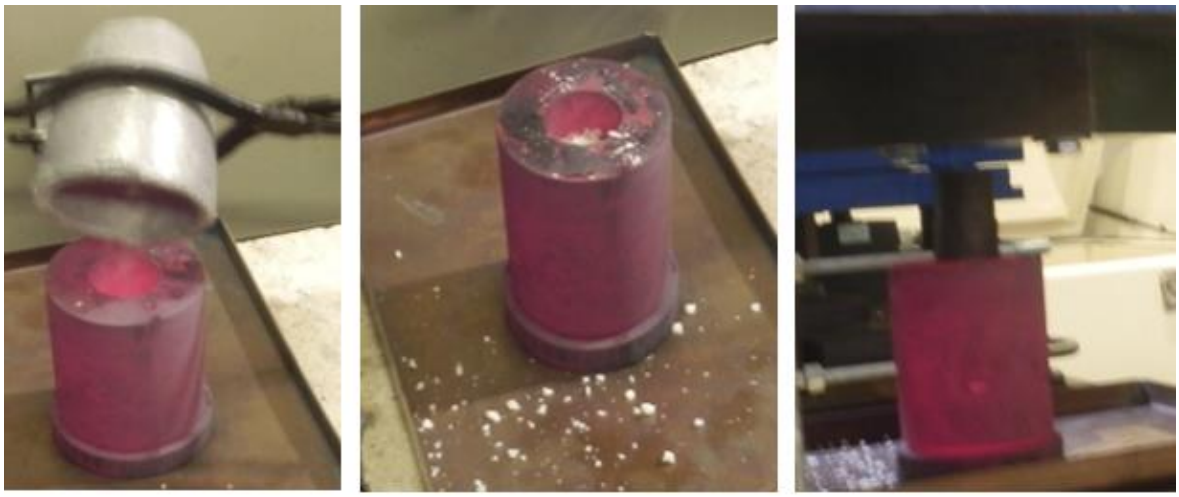

Fig. 7.19 Filling a foundry mould (mould pressing) with melt (left); a foundry mould with melt and salt poured into the mould cavity and a view of the mould and the working parts of the hydraulic press (right)

Fig. 7.20 View of the hydraulic press and its monitor with the setting of the necessary values of the pressing parameters

Fig. 7.21 View of fabricated samples of aluminium porous material, AlSi12 alloy, perspective view (samples 1,2,3,4,5,6, and 7)

Fig. 7.22 Cross-sectional view of aluminium porous material samples used for analysis and organization of selected properties (samples 1,2,3,4,5,6, and 7).

The porous material samples produced were analyzed, and physical values were calculated based on their material characteristics, which are shown in Table 7-19.

Table 7-19 Basic dimensions and bulk weight of fabricated samples of aluminium porous material

Basic dimensions and bulk weight of the produced samples of aluminium porous material							
Mark Sample	**Size particles NaCl [mm]**	***Basic dimensions of the sample***			***Values for density calculation***		
		Average D [mm]	**Average d [mm]**	**Height h [mm]**	**Weight sample m [kg]**	**Volume sample V [m^3]**	**Density of the sample ρ [$kg \cdot m^{-3}$]**
1	9	45.8	41.5	27.00	0.0380	$4.012 \cdot 10^{-5}$	**947**
2	6	45.5	41.0	28.30	0.0410	$4.159 \cdot 10^{-5}$	**985**
3	6	45.0	42.5	24.10	0.0360	$3.622 \cdot 10^{-5}$	**994**
4	6	46.5	42.3	25.00	0.0385	$3.870 \cdot 10^{-5}$	**995**
5	4	46.0	44.1	20.45	0.0354	$3.258 \cdot 10^{-5}$	**1086**
6	4	46.5	44.1	16.20	0.0285	$2.610 \cdot 10^{-5}$	**1092**
7	2	46.3	42.7	22.50	0.0415	$3.500 \cdot 10^{-5}$	**1186**

B) Evaluation of the properties of porous AlSi12 aluminium alloy material produced by pressing NaCl into an aluminium alloy melt

For the evaluation of the properties of the fabricated porous aluminium alloy system, a methodology has been developed which already includes the relationships for the determination of the relevant physical-material characteristics or the relevant quantities. These relations are (7.19) to (7.24). The evaluation of fabricated aluminium porous materials concerns the determination of the density of the porous material ($\rho_{Al.P.}$), the determination of the relative bulk density of the porous material (ρ_{REL}) the determination of the density of the discretised structure of the porous material.
Determination of the porosity of the material (P) - the ratio of the difference in density of the base material and the porous material (porous aluminium - Al. P.), determination

of Young's modulus of elasticity and coefficient of thermal conductivity. The determined values are given in Table 7-20 to Table 7-22.

Table 7-20 Porosity values of AlSi 12 aluminium alloy material produced by NaCl injection into the alloy melt, samples 1,2

Properties of porous samples: 1, 2		
Marking of samples	**1**	**2**
Mean particle size of sodium chloride [mm]	9	6
Density of AlSi 12 alloy sample, (base material); $\rho_{B.M.(AlSi12)}$ [kg·m^{-3}]·	2650	2650
The volume of AlSi 12 alloy samples, (base material); sample 1: ∅ 44 x 27 mm; sample 2: ∅ 43.25 x 28.3 mm; $V_{B.M.(AlSi12)}$ [m^3]	4.103·10^{-5}	4,156·10^{-5}
Weight of AlSi 12 alloy samples; sample 1: ∅ 44 x 27 mm; sample 2: ∅ 43.25 x 28.3 mm; $m_{B.M.(AlSi12)}$ [kg]	0.109	0.110
Volume of porous AlSi12; $V_{P\ (AlSi12)}$ alloy samples [m]^3	4.012·10^{-5}	4.159·10^{-5}
Weight of AlSi 12 porous alloy samples; $m_{P.\ (AlSi12)}$ [kg]	0.0380	0.0410
Bulk weight of porous AlSi12 alloy samples; $\rho_{Al.P.\ (AlSi12)}$ [kg·m^{-3}]	947	985
Relative bulk density (porous/base) AlSi 12 alloy $\rho_{REL\ (AlSi12)}$ [1]	0.36	0.37
Porosity of porous AlSi 12 alloy samples; P [%]	64	63
Young's modulus of elasticity of porous AlSi 12 alloy samples; $E_{P.(AlSi12)}$ [MPa]	956	1013
Thermal conductivity coefficient of porous AlSi 12 alloy samples; $\lambda_{P.(AlSi12)}$ [W·m^{-1}·K^{-1}]	27	29

Note: $E_{B.M.\ (AlSi12\ )}$ ***- Young's modulus;*** E_{AlSi12} ***= 75000 [MPa]; k = 0.1; m = 2; a =1.65***

Table 7-21 Porosity values of AlSi 12 aluminium alloy material produced by NaCl injection into the alloy melt, samples 3,4

Properties of porous samples: 3, 4		
Marking of samples	**3**	**4**
Mean particle size of sodium chloride [mm]	6	6
Density of AlSi 12 alloy sample (base material); $\rho_{B.M.(AlSi12)}$ [kg·m^{-3}]	2650	2650
The volume of AlSi 12 alloy samples, (base material); sample 3: ∅ 43.75 x 24.1 mm; sample 4:∅ 44.4 x 25.1 mm; $V_{B.M.(AlSi12)}$ [m^3]	3.621·10^{-5}	3.884·10^{-5}
Weight of AlSi 12 alloy samples; sample 3: ∅ 43.75 x 24.1mm; sample 4: ∅ 44.4 x 25.1 mm; $m_{B.M.(AlSi12)}$ [kg]	0.0956	0.103
Volume of porous AlSi12; $V_{P\ (AlSi12)}$ alloy samples [m^3]	3.622·10^{-5}	3.870·10^{-5}
Weight of AlSi 12 porous alloy samples; $m_{P.\ (AlSi12)}$ [kg]	0.0360	0.0385
Bulk weight of porous AlSi12 alloy samples; $\rho_{Al.P.\ (AlSi12)}$ [kg·m^{-3}]	994	995
Relative bulk density (porous/base) AlSi 12 alloy $\rho_{REL\ (AlSi12)}$ [1]	0.38	0.38
Porosity of porous AlSi 12 alloy samples; P [%]	62	62
Young's modulus of porous AlSi 12 alloy samples; $E_{P.\ (AlSi12)}$ [MPa]	1055	1060
Thermal conductivity coeff. of porous AlSi 12 samples; $\lambda_{P.(AlSi12)}$ [W·m^{-1}· K^{-1}]	30	30

Note: $E_{B.M.\ (AlSi12\ )}$ ***- Young's modulus;*** E_{AlSi12} ***= 75,000 [MPa]; k = 0.1; m = 2; a =1.65***

The porous structure of the fabricated samples was observed on a scanning electron microscope (Vega 3 Tescan, SEM HV 20.0 kV). On this microscope, the interconnection of open cells in the structure of the individual porous samples made from AlSi12 alloy was observed. Furthermore, EDX analysis was also performed and the chemical composition of the AlSi12 alloy used in the selected sample location was evaluated. In the following section, the structures of the individual samples from the electron microscop excluding sample 2 (which was used for the compression test), are shown in Fig. 7.23, Fig. 7.25, Fig. 7.27, Fig. 7.29, Fig.

7.31 and Fig. 7.33. The EDX analyses of the individual samples are shown in Fig. 7.24, Fig. 7.26, Fig. 7.28, Fig. 7.30, Fig. 7.32 and Fig. 7.34.

Table 7-22 Porosity values of AlSi 12 aluminium alloy material produced by NaCl injection into the alloy melt, samples 5, 6 and 7

Properties of porous samples: 5, 6 and 7			
Marking of samples	**5**	**6**	**7**
Mean particle size of sodium chloride [mm]	4	4	2
Density of AlSi 12 alloy sample (base material); $\rho_{B.M.(AlSi12)}$ [kg·m^{-3}]	2650	2650	2650
Volume of AlSi 12 alloy samples (base material); sample 5: ∅ 45.05 x 22.45 mm; sample 6:∅ 45.30 x 16.20 mm; Sample 7∅ 44.50 x 22.5 mm; $V_{B.M.(AlSi12)}$ [m^3]	3.258·10^{-5}	2.610·10^{-5}	3.500·10^{-5}
Weight of AlSi 12 alloy samples; sample 5:∅ 45.05 x 22.45 mm; sample 6:∅ 45.30 x 16.20.3 mm; sample 7: 44.50 x 22.5 mm; $m_{B.M.(AlSi12)}$ [kg]	0.0863	0.0691	0.0928
Volume of porous AlSi12; $_{VP\ (AlSi12)}$ alloy samples [m^3]	3.258·10^{-5}	2.610·10^{-5}	3.500·10^{-5}
Weight of porous AlSi 12 porous alloy samples; $m_{P.(AlSi12)}$ [kg]	0.0354	0.0285	0.0415
Bulk weight of porous AlSi12 alloy samples; $\rho_{Al.P.\ (AlSi12)}$ [kg·m^{-3}]	1086	1092	1186
Relative bulk density (porous/base) AlSi 12 alloy $\rho_{\ REL\ (AlSi12)}$ [1]	0.41	0.41	0.45
Porosity of porous AlSi 12 alloy samples; P [%]	59	59	55
Young's modulus of porous AlSi 12 alloy samples; $E_{P.\ (AlSi12)}$ [MPa]	1260	1274	1502
Thermal conductivity coefficient of porous AlSi 12 alloy samples; $\lambda_{\ P.(AlSi12)}$ [W·m^{-1}·K^{-1}]	34	35	40

Note: $E_{B.M.\ (AlSi12\ )}$ ***- Young's modulus;*** E_{AlSi12} ***= 75,000 [MPa]; k = 0.1; m = 2; a =1.65***

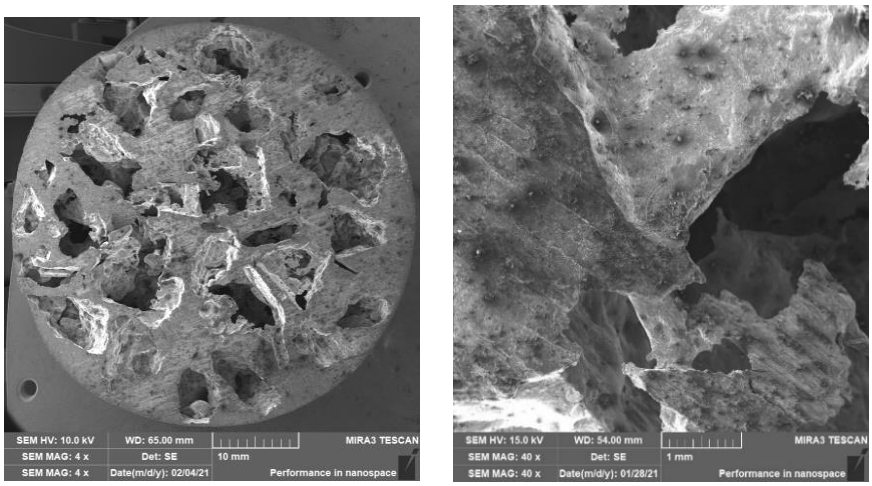

(a) **(b)**

Fig. 7.23 View of the structure of the porous AlSi12 alloy material (a), detail of the material (b); scanning electron microscope (Vega 3 Tescan, SEM HV 20.0 kV), sample 1.

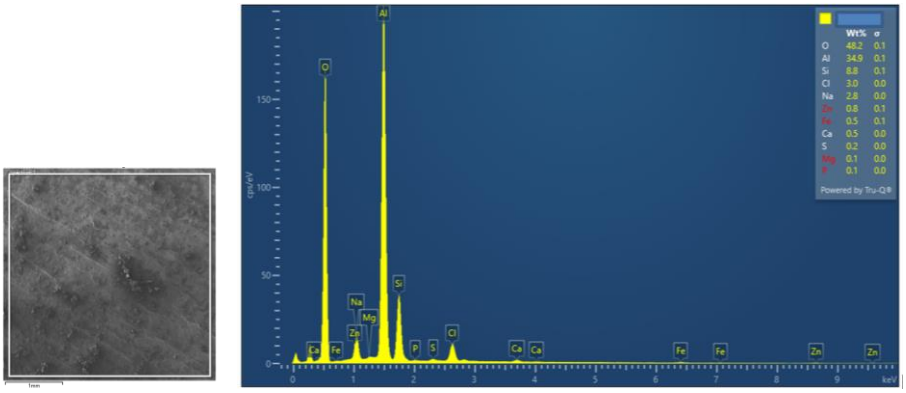

(a) **(b)**

Fig. 7.24 EDX analysis and its evaluation with respect to local chemical composition (a), chemical composition of the AlSi12 alloy used (b); sample 1

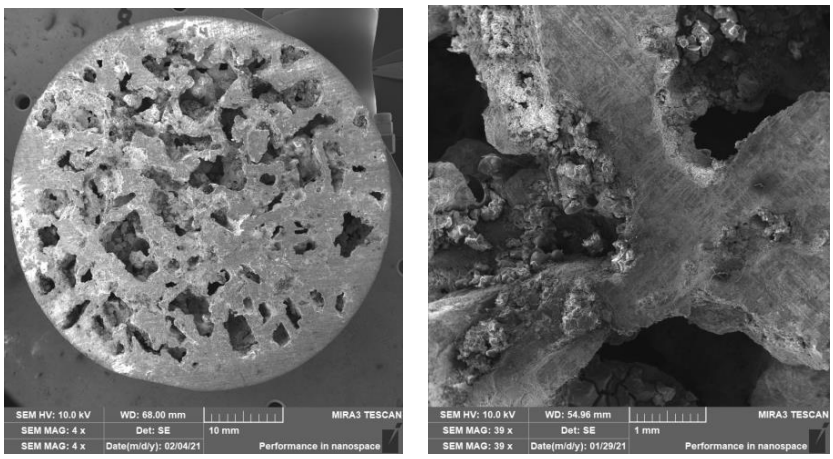

(a) **(b)**

Fig. 7.25 View of the structure of the porous AlSi12 alloy material (a), detail of the material (b); scanning electron microscope (Vega 3 Tescan, SEM HV 20.0 kV), sample 3 .

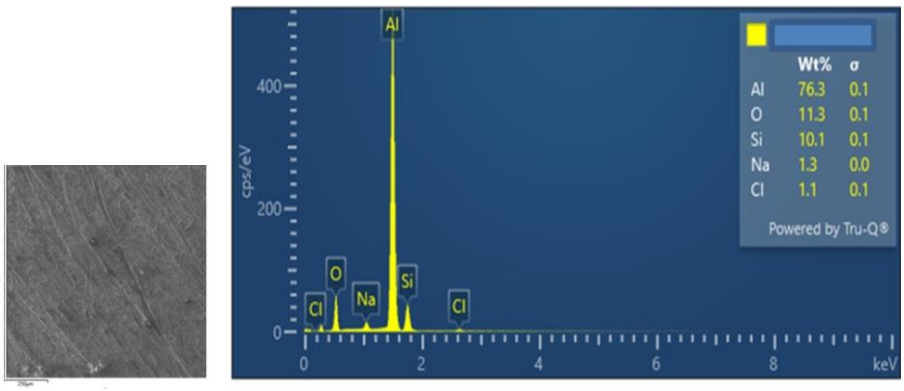

(a) **(b)**

Fig. 7.26 EDX analysis and its evaluation with respect to local chemical composition (a), the chemical composition of the AlSi12 alloy used (b); sample 3

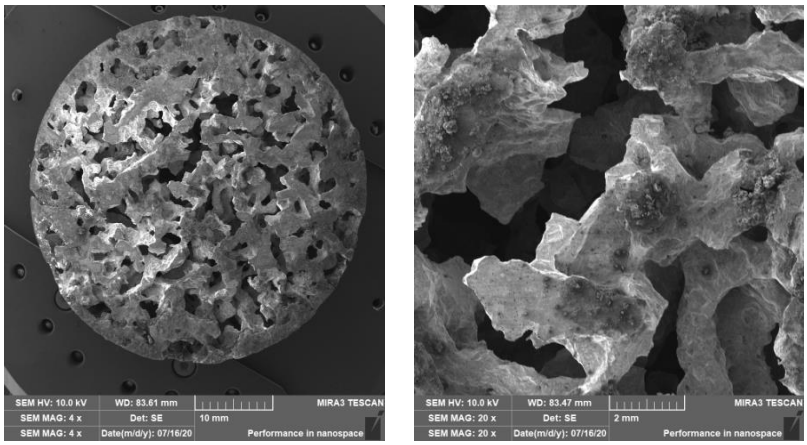

(a) **(b)**

*Fig. 7.27 View of the structure of the porous AlSi12 alloy material (a), detail of the material (*b); scanning electron microscope (Vega 3 Tescan, SEM HV 20.0 kV), *sample 4*

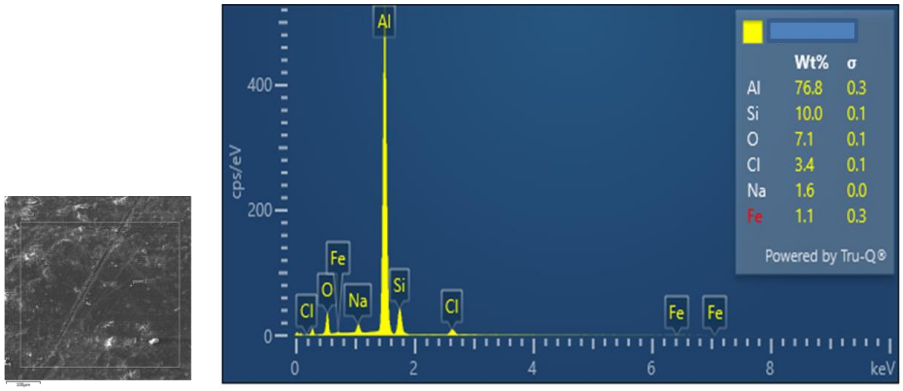

(a) **(b)**

Fig. 7.28 EDX analysis and its evaluation with respect to local chemical composition (a), chemical composition of the AlSi12 alloy used (b); sample 4

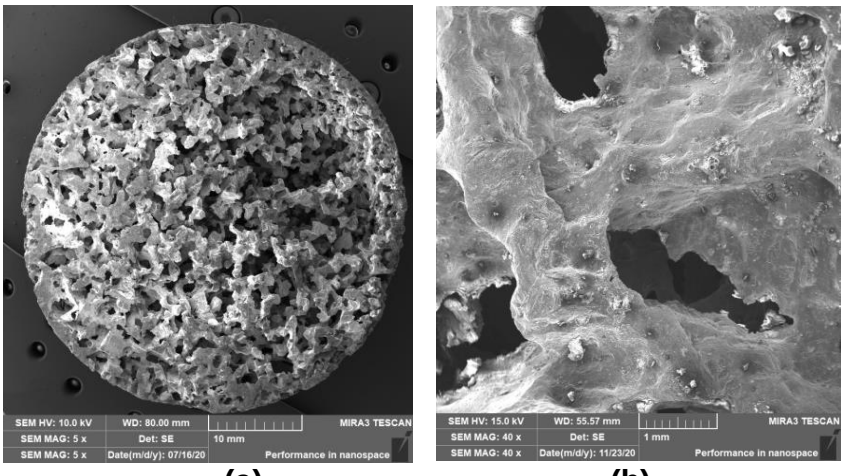

(a) **(b)**

*Fig. 7.29 View of the structure of the porous AlSi12 alloy material (a), detail of the material (*b); *scanning electron microscope (Vega 3 Tescan, SEM HV 20.0 kV), sample 5*

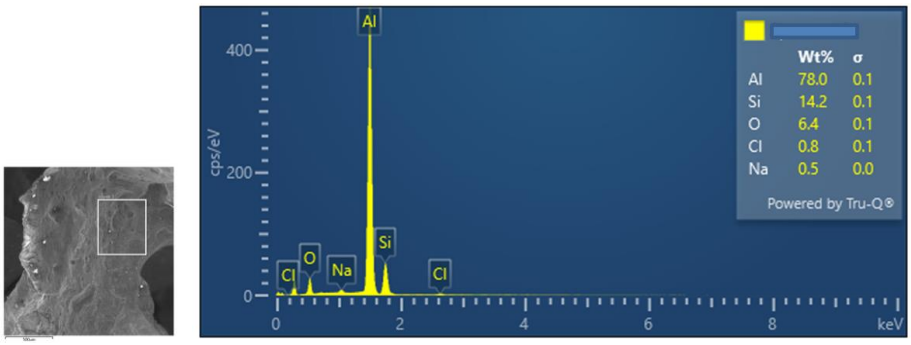

(a) **(b)**

Fig. 7.30 EDX analysis and its evaluation with respect to local chemical composition (a), chemical composition of the AlSi12 alloy used (b); sample 5

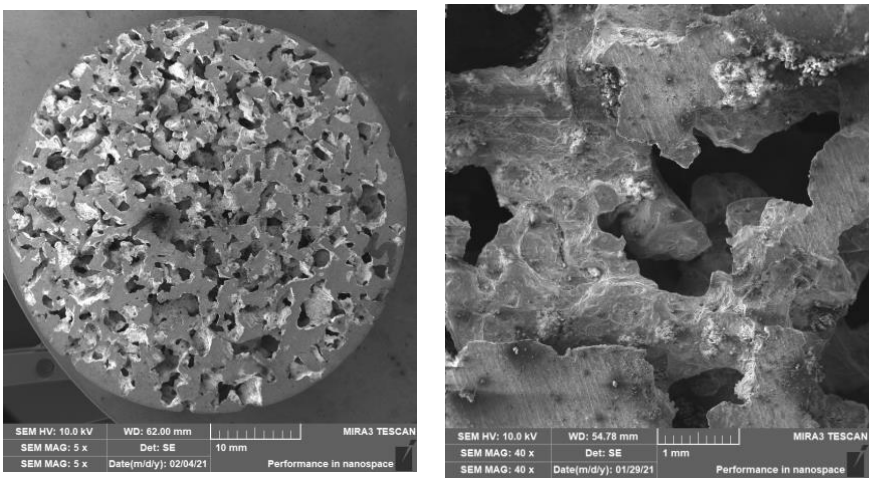

(a) **(b)**

*Fig. 7.31 View of the structure of the porous AlSi12 alloy material (a), detail of the material (*b); *scanning electron microscope (Vega 3 Tescan, SEM HV 20.0 kV), sample 6*

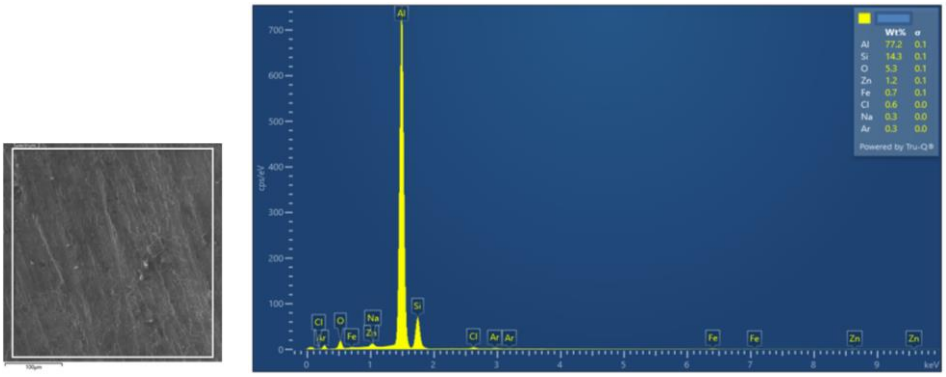

(a) **(b)**

Fig. 7.32 EDX analysis and its evaluation with respect to local chemical composition (a), chemical composition of the AlSi12 alloy used (b); sample 6

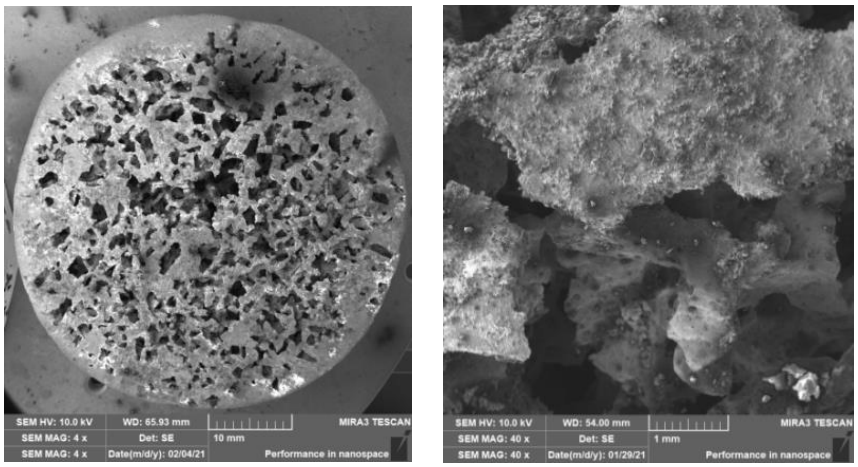

(a) **(b)**

*Fig. 7.33 View of the structure of the porous AlSi12 alloy material (a), detail of the material (*b); *scanning electron microscope (Vega 3 Tescan, SEM HV 20.0 kV), sample No. 7*

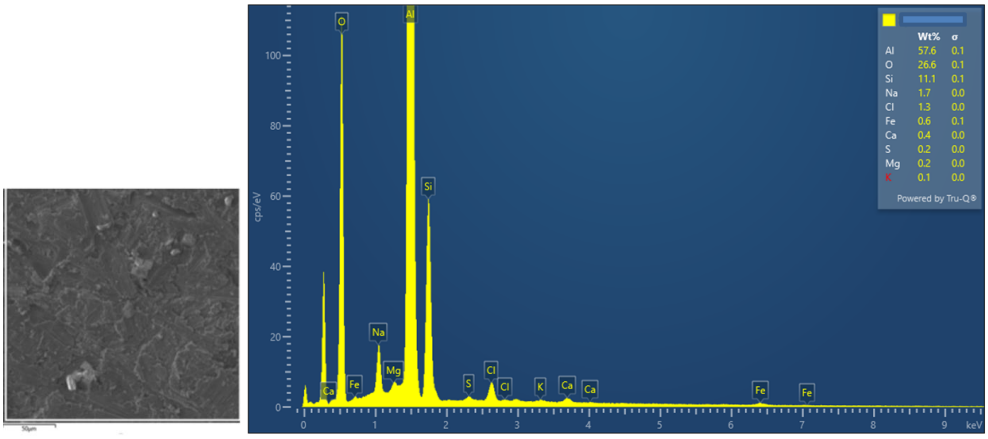

(a) **(b)**

Fig. 7.34 EDX analysis and its evaluation concerning local chemical composition (a), the chemical composition of the AlSi12 alloy used (b); sample 7

The porosity of the fabricated AlSi12 alloy specimens was also monitored using a ZEISS METROTOM 1500 CT industrial computed tomograph (model 1500 from ZEISS, Oberkochen, Germany). The observed structures are shown in Fig. 7.35, Fig. 7.36 and Fig. 7.37. The observed porosity is well related to the particle size of sodium chloride used for their production. At the same time, the interconnectedness of the individual cells can be seen in the above figures.

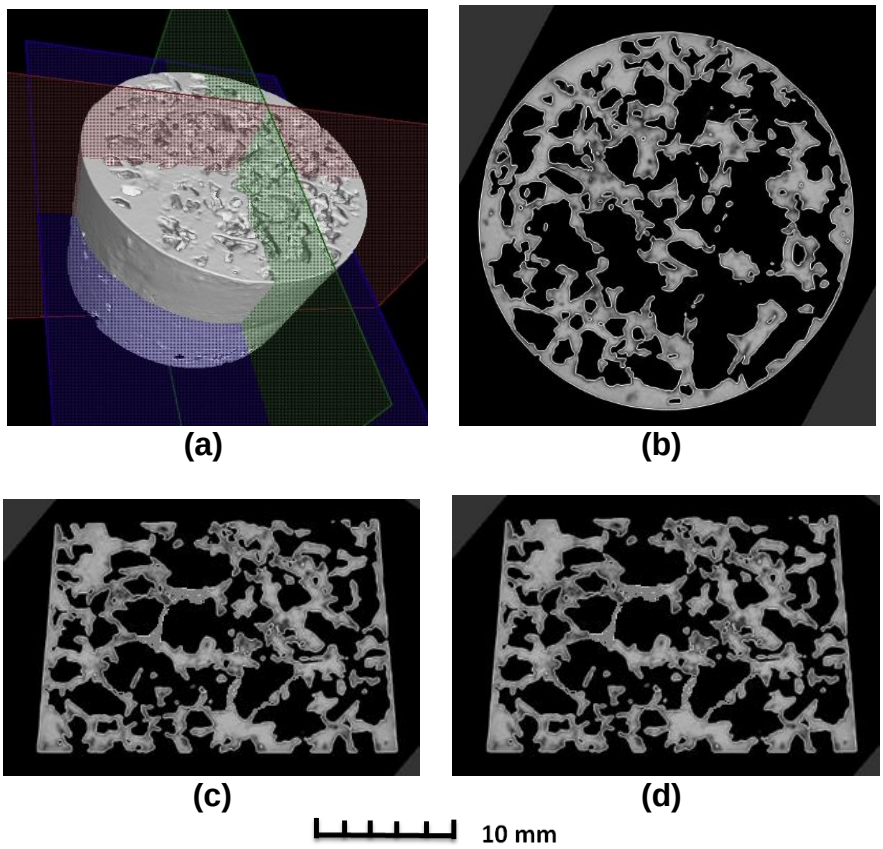

Fig. 7.35 Example of porosity in selected planes of aluminium porous material, AlSi12 sample 4, evaluated on a METROTOM 1500 CT ZEISS industrial computed tomography scanner: planes of porous sample section (a); plane section-purple colour (b); plane section - red colour (c); plane section - green colour (d).

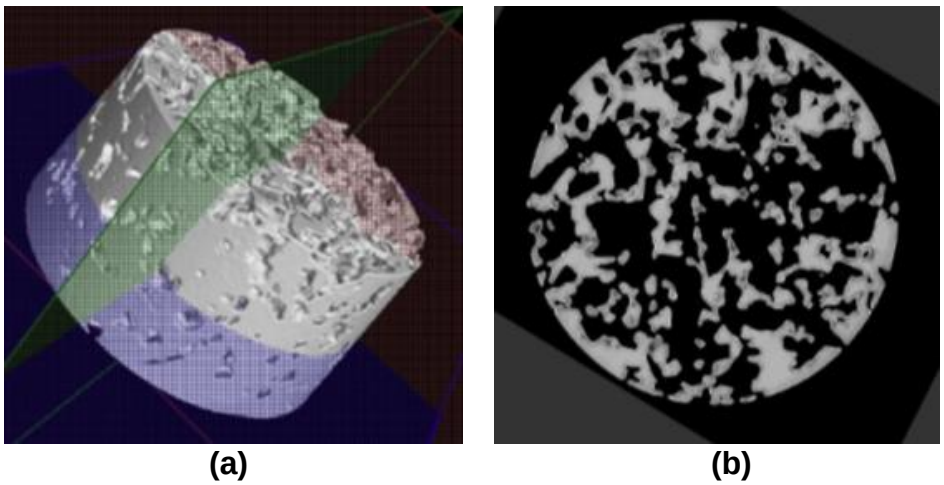

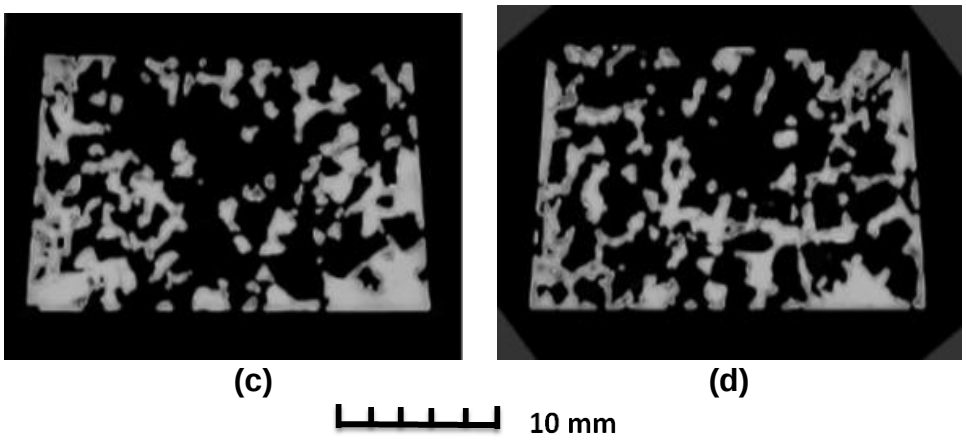

Fig. 7.36 Example of porosity in selected planes of aluminium porous material, AlSi12 specimen 5, evaluated on a METROTOM 1500 CT ZEISS industrial computed tomography scanner: planes of porous specimen section (a); plane section - purple colour (b); plane section - red colour (c); plane section - green colour (d).

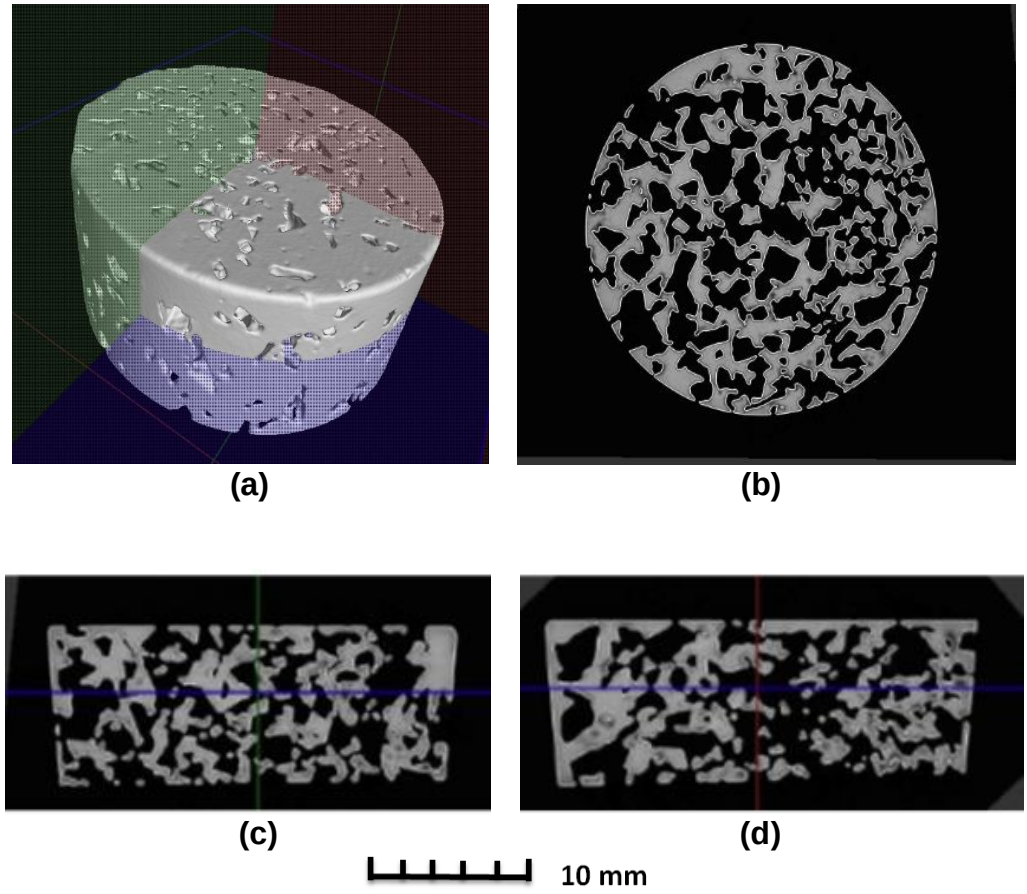

Fig. 7.37 Example of porosity in selected planes of aluminium porous material, AlSi12 sample 6, evaluated on a METROTOM 1500 CT ZEISS industrial computed tomography scanner: planes of porous section (a); plane section-purple colour (b); plane section - red colour (c); plane section - green colour (d).

C) Monitoring of mechanical properties of selected porous aluminium materials from AlSi12 alloy

The compressive strengths of the fabricated specimens were monitored on a TIRA Test blast machine, see Fig. 7.38, this figure also shows two specimens of the aluminium porous material AlSi12 after the compressive test (sodium chloride particle size 5 to 7 mm and 8 to 10 mm.

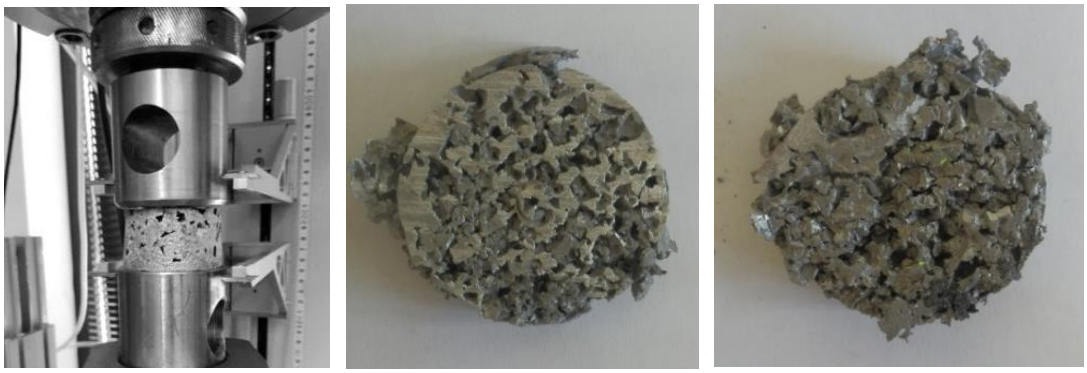

Fig. 7.38 Strength measurements on the TIRA Test machine and samples after the compressive test

The effect of the cavity size on the compressive strength of the material was also investigated in the context of the porosity of the samples. The compressive strength values obtained are shown in Fig. 7.39.

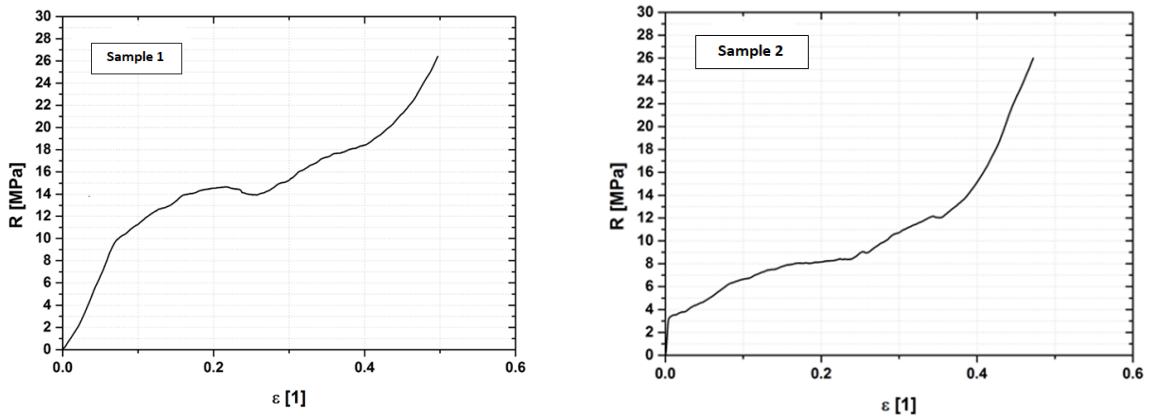

Sample 1 - Young's modulus, $E_{P\,(AlSi\,12)\text{-}1}$ = 160 MPa;
Sample 2 - Young's modulus, $E_{P\,(AlSi\,12)\text{-}2}$ = 1027 MPa;

Fig. 7.39 Compressive strengths of aluminium porous materials made from AlSi12 alloy

Porous aluminium materials are most commonly produced by infiltrating the melt between particles of sodium chloride or other suitable materials. For this purpose, there must be a specially designed melting furnace with an opening at the top, as well as a foundry mould which is designed for the introduction of argon and for connecting the mould to the die. We have developed a methodology for the production of porous aluminium materials by pressing sodium chloride particles into the aluminium alloy

melt, as published in this paper. The results obtained confirmed that for pressing sodium chloride particles into the aluminium alloy melt, a hydraulic press with the ability to generate a pressure of 100 to 150 MPa must be available. At the same time, a metallurgical mould is required, the cavity of which is used for the production of test samples of the produced aluminium materials. This mould must be well heat-prepared and metallurgically treated, including the use of a suitable separating agent (e.g. graphite-based) when producing the samples.

The results obtained from the fabricated samples confirmed that porous aluminium materials with simple geometrical shapes can be produced in this way. In the fabrication process, we focused on the use of 50 % by volume of sodium chloride and 50 % by volume of AlSi 12 aluminium alloy. With the possibility of applying particle sizes of sodium chloride of 8 to 10 mm; 5 to 7 mm; 3 to 5 mm and 1 to 3 mm. At the same time, samples of porous aluminium alloy material were obtained with porosity from 55 to 64 % and density from about 950 $kg \cdot m^{-3}$ to 1190 $kg \cdot m^{-3}$.

Experiments have shown that it is necessary to ensure a homogeneous distribution of sodium chloride particles so that the porosity of the material produced is uniform throughout its volume. The results have shown that the use of large particles (8 to 10 mm) of sodium chloride is not suitable for the production of small-sized samples, because the grains often collapse the walls between the cavities of the material, which also leads to its low Young's modulus value, see sample 1, as confirmed by the calculated value from the stress-strain relationship, which is about 160 MPa. When using sodium chloride particles of 5 to 7 mm in size, see sample 2, the calculated value of Young's modulus from the stress-strain curve is 1027 MPa. The Young's modulus value calculated from equation (7.23) is 1013 MPa. As can be seen from Fig. 7.39 the stress-strain curve of porous aluminium material corresponds to that of mild steel.

The curve consists of three areas. The first area is the steep stress curve. The walls around the cavities are quite solid and contribute to a small deformation. As can be clearly seen in Fig. 7.39, right. In the second region, the stress-strain curve is more gradual and less steep with large deformation. The lower strength of the walls around the cavities already contributes to this deformation.

With increasing tension, the cell walls gradually deform, and the walls collapse and gradually the porous material begins to compact (collect). In the third region, the already compact material is deformed, so the stress rises more steeply until its integrity is broken.

The results of the samples obtained from the experiments have been published:
NOVÁ, I. FRAŇA, K. SOLFRONK, P. and D. KOREČEK. Monitoring the Influence of Sodium Chloride Particle Size on the Physical, Mechanical Properties and Structure of Samples of Porous Aluminium Materials. Manufacturing Technology. 2021, Vol. 21, No. 1. pp. 109-116.
NOVÁ, I. FRAŇA, K. and T. LIPINSKI. Monitoring of the Interaction of Aluminium Alloy and Sodium Chloride as the basis for Ecological Production of Expanded Aluminium. Physic of Metal and Metallography, 2021. Vol. 122, No 13, pp. 1288-1300. Pleiades Publishing, Ldi., 2021. ISSN 0031-918X.

NOVÁ, I. FRAŇA, K. SOLFRONK, P. SOBOTKA, J. KOREČEK, D. and M. ŠVEC. Characteristic of Porous Aluminium Materials Produced by Pressing Sodium Chloride into Their Melts. Materials. 2021, 14, 4809, https./doi.org./10.3390/ma14174809.
NOVÁ, I. JELÍNEK, M. SOLFRONK, P. and D. KOREČEK. Production of Non-compacted, Lightweight Zinc-Tin Alloy Materials for Possible Storage of Liquid Hydrogen. Manufacturing Technology. 2024, Vol. 24, Iss. 1. ISBN 2787-9402 (online).

7.3 Implementation of a translational magnetic field for the production of aluminium cellular materials

As part of the "HYHI" project, a specific plant for the production of cellular aluminium materials or metal foams was designed (see Fig. 7.40). A metal foam is a specific material whose base is a metal (usually aluminium or an aluminium alloy) and whose structure is lightened by air bubbles. Despite this relatively high porosity, it retains the mechanical properties of the base metal and achieves a high strength-to-weight ratio; at the same time, it has good thermal insulation properties, the ability to absorb sound and shock, and to shield certain types of ionising radiation (X-rays, gamma rays and neutron radiation). The use of this material makes it possible to reduce the weight of various components without compromising strength and durability and entire structures. This makes metallic foam very useful in several different fields - construction (e.g. as an insulating building material), transport (reduction of the weight of vehicles, especially vessels), military industry (production of lightweight yet effective armour), healthcare (production of lightweight prostheses), aerospace, etc.

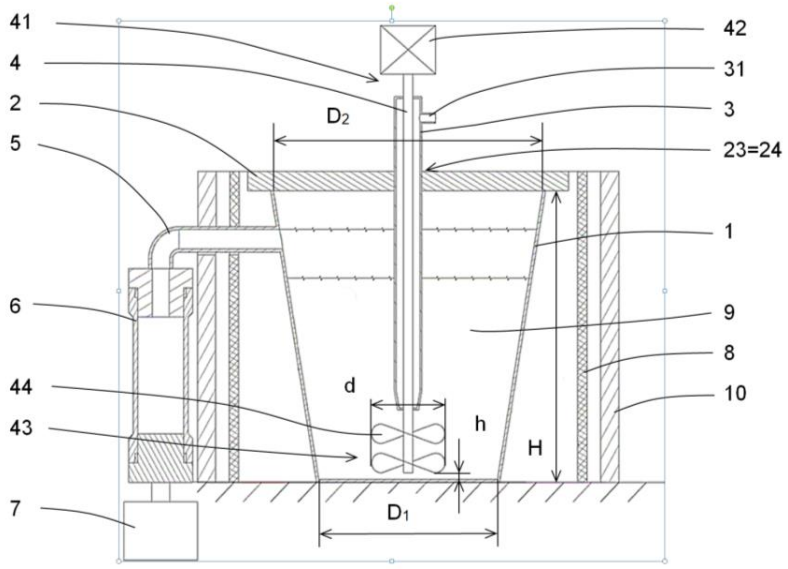

Fig. 7.40 Schematic diagram of the equipment for the production of aluminium foam by direct melt foaming from an external source

The device for producing metal foam, see Fig. 7.40, according to the invention comprises a foaming vessel **1,** which is closed by a lid **2.** Filling vessel 1 and all its components are made of a suitable refractory material, such as steel 1.4841

(AISI314, CSN 17 252), steel 1.4845 (AISI 310, CSN 17 252), quart, etc. A passage 23 is formed in the lid **2 of** the filling vessel 1 for a pressure gas supply tube 3 provided outside the filling vessel **1** with a pressure gas inlet **31** for connecting an unshown pressure gas source, and a passage 24 for the shaft **4 of** the agitator **41** which is connected to the actuator **42** arranged outside the filling vessel **1**. In the variant embodiment shown in Fig. 1, the agitator shaft **4 of the** agitator **41** is housed for part of its length in the pressure gas inlet tube **3**, so only one passage **23=24** is formed in the lid **2** of the filling vessel **1**.

In a preferred embodiment, the agitator **41** has two superimposed impellers **43,** each comprising four evenly arranged impellers **44** formed of heat-resistant steel. In the most preferred embodiment, these impellers **44** incline relative to the longitudinal axis of the agitator shaft **41 of** 30 to 45°, and the agitator **41** is arranged in the filling vessel **1** such that the height h of the lower edge of the impellers **44** of its lower impeller **43** above the bottom of the filling vessel **1** is equal to 1/3 to 3/4 of the diameter d of these impellers **44**.

In other embodiments, however, it is possible to use an agitator 41 of any other design or type – for example, the agitator **41** may comprise a different arrangement and/or a different number of impellers **43** and/or blades **44**, or it may comprise so-called turbine blades - i.e. blades whose surface is arranged parallel or nearly parallel to the longitudinal axis of the shaft of the agitator **41,** etc.

Around the periphery of tension vessel **1,** preferably on the outer side of thermal insulation **8,** electromagnetic coil **10** is arranged and provided with a non-displayed means for connection to a non-displayed source of electric current. This electromagnetic coil **10** is preferably arranged along the entire height of the straining vessel **1.** Electromagnetic coil **10** is designed to generate a shifting magnetic field with a sinusoidal waveform.

7.3.1 Translational magnetic field

A translational magnetic field will be implemented in the above device. The magnetic field acts on an electrically conductive melt and induces a current j in it. This force that arises in the melt due to the magnetic field is called the Lorentz force and is usually denoted by f_L. This force causes an imbalance in the melt. As a consequence, a pressure difference (pressure gradient) is created in the melt, which furthermore, according to the shape of the vessel (height H and radius R), leads to a movement of the melt. This movement of the melt in the vessel will influence the behaviour of the bubble in the melt. Forces are exerted on the gas bubble:

c) lift force $F_{VZ;}$
d) resistive force F_{OD}
e) Lorentz melt force f_L

According to the nature of the action of the translational magnetic field:

Vector: $F_{VZ} - F_{OD} - f_L = 0,$ (7.29)

$F_{VZ} + f_L - F_{OD} = 0.$ (7.30)

The translational magnetic field in a cylindrical vessel (of height H and radius R) can act either upwards at the vessel wall or downwards in the central part of the filling vessel. Then the Lorentz force on the bubble acts downward (see Fig. 7.41, left). Alternatively, the translational field may act downwards at the vessel wall and upwards in the central part of the frothing vessel (see Fig. 7.41, right).

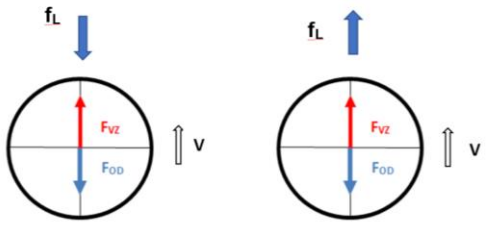

Fig. 7.41 Diagram of the buoyancy, drag and Lorentz forces on a bubble of a gas in a melt

The buoyancy force is calculated:

$$F_{VZ} = V_B \cdot \rho_K \cdot g, \tag{7.31}$$

The resistance force is calculated:

$$F_{OD} = 4 \cdot \pi \cdot R \cdot \eta \cdot v, \tag{7.32}$$

where: R is the radius of the gas bubble [m]; η is dynamic viscosity [Pa·s; $kg \cdot s^{-1} \cdot m^{-1}$]; v is velocity of the gas bubble [$m \cdot s^{-1}$]; V_B is volume of the air bubble [m^3], assuming the air bubble is spherical then $V_B = 4/3 \cdot \pi \cdot R^3$; ρ_K is the density of the melt to be gassed [$kg \cdot m^{-3}$]; g is the gravitational acceleration [$m \cdot s^{-2}$]; ν is the kinematic viscosity of the melt [$m^2 \cdot s^{-1}$],$\nu = \eta/\rho$.

The Lorentz force is calculated:

$$f_L = \frac{1}{8} \cdot B_0^2 \, \sigma \cdot \omega \cdot a_m \cdot R^2 \cdot e_Z, \tag{7.33}$$

where: σ is the specific electrical conductivity coefficient of the melt [$m \cdot \Omega^{-1}$], [$S \cdot m^{-1}$]; ω is the angular frequency [s^{-1}],$\omega = 2 \cdot \pi \cdot f$, f = 50; B_0 is the magnetic field induction (excluding the effect of fluctuations) [T], [$kg \cdot A^{-1} \cdot s^{-2}$]; a_m is wave number of the translational magnetic field [m^{-1}], $a_m \approx 1$, R is radius of the vessel where the translational magnetic field acts [m]; e_z is the unit vector of cylindrical coordinates.

Derivation of air bubble escape velocity in a melt under conditions of

A) **$F_{VZ} - F_{OD} = 0$** (no translational magnetic field);

$$V_B \cdot \rho_K \cdot g = 4 \cdot \pi \cdot R \cdot \eta \cdot v, \tag{7.34}$$

$$v = \frac{1}{3} \cdot \frac{R^2 \cdot g}{\nu} \qquad (7.35)$$

B) A translational magnetic field acts on the bubble in addition to the buoyancy and drag forces on the bubble:

$F_{VZ} + F_{OD} = 0$ (a translational magnetic field acts on the melt, a velocity *u* is established in the melt which acts against the outflow velocity *v*).

This is the case when the translational magnetic field causes the melt to move upwards against the wall of the frothing vessel. This movement contributes to a positive effect on the development of the gas bubble during foaming. Fig. 7.30 shows a diagram of the velocities acting on the gas bubble in the melt when a translational magnetic field is applied.

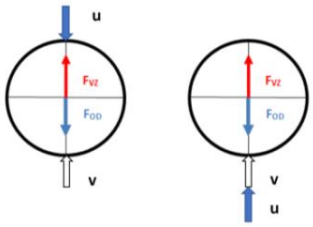

Fig. 7.42 Diagram of the velocities acting on a gas bubble in a melt

For the technical application of the translational magnetic field, the value of the criterion number F of the translational magnetic field is decisive.
For small values of the criterion number F of the translational magnetic field ($F = 1 \cdot 10^2$ to $5 \cdot 10^2$), the magnetically generated melt flow in the kelin is axisymmetric and no oscillations in the melt velocity field occur. This fact can be advantageously used in melt foaming (in a cylindrical vessel of height H and radius R) to achieve good homogenization of the ceramic particles necessary to increase the melt viscosity. At the same time, the velocity field thus created also influences and positively generates and refines the size of the gas bubbles as they exit to the melt surface and also homogenises the melt temperature.

The melt flow velocity depends on the intensity of the magnetic induction of the translational magnetic field, or the criterion number *F* of the translational magnetic field:

$$\boldsymbol{F = \frac{\sigma \cdot \omega \cdot B_0^2 \cdot a_m \cdot R^5}{4 \cdot \rho \cdot \nu^2}}, \qquad (7.36)$$

where: σ is the specific electrical conductivity coefficient of the melt [$m \cdot \Omega^{-1}$], [$S \cdot m^{-1}$]; ω is the angular frequency [s^{-1}], $\omega = 2 \cdot \pi \cdot f$, $f = 50$; B_0 is the magnetic field induction (excluding the effect of fluctuations) [T], [$kg \cdot A^{-1} \cdot s^{-2}$]; a_m is the wave number of the translational magnetic field [m^{-1}], $a_m \approx 1$, R is the radius of the vessel where the translational magnetic field acts [m]; ρ is the density of the melt in which the

translational magnetic field acts [kg·m^{-3}]; ν is the kinetic viscosity of the melt in which the translational magnetic field acts [m^2·s^{-1}], ν =η /ρ.

At the same time, the value of the translational magnetic field criterion number F is important for the derivation of the translational magnetic field.

A low value of the magnetic field criterion number F = 1·10^2 to 5·10^2 is required for an intense melt velocity in the middle of the vessel (height H and radius R). Conversely, a higher value of the F-number causes intense melt motion only in the lower part of the vessel. A translational magnetic field with a magnetic induction value of max. 6 mT was designed for the device in Fig. 7.40. The calculation of the criterion number F can be done based on equation (7.36).

$$\boldsymbol{F} = \frac{4 \cdot 10^6 \cdot 2 \cdot \pi \cdot 50 \cdot 0.006^2 \cdot 1 \cdot 0{,}03^5}{4 \cdot 2380 \cdot (5.65 \cdot 10^{-7})^2} = 361802$$

The calculated value of the criterion number, F = 361802, is too high. It can be influenced by a higher viscosity value due to the incorporation of ceramic particles in the melt, which better conditions the formation of aluminium foam. The kinetic viscosity value can be calculated:

$$\boldsymbol{\nu^2} = \frac{4 \cdot 10^6 \cdot 2 \cdot \pi \cdot 50 \cdot 0{,}006^2 \cdot 1 \cdot 0.03^5}{4 \cdot 2380 \cdot 1 \cdot 10^2} = 1.15 \cdot 10^{-9}$$

$\nu = \sqrt{1.15 \cdot 10^{-9}} = 3.39 \cdot 10^{-5}\ [m^2 \cdot s^{-1}]$.

As is clear from the calculation, the kinetic viscosity of the melt should be $3{,}39 \cdot 10^{-5}\ [m^2 \cdot s^{-1}]$. Fig. 7.43 shows the simulated translational magnetic field velocities, where the criterion number F = 1·10^2.

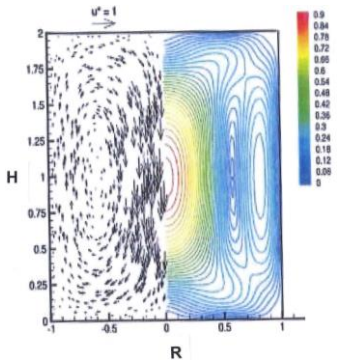

Fig. 7.43 Simulated translational magnetic field *velocities*, Criterion number F = 1·10^2

7.4 Numerical simulation calculation of aluminium melt gassing with air

Within the framework of the grant project "HYHI", it proceeded to perform numerical simulation calculation of the conditions of gassing of aluminium melt, respectively to

predict the gas deposition in a two-phase mixture, i.e. aluminium melt and particles increasing the viscosity of aluminium melt. The effect of gas deposition was studied concerning different viscosities of the liquids. It was found that the shape and volume fraction of the bubbles depends on the magnitude of the liquid or aluminium melt viscosity. Fig. 7.44 shows the structure of the cellular material produced by melt foaming from an external gas source. The numerical simulation calculations performed were based on the problem of the two-phase, laminar, non-stationary flow of a mixture of aluminium melt and gas. The facts about the change of liquid viscosity due to small particles in suspension were investigated.

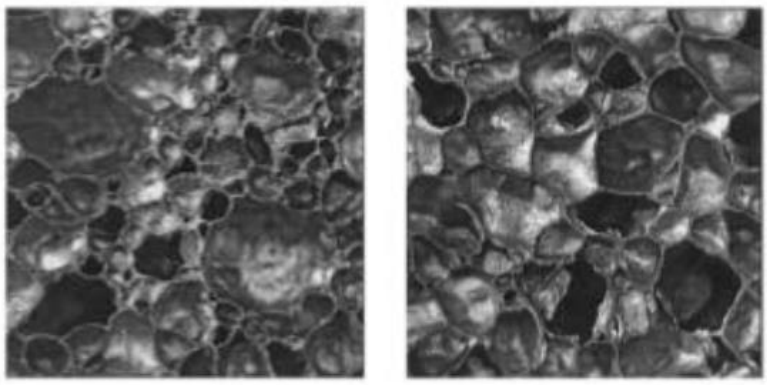

Fig. 7.44 Example of a foamed aluminium structure based on direct pouring with air from an external gas source [4]

The numerical study was focused on the prediction of bubble formation at different melt viscosity values. The two-phase gas-liquid or gas-melt flow inside a double inlet cyclone for gas separation was numerically simulated using a discrete phase model, e.g., in [1]. The numerical approach was verified with experimental data and the results agreed well when compared with each other. A second example, which presents the calculation of a dispersed water wave as a compressible mixture of air and water with homogeneous material properties, was investigated in [3].

The corresponding mathematical equations were based on a multiphase flow model based on the laws of conservation of mass, momentum and energy and the equation of advection of the volume fraction of the gas phase. A similar model (based on equations) was applied in this simulation calculation. The two-phase problem with porous materials investigated numerically is presented in reference [2].

The solution of the numerical simulation calculation was based on the solution of three areas:

Area I. presents the problem under investigation and describes the computational area and the techniques used for numerical simulation. The basic theoretical background is presented on bubble formation.

Area II. contains the simulation results and demonstrates the feasibility of the computational solution used for the two-phase mixture simulation problem.

Area III. discusses the main conclusions about the two-phase flow result discovered through numerical simulations.

7.4.1 Characteristics of numerical simulation calculation

a) Material properties and simulation calculation area

The problem under study is characterized by a multiphase flow, which is a liquid-gas mixture system. The liquid phase is represented by an aluminium melt and is defined as a perfect fluid in the numerical simulation. Since the temperature change in the aluminium melt is relatively small, the bulk mass remains mostly constant. The second phase is air, which is considered an ideal gas in the simulation.

In the case of different material properties, a multiphase approach was used. Each component n of the mixture is considered a compressible and non-isothermal immiscible liquid. The actual material properties of the aluminium and air used are given in Table 7-23.

Table 7-23 Physical properties of aluminium and air for foaming simulation calculation

Properties of pure aluminium melt	
Dynamic viscosity	0.014 Pa·s
Density	2380 $kg \cdot m^{-3}$
Molar mass	26.98 $g \cdot mol^{-1}$
Prandtl's number	0.07
Air properties	
Dynamic viscosity	$1.84 \cdot 10^{-5}$ Pa·s
Molar mass	28.9 $g \cdot mol^{-1}$
Heat capacity at constant pressure	1007 $J \cdot kg^{-1} \cdot K^{-1}$
Prandtl's number	0.7
Surface tension of aluminium when exposed to air (temperature dependence)	0.85 $N \cdot m^{-1}$

The computational domain, see Fig. 7.46, is in the form of a cube-shaped container. The general dimensions are L x B x H, with a size of 0.4 m x 0.4 m x 1 m and a spacing of 100 x 100 x 120, resulting in 1.28 million hexahedral cells. Boundary conditions are applied to all sidewalls. A type of input/output boundary condition is prescribed for the top of the enclosure, which has zero values for all phases except the air phase, for which the input/output velocity magnitudes are calculated. A parabolic inlet velocity profile is defined for the lower part of the air phase. The peak flow velocity is constant 0.084 $m \cdot s^{-1}$ or varies (if the bubble formation intensity is the objective of the investigation).

b) Mathematical equations

A volumetric approach (VOF) [1], based on interface application methods, was used to address the phase-interface interaction. In general, the material properties of a homogeneous mixture is described by a volume fraction function for phase 1, which is defined as :

$$\alpha_1 = \frac{\Omega_1}{\Omega_1+\Omega_2}, \tag{7.37}$$

where denotes: Ω_1 is phase 1 volume; Ω_2 is phase 2 volume.

Accordingly, the parameter for the second phase can be defined as $\alpha_2 = 1 - \alpha_1$. A simplified two-phase approach can be used to implement the mathematical model instead of the multiphase model. The volume fraction α_1 represents the liquid or melt of aluminium. The volume fraction α_2 represents a gas (in this case, air).
The mathematical model used for the flow of a two-phase mixture consists of the laws of conservation of mass, momentum and energy. At the same time, the law of conservation of mass for each component separately must also be included. Fig. 7.45 shows a schematic of the computational domain with boundaries. The cube represents a container where a melt of aluminium is injected with gas. Gas bubbles are formed at the bottom of the melt and rise to the surface of the aluminium melt. This simulation calculation is aimed at observing the different melt and gas contexts for the formation of bubbles in the melt.

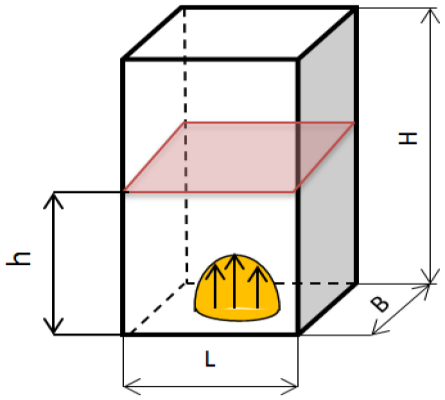

Fig. 7.45 Sketch of the calculation area with boundaries

For the simulation calculation, it was necessary to consider, but also include in the simulation calculation, the effects of bubble gravity as well as wave problems in the liquid phase. The basic "conservative" part of the flow model can be expressed in the following form:

$$\frac{\partial \bar{U}}{\partial t} = \frac{\partial \overline{F_1}}{\partial x} + \frac{\partial \overline{F_2}}{\partial x} + \frac{\partial \overline{F_3}}{\partial x} = \bar{G}, \tag{7.38}$$

where denotes: U is the vector of conservative variables; F is flow function; G is source terms. The source terms are defined as:

$$\bar{U} = \begin{bmatrix} \alpha_1\rho \\ \alpha_2\rho \\ \rho u \\ \rho v \\ \rho w \\ \rho e \end{bmatrix}, \quad \bar{F_1} = \begin{bmatrix} \alpha_1\rho u \\ \alpha_2\rho u \\ \rho u^2 + p - \tau_{xx} \\ \rho vu - \tau_{xy} \\ \rho wu - \tau_{xz} \\ \rho hu - u\tau_{xx} - v\tau_{xy} - \tau_{xz} + q_x \end{bmatrix}, \tag{7.39}$$

$$\overline{F_2} = \begin{bmatrix} \alpha_1\rho v \\ \alpha_2\rho v \\ \rho uv - \tau_{yx} \\ \rho v^2 + p - \tau_{yy} \\ \rho wv - \tau_{yz} \\ \rho hv - u\tau_{yx} - v\tau_{yy} - \tau_{yz} + q_y \end{bmatrix}, \tag{7.40}$$

$$\overline{F_3} = \begin{bmatrix} \alpha_1\rho w \\ \alpha_2\rho w \\ \rho uw - \tau_{zx} \\ \rho vw - \tau_{zy} \\ \rho w^2 + p - \tau_{zz} \\ \rho hu - u\tau_{zx} - v\tau_{zy} - \tau_{zz} + q_z \end{bmatrix}, \text{ and } \bar{G} = \begin{bmatrix} 0 \\ 0 \\ 0 \\ 0 \\ -\rho g \\ \rho hv \end{bmatrix}, \tag{7.41}$$

where denote: u, v, w is velocity components along x, y, z axes; g is gravitational acceleration; p is pressure; τ is component of the Reynolds stress tensor; e is inertial energy; h is the enthalpy given in Eq. (7.42).

Enthalpy (h) can be calculated:

$$h = \frac{\rho \cdot e + p}{\rho}. \tag{7.42}$$

For the simulation calculation of the initialisation process, the phase volume fractionα_1 must be prescribed as a value of 1 for the entire domain defined by a vessel height of 0.52 m. The space above this aluminium melt is air with α_2 equal to 0 (the rest of the cube container). This initial boundary prescription is common for a typical two-phase solution concept.
The calculation was performed in Open FOAM code using the PIMPLE scheme. A Gaussian linear scheme was used for most of the variables. A compressible multiphase solver with different time steps determined by a stability condition based on a maximum Courant number of 0.25 was used.

c) Properties of bubbles

To predict the behaviour of bubbles, it is necessary to consider the following numbers: the Reynolds number *(Re)*, the Weber number *(We)* and the Haberman-Morton number. The intensity of the surface tension affects the bubble deformation, which is the characteristic force that maintains the sphericity of the bubble. It is known from

theory that bubble deformation occurs when We/Re approaches unity for Re << 1 or when we approach unity for Re >> 1. This Reynolds (Re) number is defined:

$$Re = \frac{2 \cdot \rho \cdot R \cdot W}{\eta}, \tag{7.43}$$

where: R is the instantaneous radius of the spherical bubble; w is the magnitude of the translational velocity; η is viscosity; ρ is density.

The characteristic properties of the materials used are given in Table 7-23:

$$We = \frac{2 \cdot \rho \cdot W_{\infty}^{2} \cdot R}{\sigma} \tag{7.44}$$

where: w_∞ is the terminal velocity of the bubbles and σ is the surface tension (see values in Table 7-21). The terminal velocity is a function of the shape, and this value must be known to calculate the Weber number.

According to [3], the terminal velocity of bubble motion can be replaced by ΔW, which expresses the relative velocity of the gas-liquid system. The generation of small-scale dynamics must take into account the ratio of the hydrodynamic force related to the dynamic pressure to the surface tension force. This is expressed in fluid mechanics by Weber's number. The hydrodynamic force is conveniently defined as $\rho \cdot \Delta W_2$, so it captures both the case of a high-velocity gas over a slow fluid and a high-velocity fluid flow in a static gas that breaks into droplets. Depending on the local shape, bubble bursting may occur above a certain critical value of *We*. Below this value, the surface tension forces are large enough to overcome the dynamic pressure, and no local breakup occurs. At higher Weber numbers, the predominance of aerodynamic force leads to deformation and splashing. This process produces small bubbles with a lower Weber number. If their size is small enough, they drop below a critical level, and the disintegration process stops. Another way to predict the behaviour of the bubble is to express the Haberman-Morton number, according to the equation:

$$H_m = \frac{g \cdot \eta^4}{\rho \cdot \sigma^3}, \tag{7.45}$$

where: g is the acceleration of gravity [$m \cdot s^{-2}$]; η is the viscosity of the surrounding fluid [Pa·s]; ρ is the density [$kg \cdot m^{-3}$], and σ is the surface tension coefficient [$N \cdot m^{-1}$].

In this case, if Hm < 1, all bubbles for which Re << 1 remain spherical. However, there are some unusual circumstances in which Hm > 1 and then there will be a range of Re in which there can be a significant departure from sphericity [2]. For the assumed two-phase flow problem, it has been calculated that Re >> 1 and will be approximately Hm = 3 $x10^{-10}$. In this particular case, the finite velocity is given by the Froude number Fr ≈ O(1), the bias occurs when We > 1. Using Fr = 1 and Hm implies that the departure

from bubble sphericity occurs when Re >> $Hm^{-1/4}$. Consequently, under normal circumstances in which Hm < 1, there is a range of Reynolds numbers, Re < $Hm^{-1/4}$, in which sphericity is preserved; non-spherical shapes occur when Re > $Hm^{-1/4}$. It has been observed experimentally that the initial deviation from sphericity causes ellipsoidal bubbles that can oscillate in shape and have oscillatory trajectories. As the bubble size increases further, that is, up to the point where We ≈ 20, the bubble acquires a new asymptotic shape, known as a spherical cap bubble [2].

d) Results achieved

A) Formation of a bubble bath for a liquid phase viscosity of 0.014 Pa.s

Fig. 7.46 shows the instantaneous flow of bubble formation for different time steps. Firstly, to investigate the bubble formation behaviour, the dynamic viscosity of the liquid (aluminium melt) was kept constant at 0.014 Pa.s (see Table 7-23).

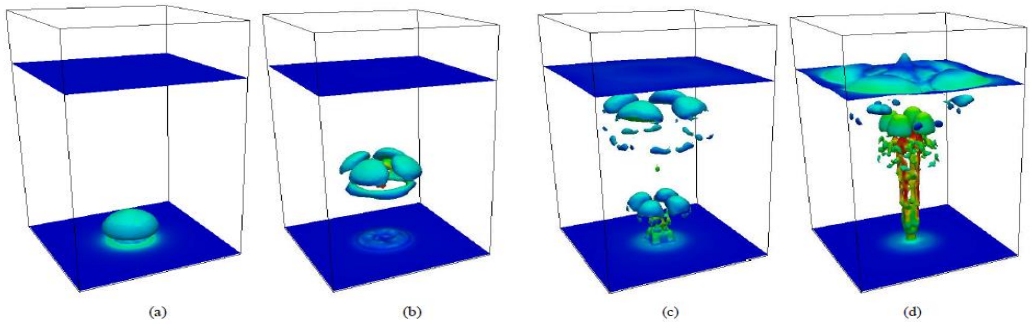

Fig. 7.46 Instantaneous bubble patterns for (a) 0.3s; (b)0.6s; (c) 0.9s and (d) 1.2s

The colour representation in Fig. 7.46 indicates the intensity of the flow velocity. The first bursting of the main bubble was observed, and other small bubbles remained entrained in the fluid and slowly floated to the surface. The first bubble broke up into other small bubbles, and this process continued as the bubbles floated to the surface of the mixture. Fig. 7.46(d) shows the tracking of the path of different-sized bubbles between the bottom and the surface of the aluminium melt (liquid phase) for 1.2 s. It was observed that the smaller bubbles formed later, after the first burst, reached a higher velocity (marked in red). The surface of the liquid or aluminium melt was deformed by the incoming bubbles.

At the same time, Fig. 7.46 shows the formation and behaviour of the first main bubble at 0.55 s. The vector representation shows the flow orientation and velocity intensity represented by colours. It was found that the center of the bubble has the highest velocity, taking values up to 1.5 $m \cdot s^{-1}$. This intense translational velocity is about 180 times higher than the initial air velocity used to form the bubble at the bottom.

This motion causes the bubble to deform from its spherical shape (see Fig. 7.46a for 0.3 s). There is a significant flow around the bubble, which draws material from the

upper part of the bubble to the lower part, which is later pumped back into the centre of the bubble. This flow exists because of the translational motion of the bubble as the liquid passes around the bubble´s body. The differential flow around the bubble was investigated in [2].

Fig. 7.47 shows the temperature distribution in the two-phase mixture at 1.15 s. From Fig. 7.47 it can be seen that a slight heat flux has formed at the bottom of the vessel, causing a cooler bottom effect, resulting in a lower temperature of approximately 719.6 K. The circulating ambient air has a temperature of 295 K (area above the aluminium surface). On this surface, the cooling effect of the ambient air is considered, leading to a significant temperature drop.

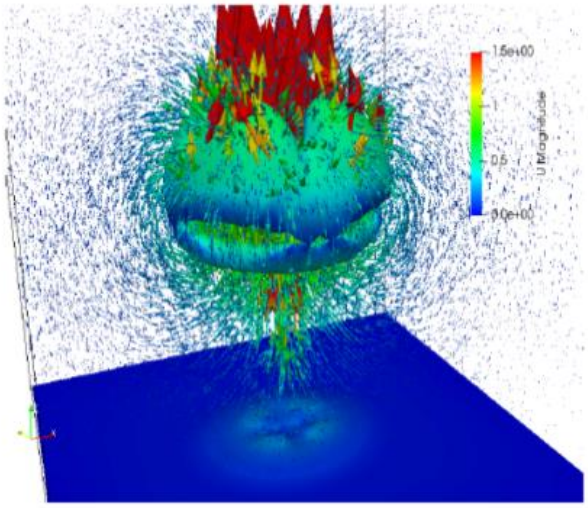

Fig. 7.47 Formation of bubbles with velocity vectors at time 0.55s

The airflow above the aluminium surface is driven by buoyancy due to a strong temperature gradient. Inside the aluminium melt, the temperature is homogeneous at around 720 K. The effect of temperature has been taken into account in the calculation due to the existence of a slight temperature gradient between the bottom and the top of the vessel. In general, this existing temperature gradient can be caused by the flow of the aluminium melt driven by the buoyancy force, which also influences the overall bubble motion. In terms of the forces acting on the bubble at a small relative Reynolds number Re << 1, only the forces due to buoyancy and the mass of the particle need to be considered in addition to the total force acting on the bubble. However, at high relative Reynolds numbers, Re >> 1, we must resort to a heuristic approach in which the fluid forces are supplemented by drag (and lift) forces [2]. Fig. 7.48 shows the temperature field when the aluminium melt gushes in chae1.15 s.

B) Effect of viscosity on bubble path formation

The effect of viscosity on bubble path formation was investigated for the simulation calculation or bubble formation study. For this purpose, several different values of the viscosity of the aluminium melt or liquid phase were calculated, η from 0.14 Pa.s to 0.014 Pa.s.

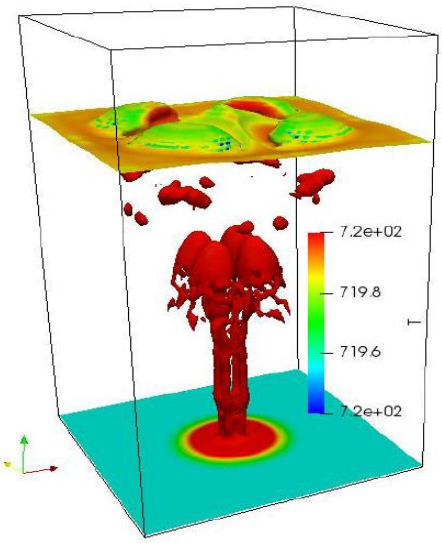

Fig. 7.48 Instantaneous temperature field during aluminium melt gassing in time 1.15 s

In previous work, it has been experimentally found and discussed above that as the volume fraction of gas in the liquid phase increases, a stabilising effect must be achieved due to small particles of different sizes. The small particles caused a slightly higher viscosity of the liquid. To assume these small particles in the simulation would be difficult, so the effect of the small particles was replaced by a change in the viscosity of the liquid (as experimentally observed).

Fig. 7.49 shows the simulated volume fraction of gas in the liquid phase at a time instant of 1.15 s, using a dynamic viscosity value of η = 0.014 Pa.s, see Fig. 7.49a). And using the dynamic viscosity value η = 0.14 Pa.s, see Fig. 7.49b). In the case of higher viscosity, more bubbles can be detected below the surface of the liquid phase. The formed path of gas bubbles between the bottom and the top of the vessel had a slightly different shape. The magnitude of the translational velocity remains the same. At the same time, Fig. 7.49 shows the amount of gas phase in the liquid phase at the time 1.15 s. While the amount of gas for the dynamic viscosity values η = 0.14 Pa.s and η = 0.014 Pa.s was at the same level, for the dynamic viscosity of the liquid phase, i.e. for the aluminium melt η = 0.07 Pa.s, the volume fraction of the gas phase was about 30% higher. Unfortunately, there were few telling results to explain this observed effect.

In general, the amount of gas increased during the bubble formation period for all viscosity values. No decrease in the amount of gas in the liquid was detected until 1.0 s. Fig. 7.50 shows a simulation calculation of the amount of gas volume fraction in the aluminium melt for a time of 1.15 s for different values of the dynamic viscosity of the aluminium melt.

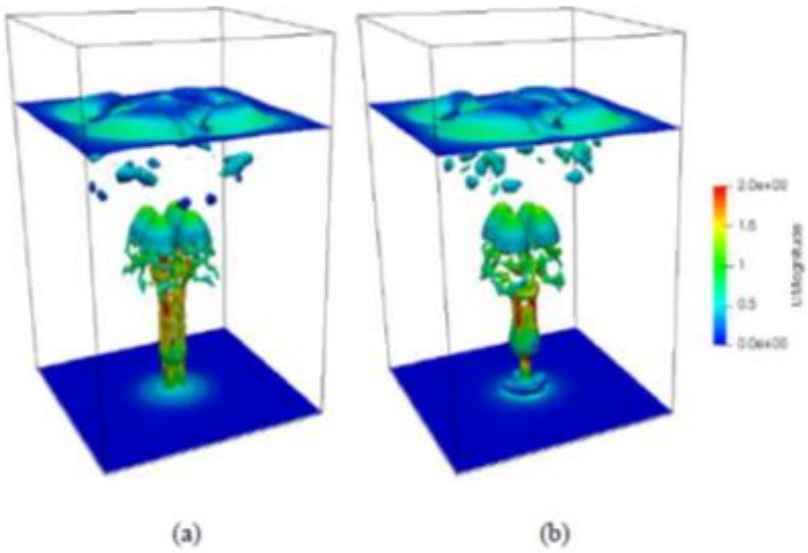

Fig. 7.49 Simulation calculation of the instantaneous gas volume fraction of gas in time 1.15 s for dynamic viscosities of 0.014 Pa.s (a) and 0.14 Pa.s (b)

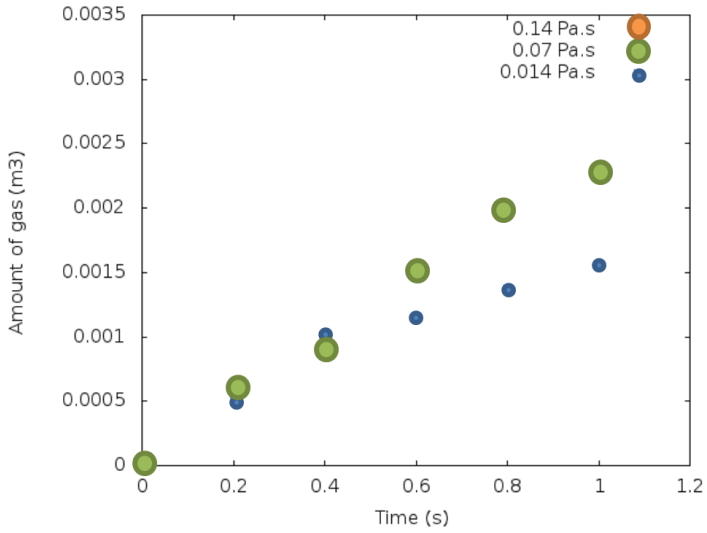

Fig. 7. 50 The amount of the gas volume fraction in aluminium melt for different times

Based on the numerical simulation calculation performed above, it can be concluded that the bubble formation in the mixture represented by the two-phase problem was investigated by numerical simulation. The flow problem was considered as non-stationary, laminar and non-isothermal. The effect of mixture viscosity on bubble path formation was studied on several samples defined by different fluid viscosities. A compressible multiphase OpenFOAM computational code solver was successfully applied.

Reasonable results were found considering the theoretical knowledge and current experience with similar flow simulations in other engineering problems. It was found that the viscosity of the liquid affected the bubble formation (shape and total volume fraction of gas in the mixture). However, the effect of viscosity on the bubbles formed

could not be sufficiently confirmed. Further calculations will be required to determine which specific material properties or flow conditions may actually stabilize the foam and prevent the gas from escaping from the mixture. In terms of calculation efficiency, higher velocity magnitudes were found over the aluminium melt in the airflow region. These higher values determine the size of the time step and thus, the total time requirement for the calculation.
However, the effects associated with bubble formation, which is the objective of this investigation, did not affect the calculation efficiency.

This issue has been published:
FRAŇA, K. and I. NOVÁ. An Effect of the Fluid Viscosity on the Gas Deposition in the Two-Phase Mixture. In. Conference: 2018 International Conference on Applied Mathematics & Computer Science. Paris 2018. (ICAMCS), DOI:10.1109/CAMCS 46079.2018.00012.
FRAŇA, K. and I. NOVÁ. Interface Formation in two. Phace flow problems. International Journal of Mechanics, 2018. Vol. 12, pp. 102-108.

7.5 Structures produced by direct melt filling with an external gas source

7.5.1 Monitoring the foaming process from an external gas source

The implementation of the aluminium smelting foaming process (with gas supplied from an external source) to obtain "aluminium foam" requires experimental testing of all the necessary technological steps. For this purpose, a custom-made furnace was manufactured by the German company HTM Reetz GmbH (see Fig. 7.51a) and Fig. 51b). Furthermore, the melt has to be prepared with a precise determination of the ceramic reagent that increases the viscosity of the melt. The frothing gas was technical air. The straining sensor consisted of a heat and corrosion-resistant tube ∅ 8 mm long 1500 mm, a hose and pressure-reducing valves to achieve suitable bubbles of gas fed into the melt of the selected aluminium alloy. The temperature in the foaming furnace was about 760 °C, and the foaming process was carried out for 2 hours, with the greatest control of the feed gas. Fig. 7.52 shows Dr. Sobotka and Ing. Korecek setting up the foaming experiments and introducing the foaming sensor into the aluminium alloy melt.
The samples were produced by foaming the aluminium alloy melt. The melt was prepared in the furnace of HTM Reetz GmbH. A ceramic crucible was used for foaming based on gas supplied from an external source. The charging gas was technical air. The viscosity-increasing agent greatly reduced the fluidity of the melt. Its quantity will have to be more systematically tested; most often, it was Al_2O_3 with particle sizes up to 10 μm.

Fig. 7.51a) View of the box-shaped foaming furnace from HTM Reetz GmbHz

Fig. 7.51b) View of the HTM Reetz GmbHz box-shaped foaming furnace and the feed of the foaming medium into the metal melt

Fig. 7.52 Preparation of the foaming process and view of the introduction of the foaming sensor into the aluminium melt, Dr. Sobotka and Dr. Korecek

The strain sensor consisted of a corrosion-resistant tube ∅ 8 mm long by 1500 mm. Connected to this sensor is a hose that feeds gas from an external source into the melt. The gas supply hose is fitted with control valves. The first foaming was carried out with AlSi12 aluminium alloy melt. The temperature in the furnace during the foaming process was approximately 760 °C. The first foaming process was carried out with AlSi12 alloy and the foaming gas was argon, the foaming time was 15 minutes. Further study of the literature revealed that the AlSi12 alloy was unsuitable for direct foaming.

More suitable alloys were sought, such as AlSi7Mg0.3. This alloy was used in the testing of other foaming processes. Also in the other foaming processes, the foaming was carried out for 2 hours, while taking care to control the feed gas as much as possible so that the gas entered the melt one bubble at a time. At the same time, it was difficult to design the material for the gas supply, which exits at a melt temperature of about 760 °C. Corrosion and heat-resistant steel could not withstand the long residence time at 760 °C, so a quartz tube had to be used. Fig. 7.53 shows a view of the foamed melt in the furnace of HTM Reetz GmbHz.

Fig. 7.53 View of the foamed melt in the ceramic crucible

A) Production and structure of AlSi12 alloy sample, direct argon sputtering (sample 1)

For the production of AlSi12 alloy sample 1, argon was used for the gassing, see Fig. 7.54, left. The installation of the argon supply to the furnace to melt the 0.2 MPa aluminium alloy is shown in Fig. 7.54, right. Al_2O_3 particles were used to increase the viscosity of the aluminium alloy melt. Fig. 7.55 shows a section of the sputtered sample (∅ 52 mm, height 56 mm), the sputtering is at the top of the sample, about 10 mm thick.

ion

Fig. 7.54 Argon used for direct foaming of the aluminium alloy melt in the furnace

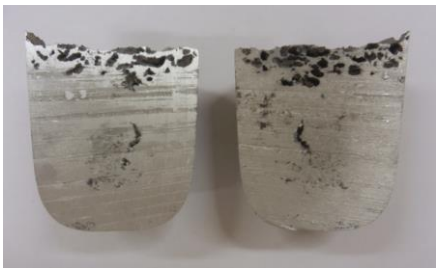

Fig. 7.55 View of the cross-sectional areas of the foamed sample∅52 mm, height 56 mm, foaming layer approx. 10 mm, foaming time 15 minutes, argon; sample No. 1

Fig. 7.56 shows a detail of the upper part of a gassed sample, approximately 10 mm thick (∅ 52 mm, height 56 mm), gassed with argon; sample 1.

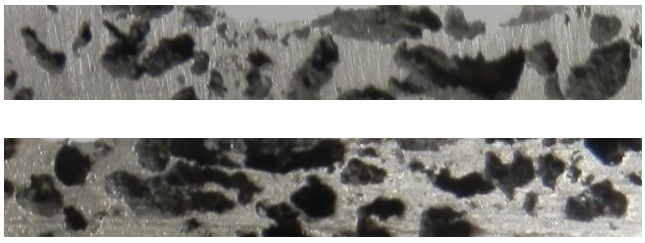

Fig. 7.56 Upper foamed part of the sample, thickness approx. 10 mm (∅52 mm, height 56 mm), argon gas used; sample No. 1

The upper sputtered part of the sample was observed on a scanning electron microscope (Vega 3 Tescan, SEM HV 20.0 kV). Fig. 7.57 and Fig. 7.58 show a view of the foamed part of the aluminium sample with the distribution of Al_2O_3 particles. These particles are added to the melt to increase the melt viscosity or stability of the foaming process.

Furthermore, EDX analysis was also performed to evaluate the chemical composition of the AlSi12 alloy used in the selected sample location. Fig. 7.59 shows the EDX analysis, the local chemical composition of the upper sputtered layer of the sample.

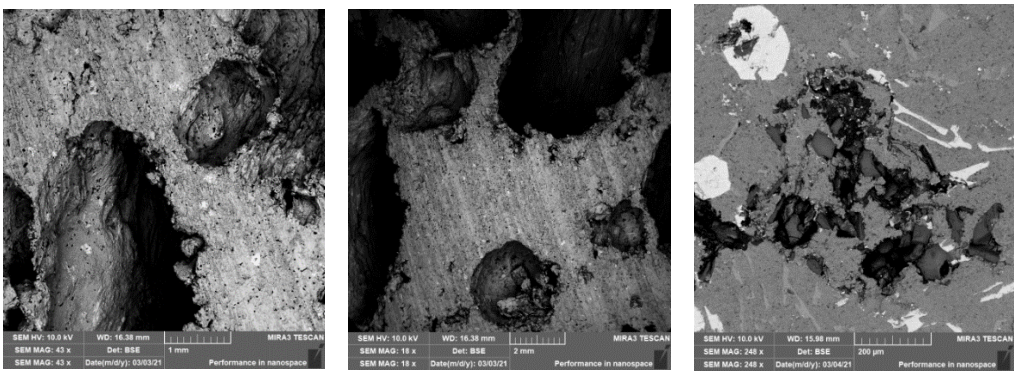

Fig. 7.57 View of the foamed part of the material with Al_2O_3 particle distribution to increase the viscosity of the AlSi12 aluminium alloy melt, sample 1

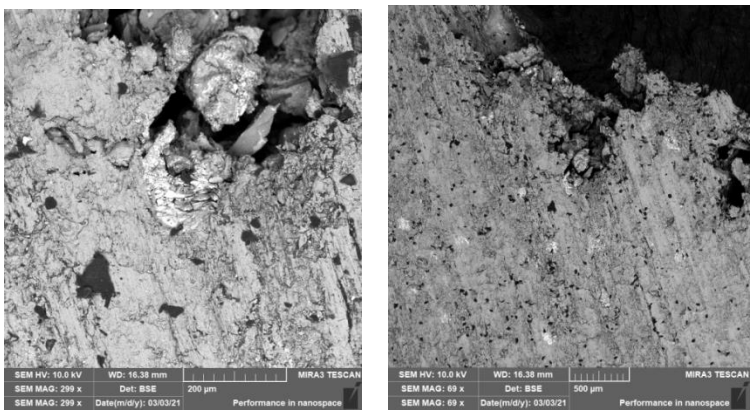

Fig. 7.58 View of the particles in the wall of the foamed alloy (intermetallic particles of the Al-Fe-Si type; Al_2O_3, Si), sample No. 1.

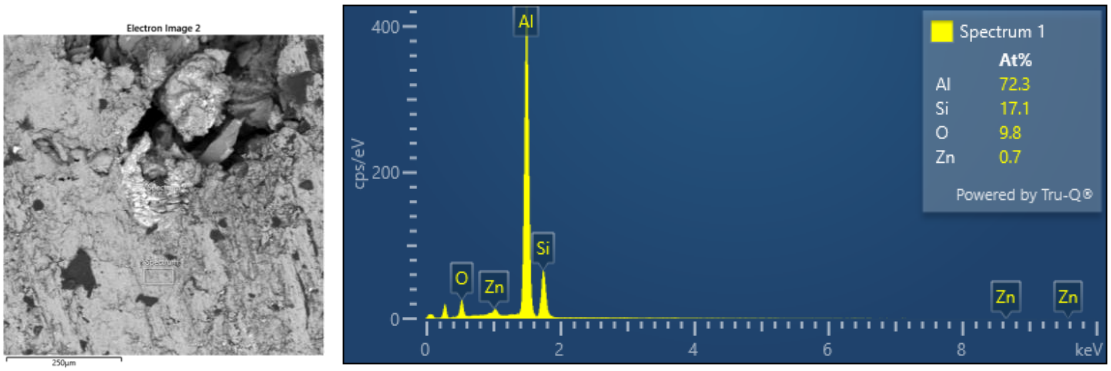

Fig. 7.59 EDX analysis of the used AlSi12 alloy, sample No. 1

B) Fabrication and structure of AlSi7Mg0.3 alloy sample, direct air foaming (sample 2)

For the production of sample No. 2, made of AlSi7Mg0.3 alloy, air was used for sputtering at a pressure of 0.2 MPa. Al_2O_3, with a sparging time of 120 minutes, was used as a reagent to increase the viscosity of the aluminium alloy melt. The gassing was carried out in a furnace at 760 °C in a ceramic crucible. Fig. 7.48 shows a section of sample 2, the structure of the sputtered AlSi7Mg0.3 alloy; sample ∅ 118 mm; maximum height 80 mm, left. Also shown in Fig. 7.60 is a plan view of a foamed section of AlSi7Mg0.3 alloy, 45 x 80 mm, right.

The structure of the foamed AlSi7Mg0.3 alloy sample 2 was analysed with a Vega 3Tescan scanning electron microscope, SEM HV 20.0 kV. At the same time, EDX analysis was performed and the chemical composition of the used AlSi7Mg,3 alloy was evaluated at the selected sample location.

An important aim of the research was to monitor the distribution of Al_2O_3 particles in the bubble wall. For this purpose, a metallographic sample was prepared, as shown in Fig. 7.61.

Fig. 7.60 View of a section through AlSi7Mg0 alloy specimen 2, left and its foamed part (foamed specimen∅118 mm; maximum height 80 mm), right, specimen 2

Fig. 7.61 View of the sample for metallographic observation of the distribution of Al_2O_3 particles

Fig. 7.62 and Fig. 7.63 show Al_2O_3 particles dispersed in a foamed AlSi7Mg0.3 alloy.

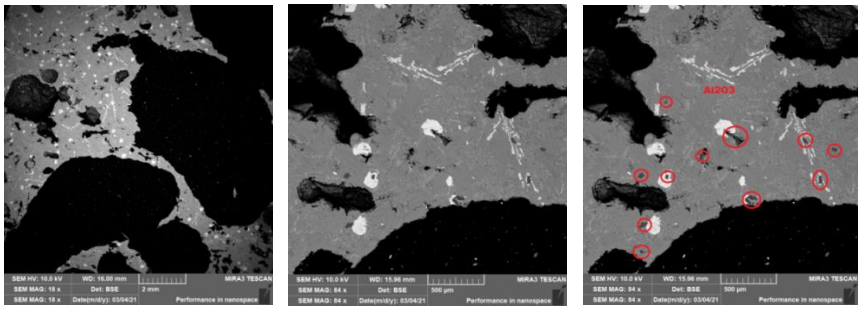

Fig. 7.62 View of the foamed part of the material with Al_2O_3 particle distribution to increase the viscosity of the aluminium alloy melt, sample 2

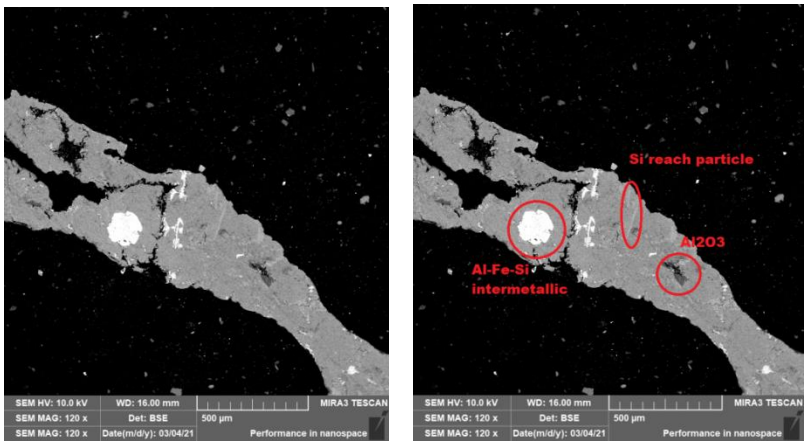

Fig. 7.63 View of the particles in the wall of the foamed alloy (intermetallic particles of Al-Fe-Si type; Al_2O_3, Si) - cell wall durability, sample 2

Fig. 7.64 is the EDX analysis, and Fig. 7.65a), Fig. 7.65b), and Fig. 7.65c) are the detailed area of EDX analysis of the aluminium alloy AlSi7Mg0.3 used, tracking the elements Al, Si, O, Fe, Cr, Mn, of sample 2.

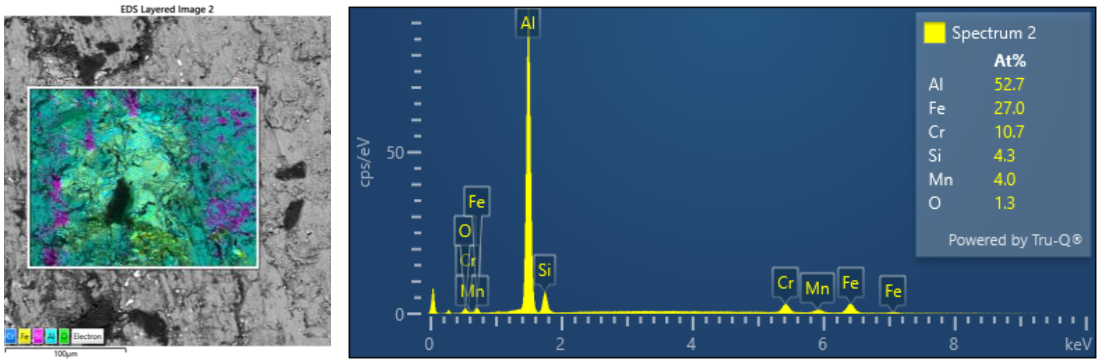

Fig. 7.64 EDX analysis of the alloy used, AlSi7Mg0.3; sample No. 2

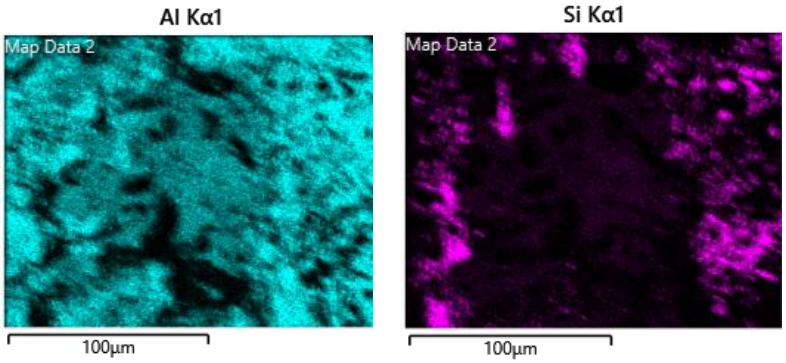

Fig. 7.65a) Detailed areas of EDX analysis of AlSi7Mg0.3 alloy; elements Al and Si; sample 2

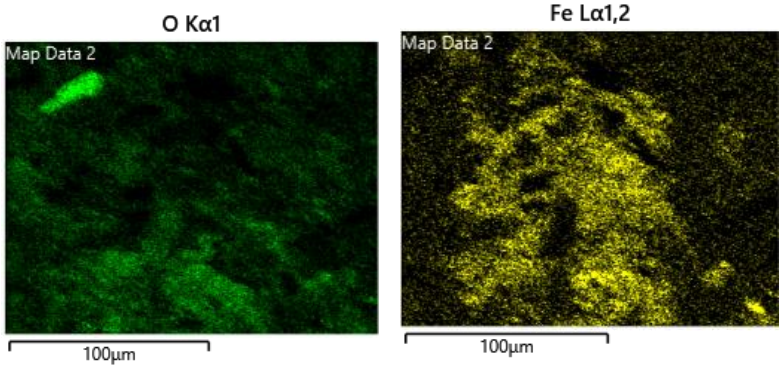

Fig. 7.65b) Detailed areas of EDX analysis of AlSi7Mg0.3 alloy; elements O and Fe; sample 2

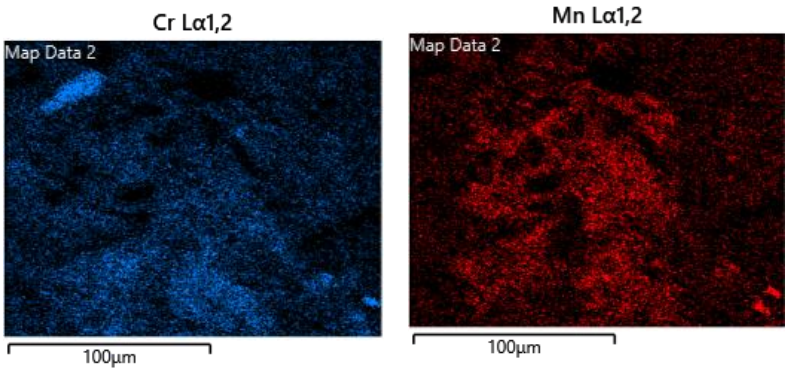

Fig. 7.65c) Detailed areas of EDX analysis of AlSi7Mg0.3 alloy; elements Cr and Mn; Sample No 2

C) Production of AlSi5Mg alloy sample by direct air foaming (sample 3)

For the production of sample No. 3, made of AlSi5Mg alloy, the direct melt foaming method with air at a pressure of 0.2 MPa was used. Al_2O_3 particles were used to increase the melt viscosity of the aluminium alloy. The frothing time was 120 minutes. The gassing was carried out in a furnace at 760 °C in a ceramic crucible. After the solidification of the gassed melt, a sample of a conical cone with, a larger diameter of 125 mm, a smaller diameter of 85 mm and a height of 105 mm was obtained. This sample was cut and its foamed structure is shown in Fig. 7.54, left. The structure of the foamed sample was observed on a scanning electron microscope, Vega 3 Tescan, SEM HV 20.0 kV. At the same time, EDX analysis was performed, and the chemical composition of the AlSi5Mg alloy used in the selected sample location was evaluated. Fig. 7.66, right, shows a detail of the foamed area of the AlSi5 Mg alloy sample. Fig. 7.67 and Fig. 7.68 are EDX analyses of the chemical composition at specific locations in the sample. Fig. 7.69 details areas of structure related to the EDX analysis.

Fig. 7.66 Section through a fabricated foamed specimen (∅125 mm;∅85 mm; maximum height 105 mm), left and plan view of the foamed part of the AlSi5Mg specimen (50 x 75 mm section), right

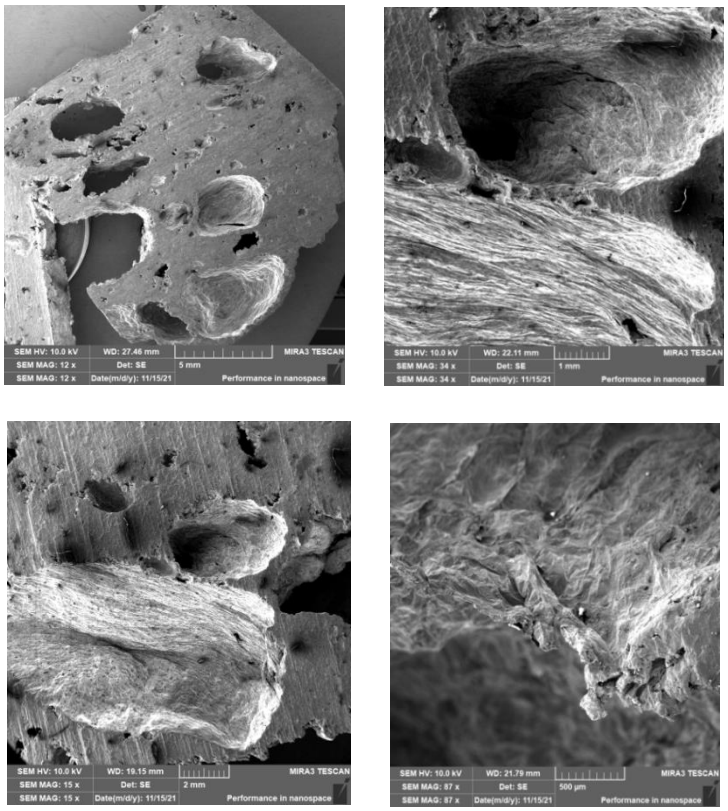

Fig. 7.67 Deatil structures of the fused AlSi5Mg alloy structure, sample 3

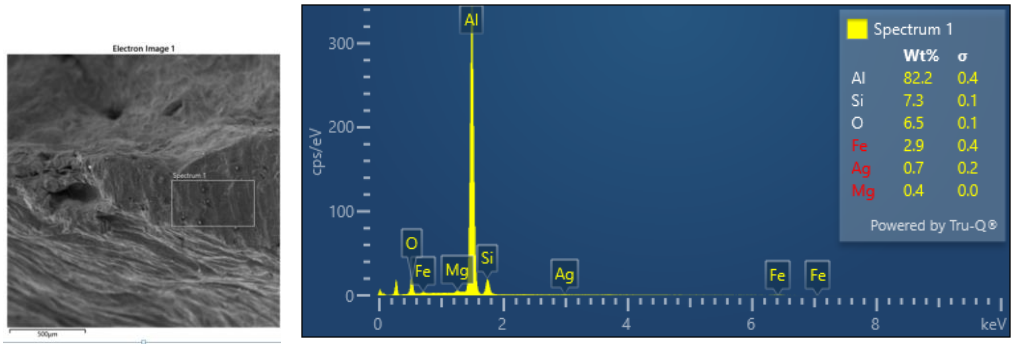

Fig. 7.68 EDX analysis of the used alloy on the surface of the used alloy in the air bubble region, sample 3

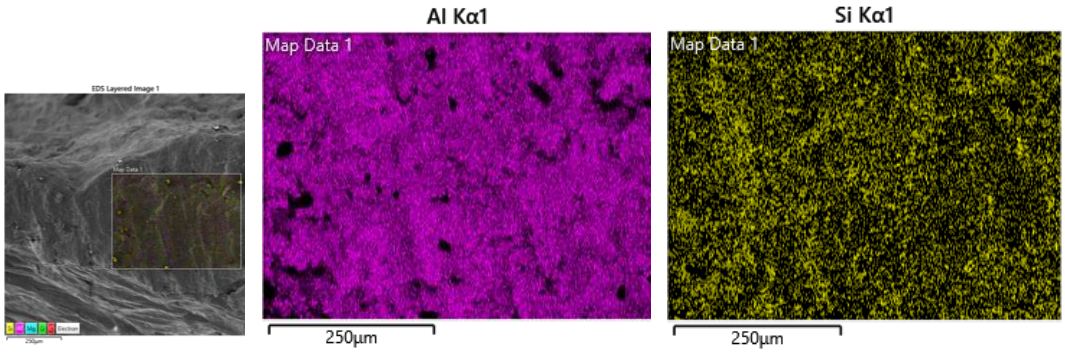

Fig. 7.69a) Detailed areas of EDX analysis with evidence of the relevant elements - aluminium and silicon, in the local location of the aluminium alloy AlSi5Mg, sample 3

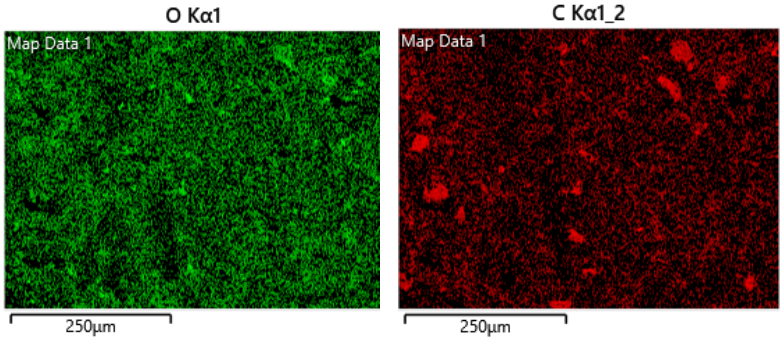

Fig. 7.69b) Detailed areas of EDX analysis with evidence of relevant elements and carbon in the local location of the aluminium alloy AlSi5Mg, sample 3

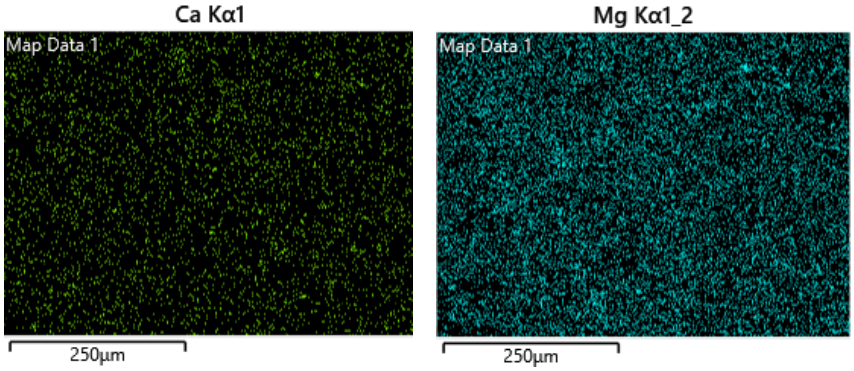

Fig. 7.69c) Detailed areas of EDX analysis with the corresponding elements – calcium and magnesium, in the local location of the aluminium alloy AlSi5Mg, sample 3

This book has been written based on the findings of the research and also on the results of our experiments conducted within the framework of the five-year development project of science and research at the Technical University of Liberec from 2018 to 2022, OP VVV: Excellent Research. CZ.02.1.01./0.0/0.0/16_019/0000843: "Hybrid materials for hierarchical purposes". In the area of research objective 2: Metal-based materials and structures, research activity 01: *Cellular lightweight metallic structures* was applied.

List of references

References to chapters Preface, Introduction

[1] DE MELLER, M.A. Produit Métallique Pour L'*obtention D'*objets Laminés, Moulés Ou Autres, *Et Procédés Pour Sa Fabrication*. French Patent (1926). 615, 147.
[2] BANHART, J. AND D. WEAIRE. Physics Today 55 (2002) p.p. 37-42.
[3] BANHART, J. Manufacturing Routes for Metallic Foams. Solidification Science: *Overview Journal JOM* 52 (12) 2000, pp. 22-27.
[4] BANHART, J. Manufacture, Characterization and Application of Cellular Metals and Metal Foams. *Progress Materials Science*, vol. 46, Iss. 6, (2001), pp.559 to 632.
[5] BANHART, John Metal Foams: Production and Stability. *Advanced Engineering Materials* 8 (9), 2006 pp. 781-794.
[6] ASHBY, M.F. et al: Metal Foams. A Design Guide. *Elsevier* 2000.
[7] BANHART, J. Light Metal Foams – History of Innovation and Technological Challenges. *Advanced Engineering Materials.* 2013, 15, No. 3, pp. 82-111.
[8] CURRAN, D.C. Aluminium Foam Production using Calcium Carbonate as a Foaming Agent. [Doktorská disertační práce]. Department of Materials Science and Metallurgy, University Cambridge, 2003.
[9] MICHNA, Š et al. Encykloperie hiníku. Adin, s.r.o. Prešov, 2005. In. JERZ, J. Výroba a průmyslové využití pěnového hliníku, kap. 10.8, s. 642 až 693.
[10] GARCIA-MORENO, F. Commercial Application of Metal Foams: Their Properties and Production. *Materials* 2016, 9, 85, pp. 1 to 27.
[11] GERGRLY, V. and B. CLYNE. The FormGRIP Process: Foaming of Reinforced Metals by Gas Release in Precursors. *Advanced Engineering Materials*, 2, No. 4, 2000. Pp. 175 - 178.
[12] HARTMANN, M. Herstellung, Struktur und Eigenschaften syntaktischer Magnesiu-mschäume. (Production, structure and properties of syntactic magnesium foams.). Doctoral Thesis. Der Friedrich-Alexander-Universität Erlangen-Nürnberg. 2015, in German.
[13] BIKERMAN, J. Foams. 1st edition, Verlag Berlin/New York, 1973.

References for Chapter 1
Characteristics of Cellular Metal Systems

[1] BANHART John. Manufacturing Routes for Metallic Foams. Solidification Science: *Overview Journal JOM* 52 (12) 2000, pp. 22-27.
[2] BANHART, J. Manufacture, Characterization and Application of Cellular Metals and Metal Foams. *Progress Materials Science*, Vol. 46, Iss. 6, (2001), pp. 559-632.
[3] ASHOLT, P. *Metal Foams and Porous Metal Structures,* ed. J. Banhart, M.F. Ashby, and N.A Fleck (Bremen, Germany: *MIT-Verlag,* 1999), p. 133.
[4] WOOD, J. *Metal Foams,* ed. J. Banhart and H. Eifert (Bremen, Germany: MIT-Verlag, (1997), p. 31.
[5] PRAKASH, SANG, H. and J. D. EMBURY, Materal Science Engineering, A199 (1995), p. 195.
[6] KENNY, L. D. Mechanical Properties of Particles Stabilized Aluminium Foam. *Material Science Forum,* 217-222 (1996), pp. 1883-1890.
[7] SIMONE, A.E. and L.J. GIBSON. Aluminium Foams Produced by Liquid State Processes. *Acta Mater*ial, 46 (1998), pp. 3109-3123.
[8] BEALS, J.T. and M.S. Thomson. Density gradient effects on aluminium foam compression. *Journal Materl Science* 1997; 32 (13), pp. 3595-3600.
[9] MIYOSHI, T., ITOH, M. AKIYAMA, S. and A. KITAHARA. Production Processes, Properties, and Applications" Advanced Engineering Materials 4, 2000, pp. 179-183.
[10] MA, L. and Z. SONG, *Scripta Materialia*,1998, 39 (11) pp. 1523-1528.
[11] SHAPOVALOV, V. Porous and Cellular Materials for Structural Applications, Vol. 521, *ed. D.S. Schwartz et al. (Warrendale, PA: MRS, 1998),* p. 281.
[12] BAUMGÄRTNER, F., DUARTE, I. and J. BANHART. Industrialization of Powder Compact Foaming Process. *Advanced. Engineering. Materials,* 2 (4), 2000, pp. 168-174.

[13] RAJAK, D.K. KUMARASWAMIDHAS, L. A and S. DAS Technical Overview of Aluminum Alloy Foam. *Material Science* 48 (2017) pp. 68-86.
[14] LEITLMEIER, D. DEGISCHER, H.P.and H.J. FLANKL. Development of a Foaming Process for Particulate Reinforced Aluminium Melts. *Advanced Engineering Materials*. 2002, Vol. 4, pp. 735-740.
[15] YUN, H. et al. Influence of Withdrawing Speed on the Porous Structures of Gasa Ingots Fabricated by Bridgman Method. *Journal of Material Processing Technology*. Vol. 245, July 2017, pp. 106-114.
[16] ASHBY, M.F. EVANS, A. FLECK, N.A. GIBSON, L.J HUTCHINSON, J.W. and H.N.G WADLEY. Metal Foams – A design guide. Butterworth Heinemann, 2000.
[17] CINGI, C. NIINI, E. DRKAS, J. Foamed aluminium parts by investment castings. Colloids and Surfaces A: Physicochemical and Engineering Aspects. Vol. 344, Iss. 1-3, 20, July 2009, pp. 113-117.
[18] CURRAN, D.C. Aluminium Foam Production using Calcium carbonate a s a Foaming Agent [Doktorská disertační práce]. Department of Materials Science and Metallurgy, University Cambridge, 2003.
[19] AKIYAMA, S. et al. US Patent 4,713, 277: Foamed Metal and Method of Producing Same. 1987.
[20] AOYAGI, N. and Y. KOJIMA, Production Process and Microstructure of Aluminium Alloy Foams by Semi-Solid Stirring Method. In 5th International Conference on Semi-Solid Processing of Alloys and Composites. 1998. Colorado, USA.
[21] ALPORAS, ALPORAS® brochure. 1998, Shinko Wire Co., Ltd., Amagasaki-shi, Japan.
[22] MIYOSHI, T. HARA, S., MUKAI, T. and K. Higashi. Development of a Closed Cell Aluminium Alloy Foam with Enhancement of the Compressive Strength. *Materials Transactions,* JIM, 2001. 42(10): p. 2118-2123.
[23] ŠIMANCIK, F. and J. KOVACIK. Porosity in Complex 3D Parts Prepared from Aluminium Foam. In. *Metal Foams.* 1997. Bremen, Germany: MIT-Verlag Publishing, Bremen.
[24] MELZNER, A. BANHART, J. BAUMEISTER, J. and M. WEBER German patent 19813176.
[25] GERGELY, V. and T.W. CLYNE. The FORMGRIP: Proces: Foaming of Reinforced Metals by Gas Release in Precursors. *Advanced Engineering Materials* 2, (200175-178.
[26] GERGELY, V. CURRAN, D.C. and T.W. CLYNE. The FOAMCARP Process. *Composites Science and Technology*, 63 (16), 2003, pp. 2301-2310.
[27] WIGHTMAN, G. and D.J. FRAY. *Metallurgical Transaction* 14 B (1983), pp. 625 to 631.
[28] IBRAHIM, A.H. Efecct of Materiál and Processing Parameters on the Morphology of Aluminium Foams Produced by the PM Route. Faculty of Engineering – University of Erlangen-Nürburg, Eelangen, 2005.
[29] BAUMEISTER, J., German Patent 40 18 360, (1990); US Patent 5,151,246 (1992), European Patent EP 0460392A1 (1996).
[30] BAUMEISTER, J. and H. SCHRADER. German Patent DE 41 01 630 (1991).
[31] BAUMEISTER, J. BANHART, J. and M. WEBER. German Patent DE 44 26 627, (1997).
[32] Alulight – Brochure (MEPURA, Ranshofen, Austria).
[33] ZEPPELIN, F. Composite Science and Technology 63 (2003), pp. 2293.
[34] BANHART, J. In: Proc. Symp. Metallschaume (MIT- Verlag, Bremen, 1997), p. 225.
[35] DEGISCHER, H.P. and B. KRISZT. Handbook of Cellular Metals (Wiley-VCH, Weinheim 2002).
[36] COHRT, H. and F. BAUMGARTNER. Proceedings Werkstoffwoche 98 (1999), p. 159.
[37] BANHART, J. Production Methods for Metallic Foams. Personal Internet homepage, Fraunhofer-Institute for Applied Materials Research, Bremen, Germany, 1998, pp. 3-12, XP002349180.
[38] BANHART, J. and BAUMEISTER, J. Deformation Characteristics of Metal Foams. Journal of Materials Science 33, 1998, pp. 1431-1440.
[39] KRISZT, B., FALAHATI, A. and H.P. DEGISCHER In „Metallschäume“, Proc. Symp. Metal Foams, ed.: J. Banhart, MIT-Verlag, Bremen, (1997), p. 59, (in German).
[40] BANHART, J. Advanced Engineering Materials 8, 2006, p. 781.

[41] NAVACERRADA, M. A. FERNANDEZ, P. DIAZ, C and A. PEDRERO. Applied Acoustics 74 (2013) 496.
[42] OAK, S.M. KIM, B.J. KIM, W.T. CHUN M. S. and Y.H. MOON. *Journal of Materials Processing Technology,* 2002*,* 130-131, p. 304.
[43] HAESCHE, M. LEHMHUS, D. WEISE, J. WICHMANN M. and I. C. M. MOCELLIN *Journal of Materials Science & Technology* 26, 2010, p. 845.
[44] BAUMGÄRTNER, F. DUARTE, I. and J. BANHART. Industrialization of Powder Compact Foaming Process. *Advanced Engineering Materials*, 2000, 2, No. 4. pp. 168-174.
[45] KAMMER, Katrin Aluminium foam. TALAT, Lecture 1410, EAA – Europen Aluminium Association, 1999.
[46] ŠIMANĆÍK, F. RAJNER, W. and J. JERZ. Alulight – Highly Porous Foamed Aluminium Panels with Outstanding Properties at Low Density. Europen Automotive Congress Bratislava 2001, SAITS 01112, pp. 1 to 6.
[47] DEGISCHER, H.P. and B. KRISZT. Handbook of Cellular Metals: Production, Processing, Applications, Eds., Wiley-VCH, Weinheim, 2002.
[48] BANHART, J. Aluminium Foams for Light Vehicles. *International Journal of Vehicle Design* 37, 2005, pp. 114-125.
[49] BANHART, J. SCHMOLL, C. and U. NEUMANN. Lightweight aluminium foam structures for ships. In Materials in Oceanic Environment (Euromat ’98), Ed: L. Faria, Federation of European Materials Societies (FEMS), 1998, pp. 55.
[50] YU, C.J. EIFERT, H.H. BANHART, J. and J. BAUMEISTER. Materials Research Innovations 1998, 2, pp. 181-188.
[51] ASHBY, M.F. EVANS, A. G. FLECK, N. A. GIBSON, L. J. HUTCHINSON, J. W. and H. N. G. WADLEY. Metal foams: A design guide, Butterworth-Heinemann: Boston, 2000.
[52] ŠIMANČÍK, F. RAJNER, W. and R. LAAG. Reinforced 'Alulight' for structural use. In Processing and properties of lightweight cellular metals and structures (Eds: A. Ghosh, T. H. Sanders, T. D. Claar), TMS, 2002.
[53] ŠIMANČÍK, F. LÚČAN, L. and J. JERZ. Reinforced aluminium foams, In Cellular Metals and Metal Foaming Technology (MetFoam2001) (Eds: J. Banhart, M. F. Ashby, N. A. Fleck), Verlag MIT Publishing, 2001, pp. 365.
[54] BANHART, J. GARCÍA-MORENO, F. HEIM, K. and. H.W. SEELIGER. Light-Weighting in Transportation and Defence Using Aluminium Foam Sandwich Structures. International Symposium on Light Weighting for Defence, *Aerospace and Transportation Indian Institute of Metals,* Goa, 11 November 2017.
[55] Podkladové a propagační materiály firmy LKR.
[56] JERZ, J. Foamed Aluminium and Aluminium Alloys Prepared by Powder Metallurgy. [Disertační práce]. TU Vienna, 1995.
[57] LEHMHUS, D. and J. BANHART. Properties of heat-treated aluminium foams. Materials Science and Engineering A 349 (2003), pp. 98-110.
[58] KENNEDY, A.R. The effect of TiH_2 heat treatment on gas release and foaming in Al-TiH_2 preformes. Scripta Materialia Vol. 47, Iss. 11, 2002, pp. 763-767.
[59] Podkladové materiály MEPURA – NEUMAN, Rakousko.
[60] DUOCELL product information, ERG Inc., Oakland Ca., USA, (1996).
[61] YOSIDA, Y. HAYASHI, C. Conf. Casting Science and Technology, Sept. 1990, p.103.
[62] Podkladové a propagační materiály firmy ERG and Aerospace Corporation, USA.
[63] MALEKJAFARIN, M. and S. K. SADRNEZHAAD. Effect of SIC on MIcrostructural Features and compressive properties of aluminium foam. *Sciencia Iranica 2014* (A) 21 (4) pp. 1325-1329.
[64] ZHOU, Y. LI, Y. and J. YUAN. The stability aluminium foams at the accumulation and condensation stage in the gas injection foaming process. *Colloids and Surfaces A: Physicochemical and Engineering Aspects.* 482*,* 2015, pp. 468–476.
[65] Allen, B.C., Mote, M.W. Sabroff, A.M. US Patent 3, 087 807, 1963.

Reference for Chapter 2

Method of producing porous metal materials using SHP

[1] PAPATONIOU, I.G. et al. Application of Aluminium Flakes in Fabrication of Open-Cell Aluminium Foams by Space Holder Method. *Materials* 2018, 11(8), p. 1420.

[2] BAKAN, H.I. A Novel Water Leaching and Sintering Process for Manufacturing Highly Porous Stainless Steel. *Scripta Materialia* 2006, *55*, pp. 203–206.

[3] El-HADEK, M.A. and S. KAYTBAY. Mechanical and Physical Characterization of Copper Foam. *International Journal of Mechanics and Materials in Design* 2008, *4*, pp. 63–69.

[4] NABAWY, A.M.; KHALIL, K.A.; AL-AHMARI, A.M.; SHERIF, E. and S.M. MELT. Processing and Characterization of Al-SiC Nanocomposite, Al, and Mg Foam Materials. *Metals* 2016, *6*, 110, pp. 1-11.

[5] BAFTI, H. and A. HABIBOLAHZADEH. Production of Aluminum Foam by Spherical Carbamide Space Holder Technique-processing Parameters. *Materials and Design* 2010, *31*, 9, pp. 4122–4129.

[6] HU, L. NGAI, T. PENG, H. LI, L. ZHOU, F. and Z. Peng. Microstructure and Properties of Porous High-N Ni-Free Austenitic Stainless Steel Fabricated by Powder Metallurgical Route. *Materials* 2018, *11*, 1058.

[7] JAKUBOWICZ, J. ADAMEK, G. and M. DEWIDAR. Titanium Foam made with Saccharose as a Space Holder. *J. Porous Materials.* 2013, *20*, pp. 1137–1141.

[8] ARIFVIANTO, B.; LEEFLANG, M. and J. ZHOU, A. New Technique for the Characterization of the Water Leaching Behavior of Space Holding Particles in the Preparation of Biomedical Titanium Scaffolds. *Mater. Lett.* 2014, *120*, pp. 204–207.

[9] ESEN, Z. and S. BOR. Processing of Titanium Foams Using Magnesium Spacer Particles. *Scripta Materialia* 2007, *56*, pp. 341–344.

[10] LICHÝ, P. BEDNÁŘOVÁ, V. ELBEL, T. and I. LÁNA. Kovové pěny – perspektivní materiál dalšího tisíciletí, 49. Slévárenské dny, Brno, 2012, ISBN 978-80-02-02405-7 (in Czech).

[11] MOHAMMED, S. H. and A.A. ALJUBOURI. Manufacturing of Aluminium Foam as a Light Weight Structural materiál. Engineering and Technical Journal, 2016, Vol. 34. Part. (b) No. 5, pp. 697-702.

[12] ZHAO, Y.Y. FUNG, T. ZHANG, L.P. and F.L. ZHANG Lost Carbonate Sintering Process for Manufacturing Metal Foams. *Scripta Materialia* 2005, Vol. 52, pp. 295 to 298.

[13] LI, D.S. ZHANG, Y.P. EGGELER, G. and X.P. ZHANG, High Porosity and High-Strength Porous Niti Shape Memory Alloys with Controllable Pore Characteristics. *Journal of Alloys and Compounds.* 2009, Vol. 470, pp. 1 to 5.

[14] LAPTEV, A. BRAM, M. BUCHKREMER, H.P and D. STÖVER, Study of Production Route for Titanium Parts Combining Very High Porosity and Complex Shape. *Powder Metallurgy*, 2004, Vol. 47, pp. 85 to 92.

[15] LUNA, E. E. M. BARARI, F. WOOLLEY, R and R. CODDALL. Casting Protocols for the Production of Open Cell Aluminium Foams by the Replication Technique and the Effect on Porosity. Department of Materials Science and Engineering. University of Sheffield.

[16] BARARI, F. Metal Foam Regenerators, Heat Transfer and Pressure Drop in Porous Metals. [Doctoral Thesis]. The University of Sheffield, 2014.

[17] Underlying materials of the Exxentis – porous materials Swiss company (2018).

[18] CURRAN, D.C. Aluminium Foam Production using Calcium carbonate a s a Foaming Agent [Doktorská disertační práce]. Department of Materials Science and Metallurgy, University Cambridge, 2003.

[19] Professional materials of the company Material District Naarden.

[20] Professional materials of the company Composite Material, Ltd., ALUPOR.

[21] Professional materials of the company Alumeco Group, Denmark.

[22] WANG, Z. et al. Manufacturing of Open-cell Aluminum Foams *via* Infiltration Casting in Super Gravity Fields and Mechanical Properties. *Royal Society of Chemistry* 2018, 8, pp. 15933-15939.

[23] BANHART, J. Manufacture, Characterisation and Application of Cellular Metals and Metal Foams, *Prog. Mater. Sci.*, 2001, 46, pp. 559–632.

[24] FABRIZIO, Q. BOSCHETTO, A. ROVATTI L. and L. SANTO. Replication Casting of Open-cell $AlSi_7Mg_{0.3}$ Foams. *Mater. Lett.*, 2011, 65, pp. 2558–2561.

[25] LARA-RODRIGUEZ, G. FIGUEROA, I. SUAREZ, M. NOVELO-PERALTA, O. ALFONSO, I. and R. GOODALL, A Replication-Casting Device for Manufacturing Open-cell Mg Foams, *J. Mater. Process. Technol.*, 2017, 243, pp. 16–22.
[26] WANNASIN, J. and M. FLEMINGS. Fabrication of Metal Matrix Composites by a High-Pressure Centrifugal Infiltration Process. *J. Mater. Process. Technol.*, 2005, 169, pp. 143–149.
[27] PIMIENTO, S. B. ROJAS, M.E.H. and M.E.P. PARDAVÉ. Processing and Characterization of Open–cell Aluminum Foams Obtained Through Infiltration Processes. International Congress of Science and Technology of Metallurgy and Materials SAM – CONAMET 2014. *Procedia Materials Science*, 2015, 9, pp. 54-61.
[28] BAFTI, H. and A. HABIBOLAHZADEH. Production of Aluminum Foam by Spherical Carbamide Space Holder Technique-processing Parameters. Materials and Design 31, 2010, pp. 4122–4129.
[29] AIDA, S.F. HIJRAH, M.N. AMIRAH, A.H. ZUHAILAWATI, H. and A.S. ANASYIDA. Effect of NaCl as a Space Holder in Producing Open Cell A356 Aluminium Foam by Gravity die Casting Process. *Procedia Chemistry* 2016, 19, pp. 234–240.
[30] NANSAARNG, S. and S. SOPHA. A Synthesis of Aluminium Foam from Ingot Compressing Method. Proceedings of the 1st WSEAS International Conference on Material Science (Materials´ 08), 2008, pp. 130 -133, ISSN: 1790-2769.
[31] HUSSAIN, Z and N.S. SUFFIN. Microstructure and Mechanical Behaviour of Aluminium Foams Produced by Sintering Dissolution Process Using NaCl Space Holder. *Journal of Engineering Science,* 2011, Vol. 7, pp. 37-49.
[32] MICHAILIDIS, N. and F. STERGIOUDI. Establishment of Process Parameters for Producing Al–Foam by Dissolution and Powder Sintering Metdod. *Materials and Design, 2011, 32, 3, pp. 1559-1564.*
[33] XIAO-QING, C., ZHI-HUA, W., HONG-WEI, M., LONG-MAO, Z. and Y. GUI-TONG. Effects of Cell Size on Compressive Properties of Aluminium Foam. Trans. Nonferrous Met. Soc. China, 2006, 16, pp. 351–356.
[34] LUNA, E.M.E. Investigation of Porous Metals as Improved Efficiency Regenerations. Doctoral thesis. The University of Sheffield, 2016.
[35] CONDE, Y. DESPOIS, J.F. GOODALL, R. MARMOTTANT, A. SALVO, L. SAN MARCHI C. AND A. MORTENSEN. Replication Processing of Highly Porous Materials. *Advanced Engineering Materials,* 2006, Vol. 8, No. 9, pp. 795-803.
[36] GOODALL, R. Chapter 10 - Porous Metals: Foams and Sponges, In I.T. Chang and Y.Y. Zhao eds. Advances in Powder Metallurgy: Properties, Processing and Applications, Cambridge: Woodhead Publishing Limited, 2013, pp. 273-307.
[37] ASHBY, M. F. EVANS, A. G. FLECK, N. A. GIBSON, L. J. HUTCHINSON J. W. and H. N. G. WADLEY. Metal Foams: A Design Guide, Boston: Butterworth Heinemann, 2000, pp. 1-39.
[38] CZYZEWSKI, A. Nature Inspires New Methods of Making Porous Materials [Online]. Available:http://www.theengineer.co.uk/civil/news/nature-inspires-new-methods-of-making-porous materials/1009543.article. (2011, August 1).
[39] ROUQUEROL, J. ANVIR, D. FAIRBRIDGE, C.W. EVERETT, D.H. HAYNES, J.H. PERNICONE, N. RAMSAY, J. D. F. SING, K. S. W. and K. K. UNGER. Recommendations for the Characterization of Porous Solids. *Pure & Applied Chemistry,* Vol. 66, No. 8, 1994, pp. 1739-1758.
[40] LIU, P. HU, B. YU, A. LIANG, K. AND S. GU. Development in Applications of Porous Metals. *Trans. Nonferrous Met. Soc. China,* 2001. Vol. 11, No. 5, pp. 629-638.
[41] ALOTHMAN, Z. A. A. Fundamental aspects of silicate mesoporous materials. *MDPI Materials.* Vol. 5, No. 12, 2012. pp. 2874-2902.
[42] ARRUA, R.D. STRUMIA, M.C. AND C.I. ALVAREZ-IGARZABAL. Macroporous Monolithic Polymers: Preparation and Applications. *MDPI Materials.* Vol. 2, No. 4, 2009, pp. 2429-2466.

References for Chapter 3

Physical nature of the foaming process

[1] KÖRNER, C. Integral Foam Molding of Light Metals. *Springer – Verlag Berlin Heidleberg,* 2008. ISBN 978-3-540-66838-9.

[2] LANGE, H. Schäume und ihre Stabilität. VDI-Berichte, 182, 1972, pp. 71–77.

[3] PUGH, R.J. Foaming, Foam Films, Antifoaming and Defoaming. *Advances in Colloid Interface Science,* 64, 1996, pp. 67–142.

[4] LUTZE and J. RUGE. Wasserstoff in Aluminium und seinen Legierungen. *Metall,* 44 (8), (1990), pp. 741–748 (in German).

[5] EICHENAUER, W. and J. MAKROPOULUS, Messung des Diffusionkoefizienten von Wasserstoff in flüssigem Aluminium. *Zeitschrift für Metallkunde,* 65(10), 1974, pp. 649–652 (in German).

[6] EICHENAUER, W. HATTENBACH, K., and H. WITTE. Zeitschrift für Metallkunde, 54, (1963), pp. 402.

[7] ROUČKA, J. Metalurgie neželezných slitin (Metallurgy of Non-Ferrous Alloys). 1. vyd. Brno: Akademické nakladatelství CERM, 2004. 148 s. ISBN 80-214- 2790-6 (in Czech, Europe).

[8] AMBRIZ, R.R. and D. JARAMILLO. Mechanical Behavior of Precipitation Hardened Aluminium Alloys Welds. *INTECH,* 2014.

[9] KOUKAL, J. et al. Materials and their Weldability. 1st ed. VŠB-TU Ostrava, 2009, ISBN 978-80-248-2025-5 (in Czech).

[10] TALBOT, D. E. J. Effects of Hydrogen in Aluminium, Magnesium, Copper, and their Alloys. *International Metallurgical Reviews,* 20, 1975, pp.166–184.

[11] KALOUSEK, J. et al. Physical Chemistry of Metallurgical Processes. 1st ed. Technical University of Liberec (in Czech, Europe).

[12] RANSLEY, C.E. and H. NEUFELD*. Journal of the Institute of Metals, 1947*-1948*, vol.* 74*, pp.* 559-*620.*

[13] OPIE, W.R. and N.J. GRANT. Hydrogen Solubility in Aluminium and Some Aluminium Alloys. *Transaction AIME*, vol. 188, 1950, pp. 1237-1241.

[14] TALBOT, D. E. J. and P. N. ANYALEBECHI. Solubility of Hydrogen in Liquid Aluminum.*Materials Sciences and Technology*, 4 1988, p. 1-4.

[15] EICHENAUER, W. HATTENBACH, K. and Z. PEBLER. The Solubility of Hydrogen in Solid a Liquid Aluminium, *Zeitschrift für Metallkunde.* Vol. 52, 1961, pp. 682-684.

[16] GRIGORENKO, G.M. and V. I. LAKOMSKY. Solubility of Hydrogen in Aluminum at Temperatures Characteristic of Arc Melting. *Auto. Weld.*, Vol 20, 1967, pp. 27–29.

[17] ICHIMURA, M. IMABAYASHI, M. and M. HAYAKAWA. Measurement of the Diffusion Coefficient and Solubility of Hydrogen in Solid Aluminium, *Journal of the Japanese Institute of Metals and Materials.* Vol 43, 1979, pp. 876- 883 (in Japanese).

[18] IMABAYASHI, M. ICHIMURA, M. and Y. Sasajima. Solubility of Hydrogen in Molten Aluminium. *Light Metals,* Vol 45, 1995, p 278-283 (in Japanese).

[19] ICHIMURA, M. and IMABAYASHI, M., Japan. Inst. Metals, 1979, 43, p. 876.

[20] LIU, H. BOUCHARD, M. and L. ZHANG. An Experimental Study of Hydrogen Solubility in Liquid Aluminium. *Journal of Materials Science* 30, 1995, pp. 4309-4315.

[21] BHAKTA, A. and E. RUCKENSTEIN. Decay of Standing Foams: Drainage, Coalescence and Collapse. *Advances in Colloid and Interface Science*, 70, 1997, pp. 1-124.

[22] KÖRNER, C. ARNOLD, M. and R.F. SINGER. Metal Foam Stabilization by Oxide Network Particles. *Materials Science and Engineering*, A 396: 28–40, 2005.

[23] BANHART, J. Manufacturing Routes for Metallic Foams. *The Journal of the Minerals, Metals and Materials Society*, 52: 22–27, 2002.

[24] PARK, S.H. and B.Y. HUR. A Study on the Viscosity and Surface Tension in Molten Al and the Effect of Additional Elements. In J. Banhart et al., editor, Cellular Metals. Manufacture, Properties, Applications, pp. 123–128. Verlag MIT Publishing, Berlin 2003.

[25] Mc NAMARA, G.R. and G. ZANETTI. Use of the Boltzmann equation to simulate lattice gas automata. Physical Review Letters, 61, 1988, pp. 2332–2335.

[26] WOOD, J.T. Production and Application of Continuously Cast, Foamed Aluminum. In J. Banhart and H. Eifert, editors, Proceedings of the Fraunhofer USA Metal Foam Symposium, Stanton, USA, pp. 31–36. MIT Press-Verlag, 1998.
[27] BAUMEISTER, J. German Patent, 4,018,360, 1990.
[28] STANZICK, H. WICHMANN, M. WEISE, J. HELFEN, L. Baumbach, T. and J. BANHART. Process Control in Aluminum Foam Production Using Real-time X-ray Radioscopy. *Advanced Engineering Materials,* 4, 2002, pp. 814–823.
[29] THIES, M. Lattice Boltzmann with Free Surface Applied to Formation of Metal Foams. [Doctoral thesis]. University Erlangen-Nürnberg, 2005.
[30] BINKS, B. P. Particles as Surfactants – Similarities and Differences. *Current Opinion in Colloid & Interface Science,* 7, 2002, pp. 21–41.
[31] PLESSET, M.S. and A. PROSPERETTI. Bubble Dynamics and Cavitation. *Annual Reviews of Fluid Dynamics,* 9, 1977, pp. 145–185.
[32] LANDAU, L.D. and E.M. LIFSCHITZ. Hydrodynamik. *Akademie-Verlag-Berlin*, 1974.
[33] IP, S.W. Wang, Y. and J. M. TOGURI. Aluminum Foam Stabilization by Solid Particles. Canadian Metallurgical Quarterly, 1999, 38, pp. 81–92.
[34] DIPPENAAR, A. The Destabilization of Froth by Solids. I. The Mechanism of Film Rupture. International *Journal of Mineral Processing*, 9, 1982, pp. 1-14.
[35] BABCSÁN, N. LEITLMEIER, D. and H.P. DEGISCHER. Foamability of Particle Reinforced Aluminum Melt. *Materialwissenschaft und Werkstofftechnik*, 34, 2003, 22–29.
[36] MIYOSHI, T. ITOH, M. AKIYAMA, S. and A. KITAHARA. ALPORAS Aluminum Foam: Production Process, Properties, and App
lications. *Advanced Engineering Materials,* 2, 2000, pp.179–183.
[37] KRIEGER, I.M. and T. DOUGHERTY. A Mechanism for Non-Newtonian Flow in Suspensions of Rigid Spheres. *Transactions of the Society of Rheology*, 3, 1959, pp. 137-152.
[38] KOKE, J. and M. MODIGELL. Flow Behaviour of Semi-solid Metal Alloys. *Journal of Non-Newtonian Fluid Mechanics,* 112, 2003, pp. 141–160.
[39] CHEN, J.Y. and Z. FAN. Modelling the Rheological Behavior of Semisolid Metal Slurries. Part 1 – Theory. *Materials Science and Technology*, 18, 2002, pp. 237–242.
[40] PARK, S.H. and B.Y. HUR. A Study on the Viscosity and Surface Tension in Molten Al and the Effect of Additional Elements. In J. Banhart et al., editor, *Cellular Metals. Manufacture, Properties, Applications,* Vorlag MIT Publishing Berlin, pp, 123-128.
[41] GUDEN, M. and S. YUKSEL The Particulate Composite Foams Used for Powder Compacts: Foaming Compression Behavior. *Journal of Materials Science* 41 (13), 2006, pp. 4075-4084.
[42] RAVI, K.R., PILLAI, R.M., AMARANATHAN, K.R., PAI, B.C. AND CHAKRABORTY, M. 2008, Fluidity of Aluminum Alloys and Composites: A review. Journal of Alloys and Compounds, 456: p. 201-210.
[43] WANG, J., GUO, Q., NISHIO, M., OGAWA, H., SHU, D., LI, K., HE, S. AND SUN, B., The Apparent Viscosity of Fine Particle Reinforced Composite Melt. *Journal of Materials Processing Technology*, 136, 2003, p. 60-63.
[44] SONG, Z. L., MA, L. Q., WU, Z. J. AND HE, D. P., 2000, Effects of Viscosity on Cellular Structure of Foamed Aluminum in Foaming Process. *Journal of Materials Science*. 35(1): p. 15-20.

***References for Chapter** 4*
Foaming agents for the production of cellular metal materials

[1] KÖRNER, C. Integral Foam Molding of Light Metals. *Springer - Verlag Berlin Heidleberg,* 2008. ISBN 978-3-540-66838-9.
[2] MATIJASEVIC-LUX, B. and J. BANHART. Improvement of Aluminium Foam Technology by Tailoring of Bloving Agent. *Sceipta Materrialia,* vol. 54 (4) February 2006, pp. 503-508.
[3] DAVIES, J. R. Aluminum and Aluminum Alloys ASM International, *Materials Park* 1993.
[4] KAMMER, C. (Ed.) Aluniniumtaschenbuch, vol. 1, Aluminium verlag Düsseldorf, 1995.

[5] KOIZUMI, T. et al. Foaming Agents for Powder Metallurgy Production of Aluminium Foam. *Material Transaction,* vol. 52, No. 4, pp. 728-773.
[6] BINKS, B.P Particles as Surfactants - Similarities and Differences. Current Opinion in *Colloid & Interface Science,* 7, 2002, pp. 2-41.
[7] DEGISCHER, H. P. and B. KRISZT, (Ed.) Handbook of Cellular Metals. WILEY-VCH, 2002.
[8] GERGELY, V. and T. W. CLYNE. The FORMGRIP Process: Foaming of Reinforced Metals by Gas Release in Precursor. *Advanced Engineering Materials,* 2000, 2, pp. 175-178.
[9] GERGELY, V. CURRAN, D.C. and T.W. CLYNE. The FOAMCARP Process: Foaming of Aluminium MMCs by the Chalk-Aluminium Reaction in Precursors. *Composites Science and Technology,* 63, 2003, pp. 2301-2310.
[10] GUI, M. C. WANG, D. B. WU, J. J. YUAN, G. J. and C. G. LI. Deformation and Damping Behaviors of Foamed Al-Si-SiCp Composite. *Materials Science and Engineering A*, 286, 2000, pp. 282-288.
[11] HASHIMOTO, Y. and H. OHASHI. Droplet Dynamics Using the Lattice-gas Method. *International Journal of Modern Physics C*, Vol. 08. No. 04, 1997, pp. 977-983.
[12] IBRAHIM, A.H. Effect of Material and Processing Parameters on the Morphology of Aluminium Foams Produced by the PM route. [PhD. Thesis], University of Erlangen Nürnberg, 2005.
[13] SASTRI, M. V. C. VISWANATHAN, B. and S. S. MURTHY. (Eds.) Metal Hydrides. *Narosa Publishing House,* 1998.
[14] GREENWOOD, N. and A. EARNSHAW. Chemistry of the Elements (2nd ed.). 1997 *Butterworth-Heinemann*. ISBN 0-08-037941-9.
[15] HOLLEMAN, A. F. WIBERG, E. Inorganic Chemistry Academic Press San Diego, 2001. ISBN 0-12-352651-5.
[16] RITTMEYER, P. and U. WEITELMANN. Hydrides. *Ullmann's Encyclopedia of Industrial Chemistry*. Wiley-VCH, 2005, pp. 13-199.
[17] MILLENBACH, P. and G. MEIR The Electrochemical Formation of Titanium Hydride. *Journal of the Less Common Metals*. 87 (2), October 1982, pp. 179-184.
[18] ZHANG, H. and E. H. KISI. Formation of Titanium Hydride at Room Temperature by Ball Milling. *Journal of Physics: Condensed Matter*. 9 (11), 1997, pp. 185-190.
[19] BROWN, *Ch. C. and R. E.* BUXBAUM, Kinetics of Hydrogen Absorption in Alpha Titanium". *Metallurgical Transactions A.* 19 (6), June 1988. pp. 1425-1427.
[20] FUKAI, *Y.* The Metal-Hydrogen System, Basic Bulk Properties, 2nd. edition. *Springer. 2005.* ISBN 978-3-540-00494-3.
[21] NUMAKURA, H; KOIWA, M; ASANO, H, and F. IZUMI Neutron Diffraction Study of the Metastable Titanium Deuteride. *Acta Metallurgica.* 36 *(8), 1988, pp. 2267-2273.*
[22] DONACHIE, M. J. Titanium a Technical Guide. *ASM International, 2000.* ISBN 0-87170-686-5.
[23] LU, G. BERNASEK, *S. and J.* SCHWARTZ. Oxidation of a Polycrystalline Titanium Surface by Oxygen and Water. *Surface Sci.* 458, (1-3), 2000, pp. 80-90.
[24] YANG, D. HUIWANG, J.CH. JANG, J. MA, A. and Z. P. LU. Effect of Decomposition Kinetics of Titanium Hydride on the AL Alloy Melt Foaming Process. Journal of Material Science and Technology, Vol. 31, Iss. 4, Apr. 2015, pp. 361-368.
[25] BOWMAN, R. CRAFT, B. CANTRELL, J. and E. VENTURINI, Effects of Thermal Treatments on the Lattice Properties and Electronic Structure of ZrH_x ". *Physical Review B*. 31 (9), 1985), pp. 5604-5615.
[26] BOWMAN, R. VENTURINI, E. CRAFT, B. and A. ATTALLA, A. Occupational Safety and Health Guideline for Zirconium & Compounds, Archived July 21, 2011, at the Wayback Machine. Occupational Safety & Health Administration, U.S. Department of Labor.
[27] MATIJASEVIC, B. Gorke, O. SCHUBERT, H and J. BANHART. Zirconium Hydride a Possible Blowing Agent for Making Aluminium Alloy Foams. *Porous Metals and Metal Foaming Technology,* 2005. Edited by H. Nakajima and N. Kanetake, The Japan Institute of Metals.
[28] SPEED, S.E. Foaming of Metal by Catalysed and Controlled Decomposition of Zirconium Hydride and Titanium Hydride. US Patent 3,981, 720, 1976.

[29] BLACK, J. P. Edge. An Introduction to the Nature and Technology of Hydrides, Metal Hydrides, ed. by W. M. Muller, J. P. Blackledge and G. G. Libowitz (Academic Press, New York, 1968), pp. 1-20.
[30] HELFEN, L. BAUMBACH, T. STANZICK, H. BANHART, J. ELMOUTAOUAKKIL J. A. and P. CLOETENS. Viewing the Early Stage of Metal Foam Formation by Computed Tomography Using Synchrotron Radiation. *Advanced Engineering Materials*, 4, 2002, pp. 808-813.
[31] MATIJASEVIC, B. FIECHTER, S. ZIZAK, I. GORKE, O. WANDERKA, N. SCHUBERT-BISCHOFF, P. and J. BANHART. PM Lightweight and Porous Materials, Powder Injection Moulding, *PM Functional Materials*, ed. by H. Danninger, R. Ratzi (European Powder Metallurgy Association, 2004) pp. 149-155.
[32] PAPADOPOULOS, D. P. OMAR, H. STERGIOUDI, F. TSIPAS S. A. MICHAILIDIS, N. The Use of Dolomite as a Foaming Agent and Its Effect on the Microstructure of Aluminium Metal Foams - Comparison to Titanium Hydride. *Colloids and Surfaces A: Physicochemical and Engineering Aspects.* Vol. 382, Iss. 1-3, 5., June 2011, pp.118-123.
[33] PAPADOPOULOS, D. P. [Thesis Ph.D]. Aristotle University of Thessaloniki, Department of Mechanical Engineering, 2008.
[34] BANHART, J. Manufacture, Characterization and Application of Cellular Metals and Metal Foams. *Progress in Materials Science* 46, 2001, pp. 559-632.
[35] HAESCHE, M. LEHMHUS, D. WEISE, J. WICHMANN, M. and I. C. MOCELLIN. Carbonates as Eoaming Agent in Chip-base Aluminium Foam Precursor. *Journal Matter Science Technology*, 2010, 26 (9) pp. 845-850.
[36] BAUMEISTER, J. WEISE, J. JESWEIN, A. BUSSE, M. and M. HAESCHE. Metal Foam Production from AlMg4.5Mn Recycling Machining Chips by Means of Thixocasting and the Effects of Different Additives for Stabilization, in Proc. 5th Int. Conf. on Porous Metals and Metallic Foams, eds. L.P. Lefebvre, J. Banhart, D.C. Dunand, DEStech Publications, Inc., Lancaster, 2008, 83.
[37] ESMAEELZADEH, S. SIMCHI, A. and D. LEHMHUS. Materials Science Engineering A, 2006, pp. 424-290.
[38] LEHMHUS, D. WICHMANN, M. and M. BUSSE. Kinetic Analysis of Foaming Agent Variants as a Means Toward Optimized Temperature Cycles and Foaming Agent/Matrix Alloy Combinations. *Porous metal metallic foam.* Conference METFOAM, 2007.
[39] BRYANT, J.D. United States Patent 2006/0243094 A1, 2006.
[40] KEVORKIAN, V. Low-Cost Aluminium Foams Made by $CaCO_3$ Particulates. *MJoM* Vol. 16 (3) 2010 pp. 205-219.
[41] CURRAN, D.C. Aluminium Foam Production using Calcium carbonate and with a Foaming Agent [Doctoral dissertation]. Department of Materials Science and Metallurgy, University Cambridge, 2003.
[42] GERAMIPOUR, T. and H. OVEISI. Effects of Foaming Parameters on Microstructure and Compressive Properties of Aluminium Foams Produced by Powder Metallurgy Method. *Transaction Nonferrous Metals Society.* China 27, 2017, pp. 1569-1579.
[43] NAKAMURA, T. GNYLOSKURENKO, S. V. SAKAMOTO, K. BYAKOVA, A. V. and R. ISHIKAWA. Development of a New Foaming Agent for Metal Foam. *Mater. Transactions,* 2002, 43, pp. 1191-1996.
[44] LÁZARO, J. SOLÓRZANO, E. RODRÍGUEZ-PÉREZ, M.A. Alternative carbonates to produce aluminium foams via melt route. *Procedia Materials Science* 4 2014, pp. 275-280.
[45] MIYOSHI, T., ITOH, M. AKIYAMA, S. and A. KITAHARA. 2000. ALPORAS Aluminium Foam: Production Process, Properties and Applications. *Advanced Engineering Materials,* 2, pp. 179-183.
[46] GERGELY, V., CURRAN, D.C. and T.W. CLYNE. The FOAMCARP Process: Foaming of Aluminium MMCs by the Chalk-Aluminium Reaction in Precursor. *Composites Science and Technology,* 63, 2003, pp. 2301-2310.
[47] BRYANT, J. D. CLOWLEY M. D. WILHELMY, M. D. KALLIVAYALIL, J. A. and W. WANG. In Metfoam 2007, Destech Publications, Inc., Lancaster, PA, 2008, p. 27.
[48] BARIN, I., KNACKE, O. and O. KUBASCHEWSKI. Thermodynamic properties of inorganic substances. 1977, Berlin: Springer-Verlag.

[49] SOLOKI, A. and H. ESMAILIAN. Carbonate Foaming Agents in Aliminum Foams: Advantage and Perspectives. Metallurgical and Materials Translations B, 2015, Vol. 46 B, pp. 1052-1057.

References for Chapter 5

Metals for the production of cellular materials and substances increasing the viscosity of their melts

[1] KALOUSEK, J. et al. Physical chemistry of metallurgical processes. VŠST Liberec 1980.
[2] BANHART, J. Manufacture, Characterisation and Application of Cellular Metals and Metal Foams. *Progress in Materials Science* 2001, 46, pp. 559-632.
[3] JIN, I. KENNY, J. I. and H. SANG. US Patent 5112697, 1992.
[4] BABCSÁN, N., BANHART, J. and D. LEITLMEEIER. Metal Foams - Manufacture and Physics of Foaming. In: International Conference *Advanced Metallic Materials*, 2003, 5-7 November, Smolenice Slovakia.
[5] JIN, I. KENNY, L.D and H. SANG US Patent 5112 697 (1992).
[6] GERGELI, V. JONES, L. and T. W. CLYNE. The Effect of Capillarity-Driven Melt Flow and Size of Particles in Cell Faces on Metal Foam Structure Evolution Trans. JWRI 30 (2001), pp. 371-376.
[7] LEITLMEIER, D. DEGISCHER H. P. and H.J. FLANKL. Development of a Foaming Process for Particulate Reinforced Aluminum Melts. *Advanced Engineering Materials* 4 (2002) pp. 735-740.
[8] BABCSÁN, N. LEITLMEIER, D. Degischer H. P. and J. Banhart, The Role of Oxidation in Blowing Particle-Stabilised Aluminium Foams. *Advanced Engineering Materials* 6, 2004, pp. 421-428.
[9] CAPTAY, G. Interfacial Criteria for Stabilization of Liquid Foams by Solid Particles. *Colloid and Surfaces* A: Physicochemical Engineering Aspects 230, 2003, pp. 67-80.
[10] KENNEDY, A.R. Proc. Int. Conf. High Temperature Capillarity, 29. June 2. July 1997, Cracow, Poland, Edited by N. Eustathopoulos and N. Sobczak, (1997), pp. 395-399.
[11] BABCSÁN, N. Ceramic Particles Stabilized Aluminium Foams. [Ph.D. dissertation], University of Miskolc, (2003).
[12] YÜKSEL, S. The Effects of SiC Particle Addition on the Foaming and Mechanical Behavior of Aluminum Closed-Cell Foams Produced by Foaming of Powder Compacts. Institute of Technology-Graduate School of Engineering and Sciences of İzmir, July 2010.
[13] MALEKJAFARIAN, M. and S.K. SADRNEZHAARD. Effect of SiC on Microstructure Features and Compressive Properties of Aluminium Foams. *Scientia Inranica - Transaction A*: Civil Engineering 21(4), 2014 pp. 1325-1329.
[14] KAPTAY, G. A Unified Equation for the Viscosity of Pure Liquid Metals. *Z. Metallkd* 96 (2005), pp. 1-8.
[15] FERREIRA, I. L et al. Dependence of Surface Tension and Viscosity on Temperature in Multicomponent Alloys. *Implication for Material Processing,* March 2019.
[16] SHI, D. et al. Effect of the Degassing on Surface Tension of Eutectic Al-Si alloys. *Metal Materials,* 47, 2009, pp. 51-54.
[17] SHIRANGAM, P. et al. Partial Pair Correlation Functions and Viscosity of Liquid Al-Si Hypoeutectic Alloys via High-energy X-ray Diffraction Experiments. *Philosophical Magazine A 91* (30) 2011, pp. 3867-3904.
[18] SRIRANGAM, P. KRAMER, M. J. and S. SHANKAR. *Acta Materialia* 59, (2) 2011, pp. 503- 513.
[19] XIGUI, S. et al. Temperature Dependent Viscosities of Eutectic Al-Si Alloys Modified with Sr and P. *Journal of Alloys and Compounds,* vol. 479, Iss. 1-2, 2009, pp. 670-673.
[20] YAN, M. and W. LUO, *Materials Chemistry and Physics,* 2007, 104 pp. 267-270.
[21] HRMA, P. Glass Viscosity as a Function of Temperature and Composition: A Model Based on Adam-Gibbs Equation. *Journal Non-Crystalline Solids*, 2008, 354, pp. 3389-3399.
[22] KOBATAKE, H. et al. Surface Tension of Binary Al-Si Liquid Alloys. Journal of Materials Science, 2015, vol. 50, Iss. 9, pp. 3351-3360.

[23] BANHART, J. Ligh-Metal Foams - Hystory of INNOVATION and Technological challenges. *Advanced Engineering Materials*, 2013. DOI: 10.002/adem. 201200217.
[24] KINGREY, W.D. and M. HUMENIK. Surface Tension at Elevated Temperatures. I. Furnace and method for use of the sessile drop method: surface tension of silicon, iron and nickel. J. Phys. Chem. 1953, 57, pp.359-363.
[25] DZHEMILEV N.K. POPEL S.I. and B.V. TSAREVSKII. Isotherm of the Density and Surface Tension of Iron-Silicon Melt. Fiz. Met. Metalloved. 18, 1964, pp. 83-87.
[26] ELYUTIN V.P, KOSTIKOV V.I. and V. LEVIN. Surface and Density of Si-Ti Melts, Fizichekaya Khimiay Poverkhnostnykh Yavlenii v Rasplavakh. Naukova Dumka, Kiev, 971, pp. 153-159.
[27] MUKAI, K. YUAN, Z. Nogi, K. and. T. HIBIYA. Effect of Oxygen Partial Pressure on the Surface Tension of Molten Silicon and its Temperature Coefficient. ISIJ Int. 40, 2000, pp. 148-152.
[28] GOUMIRI, L. JOUD, J.C. RESRE, P. MICHTER, J.M. Sensions Superficielles D' alliages liquides binaires presentant un caractere d'immiscibilite: Al-Pb, Al-Bi, Al-Se et Yn-Bi. Sur Sci 83, 1979, pp. 471-486.
[29] LEVIN, E.S. AYUSHINA, G.D. GEL'D, P.V. Density and Surfaceenergy Polytherms of Liquid (molten) Aluminum. Vysokika Temp. 6, 1968, pp. 416-418.
[30] POPEL, S.I. KOZHURKOV, V.N. ZHUKOV, A.A. Izv Akad Nauk SSSR Met 5,1975, p. 69 (in Russian).
[31] YATSENKO, S.P. KONONENKO, V.I. SUKHMAN, A.L. Experimental Investigation of Temperature Dependence Between Surface Tension and Density of Tin, Indium, Aluminum and Gallium. *Term Phys High temp* 10, 1972, pp.66-71. Translated from Teplofixika Vysokikh Temperatur (in Russian).
[32] CORDOVILLA, C.G. LOUIS, E. PAMIES, A. The Surface Tension of Liquid Pure Aluminum and Aluminum-Magnesium Alloy. *J Mater Sci* 21, 1986, pp. 2787-2792.
[33] SARAVANAN, R. A, MOLINA, J. M, NARCISO, J. GARCÍA-CORDOVILLA, C. and E. LOUIS. Effects of Nitrogen on the Surface Tension of Pure Aluminium at High Temperatures. *Scripta Mater* 2001, 44 (6), pp. 965-970. DOI: 1016/S1359-6462(00)00688-6.
[34] MOLINA J.M, et al. The Surface Tension of Liquid Aluminium in High Vacuum: The role of surface condition. *Int J Adh Adhesives* 27, 2007, pp. 394-401.
[35] LEVIN, E.S, AYUSHIMA, G.D, GEL'D, P.V, RYSS, M.A and V.F. SERYI. In: Eremenko VN (ed) Phys. Khim. Poverkh Yavleni, vol 120. Naukova Dumka, (1971) Kiev, pp. 153-156 (in Russian).

References for Chapter 6
Characteristics of physical and mechanical properties of cellular metallic materials

[1] KRETZ, R. PM-Schaumaluminium, Legierungen Mechanische Eigenshaften, LKR, 2003, Ransdofen Österreich.
[2] ASHBY, M. F. EVANS, A. FLECK, N. A. GIBSON, L. J HUTCHINSON, J. W. and H. N. G WADLEY. Metal Foams - A design guide. Butterworth Heinemann, 2000.
[3] XIA, X.C. et al. Effect of Porosity and Pore Size on the Compressive Properties of Closed Cell Mg Alloy Foam. *Journal Magnesium and Alloys* Vol. 1, Iss. 4, 2013, pp. 330-335.
[4] ANDREWS, E. SANDERS, W. and L. J. GIBSON, Compressive and Tensile Behaviour of Aluminum Foams. *Materials Science Engineering*, A 270, 1999, pp. 113-124.
[5] MAHAJAN, S. M. JADHAV, G. A. Aluminium Foaming for Lighter Structure. *International Journal Computational Engineering Research* (IJCER) vol. 05, Iss. 01 January 2015, pp. 70-74.
[6] SHIM, J.D. and B.Y. BYUN. Production Process of Porous Materials and their Applications. *Korean Journal of Material Research*. Vol. 25. No. 3, 2015, pp. 155-164.
[7] ŠIMANČÍK, F. JERZ, J. KOVÁČIK, J. and P. MINÁR. Aluminium Foam a New Lightweight Structural Material. *Metal Materials*, 35, 1997, no. 4, pp. 265-277.
[8] WANG, ZHAO, H. M. L. and G. YANG. *Scripta Materialia* 54, 2006, p. 83.
[9] RAJ, R.E. PARAMESWARAN, V. and B. S. DANIEL. *Materials Science and Engineering* A 526, 2009, p. 11.

[10] KRETZ, R. PM-Schaumaluminium, Legierungen Mechanische Eigenschaften, LKR, 2003, Ranshofen Österreich.
[11] ORT, M. Use of metal foams in automotive parts. Master thesis, KSP-FS, TUL, 2008.
[12] GIBSON, L.J. ASHBY M.F. Cellular Solids. Cambridge University Press, New York, 1997.
[13] MATA, A. SANTOS, A. D. PARENTE, M. P. L. VALENTE, A. A. FERNANDES, A. A. and R. N. JORCE. Study on the Forming of Sandwich Shell with Closed Cell Foam Cores. *International Journal of Material Foaming*, vol. 7, Iss. 4, 2014, pp. 413-424.
[14] GUDEN, M. and S. YÜKSEL. SiC Particulate Aluminium Composite Foams Produced From powder compacts: foaming and compression behaviour. *Journal of Materials Science* 41(13) 2006, pp. 4075-4084.
[15] ANDREWS, E. SANDERS, W. and. L. J. GIBSON. Compressive and Tensile Behaviour of Aluminium Foams. *Materials Science Engineering*, A 270, 1999, pp. 113-124.
[16] ASTM International, ASTM E9-89a Standard Test Method of Metallic Materials at Room Temperature, ASTM International Standard, 100 Barr Harbor Drive, PO Box C 700, West Conshohocken, PA 19428-2959, United States, 2000.
[17] KOVÁČIK, J. OROVČÍK, Ľ. and J. JERZ. High-temperature Compression of Closed-cell Aluminium Foams. *Kovove Materialy.* 54, 2016, pp. 429-440. DOI: 10.4149/km 2016 6 429.
[18] SGIMURA, Y et al. On the Mechanical Performace of Closed Cell Al Alloy Foams. *Acta Materialia,* vol. 45, Iss. 12, 1997, pp. 5245-5249.
[19] MARKAKI, A. Mechanical Behaviour of Layered Metal Foam/Ceramic Composites. [PhD. Thesis]. Cambridge, Cambridge University 2000, p. 95.
[20] SIMANČÍK, F. KOVÁČIK, J. and N. SEDLIAKOVÁ. In: Proceedings of Powder Metallurgy World Congress and Exhibition. Shrewsbury, EPMA 1998, p. 245. ISBN 1 899072 09 8.

References for Chapter 7

References chapter 7.1.1.

[1] MATIJASEVIC-LUX, B. BANHART, J. FIECHTER, S. GÖRKE, O. and N. WANDERKA. Modification of Titanium Hydride for Improved Aluminium Foam Manufacture. *Acta Mater*, 54, 2006, pp.1887-1900.
[2] KOIZUMI, T. et al. (2011). Foaming Agents for Powder Metallurgy Production of Aluminium Foam. *Materials Transactions*, Vol. 52, No. 4, pp. 728 to 733.
[3] ASHBY, M.F. et al. Metal Foams: A Design Guide. 2000 Ed. Betterwort-Heinemann.
[4] BANHART, J. Light - Metal Foams History of Innovation and Technological Challenges. *Advanced Engineering Materials* 2013, No 3, pp. 82-111.

References for chapter 7.1.2

[1] The Lincoln Electric Company the Procedure Handbook of Arc Welding 9.1(1-9.4-12).
[2] HASHIMOTO, Y. and H. OHASHI. Droplet Dynamics Using the Lattice-gas Method. *International Journal of Modern Physics* C, 8, 1997, p.977-983.
[3] AMBRIZ, R. R. and D. JARAMILLO. Mechanical Behavior of Precipitation Hardened Aluminium Alloys Welds. INTECH, 2014.
[4] EICHENAUER, W. and J. MAKROPOULUS. Messung des Diffusionkoefizienten von Wasserstoff in flüssigem Aluminium. Zeitschrift für Metallkunde, 65(10), 1974, p. 649-652.
[5] ROUČKA, J. Metallurgy of non-ferrous alloys. 1st ed. Brno: Akademické nakladatelství CERM, 2004. 148 s. ISBN 80-214- 2790-6 (in Czech, Europe).
[6] TALBOT, D. E. J. Effects of Hydrogen in Aluminium, Magnesium, Copper, and Their Alloys. *International Metallurgical Reviews*, 1975, 20, pp.166-184.
[7] SAN-MARTIN, A. and F. D. MANCHESTER. The H-Ti (hydrogen-titanium) system. Bulletin of alloy phase diagrams, 8(1), 1987, p. 30-42.
[8] LIU, H. BOUCHARD, M. and L. ZHANG. An Experimental Study of Hydrogen Solubility in Liquid Aluminium. *Journal of Materials Science* 30, 1995, p. 4309-4315.
[9] TALBOT, D. E. J. and P. N. ANYALEBECHI. Materials Sciences and Technology 4 1988, p. 1-4.

[10] RANSLEY, C.E. and H. NEUFELD. J. Inst. Metals, *1947-1948,* vol. *74*, pp. *559-620*.
[11] OPIE, W. R. and N.J. Grant. Hydrogen Solubility in Aluminium and Some Aluminium Alloys. Transaction AIME, vol. 188, 1950, pp. 1237-1241.
[12] ANYALEBECHI, P. N. Analysis of The Effects of Alloying Elements on Hydrogen Solubility in Liquid Aluminium Alloys. Scripta Metallurgica at Materialia, Vol. 33, No. 8 (1995) pp. 1209-1216.
[13] GRIGORENKO, G. M. and and V. I. LAKOMSKY. Solubility of Hydrogen in Aluminum at Temperatures Characteristic of Arc Melting. *Auto. Weld.*, Vol 20, 1967, pp. 27-29.
[14] FEICHTINGER, H. and R.A. MORACH. Solubility of Hydrogen in Molten Aluminum at High Pressures, Aluminium, Vol 63, 1987, pp. 181-187 (in German).
[15] ICHIMURA, M. IMABAYASHI, M. and M. HAYAKAWA. Measurement of the Diffusion Coefficient and Solubility of Hydrogen in Solid Aluminium. *Japanise Inst. Met.,* Vol. 43, 1979, pp. 876-883 (in Japanese).
[16] TALBOT, D.E.J. The effects of Hydrogen in Aluminium and its Alloys, Maney Publishing on behalf of the Institute of Materials, London 2004, ISBN 1-902-653-73-4.
[17] PAPP, K. and KOVACS-CSETENYI, E. Scripta metall., 1981, 15, p. 161. 17.
[18] EICHENAUER, V.W. The Solubility of Hydrogen and Deuterium in Extremely Pure Aluminium at Temperature Ranging from 400 to 600°C, Z. Metallkunde., Vol. 59, 1968, pp. 613-616 (in German).
[19] OUTLAW, R. A. et al., Scripta Metall., 1982, 16, p. 287.
[20] KALOUSEK, J. et al. Physical Chemistry of Metallurgical Processes. 1st ed. Technical University of Liberec (in Czech, Europe).
[21] IMABAYASHI, M. ICHIMURA, M. and Y. Sasajima. Solubility of Hydrogen in Molten Aluminium, Keikinzoku (Light Metals), Vol 45, 1995, p 278-283 (in Japanese).
[22] [16] GERGELY, V. CURRAN, D.C. and T.W. CLYNE. The FOAMCARP Process: Foaming of Aluminium MMCs by the Chalk-aluminum Reaction in Precursors. Composites Science and Technology, 63, 2002, pp.2301-2310.
[23] ICHIMURA, M. and Imabayashi, M., Japan. Inst. Metals, 1979, 43, p. 876.
[24] PAPP, K. and KOVACS-CSETENYI, E., Scripta metall., 1977, 11, p. 921.
[25] TALBOT, D.E.J. The effects of Hydrogen in Aluminium and its Alloys, Maney Publishing on behalf of the Institute of Materials. London 2004, ISBN 1-902-653-73-4.

References for chapter 7.2.2

[1] JERZ, J. Foamed Aluminium and Aluminium Alloys Prepared by Powder Metallurgy. Ph.D. thesis, TU Vienna, 1995.
[2] MORENO, F.G. Commercial Application of Metal Foams: Their Properties and Production. *Materials,* 9. 85, 2016, pp. 1-27.
[3] PIMIENTO, S. B. ROJAS, M. E. H. and M. E. P. PARDAVÉ. Processing and Characterization of Open-cell Aluminum Foams Obtained Through Infiltration Processes. International Congress of Science and Technology of Metallurgy and Materials SAM CONAMET 2014. *Procedia Materials Science*, 9, 2015, pp. 54-61.
[4] HASSANI, A. HABIBOLAHZADEH, A. AND H. BAFTI. *Materials at Design.* Vol. 40, September 2012, pp. 510-515.
[5] Technical Materials of the Company Alumeco Group, Denmark. (www.alumeco.com).

References for chapter 7.2.3

[1] LUNA, E.M.E. at al. (2014). Casting Protocols for the Production of Open Cell Aluminium Foams by the Replication Technique and the Effect on Porosity. *Journal of Visualized Experiments.* 94, e52568. www.jove. com.
[2] LUNA, E.M.E. Investigation of Porous Metals as Improved Efficing Regeneration. [Doctoral thesis], The University of Sheffield - Faculty of Engineering, March 2016.
[3] ASHBY, M. F. et al. (2000). Metal Foams: A Design Guide. Ed. Betterwort-Heinemann.
[4] CONDE, Y. DESPOIS, J.F. GOODALL, R. MARMOTTANT, A. SALVO, L. SAN MARCHI, C. and A. MORTENSEN. Replication processing of highly porous materials. *Advanced Engineering Materials,* Vol. 8, No. 9, (2006). pp. 795-803.

[5] MORENO, F.G. Commercial Application of metal Foams: Their properties and production. *Materials,* 9. 85, 2016, pp. 1-27.
[6] PIMIENTO, S. B. ROJAS, M.E.H. and M. E. P. PARDAVÉ. Processing and Characterization of Open-cell Aluminum Foams Obtained Through Infiltration Processes.International Congress of Science and Technology of Metallurgy and Materials SAM-CONAMET 2014. *Procedia Materials Science*, 9, (2015). pp. 54-61.

References for chapter 7.3

[1] FRAŇA, K. CFD - Computational Fluid Dynamics in magneto-hydrodynamics and industrial applications. ES TUL Liberec 2015.
[2] FRAŇA, K. Computational Fluid Dynamics in Magneto-hydrodynamics and Application. ES TUL Liberec 2015.

References for chapter 7.4

[1] YANG, Y. WANG, S. and C. WEN. Gas-Liquid Two-Phase Flows in Double Inlet Cyclones for Natural Gas separation. *Cogent Engineering,* 4(1), 2017.DOI: 10.1080/23311916.2017-1373421.
[2] BRENNEN, Ch. E. Fundamentals of the Multiphase Flow. Cambridge University Press, 2005.
[3] MA, Z. H. et al. A Compressible Multiphase Flow Model for Violent Aerated Wave Impact Problems. Proc. R. Soc. A vol. p. 470, http://dx.doi.org/10.1098/ rspa.2014.0542, 2017.
[4] JANG, W.Y. HSIEH, CH. MIAO, CH. and Y. CH. YEN. Microstructure and Mechanical Properties of Alporas Closed-cell Aluminium Foam. *Mat. Character.* 107, 2015, pp. 228-238.

Annex 1

Table P1 List of manufacturers or suppliers of metal foams

Firms engaged in the manufacture of aluminium foams and metallic porous materials		
Company name	**Product/process name**	**Characteristics**
Alantum (Korea/Germany)		Nickel and iron-based open foams, special foams for filtration, catalysis or electrodes.
Al Carbon (Germany)		Composites, combinations of composites and Al-foams. Open and closed cell foams.
Alcarbon, GmbH (Switzerland)		Composites, combinations of composites and Al-foams. Open and closed cell foams.
Aluinvent Inc. (Hungary)		Aluminum foams with small and regular pores, gas injection and aluminum composite matrix.
Alulight (Austria)		Development and production of aluminium foams based on powder metallurgy, production of crusted plates and various foam shapes,
Alusion (Canada)		Production of aluminium foam plates and foam products (a division of CYMAT)
Alveotec (France)	CASTFOAM	Production of aluminium foams by the usual foundry process.
American Elements (USA)		Production of high quality aluminium foams.
Chand Eisenmann Metallurgical (USA)		Production of porous sintered material for filters, sales media, etc.
China Beihal Building Material Co. Ltd. (China)	ALPORAS	Production of aluminium foam panels and sandwiches, production by the process Alporas.
Composite Materials Ltd. (Russia)		Production of aluminium foams for structural parts.
Corex Honeycome (UK(		Production of aluminium cores.
CYMAT (Canada)	SAF	Aluminium foamed panels are produced by direct fusion of aluminium melt. SAF foamed aluminium (Stabilized Aluminium Foam).
Dunlop Equipment (England)		Production of open cell foams for high temperatures\ 900 °C, gas flow control applications and noise dampening.
ERG Materials and Eirospace Corporation (USA)	DUOCEL	Production of metal foams by open-cell casting
ECOCONTACT (France)		Production of foams with abraded cells for the abrasion of Al, Cu and steel for electrical purposes.
Exxcentis (Switzerland)		Production of aluminium porous materials, i.e. open-cell "space holder" materials, based on the use of NaCl.
FOAMTECH (Korea)	ALPORAS	Aluminium plates and sandwiches made by the Alporas method
Franhofer Institute (Germany)	IFAM	Production of aluminium foams, aluminium foam sandwiches and aluminium foam-steel sandwiches based on powder metallurgy.
Freund GmbH (Austria)		Foam materials for interior furnishing, foam distribution.
Goodfellows Corporation (USA)		Distribution of Al, Cu, Zn, Ni and foamed materials.
Havel metal foam GmbH (Germany)		Production of aluminium foam sandwich materials.
Hollоment GmbH (Germany)		Production of stable lightweight and multifunctional cellular materials.
Integran Technologies Inc. (Canada)		Production of metal foams for energy and noise absorption.

IWE Greiswald (Germany/Austria)		Production of Al foams and industrial honeycombs based on powder technology.
Korea Metal Foams (Korea)		Casting of open-cell metal sponges based on Al, Cu and Ni.
ERG Matal Foam (USA)		Production of Duocel, Al, Cu open cell foam system.
Liaoning Rontec Advanced Co. Ltd.(China)		Production of aluminium foam blocks and plates.
LKR, Ligh metallkomponenten zentrum (Austria)	METCOMB	Production of aluminium foam by injecting gas from an external source using a bubbling agent. The foamed melt is fed into a mould.
MEPURA Ranshofen (Austria)	MEPURA ALULIGHT	Production of aluminium foams based on powder metallurgy
Mitshubishi Material(Japan)		Production of metal foams with open cells.
M-Pore (Germany)		Casting of metal sponge materials with open cells Al, Cu, and hard polymers.
Pohltec Metalfoam GmbH (Germany)		Production of Al foam sandwiches (AFS) and aluminium foam plates.
Porometal (China)		Production of open-cell metal sponge materials based on Ni, Cu, Ni+Fe, and Al1Cr+Al for the production of electrode and filter components.
Reade Advenced Materials (USA)		Production of metals with open cells by electrical and foundry methods, processing of the following metals: Al, Cu, Hf, Pb, Ni, Nb, Ti, W, Zr.
RECEMAT BV (Netherlands)		Supplier of open-cell metal foams based on Ni, Ni alloys, Cu and Al alloys and Al alloys.
SELEE Corporation (USA)		Production of porous ceramics, metals and carbon for various industrial purposes.
Shanxi Putal Aluminium Fo am Manufacturing Co. Ltd (China)		Production of aluminium foams and foam products.
Shinko Wire Company (Japan)	ALPORAS	It produces aluminium foam based on the melting of aluminium with calcium and the addition of the foaming agent TiH_2
Spectra-Mat (USA)		Production of open-cell sponge materials from tungsten and molybdenum.
Veber Industriale (Italy)		Distribution of FOAMTECH products.

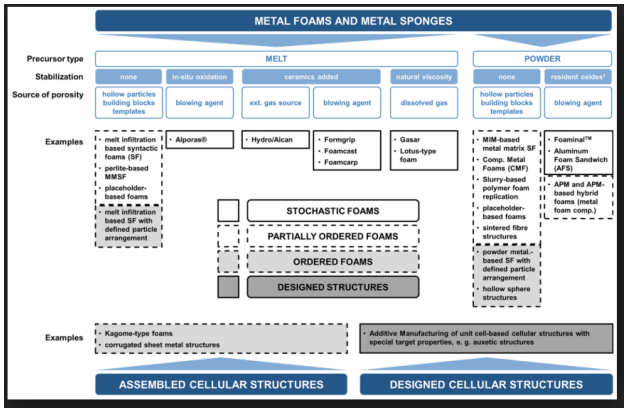

Reference: Lehmhus, D., Vesenjak, M., Schampheleire, S., Fiedler, T. (2017). From Stochastic Foam to Designed Structure: Balancing Cost and Performance of Cellular Metals. Materials, vol. 10, no. 8, p. 922, DOI:10.3390/ma10080922.

Index

Název	Cellular Metal Materials
Autor	prof. Ing. Iva Nová, CSc. prof. Ing. Karel Fraňa, Ph.D. doc. Ing. Jiří Machuta, Ph.D. .
Vydavatel	Technická univerzita v Liberci Studentská 1402/2, Liberec
Schváleno	Rektorátem TUL dne 17. 3. 2025, čj. RE 10/25
Vyšlo	v dubnu 2025
Vydání	1.
ISBN	978-80-7494-729-2
Č. publikace	55-010-25

Tato publikace neprošla redakční ani jazykovou úpravou